ENHANCED INTEGRATION OF SHEAR WAVE VELOCITY PROFILING IN DIRECT-PUSH SITE CHARACTERIZATION SYSTEMS

A Dissertation
Presented to
The Academic Faculty

by

Alexander Vamie McGillivray

In Partial Fulfillment
of the Requirements for the Degree
Doctor of Philosophy in the
School of Civil and Environmental Engineering

Georgia Institute of Technology
December 2007

ENHANCED INTEGRATION OF

SHEAR WAVE VELOCITY PROFILING IN

DIRECT-PUSH SITE CHARACTERIZATION SYSTEMS

Approved by:

Dr. Paul W. Mayne, Advisor
School of Civil & Environmental Engrg
Georgia Institute of Technology

Dr. L. Timothy Long
School of Earth & Atmospheric Sciences
Georgia Institute of Technology

Dr. J. David Frost
School of Civil & Environmental Engrg
Georgia Institute of Technology

Dr. Robert C. Bachus
Principal Engineer
Geosyntec Consultants, Inc.
Atlanta, GA

Dr. Glenn J. Rix
School of Civil & Environmental Engrg
Georgia Institute of Technology

Date Approved: November 12, 2007

This is for you Dad

.

ACKNOWLEDGMENTS

The first thank you goes to my advisor Dr. Paul W. Mayne for giving me the opportunity to pursue this research and for having the patience to help me see it through. I am eternally grateful for the invaluable experience and all of the wonderful in-situ testing toys that you entrusted to me. I would also like to thank Dr. David Frost for his hospitality and generosity in taking me in at the Savannah campus, and for keeping the pressure on me to get this finished. Moving to Savannah was just what I needed to get focused on the prize.

I owe a debt of gratitude to Ken Thomas, our happily retired lab manager/building manager/problem solver/equipment scavenger/grumpy old man. I don't know how the department will make it without you. Your creative problem solving really made this possible. Congratulations to you for beating me to the finish line. I wasn't too far behind.

My fellow students were always there for me, including Andrew Fuggle, Laura and Todd Spencer, Jenn Knapp (Gray), Tammy Hebeler. Special thanks to Robert Hurt for rebuilding my old Toyota truck in the parking lot behind the CE building. My new electrical engineering friend Sriraaman Sridharan (Sri) saved the day to give me the electronics help I needed to pull the data acquisition together for my final field trip.

To my good friends and former students Julio Valdes, Greg Hebeler, Matt Evans, and James Schneider, thank you all for your inspiration, support, and great memories. I always knew that I wanted to study Geotechnical Engineering, but I never realized what is so great about it until I got the chance to work with all of you. I'm also grateful to my field testing companions and friends Tianfei Liao and Guillermo Zavala. Traveling around the country with the two of you drove me insane, but I wouldn't trade a minute of it for anything. You guys are the best. Thanks also to the rest of the research group, Amr Elhakim, Fikret Atalay, and Joan Larrahondo. Billy Camp bailed me out on multiple occasions with much needed advice and help getting access to test sites. Mark Quinn

deserves credit for this work too as co-inventor of the RotoSeis. He turned my words into a working wooden RotoSeis that made me realize that we might actually have something.

I depended on my non-engineering friends to keep me sane, and to deliver a steady stream of jokes at my expense to keep me motivated to graduate. Steve Pejza even went so far as to provide me with a second home in Atlanta whenever I needed a place to stay.

I would like to recognize the support of my family during my time at Georgia Tech. That includes Dr. Leroy Emkin who looked out for me all these years and convinced me that I can do great things.

The one person that outshines all the others is my incredible wife Catherine. I'd be lost without her.

TABLE OF CONTENTS

LIST OF TABLES

LIST OF FIGURES

SUMMARY

Shear wave velocity (V_S) is a fundamental property of soils directly related to the shear stiffness at small-strains. Therefore, V_S should be a routine measurement made during everyday site characterization. There are several lab and field methods for measuring V_S, but the seismic piezocone penetration test (SCPTu) and the seismic dilatometer test (SDMT) are the most efficient means for profiling the small-strain stiffness in addition to evaluating large-strain strength, as well as providing evaluations of the geostratigraphy, stress state, and permeability, all within a single sounding.

Although the CPT and DMT have been in use for over three decades in the USA, they are only recently becoming commonplace on small-, medium-, and large-size projects as more organizations begin to realize their benefits. Regrettably, the SCPTu and the SDMT are lagging slightly behind their non-seismic counterparts in popularity, in part because the geophysics component of the tests has not been updated during the 25 years since the tests were envisioned. The V_S measurement component is inefficient and not cost effective for routine use. The purpose of this research is to remove the barriers to seismic testing during direct-push site characterization with SCPTu and SDMT.

A continuous-push seismic system has been developed to improve the integration of V_S measurements with SCPTu and SDMT, allowing V_S to be measured during penetration without stopping the progress of the probe. A new type of portable automated seismic source, given the name *RotoSeis*, was created to generate repeated hammer strikes at regularly spaced time intervals. A true-interval biaxial seismic probe and an automated data acquisition system were also developed to capture the shear waves. By not limiting V_S measurement to pauses in penetration during rod breaks, it is possible to make overlapping V_S interval measurements. This new method, termed *frequent-interval*, increases the depth resolution of the V_S profile to be more compatible with the depth intervals of the near-continuous non-seismic measurements of the SCPTu and the SDMT.

1. INTRODUCTION

1.1. Objectives and Motivation

Accurate characterization of subsurface conditions is the basis for all geotechnical analyses and designs involving the construction of foundation systems, walls, dams, embankments, and excavations, as well as the evaluation of earthquake ground motions and liquefaction susceptibility. Proper site characterization consists of a multifaceted program of drilling, sampling, laboratory testing, and in situ testing. Combinations of the multiple characterization techniques, often within the same test, can be used to determine the behavior of soils from small-strain to large-strain levels.

Shear wave velocity is a particularly important characteristic of geomaterials because it directly relates to the shear stiffness of the material at small-strains. In combination with large-strain strength testing, the entire strain range of the material can be defined. The measurement of shear wave velocity is often overlooked in routine site characterization because of difficulties in obtaining sufficiently high quality samples for lab testing, and because of seemingly complex and expensive field measurement methods, such as the crosshole test (CHT) and downhole test (DHT) which are performed inside boreholes that are drilled, cased, and grouted.

The seismic piezocone penetration test (SCPTu) and the seismic dilatometer test (SDMT) are hybrid tests that combine near-continuous penetration measurements with an intermittent geophysics operation. These tests employ alternating phases of penetration-type readings with downhole geophysical testing. Both the SCPTu and the SDMT are valuable tools for quickly and reliably characterizing the initial shear modulus (G_{max} or G_0) from shear wave velocity (V_S), such that $G_0 = \rho_t \cdot V_S^2$, where ρ_t = total soil mass density. Both the SCPTu and SDMT also provide concurrent data on geostratigraphy, soil type, strength, and stress-state parameters from their penetration measurements.

Even though the SCPTu and SDMT are readily available tools, V_S measurements

are often not considered necessary for standard site characterization, in part because a "seismic" test implies that the purpose is for investigations involving earthquake or other dynamic concerns, and not for application to static concerns. In these instances, V_S measurements are used to determine the dynamic shear modulus (G_{dyn}). Yet, it has now been well-documented that the dynamic stiffness is identical with the static (monotonic loading) small-strain modulus, such that $G_0 = G_{max} = G_{dyn}$.

The SCPT was introduced in the mid-1980's (Rice, 1984; Campanella et al., 1986; Robertson et al., 1986), with the SDMT introduced in 1988 (Hepton, 1988). The procedures for performing the penetration portions of the SCPTu and SDMT are the same as for their CPT and DMT counterparts, with the addition of an intermittent downhole seismic testing phase every one meter as new rods are added during penetration of the cone penetrometer or dilatometer blade.

Surprisingly, the geophysics portions of the SCPT and SDMT today are performed in the same antiquated manner as envisioned some two decades ago. Back then, wavelet signals were captured with analog oscilloscopes having no permanent storage capability. The procedures required paired sets of left- and right-strikes of the hammer, which were captured and displayed on the screen together so the arrival time could be determined by picking the crossover point of the oppositely polarized shear waves. The later development of digital signal storage made post-processing of seismic signals possible, reducing testing time in the field. However, given the ability to store the data, recording duplicate signals to ensure repeatability became common practice. Today, the common procedure for SCPT and SDMT (as well as conventional borehole DHT) is to record two left- and two right-strikes at each test depth, despite the availability of advanced data acquisition and digital signal processing techniques that make oppositely polarized signals unnecessary for analysis. That is, only right-strikes (or left-strikes) are needed for accurate V_S profiling with downhole methods (Liao, 2005).

For the borehole DHT, a vertical measurement interval of 1.5 m (5 feet) is

common. For the direct-push DHT methods with SCPT and SDMT, more closely spaced measurements of 1 m (3.28 feet) are common. By obtaining seismic velocity measurements only at the typical 1 m or even 2 m meter intervals between rod breaks, the V_S profile appears much coarser than the finer details reflected in the 1 cm to 20 cm readings that are characteristic of vertical and lateral resistances obtained by the CPT and DMT penetration profiles respectively. Such a discrepancy in measurement intervals reduces the correlation between the large-strain and small-strain parameters. Perhaps more importantly, the resulting coarse velocity profiles and extended testing times discourage engineers from insisting on shear wave velocity measurements as a normal part of their routine site characterization programs.

The purpose of this research effort is towards improved field techniques for measuring shear wave velocity with three primary objectives: (a) reduce field time for data collection, (b) enhance the quality of recorded seismic signals, and (c) increase the depth resolution of the measured V_S profile. Aspects included herein concern the field procedures, equipment, and post-processing of recorded shear wave signals. This research effort is particularly directed towards direct-push downhole methods, including the seismic cone penetration test and seismic flat dilatometer test, yet is also applicable to traditional borehole type downhole geophysical testing. The improvements will enhance the quality of the measured velocity profiles, as well as the procedures for making the measurements.

1.2. Overview of Thesis Content

An introductory section on wave propagation is presented in Chapter 2 that describes the different types of mechanical waves within the context of elasticity theory and details their measurement in soils. Following this is a review of the relationship between shear modulus and shear wave velocity and their significance in the non-linear stress-strain-strength response of geomaterials. The chapter ends with a brief review of

laboratory and field methods for measuring V_S and G_0.

Chapter 3 describes the components of a proposed continuous-push seismic system intended to better incorporate the measurement of shear wave velocity within the procedures for direct-push site characterization systems such as the SCPT and SDMT. A new frequent-interval seismic method is introduced for improving the depth resolution of velocity profiles. The equipment utilized for this research is described, including the construction of three versions of true-interval seismic probes, the development of a portable automated seismic source, and the data acquisition systems utilized for capturing the seismic signals. A review of existing seismic sources is given, with discussion of wave types and source/sensor alignment. The magnitudes of velocity errors related to timing and depth errors are also discussed.

Chapter 4 provides an overview and summary of the field testing program conducted for this research effort. A variety of soil types and conditions with differing geologic origins was considered for study. Of the sixteen sites visited for testing, eight primary sites are described in detail. The procedures for the tests at those eight sites are also discussed.

Chapter 5 provides detailed information about the components of the continuous-push seismic system. The characteristics and performance of the geophone receivers are examined, as well as the effects of relative alignment between source and receivers on the signal appearance. Other factors affecting signal appearance are also discussed, such as the influence of noise, reflections, and the specifications of the data acquisition system. The RotoSeis automated seismic source devices are evaluated for signal appearance, repeatability, reliability, and depth. Lastly, signals collected utilizing the RotoSeis during a continuous-push SCPT sounding are studied to determine the differences between signals recorded by stationary receivers and non-stationary receivers.

Chapter 6 presents the results of frequent-interval and continuous-push seismic tests and analyses of the profiles. Test results using standard methods are compared with

the results of the new frequent-interval procedures.

A summary set of conclusions and recommendations for future work are presented in Chapter 7. The dissertation contains three appendices with additional supporting materials for background data and developed methodologies.

Appendix A provides the detailed results for the soundings presented within the chapter text. Also included are the results of companion tests that were conducted for reconnaissance purposes as part of this research, but not discussed in the text due to space constraints.

Appendix B contains the circuit diagrams for the amplifiers and trigger circuitry described in Chapter 3.

Appendix C provides a GIS database containing the dates, locations, and other important details of all the soundings performed by the In-situ Research Group at Georgia Tech from 1997 to 2007.

One final note, is that the research results have already helped make an impact on two fronts of geotechnical practice, including: (a) commercialization of a seismic dilatometer device now available to geoengineers for routine site investigation, and (b) commercialization of an automated seismic source (patent pending) to facilitate shear wave data collection. Hopefully, other additional important aspects of this research effort will be realized and integrated into site investigation practice in due time.

2. LABORATORY AND IN-SITU METHODS FOR THE MEASUREMENT OF SHEAR WAVE VELOCITY

2.1. Introduction

The shear wave velocity (V_S) is a fundamental material property common to all solids in civil engineering. It applies to all types of geomaterials. It is a valuable measurement for characterizing the behavior of soils, rocks, subgrades, foundation systems, compacted fills, and earthen structures for both static and dynamic load conditions. The in-place shear wave velocity is versatile and can be used to evaluate dynamic foundation stiffness (Richart et al., 1970), earthquake site response (Schnabel et al., 1972), sample disturbance (Sasitharan et al., 1994; Shibuya et al., 1995), liquefaction potential (Andrus and Stokoe, 1997; Seed et al., 2003), soil density (Mayne et al., 1999), foundation settlements (Burland, 1989; Lehane and Fahey, 2002), and soil stratigraphy (McGillivray and Mayne, 2004). The primary significance of V_S lies in the relationship between mechanical wave velocity and material stiffness. Elastic theory defines that the small-strain shear modulus (G_0) is determined according to the following relationship (Equation 2.1) between the total soil mass density (ρ) and V_S, with the subscript "naught" denoting that G_0 is the initial shear modulus in the elastic strain range.

$$G_0 = \rho \cdot V_s^2 \qquad 2.1$$

The stiffness (G_0) has been previously termed as G_{dyn} because of its early recognition and relevance to dynamic problems (e.g. Hardin and Drnevich, 1972). The shear modulus G_0 has also been designated G_{max}, because it is the maximum stiffness achievable (e.g. Woods, 1978). Most recently, the nomenclature has become G_0 (e.g. Tatsuoka et al., 1999) to signify its fundamental significance and relevance as a state parameter (e.g. Mayne, 2005).

2.2. Wave Propagation in Soils

In order to discuss the measurement of V_S and its applicability to geotechnical problems, a brief introduction of wave propagation is appropriate. A more comprehensive explanation of wave propagation in geomaterials can be found elsewhere (e.g. Ewing et al., 1957; White, 1983; Santamarina et al., 2001). In the context of this research, the concept of wave propagation describes the transmission of stresses and strains through soil and rock. There are several mechanical wave types, or modes, which can propagate through the subsurface. Some common wave modes encountered in geotechnical investigations are illustrated in Figure 2.1. The modes can be categorized into two basic types: body waves and interface waves. Body waves can travel through material reflecting from and transmitting through boundaries, or interfaces. Interface waves are restrained to the region surrounding material and stress boundaries (e.g. soil and air or soil and rock). The body waves include *compression waves* (P-waves) and *shear waves* (S-waves). Common interface waves in geotechnical applications are surface waves known as *Rayleigh waves* (R-waves) that exist at stress free boundaries, and *Love waves* (L-waves) that propagate along the interface between two layers.

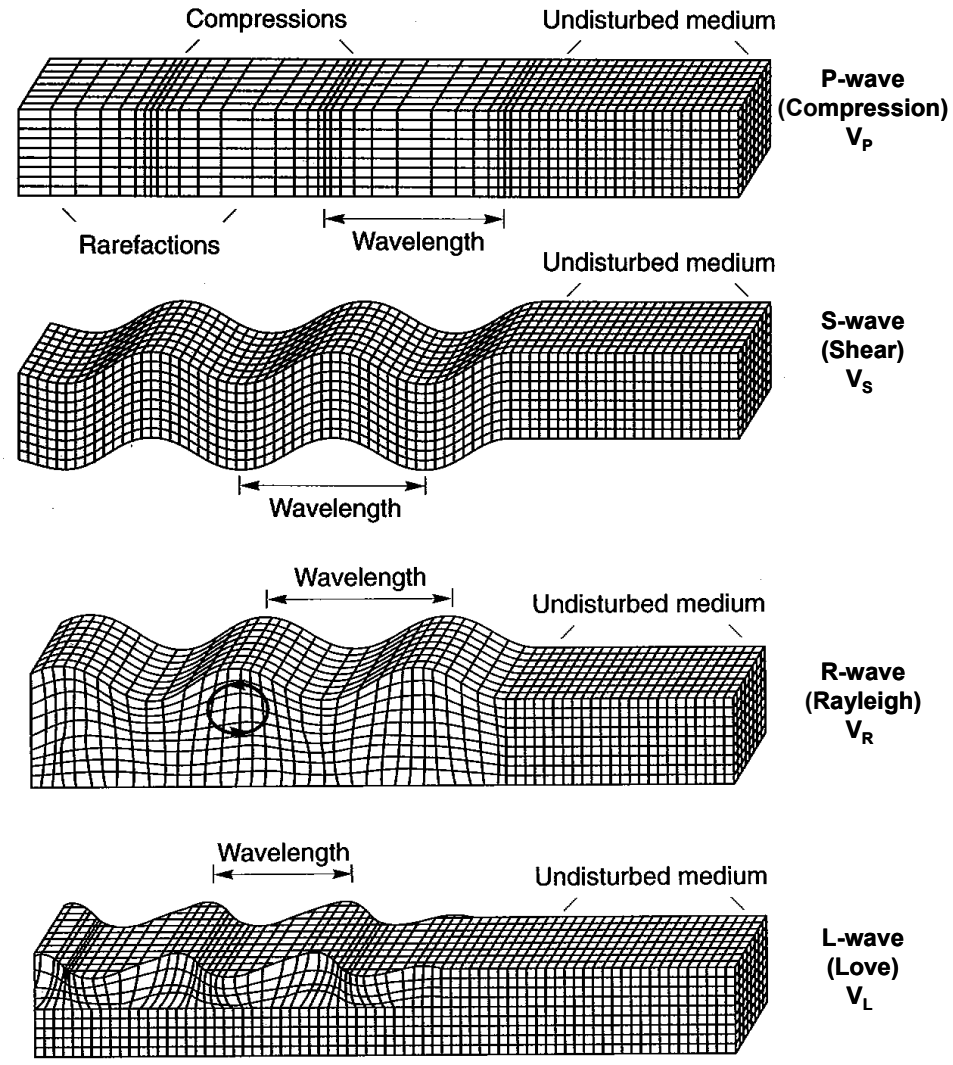

Figure 2.1 Illustration of body wave modes (compression and shear) and surface/interface wave modes (Rayleigh and Love) modified from Kramer (1996)

The P-wave (primary mode wave) is a compression wave. The particle motion is parallel to the direction of propagation, creating repeating cycles of compression (compactness) and rarefaction (extension). The P-wave is the fastest moving of the waves. However, the P-wave velocity of water lies between that of loose sand and dense sand, and between that of soft clay and hard clay. Thus, the presence or lack of water may cause some confusion and/or uncertainty in the interpretation of P-wave measurements.

The secondary mode wave (S-wave) is a shear wave (also known as a transverse

wave or dilational wave). The particle motion is perpendicular to the direction of propagation. Because water cannot support shear stresses, the S-wave is transmitted only by the soil skeleton, even in saturated soils. Thus, the presence of water does not affect our ability to measure V_S in the field. However, partial saturation causes increased effective stress, which may result in much higher measured velocities if the material becomes desaturated (Cho and Santamarina, 2001).

The propagation of interface waves is more complex than that of body waves. Rayleigh waves, for example, occur at the ground surface boundary and have retrograde elliptical particle motion. Love wave particle motion is parallel to the interface and perpendicular to the direction of propagation. The penetration depths of these waves are a function of the frequency content of the wave cycles or more specifically, dependent upon their wavelengths. The relationship between wavelength and frequency is defined in Equation 2.2, where λ is the wavelength, f is the frequency, and V is the wave velocity related to a particular wave type.

$$\lambda = \frac{V}{f} \qquad 2.2$$

The velocity of shear wave propagation in soils is the primary focus of this research because of its importance in geotechnical applications. The initial shear modulus defined by V_S is well appreciated in soil dynamics (e.g. Hardin and Drnevich, 1972), yet also relevant (but not so well-recognized in practice) to basic static deformation problems (e.g. Burland, 1989).

2.3. Shear Modulus

Initial shear modulus is controlled by a number of factors such as: cementation, void ratio, effective confining stress, number of particle contacts, ageing, mineralogy, loading frequency, and other influential variables (Hardin and Black, 1968; Hardin and Drnevich, 1972; Woods, 1978; Tatsuoka and Shibuya, 1992). Consequently, G_0 (and/or

V_S) can be used to infer a number of important engineering characteristics and behavioral aspects about geomaterials.

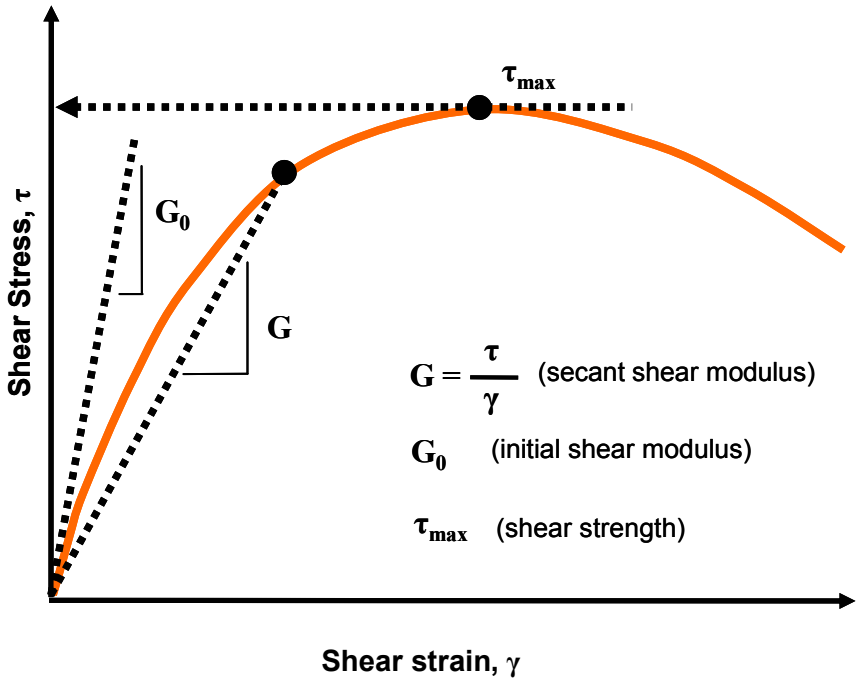

Figure 2.2 Representative shear stress–strain behavior with shear modulus

The relationship between shear stresses (τ), shear strains (γ), and shear modulus (G) can be defined for different strain ranges (Figure 2.2). As the stress level increases, the secant value of shear modulus reduces, where $G = \tau/\gamma$. Also, as strains increase, G is reduced. The initial modulus, G_0, is in the small-strain linear-elastic region of the stress-strain response, well below the strain range of common geotechnical problems, such as retaining walls, foundations, and tunnels (Figure 2.3). This partly explains why G_0 (often determined from dynamic lab tests) is typically considered applicable only to dynamic problems, such as earthquakes and machine vibrations involving wave propagation. However, G_0 is the starting point for the stress-strain behavior for all stress-strain curves, including static (monotonic) loading, as well as cyclic and dynamic loading. Though the initial modulus is the same for both modes, the modulus reduction curves are different

under static and dynamic loading. Differences can be attributed to strain rate effects (Alarcon-Guzman et al., 1989; Lo Presti et al., 1996; Shibuya et al., 1996) and cyclic strain hardening/softening involved in dynamic loading (Puzrin and Shiran, 2000), as illustrated by Alarcon-Guzman et al. (1989) in Figure 2.4. Specifically, static loading has a faster reduction from G_0 (backbone curve) compared with cyclic, or dynamic, loading.

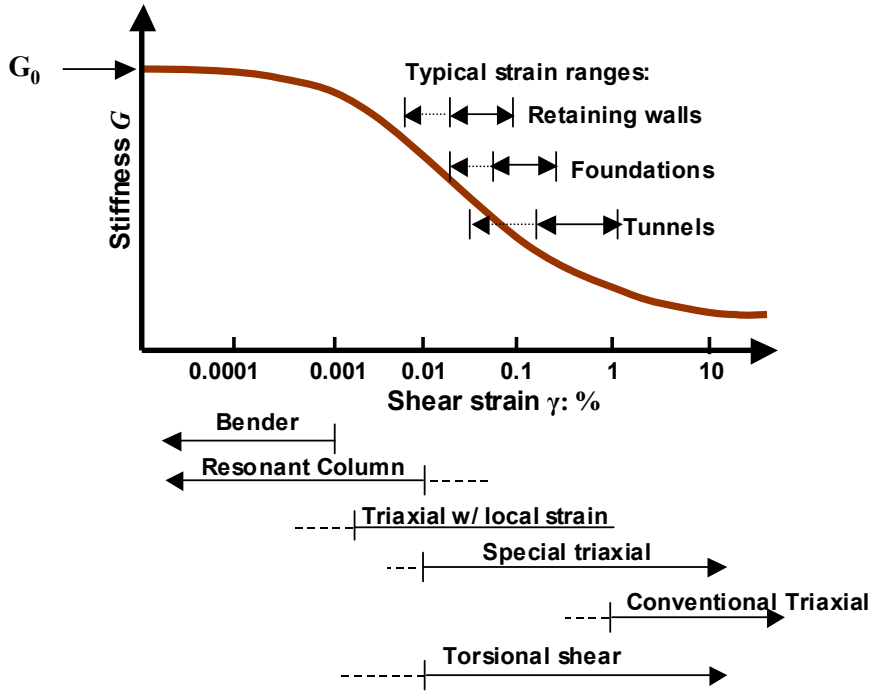

Figure 2.3 Strain levels of common geotechnical applications and laboratory tests modified after (Simons et al., 2002)

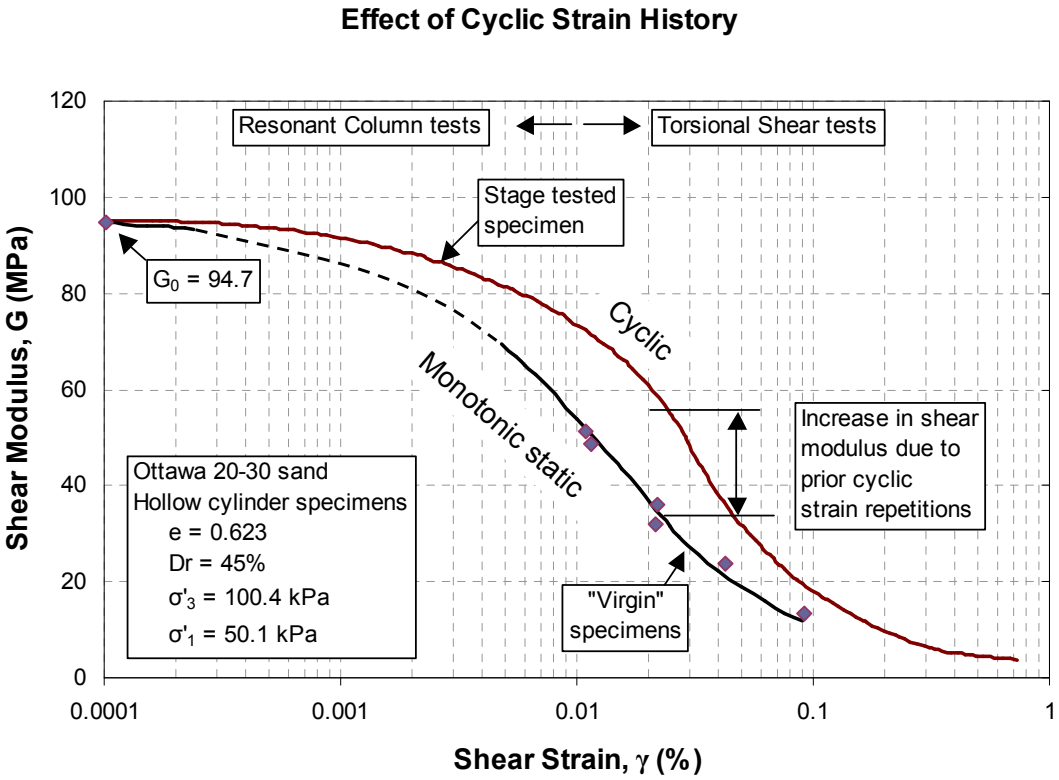

Figure 2.4 Comparison of monotonic versus dynamic modulus reduction trends (Alarcon-Guzman et al., 1989)

The stress-strain-strength behavior of soil is highly non-linear at all levels (Jardine et al., 1984; Jardine and Potts, 1991). As a result, the operational value of shear modulus depends on strain level (Figure 2.5). Four primary regimes of strain level can be delineated. The modulus reduces continually once strains exceed the linear elastic threshold strain, designated γ_{tl} (Vucetic, 1994). The linear threshold strain (γ_{tl}) is the limit of small-strain, linear-elastic behavior over which G_0 applies. Beyond γ_{tl}, the modulus begins to reduce with minor fabric changes, but cyclic pore pressures are not yet generated. Though the linear threshold limit (γ_{tl}) depends on plasticity and confining stress, the strain below which G_0 applies is somewhere between 5×10^{-4} % for non-plastic soils with low confinement, and 5×10^{-2} % for soils with either high confinement or high plasticity (Leroueil and Hight, 2003). The degradation threshold strain (γ_{td}) is a limit of

the medium-strain region, with a modulus reduction of 0.6 G_0 to 0.85 G_0 and is typically one to two orders of magnitude greater than γ_{tl} in fine grained soils (Vucetic, 1994; Santamarina et al., 2001). Beyond γ_{td}, permanent fabric and volume changes will occur leading to a loss of strength and/or excess pore water pressure build-up in undrained loading until peak strength is reached. Beyond peak, the residual threshold strain (γ_{tr}) applies to platy particles and is reached at very large strains. In this region, the particles become aligned along slip surfaces or localizations and shear strength is at its minimum.

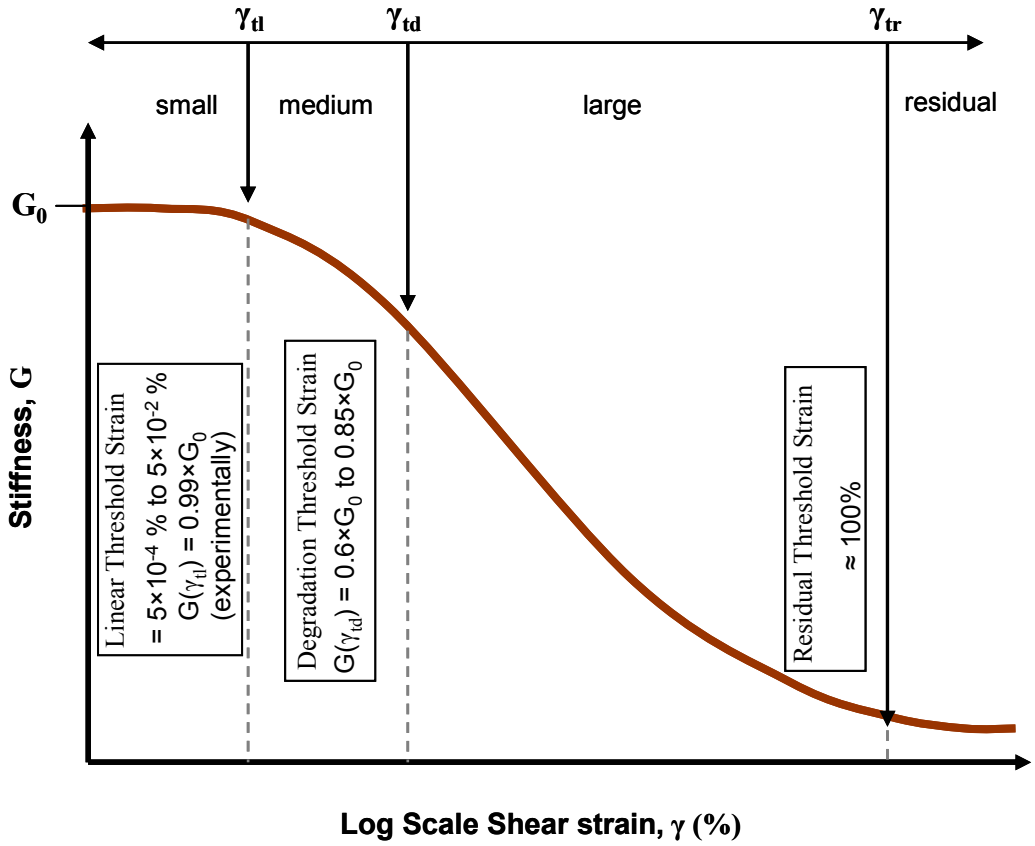

Figure 2.5 Approximate threshold strain regimes after Santamarina et al. (2001)

To extend the application of G_0 to large strain geotechnical problems, a number of mathematical algorithms, empirical expressions, and/or constitutive soil models have been developed which can model the stress-strain behavior over broad strain ranges,

beginning with G_0 and utilizing medium- or large-strain parameters determined from other measurements to represent the stress-strain behavior above the linear threshold strain (γ_{tl}) and even up to the shear strength, τ_{max} (e.g. Ramberg and Osgood, 1943; Kondner, 1963; Fahey and Carter, 1993; Puzrin and Burland, 1998).

2.4. Review of Methods for Obtaining V_S and G_0

Historically, V_S and G_0 measurements have been reserved for critical, high visibility projects. However, small-strain properties are now recognized as relevant to the situations of foundation displacements, wall deflections, and pile movements (Burland, 1989; Tatsuoka et al., 1999; Jardine et al., 2005). Complex numerical modeling techniques (e.g. finite element, finite difference), requiring the initial shear modulus, are being used increasingly on small, medium, and large projects so that realistic assessments of ground movements near excavations, piled rafts, and civil engineering works are reasonably predicted. In addition, new building codes are also increasing the demand for V_S measurements, including the International Building Code (IBC 2003) that requires structural engineers and architects to change the severity and level of detailing in their designs according to the site-specific shear wave velocities.

There are a variety of methods available for determining G_0 values of soil and rock, either by measuring the V_S and calculating G_0 based on Equation 2.0 or by measuring G_0 directly from the results of stress-strain tests. Figure 2.6 is a summary of the current methods for obtaining G_0 for soil materials, grouped into laboratory and field (in-situ) methods. A brief summary of each lab and field technique is given in the subsequent sections. Comprehensive reviews of lab methods for determining small-strain properties, focusing on cyclic torsional shear, resonant column, and direct wave propagation techniques using bender elements are given by Woods (1978; 1994). Detailed information on the field testing techniques for measuring V_S in soils can be found in Hoar and Stokoe (1978), Woods (1978), and Campanella (1994).

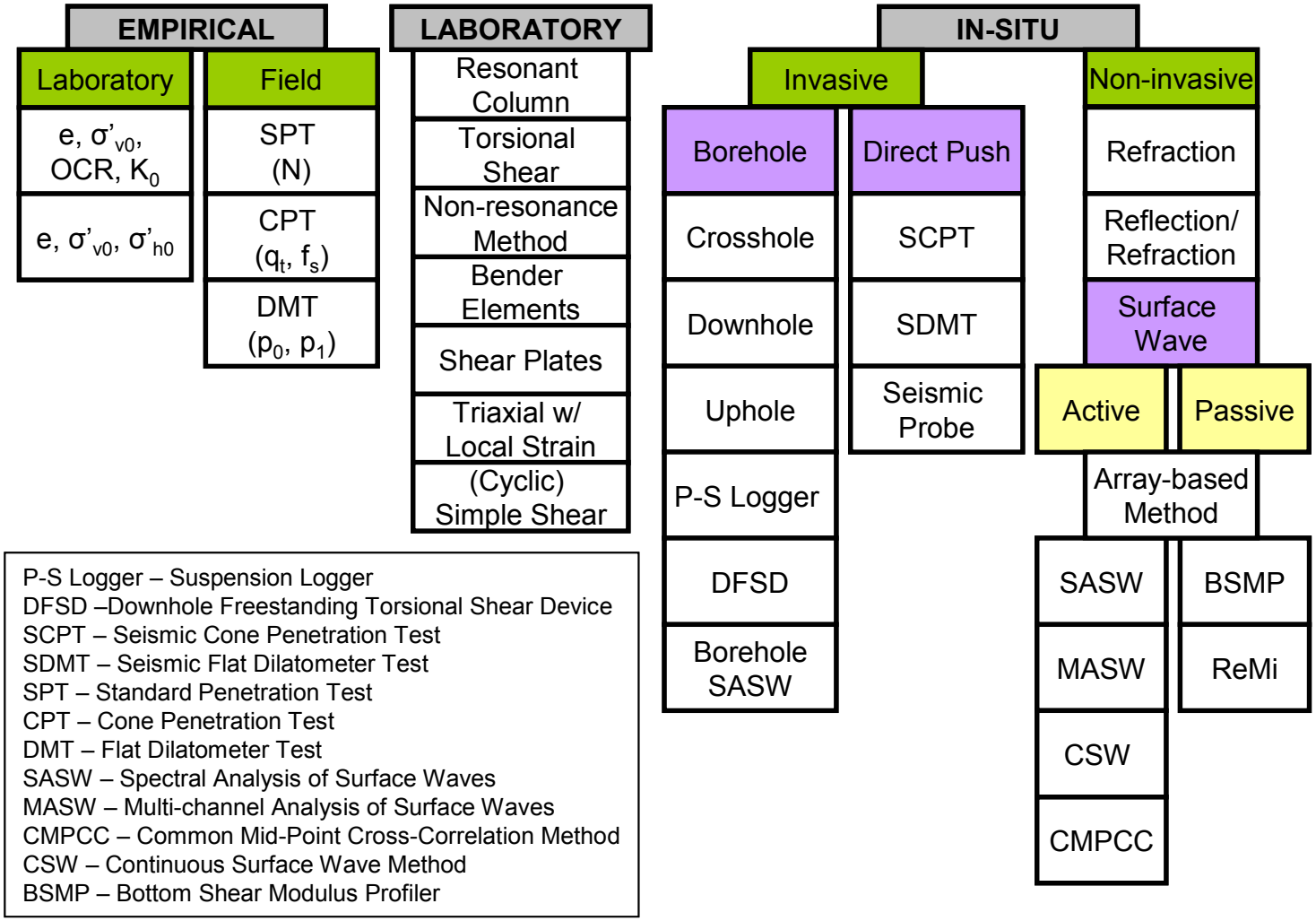

Figure 2.6 Laboratory and field methods for evaluating initial shear modulus (G_0) of soils (modified after Casey, 2000)

2.4.1. Laboratory methods for V_S and G_0

Laboratory measurements of V_S and G_0 have the advantage that the samples can be touched and seen, thus material identification is assured. The specimen conditions can be controlled for stress states, drainage, and boundary conditions, whereas this is not possible in the field. However, the cost of retrieving samples and performing the tests can be expensive. Moreover, the disturbance caused by the sampling process may induce strains well beyond the elastic threshold, thereby destroying the soil fabric and misrepresenting the in-situ state (Shibuya et al., 1995). When the soil is disturbed, the apparent value of V_S is altered from its true in-situ value. In fact, the lab shear wave velocity measurements on "undisturbed" samples can be compared to the field shear wave velocities to determine the level of sample disturbance that has occurred (Tan et al., 2002). In certain soils, such as clean sands and gravels, undisturbed sampling is extremely difficult, so the lab specimens may even have to be built from reconstituted material. Such data are subject to careful scrutiny as the values may, however, be quite different from the true undisturbed samples.

2.4.1.1.Resonant Column

The resonant column test (RCT) is performed according to ASTM procedures (ASTM D4015-92, 2000) and consists of a dynamic test utilizing wave propagation to determine soil stiffness in the elastic range (Figure 2.7). The device can measure V_S of cylindrical specimens based on one-dimensional wave propagation theory of a torsional wave in a rod (Hardin and Drnevich, 1972) within the shear strain range from 10^{-5} % to about 10^{-3} % (Meng, 2003). The resonant column device has enjoyed about four decades of use primarily related to defining G_{dyn} (alias G_0), and the resulting G/ G_0 reduction curves with shear strain (γ). The RCT also evaluates the increase of damping (D) with γ for soil dynamics problems (Woods, 1994).

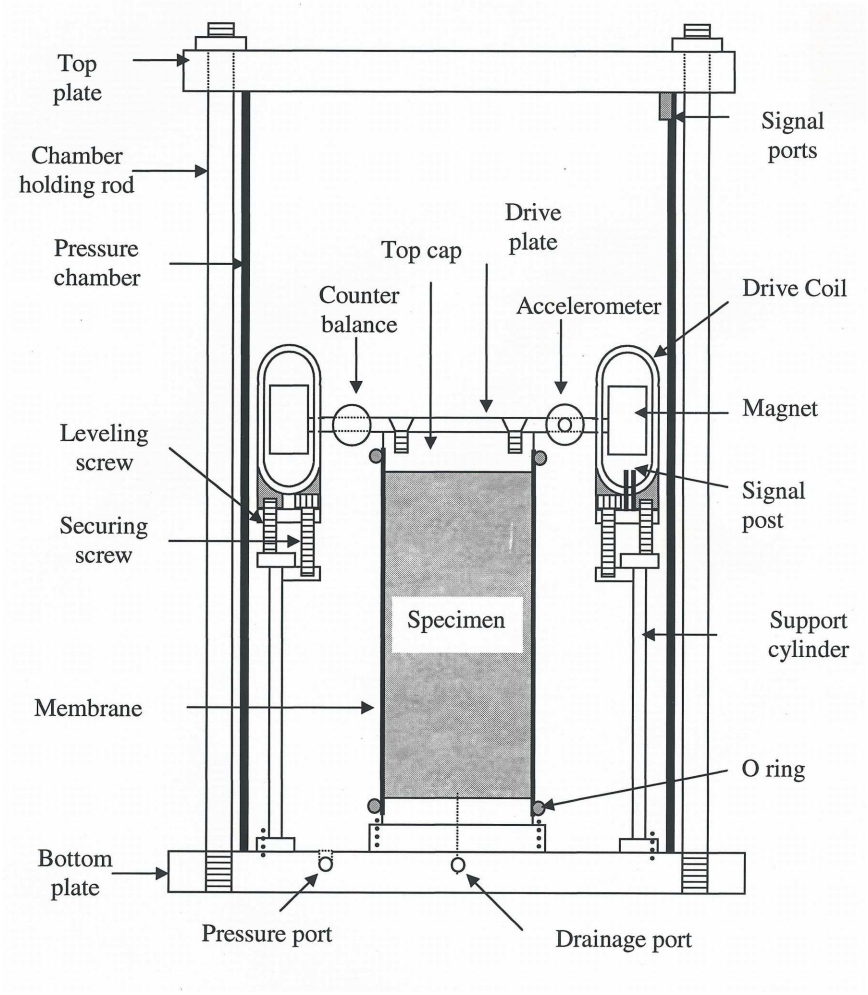

Figure 2.7 Schematic of Georgia Tech resonant column device (Meng, 2003)

With the bottom of the sample fixed to the base of the chamber, harmonic torsional stresses are applied to the top cap for a range of frequencies. At the natural frequency of the first fundamental mode of vibration for the sample, somewhere between about 20 and 260 Hz (Meng, 2003), the motions will resonate allowing the calculation of velocity and ultimately the initial shear modulus at that particular frequency. A special electronic servo system developed by Li et al. (1998) enabled the resonant frequency to be changed during the test in order to make measurements over a range of resonant frequencies, with 20 Hz being the lower limit.

The resonant column is also popular for obtaining estimates of the material

damping (D) of the tested samples, although the equipment-generated damping, or back EMF (electromagnetic force) effect caused by the solenoids and magnets, has long been realized to have an significant influence on the damping measurements (Kim, 1991; Hwang, 1997; Wang, 2001; Cascante et al., 2003). By replacing the conventional voltage-mode power supply with a current-mode power supply, the equipment-generated damping may be reduced by several orders of magnitude (Meng, 2003).

2.4.1.2.Torsional Shear

Similarly to the resonant column, the torsional shear test (TS) involves the application of torsional stress to the top of a cylindrical specimen (Figure 2.8), but the method of calculating shear modulus does not involve wave propagation theory or resonance. In many instances, the RCT and TS are married, whereby the specimen is first tested dynamically at low strains (RCT), then switched to quasi-static monotonic, or cyclic, shear for high strains up to failure (TS). Stress-strain hysteretic loops are generated at quasi-static frequencies (low frequencies) less than 2 Hz to avoid inertial affects of the top cap (Hardin and Drnevich, 1972). The strain range of the typical device covers shear strains from 10^{-2} % to 10 % (Frost and Drnevich, 1994). Shear modulus can be determined from the stress-strain data, and the hysteresis is used to determine the damping. The torsional shear is perhaps the best suited lab device for obtaining static (monotonic) G/G_0 reduction curves with shear strain in soils (e.g. Tatsuoka and Shibuya, 1992).

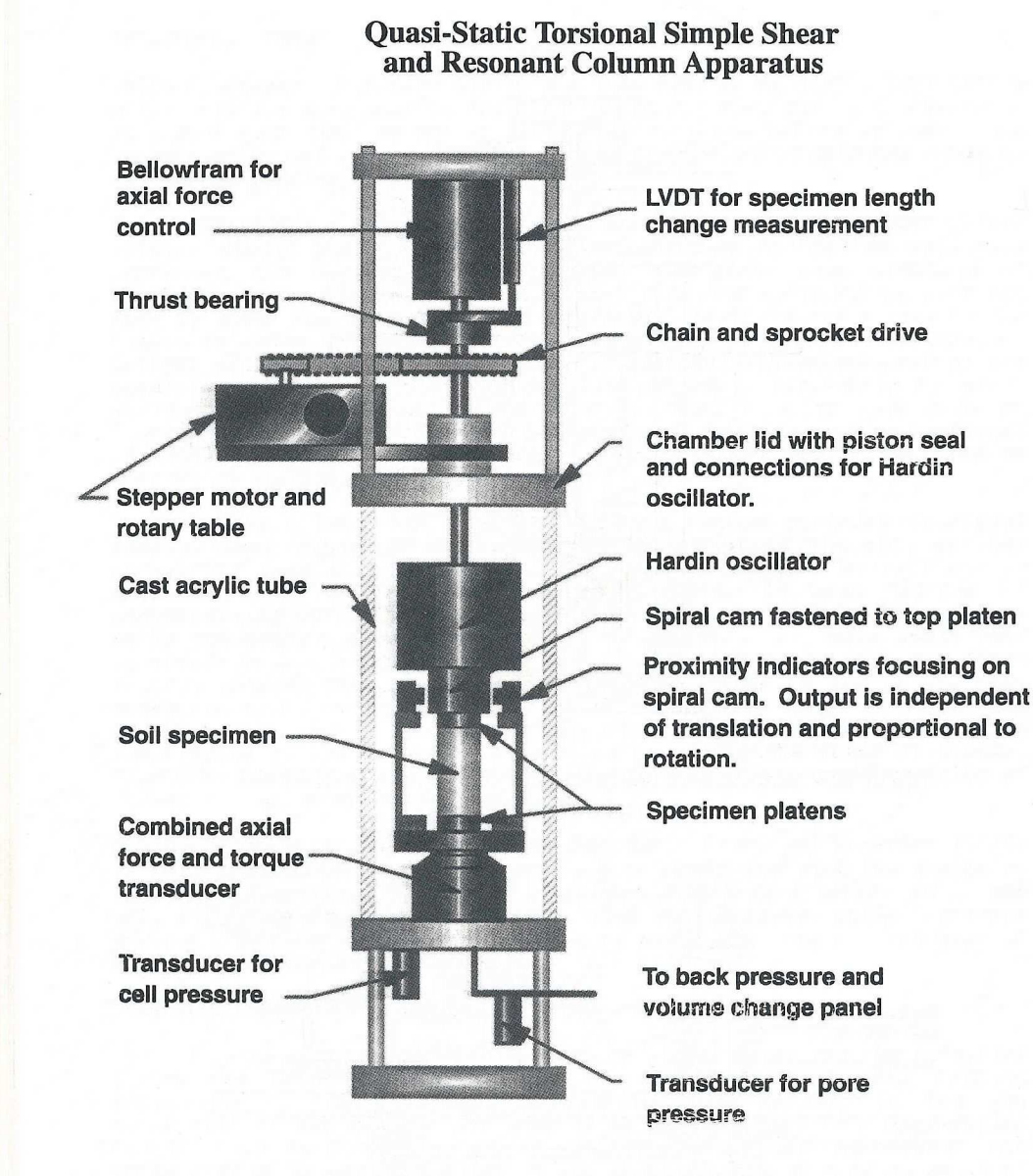

Figure 2.8 Torsional shear / resonant column device (Frost and Drnevich, 1994)

The resonant column device can be used to perform both resonant column tests as well as torsional shear tests (Hardin and Drnevich, 1972; Alarcon-Guzman et al., 1986; Woods, 1994). However, the frequency ranges of the test methods, 0.1 Hz to 2 Hz and 20 to 260 Hz respectively, do not overlap and the analysis methods are different, making the results difficult to combine.

2.4.1.3.Non-resonance method

A method termed non-resonance, originally developed for characterizing polymeric materials, is a new technique that increases the frequency range of the resonant column / torsional shear device for the evaluation of G_0 and damping ratio, D (Lai, 1998; Lai et al., 2001; Meng, 2003). The system relies on a current-mode power supply rather than the typical voltage-mode power supply of the standard resonant column. The components of the system are illustrated in Figure 2.9.

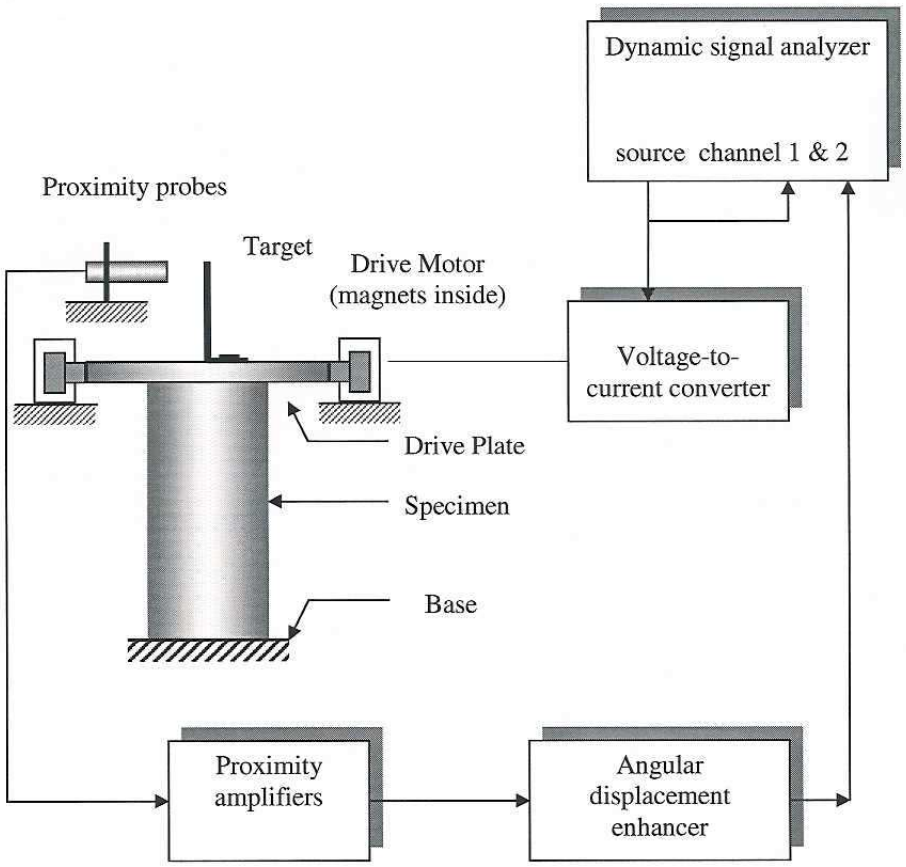

Figure 2.9 Modified resonant column device for performing non-resonance method (Meng, 2003)

This new approach assumes a visco-elastic model to analyze the frequency

response of the system to applied harmonic torsional stresses. The result is a complex valued modulus containing both the shear modulus and the damping. The resonant column test is only able to evaluate G_0 and D at a single resonant frequency between 20 Hz and 260 Hz, and torsional shear is capable of making measurements at frequencies less than 2 Hz. With the non-resonance procedure, the frequency range is increased, spanning from 0.01 Hz to 30 Hz (Meng, 2003). The range of shear strains is equivalent to the standard resonant column, generally from 10^{-5} % to about 10^{-3} %.

2.4.1.4.Triaxial with local strain measurements

The triaxial test is a common method for evaluating the stress-strain behavior of soil. However, for the normal triaxial apparatus available in commercial testing, there are considerable errors caused by poor seating of the platens, misalignment of the specimen and/or loading system, uneven bedding of the porous stone, and compliance of the pressure cell and load cell, that mask the true response of the specimen (Jardine et al., 1984; Baldi et al., 1988). Special triaxial systems are available at research institutions to overcome these shortcomings. By monitoring displacements directly on the specimen, rather than at points located outside the triaxial pressure cell, the errors listed above can be eliminated.

Investigations performed by Lo Presti et al. (1993) and Jamiolkowski et al. (1994) examined the sources of error by placing strain measurement devices at multiple locations to compare the displacement of the piston from outside the cell with: (1) the displacement between the loading caps, and (2) the displacement locally within the central portion of the specimen. The results showed that the measured displacements were several tens of percent less when measured directly on the central part of the specimen as compared to the internal measurements made between the caps or to the standard external measurements. Also, the error sources had little effect on the displacements measured at strains less than 10^{-3} %, but became noticeable when strains

exceeded 10^{-3} %.

Scholey et al. (1995) examined internal versus external measurements and reviewed the performance of several types of instrumentation for measuring local strains. The authors recommend that strain measurements be made to an accuracy of 10^{-3} %. An example of the placement of the instrumentation for making local measurements is shown in Figure 2.10 with the displacement transducers monitoring the center portion of the specimen. These specially instrumented triaxial apparatuses with local strain measurements are now widely used in European (e.g. Jardine et al., 1984) and Asian research laboratories (e.g. Tatsuoka and Shibuya, 1992).

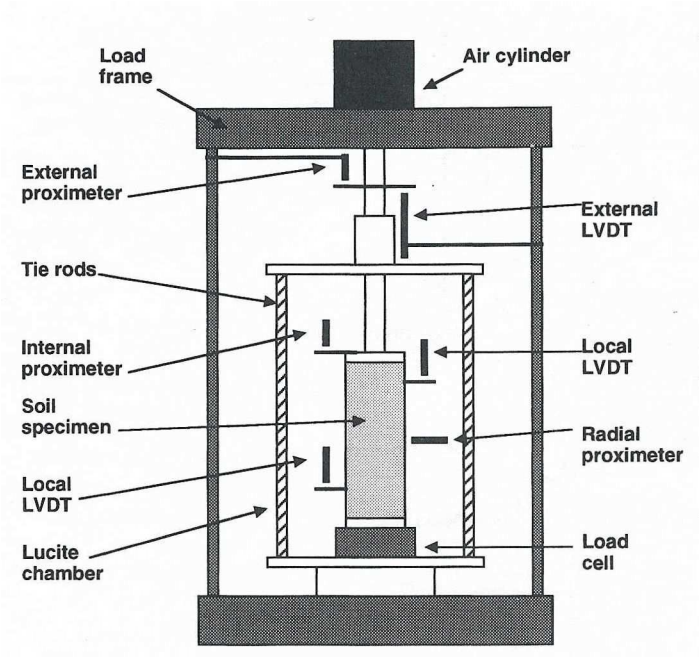

Figure 2.10 Placement of instrumentation for triaxial test with local strain measurements (Scholey et al., 1995)

2.4.1.5.Bender elements and shear plates

Direct wave propagation is a method for determining V_S and G_0 of laboratory specimens. Elastic waves are generated and received by piezoceramic elements, and the

velocity can be determined from the travel time of the waves between the source and receiver (Woods, 1994).

The piezoceramic elements are small ceramic wafers that convert electrical energy into mechanical motion, and can also convert mechanical motion into electrical energy. In this way, they can act as both sources and receivers. There are several varieties of piezoceramic elements including: bender elements, shear plates, and compression elements. Each type is designed to deform in a particular way in response to an applied electric field (i.e. bending, shear, and axial extension), as illustrated in Figure 2.11. Bender elements and shear plates are used to send and receive shear waves. A compression element would be used to generate and detect compression waves.

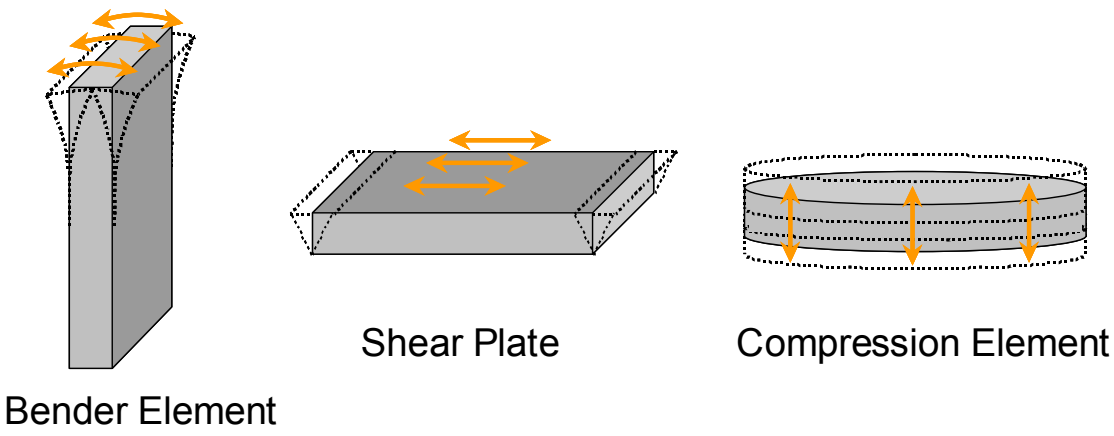

Figure 2.11 Three types of piezoceramic elements: bender element, shear plate, and compression element

Due to their small size and relatively simple setup, recent research has seen the proliferation of bender elements incorporated into all types of conventional bench top apparatuses, including oedometers, triaxial cells, resonant columns, and other devices. Many researchers have used V_S from bender elements to monitor the progress of skeleton formation during sedimentation experiments (Dyvik and Madshus, 1985; Woods, 1994; Klein, 1999; Santamarina et al., 2001). Figure 2.12 shows how bender elements, shear

plates, and compression elements can be used to monitor V_S and V_P in triaxial specimens. The frequency of loading with bender elements is between 1 kHz and 10 kHz with shear strains less than 10^{-3} % (Santamarina et al., 2001). However, they measure only V_S relating to G_0 and do not describe the variations of G/G_0 and damping (D) with shear strain (γ).

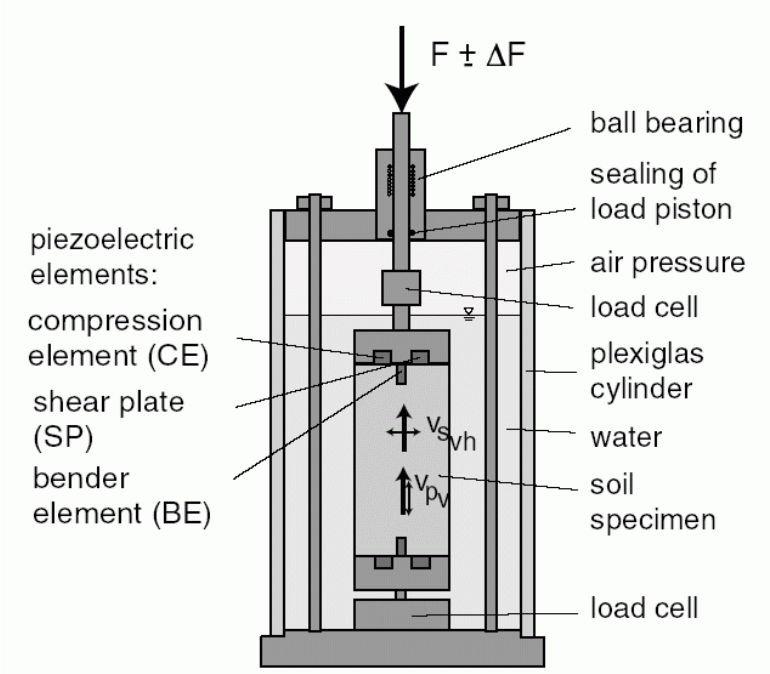

Figure 2.12 Instrumentation of a triaxial specimen with piezoceramic elements to monitor P-wave and S-wave velocities during strength testing (Triantafyllidis et al., 2004)

2.4.2. Field measurement of V_S and G_0

The major advantage of field measurements of V_S is that the soil is tested in its natural state, thus mitigating the dramatic affects of sample disturbance caused by drilling, tube insertion, extraction, transportation, storage, trimming, and reconsolidation. Figure 2.13 follows the stress history of a soil sample from sampling to reconsolidation for testing. The final state can sometimes be significantly different than the real soil in

situ. With field geophysics, larger volumes of soil can be tested, in many cases more rapidly and at lower cost than comparable lab tests. Field tests for V_S fall into categories of intrusive and non-intrusive. The intrusive methods require the installation of sources and/or receivers at or beneath the ground surface either inside a borehole or by direct push methods. The non-intrusive methods include surface geophysics, which utilize surface receivers as well as surface sources.

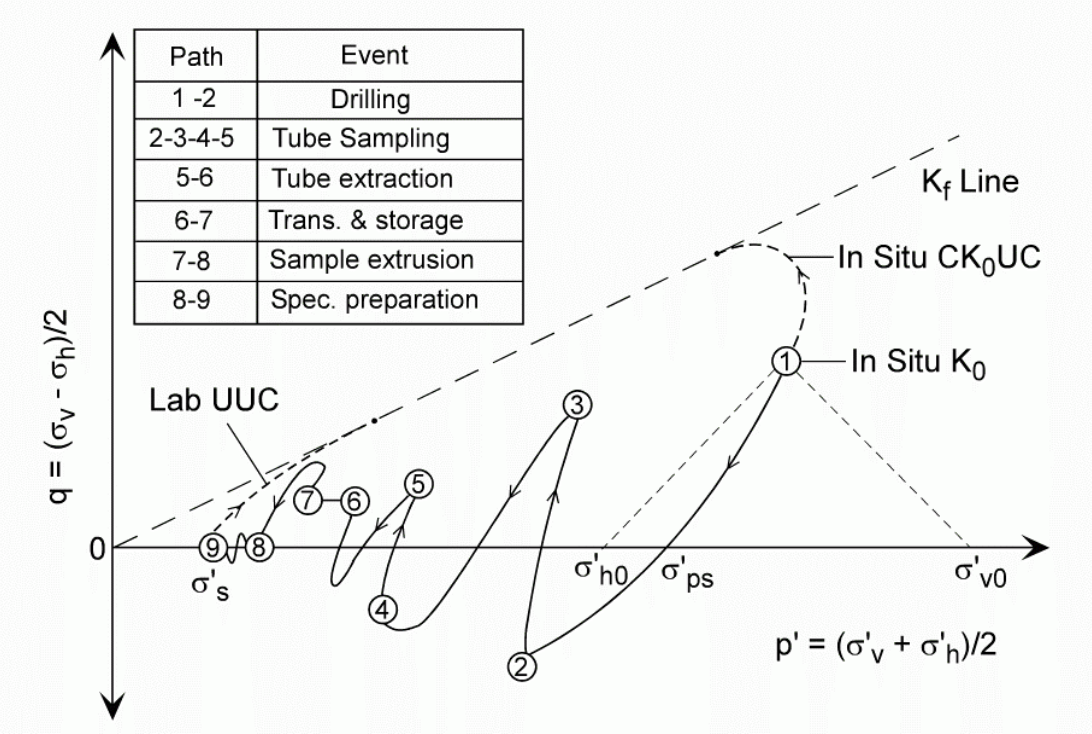

Figure 2.13 Hypothetical stress history caused by tube sampling of a low OCR clay (Ladd and DeGroot, 2003)

2.4.2.1.Crosshole

The crosshole test (ASTM D 4428/D 4428M, 2000) is often considered the reference standard by which other in-situ shear wave velocity tests are compared. The tests are performed in a series of 2 or more cased boreholes. A borehole seismic source generates waves that propagate past receivers at the same depth in adjacent boreholes

(Figure 2.14). The velocity is determined from the travel time of the waves over the distances between boreholes. The layering is considered to be essentially horizontal between the boreholes and the measured velocity is applicable to a particular layer. The classical reviews of crosshole test (CHT) procedures can be found in Hoar and Stokoe (1978) and Woods (1978). One major advantage of crosshole testing is the direct measurement through only the desired material of a particular select layer. Because of the direct measurement and the reasonable certainty of the travel path of the source waves, the results are considered to be accurate. The test can be conducted in soil and or rock materials, and testing depths can be taken quite deep, up to 300 m or more. The greatest disadvantage of CHT is the need for multiple cased and grouted boreholes with accurate inclination records. The results are sensitive to variations in the spacing between the boreholes. As a consequence, the CHT is slow, time consuming, and very expensive. As of 2007, the cost for a 30 m deep CHT is about $12,000 to $15,000 or more for a two-borehole array in the USA. Such expense has discouraged V_S profiling by CHT for routine small to medium projects.

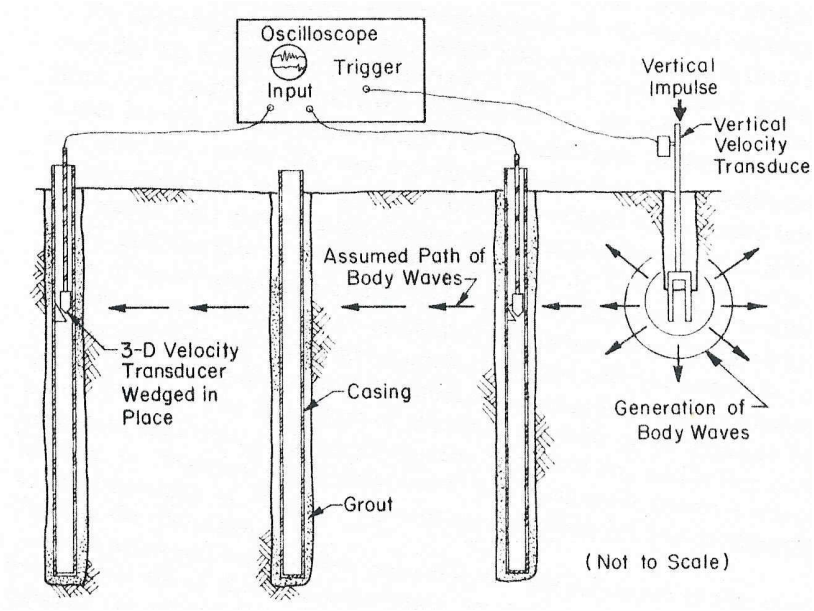

Figure 2.14 Crosshole test configuration (Hoar and Stokoe, 1978)

2.4.2.2.Downhole

The downhole test (DHT) utilizes a source at the surface and receivers lowered down a borehole, coupled to the side of the borehole by an inflatable tube (Figure 2.15) to measure interval velocities with depth. Again, a complete review is available in Hoar and Stokoe (1978) and Woods (1978). Only a single receiver is required, but additional receivers can reduce measurement uncertainty and testing times. The single receiver method is referred to as a pseudo-interval analysis. A true-interval analysis is performed utilizing two or more receivers separated by a known depth. These methods will be discussed in detail in the chapter corresponding to analysis methods.

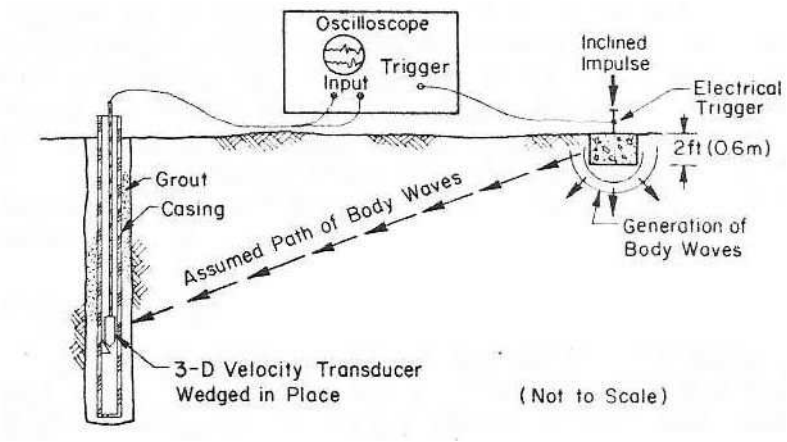

Figure 2.15 Downhole test configuration (Hoar and Stokoe, 1978)

A benefit of the DHT is that only a single cased borehole is required, and the inclination of the borehole is not so critical to V_s measurements as with CHT. Whereas the CHT measurements are made entirely within the interval of concern, in the DHT, the wave must travel from the surface down to the receiver(s), with the propagation distance increasing with depth. Attenuation of the source energy limits the practical depth of the test to approximately 100 m, unless high energy, explosive type, sources are used. When signal amplitudes are low, several signals may be added together to amplify the arriving

wavelet while averaging out the variable noise, but this requires additional field time for generating multiple source events. The calculation of the travel distance for the raypath can be a potential source for errors. The raypath of the wave is assumed to follow a straight path from the source to the receiver. Methods exist for analyzing the results considering curved raypaths (Hryciw, 1989), but this has a decreasing significance as depth increases and is not significant if the source is placed close to the borehole at the surface. In 2007, a 30 m deep DHT may cost on the order of $6,000 to $8,000. This is still considered too expensive for routine use on site investigations for small to medium projects.

2.4.2.3.Uphole

The uphole test is similar to the downhole test except that the source is lowered down the borehole and the receivers remain on the surface. The advantage of this method is better source coupling at depth where confinement is higher. Also, an array of receivers can be placed on the surface to capture effects of horizontal nonuniformity. A major disadvantage is that the energy of the borehole source is limited to prevent damage to the borehole. Despite the limitations on the source energy, early investigators found that profiled depths could reach as much as 3 km (Kokesh, 1952). However, the type of source wave is more difficult to control in deep boreholes, as the sources are explosive types, which generate mostly P-waves.

2.4.2.4.Seismic refraction

The seismic refraction test (ASTM D 5777-00, 2006) is a noninvasive method for determining V_S profile with depth. A surface source generates waves that propagate into the ground, reflecting and refracting waves at layer boundaries where velocity changes sharply. A linear array of receivers extends outward from the source to detect waves that reflect to the surface (Figure 2.16). The critically refracted waves along the layer interfaces travel at the velocity of the faster layer. If the velocity increases with depth,

critically refracted waves that travel along the layer boundaries will arrive at the surface, some distance from the source, before the direct arrival through slower velocity material above. The technique was the original geophysical method employed for deep oil exploration, and became popular for relatively shallow, geotechnical applications much later (Stam, 1962; Richart et al., 1970; Redpath, 1973). The most serious limitations of the method are the inability to detect slow layers below fast layers, as well as thin layers with sharp velocity contrasts (Redpath, 1973). Analysis methods have been developed to account for dipping or curved layers and forming tomographic images (Zhang and Toksoz, 1998).

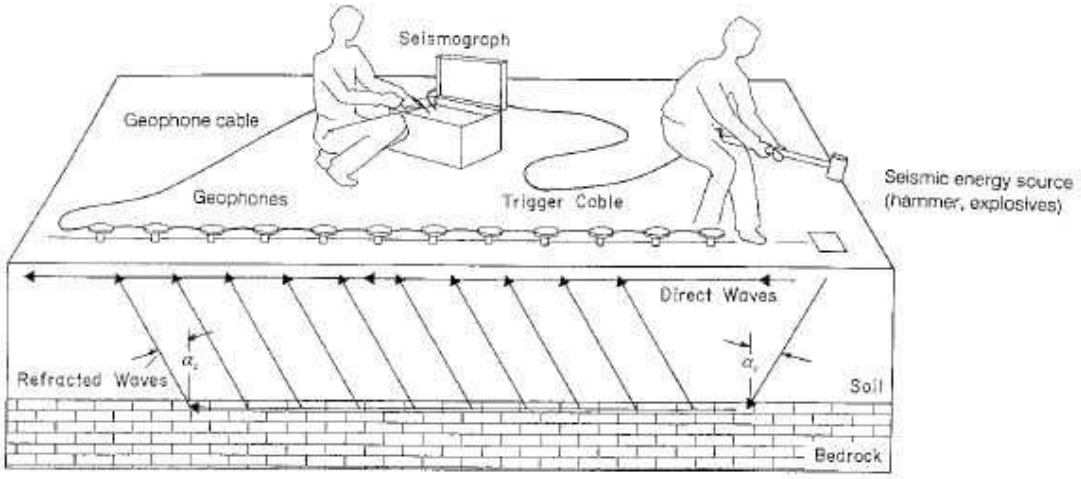

Figure 2.16 Schematic of a seismic refraction survey (ASTM D5777-00, 2006)

2.4.2.5.Seismic reflection

Seismic reflection is a non-invasive technique for determining velocity profiles as well as creating cross-sectional images of subsurface layering. The configuration of source and receivers is similar to the seismic refraction method (Figure 2.17). Instead of only looking at the first arrival of signals at the receivers, the entire record of each

receiver is considered. The recordings are lined up side-by-side according to their spatial locations, and corrections are applied to adjust the time delays of the signals to allow comparison of the records as a whole. The result is a cross-sectional representation of soil and rock layers based on reflections at layer boundaries or objects. The method requires sharp velocity contrasts, but is not affected by low velocity layers below high velocity layers. The analysis is complicated and must be performed by computer software. Experience is required to interpret the results in the presence of sloped or curving reflectors. The seismic reflection technique is commonly used in oil exploration. Depending on the type of source and the arrangement of receivers at the surface, tomographic images of the subsurface can be obtained to depths of several kilometers.

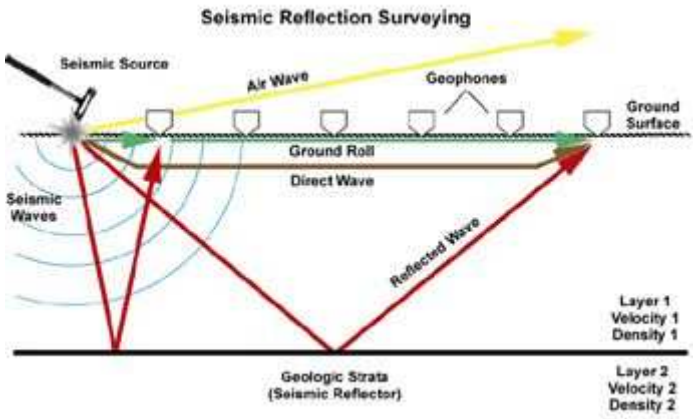

Figure 2.17 Seismic reflection test layout (Illinois State Geological Survey)

2.4.2.6.Surface wave testing

Surface wave testing is a type of noninvasive method for profiling V_S with depth and is based on propagation characteristics of Rayleigh waves. A source on the surface is used to produce vertical motions, impact or vibration, while the ground motions are monitored with two or more geophones (Figure 2.18). As shown earlier in Figure 2.1, the

particle motion of a Rayleigh wave is a retrograde ellipse moving along the surface. High frequency Rayleigh waves have short wavelengths with small ellipses, and therefore correspond to very shallow depths of influence. Low frequency Rayleigh waves have large wavelengths with bigger ellipses and consequently correspond to greater depths of influence. If the velocity changes with depth, as it does in geologic strata, the Rayleigh wave velocity will change as a function of frequency. Waves that change velocity as a function of frequency are said to be dispersive. The primary goal of surface wave testing is to determine the dispersion relationship, or Rayleigh wave phase velocity as a function of frequency. Using inverse problem solving techniques, the profile is then separated into layers of different shear wave velocities that can be used along with Poisson's ratio and density to calculate a synthetic dispersion curve fitting the measured dispersion curve (Park et al., 1999).

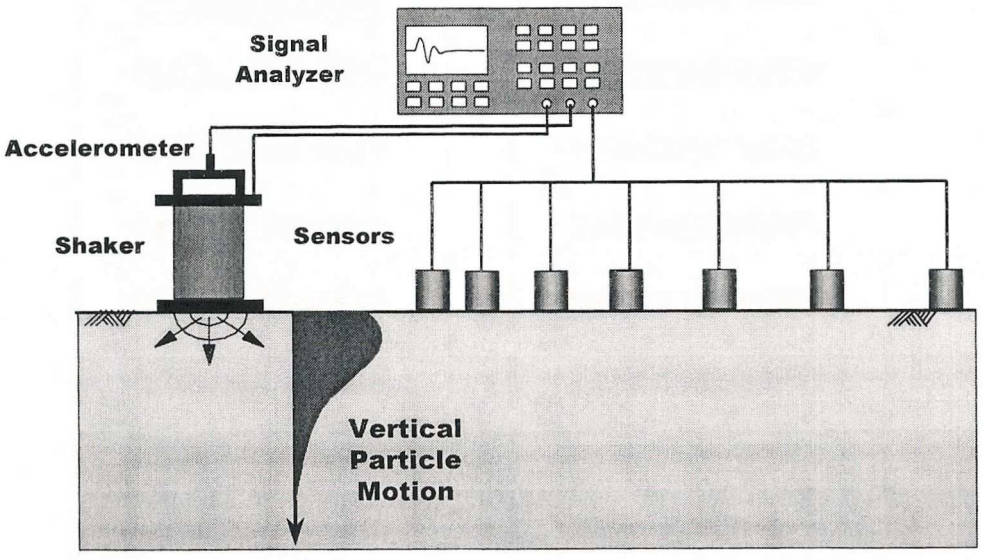

Figure 2.18 Configuration of surface wave testing equipment for a typical MASW method with an active source (Hebeler, 2001)

There are a number of variations of this type of method, all falling under the description of surface wave testing, including: spectral analysis of surface waves (SASW)

(Nazarian and Stokoe, 1984), continuous surface wave (CSW) (Tokimatsu et al., 1992), multi-channel analysis of surface waves (MASW) (Park et al., 1999), frequency-domain beamforming (Tokimatsu, 1995; Zywicki, 1999), spatial autocorrelation (SAC) (Aki, 1965), extended spatial autocorrelation (ESAC) (Ohori et al., 2002), common mid-point cross correlation (CMPCC) (Hayashi and Suzuki, 2004), and even seafloor methods such as the bottom shear modulus profiler (BSMP) (Yamamoto et al., 1991). They all operate on the same principles, but differ in source type, number and configuration of receivers, and analysis techniques. Consequently, there is some challenge in designating specific methods, with researchers assigning unique acronyms to methodologies that are, in fact, quite similar in concept. Generally, the methods can be grouped into four categories (Rix, 2004): Spectral Analysis of Surface Waves (SASW), multi-offset phase analysis (MOPA), spatial autocorrelation (SAC), and conventional frequency-domain beamforming, which describes MASW.

Viable sources for these tests can provide either harmonic excitation (e.g. heavy mass vibrator) or transient excitation (e.g. hammer impact), but only SAC and MASW can accommodate two-dimensional arrays necessary for passive sources (e.g. traffic vibrations, passing trains, ocean waves, or seismic activity). The excitation of a transient source can generate broad frequency ranges, speeding up testing, but ambient noise can be detrimental. Harmonic sources can generate individual sine signals that permit accurate filtering and high noise rejection. Though active sources, transient and harmonic, can be used to measure velocities hundreds of meters deep, passive sources can generate very low frequencies, enabling data to be collected on the order of kilometers deep.

The noninvasive nature and deep profiling capabilities of surface wave testing are major advantages to the method. The equipment is highly specialized, but the tests can be run quickly, keeping costs low. However, the profile is not determined directly, and has to be determined by fitting an estimated dispersion curve to the measured dispersion

curve (Figure 2.19). There may be multiple interpretations to the same profile, thus uniqueness is not guaranteed. Also, as depth increases, the depth resolution decreases and layer thicknesses appear to increase.

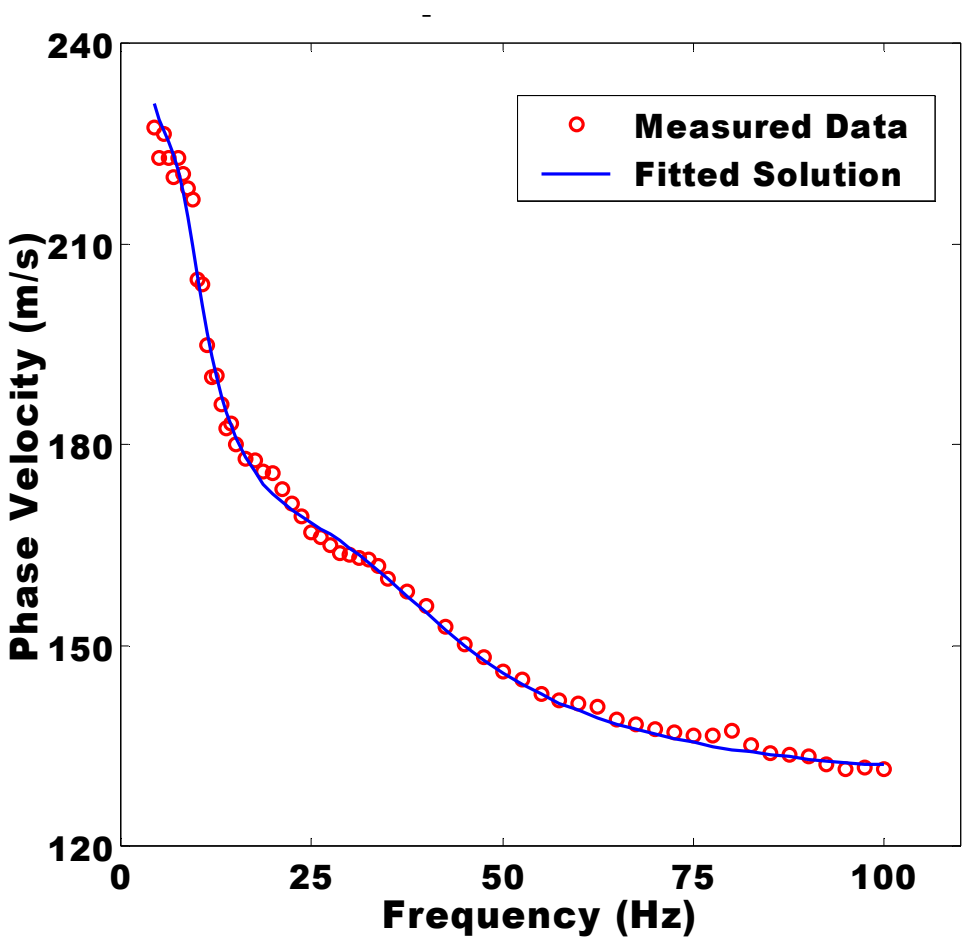

Figure 2.19 Measured dispersion data using an active source and beamforming method at Shelby Forest near Memphis, TN fit with analytical dispersion solution (Hebeler, 2001)

2.4.2.7.Borehole SASW

The borehole SASW utilizes a pressuremeter-like device for performing a surface wave test along the walls of a borehole. The device is contained within a pressurized bladder, similar to the pressuremeter test (PMT) device (Figure 2.20). The device is

lowered down a borehole and then pressurized, expanding outward against the walls of the borehole. The purpose of the pressurized bladder is to reconsolidate the surrounding soil back to the undisturbed conditions. The device has been unsuccessful at eliminating the disturbance caused by excavating the borehole, but the technique was able to evaluate the extent of the disturbed annulus, as well as measure velocities beyond and into undisturbed soil (Kalinski and Stokoe, 2003).

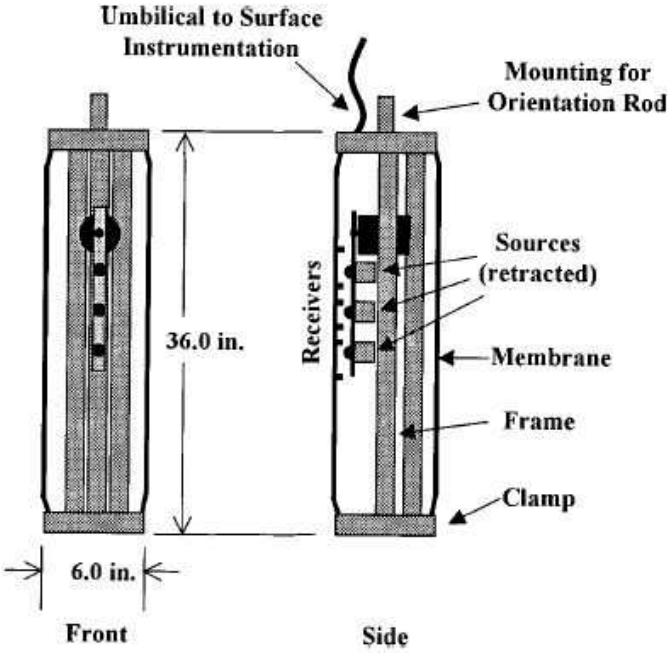

Figure 2.20 Borehole SASW device (Kalinski and Stokoe, 2003)

2.4.2.8.Bottom shear modulus profiler

The bottom shear modulus profiler (BSMP) is a method for measuring the shear modulus of the seafloor based on the propagation of surface waves (Yamamoto et al., 1991). The surface waves are generated by pressure changes caused by passing ocean waves.

2.4.2.9.P-S Logger

The P-S Logger is a borehole seismic device containing a source and receivers, capable of measuring both P-wave and S-wave velocities in soil as well as rock. Developed by the OYO Corporation (Kitsunezaki, 1980; Kaneko et al., 1990; Nigbor and Imai, 1994). Similar devices have been in use for several decades by geophysicists involved in oil prospecting (Summers and Broding, 1952; Vogel, 1952).

Aside from improved computing and data acquisition, the components of the device have remained essentially unchanged from the earlier versions. As seen in Figure 2.21, the tool has two receiver packages separated by 1 m, with the source suspended 3 to 5 m below the receivers. The components are separated from one another by rubber tubes in order to reduce the coupling between them. The entire device, approximately 7 m in length, is suspended by a cable in the fluid-filled borehole.

The source consists of a horizontal solenoid, which creates an impulse in the borehole fluid, directed at the wall of the borehole, generating P-waves and S-waves in the surrounding material. The frequency of the generated wave is low, between 100 Hz and 1000 Hz, depending on the soil/rock stiffness, so that the wavelength is much larger than the borehole diameter. Because the wavelength is larger than the borehole, the motions are independent of the borehole fluid. As a result the device is coupled to the borehole through the fluid without the need for mechanical connection. To ensure the device responds in phase with the borehole fluid, the specific gravity of the device is calibrated to match that of the fluid. The result is a direct measurement of wave velocities.

Earlier devices made indirect velocity measurements, based on refraction methods. The source in the device generated high frequency, short wavelength, pressure waves in the fluid that critically refracted along the walls of the borehole. The S-waves were created by mode conversion of the P-waves upon intersecting the borehole wall. The waves then transmitted back into the fluid where they could be detected by the

receivers.

The advantage of the P-S Logger is the ability to make direct velocity measurements over discrete intervals to depths more than 1000 m. However, for shallow investigations, the cost is prohibitive.

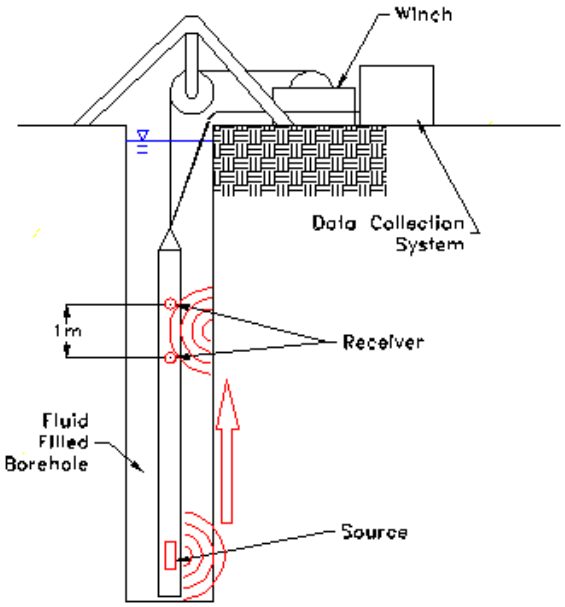

Figure 2.21 Suspension logger configuration (Casey, 2000)

2.4.2.10. Seismic cone penetrometer

The seismic cone penetration test (SCPT) , introduced in 1984 at the University of British Columbia (Rice, 1984; Campanella et al., 1986; Robertson et al., 1986), combines the versatility and simplicity of the downhole test (DHT) with the speed and efficiency of the direct push method of the traditional standardized cone penetration test (ASTM D5778-95, 2000). Figure 2.22 illustrates the components of the typical test equipment the basic procedures for the SCPT have changed little since its development. A cone penetrometer, including one or more horizontally aligned seismic sensors, is pushed into the ground vertically at a rate of 20 mm/s. As with the DHT, the seismic measurements can be made using a single receiver and the pseudo-interval method, or with two

receivers and the true-interval method. During penetration, readings of tip stress, friction sleeve stress, and porewater pressure are taken at 1 cm to 5 cm intervals. The pseudo-interval or true-interval seismic signals are only recorded during pauses in penetration at each 1 m rod break. In the United States, where English Imperial units are still prevalent, a common depth interval for DHT is 5 feet (1.5 m), thereby obtaining a V_S profile that is 50% more coarse than accepted international practice.

In usual practice, a horizontal beam or plate coupled to the ground surface by the weight of a support vehicle or the testing vehicle is the source of the seismic energy. The beam is struck on end with a hammer to generate horizontally polarized vertically propagating shear waves that can be detected by the horizontal receiver(s) within the cone penetrometer embedded below. The velocity is determined from the travel-time differences between recorded waves and the difference in the assumed travel path length for different receiver depths.

This is a cost effective method for characterizing subsurface profiles, capable of measuring five separate parameters including, tip resistance, local friction, penetration porewater pressures, time for porewater dissipations, and V_S, all within the same test. As such, a single SCPTu sounding conducted to 30 m costs approximately $2,000 in 2007 dollars.

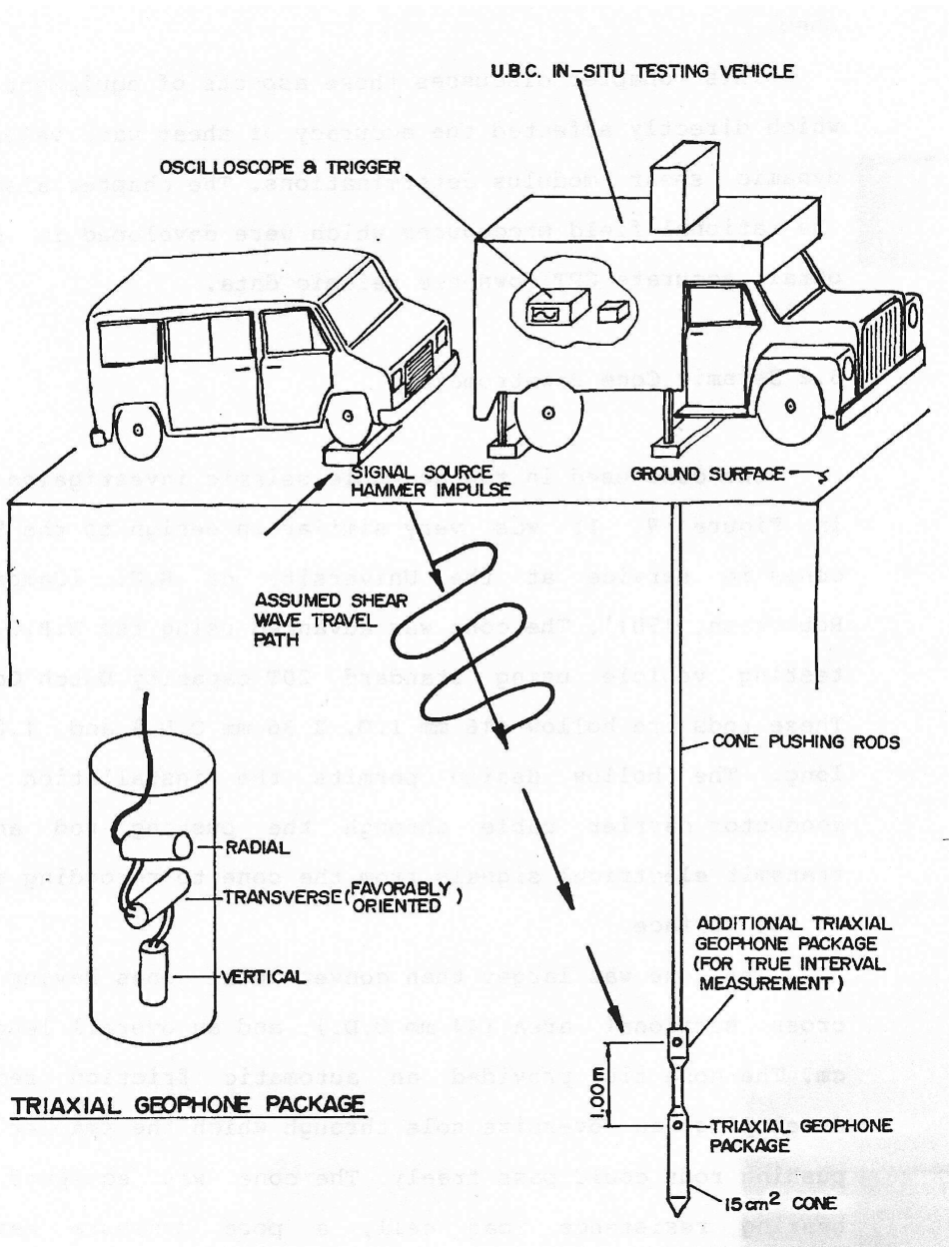

Figure 2.22 Layout of seismic cone penetration test (Rice, 1984)

2.4.2.11. Seismic flat dilatometer

The seismic flat dilatometer test (SDMT) is a direct push test method that is the combination of the traditional flat plate dilatometer test (DMT), developed by Marchetti (1980), with seismic receivers added behind the blade to incorporate V_S measurements

(Hepton, 1988; Martin and Mayne, 1998; McGillivray and Mayne, 2004). The SDMT is capable of providing 5 measurements from a single test: initial contact pressure (p_0), expansion pressure (p_1), closing pressure (p_2), A-reading dissipation (t_{flex}), and V_S. The combination of these measurements can be used to evaluate soil layering as well as strength parameters (Kates, 1997; Mayne et al., 1999). Unlike the CPT measurements, DMT readings are made while penetration is stopped, typically every 20 cm or 1 ft in the USA. Because penetration is stopped, SDMT shear wave velocity could be measured more frequently than with standard SCPT methods.

The commercially available SDMT device, shown in Figure 2.23, was developed by Marchetti following a joint testing program with Georgia Tech in Venice, Italy for which the true-interval seismic dilatometer presented in Chapter 3 was constructed. The recently developed commercial SDMT unit is a true-interval device having a 0.5 m spacing between receivers. A unique feature is that the signals are digitized downhole and broadcast up the single wire contained within the standard dilatometer tubing.

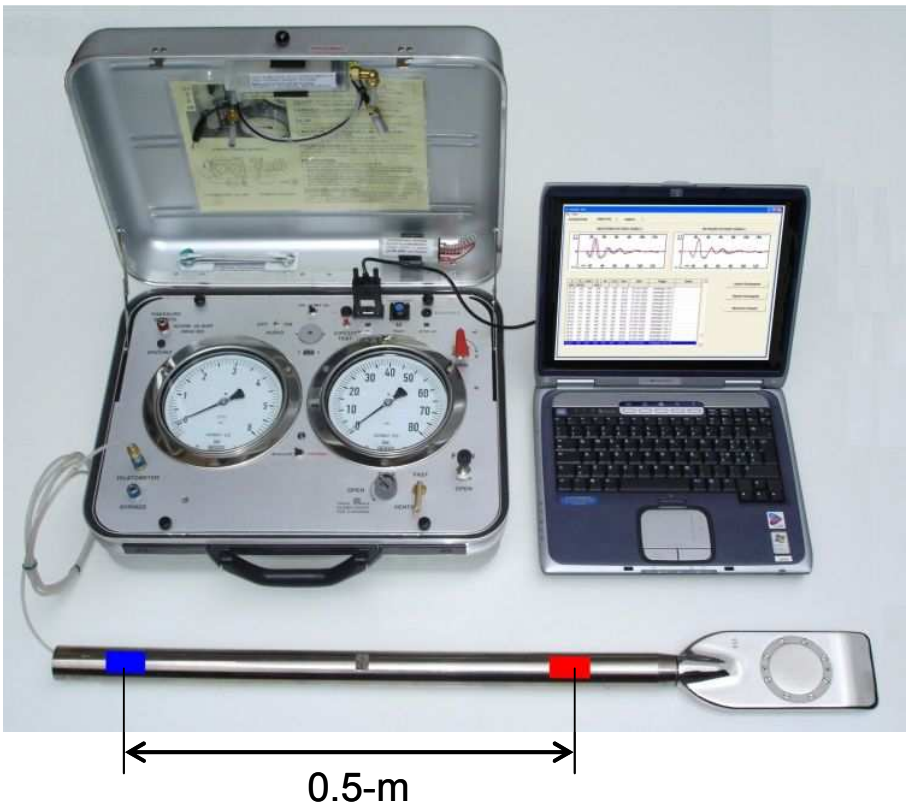

Figure 2.23 The commercial seismic dilatometer system (Marchetti et al., 2007)

2.4.2.12. Downhole freestanding torsional shear

The downhole freestanding torsional shear device (DFSD) is a borehole device for performing torsional shear tests in-situ (Roblee et al., 1994; Roblee and Riemer, 1998). The method is intended to be a borehole version of the resonant column / torsional shear device. The in-situ "specimen" is prepared below the bottom of the borehole by carefully carving out a cylindrical column of soil (Figure 2.24). A loading cap placed on top of the specimen applies torsional loads in either resonant column mode or torsional shear mode. The loading frequencies and strain ranges are comparable to the resonant column and torsional shear values. The device is based on the design of a similar device developed by (Henke and Henke, 1993) for performing impulse shear tests on cylinders of soil below the base of a borehole.

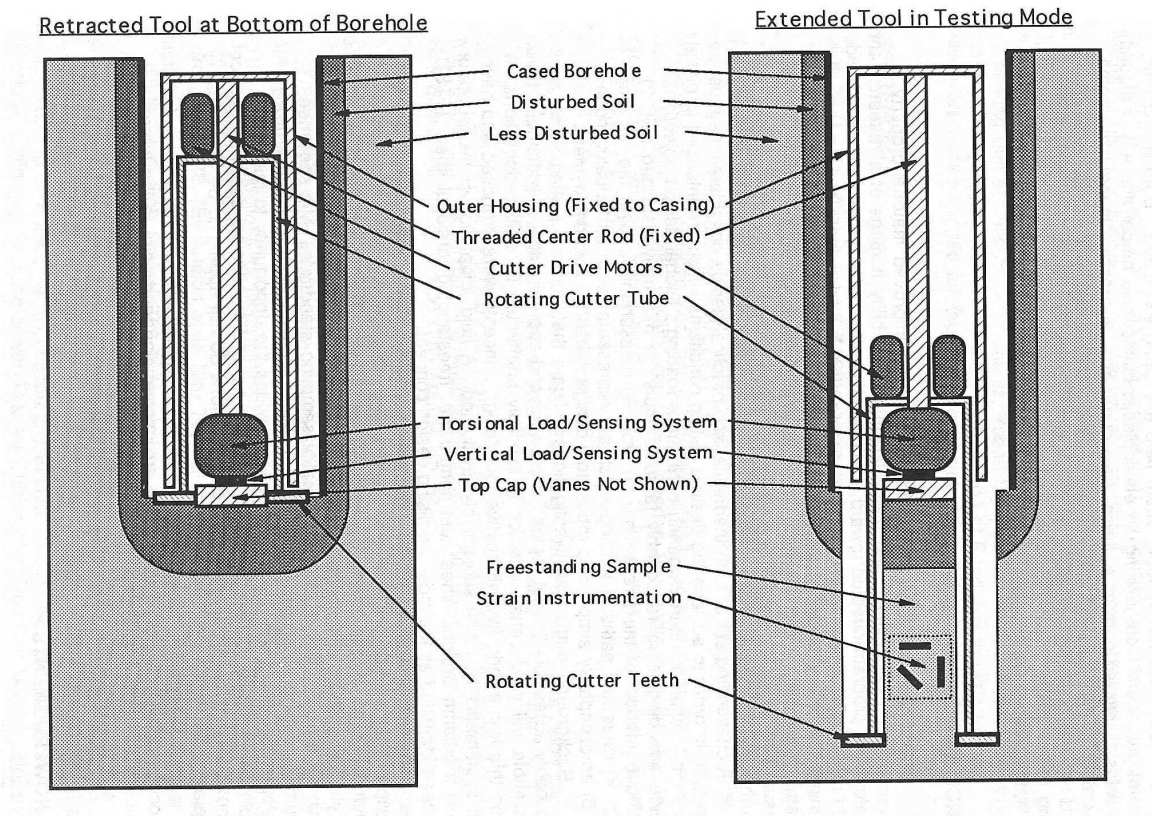

Figure 2.24 Schematic of Freestanding Torsional Shear device (Roblee et al., 1994)

Though this test is performed in-situ, the soil specimen can suffer sampling disturbance from stresses applied and relieved during the carving process. Additionally, in resonant column mode, energy leakage through the base of the specimen is significantly greater than through the comparatively rigid base of the laboratory resonant column device.

2.5. Summary

Investigators have a range of laboratory and field methods at their disposal for evaluating V_S (and corresponding G_0) of geomaterials. Figure 2.25 presents a summary of several common methods. While it is generally beneficial to obtain as much information as possible, test selection depends on several factors including time, budget, type of

material, and application of results. Laboratory specimens are subjected to potentially damaging stress histories during sampling and test preparation. Also, the results are based on discrete elements and may not be representative of larger systems. In-situ test methods offer the benefit of characterizing large volumes of soil, as well as identifying the locations and interactions of boundaries, in a manner that preserves natural conditions.

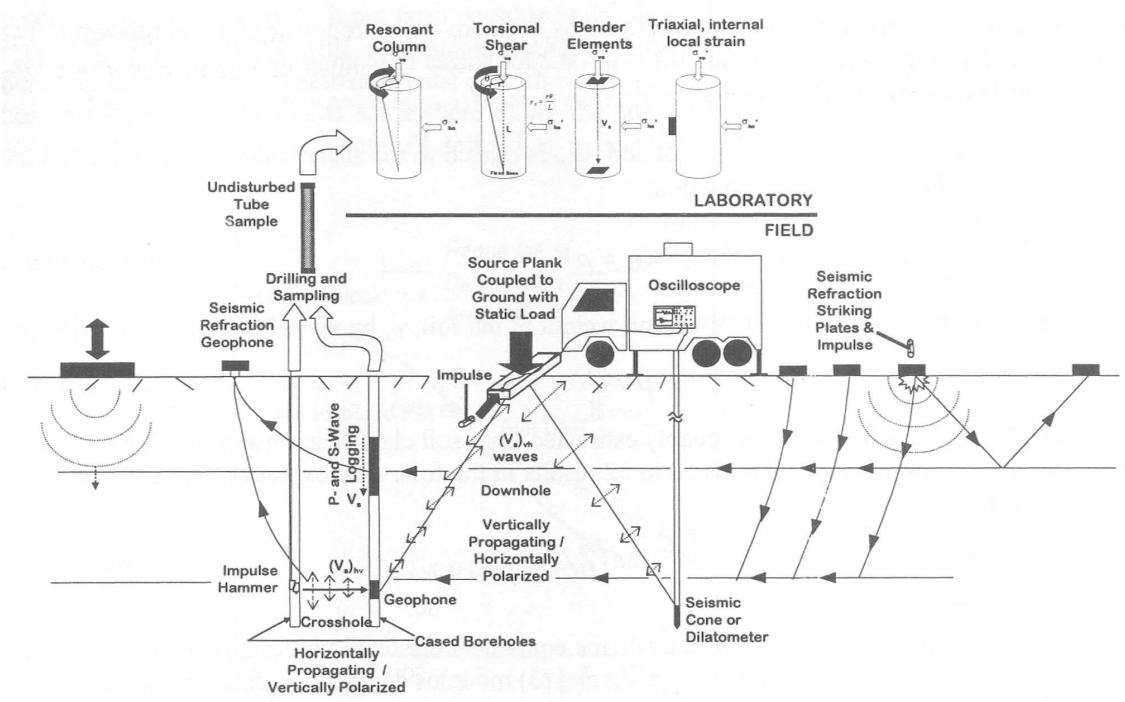

Figure 2.25 Laboratory and field methods to evaluate V_S in soils (Schneider et al., 1999)

3. DEVELOPMENT TOWARDS A CONTINUOUS-PUSH SEISMIC SYSTEM FOR DIRECT-PUSH SITE CHARACTERIZATION

3.1. Introduction

A new continuous-push seismic system for the SCPT and SDMT was investigated to examine how shear wave velocity measurements could be incorporated more seamlessly into these in situ test procedures. Such a system would shorten field testing times, helping to promote regular V_S profiling in practice. The continuous-push system also has the potential to enhance the quality of the test results by allowing V_S measurements to be made on a scale more directly comparable with other direct-push probe measurements made within the same interval. Currently available seismic sources and testing methodologies were not well-suited for this type of system. As part of this research, a new automated seismic source was developed and tested with new procedures to measure V_S without halting the penetration of the probe or requiring additional work by the operator. Existing commercial devices utilize proprietary hardware and software, and were consequently not adaptable for researching continuous-push testing. For this reason, three separate configurations of a true-interval seismic device were designed and built to evaluate optimal arrangements for the source, geophone configurations, and procedures.

3.2. Frequent-Interval Procedure for Continuous-Push Velocity Measurement

One of the goals for improving the integration of the seismic component of the SCPTu and the SDMT is to make the depth resolution of V_S more similar with the depth intervals of the other penetration measurements. The two types of standard downhole seismic testing methods (pseudo-interval and true-interval method) measure velocity only during rod breaks. In the United States, the V_S interval is often 1.5 m (5.0 feet), while international operations commonly use a 1 m (3.3 feet) interval. The resulting V_S profiles

are much coarser than the other measurements made during the sounding, such as q_T measured every 1 to 5 cm. Therefore, a new method, termed frequent-interval, which is a variation of true-interval, was introduced to make measurements of V_S at closer depths resulting in a more detailed velocity profile.

3.2.1. Assessment of current interval velocity methods

The value of V_S cannot be measured discretely (at a point). Measurements of V_S represent an average velocity over the length of material through which the wavelets are propagated. The V_S can be measured directly by dividing the distance between two points by the time it takes a transient shear wave to propagate from the first point to the second point. Figure 3.1 demonstrates this concept, showing a wave passing through Point A to Point B and beyond. The resulting measured wave velocity is an average value for the length of material within the interval A to B.

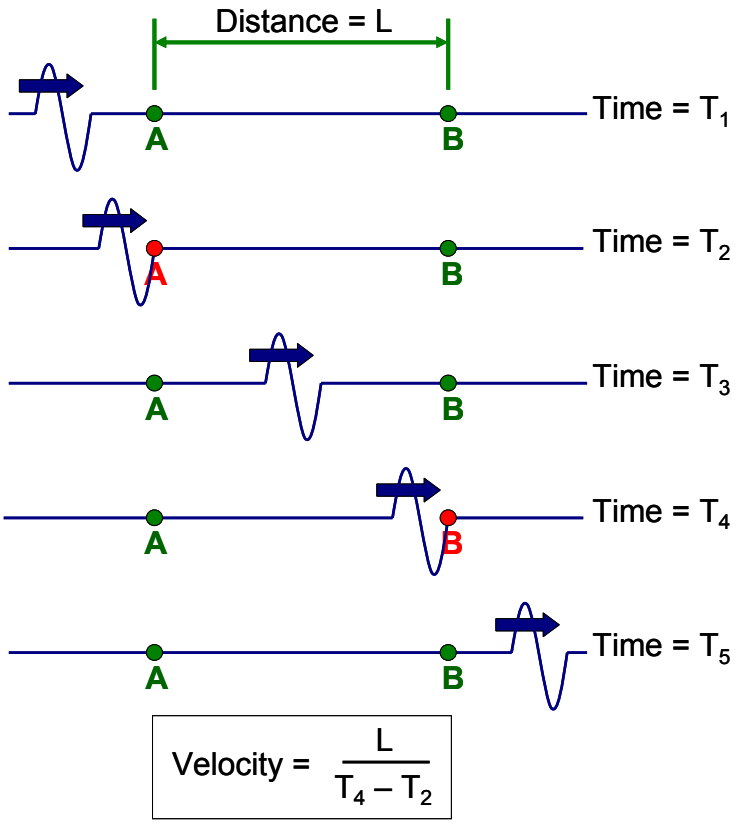

Figure 3.1 Direct wave velocity measurement within an interval between two points

The same concept of interval measurement applies to direct-push downhole tests such as the SCPT, except that the seismic source is offset to the side of the receivers. The distance between recorded signals is thus taken as the difference in the lengths of the assumed raypaths rather than simply the distance between receivers. In Figure 3.2, two methods are presented for measuring shear wave velocity with the SCPT. The pseudo-interval method utilizes multiple source events recorded by a single receiver at different depths, while the true-interval method utilizes two receivers separated by a fixed distance. The calculation of V_S is the same for both methods. These techniques are also applicable to other types of downhole velocity tests. The advantage of the pseudo-interval method is the simplicity of a device containing only a single receiver. However, accurate depth measurement is critical for correctly determining the differences in raypath lengths.

The seismic source also needs to be repeatable with respect to signal quality and trigger timing in order to determine differences in travel times for the source waves. True-interval has the advantage of fixed distance between receivers so depth errors have less significance, and the same source wave is captured at both receivers, eliminating trigger timing errors completely.

The interval length between receiver locations affects the accuracy of the measured velocities. At Georgia Tech, the interval spacing used for the pseudo-interval and true-interval methods for SCPT and SDMT is approximately one meter. The standard depth between each measurement is one meter, corresponding to the rod breaks. In this way, interval velocity is measured end-to-end, without overlapping. As a result, the V_S profile is much less detailed than the CPT or DMT resistance profiles recorded at intervals of 1 cm to 20 cm.

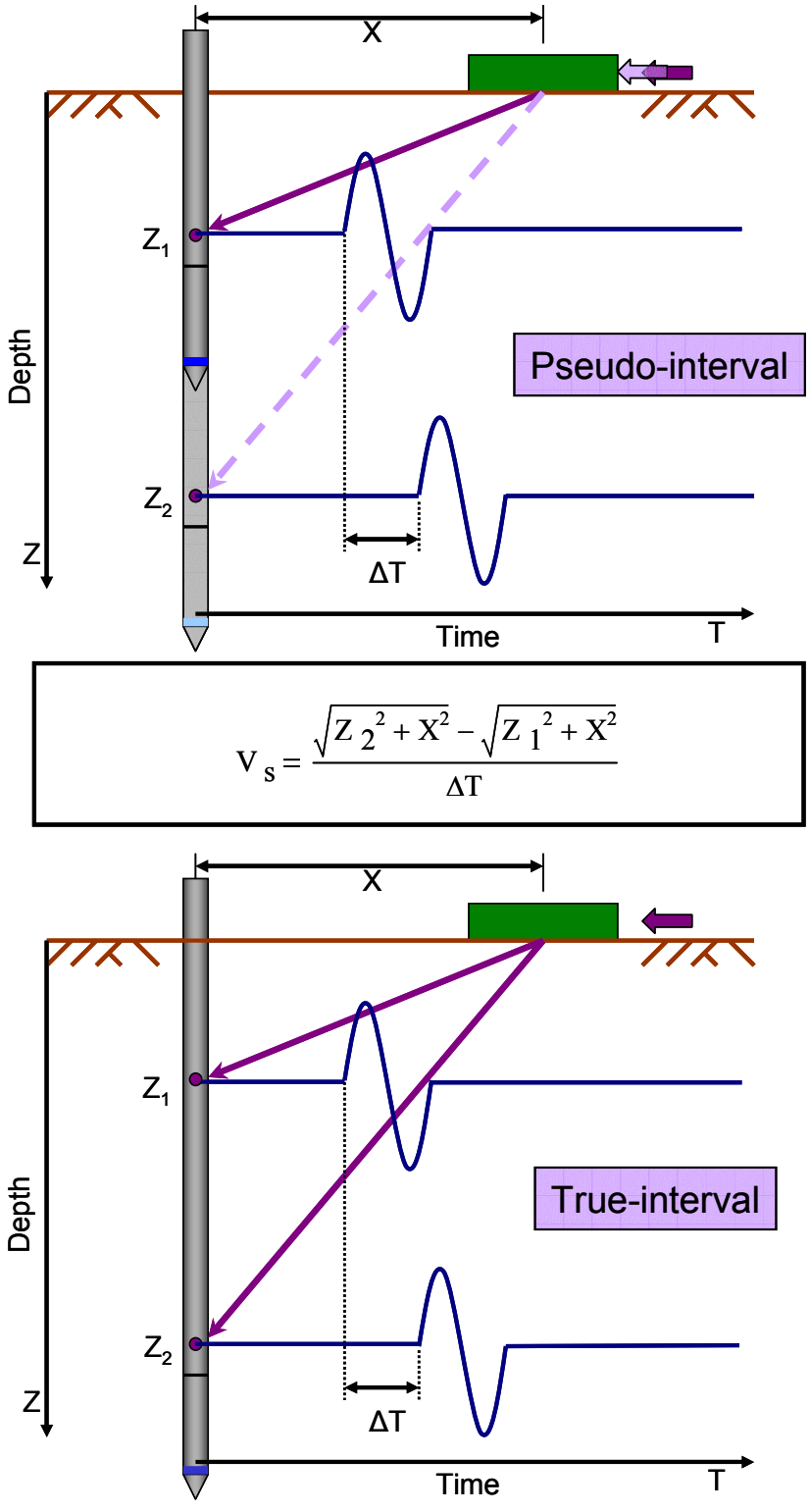

Figure 3.2 Methodology for pseudo-interval and true-interval shear wave velocity measurement with SCPT

One approach to improving the depth resolution of the velocity profile is to shorten the interval between receivers to make the measurements more discrete. The commercially available SDMT (Figure 2.23) has a short interval spacing of 0.5 m. However, this approach actually reduces the accuracy of each V_S measurement. Remember that the velocity is determined by the travel time for a wave passing between two points. If the distance is shortened, the travel time is also shortened. The effect of inaccuracy in travel times becomes magnified as travel times are shortened. Table 3.1 and Table 3.2 show the amount of velocity error caused by various time errors, for a 1 m interval and a 0.5 m interval respectively. By shortening the interval length from 1 m to 0.5 m, the velocity error can double for a given amount of error in the time measurement. The tables also reveal that lower velocities can be measured more accurately than higher velocities.

Table 3.1 Velocity error as a function of travel time error and velocity for a 1 m interval between receivers

Interval Length	1.0 -m				
Time Error (msec)	Actual Velocity (m/s)				
	100	200	300	400	500
	Actual Travel Time (msec)				
	10.00	5.00	3.33	2.50	2.00
	Velocity Error (m/s)				
0.001	0.0 (0%)	0.0 (0%)	0.1 (0%)	0.2 (0%)	0.2 (0%)
0.01	0.1 (0%)	0.4 (0%)	0.9 (0%)	1.6 (0%)	2.5 (1%)
0.1	1.0 (1%)	3.9 (2%)	8.7 (3%)	15.4 (4%)	23.8 (5%)
1	9.1 (9%)	33.3 (17%)	69.2 (23%)	114.3 (29%)	166.7 (33%)
2	16.7 (17%)	57.1 (29%)	112.5 (38%)	177.8 (44%)	N/A

N/A - time error is greater than actual travel time
(#%) - percent error

Table 3.2 Velocity error as a function of travel time error and velocity for a 0.5 m interval between receivers

Interval Length	0.5 -m				
Time Error (msec)	Actual Velocity (m/s)				
	100	200	300	400	500
	Actual Travel Time (msec)				
	10.00	5.00	3.33	2.50	2.00
	Velocity Error (m/s)				
0.001	0.0 (0%)	0.1 (0%)	0.2 (0%)	0.3 (0%)	0.5 (0%)
0.01	0.2 (0%)	0.8 (0%)	1.8 (1%)	3.2 (1%)	5.0 (1%)
0.1	2.0 (2%)	7.7 (4%)	17.0 (6%)	29.6 (7%)	45.5 (9%)
1	16.7 (17%)	57.1 (29%)	112.5 (38%)	177.8 (44%)	N/A
2	28.6 (29%)	88.9 (44%)	N/A	N/A	N/A

N/A - time error is greater than actual travel time
(#%) - percent error

3.2.2. Proposal of a new frequent-interval V_S measurement method

The interval length cannot be reduced to significantly improve V_S depth resolution without magnifying timing errors. Another option for improving depth resolution while maintaining accuracy, is to keep the interval length the same, but make overlapping measurements, rather than end-to-end measurements. This proposed method is called frequent-interval (Figure 3.3). For this research task, a true-interval receiver configuration was used with approximately 1 m between receivers, and the measurements were made every 0.2 m, so that each V_S measurement is overlapped five times.

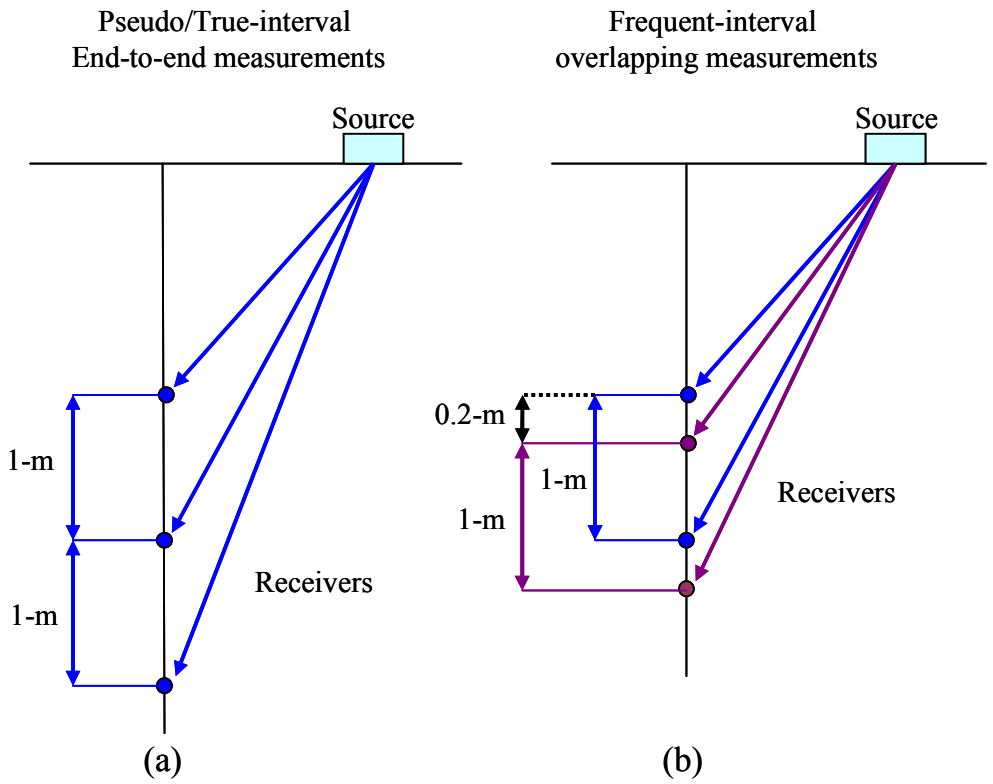

Figure 3.3 Schematic of (a) traditional interval-measurements made end-to-end and (b) frequent-interval with overlapping measurements

As described in Section 3.2.1, downhole velocity measurements are not discrete. Each value is the average velocity between the receivers. The configuration of the receivers for the frequent-interval method is identical to that of the true-interval method. However, because the frequent-interval measurements overlap one another, the frequent-interval velocity can be viewed as a moving average velocity of five smaller 0.2 m intervals (Figure 3.4). A mathematical description of the moving average velocity is given by Equation 3.1. Note that because the units of velocity contain time (seconds) in the denominator, average velocity must be calculated by the harmonic mean rather than the arithmetic mean.

$$V_{n+3(\text{measured})} = \frac{5}{\frac{1}{V_{n+1}} + \frac{1}{V_{n+2}} + \frac{1}{V_{n+3}} + \frac{1}{V_{n+4}} + \frac{1}{V_{n+5}}} \qquad 3.1$$

Utilizing inverse problem solving techniques, it may be possible to deconvolve the moving average relationship for measured 1 m interval results into more discrete 20 cm intervals. The same concept has been examined previously for deconvolving CPT friction sleeve measurements into more discrete values (Saussus et al., 2004; Frost et al., 2006). The potential of such analysis in V_S profiling is encouraging, but the solution is outside the intended scope of this research to develop practical tools for routine V_S measurement. This concept of a moving average is presented here to provide insight into the differences between measured profiles and actual profiles. A moving average is a low-pass filter, so the measured frequent-interval profile is a smoothed version of the true-profile. Figure 3.5 shows a synthetic layered V_S profile on the left, the results from a simulated conventional pseudo- or true-interval test in the center, and a simulated frequent-interval test on the right. The depth increment with conventional methods is too coarse to reliably detect the presence of thin layers. The frequent-interval can detect thinner layers, but there is a smoothing effect because of the distance between receivers. Sharp transitions appear more gradual, and for layers thinner than the interval length, high values will be underestimated and low values will be overestimated.

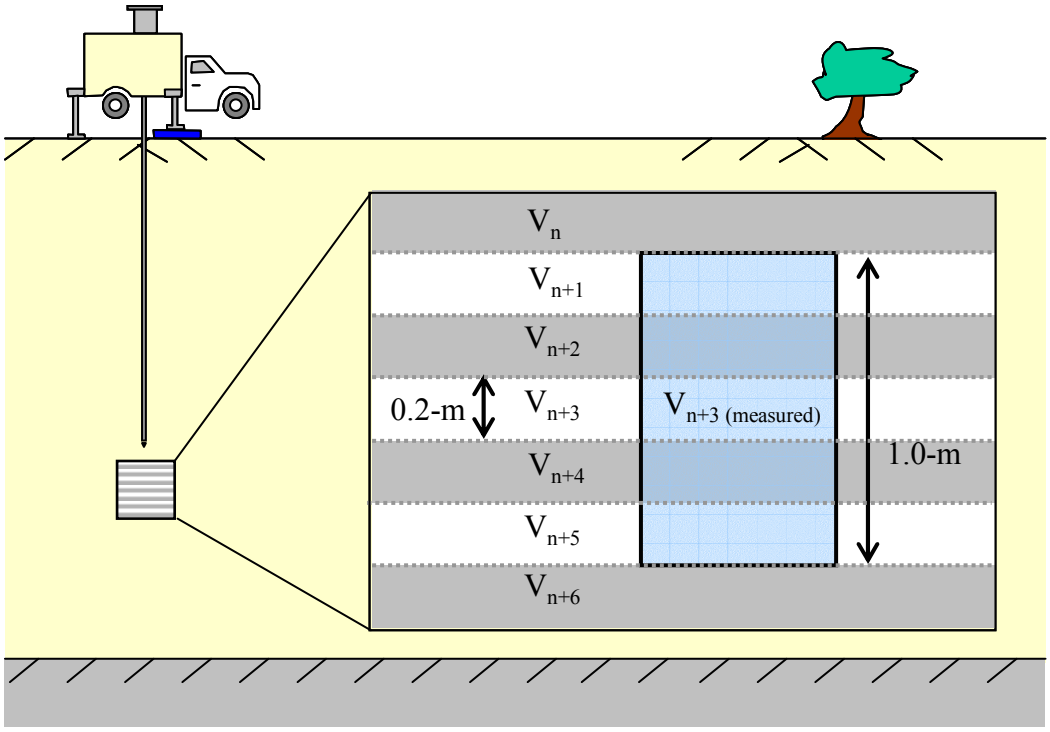

Figure 3.4 Averaging of the 20 cm incremental depths by the 1 m frequent-interval receiver spacing

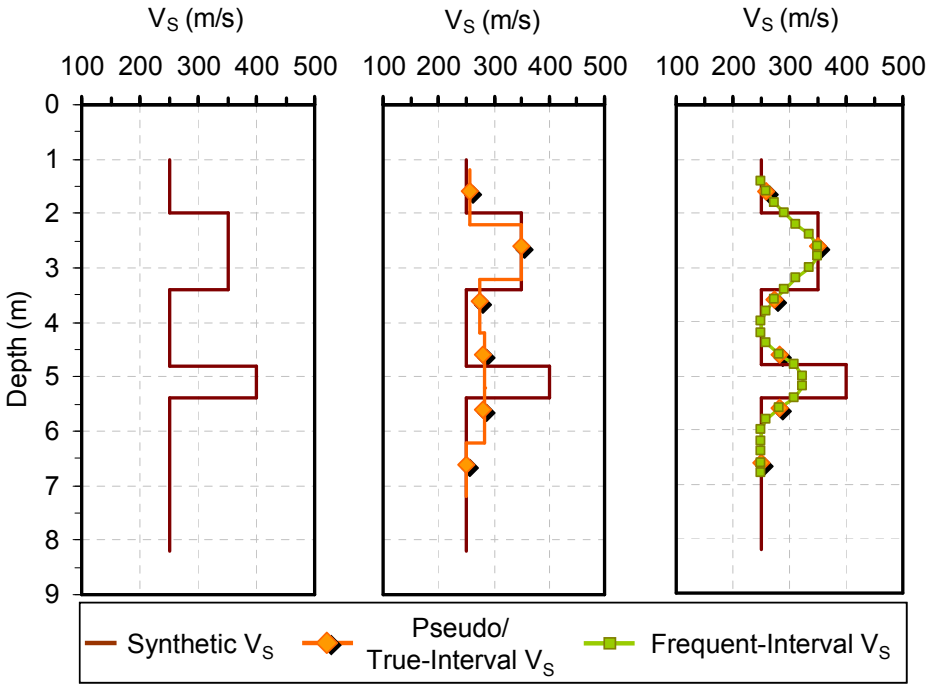

Figure 3.5 Synthetic V_S with simulated coarse pseudo/true-interval results, and simulated frequent-interval results with more depth resolution

3.3. Non-Stationary Receivers

A continuous-push seismic system would permit the use of the frequent-interval method, by eliminating the need to stop penetration in order for V_S measurements to be made. For the SDMT, this is not as much of a problem because penetration is already stopped every 20 cm to make pressure readings. In contrast, the pauses during SCPTu occur only at standard 1 m rod breaks. However, each time penetration is stopped, and the load is released, consolidation of the soil allows stresses to relax as porewater pressures dissipate. Pausing for seismic testing every few centimeters may cause some discontinuity in the tip, sleeve, and porewater pressure results. In order to incorporate the frequent-interval method into the SCPTu to create a continuous-push system, seismic data must be recorded while the receivers are in motion.

Traditionally, seismic tests have always been conducted with stationary receivers. For instance, with surface wave tests or seismic refraction surveys, the receivers are positioned at precise locations while data recording is in progress. Similarly, for downhole and crosshole seismic tests in a borehole, the receivers maintain their position during measurements, coupled to the borehole wall by an inflatable packer. Naturally, the SCPTu and SDMT devices were developed following the same procedures, recording only while penetration is stopped. However, the direct-push tests have the distinct advantage of maintaining continuous coupling even while the probe is in motion.

The probe steadily moving away from the source results in a Doppler Shift. Recorded waves seem to propagate more slowly, and with an apparently lower frequency because the wave front has to catch-up to the receivers. Fortunately, the Doppler Effect for the SCPTu is negligible. The penetration rate for the SCPTu probe is only 0.02 m/s compared to the 100 to 700 m/s propagation speed of the shear waves. There is only a 0.02 m/s underestimation of V_S, which is well below the threshold of measurement resolution.

The receivers have also been kept stationary in order to minimize any unwanted

vibrations. Any operator is familiar with vibrations from nearby vehicles, including the testing vehicle, or from construction activities, obscuring the generated source waves, making analysis difficult or impossible. Concerns are justified in that a penetrating probe is subjected to even more noise sources than stationary receivers. During penetration, the testing vehicle transfers vibrations through the grips, clamps, or pushing cap, directly to the probe rods, while during a standard static seismic test, the connection to the rods can be released during recording. Other noise is created as the probe is pushed into the ground. Particles are crushed and displaced, thereby causing vibrations that are detectable by the seismic sensors. Researchers have actually used these vibrations to their benefit to help characterize the soil. Villet et al. (1981), Tringale and Mitchell (1982), and Massarsch (1986) developed cone penetrometers with microphones built into the cone tip in order to measure vibratory noises during penetration. Termed the Acoustic Cone Penetration Test (ACPT), the vibratory amplitudes of the frequency responses were utilized to determine soil type and layer changes. In later experiments, Houlsby and Ruck (1998) attempted to extend the application of the ACPT to identify sand mineralogy along with density and stress state.

Just as ambient noise sources are handled during stationary seismic tests, the influence of penetration-induced noise sources can be minimized using signal processing techniques as well as careful testing procedures. To investigate the influence of penetration-induced noise, tests results of stationary and non-stationary receivers will be characterized later in Chapter 5.

3.4. True-Interval Seismic Probes

Three separate seismic probes were constructed for recording shear wave signals during the investigation of the continuous-push seismic system. These devices include: (a) a true-interval seismic dilatometer, (b) a true-interval seismic probe, and (c) a true-interval seismic probe with biaxial geophone arrays at three elevations. True-interval

devices allow comparison of the same source event recorded at separate locations, and the interval distance is fixed, eliminating the potential for uncertain receiver spacing. In the pseudo-interval method, signals from different source events are compared as if they were the result of the same source event. Any trigger timing inconsistency will cause time errors, which were shown previously in Table 3.1 and Table 3.2 to translate into V_S errors. Inaccurate depth measurement with pseudo-interval is also a potential for error. Depending on the type of system, it is not unusual to have a depth measurement error of 5 cm within a one meter stroke. A 5 cm depth error within a 1 m interval translates to a 15 m/s velocity error for a 300 m/s soil layer (Table 3.3). The same depth error in soil with V_S equal to 500 m/s would result in a velocity error of 25 m/s. The amount of the error increases with increasing velocity, but the percent error in velocity remains equal to the percent error in the depth measurement. The true-interval configurations for the new devices were used in order to reduce potential errors associated with trigger timing and depth measurement (Butcher and Powell, 1996).

Table 3.3 Velocity error as a function of depth error for pseudo-interval velocities

Actual Interval	1.0 -m				
Depth Error (cm)	Actual Velocity (m/s)				
	100	200	300	400	500
	Velocity Error (m/s)				
0.01	0.0 (0%)	0.0 (0%)	0.0 (0%)	0.0 (0%)	0.1 (0%)
0.1	0.1 (0%)	0.2 (0%)	0.3 (0%)	0.4 (0%)	0.5 (0%)
1	1.0 (1%)	2.0 (1%)	3.0 (1%)	4.0 (1%)	5.0 (1%)
5	5.0 (5%)	10.0 (5%)	15.0 (5%)	20.0 (5%)	25.0 (5%)
10	10.0 (10%)	20.0 (10%)	30.0 (10%)	40.0 (10%)	50.0 (10%)

(#%) - percent error

The primary requirement for a continuous-push seismic probe is that the device has a true-interval configuration of seismic receivers to avoid undue errors from inability

to accurately monitor the depth. Another significant characteristic is that the receivers are not integrated with any other instrumentation built into the device. The seismic sensors must be able to be monitored independently. Lastly, the receivers in the device must be responsive and sensitive within the frequency range compatible with the seismic source being used.

An ideal device for continuous-push SCPTu would be a true-interval seismic cone with the ability to monitor seismic sensors continuously. There are currently no commercial-devices configurable for continuous-push seismic testing. True-interval seismic cones are uncommon, because increasing the number of sensors increases the complexity and expense of the device. Any commercially available devices that do exist are tied to proprietary data acquisition software, which is not adaptable for research purposes. Rather than construct a fully-integrated true-interval seismic cone, seismic-only probes were built.

3.4.1. Geophone seismic sensors

Seismic sensor choices for direct-push applications are restricted by the diameters of drill rods and cone rods. In addition to the limiting rod diameter, sensor size is further limited due to the need to keep significant open space in the middle of the rod to permit the passing of cables and tubing up and around the sensors to connect with the data acquisition at the surface. Piezoelectric accelerometers and Micro-Electro-Mechanical Systems (MEMS) accelerometers are available in very small packages, but they can be costly, and the circuitry and power requirements add complexity. There are a few geophones, or velocity transducers, available in the necessary sizes. These are inexpensive simple devices, and they have the advantage of not requiring a power source.

Each of the three seismic probes built for this research were fitted with model GS-14-L3 geophones from GeoSpace, LP (Figure 3.6). The specifications for this model geophone are listed in Table 3.4. With a diameter of 16.7 mm and a height of 17.3 mm, it

is small enough to fit inside of a 44.45 mm rod with enough space left over for cables and DMT tubing. However, the physical size of a geophone affects the response characteristics of the device, and the GS-14-L3 geophone compromises some aspects of performance for its convenient size.

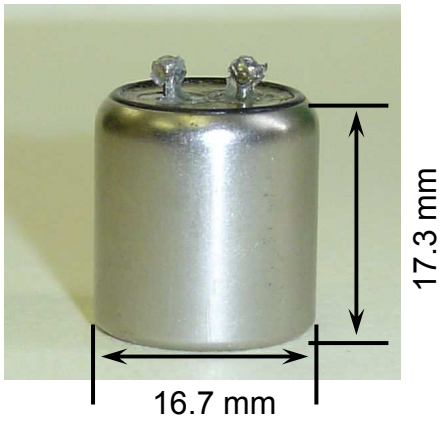

Figure 3.6 Image of GS-14-L3 geophone contained in the seismic devices

Table 3.4 Specifications for the model GS-14-L3 geophone from GeoSpace, LP (www.geospacelp.com)

Property	Specification
Sensitivity (± 15%)	114 mV/cm/sec
Natural Frequency (± 20%)	28 Hz
Coil Resistance (± 5%)	570 ohms
Coil Inductance	45 mh
Damping Factor (± 30%)	0.18
Damping Constant	172
Displacement Limit	2.3 mm
Inertial Mass	2.15 g
Orientation Angle	± 180°
Height	17.3 mm
Diameter	16.7 mm
Total Mass	19 g
Operating Temperature	-45° to 100°C
Storage Temperature	-45° to 100°C
Shock	5000 G

The frequency response curve for this geophone is shown in Figure 3.7. The resonant frequency of the geophone is approximately 28 Hz. Input signals with frequencies at or below the resonant frequency become distorted by phase shifts and a variable output scaling factor. The expected frequency content for a sledgehammer seismic source ranges from 0 to less than 150 Hz (Keiswetter and Steeples, 1994), which falls within the non-linear range for the geophone. Therefore, the recorded signals are distorted from the actual motions.

Distorted signals are an unfortunate consequence of having the seismic source frequency at or near the resonant frequency of the sensor. However, signal distortion is less of a problem than it may seem. As long as the same model sensor is used to record all of the signals, the distortion effects will cancel when comparing signals to each other. The V_S measurements are made by determining travel time differences between signals, so amplitude scaling is relatively unimportant.

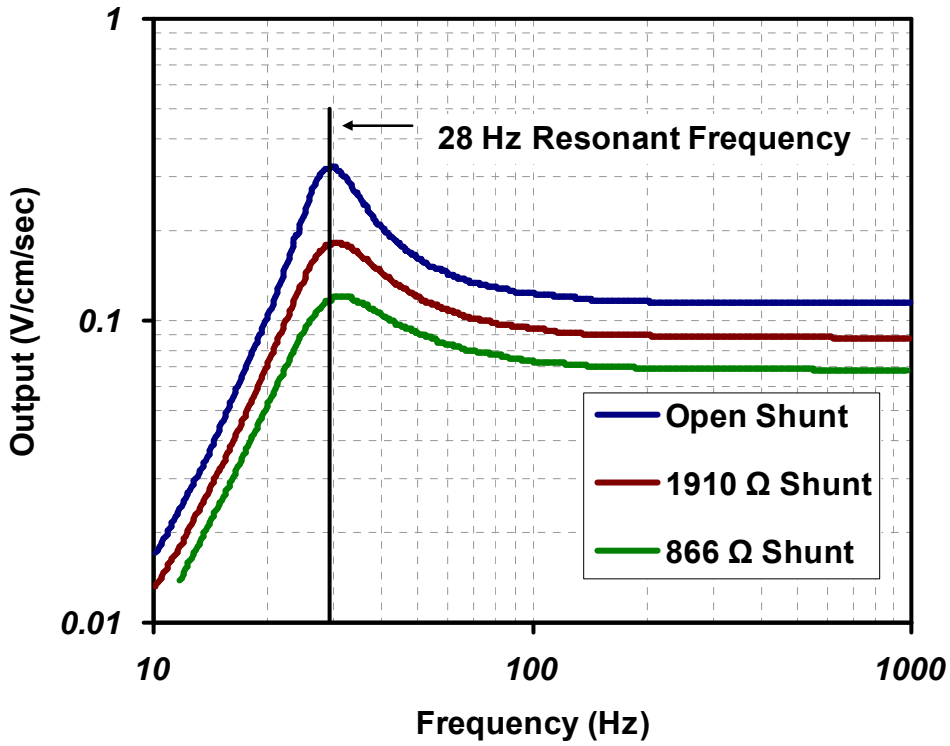

Figure 3.7 Frequency response curves for the GS-14-L3 geophone as provided by the manufacturer on their website (www.geospacelp.com)

The electrical connections can also affect the output response. A geophone consists of a mass on springs. The mass is a coil of fine wires which encircles a permanent magnet. As the mass, or wire coil, moves up and down relative to the magnet, an electric field is generated which creates a difference in potential between the terminals of the geophone. The mass-spring system is damped slightly to limit some of the bouncing, or ringing, which keeps the mass moving after the applied motion has ceased. The damping can be increased, to minimize the ringing, by adding shunt resistors between the terminals to dissipate some of the energy, but this also reduces the output levels. To maximize the output levels of the geophones, they were connected with open shunt, meaning no additional damping was added. The low damping can cause ringing which means the recorded signals vibrate more cycles than desired.

3.4.2. True-interval seismic dilatometer

Adding seismic sensors to a standard flat dilatometer transforms the DMT into the SDMT, the history of which is described in Section 2.4.2.11. For this research, a true-interval seismic dilatometer was developed that allowed the measurement of frequent-interval shear wave velocities. This prototype inspired a new commercially available SDMT. The Georgia Tech SDMT device consists of two horizontal single-axis geophone modules separated by a length of rod. A pair of small diameter coaxial cables carries the signals to the surface. Figure 3.8 shows a schematic of the device accompanied by an image of the assembled device in the field.

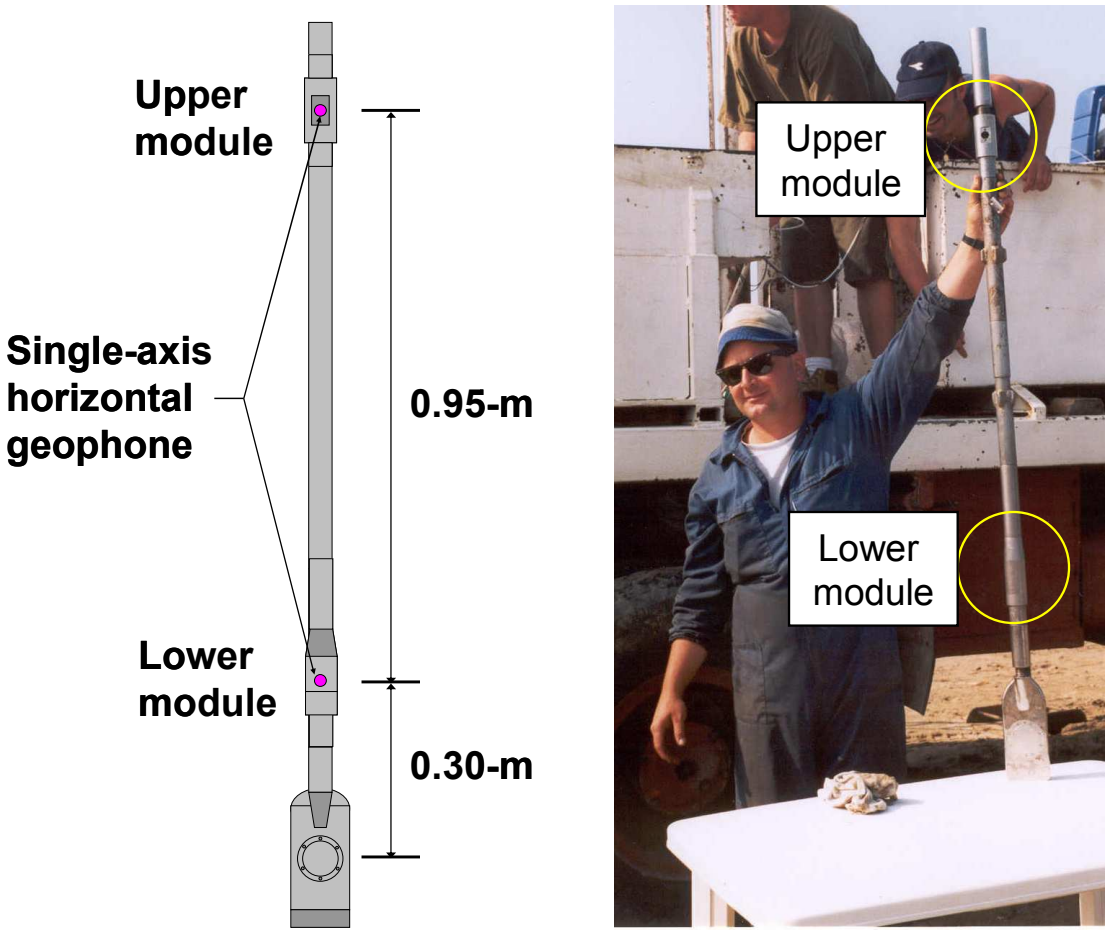

Figure 3.8 Receiver configuration of the true-interval seismic dilatometer

3.4.2.1.Seismic modules

For true-interval testing, the seismic sensors have to be separated by some distance, typically about one meter, so that the travel time difference between the receivers can be resolved. Rather than build the device as a single lengthy unit, two small individual modules were made to house the geophones. A short length of rod was used to separate the modules, resulting in a geophone spacing of 0.95 m.

Each module holds a single horizontal geophone. The seismic modules are machined from stainless steel to prevent corrosion, while the adapters to connect the modules to the rods are made from short pieces of the rods themselves.

The lower seismic module (Figure 3.9) consists of 4 parts, the core of the module, a protective housing, and two cone rod adapters. The geophone mounts inside a precision hole in a center post within the module, held in place by friction. Just enough space was allowed inside the module for the dilatometer tubing to pass through. The protective housing fits down over the geophone to enclose it. A small divot was drilled in the outside of the core of the module and filled with brass weld to indicate the direction of the geophone once assembled. The outside diameter of the module was machined to 44.45 mm, so that it would be larger than the diameter hole created by the leading DMT blade. This ensures that the module will be coupled to the surrounding soil.

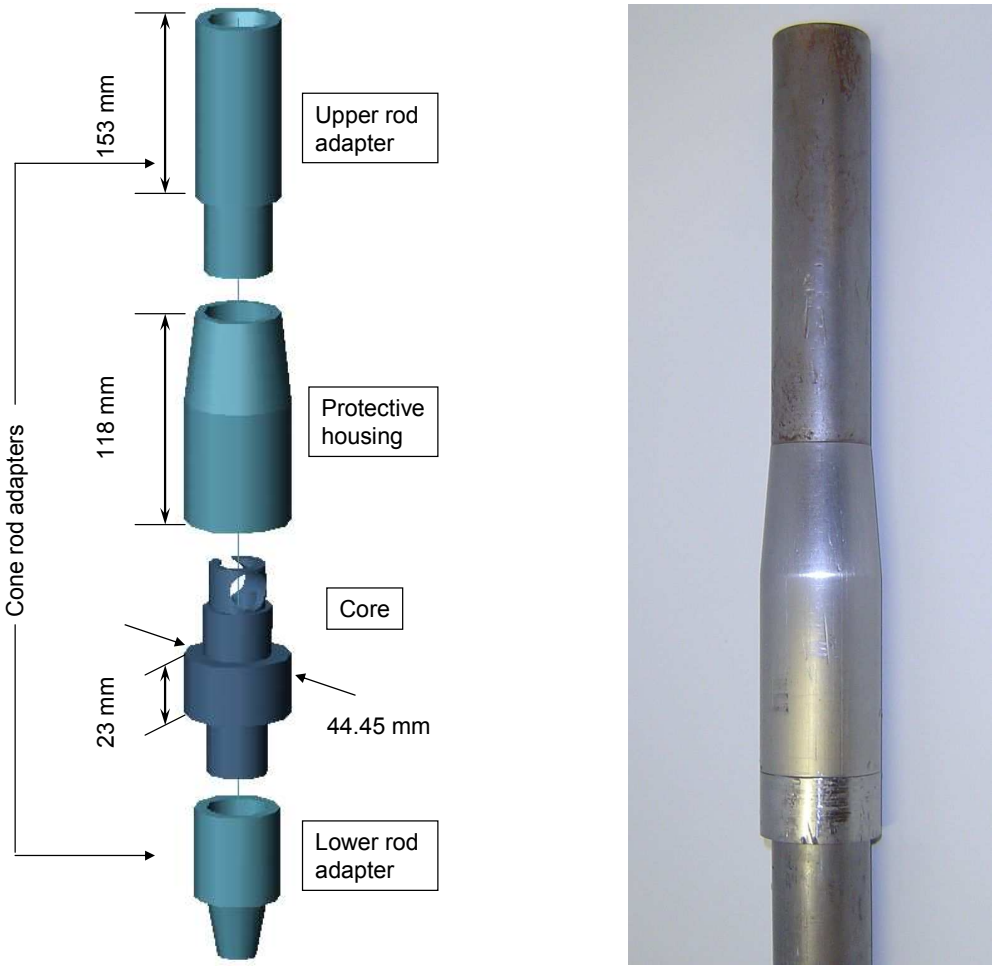

Figure 3.9 Lower seismic module of the true-interval seismic dilatometer

The upper seismic module (Figure 3.10) consists of 5 components, the geophone housing, a detachable cover plate, two rod adapters and assorted adjustment washers. With this module, both the dilatometer tubing and the coaxial cable from the lower geophone have to pass through to the surface. As a result, the geophone has to mount off-center, closer to the outside edge of the module, leaving more open space in the center. A door, cut into the side of the module allows the geophone to be inserted after the module is attached to the rods. The diameter of the upper module is slightly larger than the lower module at 45.72 mm, again to ensure coupling to the soil.

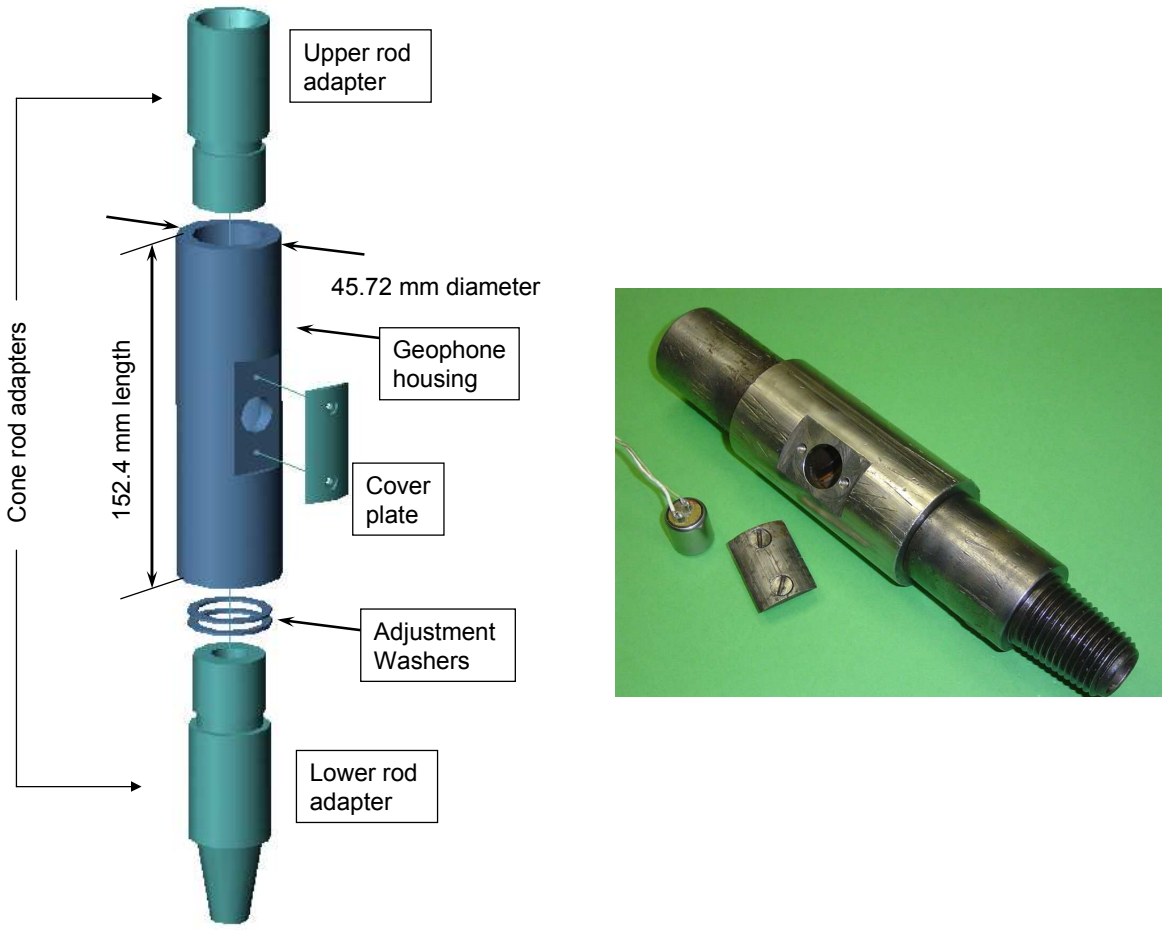

Figure 3.10 Upper seismic module of the true-interval seismic dilatometer

The geophones in the probe must be aligned in the same direction in order be comparable. The adjustment washers in Figure 3.10, which are placed between the geophone housing and the lower cone rod adapter, are used to align the upper seismic module with the lower module. The geophones are fixed within their respective modules. When modules are threaded together with a rod in-between, they are not guaranteed to be aligned in the same direction. To account for misalignment, steel washers of varying thicknesses were made to manipulate the amount of rotation needed to tighten all the components together.

Figure 3.11 illustrates the relationship between washer thickness and rotation. The thread pitch of the straight threads of the lower cone rod adapter is the reciprocal of 5.5

threads/cm. For this pitch, varying the thickness of the washer by 0.05 mm relates to a 10° rotation. By combining multiple washers, the rotation of the upper module can be adjusted to within 10° of the lower module. The washers can only be used on the straight threads of the lower cone rod adapter and not the tapered cone rod threads. Washers would prevent full thread engagement of the tapered threads.

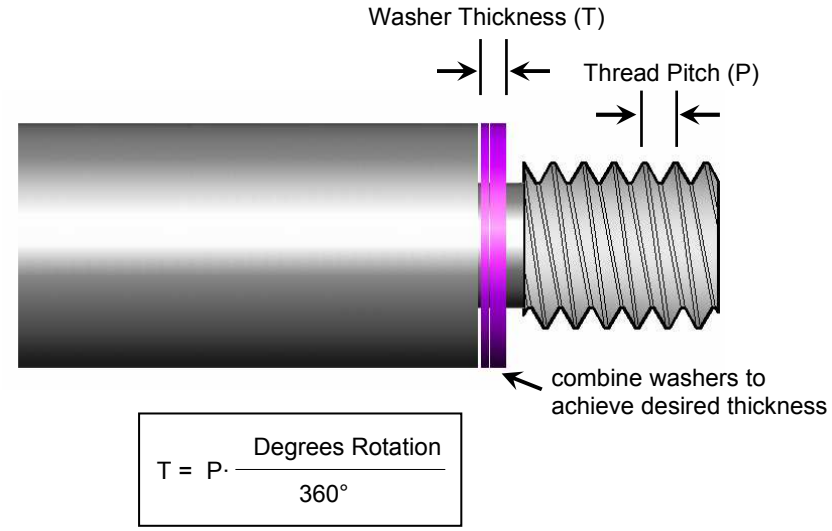

Figure 3.11 Relationship between thickness and rotation for the seismic module adjustment washers

In order to determine the proper combination of washers, the two modules are first assembled without geophones, cables, or washers. Once the modules are both attached to the rod that separates them, the geophone housing of the upper module is unthreaded until the modules are aligned. The necessary combination of washers is then chosen by slipping them into the resulting gap. After determining the required number of washers, the entire device is disassembled and then reassembled with the DMT blade, cables, geophones, and washers.

3.4.2.2.Electrical connections

The cable and connectors for the seismic components of the SDMT device are shown in Figure 3.12. Two 45 m lengths of coaxial cable, having a diameter of only 2.8 mm, were used to transmit the geophone signals to the surface. Crimp-style BNC connectors (shown in the lower right corner of Figure 3.12) were attached on the above-ground ends for connecting to the data acquisition system. To conserve space within the seismic modules, the downhole connectors between the geophones and the coaxial cables were made from small pins and sockets taken from a PC printer cable. The pins and sockets (shown in the upper left corner of Figure 3.12) were soldered to wires and covered with heat-shrink tubing to strengthen them. The wire leads with the sockets were soldered to the downhole ends of the coaxial cables, and the wire leads with the pins were soldered to the terminals of the geophones. With the pin and socket plugged together, the diameter of the connection is only slightly larger than the wire diameter alone.

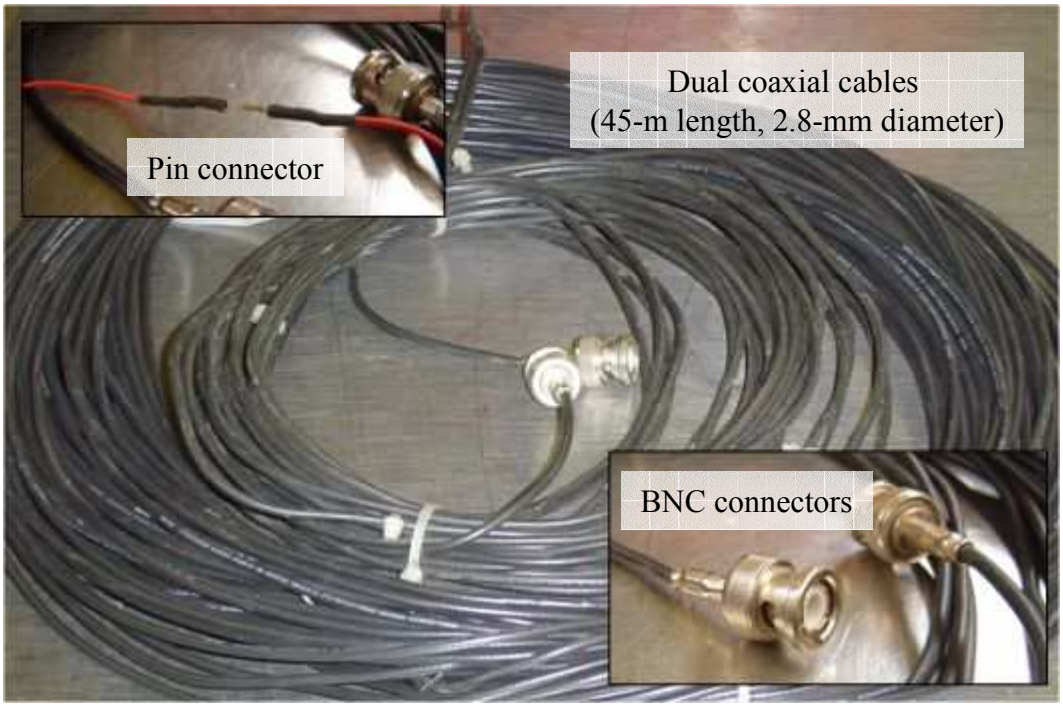

Figure 3.12 Coaxial cables and connectors of the SDMT device

The soldered terminals on the geophones were sprayed with a varnish designed to protect electronics in wet conditions. This water proofing method is moderately effective, but can not withstand several hours submerged below the water table. Field results suggested that more substantial water proofing is necessary.

In the field, the two coaxial cables and the plastic DMT tubing were tied to each other with small plastic cable ties. While threading the cables through the rods during set-up, the downhole ends of the coaxial cables were also taped securely to the device end of the dilatometer tubing. The tape protects the small connectors as the cable is pulled through the rods. Once the geophones were plugged into the coaxial cables during assembly, each pin/socket joint is wrapped in another layer of heat-shrink tubing to improve water resistance as well as prevent the connections from being accidentally pulled apart.

3.4.3. True-interval seismic probe

Later, based on experience gained from the SDMT device, a second true-interval prototype seismic probe was constructed to further investigate the frequent-interval shear wave velocity method. The device utilizes the upper geophone module and the coaxial cables from the seismic dilatometer, along with a new lower module, fitted with a dummy cone tip. A single 1 m cone rod is placed in between to separate the seismic modules. A schematic of the complete probe is shown in Figure 3.13.

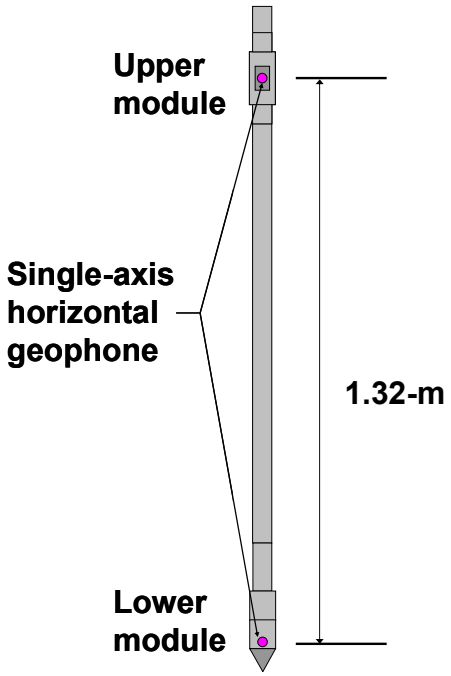

Figure 3.13 Drawing of the assembled true-interval seismic probe

The lower module consists of 3 components, the cone rod adapter, a geophone housing, and a 60° cone tip (Figure 3.14). The geophone housing is a steel disk with a hole cut in the center to fit the horizontal geophone. Rather than use the spray varnish for waterproofing, as with the seismic dilatometer, the lower geophone housing is filled with paraffin wax to protect the connections. To assemble the device, the geophone module is placed inside the tip, the cable connections are made between the geophone and the coaxial cable, and then the cone rod adapter is threaded onto the tip. A set screw through the side of the tip keeps the geophone housing from rotating during assembly, and indicates orientation of the geophone. As with the true-interval seismic dilatometer, the probe is first assembled without the geophones to determine the necessary combination of adjusting washers for aligning the modules. Then the probe is reassembled with the geophones and washers in place.

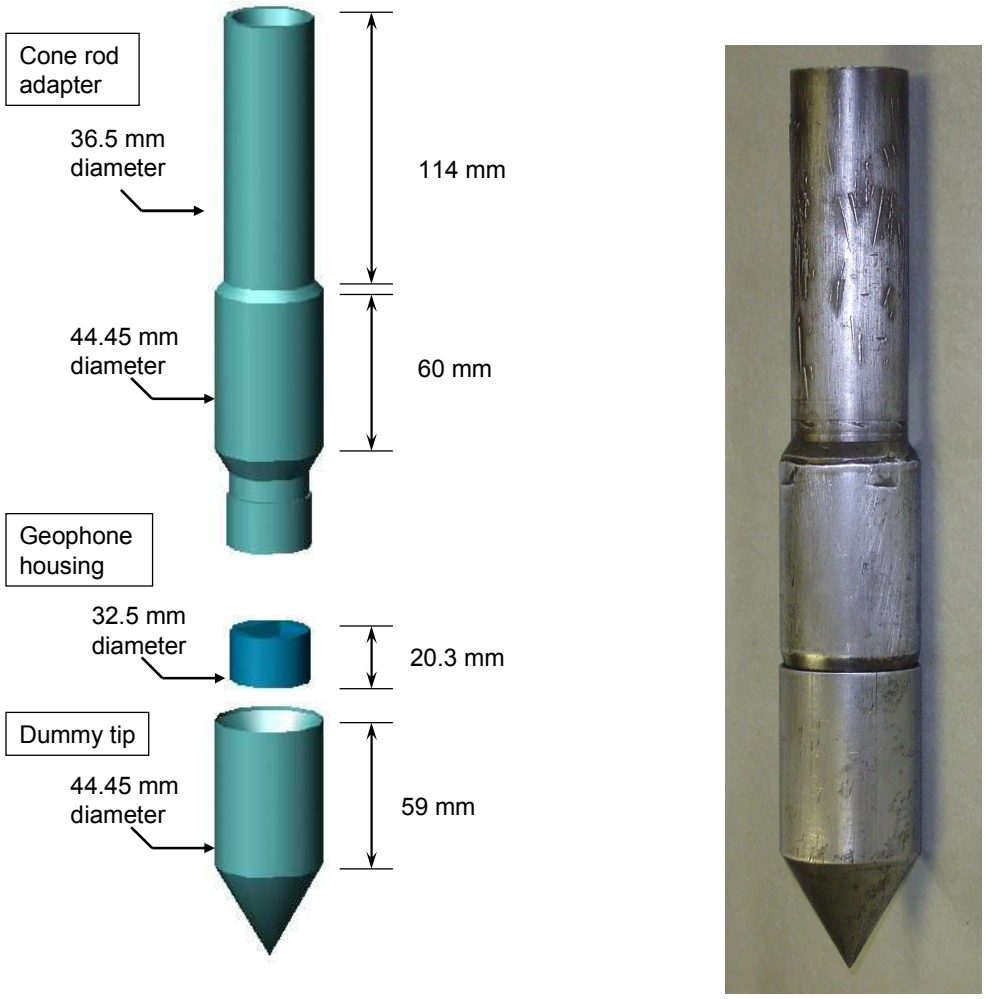

Figure 3.14 Details of the lower module of the true-interval seismic probe

3.4.4. Biaxial true-interval seismic probe

A third true-interval seismic probe was created to investigate the 2-dimensional aspects of the shear waves generated in a horizontal plane during testing with the frequent-interval and continuous-push seismic methods (Figure 3.15). The previously described devices only detected motion in a single horizontal axis. This third prototype device consists of 3 horizontal orthogonal pairs of geophones inserted into a single continuous rod.

Figure 3.15 Biaxial true-interval seismic probe with pairs of horizontal orthogonal geophones at three set elevations

A detailed depiction of the biaxial true-interval seismic probe is shown in Figure 3.16. The body of the probe is a single probe rod, which is used commercially for high quality discrete water sampling with a BAT (Bengt-Arne Torstensson) sampler. The BAT rod is 1 m in length, having a 25.4 mm inside diameter and a 44.5 mm outside diameter. The probe rod is fitted with a 60° cone tip and a cone rod adapter for connecting the probe to 37 mm cone rods. The horizontal pairs of geophones are mounted in separate modules that are connected together in a single removable unit. The geophone modules are connected together by lengths of threaded rod, which fix the spacing at 0.45 m between the centers of each module. The modules are aligned so that the upper geophones all point in the same direction, and the lower modules all point in the same direction and are orthogonal to the upper geophones. At the top of the probe is a short length of 18-pin cable fitted with a LEMO connector. The cable is held to the array of geophones by a watertight cord-grip. O-ring grooves have been cut into the outside perimeter of the cord-grip to prevent water from flowing down around the connection.

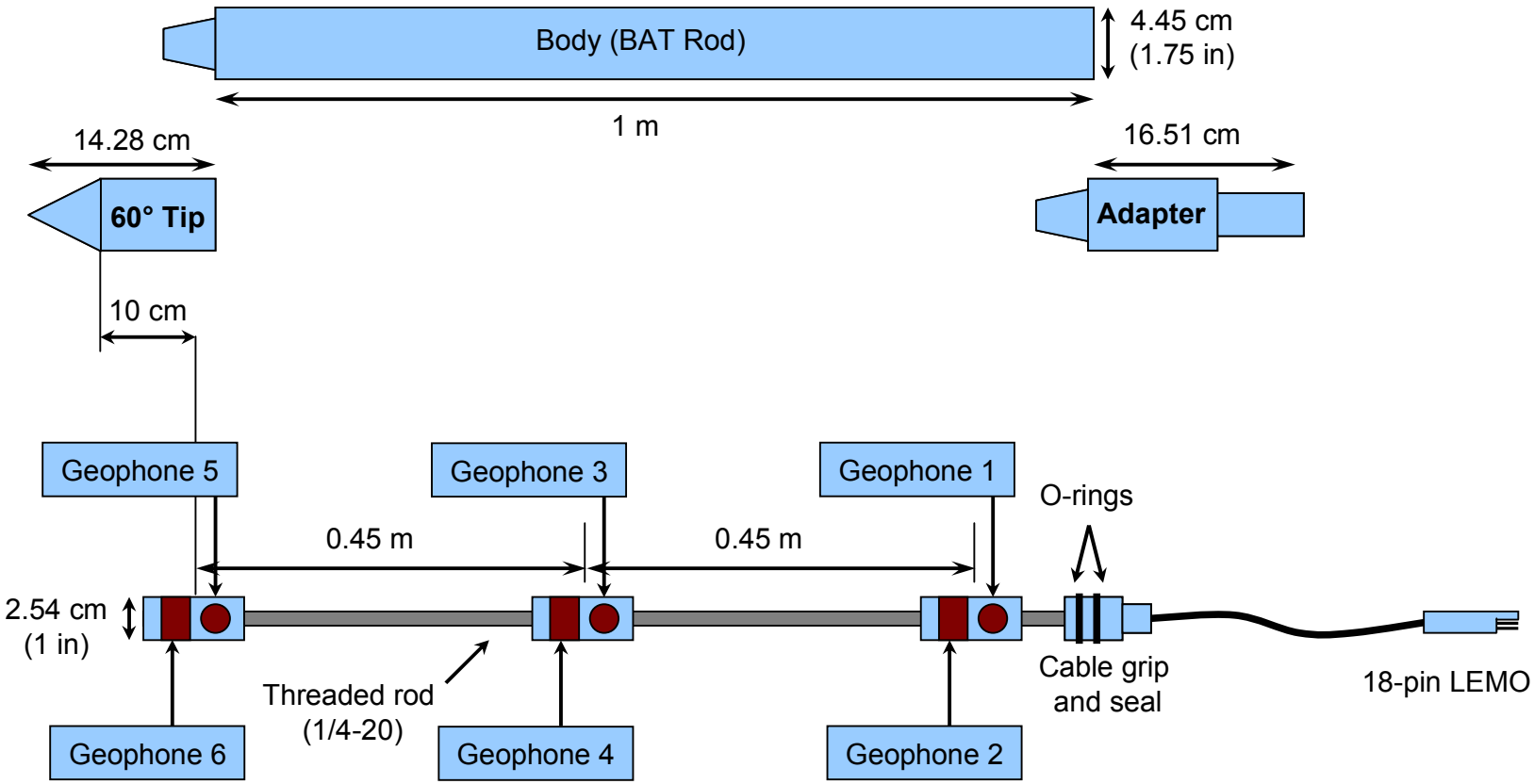

Figure 3.16 Illustration of the components of the true-interval seismic probe with biaxial geophone pairs at three levels

Each geophone module (Figure 3.17) is an aluminum cylinder with two holes drilled at right angles to fit the geophones. The ends of the modules are drilled and tapped to accept the threaded rods. Slots cut along the lengths of the modules allow the signal wires to pass up through the probe. The geophones are glued within their respective modules, but the modules are coupled to the body of the probe by friction. The inside of the BAT rod has been polished until smooth and the aluminum cylinders have been machined to fit snugly inside the rod.

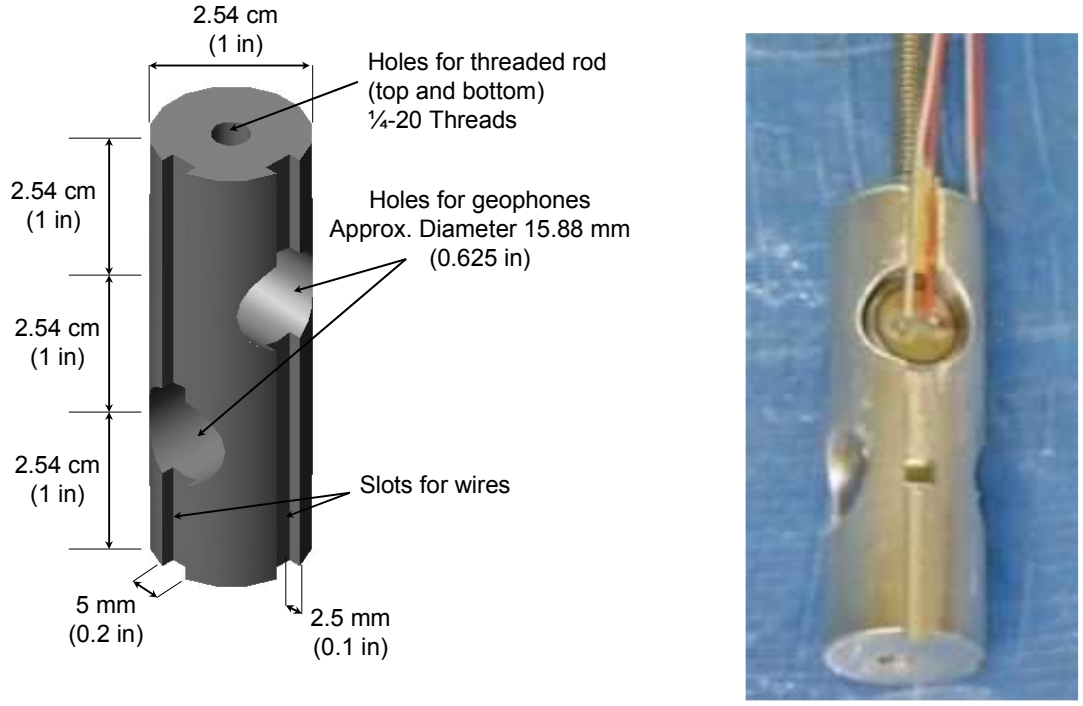

Figure 3.17 Detailed dimensions of a biaxial true-interval geophone module along with an image of the lowermost module with the geophones and wires in place

The cable for the biaxial true-interval seismic probe (Figure 3.18) is a cone cable manufactured by Vertek for their analog cone penetrometers. It is 45 m in length and contains 9 individually shielded pairs of wires. The LEMO connector at one end of the cable was removed and replaced with a female 25-pin SUB-D connector. The end that was removed is the short length of cable that is attached to directly to the geophones.

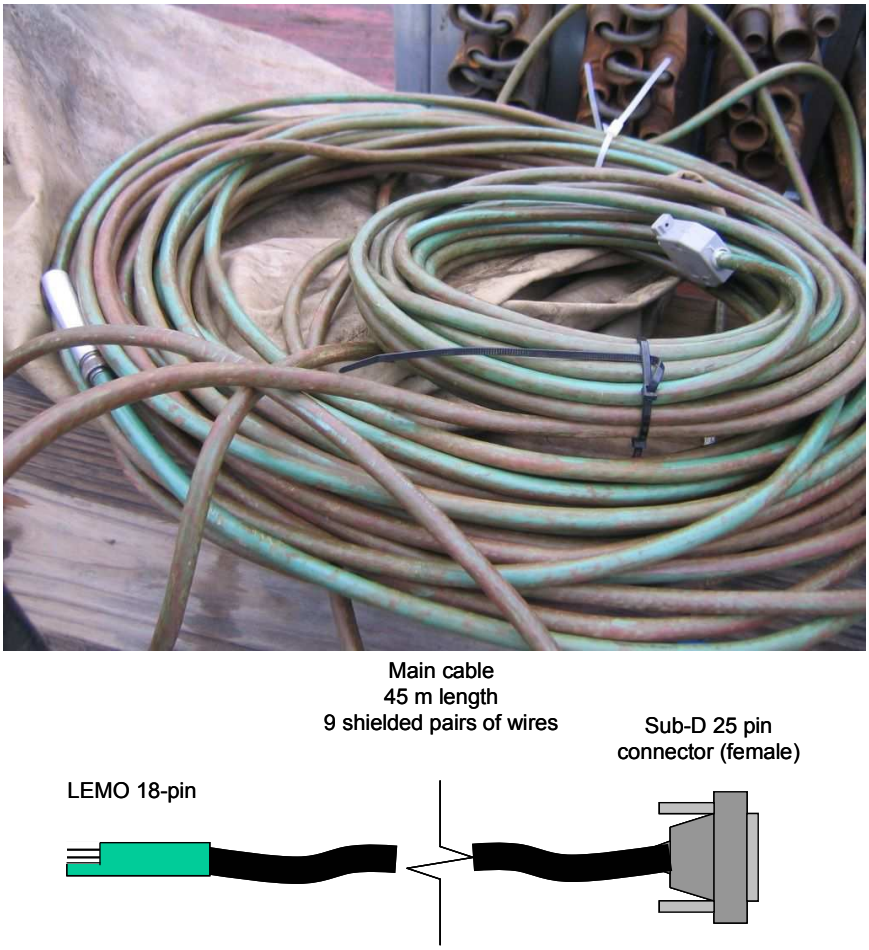

Figure 3.18 Image and diagram of the main cable for the biaxial true-interval seismic probe, 45 m long, 18-wires, an 18-pin Lemo connector (downhole) and a 25-pin Sub-D connector uphole

At the surface, the 18-pin cable is converted to BNC connectors with a breakout box (Figure 3.19). The box has a 25-pin male SUB-D connector for mating with the 25-pin female connector on the main cable. Each BNC connector is isolated from the others. The body of the box is connected to the shield of the main cable, which is connected to the body of the probe. A wing nut on the breakout box is used to ground the data acquisition hardware.

Figure 3.19 Breakout-box for biaxial true-interval seismic probe from 25-pin Sub-D connector to 6 isolated BNC connectors

3.5. Automated Seismic Source

For downhole seismic testing, the choice of seismic source has a significant effect on the in situ measurement of V_S, particularly the common pseudo-interval method. The wave propagation characteristics of the source can influence the procedure, testing depths, time and cost, as well as the quality of the results. For a continuous-push seismic system, a seismic source is required which generates consistent, clean, shear wave impulses at regular intervals during penetration, and more frequently than the 1.0 m or 1.5 m depth increments as with the conventional stationary receiver seismic methods.

Continuous repetition of source events is a daunting task for any manual source operator. There are commercial sources that have remote-control, but such sources are not designed for continuous automated repetition. As part of this research to develop a continuous-push seismic SCPTu system, a new portable seismic source has been developed to automate the generation of successive and consistent shear waves during penetration.

3.5.1. Generating and detecting shear waves

Seismic sources produce either pulses or continuous waves through impact, explosion, or vibration. Fernandez (2000) provides a thorough review of seismic sources for several types of geophysical tests, but not all sources are appropriate for measuring downhole shear wave velocity. Regardless of the type of source, they produce complex combinations of compression waves (P-waves), shear waves (S-waves), and surface waves (R-waves). However, to analyze V_S, the S-waves must be clearly identifiable within the complex wave-field so the shear wave travel times can be observed. Identification of the shear wave energy within the recorded signal is dependent on the amplitude and the clarity of the shear waves. Large powerful seismic sources are good for transmitting seismic energy deep into the ground with large amplitudes, minimizing the interference from ambient noise. For a smaller, lower energy, portable source, it is necessary to consider the characteristics of the source and the generated waves in order to maximize the potential of the source.

Significant effort is spent trying to isolate the shear wave components from complex and noisy recordings, but with proper procedures, it is possible to clarify the recorded signals at the time of their measurement and maximize the measurable amplitudes, reducing the difficulty of analysis.

When examining the characteristics of a seismic source, the shear waves are often subdivided into two types according to their direction of polarization, or particle motion. For shear waves, the particle motion is perpendicular to the propagation direction. If the particle motion has a vertical component, the S-wave is referred to as an SV-wave, or vertically-polarized shear wave. If the particle motion is purely horizontal, the S-wave is referred to as an SH-wave, or horizontally-polarized shear wave. Seismic sensors, such as the geophones utilized in this research program, respond to particle motion only in a single direction, so this directional distinction is important when considering sensor position and alignment. For example, a horizontally-oriented geophone will not capture

vertical motion. A horizontal geophone will capture horizontal motion as well as the horizontal component of any inclined particle motion.

The polarization direction of a shear wave also influences the propagation behavior at boundaries. When a wave intersects a boundary, some of the energy is transmitted through to the new material and some energy is reflected back away from the boundary. At the same time, as shown in Figure 3.20, if the incident wave is purely compression, some of the reflected and transmitted energy will be converted to shear. The same happens for shear waves. An incident shear wave is reflected and transmitted with some of the energy converted to compression. This conversion from one form to another is referred to as mode conversion. However, if the particle motion is parallel to the boundary intersected, mode conversion does not occur. Therefore, if the subsurface layering is horizontal, no mode conversion will occur with a horizontally-polarized shear wave. The lack of mode conversion can help to simplify the wave field, making the shear wave impulse signal easier to identify.

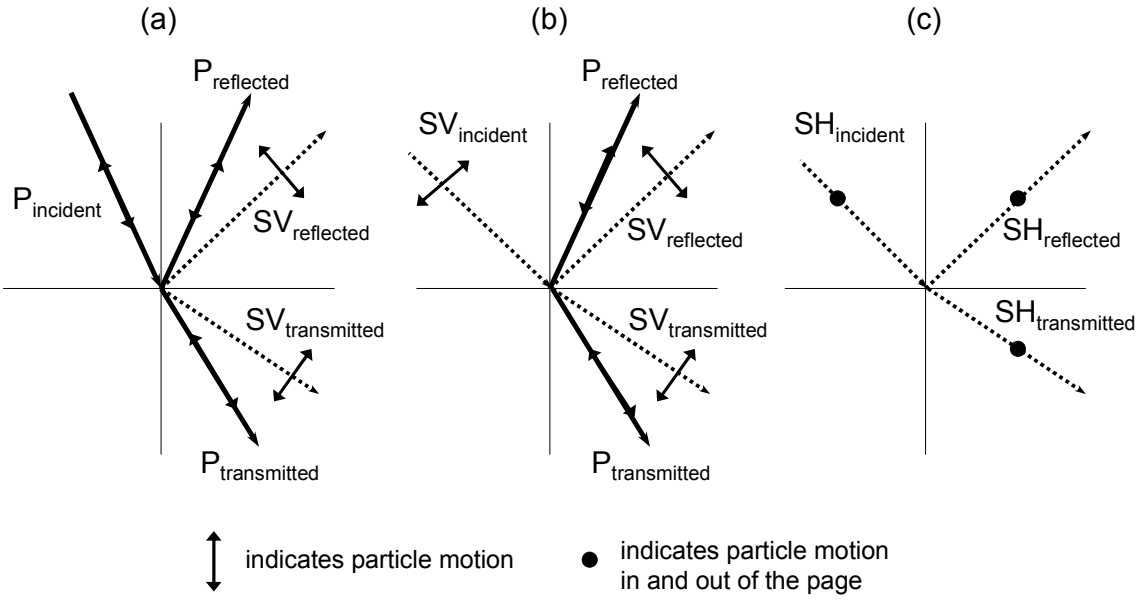

Figure 3.20 Mode conversion of P, SV, and SH incident waves upon reflection and refraction at a boundary (Richart et al., 1970)

Figure 3.21 shows the component radiation patterns of body waves for idealized horizontal and vertical point sources. For the vertical point source, no SH waves are produced, which may seem to simplify the wave-field, but the P-wave and SV-wave fields overlap, which may actually complicate interpretations of the SV-waves. Also, the optimum sensor alignment and position is unclear because the resultant direction of the SV particle motion is inclined somewhere between vertical and horizontal. The horizontal point source produces P-, SV-, and SH-waves with relatively little overlap of the SH-waves with the P- and SV-wave-fields. Additionally, the direction of the SH-wave particle motion is completely horizontal, so horizontal receivers deployed directly below the source, such as with the SCPTu, will be able to detect the maximum amplitude of the SH wave motion, free of P and SV interference.

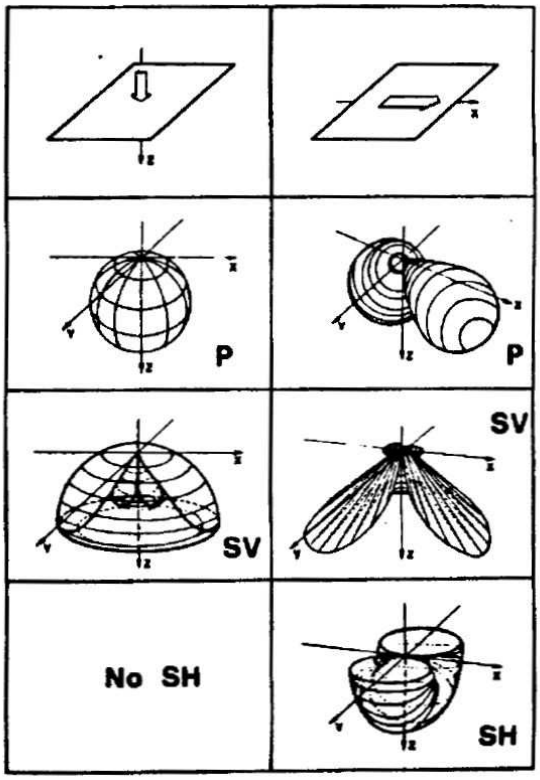

Figure 3.21 Radiation patterns for compression (P), vertically-polarized shear (SV), and horizontally-polarized shear (SH) waves for a vertical point source (left) and a horizontal point source (Kahler and Meissner, 1983)

Incorrect source-receiver alignment is a common reason for poor signal quality and low amplitude. It was demonstrated in Figure 3.21 that the position of the receivers within the wave-field is important for detecting horizontally-polarized shear waves. The alignment of the receivers in the direction of particle motion is also important. To minimize the influence from P and SV waves and maximize the amplitudes of the recorded signals, the seismic receivers in the cone should be parallel to the horizontal motion of the source. Additionally, the cone should be centered on the source, such that a line drawn along the ground surface from the rods to the center of the source is perpendicular to the axis of the source. In Figure 3.22, correct and incorrect source-receiver alignments are shown for sources placed under the leveling legs of the testing vehicle.

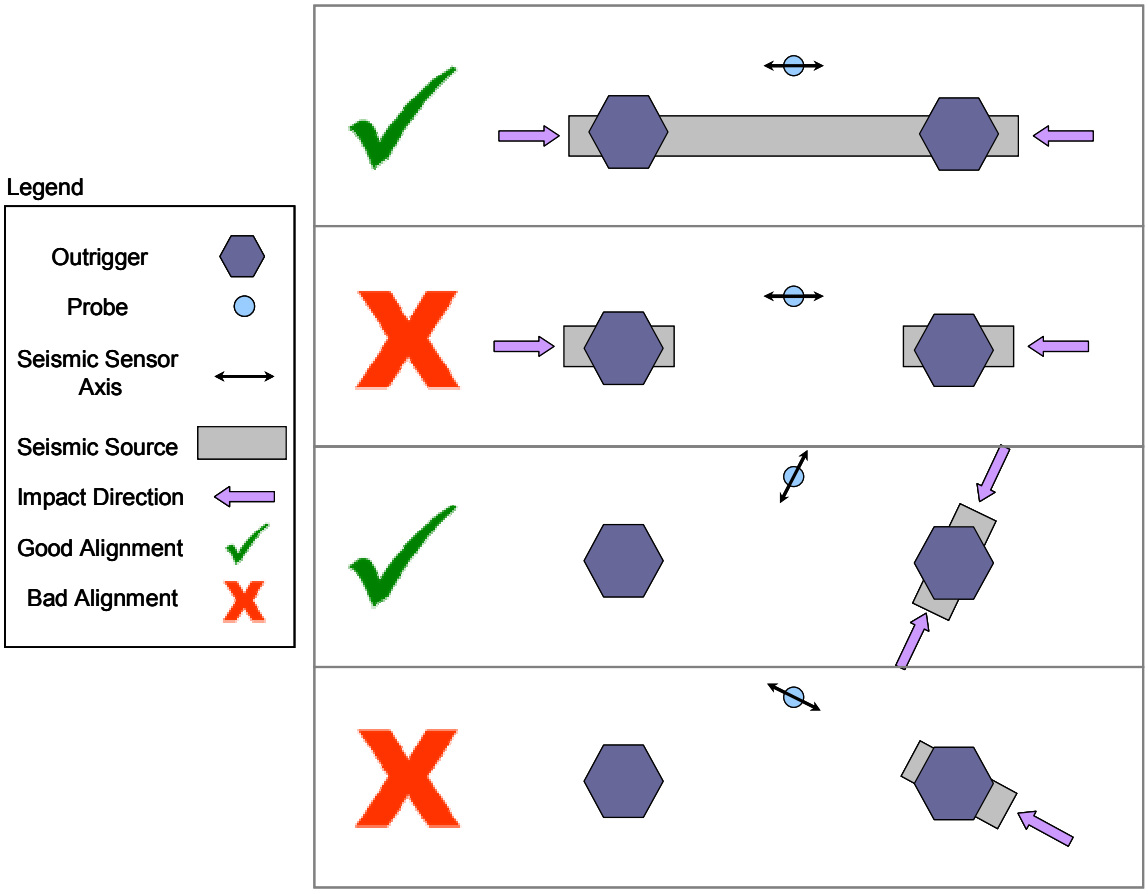

Figure 3.22 Proper and improper alignment of the seismic source relative to the orientation of the seismic receivers

The coupling between the source and the ground surface is another critical factor affecting the source performance. For downhole testing to be successful, the energy of the source impact must be transmitted from the seismic source into the subsurface. If the source slips along the surface because of inadequate normal force, the energy is not transmitted and the amplitude is lost. Similarly, if the energy level of the source is so high that the supporting surface is permanently deformed, again, the energy is not effectively transmitted.

The quality of the contact between the source and the ground surface has an effect on the frequency content of the generated waves as well as the amplitude. A soft

deformable contact, or a slipping contact, eliminates any high frequencies generated by the source. To improve the transfer of energy from the source into the ground, and reduce energy losses into the leveling pad of the testing vehicle, Aerias et al. (2004) placed a roller system between the top of the source and the leveling pad (Figure 3.23) so that all of the source energy was transferred to the soil and essentially none into the cone truck. This is an attractive concept for small, low power, portable sources for which low amplitudes are problematic. However, stability issues should be considered when creating a frictionless surface under the leveling pad of the testing vehicle.

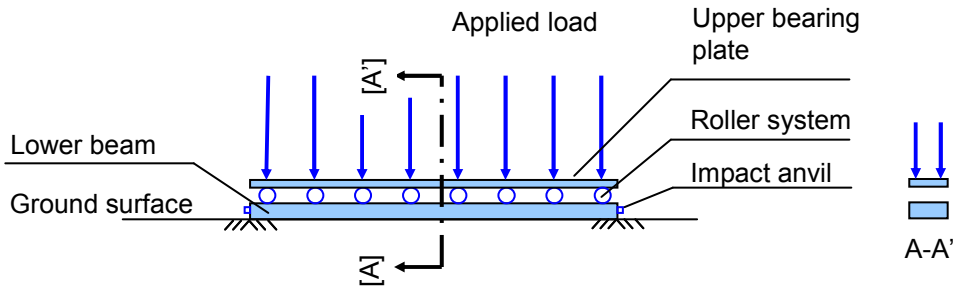

Figure 3.23 Concept of a mechanism for de-coupling a seismic source from the horizontal resistance of the testing vehicle (after Areias et al., 2004)

3.5.2. Review of seismic sources

Several types of horizontal impact shear wave sources are available for generating wavelets for downhole shear wave velocity testing. Because it is inexpensive and reliable, the most simplistic and common shear wave source is a wooden or steel beam coupled to the ground by the weight of the testing vehicle or support vehicle, which is struck on end with a sledgehammer to produce a horizontally-polarized vertically propagating shear wave pulse (left half of Figure 3.24). Variations of the sledgehammer source were developed with sliding weights to improve the consistency of the delivered energy (right half of Figure 3.24).

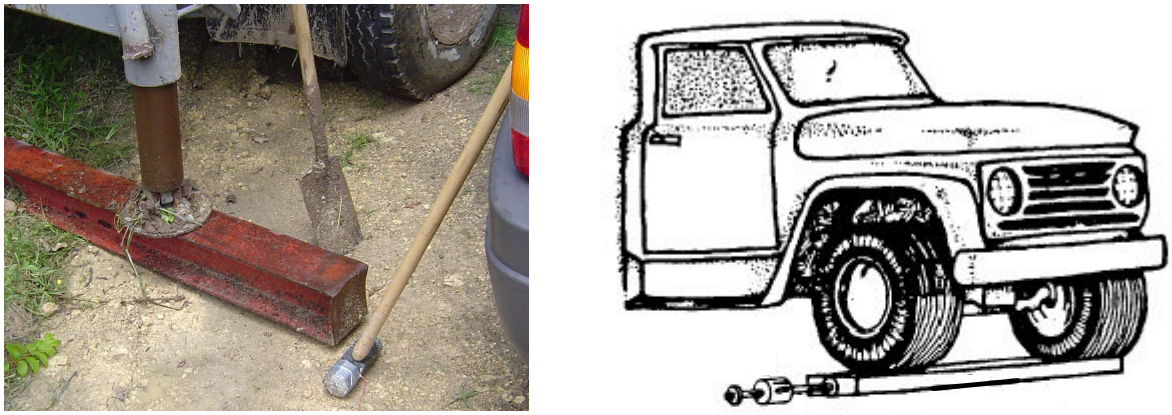

Figure 3.24 Image of a sledgehammer seismic source with the steel beam coupled to the ground by the leveling pad of a drill rig (left) and a diagram of a similar source with a sliding hammer coupled to the ground by the wheels of a vehicle (after Elzeftawy and Cartwright, 1981) (right)

In order to make the sledgehammer source more consistent with regard to amplitude and alignment, Robertson et al. (1986) modified a cone truck at the University of British Columbia to accommodate a pivot for the sledgehammer, allowing it to be used as a pendulum. The pendulum also helped standardize the energy imparted to the source keeping the waveforms consistent so that signals from consecutive hammer blows could be compared. A similar, yet portable version of the pendulum source, shown in Figure 3.25, was used for part of this research. The beam consists of a welded steel tube with a textured bottom, and welded end caps. A vertical hammer support is attached to one end of the beam. A 4.5 kg sledgehammer hangs from the support on a pin drilled through the handle of the hammer.

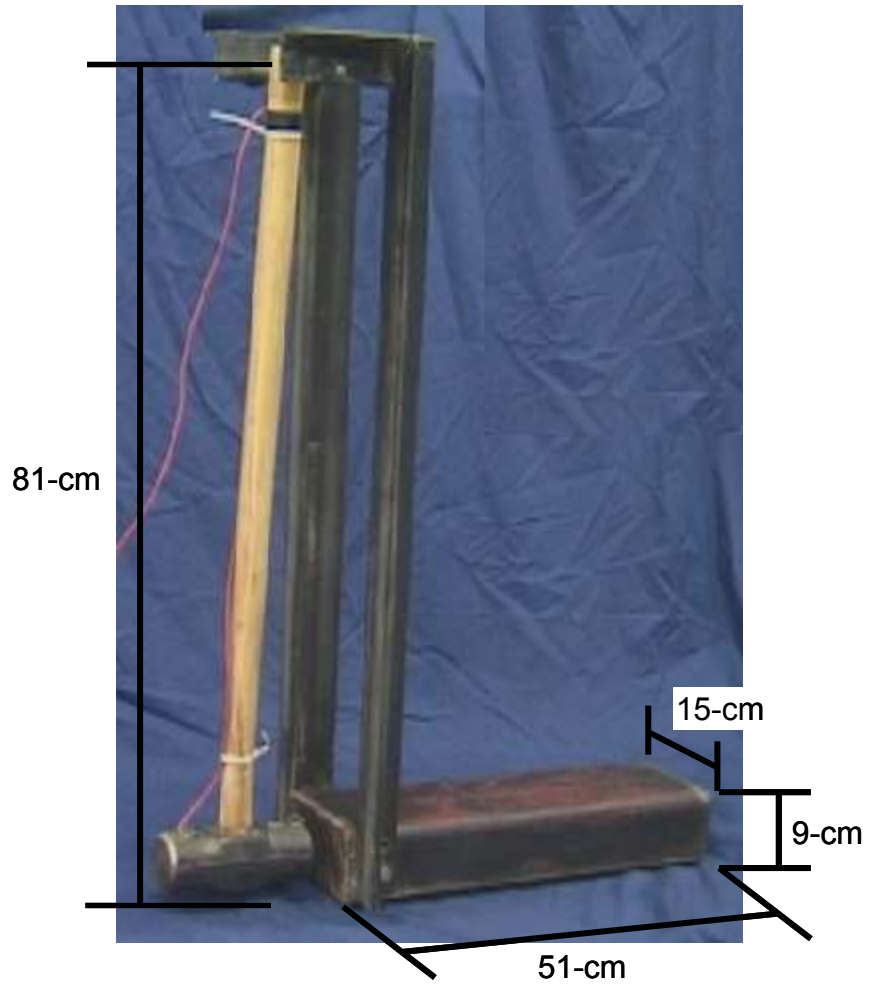

Figure 3.25 A portable pendulum seismic source consisting of a sledgehammer and a steel beam

In order to increase the source energy and increase the wave penetration depth, as well as reduce the operator-induced variability, researchers have developed sources utilizing high energy methods for accelerating and impacting masses, such as explosives, hydraulics, pneumatics, and electromagnetism. Shima and Ohta (1967) describe a gun-like source with an explosive charge used to accelerate a metal slug through a steel tube attached to the beam (Figure 3.26). Schwarz and Conwell (1974) developed a powerful electromagnetic source for generating shear waves on the sea floor (Figure 3.27), which consisted of two opposing electric solenoids that could send a 77 kg iron slug from one end to the other. A reversible pneumatic device was developed by Liu et al. (1988), in

which a pneumatic cylinder accelerated a mass, into an anvil, or striking plate (Figure 3.28). The modern commercial source mounted to the leveling jacks of the cone truck shown in Figure 3.29, is based on a hydraulic cylinder striking a plate integrated with the front leveling jacks of the vehicle.

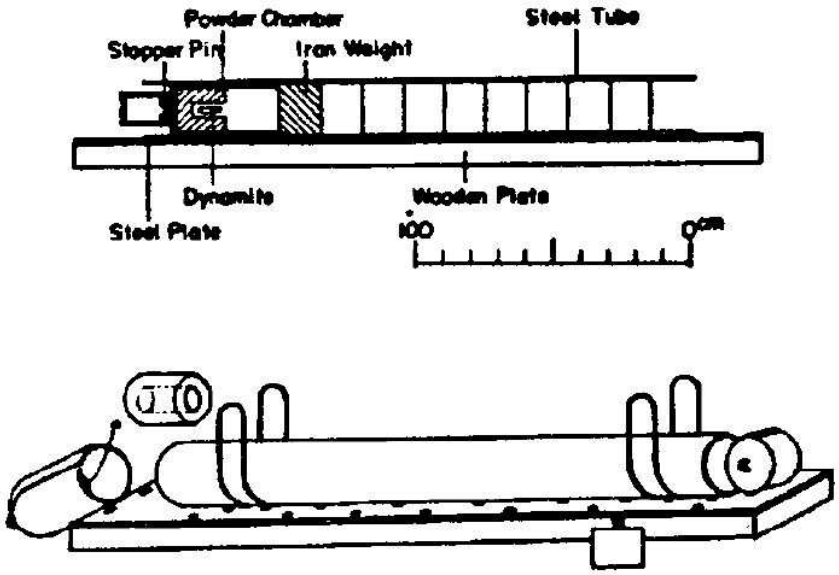

Figure 3.26 Diagram of an explosive- or gun-type seismic source in which an explosive charge is used to horizontally accelerate an iron slug into the end of a length of metal tube (Shima and Ohta, 1967)

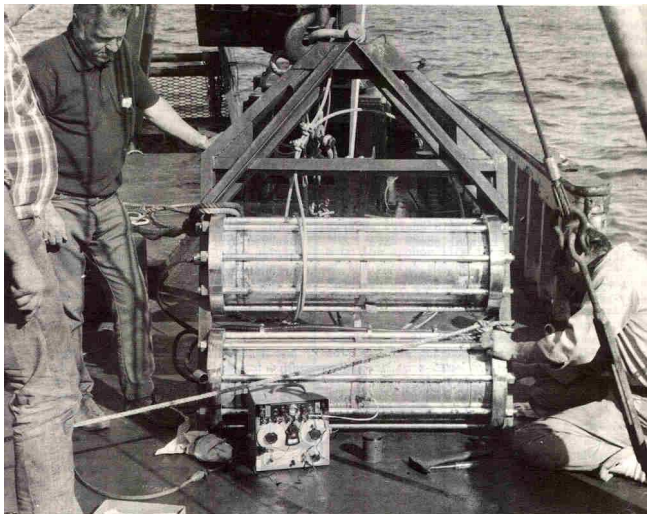

Figure 3.27 Image of an electromagnetic seismic source for undersea applications and a diagram of the mechanism (Schwarz and Conwell, 1974)

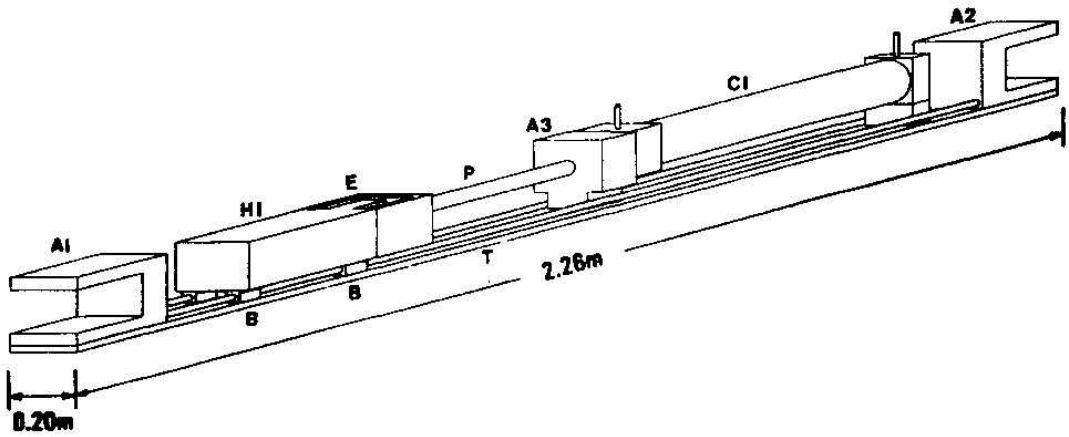

Figure 3.28 Diagram of a double-acting pneumatic seismic source (Liu et al., 1997)

Figure 3.29 A modern cone truck with an integrated, remotely controlled hydraulic seismic source

The means used to provide the power should not affect the resulting source signal, so the choice of electric, hydraulic, or pneumatic, is an issue of constructability and implementation. For example, an electromagnetic source may be more desirable for offshore applications because it is easier to transmit electrical power over large distances than hydraulic or pneumatic power. Another example would be to choose a hydraulically powered source for use on a cone truck where all of the other systems are powered by hydraulics.

High-powered seismic sources can be expensive and are usually too large to be considered portable. Large commercial sources, like the hydraulic source permanently mounted to the underside of the cone truck in Figure 3.29, are capable of generating waves that propagate to depths more than 100 m, but they are expensive (more than $18,000 for this source). The size and weight are not of concern when the source is integrated into the structure of a massive cone truck, but they are significant when portability is required.

The performance of any of the commercial sources is an improvement over the manual sledgehammer source, in that they are operator independent and there is automation and repeatability. However, none of them were designed to meet the requirements for a continuous-push seismic system as they cannot keep up with the rate of hammer strikes required for the frequent-interval method. The popular hydraulic seismic source has a surge tank that takes several seconds to pressurize and while the pump is charging the surge tank, penetration must be halted. A small source, which can operate continually, is lightweight, portable, and low cost, is a necessity for small cone trucks, drill rigs, and portable CPT devices.

Several of the shear wave sources are capable of generating reversible polarity shear waves. These sources generate a shear wave with a left-facing hammer strike and another with a right-facing hammer strike. The reason is that the compression wave polarity would remain unchanged, while the shear wave will have opposite polarity which can be used to identify the shear wave arrival within a complex wave field. Figure 3.30 illustrates the concept of the left-strike/right-strike testing method, which requires at least two strikes to be recorded at each test depth.

The analysis technique based on this method, known as the first cross-over method (Hoar and Stokoe, 1978), is quite common because of its simplistic nature. Cross-correlation is well-known to be a more robust analysis method which requires only a single strike to be recorded at each test depth (Campanella, 1994), but the method has been too inaccessible to practitioners because of a lack of software. A cross-correlation shear wave processing software package (ShearPro), developed at Georgia Tech to make advanced analysis available for practitioners (Liao, 2005), can be downloaded for free from http://geosystems.ce.gatech.edu/Faculty/Mayne/papers/index.html, eliminating the need to record both left-strikes and right-strikes. A review of various post-processing methods can be found in Sanchez-Salinero et al. (1986) and more recently in Liao (2005).

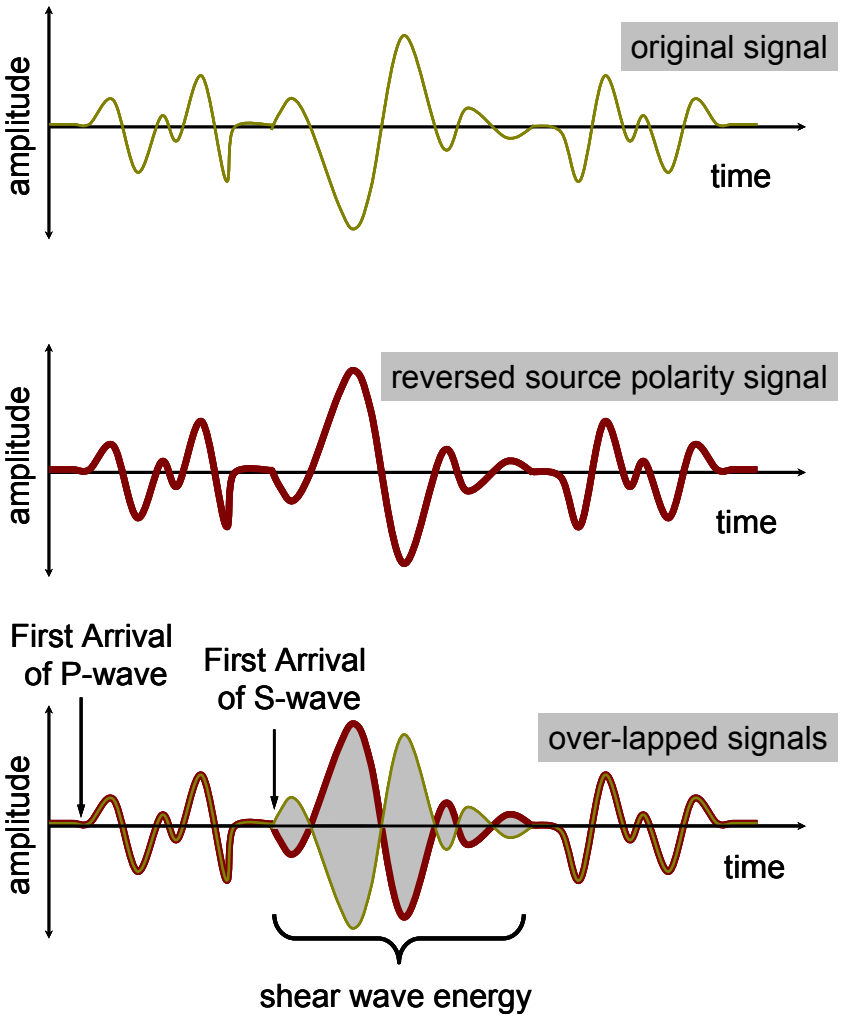

Figure 3.30 Utilization of reversed polarity shear waves to identify arrival of the shear wave component within a signal

3.5.3. Georgia Tech seismic sources

In order to encourage the collection of seismic measurements during all direct-push site characterization, the seismic source requirements for the continuous-push system included that the unit be automated, reliable, portable, low cost to build, and be able to generate consistently repeatable shear waves at regular intervals. A previous effort provided an early AutoSeis design with paired left- and right-strikes (Casey, 2000). Reversible polarity capability was not a requirement for this unit, given that analysis methods are available which require only a single source signal at each test depth. For

practicality, the design depth for transmitting detectable waves was set at 30 m. That depth is more than adequate for determining liquefaction susceptibility, and meets the depth requirement for determining site-specific earthquake site class required by international building codes. The seismic source designs progressed through several versions, until the desirable performance was obtained.

3.5.3.1.Electromagnetic AutoSeis

AutoSeis was the original portable, remote-controlled seismic source developed at Georgia Tech by Casey (2000) (Figure 3.31). It was a double-acting electromagnetic source, similar to the source described earlier in Figure 3.27 developed by Schwarz and Conwell (1974), but on a smaller scale. The device contained two, 12 V electric solenoids that accelerated a 2.3 kg mass horizontally into an impact plate. The source, controlled from the deck of the truck, was capable of generating reversible polarity shear waves, known as left-strikes and right-strikes. The left- and right-strike feature was considered desirable at the time, but later deemed unnecessary as computer advances led to changes in analysis methods.

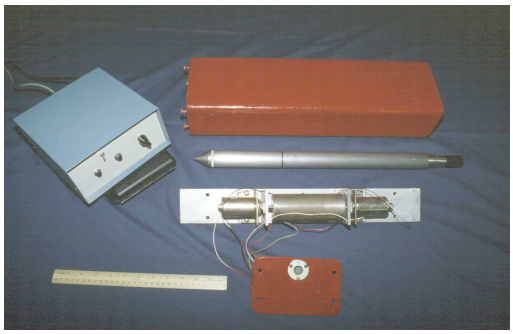

Figure 3.31 Components of the first Georgia Tech AutoSeis, a portable electromagnetic source (Casey and Mayne, 2002)

The impact energy of the 12 V solenoids was small, but at one particular test site, the signals were detectable to a depth of 21 m, as seen in Figure 3.32 showing a pasteup

plot of signals collected by Casey (2000) at a test site near Memphis, TN. Below this depth, the signal amplitude was generally too low to be useful for analysis. For a single strike per test depth, a greater energy would be required to generate larger amplitude signals, which could propagate deeper. However, the solenoids could not accelerate the mass fast enough to deliver the necessary energy. More powerful solenoids were required to increase acceleration, but upgrading the power requirements would have reduced the portability. Stacking multiple duplicate signals together, a technique for magnifying weak signals while canceling noise components can be used to increase the source effectiveness for conventional testing methods utilizing stationary receivers. However, for continuous-push soundings, signal stacking is not possible because the receiver position is not constant.

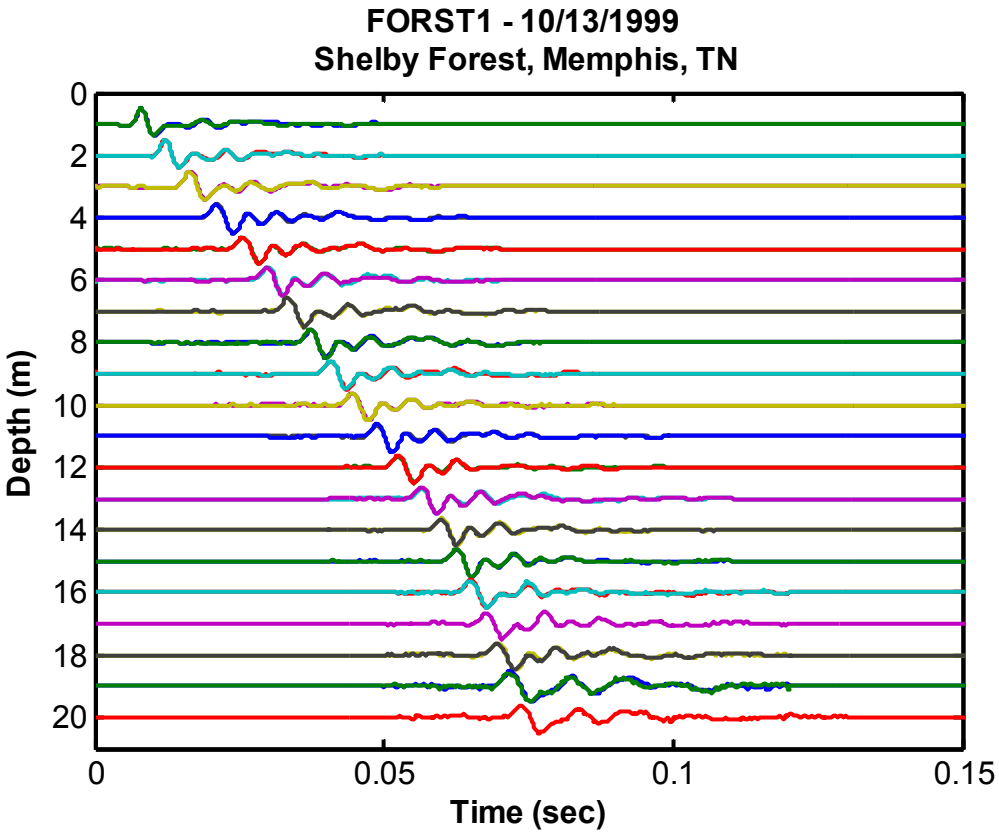

Figure 3.32 Pasteup of seismic signals measured with the Georgia Tech electromagnetic AutoSeis

3.5.3.2.Pneumatic AutoSeis

The second generation remote-controlled source, AutoSeis II, was a pneumatic device (Figure 3.33) designed to improve upon the energy level over the electromagnetic version. The mass was connected to a pneumatic cylinder, which was connected to an adjacent small surge tank by an electrically operated valve. An air compressor or compressed air cylinder was used to charge the tank. To activate the source, the operator remotely opened the valve, allowing the air from the surge tank to flow into the cylinder. The cylinder horizontally accelerated the mass into the steel striking plate.

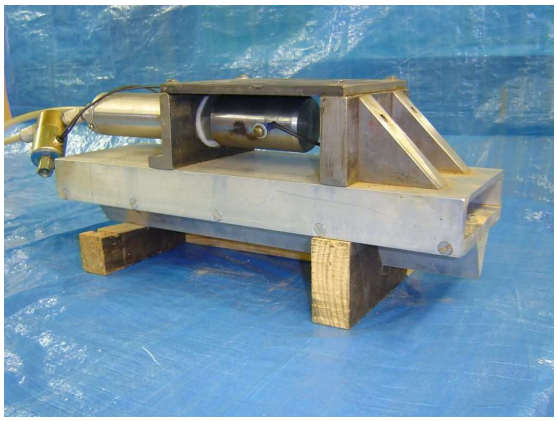

Figure 3.33 Image of the single-acting pneumatic Georgia Tech AutoSeis

The pneumatic AutoSeis II was able to deliver more power than the electric solenoids of the electromagnetic AutoSeis. Increasing the energy of the impact only required increasing the pressure in the surge tank. The mass of the hammer remained unchanged at 2.3 kg. Although the amplitude of the pneumatic source signal was higher than that of the electromagnetic signal, the pneumatic source signal was unfortunately of lower quality. Figure 3.34 is a pasteup plot of signals recorded at a sewage treatment plant near Memphis, TN, showing well-defined impact peaks.

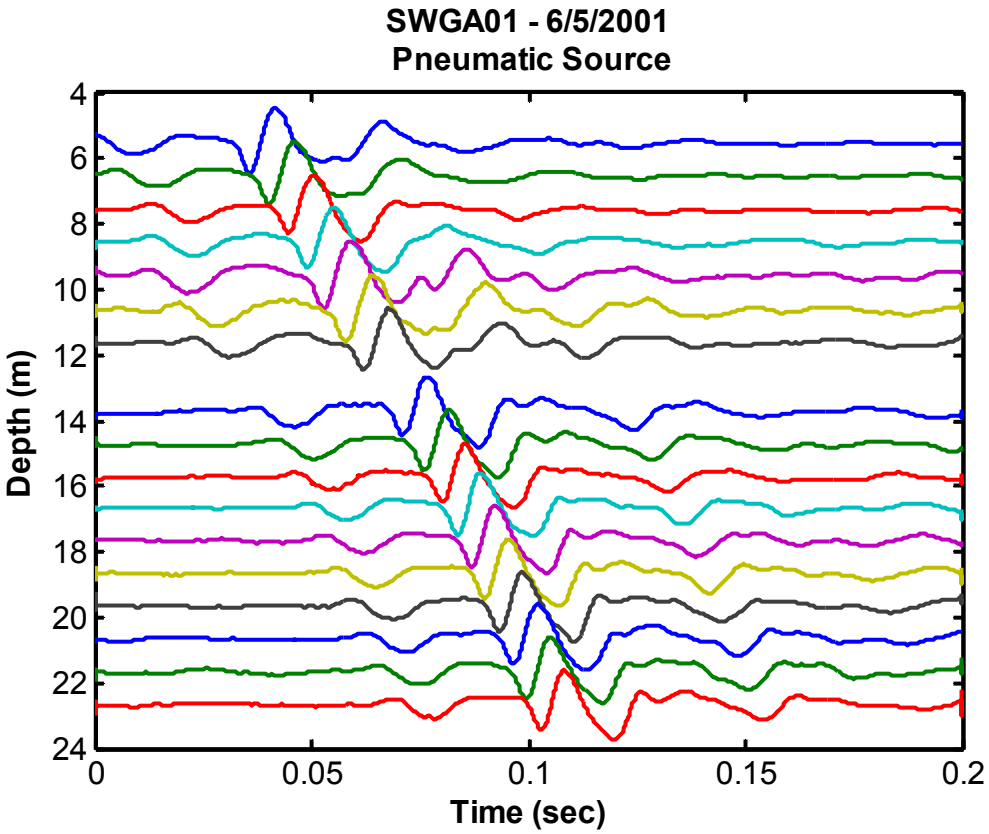

Figure 3.34 Pasteup of seismic signals recorded with the pneumatic AutoSeis

The signal generated by the pneumatic AutoSeis is free from noise and interference from other wave modes, but there is a low frequency dip preceding each impact peak. The timing of the dip is inconsistent with respect to the impact peaks, which could interfere with comparisons of signals from different depths.

Figure 3.35 highlights the reaction wave energy by superimposing signals generated by the AutoSeis with signals generated by the pendulum source at the same depths. The characteristics of the signals resulting from the different sources are very similar except that the pendulum source signal is flat all the way leading up to the peak, while the pneumatic signals show a dip before the impact. The difference between the source signals is due to the reaction force generated by the horizontal acceleration of the AutoSeis' hammer. The same finding was described by Liu et al. (1996) for their

pneumatic seismic source shown in Figure 3.28. The proposed solution was to allow the air to flow into the cylinder more slowly, reducing the shock created when the hammer is initially accelerated. This has the affect of reducing the frequency bandwidth of the reaction wave, making it less visible, but does not eliminate it. For deep soundings, a small portable source would still be affected. The electromagnetic AutoSeis was not significantly affected by the reaction forces because the acceleration of the mass was low, and as a result the penetration depth was also low.

The problem with the pneumatic source reaction wave is that prior to the impact of the mass against the impact plate, low frequency waves were already being transmitted through the soil as a reaction to accelerating the hammer mass. The frequency of the reaction wave is too low to be useful for comparing signals. Also, the consistency of the source signal suffers because the timing of the reaction signal is not as repeatable as the impact signal. It was found that adding more pressure in order to increase the amplitude, increased the amplitude of the impact signal, but also increased the amplitude of the reaction signal. This same behavior is not apparent in large truck-mounted hydraulic sources with the source rigidly fixed to the truck.

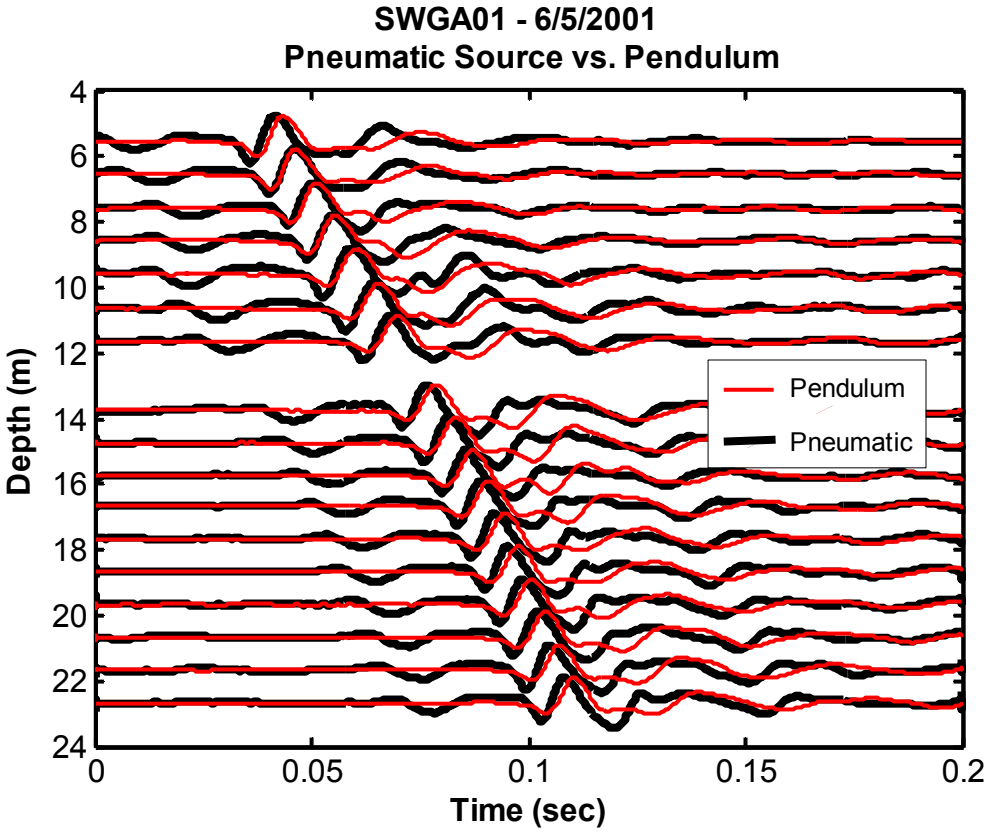

Figure 3.35 Comparison pasteup of seismic signals recorded with the pneumatic AutoSeis and the pendulum seismic source at the same depths, highlighting the low frequency reaction wave present prior to impact in the pneumatic signals

3.5.3.3.RotoSeis

Though commercial sources based on horizontal acceleration of a mass into an impact plate perform well in standard applications, the portable AutoSeis sources based on this concept were found to lack the energy needed to reach the desired 30 m depth and the reaction forces resulted in undesirable signal characteristics. Ultimately, a new type of source was developed to generate quality signals down to 30 m depths, while remaining portable.

A new source concept was developed and given the name *RotoSeis*. The source can deliver repeated impulses as fast as 1 strike every 4 seconds, which corresponds to a measurement interval comparable to that of the cone penetrometer readings, q_T, f_S, and

u_2. A United States patent application for RotoSeis is currently on file with the United States Patent Office, submitted on September 9, 2005 (Application Number – 20060118353). Georgia Tech has licensed the rights to Finite Designs, Inc. in Ball Ground, GA to produce and sell RotoSeis sources to the in-situ testing community.

In order to produce clear impulse signals while increasing the amplitude at the same time, a rotational motion for the hammer was implemented. The solution was to replace the horizontal acceleration of the mass with a rotational motion, in which, the reaction force is directed vertically rather than horizontally. The purpose was to change the particle motion direction of the undesirable reaction waves, to make them less detectable. Unwanted particle motions caused by reacting forces would be in the vertical direction and would not be detectable with horizontal sensors in a seismic probe. The source based on this concept, has been given the name RotoSeis. A simplified diagram of the RotoSeis is presented in Figure 3.36.

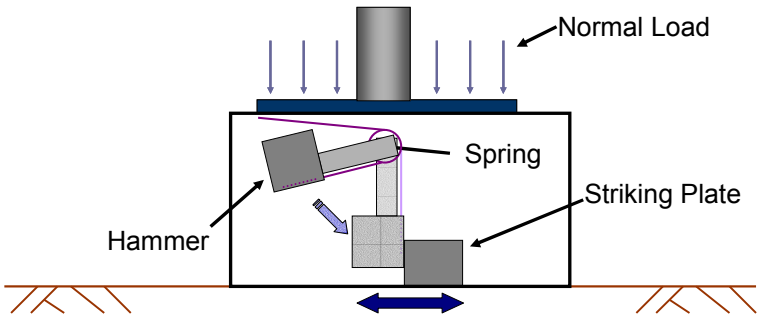

Figure 3.36 Cross-sectional diagram of the RotoSeis source concept illustrating the spring driven rotational hammer motion within a device coupled to the ground under the leveling pad of a cone truck

The RotoSeis source consists of a mass (hammer) rotating in a plane perpendicular to the ground surface that transfers its energy to the ground surface in the direction parallel to the surface when the mass impacts against a thick steel plate, or anvil, fixed to the base of the source. Torsion springs on each side of the hammer help to accelerate the mass in an angular mode towards the anvil. An electric motor is used to wind the hammer up each time to a point where it is released and driven by the springs into the anvil. A horizontally-polarized vertically propagating shear wave is generated by the impact. The reaction forces of the springs accelerating the mass are directed against the body of the source in the vertical direction.

Gears connected to the electric motor and to the hammer are used to raise and release the hammer. The process is illustrated in Figure 3.37. A large diameter gear is attached to the hammer and a small diameter gear to the motor. The small drive gear engages the hammer-gear, raising the hammer. Missing teeth on the motor's small gear cause the hammer to slip free after a predefined amount of rotation. When the hammer is free of the small gear, springs drive the hammer into the anvil, and the process repeats as long as the motor is spinning. The rate of repetition is controlled by changing the motor speed with a speed controller device. Electricity in the field is available from the electrical system of the cone truck. A DC/AC inverter connected to the cigarette lighter outlet provides 110 VAC. Alternatively, power can be supplied by a deep-cycle marine battery or a portable generator. The motor operates on DC power, but the speed controller device converts 110 VAC to 90 V DC to drive the motor.

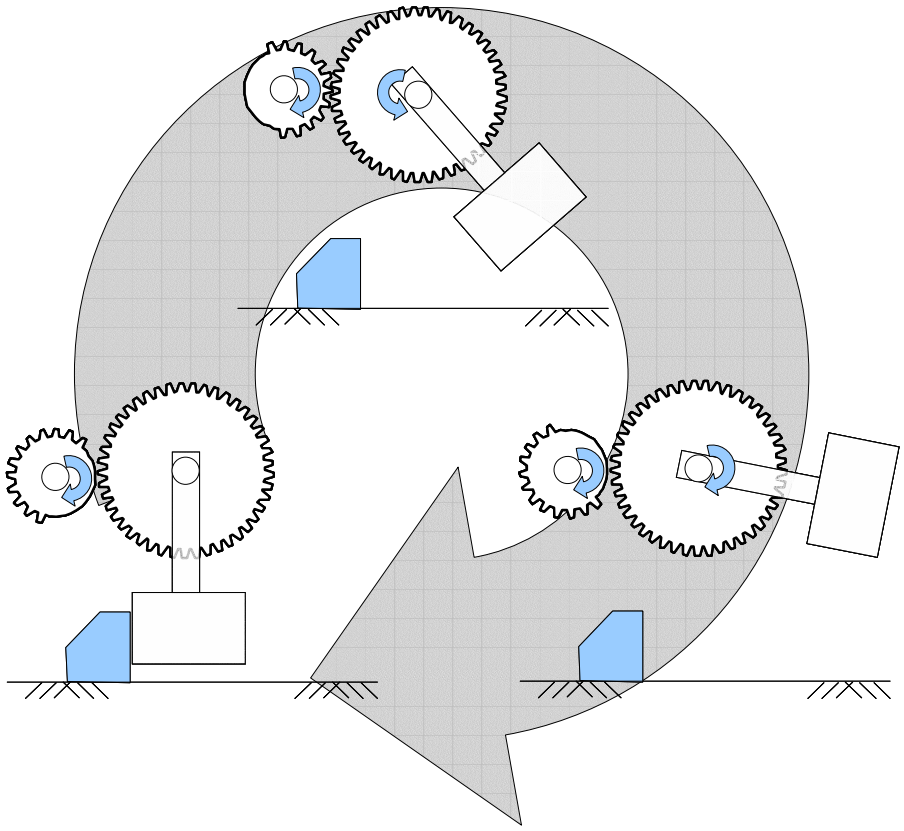

Figure 3.37 Diagram of RotoSeis gear system in continuous operation

Several RotoSeis sources, spanning 6 versions from initial prototype to a commercial version, were constructed in order to achieve the desired characteristics for performance as well as packaging. Pictures and descriptions of each of the non-commercial RotoSeis versions are shown in Table 3.5. With each version the sizes of the hammers and the packaging were changed until the most compact and robust enclosure was finalized. Each of the sources had a gearing system to raise and release the hammer. The sizes of the gears changed depending on the mass of the hammer and the stiffness of the springs for different versions.

Table 3.5 Images and descriptions of the RotoSeis prototype evolution

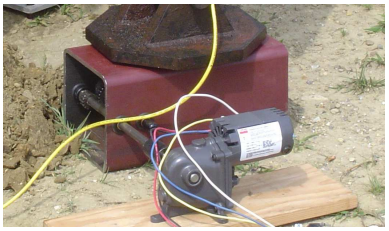	RotoSeis I Open-ended steel monotube body Smooth base surface 0.45 kg internal hammer 90V AC/DC gearmotor Internal gears
	RotoSeis II Open-ended steel monotube body Smooth base surface 2.6-kg internal hammer 90V AC/DC gearmotor External gears
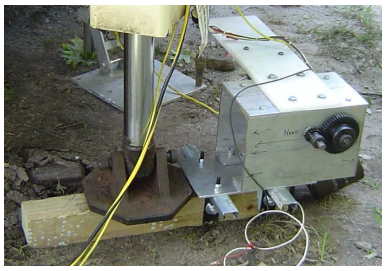	RotoSeis III Open-ended aluminum body attached to a smooth wooden base with a metal endcap 9.5-kg hammer (external) 90V AC/DC gearmotor External gears
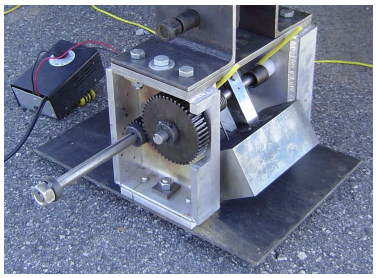	RotoSeis IV Open-frame body with steel base and top, and aluminum side walls Smooth base surface 11.5-kg hammer 90V DC gearmotor (internal) Internal but exposed gears
	RotoSeis V Closed-ended steel monotube body metal screen textured base 6-kg hammer 90V DC gearmotor (internal) External Gears

The first RotoSeis was intended just to demonstrate the concept, and had a hammer mass of just 0.45 kg. Preliminary results at a test site in Mooring, TN showed promise towards this approach. Signals from the small source were weak, but repeatable and detectable to a depth of 21 m at this site (Figure 3.38).

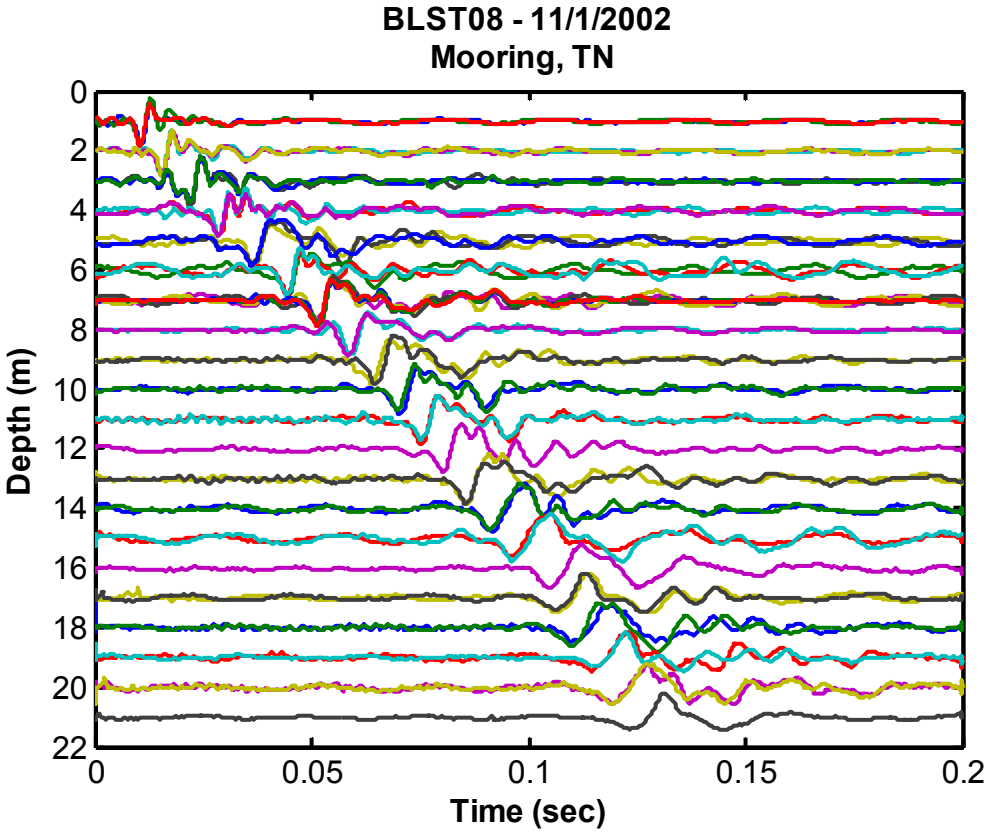

Figure 3.38 Preliminary results of RotoSeis I to a depth of 21 m in Mooring, TN

The hammer size was changed with RotoSeis II, initially a 2.6 kg hammer and later increased to 5.5 kg, to try to increase the depth capability. However, the base of the source was smooth, and with the 5.5 kg mass, the source slipped along the ground surface. The hammer mass was increased again with RotoSeis III, to 9.5 kg, but the base of the device was changed from steel to wood to check for any material effects on the appearance of the signals and slippage. For RotoSeis IV, the mass was increased to 11.5

kg, and the shape of the device was changed to enclose the motor inside with the hammer. The source was fixed rigidly to the cone truck leveling pad to prevent sliding. At last, the hammer mass for the final prototype, RotoSeis V, was reduced to 6 kg, and the motor and hammer were completely enclosed with only the gears mounted on the outside. Expanded metal screen was welded to the bottom to increase the surface roughness and interface stiffness.

RotoSeis V has the most compact arrangement of the hammer, motor, springs, and gears of all the RotoSeis devices. As seen in Figure 3.39, the gear motor is mounted upside down and shifted to the side in order to provide clearance for the hammer shaft. The completed RotoSeis device is 45.7 cm × 17.8 cm × 17.8 cm with a total mass of 30 kg.

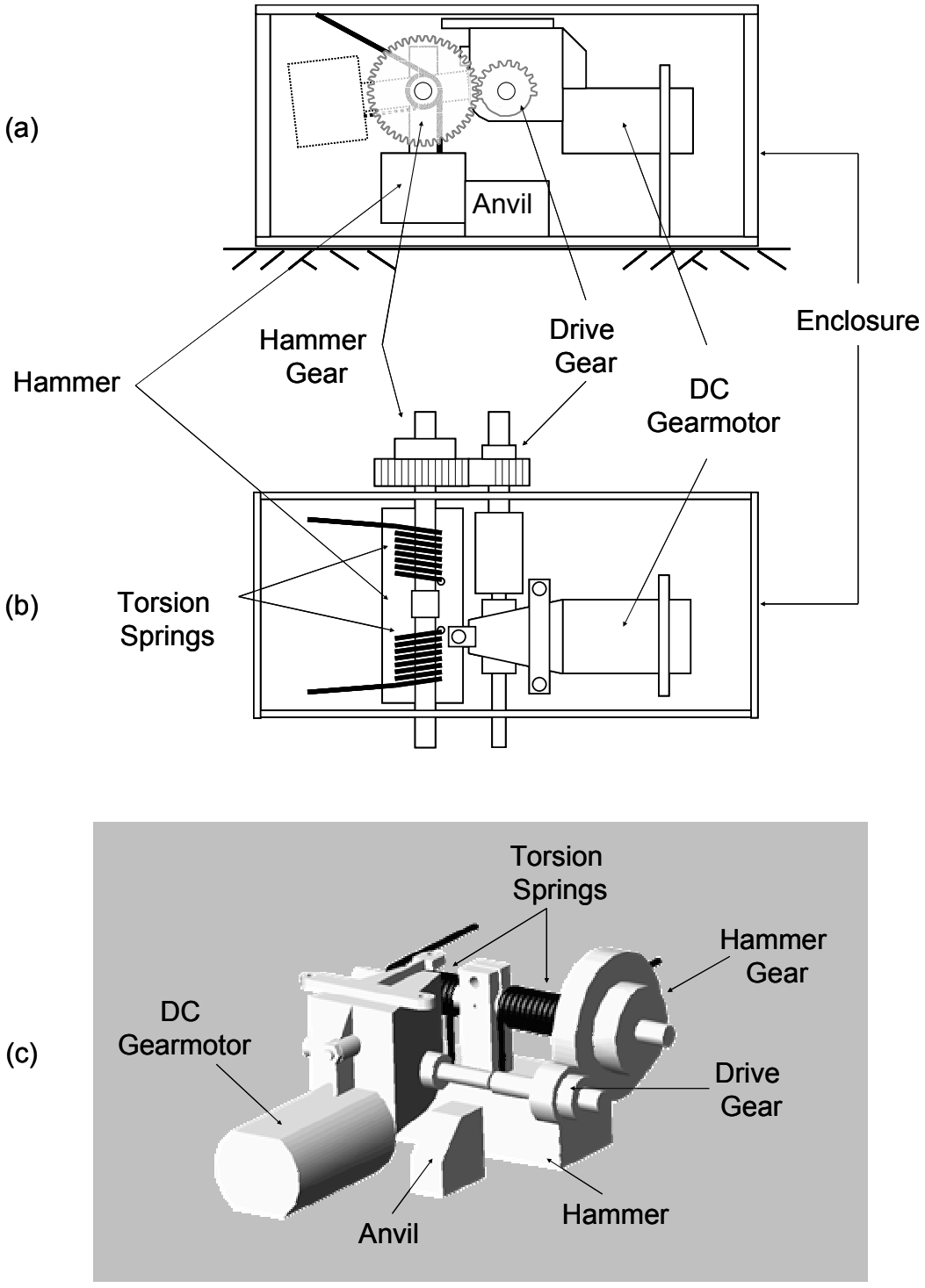

Figure 3.39 Schematic of RotoSeis V, (a) top view, (b) side view, and (c) 3-D view

During continuous operation, RotoSeis V generates horizontally-polarized, vertically-propagating shear waves at regular time intervals. The rate of the motor is remotely-controlled with a variable speed control device connected to the source by a cable (Figure 3.40). For this research the source was set to impact every 10 seconds. The 10 second time interval corresponds to a measurement every 20 cm of penetration at the standard 2 cm/s penetration rate for CPT. The source continues operating during rod breaks, at which time several redundant records will be recorded. These additional records are advantageous for determining the consistency of the analyses, and they provide an opportunity for signal stacking during processing of the results.

There is now a commercially available RotoSeis, which is a product of Finite Designs, Inc. Commercial RotoSeis has essentially the same internal components and configuration as the prototype RotoSeis V. However, improvements have been made to the body of the source, with the addition of handles and watertight seals. Figure 3.41 is a transparent rendering of the new commercial device illustrating the components within the upgraded housing. A photograph of the completed device with the control box is shown in Figure 3.42 (a). The lower part of the figure (Figure 3.42 (b)) is a view of the base of the source with the expanded metal screen texture. The device has been featured at the 2006 International Conference on Flat Dilatometer in Washington D. C., and several units have been purchased by in-situ testing companies around the world.

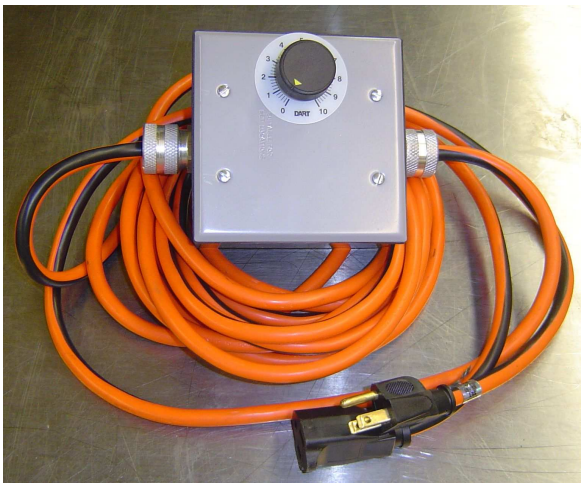

Figure 3.40 Motor control box for RotoSeis V

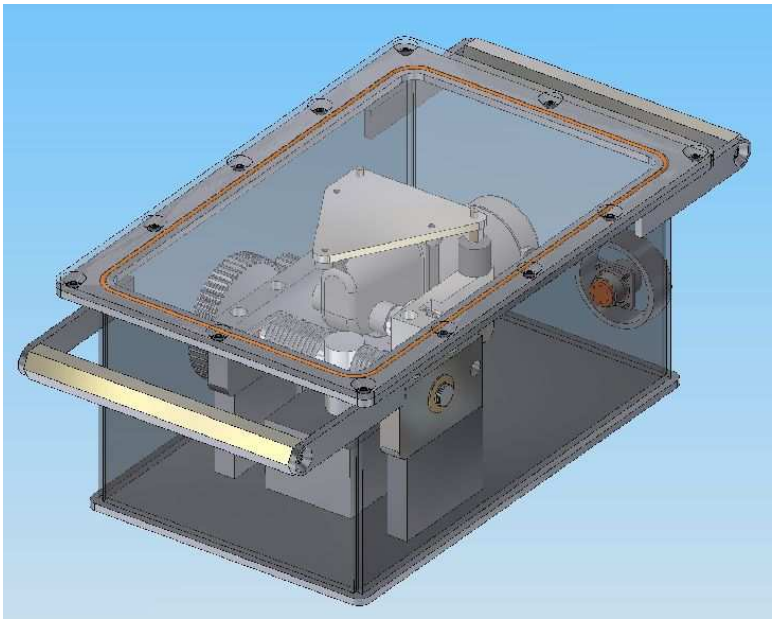

Figure 3.41 Conceptual image of Commercial RotoSeis, produced by Finite Designs, Inc., Ball Ground, GA (www.finiteprecision.com)

(a)

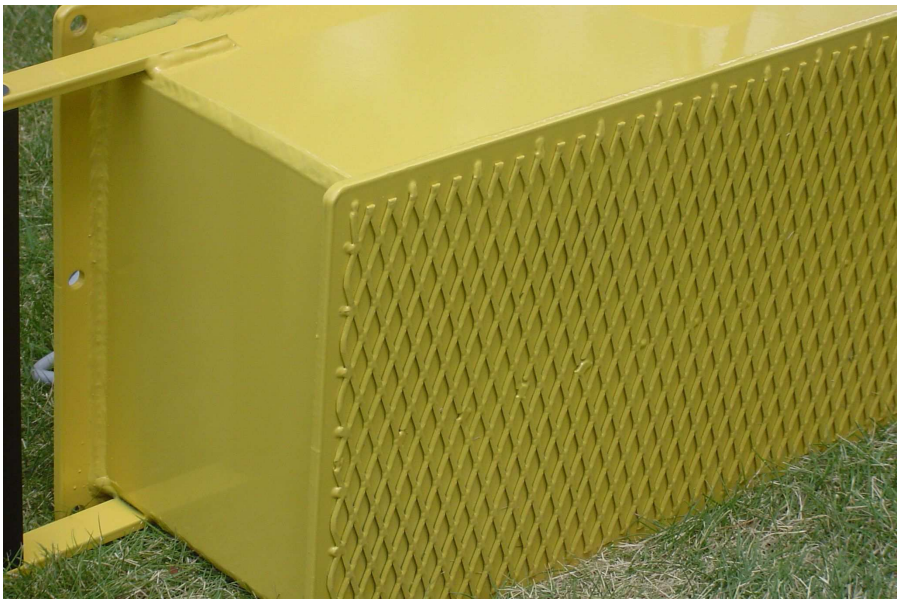

(b)

Figure 3.42 Commercial RotoSeis seismic source produced by Finite Designs, Inc. (a) complete unit with digital control box and (b) expanded metal screen welded to base to prevent slipping between the source and the ground surface

3.6. Data Acquisition Systems

Multiple data acquisition systems were utilized during the search for the optimal system for a continuous-push seismic system in order to identify components and characteristics for an efficient and affordable system. Slow recording devices were used to measure tip, sleeve, and pore pressure data from the cone penetrometer. High sampling rate systems were used to record seismic signals from the geophones in the true-interval seismic devices. For the continuous-push seismic soundings, a slow sampling rate system was used to monitor depth while a high speed recording system monitored the seismic channels.

3.6.1. True-interval seismic dilatometer data acquisition

Pressure readings and seismic signals are recorded simultaneously during the SDMT. Penetration is halted every 20 cm to manually record pressures from the system's pressure panel, and at the same time, a FLUKE 123 ScopeMeter is used to collect the seismic data. As seismic data are recorded they are transferred to a notebook computer through a serial cable. The measurement set-up as used in the field is shown in Figure 3.43.

The FLUKE 123 ScopeMeter is a 2-channel, hand-held, battery-operated oscilloscope. The voltage resolution is 8-bits, with selectable voltage ranges from 5 mV/division to 500 V/division. There are 8 voltage divisions, so the best voltage resolution is approximately 0.15 mV. The sampling frequency is also selectable, but the length of the recording is constant at 252 points per channel. Recording at higher sampling rates shortens the time span of the records. For example, recording at 1250 Hz yields a 200 ms length signal, while a sampling rate of 2500 Hz results in a 100 ms length signal. For true-interval tests, the sample length is 100 ms, for pseudo-interval the sample length is 200 ms. Recording is triggered off of the one of the two channels. After each recording, the signals are transferred to the notebook computer and stored as a text file

for later analysis.

Figure 3.43 Data acquisition system for the true-interval seismic dilatometer, including the DMT pressure panel, Fluke 123 ScopeMeter oscilloscope, and a notebook computer

3.6.2. SCPTu data acquisition

Two different data acquisition systems were utilized during this research to perform standard SCPTu and CPTu soundings: (1) a commercial CPT system manufactured by Hogentogler & Co., Inc., and (2) a 34970A multi-channel data acquisition unit from Agilent Technologies.

3.6.2.1.SCPTu for pairing with static frequent-interval seismic tests

The Hogentogler SCPTu data acquisition system was used to collect the CPTu and conventional stationary receiver SCPTu data. The components of the Hogentogler system are shown in Figure 3.44, consisting of the E3 field computer, penetrometer probe, and an encoder wheel for monitoring penetration values with depth in 2.5 cm increments. The system tracks depth using the encoder wheel and acquires data on 5 channels from the penetrometer, including: tip resistance, sleeve friction, porewater

pressure, inclination, and seismic. However, the seismic acquisition cannot be run concurrently with the other channels. Utilizing conventional methods, the seismic component is operated at 1 m rod breaks.

Figure 3.44 Components of the Hogentogler SCPTu system including the field data acquisition computer, depth wheel, and a seismic piezocone with u_2 porous filter element

3.6.2.2.CPTu data acquisition for continuous-push seismic tests

The Agilent 34970A multiplexing digital multi-meter was used to record CPTu penetration data for use in combination with static, as well as continuous-push frequent interval, seismic soundings in order to simulate a complete continuous-push seismic system. A notebook computer running Microsoft Excel stores and displays the data in real-time. Figure 3.45 shows the Agilent system as connected in the field. The data acquisition device is configured to measure tip, sleeve, porewater pressure, and inclination channels from the penetrometer, as well as depth from a wireline potentiometer (Figure 3.46). The wireline monitors the position of the pushing system relative to the ground surface. A recording sweep of all the channels is performed every second, which corresponds to a depth increment of 1 cm during penetration. A 9 V

indicator button (Figure 3.47) is also connected to the 34970A in order to differentiate data recorded during penetration and data recorded during rod changes. The button is depressed during penetrometer pushing and released during other times.

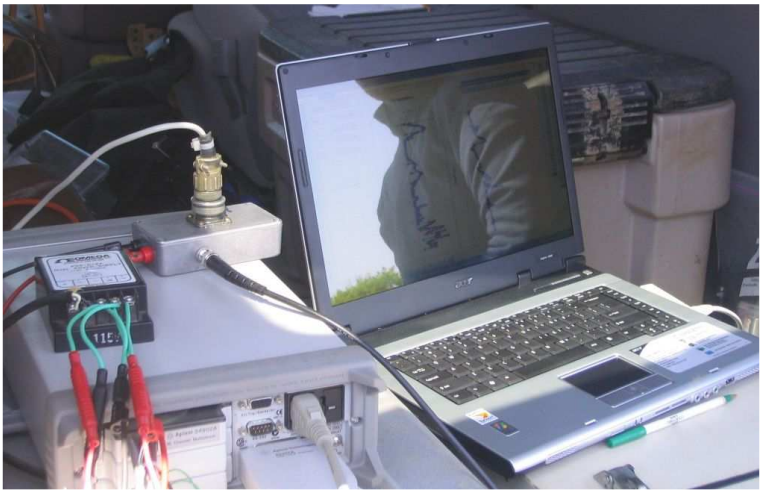

Figure 3.45 Image of the Agilent 34970A data acquisition unit in use

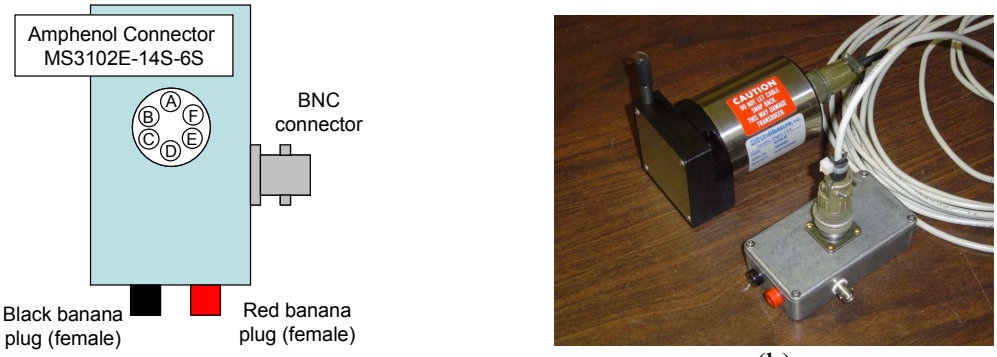

(a) (b)

Figure 3.46 (a) Diagram of junction box for connecting the depth-monitoring potentiometer to the Agilent Technologies 34970A and (b) the potentiometer connected to the junction box

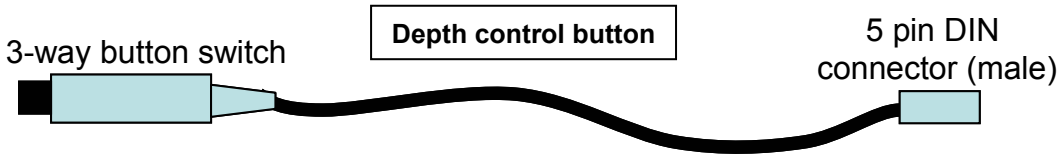

Figure 3.47 Push-button device for use with the Agilent 34970A to monitor depth

3.6.3. True-interval seismic probe data acquisition

Seismic data for the true-interval seismic probe were collected with an HP3560A Dynamic Signal Analyzer (Figure 3.48). The device has 2-channel capability and is battery-operated. Channel 1, connected to the upper geophone in the probe, was used as the trigger. Voltage ranges and sampling rates are selectable, similar to an oscilloscope. Signals were recorded at 5120-S/s for 0.1 seconds. The analyzer has onboard storage for data, but not enough for an entire 30 m frequent-interval sounding. When the storage is full, individual data files are transferred to a computer through a serial cable, and the file format is converted for importing into MATLAB software for processing.

Figure 3.48 Field image of the HP3560A Dynamic Signal Analyzer in use as the data acquisition for the true-interval seismic probe

3.6.4. Biaxial true-interval seismic probe data acquisition

Three different systems were used to record data for static frequent-interval and continuous-push seismic soundings: (1) An Agilent 1432A 16-channel signal analyzer was used for static seismic tests, and both a (2) Geode seismograph from Geometrics, Inc. and (3) National Instruments CompactDAQ system were used to make static as well as continuous-push seismic measurements.

3.6.4.1.Static frequent-interval seismic tests

The Agilent 1432A, shown in Figure 3.49, connected to the notebook computer, has 16-channel capability with recording rates up to 50 kS/s. There is no front panel on the device, so the interface is controlled from the computer running MATLAB software via an IEEE1394 interface. A geophone, connected to the seismic source at the surface and to Channel 7 on the analyzer, was used to trigger recordings on Channels 1-6 from the biaxial true-interval seismic probe. The recording rate was set to 5120 S/s during initial trails and 40 kS/s in later tests. The duration of each record was 0.4 s long. After each trigger event, the signals were displayed on the computer screen for monitoring the quality. Power for the system was supplied in the field by a portable gasoline-powered generator.

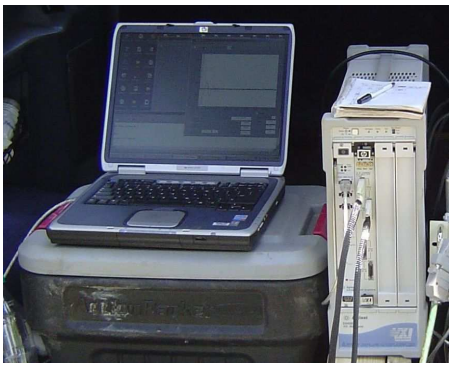

Figure 3.49 Field set-up of the Agilent 1432A 16-channel Analyzer and notebook computer for recording data from static tests with the biaxial true-interval seismic probe

3.6.4.2.Continuous-push seismic tests

Seismic signals for both static and continuous-push seismic soundings were collected with a Geometrics Geode seismograph (Figure 3.50). The device was provided on loan from Geometrics for evaluation purposes. This particular model was 16-channel capable, but the sensor interface cable only allowed for 4-channels to be input via BNC connectors. Device control is managed through a network connection to a notebook PC running the manufacture's control software. The selectable sampling rate was set for 48 kS/s with a recording time of 0.5 s and a resolution of 24-bits. Triggering was performed with a piezoelectric hammer switch connected directly to the hammer of the seismic source. After each trigger, the signals display momentarily on the computer screen and are stored in separate numbered files for each source event. The output is a standard SEG-2 format of the Society of Exploration Geophysicist, which is later converted to MATLAB compatible matrices during processing. The Geode is waterproof and shock resistant. Power is supplied through battery clips connected to a 12 V car battery.

Figure 3.50 Image of the Geode seismograph for recording continuous-push seismic data from the biaxial true-interval seismic probe

For continuous-push seismic data acquisition, the Geode was used in conjunction with the Agilent 34970A and the wireline potentiometer to measure the depth. The Geode and the 34970A operate independently, so the clocks were synchronized on each device so that the time stamps on each recording could be used to match the seismic records with the appropriate depths.

Continuous-push seismic soundings were also conducted with a CompactDAQ system from National Instruments (Figure 3.51). The CompactDAQ is a modular system consisting of a chassis with 8 slots for accepting any of 30 different hot-swappable measurement modules. Two modules were used for recording the seismic signals from the biaxial true-interval seismic probe. The NI 9239 module is a 4-channel, ± 10 V, 24-bit, 50,000 samples/s analog-to-digital converter. Triggering was performed with a NI 9411 8-channel, 5 to 24 V digital input module. The chassis connects to the notebook field computer via USB 2.0 interface. LabView software was used to control the data acquisition hardware.

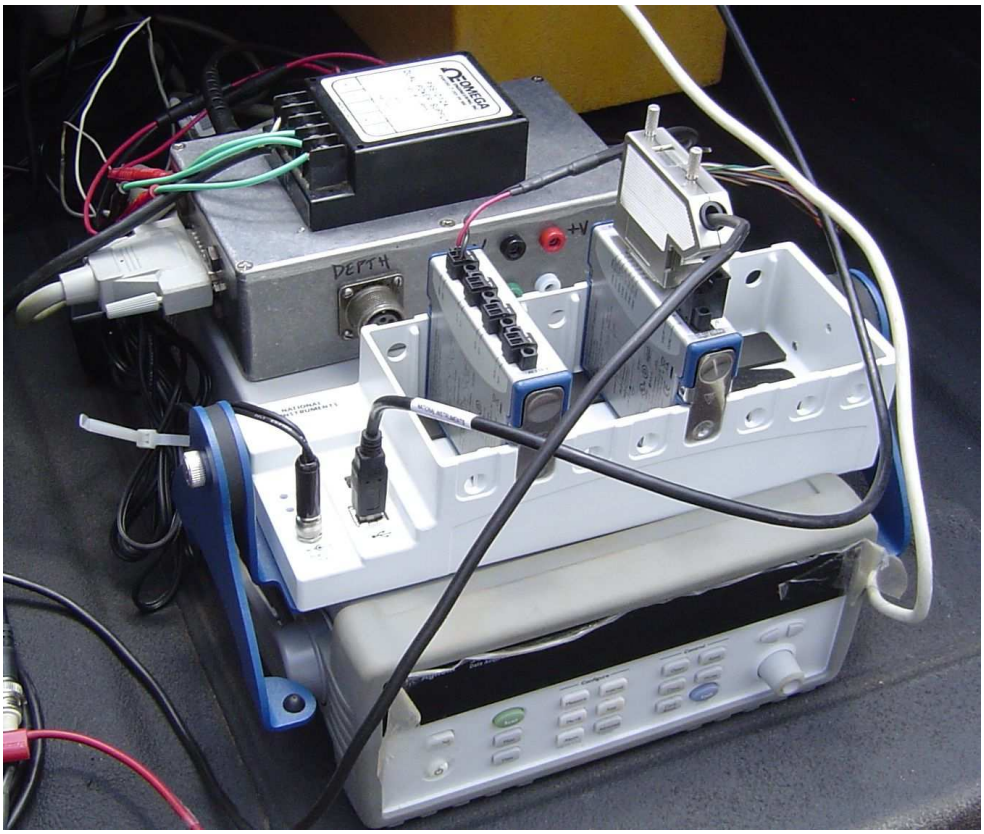

Figure 3.51 National Instruments CompactDAQ 4-channel seismic data acquisition system with Agilent 34970A CPT data acquisition

The sampling rate for the 4-channel seismic recording was set to 5,000 samples/s and the duration of the records was set to 1.4 s. For each strike of the RotoSeis seismic source, the 4-channels were recorded, momentarily displayed on the notebook computer screen, and automatically stored on the computer's hard drive as a tab delimited text file. The file name, containing a number, was incremented for each subsequent record.

Four instrumentation amplifiers were built to individually amplify the low-voltage geophone signals by a factor of 100 in order to use more of the ±10 V input range of the NI 9239 data acquisition module. The complete device with circuit boards mounted in an enclosure is shown in Figure 3.52. Each amplifier is constructed utilizing three LM741 operational amplifier ICs (integrated circuit) and powered with two 9 V batteries. The amplifier gain is fixed at ×100, and has a bandwidth of 1 kHz. There are two amplifiers

per circuit board, and the four amplifiers are installed together in a single enclosure. The circuit diagram for the LM741 instrumentation amplifiers can be found in Figure B.1 in Appendix B.

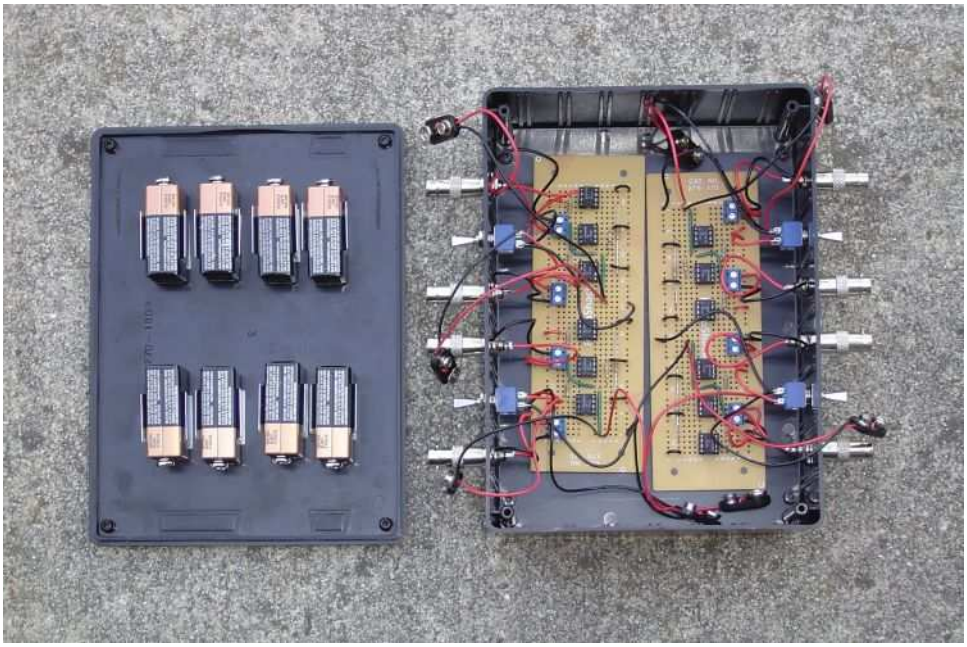

Figure 3.52 Four-channel LM741 instrumentation amplifier device for applying ×100 gain for inputs less than 0.18 V with bandwidth less than 1 kHz

Triggering for the Commercial RotoSeis utilizes a built-in piezoelectric hammer switch, mounted to the anvil inside the unit. Upon impact, the hammer switch closes for 5 ms. With a 9 V battery placed in series with the switch, the NI 9411 digital input module can detect the switch closure and trigger the NI 9239 to begin recording. However, the electric motor within the RotoSeis induces electrical noise in the wires of the hammer switch, which causes false triggering of the data acquisition system. Additionally, the electrical noise is carried through the hammer switch wires into the CompactDAQ chassis and appears in the recorded seismic signals. Two circuits were built to alleviate the trigger noise problems, one to block the noise from reaching the data acquisition and another circuit to regulate the trigger signal. The circuits are described below and

diagrams can be found in Appendix B.

The first trigger circuit is an optical isolator (see diagram in Figure B.3) that was constructed in order to block electrical noise from reaching the data acquisition (Figure 3.53). A current-limited infrared LED connects in series with the hammer switch and a 9 V battery. Each hammer strike closes the switch for 5 ms causing the LED to light-up. The LED does not respond to the electrical noise in the circuit. On the other end of the circuit board is an infrared phototransistor circuit, powered by another 9 V battery, which detects the light from the LED and causes a voltage drop at the output terminals while the LED is on. The LED and the phototransistor are mounted inside a short length of plastic tubing in order to keep them aligned with each other.

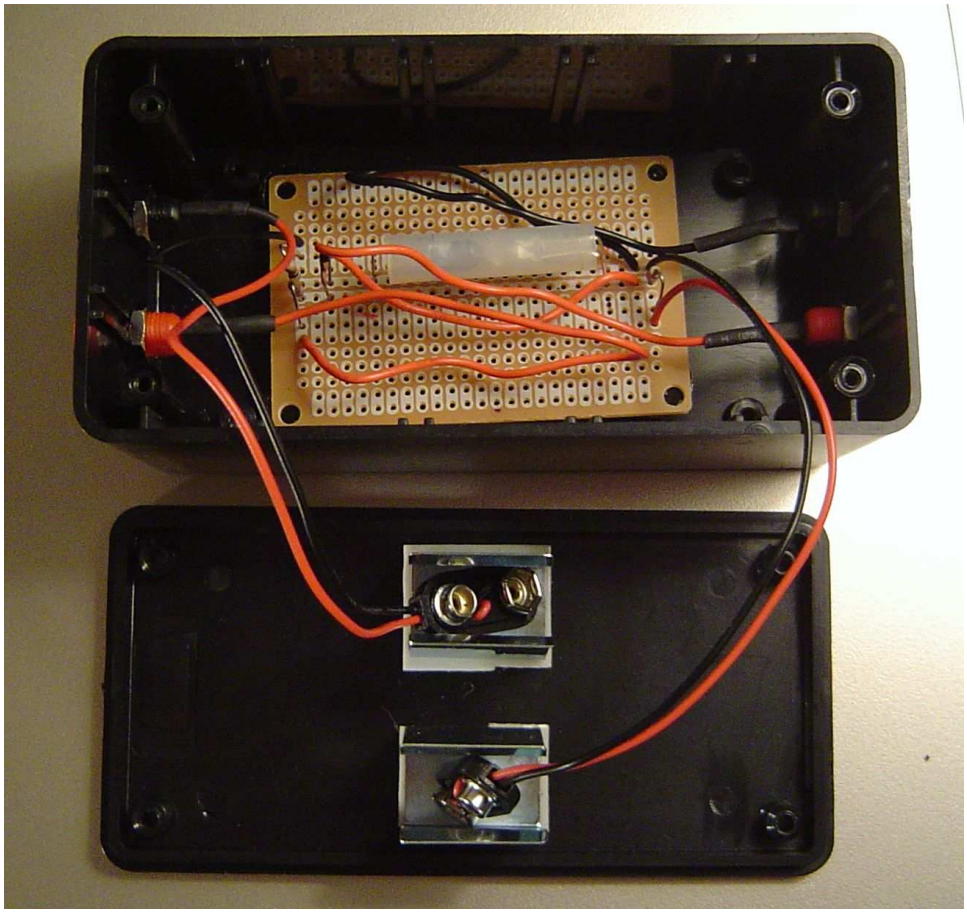

Figure 3.53 Optical isolator circuit built to block electrical interference in the hammer switch lines from reaching the data acquisition system

Although, the voltage drop from the optical isolator creates a falling-edge signal that could be used to trigger the data acquisition system, the circuit shown in Figure 3.54 was built to regulate the voltage level and lengthen the duration of the trigger signal from 5 ms to 2.5 s (see diagram in Figure B.2). Lengthening the width of the trigger pulse eliminates accidental re-triggering once recording has already begun. This circuit utilizes an LM555 timer IC powered by a 9 V battery, with just a few resistors and capacitors required to control the circuit operation. The design for the circuit is based on the circuit recommended by Stewart and Campanella (1993).

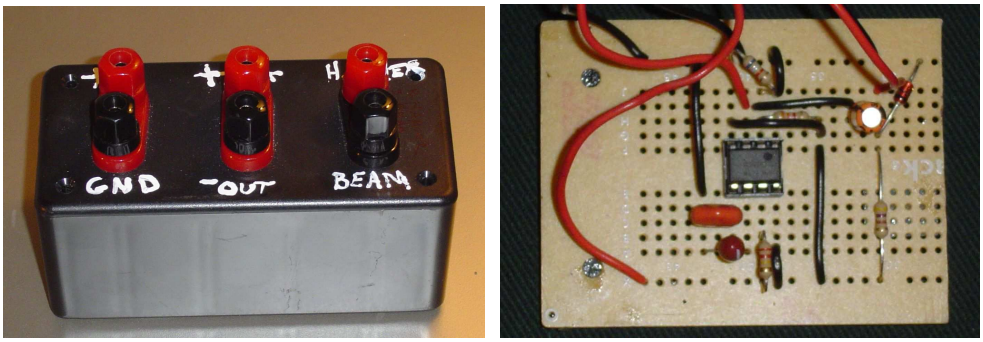

Figure 3.54 LM555 timer circuit for regulating trigger voltage and pulse width

3.7. Summary

In-situ V_S profiles from routine direct-push methods such as the SCPTu and SDMT are undervalued because the velocity profiles lack significant detail and the seismic procedures are poorly integrated with the other penetration procedures. A frequent-interval shear wave velocity method is proposed that can improve the depth resolution and the confidence levels associated with V_S by making overlapping, rather than end-to-end, measurements. For SCPTu, there are no pauses between rod breaks, so the frequent-interval method must be incorporated with continuous-push seismic measurements. Although the SDMT penetration is halted at sufficiently frequent intervals for the frequent-interval method, continuous-push seismic measurements are also required because the operator's time is consumed with obtaining and recording pressure

readings from the DMT pressure panel.

The true-interval SDMT and true-interval seismic probe were built to investigate the frequent-interval method, and the biaxial-true-interval seismic probe was developed for determining the feasibility of recording while the receivers were in motion and examining the characteristics of the RotoSeis seismic source.

Continuous-push seismic testing requires an automated source for generating the source events at regular intervals. There are several types of sources available. However, they are ill-suited for continuous-push seismic systems because they are intended to operate continuously. Several of the systems are quite large, especially hydraulic systems, and require permanent mounting or 2 or more people to set up. The horizontal acceleration of the mass used to generate impact with large commercial sources was found to be problematic for smaller portable sources.

The RotoSeis was developed with rotational motion to direct the reaction forces in the vertical direction and out of the plane of seismic sensor sensitivity. The source is rate controlled, and for the purposes of the continuous-push seismic system, is operated at 10-second intervals corresponding to 20 cm depth increments during penetration. A patent pending for the RotoSeis concept has been filed and several units of the Commercial RotoSeis are now in use around the world.

The disparity between sampling rates for seismic signals and other penetration measurements of necessitates that the seismic data acquisition for the continuous-push seismic system be separated from the recording of the CPTu channels. The Synchronization of the seismic records with the appropriate depth values can be achieved by comparing the timestamp of each seismic signal with the depth versus time for the CPTu channels. Additionally, frequent-interval testing with a continuous-push seismic system further necessitates automated triggering, recording, and storage operation from the data acquisition system.

4. FIELD TESTING PROGRAM

4.1. Introduction

During the course of this research, many field tests were conducted to verify the components of the prototype continuous-push seismic system. This chapter presents information about the various test sites, as well as details of the testing programs performed for evaluation of the RotoSeis seismic source, the true-interval seismic probes, the frequent-interval method, and the non-stationary receivers of the continuous-push seismic system.

4.2. Testing Summary

The testing program for this research spans sixteen sites located in Venice (Italy), Tennessee, Alabama, Georgia, Florida, Missouri, South Carolina, Minnesota, and Louisiana. The field trials of the new methods and field equipment, as well as other companion tests performed at the same sites, are summarized in Table 4.1. Field experiments included eleven frequent-interval tests, four of which were performed with non-stationary receivers, ten tests used the final prototype seismic source, RotoSeis V, and two tests utilized the Commercial RotoSeis.

Many of these tests were incorporated into the testing programs of other ongoing research and consulting projects. For example, the first trials of a RotoSeis prototype (BLST08 and BLST11) were performed at a site in the northwest corner of Tennessee as part of the Embayment Seismic Excitation Experiment (ESEE), a joint project between the USGS and CERI to study the propagation of Rayleigh waves in the Mississippi embayment. Georgia Tech's role in the research was funded by the Mid-America Earthquake Research Center to investigate blast-induced liquefaction, and to study post-liquefaction aging in sands. RotoSeis I was included in the testing program to evaluate changes in V_S with time after the blast (Liao, 2005).

It is not useful to discuss all of the pilot tests of each of the five seismic source prototypes in this thesis. Consequently, eight sites were selected from the sixteen for detailed analysis as presented later in the text. These sites were chosen because they involve frequent-interval or continuous-push tests, and/or represent the final stages of seismic source development. Several of the selected sites also have data from outside sources available for comparison. The results from the other eight test sites mentioned in Table 4.1, but not included in the following text can be found in Appendix A. These tests were valuable as part of the overall study in that they helped refine the author's insight into various aspects of continuous-push seismic penetration testing although their specific relevance to the findings discussed herein is less explicit.

Table 4.1 Summary of tests performed which are related to the development of the continuous-push seismic system

Sounding Name	Site	Date	Latitude N°	Longitude E°	Test Type	Seismic Method	Seismic Source	Probe	Depth (m)
SWGA01	Collierville, TN	June 5, 2001	35.09335	89.71093	$SCPTu_2$	Pseudo-interval	Pneumatic AutoSeis, Pendulum	Hogentogler 10cm²	22.9 (28.6)
SCPT19 (VENI01)	Treporti, Italy	June 10, 2002	45.46774	-12.45487	$SCPTu_2$	Pseudo-interval	Pendulum	Hogentogler 10cm²	40.8
SCPT14 (VENI02)	Treporti, Italy	June 11, 2002	45.46774	-12.45461	$SCPTu_2$	Pseudo-interval	Pendulum	Hogentogler 10cm²	40.2
SCPT15 (VENI03)	Treporti, Italy	June 11, 2002	45.46771	-12.45447	$SCPTu_2$	Pseudo-interval	Pendulum	Hogentogler 10cm²	40.6
SDMT15	Treporti, Italy	June 12, 2002	45.46770	-12.45448	SDMT	Pseudo-interval True-interval	Pendulum	True-interval Seismic DMT	15.8 (P-I) 13.2 (T-I) (32.0)
SDMT14	Treporti, Italy	June 13, 2002	45.46770	-12.45465	SDMT	Pseudo-interval Frequent-interval	Pendulum	True-interval Seismic DMT	29.8 (P-I) 16.2 (F-I) (31.0)
SDMT19	Treporti, Italy	June 14, 2002	45.46773	-12.45486	SDMT	Pseudo-interval True-interval	Pendulum	True-interval Seismic DMT	36.8 (P-I) 36.2 (T-I) (37.0)
BLST01	Mooring, TN	October 17, 2002	36.33203	89.58680	$SCPTu_2$	Pseudo-interval	Pendulum	Hogentogler 10cm²	38.9
BLST03	Mooring, TN	October 18, 2002	36.33203	89.58631	$SCPTu_2$	Pseudo-interval	Pendulum	Hogentogler 10cm²	30.9
BLST05	Mooring, TN	October 29, 2002	36.33203	89.58680	$SCPTu_2$	Pseudo-interval	Pendulum	Hogentogler 10cm²	25.8
BLST06	Mooring, TN	October 30, 2002	36.33204	89.58679	$SCPTu_2$	Pseudo-interval	Pendulum	Hogentogler 10cm²	27.9
BLST08	Mooring, TN	November 1, 2002	36.33203	89.58679	$SCPTu_2$	Pseudo-interval	RotoSeis I	Hogentogler 10cm²	21.0 (28.1)
BLST11	Mooring, TN	June 15, 2003	36.33203	89.58679	$SCPTu_2$	Pseudo-interval	RotoSeis I, Pendulum	Hogentogler 10cm²	15.0 (22.9)

( ) - indicates maximum depth of sounding, (P-I) - pseudo-interval, (F-I) - frequent-interval

Table 4.1 (continued) Summary of field tests performed which are related to the continuous-push seismic system

Sounding Name	Site	Date	Latitude N°	Longitude E°	Test Type	Seismic Method	Seismic Source	Probe	Depth (m)
FCPT04	Evanston, IL	July 14, 2003	42.05679	87.67663	$SCPTu_2$	Pseudo-interval	Sledgehammer	Hogentogler 10cm²	27.1
FCPT04SEIS	Evanston, IL	July 14, 2003	42.05679	87.67663	Downhole Seismic	Frequent-interval	Sledgehammer	True-interval seismic probe	12.0
FCPT02	Evanston, IL	July 16, 2003	42.05692	87.67689	$SCPTu_2$	Pseudo-interval	Sledgehammer	Hogentogler 10cm²	17.7
FCPT03	Evanston, IL	July 16, 2003	42.05688	87.67640	$SCPTu_2$	Pseudo-interval	Sledgehammer	Hogentogler 10cm²	21.0
FCPT05	Evanston, IL	July 17, 2003	42.05679	87.67663	$CPTu_1$	None	None	Hogentogler 10cm²	22.0
FCPT05SEIS	Evanston, IL	July 17, 2003	42.05679	87.67663	Downhole Seismic	Frequent-interval	Sledgehammer	True-interval seismic probe	3.4
FCPT01	Evanston, IL	July 18, 2003	42.05704	87.67654	$SCPTu_2$	Pseudo-interval	Sledgehammer	Hogentogler 10cm²	18.0
FDMT1	Evanston, IL	July 19, 2003	42.05704	87.67654	DMT	None	None	DMT blade	23.0
FCPT03SEIS	Evanston, IL	July 20, 2003	42.05688	87.67640	Downhole Seismic	Frequent-interval	Sledgehammer	True-interval seismic probe	23.0
MUDB1	Memphis, TN	March 5, 2000	35.15647	90.05688	$SCPTu_2$	Pseudo-interval	Pendulum	Hogentogler 10cm²	31.0
MUDBSEIS	Memphis, TN	September 19, 2003	35.15669	90.05692	Downhole Seismic	Frequent-interval	Sledgehammer	True-interval seismic probe	21.9
OPEAUT	Opelika, AL	March 1, 2004	32.59394	85.29739	$SCPTu_2$	Pseudo-interval	RotoSeis II	Hogentogler 10cm²	20.9
OPETRU	Opelika, AL	May 10, 2004	32.59391	85.29746	$SCPTu_2$	Pseudo-interval	Pendulum	Hogentogler 10cm²	12.2
OPETRUSEIS	Opelika, AL	May 10, 2004	32.59391	85.29746	Downhole Seismic	Frequent-interval	RotoSeis II, Pendulum	Biaxial true-interval seismic probe	11.8

( ) - indicates maximum depth of sounding

Table 4.1 (continued) Summary of field tests performed which are related to the continuous-push seismic system

Sounding Name	Site	Date	Latitude N°	Longitude E°	Test Type	Seismic Method	Seismic Source	Probe	Depth (m)
HENM	Sikeston, MO	August 11, 2004	36.71608	89.47210	$SCPTu_2$	Pseudo-interval	RotoSeis II	Hogentogler 10cm²	29.8 (30.9)
12ST01	Atlanta, GA	September 10, 2004	33.78452	84.37980	$SCPTu_2$	Pseudo-interval	RotoSeis III	Hogentogler 10cm²	16.8
12ST02	Atlanta, GA	September 10, 2004	33.78476	84.38018	$SCPTu_2$	Pseudo-interval	RotoSeis III	Hogentogler 10cm²	16.8
BMS02	Berea, SC	September 13, 2004	34.91513	82.45541	$SCPTu_2$	Pseudo-interval	RotoSeis III	Hogentogler 10cm²	18.0 (18.6)
HRES01	Atlanta, GA	February 11, 2005	33.79429	84.41091	$SCPTu_2$	Pseudo-interval	RotoSeis IV	Hogentogler 10cm²	16.8 (17.8)
PWRP1	St. Petersburg, FL	March 3, 2006	27.85923	82.60089	$SCPTu_2$	Pseudo-interval	RotoSeis V	Hogentogler 10cm²	13.7
PWRP2	St. Petersburg, FL	March 3, 2006	27.85915	82.60282	$SCPTu_2$	Pseudo-interval	RotoSeis V	Hogentogler 10cm²	18.5
PWRP3	St. Petersburg, FL	March 4, 2006	27.85970	82.60191	$SCPTu_2$	Pseudo-interval	RotoSeis V	Hogentogler 10cm²	12.4
PWRP4	St. Petersburg, FL	March 4, 2006	27.86038	82.60313	$SCPTu_2$	Pseudo-interval	RotoSeis V	Hogentogler 10cm²	14.4
PWRP5	St. Petersburg, FL	March 4, 2006	27.86032	82.60078	$SCPTu_2$	Pseudo-interval	RotoSeis V	Hogentogler 10cm²	14.2
BEAU01	Beaufort, SC	April 27, 2006	32.44004	80.68442	$SCPTu_2$	Pseudo-interval	RotoSeis V	Hogentogler 10cm²	11.0
BEAU02	Beaufort, SC	April 27, 2006	32.44006	80.68442	$SCPTu_2$	Pseudo-interval	RotoSeis V	Hogentogler 10cm²	17.0 (17.8)

( ) - indicates maximum depth of sounding

Table 4.1 (continued) Summary of field tests performed which are related the continuous-push seismic system

Sounding Name	Site	Date	Latitude N°	Longitude E°	Test Type	Seismic Method	Seismic Source	Probe	Depth (m)
STON1A	John's Island, SC	December 16, 1999	32.75241	80.01335	$SCPTu_2$	Pseudo-interval	Sledgehammer	Hogentogler 10cm²	25.1
STONOSEIS	John's Island, SC	May 21, 2004	32.75228	80.01317	Downhole Seismic	Frequent-interval	Sledgehammer	Biaxial true-interval seismic probe	26.0
STONO01	John's Island, SC	April 28, 2006	32.75123	80.01346	$CPTu_2$	None	None	Hogentogler 10cm²	22.1
STONO01SEIS	John's Island, SC	April 28, 2006	32.75123	80.01346	Downhole Seismic	Continuous-push frequent-interval	RotoSeis V	Biaxial seismic probe	9.7
CRBDH1	Mt. Pleasant, SC	December 17, 1999	32.80161	79.90153	$SCPTu_2$	Pseudo-interval	Pendulum	Hogentogler 15cm²	30.6
CRB01	Mt. Pleasant, SC	April 29, 2006	32.80162	79.90064	$CPTu_2$	None	None	Hogentogler 10cm²	24.9
CRB01SEIS	Mt. Pleasant, SC	April 29, 2006	32.80162	79.90064	Downhole Seismic	Continuous-push frequent-interval	RotoSeis V	Biaxial true-interval seismic probe	12.6
CRB02	Mt. Pleasant, SC	April 30, 2006	32.80165	79.90065	$CPTu_2$	None	None	Hogentogler 10cm²	26.0
CRB02SEIS	Mt. Pleasant, SC	April 30, 2006	32.80165	79.90065	Downhole Seismic	Frequent-interval	Sledgehammer	Biaxial true-interval seismic probe	27.7
CRB03	Mt. Pleasant, SC	July 24, 2007	32.80174	79.90180	$SCPTu_2$	Continuous-push pseudo-interval	Commercial RotoSeis	Hogentogler 10cm²	28.6
CRB03SEIS	Mt. Pleasant, SC	July 24, 2007	32.80174	79.90180	Downhole Seismic	Continuous-push frequent-interval	Commercial RotoSeis	Biaxial true-interval seismic probe	28.5
NEWOR01	New Orleans, LA	October 24, 2006	N/A	N/A	$SCPTu_2$	Pseudo-interval	RotoSeis V	Hogentogler 10cm²	29.7
F22Y0703C	St. Paul, MN	May 22, 2007	44.96817	93.08994	$SCPTu_2$	Pseudo-interval	Vertek Hydraulic	Vertek 15cm²	15.1

( ) - indicates maximum depth of sounding

4.2.1. Treporti, Italy

Figure 4.1 Treporti test embankment site located within the Venetian lagoon

The city of Venice, Italy is at risk from increasing incidences of already frequent flooding. The proposed solution to protect the city and the surrounding areas from inundation is to construct moveable floating gates at each of the 3 entrances to the lagoon, which could be closed during times of high water and opened when water levels are safe (Keahey, 2002). Georgia Tech was invited to take part in the research effort to thoroughly characterize the properties of the lagoonal soils for the purpose of determining the applicability of various soil tests and analysis methods for predicting settlements in the lagoonal soils (Marchetti et al., 2004; Simonini, 2004). A test embankment was built in Treporti, a town within the Venetian Lagoon, located just 9.6 km east from the heart of Venice (Figure 4.1).

The soils of the Venetian lagoon consist of complex varying mixtures of sands silts and silty-clays with peat inclusions from the uplands north of the Treporti area. The upper 50 to 60 m are believed to have been deposited during the end of the Pleistocene Epoch, with only the top few meters consisting of younger Holocene soils (Cola and

Simonini, 2002; Ricceri et al., 2002). Figure 4.2 is a soil profile of the Treporti test site from Simonini (2004) providing the relative percentages of sand, silt, and clay, index properties, and OCR determined from oedometer tests as well as embankment monitoring. The figure illustrates the highly non-uniform nature of the profile, showing large oscillations in saturated unit weight and high void ratios related to increased organic content. The OCR indicates that the soils are slightly over consolidated. In preparation for construction of the embankment, the surface of the site was graded flat, blanketed with a geotextile fabric, and then covered by approximately 15 cm of sand.

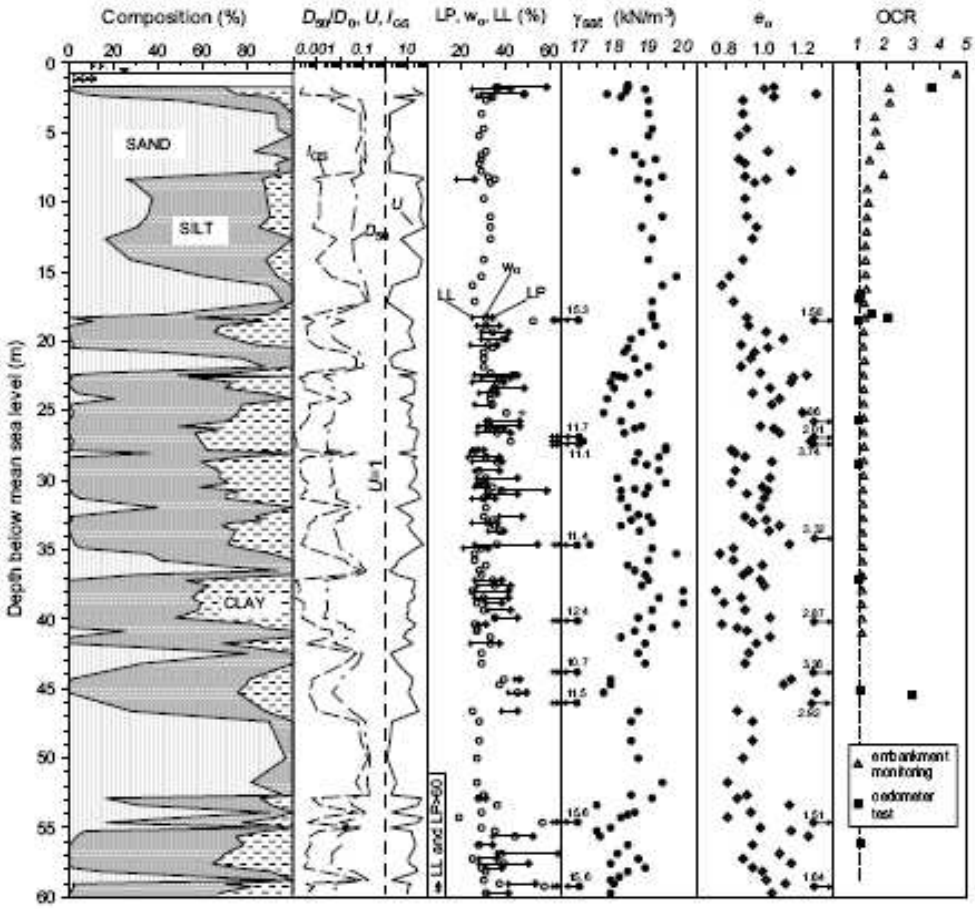

Figure 4.2 Profile of soil type, properties, and stress history for the Treporti test site (Simonini, 2004)

The test embankment, shown in the aerial photo in Figure 4.3, was completed in May 2003, several months after the Georgia Tech testing program. The final height was 6.7 m, covering a circular area 40 m in diameter. A summary of the instrumentation and resulting settlements is given by Marchetti et al. (2004). Representative reference laboratory data, mechanical properties, and soil parameters for nearby sites in the Venetian lagoon deposits are presented by Ricceri et al. (1997), Cola and Simonini (2002), and Simonini et al. (2006).

Figure 4.3 Treporti test locations superimposed onto the test embankment

A series of three conventional pseudo-interval SCPT soundings and three true-interval/frequent-interval SDMT soundings were conducted by Georgia Tech prior to construction in order to characterize the initial geostratigraphy, soil strength, and small-

strain stiffness profiles in the highly layered soils. A portable true-interval seismic dilatometer system, presented previously in Chapter 3, was developed for the project (McGillivray and Mayne, 2004). The soundings were located in pairs of one SCPTu with one SDMT across the diameter of the planned embankment with about 1 m between the soundings making up each pair and about 15 m between each of the three pairs (Figure 4.3). Table 4.2 presents a selected subset of the tests performed at this site that are to be examined further in Chapter 6 for evaluating the performance of the true-interval seismic dilatometer device as well as the frequent-interval seismic method. Other tests conducted by Georgia Tech at the site are listed previously in Table 4.1.

Table 4.2 Frequent-interval and related tests at the Treporti test site

Sounding Name	Test Type	Seismic Method	Seismic Source	Probe	Data Source
SCPT14 (VENI02)	SCPTu$_2$	Pseudo-interval	Pendulum	Hogentogler 10cm²	Georgia Tech
SCPT15 (VENI03)	SCPTu$_2$	Pseudo-interval	Pendulum	Hogentogler 10cm²	Georgia Tech
SCPT19 (VENI01)	SCPTu$_2$	Pseudo-interval	Pendulum	Hogentogler 10cm²	Georgia Tech
SDMT15	SDMT	Pseudo-interval True-interval	Pendulum	True-interval Seismic DMT	Georgia Tech
SDMT19	SDMT	Pseudo-interval True-interval	Pendulum	True-interval Seismic DMT	Georgia Tech
SDMT14	SDMT	Pseudo-interval Frequent-interval	Pendulum	True-interval Seismic DMT	Georgia Tech
S-CPT	Direct-push DHT	Pseudo-interval	Pendulum	Soil Test Seismic Probe	Soil Test

The SCPT and SDMT soundings were hydraulically pushed with a 250 kN capacity cone truck from a local company (Soil Test). The truck has four hydraulic

leveling legs used to raise the truck into a perfectly level position to ensure vertical penetration of the cone and dilatometer. The pushing system of the truck was equipped with mechanical grips for holding on to the 37 mm diameter rods as they were pushed into the ground.

A standard set of SCPTu tests were performed using a Hogentogler 10 cm², 100 kN capacity cone penetrometer and the Hogentogler E3 data acquisition computer. The shear wave velocities were measured every meter using the pseudo-interval method with a sledgehammer pendulum source.

The DMT equipment was provided by L'Aquila University. Seismic modules, described in the previous chapter, were attached above the provided DMT blade to add seismic velocity capability to the system. Seismic signals were recorded with the two-channel FLUKE 123 ScopeMeter, connected to a notebook computer, with a sledgehammer pendulum source used to generate the shear waves. Seismic recordings were made simultaneously with the DMT readings (Figure 4.4). Pseudo-interval and true-interval seismic measurements were made every meter for SDMT15 and SDMT19, and frequent-interval seismic data was collected every 20 cm with SDMT14. For pseudo-interval recordings, a surface geophone attached to the source was used to trigger the recording of a single geophone in the SDMT device. In contrast, for making true-interval measurements, both downhole receivers were connected to the FLUKE 123 which was then set to trigger off of the uppermost geophone.

Figure 4.4 Performing SDMT at test site in Treporti, near Venice, Italy

Another downhole seismic test (S-CPT) was performed at this site by Soil Test using their commercial seismic-only probe containing a single triaxial seismic array. The seismic source for this test was a different sledgehammer pendulum. Pseudo-interval signals were recorded at 1 m depth increments.

4.2.2. Northwestern University, Evanston, IL

A series of SCPT and SDMT tests were conducted on the campus of Northwestern University prior to the construction of the Ford Motor Company Engineering Design Center. The field investigations were part of a joint research project between Georgia Tech, Northwestern University, and the University of Illinois. The task for Georgia Tech was to perform high resolution characterization of the subsurface which could be utilized for modeling displacements in the excavation during construction of the building foundation. Funding for the field testing was provided by the CMS Program at NSF.

According to Finno et al. (2000), the majority of the soils in the Chicago are made up of glacial till that has been deposited under water in distinct layers during local advances and retreats of the ice during the Wisconsin stage of the Pleistocene era. The soils are derived from preexisting deposits and shale eroded from the Lake Michigan Basin.

Characterization efforts at the Northwestern University National Geotechnical Experimentation Site (NGES), just 0.55 km from the Ford Design Center test site, identify distinct layers in the subsurface profile (Figure 4.5). At the NGES, the upper 7 to 9 m is made up of fine-grained dense to very dense sand fill placed in 1966. Below the fill is 10 to 15 m of soft to medium clay, followed by approximately 4 m of stiff clay, 3-m of hard silt, and finally, dolomite bedrock. The water table is located at 4.6 m below ground surface, corresponding to the level of Lake Michigan just 60 m away (Finno, 1989,1992; Benoît, 2000; Finno et al., 2000).

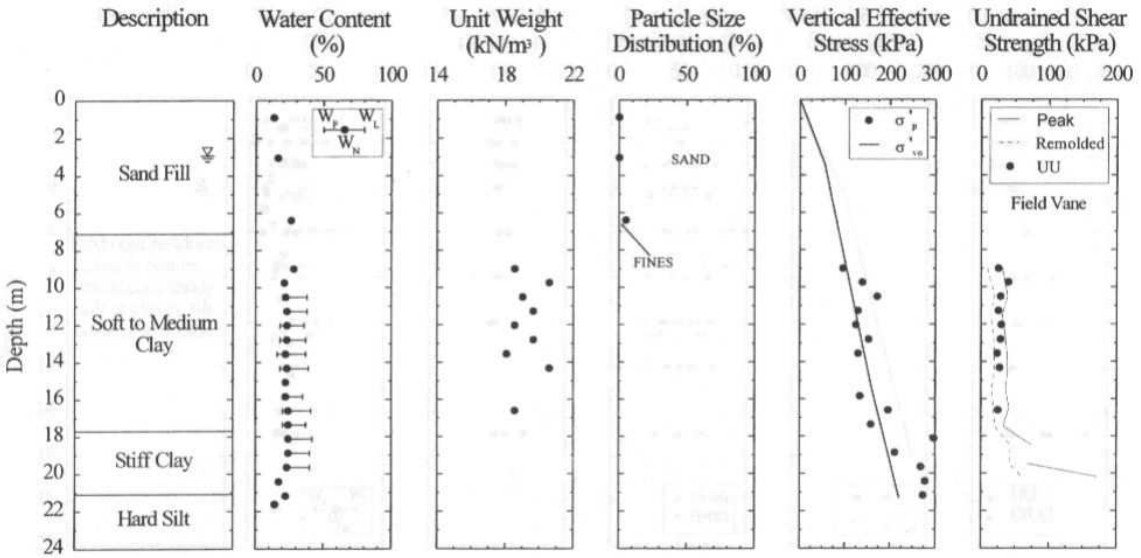

Figure 4.5 Soil profile for the Northwestern University NGES (Benoît, 2000)

Based on a boring provided by Northwestern University, the conditions at the Ford Design Center test site differ only slightly from the NGES profile. The soil profile is composed of glacial deposits of silts and clays similar to the conditions at the NGES. The elevation is 18.9 m above the mean water level in Lake Michigan. Upper soils down to 3.4 m consist of sandy fill soils containing organics. The fill overlays a 1 m layer of natural silty fine sand. Below the sand is 2 m of silty clay, 1.5 m of clayey silt, 15 m of soft to medium silty clay, and 3.3 m of hard to very hard silty clay at the end of the boring.

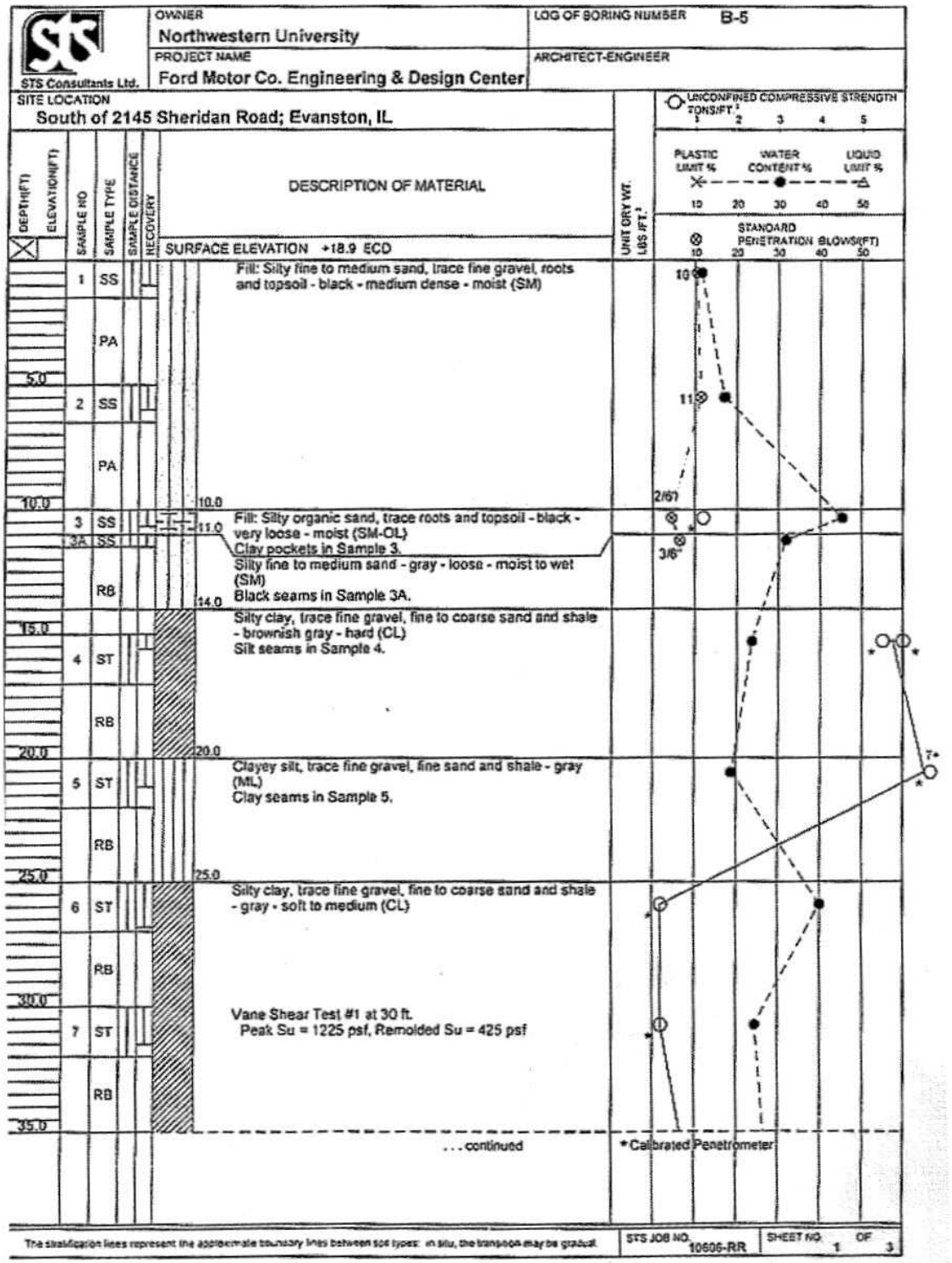

Figure 4.6 Soil boring record (page 1) provided by Northwestern which was performed at the Ford Design Center test site

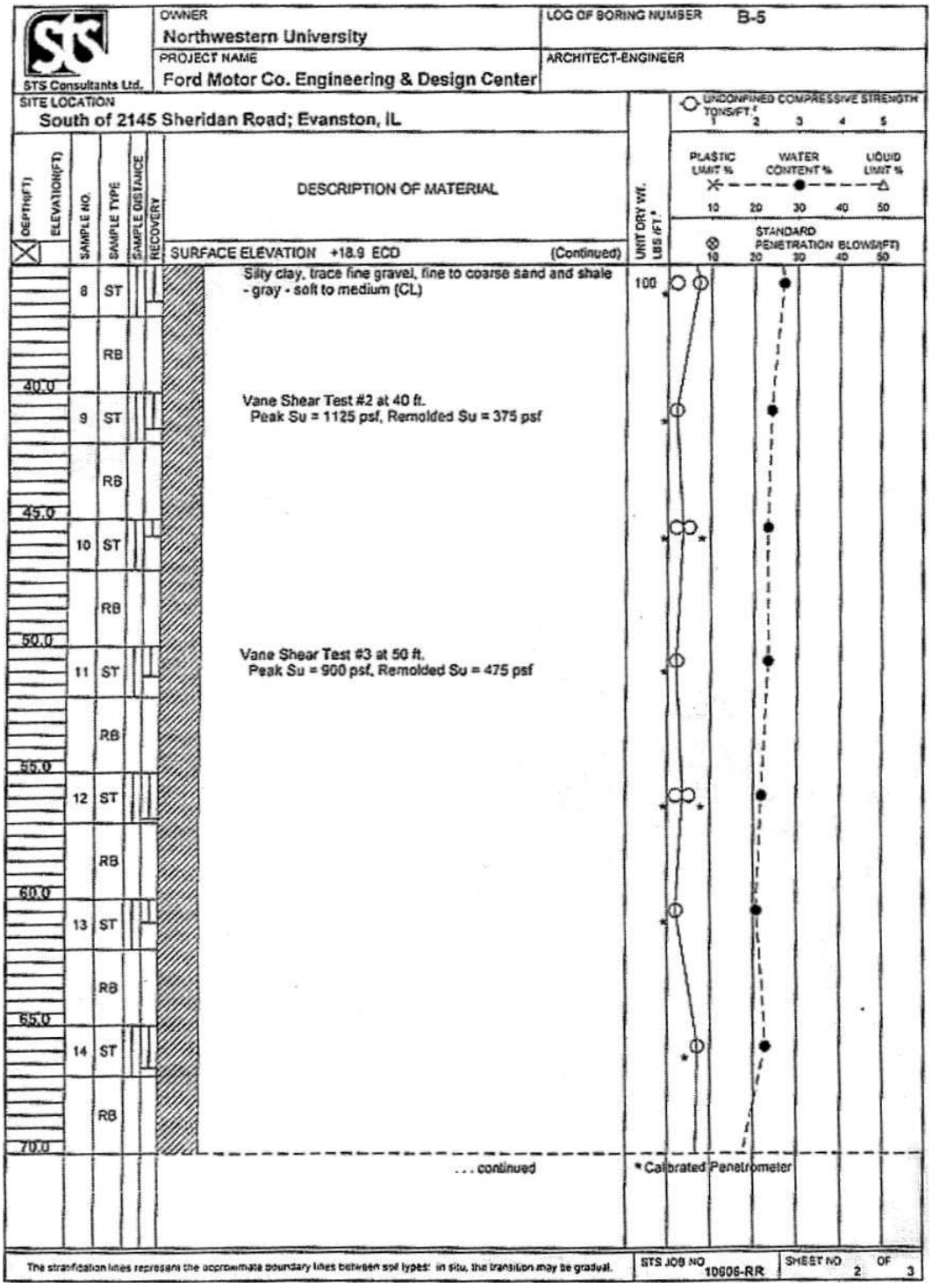

Figure 4.7 Soil boring record (page 2) provided by Northwestern which was performed at the Ford Design Center test site

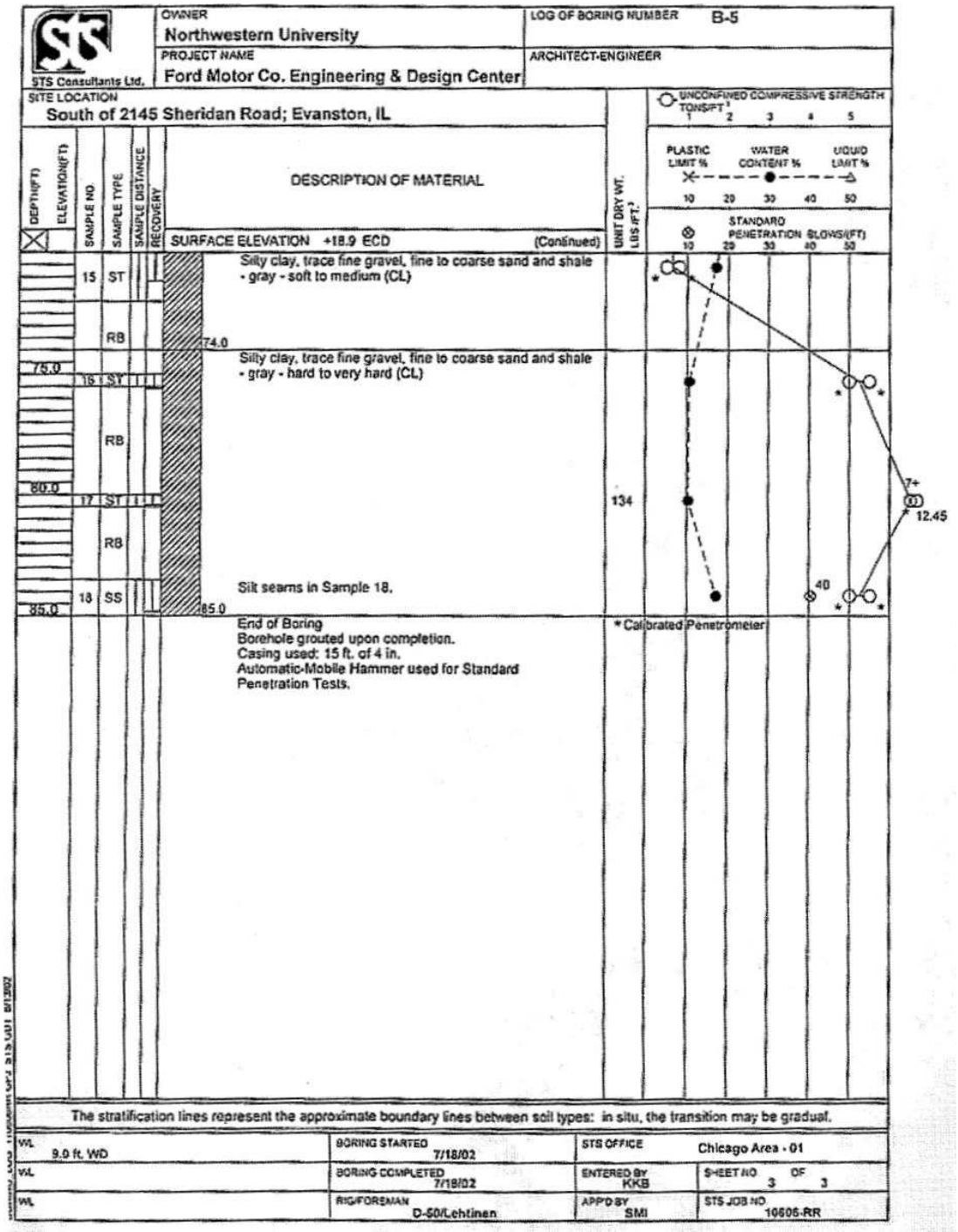

Figure 4.8 Soil boring record (page 3) provided by Northwestern which was performed at the Ford Design Center test site

The Georgia Tech cone truck was used to carry out the testing program at the site, located next to the existing engineering building on the campus (Figure 4.9) at the south end of Tech Drive. Three frequent-interval downhole seismic tests were performed along with four SCPTu, one CPTu, and one DMT. Another SCPT and DMT, not included here, were also performed at the nearby NGES.

Figure 4.9 Testing on the campus of Northwestern University

Tests were conducted at four locations distributed around the footprint of the structure (Figure 4.10). For three of the SCPTu soundings, companion frequent-interval seismic tests were conducted in order to provide detailed velocity profiles beyond the capabilities of the standard pseudo-interval method. Table 4.3 is a selection of tests from this site that relate to the evaluation of the true-interval seismic probe and the frequent-interval method. Though frequent-interval velocities were measured during FCPT05SEIS, the sounding did not penetrate to a significant depth to be considered.

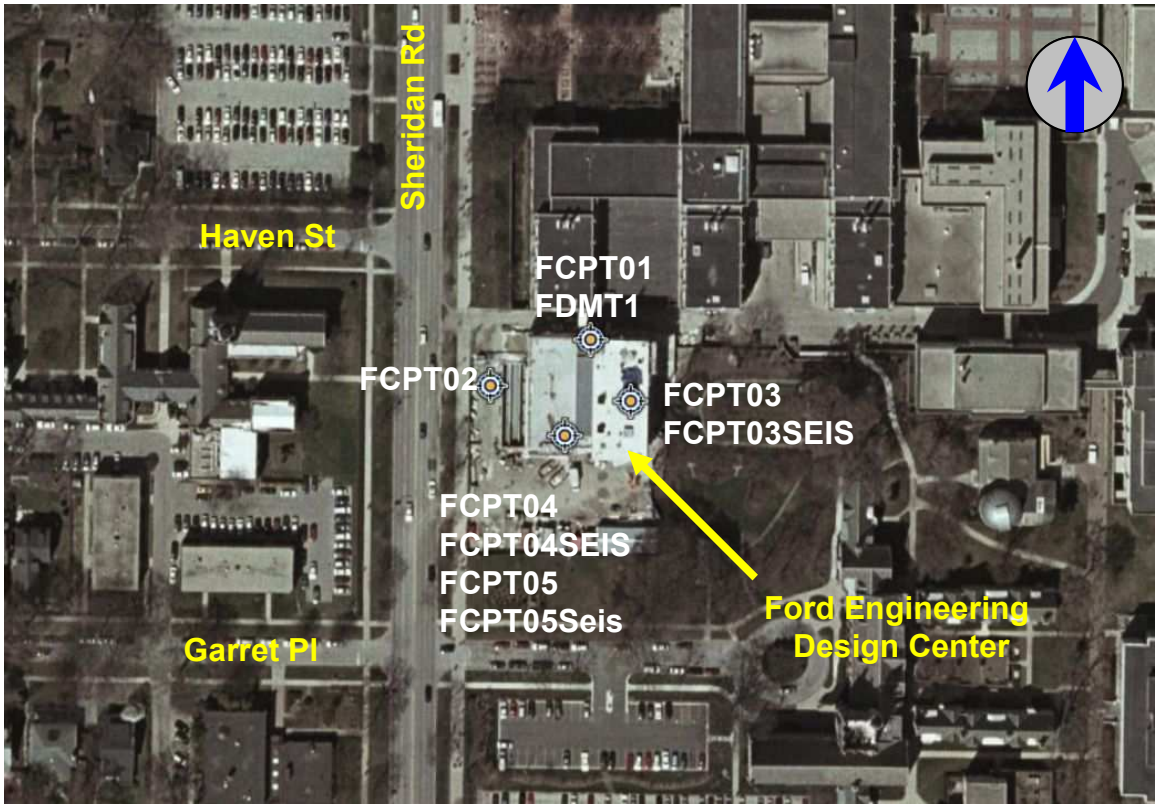

Figure 4.10 Test locations superimposed onto the Ford Design Center at Northwestern University

Table 4.3 Pertinent tests for Northwestern University, Evanston, IL test site

Sounding Name	Test Type	Seismic Method	Seismic Source	Probe	Data Source
FCPT03	SCPTu$_2$	Pseudo-interval	Sledgehammer	Hogentogler 10cm²	Georgia Tech
FCPT03SEIS	Direct-push DHT	Frequent-interval	Sledgehammer	True-interval seismic probe	Georgia Tech
FCPT04	SCPTu$_2$	Pseudo-interval	Sledgehammer	Hogentogler 10cm²	Georgia Tech
FCPT04SEIS	Direct-push DHT	Frequent-interval	Sledgehammer	True-interval seismic probe	Georgia Tech
FDMT1	DMT	None	None	DMT blade	Georgia Tech

Hogentogler 10 cm² cones and the E3 field computer were used to collect all of the SCPTu data. Shear waves were generated by striking a steel beam with a sledgehammer during each rod break. The frequent-interval tests were performed with the true-interval seismic probe, in which, two seismic receiver modules were connected to a dummy cone tip. With the same sledgehammer source, the frequent-interval shear wave velocities were measured every 20 cm. Signals from the true-interval seismic probe were recorded using the HP3560A dynamic signal analyzer by triggering on the uppermost receiver.

For FCPT04SEIS, the seismic probe was pushed into the same hole left by the FCPT04. The difference in probe diameter, 44.45 mm for the seismic probe versus 37 mm for the Hogentogler cone, ensured the seismic probe maintained coupling with the soil. The frequent-interval test FCPT03SEIS was pushed in virgin soil located within 1 m of FCPT03.

4.2.3. Mud Island, Memphis, TN

A frequent-interval seismic sounding was performed on Mud Island in Memphis, Tennessee. The "island" is actually now a peninsula. Mud Island started life as a sandbar and has been built up over the past 80 years with dredge spoil taken from the Mississippi River. The northern end has been connected to the mainland, redirecting the Wolf River. The subsurface consists of variable loose sand, silt, and clay mixtures above deeper medium dense sand, and has been determined to be at serious risk for liquefaction during an earthquake (Liao et al., 2000). Despite the danger, the land is prime waterfront real-estate with upscale housing and parks, given its location just inside the edge of the Mississippi River from downtown Memphis.

The site was selected for this research because it had been previously characterized by SCPTu for the purpose of determining the liquefaction susceptibility for the Mid-America Research Center. Additional shear wave velocity data are also available at this site, including a surface wave test performed by Georgia Tech (Hebeler, 2001), a reflection/refraction test performed by the USGS (Williams et al., 2003), and a refraction test performed by Woolery et al. (2000) of the University of Kentucky. Table 4.4 lists information about the testing efforts undertaken at this location while Figure 4.11 shows the location of the frequent-interval test, MUDBSEIS, relative to the other tests.

Table 4.4 Pertinent tests for the Mud Island test site

Sounding Name	Test Type	Seismic Method	Seismic Source	Probe	Data Source
MUDB1	SCPTu$_2$	Pseudo-interval	Pendulum	Hogentogler 10cm²	Georgia Tech
MUDBSEIS	Direct-push DHT	Frequent-interval	Sledgehammer and steel beam	True-interval seismic probe	Georgia Tech
W4	Reflection/ Refraction	Reflection/ Refraction	Sledgehammer and wood beam	N/A	USGS (Williams et al.,2003)
S4	Refraction	Refraction	Sledgehammer and steel beam	N/A	University of Kentucky (Woolery et al., 2000)
Mud Island B surface wave	Surface Wave	f-k method active and passive	Shaker and ambient energy	N/A	Georgia Tech Hebeler (2001)

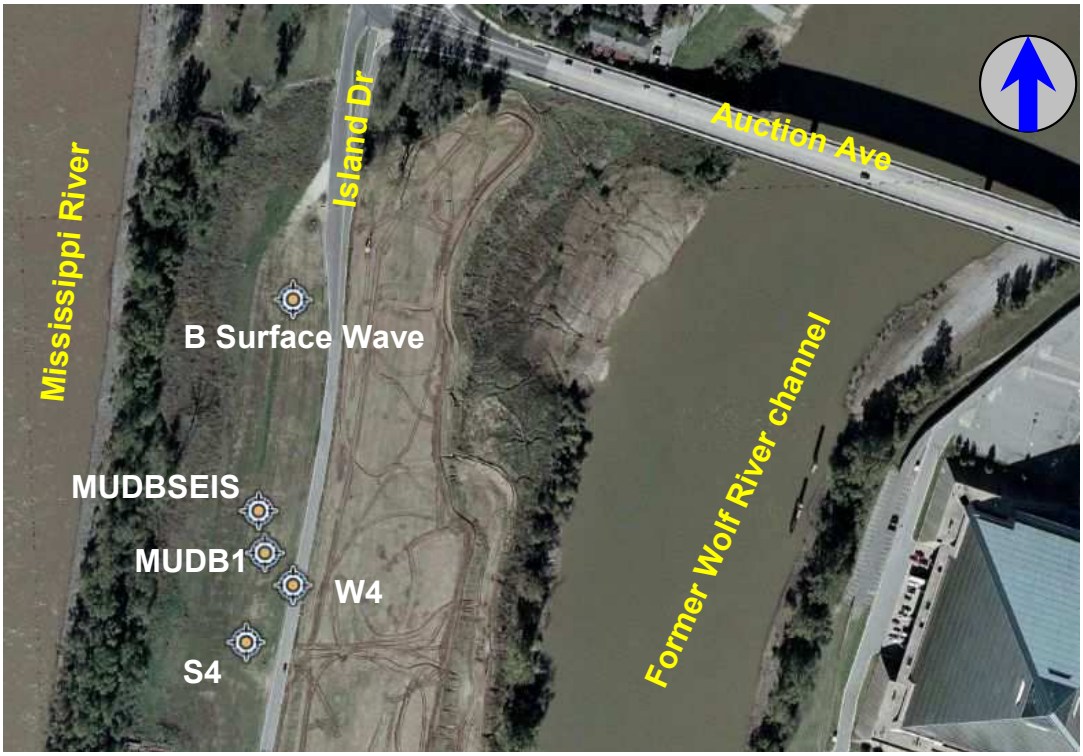

Figure 4.11 Mud Island test locations

The frequent-interval shear wave velocity test, MUDBSEIS, was performed using the true-interval seismic probe. The Georgia Tech cone truck was used to push the probe into the ground, stopping every 20 cm to measure V_S. Shear waves were generated with a steel beam and a sledgehammer. The signals from each of the two seismic receivers were recorded with the HP3560A dynamic signal analyzer, triggered by the initial response of the uppermost geophone.

Figure 4.12 Frequent-interval seismic testing on Mud Island in Memphis, TN

4.2.4. Opelika, AL

Auburn University operates a National Geotechnical Experimentation Site (NGES) in Spring Villa, near Opelika, Alabama, which occupies a corner of the National Center for Asphalt Technology test track. The site is situated in the southwest Piedmont geologic province. Locally, the profile consists of approximately 30 m of silty sands to sandy silts (SM-ML) weathered in place from high-grade metamorphic schist and gneiss bedrock.

Testing began at the site in January 1996 for the Alabama DOT to investigate highway research projects related to pavement and foundations performance. A report by Vinson and Brown (1997) provides the most comprehensive history of the site with geologic and stratigraphic descriptions, as well as compiled results of early lab and in-situ site characterization studies. The soils have been extensively characterized with laboratory and field tests (Kates, 1997; Martin and Mayne, 1998; Finke et al., 1999; Schneider et al., 1999; Casey, 2000; Mayne et al., 2000; Finke et al., 2001). The soil properties are variable but fall within a narrow range. The degree of weathering generally decreases with depth. Typical index values for the soils at the site are given in Table 4.5.

A frequent-interval seismic test was conducted in conjunction with the RotoSeis II seismic source at the NGES. Table 4.6 lists just of few of the tests that have been performed at the site that will be used later for comparison purposes. The relative locations of the tests are shown in Figure 4.13.

Table 4.5 Variation of index properties from the Auburn NGES (Schneider et al., 1999)

Property	Number of Tests	Average Value	Standard Deviation
Water Content, w_n (%)	64	34	7.5 %
Sand (%)	48	47	17 %
Silt (%)	22	33	8 %
Clay (%)	22	10	6 %
Liquid Limit, LL[1]	22	46	10
Plasticity Index, PI[1]	22	8	6
Unit Weight, γ_t (kN/m^3)	35	18.2	0.5

[1] LL and PI data do not include 20 tests, which were reported as "nonplastic"

Table 4.6 Pertinent tests for the Opelika test site

Sounding Name	Test Type	Seismic Method	Seismic Source	Probe	Data Source
OPELI2	SCPTu$_2$	Pseudo-interval	Electric AutoSeis, Sledgehammer	Hogentogler 10cm²	Georgia Tech
OPEAUT	SCPTu$_2$	Pseudo-interval	RotoSeis II	Hogentogler 10cm²	Georgia Tech
OPETRU	SCPTu$_2$	Pseudo-interval	Pendulum	Hogentogler 10cm²	Georgia Tech
OPETRUSEIS	Direct-push DHT	Frequent-interval	RotoSeis II, Pendulum	Biaxial true-interval seismic probe	Georgia Tech
S-R2 Array #2	Crosshole Seismic	CHT per ASTM D 4428	Borehole Packer	N/A	Georgia Tech (Kates, 1997)
AU-2	SDMT	Pseudo-interval	Sledgehammer	Pseudo-interval seismic DMT	Georgia Tech (Kates, 1997)
SASW-AL	Surface Wave	Multi-channel frequency sweep	Shaker	N/A	Georgia Tech (Rix, 1998)

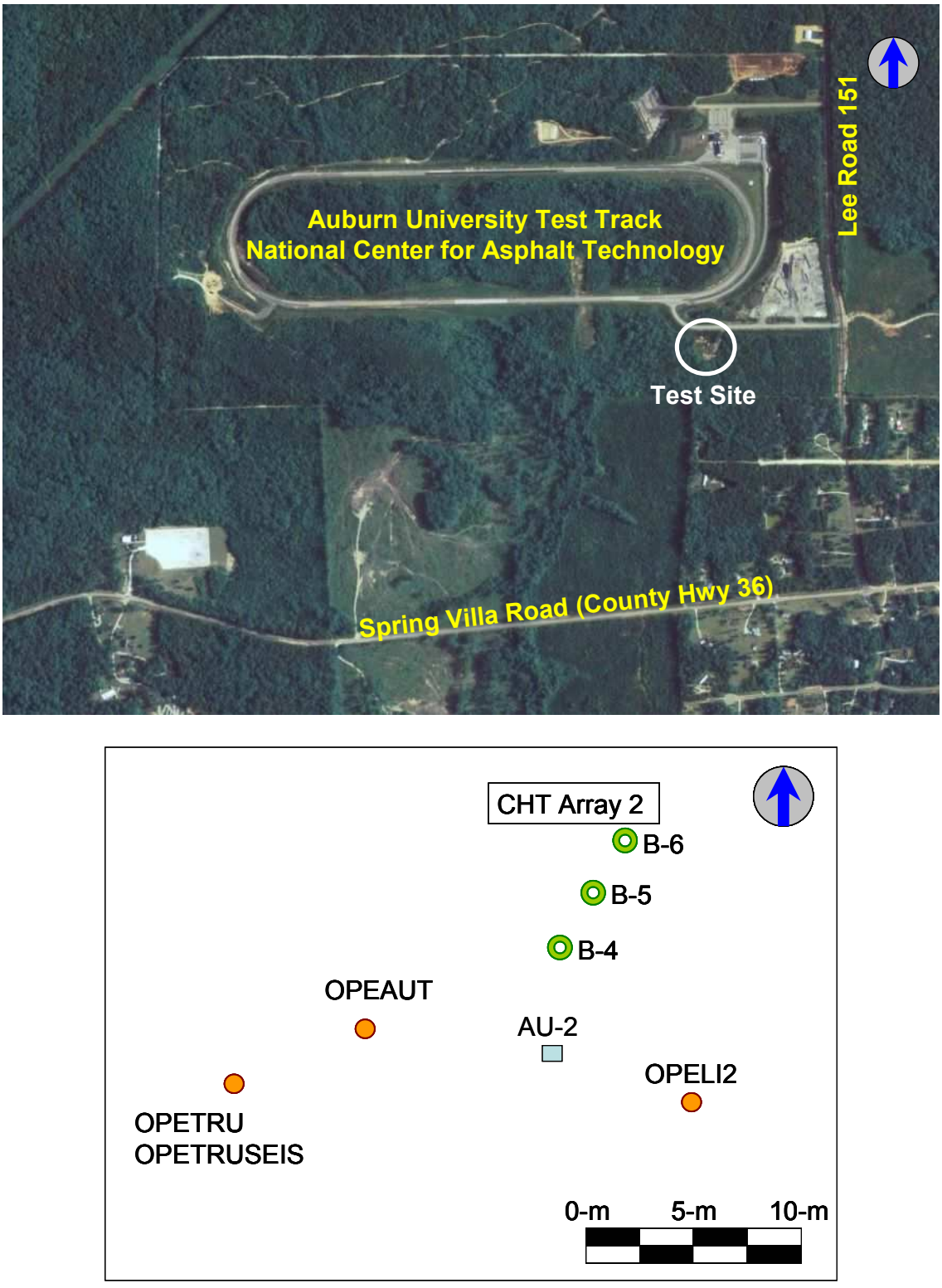

Figure 4.13 Locations of OPETRUSEIS and other compareable tests at the Opelika NGES test site in Alabama

The frequent-interval test OPETRUSEIS was performed to compare the RotoSeis II seismic source with the pendulum seismic source using the biaxial true-interval seismic probe, and to evaluate the frequent-interval velocity profile with respect to velocity profiles collected using other methods. The electromagnetic AutoSeis had been evaluated at this same site by Casey (2000) with the sounding OPELI2. Shear wave velocity results from cross-hole tests, surface wave tests, and early SDMT soundings, are also available at this location.

OPETRUSEIS, was preceded by a standard SCPTu2 (OPETRU), conducted using the Hogentogler cone and Hogentogler data acquisition with the pendulum seismic source. At the end of the SCPTu, the cone was removed and the biaxial true-interval seismic probe was pushed down the same hole. Pushing was stopped every 20 cm to measure V_S using both RotoSeis II under one leveling leg and the pendulum sledgehammer source under the other leveling leg (Figure 4.14). The probe was aligned so that the motion from the source would have equal strength in each component direction. Six channels of seismic data were recorded with the HP1432A signal analyzer. An extra geophone, mounted to the top of both sources, acted as a trigger for the data acquisition.

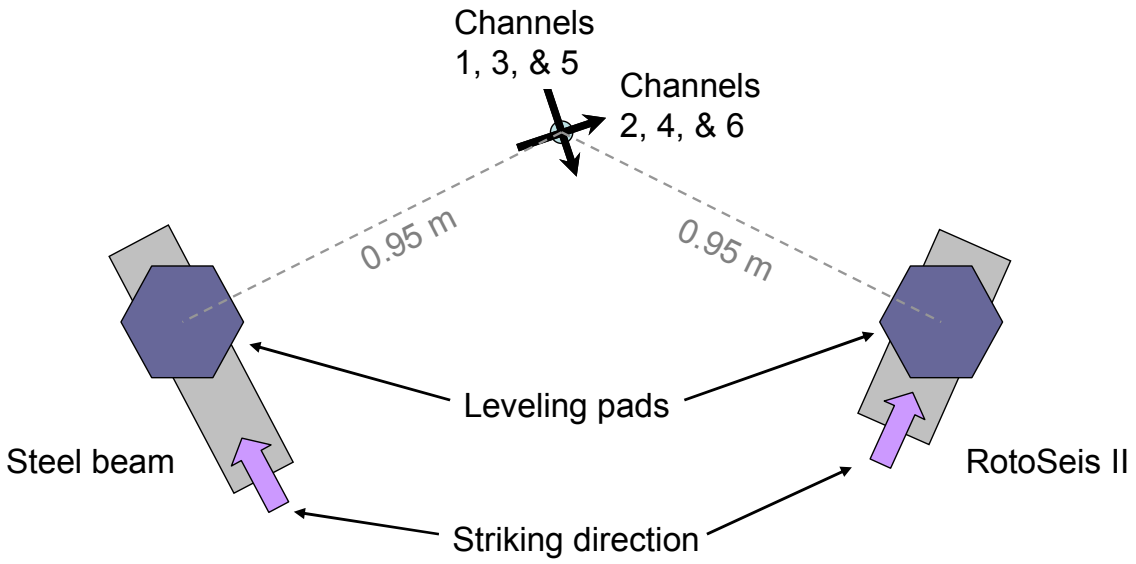

Figure 4.14 Alignment of biaxial true-interval seismic probe with the RotoSeis II and the pendulum seismic sources during the frequent-interval sounding OPETRUSEIS

Two crosshole tests were performed at the site, with the nearest comparable array being Array 2, consisting of three boreholes (B-4, B-5, and B-6). The boreholes were cased with PVC pipe, having 102 mm I.D, which were grouted in place with a cement-bentonite grout. The test was performed in accordance with ASTM D 4428.

A surface wave test was also performed at the site by Georgia Tech in the spring of 1997. The exact location was not recorded, but it is known to be within a few meters of the tests shown on the site map.

4.2.5. Johns Island, SC

Tests were conducted at the Stono Marina on Johns Island near Charleston, SC in order to evaluate the frequent-interval method, the continuous-push system, and the RotoSeis V seismic source. According to Camp (2004), the soils in the Charleston, SC area are made up from layers of alluvial and marine deposits of fine sands, silts, sandy clays, and clays to a depth ranging between 5 to 21 m. The underlying soil stratum is a deep carbonate deposit, referred to locally as the Cooper Marl. The Cooper Marl is often misclassified as a high plasticity clay, but the clay mineral content is actually less than 10%. The bulk of the material is calcium carbonate (50 to 80%) in the form of microfossils of marine organisms deposited during the Oligocene. The structure of the marl is made up of layers with varying degrees of cementation, having an open fabric, with void ratios between 1 and 2. The collapsible structure leads to the generation of characteristically large penetration porewater pressures during SCPTu, between 15 to 30 atmospheres, as in Figure 4.15 for example. A thorough examination of the Cooper Marl can be found in Camp (2004).

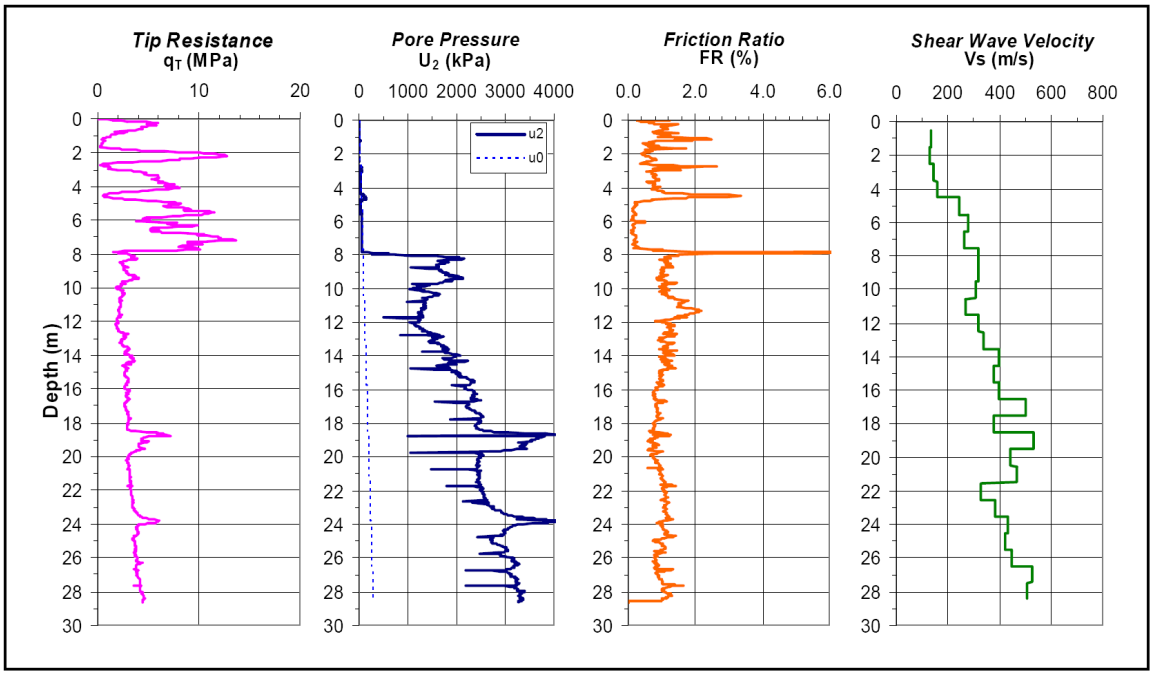

Figure 4.15 Representative profile by SCPT in the Charleston, SC area (Camp, 2004)

Andrus et al. (2006), compiled in-situ soils data from research and consulting activities in and around Charleston, in order to determine liquefaction susceptibility for the region. The test locations for the data base are superimposed on a geologic map in Figure 4.16. The locations of the Stono Marina tests correspond to the black dots immediately west of the intersection of -80° longitude and 32.75° latitude. Based on the map, the geologic unit is Qht, which is described by the authors as predominantly soft clayey soils between 5,000 and 10,000 years old.

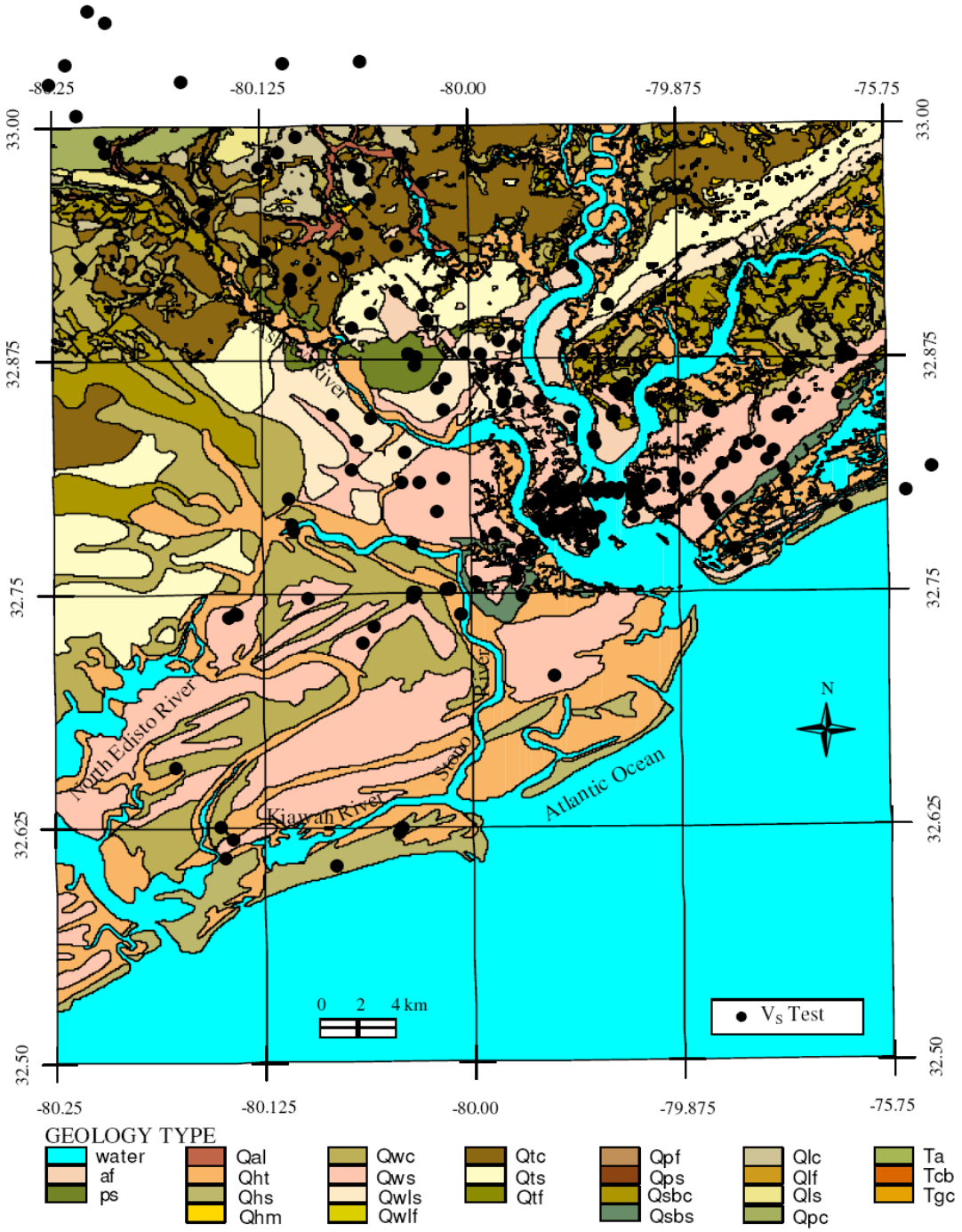

Figure 4.16 Geologic map of the Charleston area with superimposed shear wave velocity test locations used to evaluate earthquake site response and liquefaction potential for the region (Andrus et al., 2006)

One frequent-interval sounding and one continuous-push seismic sounding were performed at the Stono Marina site on Johns Island. Previous testing at this site includes a standard SCPTu (STON1A) and a deep downhole velocity test in a borehole (Table 4.7). The relative locations of tests performed at this site can be seen in Figure 4.17.

Table 4.7 Pertinent tests for the Stono Marina test site

Sounding Name	Test Type	Seismic Method	Seismic Source	Probe	Data Source
STON1A	$SCPTu_2$	Pseudo-interval	Sledgehammer	Hogentogler 10cm²	Georgia Tech
STONOSEIS	Direct-push DHT	Frequent-interval	Sledgehammer	Biaxial true-interval seismic probe	Georgia Tech
STONO01	$CPTu_2$	None	None	Hogentogler 10cm²	Georgia Tech
STONO01SEIS	Direct-push DHT	Continuous-push frequent-interval	RotoSeis V	Biaxial true-interval seismic probe	Georgia Tech
PS-1	Borehole DHT	Pseudo-interval	Sledgehammer and wood beam	BHG-2 triaxial geophone	S&ME

Figure 4.17 Test locations at the Stono Marina test site on Johns Island, SC

The true-interval biaxial seismic probe was used to measure frequent-interval shear wave velocities (STONOSEIS) near the location of a previous conventional SCPTu, STON1A (Figure 4.18). Penetration was halted in 20 cm increments to measure V_S. During each pause, a single shear wave impulse was recorded. At one meter breaks between rods, four signals were recorded, two left-strikes and two right-strikes. The sledgehammer source was used to generate the shear waves. Seismic signals were recorded using the Agilent 1432A signal analyzer connected to a notebook computer. The probe was aligned with the steel beam so that the signal strength detected by the odd-numbered channels would be equal to that recorded by the even-numbered channels (Figure 4.19).

Figure 4.18 Testing at the Stono Marina with the true-interval biaxial seismic probe and sledgehammer source during STONOSEIS

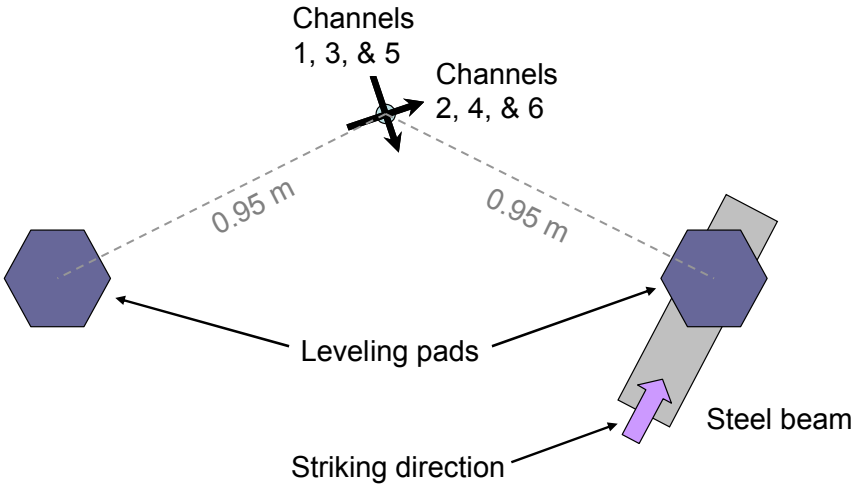

Figure 4.19 Alignment of the biaxial true-interval seismic probe with the sledgehammer source during the frequent-interval test STONOSEIS

During a subsequent field visit, the CPTu STONO01 was performed, followed by the continuous-push seismic test STONO01SEIS with the RotoSeis V seismic source, which was pushed in the same hole (Figure 4.20). The CPTu was performed with the Hogentogler 10 cm² penetrometer and Agilent 34970A data acquisition unit connected to a notebook computer. After the Hogentogler cone was removed, the larger diameter biaxial true-interval seismic probe was pushed in the same hole. The probe was aligned with the seismic source so that channels 1 through 5 were roughly parallel to the source and channels 2 through 6 were approximately perpendicular (Figure 4.21). The seismic probe was advanced at 2 cm/sec, monitoring depth with the Agilent 34970A. Seismic signals were recorded separately with the Geometrics Geode seismograph connected to the same notebook computer. The biaxial true-interval seismic probe contains six geophones, but the Geode was configured to read only four channels. The middle pair of geophones was excluded and only the upper pair (1 and 2) and lower pair (5 and 6) were monitored. Both the depth readings from the Agilent 34970A and the seismic recordings from the Geode were time-stamped for synchronizing each seismic record with a specific depth. During the test, the depth was displayed on the computer screen along with momentary snapshots of the seismic signals as they were recorded. RotoSeis V was set to generate shear waves every 10 seconds, or approximately every 20 cm of penetration. Seismic signal recording continued at 10 second intervals even while the penetration was halted between rod breaks.

Other data available at this site for comparison include a previous SCPTu (STON1A) as well as a deep downhole test (PS-1) in which shear wave velocity was measured in a borehole.

Figure 4.20 STONO01SEIS testing in progress with the RotoSeis V seismic source

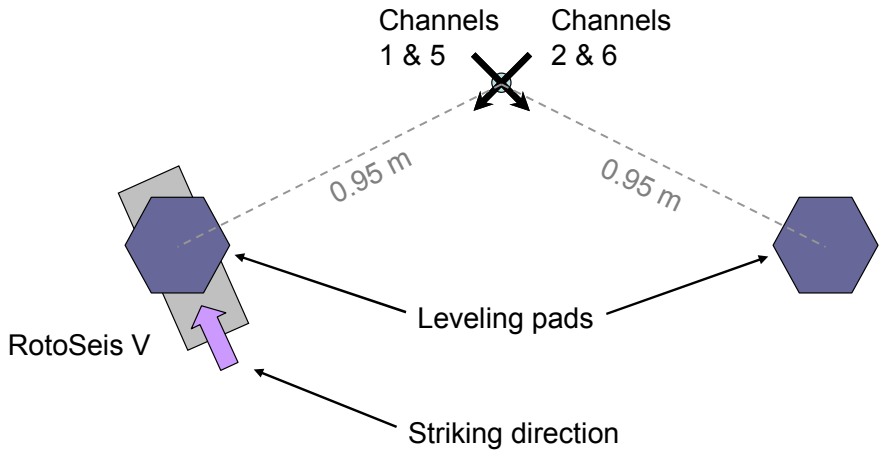

Figure 4.21 Alignment of the biaxial true-interval seismic probe with the RotoSeis V during the continuous-push seismic sounding STONO01SEIS

4.2.6. Mt. Pleasant, SC

The new Cooper River Bridge, named the Arthur Ravenel Bridge, connects the town of Mt. Pleasant with the city of Charleston, SC. The bridge was dedicated and opened on July 16, 2005. The local surface soils on the Mt. Pleasant end of the bridge are made up of predominately sandy sediments with interbedded clays between 70,000 to 130,000 years old (according to Figure 4.16 and Andrus et al. (2006)). As with the Stono Marina site and the rest of the Charleston, SC region, the site is underlain at depth by the Cooper Marl described in the previous section. Tests were performed at the site to evaluate both the RotoSeis V and the Commercial RotoSeis and also to evaluate the continuous-push seismic system. Table 4.8 lists the pertinent tests performed including 3rd party tests from the same site. The relative locations of the tests are shown in Figure 4.22.

Table 4.8 Pertinent tests at the Cooper River Bridge site

Sounding Name	Test Type	Seismic Method	Seismic Source	Probe	Data Source
CRBDH1	SCPTu$_2$	Pseudo-interval	Pendulum	Hogentogler 15cm²	Georgia Tech
CRB01	CPTu$_2$	None	None	Hogentogler 10cm²	Georgia Tech
CRB01SEIS	Direct-push DHT	Continuous-push frequent-interval	RotoSeis V	Biaxial true-interval seismic probe	Georgia Tech
CRB02	CPTu$_2$	None	None	Hogentogler 10cm²	Georgia Tech
CRB02SEIS	Direct-push DHT	Frequent-interval	Sledgehammer	Biaxial true-interval seismic probe	Georgia Tech
CRB03	SCPTu$_2$	Continuous-push pseudo-interval	Commercial RotoSeis	Hogentogler 10cm²	Georgia Tech
CRB03SEIS	Direct-push DHT	Continuous-push frequent-interval	Commercial RotoSeis	Biaxial true-interval seismic probe	Georgia Tech
DS-1	Borehole DHT	Pseudo-interval	Sledgehammer and wood beam	BHG-2 triaxial geophone	S&ME
MP-5	Suspension Logger	True-interval	Self-contained	P-S Logger tool	S&ME

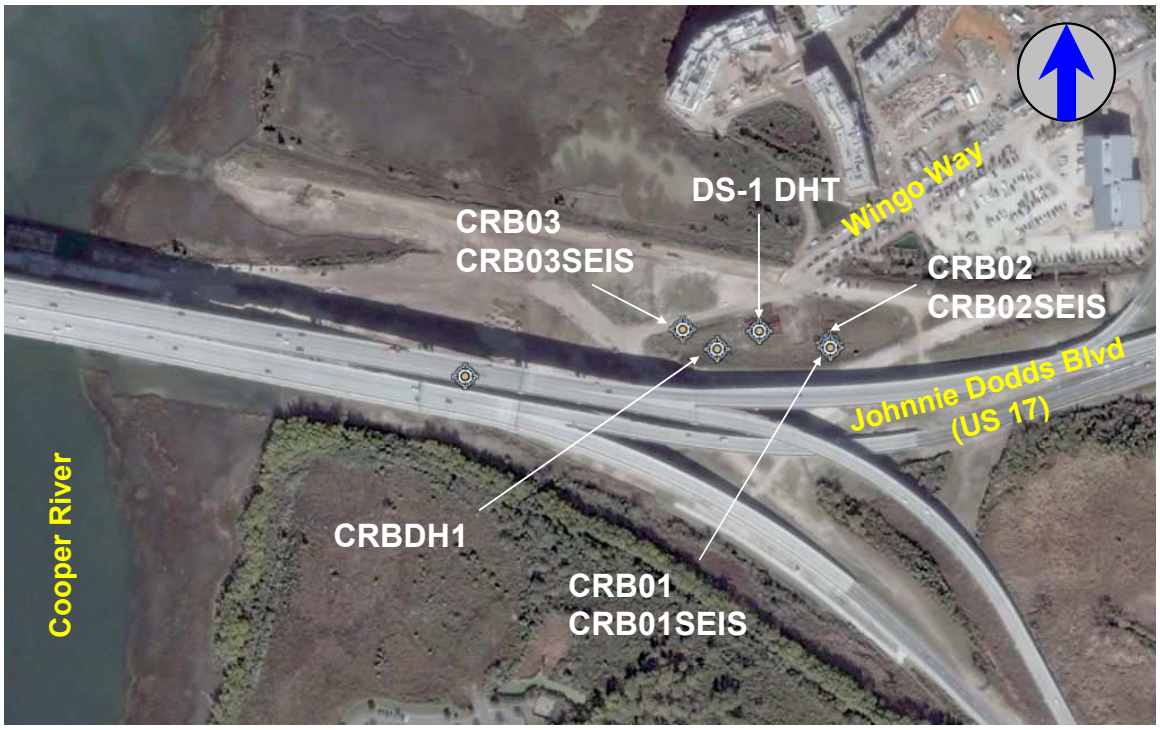

Figure 4.22 Relative test locations for the Cooper River Bridge test site

Both a CPTu and continuous-push seismic sounding (CRB01 with CRB01SEIS) were performed utilizing the same procedures and equipment as for STONO01 and STONO01SEIS at the Stono Marina on Johns Island. At the beginning of the push, the biaxial true-interval seismic probe was aligned so that channels 2 through 6 were parallel with the RotoSeis V and channels 1 through 5 were perpendicular to the source (Figure 4.23).

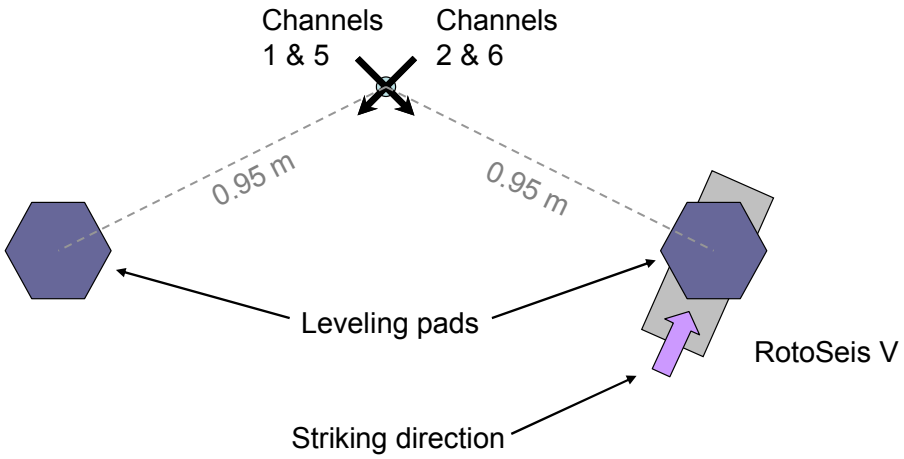

Figure 4.23 Alignment of biaxial true-interval seismic probe with the RotoSeis V seismic source during the continuous-push and continuous-pull seismic sounding CRB01SEIS

At another location, a CPTu and a stationary-receiver frequent-interval seismic test (CRB02 with CRB02SEIS) were performed with a sledgehammer seismic source. After completion of the CPTu, the biaxial true-interval seismic probe was pushed down the same hole. The sensors of the seismic probe were initially aligned with channels 1 and 5 roughly parallel to the steel beam and channels 2 and 6 approximately perpendicular to the beam (Figure 4.24). Frequent-interval seismic measurements were made using the sledgehammer seismic source to record every 20 cm, as well as at one meter intervals during rod breaks.

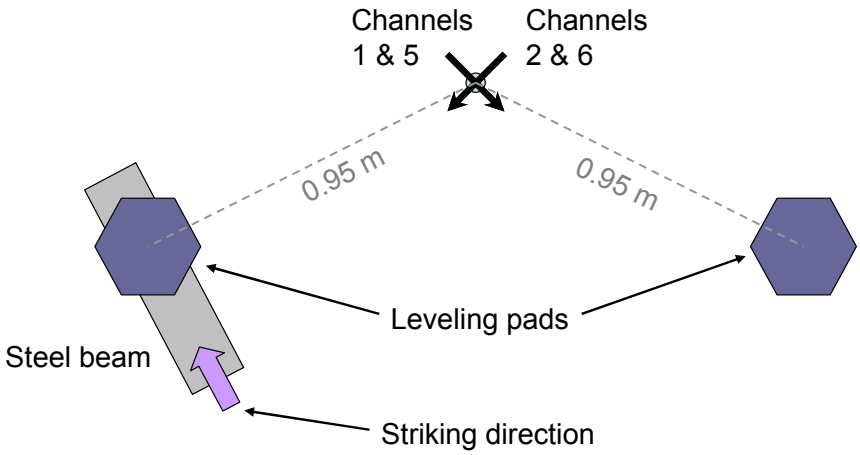

Figure 4.24 Alignment of the biaxial true-interval seismic probe with the steel beam during the continuous-pull portion of the seismic test CRB02SEIS

During a subsequent visit to the site, a continuous-push pseudo interval seismic test (CRB03) was performed with the Hogentogler 10 cm² cone and the Commercial RotoSeis seismic source (Figure 4.25). Although a pseudo-interval device is not recommended for continuous-push systems, the purpose of the test was to demonstrate the feasibility of recording seismic signals simultaneously with slower CPT channels from the same device. The Agilent 34970A was used to monitor the depth and record tip, sleeve, porewater pressure, and inclination channels, while the National Instruments CompactDAQ system recorded seismic signals from the horizontal geophone included in the Hogentogler cone. The Commercial RotoSeis was set to operate continuously, delivering hammer strikes every 10-s, which corresponds to 20 cm of separation between seismic signals during penetration. The recording settings of the CompactDAQ were configured for investigating the effect of non-stationary receivers on the seismic data. Long pre-trigger scan times were incorporated so that the "noise-only" signal, geophone response prior to hammer-impact, would be captured in the first half of the recording, and the seismic source signal would be captured in the second half.

Figure 4.25 Continuous-push seismic cone penetration testing at the Cooper River Bridge during CRB03

Following the completion of CRB03, another continuous-push seismic sounding, CRB03SEIS was performed in order to characterize the multi-dimensional appearance of the Commercial RotoSeis source wavelets, and to measure continuous-push V_S. As before with STONO01/STONO01SEIS, CRB01/CRB01SEIS, and CRB02/CRB02SEIS, the biaxial true-interval seismic probe was pushed down the same hole left by the smaller diameter Hogentogler cone during the previous sounding CRB03. During rod breaks, the source continued to operate while the next rod was added. This provided opportunities to obtain duplicate strikes for use in evaluating the consistency of the source signals, as well as to compare signals recorded with non-stationary receivers with typical signals recorded with stationary receivers.

The Georgia Tech cone truck is a light weight rig which relies on earth anchors to provide the necessary reaction force required for pushing the probes into the ground. However, the anchoring system is not rigid. As penetration force increases, the leveling pads lift up off the ground as the anchors pull out of the ground slightly, reducing or

eliminating the normal force applied to the seismic source. During conventional seismic testing with stationary receivers, the load on the probe rods can be released, lowering the leveling pads back to the ground. The seismic source could not be placed under the leveling pad for continuous-push testing. For the continuous-push soundings CRB01SEIS and STONO01SEIS, the source was placed under the leveling pad, but the tests were shallow and the soils were soft, so the truck did not lift completely off of the source.

For the deeper CRB03/CRB03SEIS soundings, the solution to the problem was to place the source on the ground away from the cone truck and anchor it to the ground in the same way that the cone truck is anchored. Small earth anchors available from the hardware store were installed on either side of the source. A cross-beam attached to the anchors could then be tightened down on top of the source in order to apply the normal force on top of the source. At the Cooper River Bridge test site, the surficial sand proved to be too much for the anchors to penetrate fully, so shims had to be inserted to allow confinement of Commercial RotoSeis. The anchored source is shown in Figure 4.26 and the source layout relative to the biaxial seismic probe is shown in Figure 4.27.

Data available for comparison, collected on previous visits, include $SCPTu_2$ CRBDH1 and $SCPTu_1$ CRBDH3. The site investigation program conducted prior to construction of the new bridge also provides additional data for comparison, including commercial DMT, SCPTu results, borehole downhole shear wave velocities, and PS-Logger shear wave velocities.

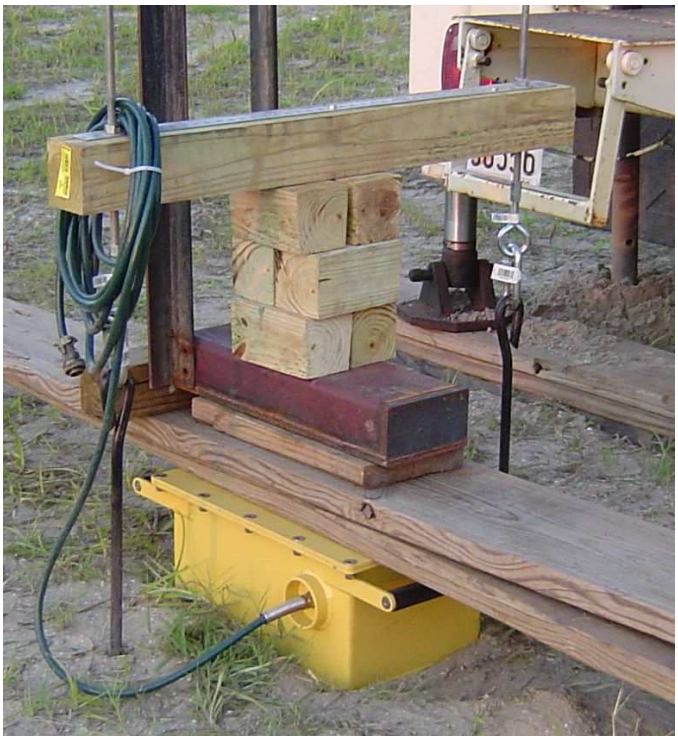

Figure 4.26 Commercial RotoSeis coupled to the ground behind the cone truck using earth anchors and a cross-beam

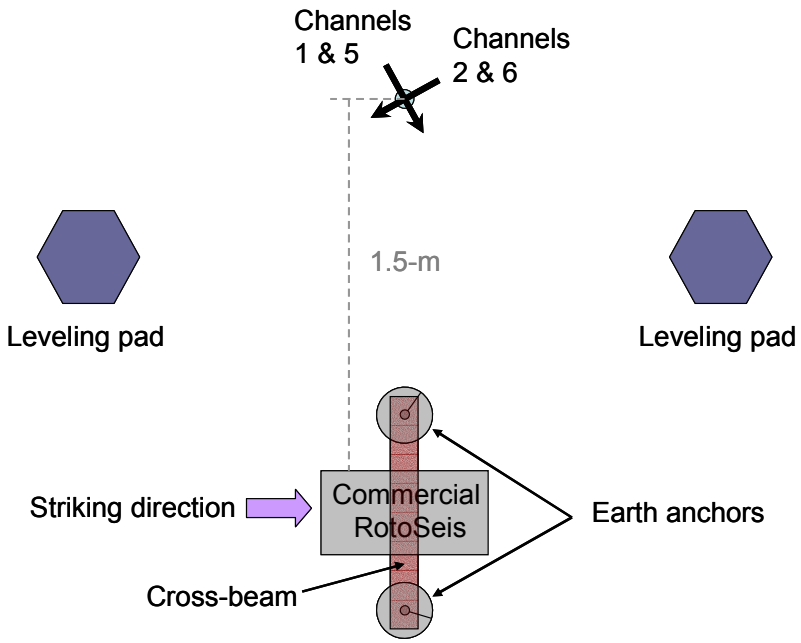

Figure 4.27 Alignment of biaxial true-interval seismic probe with the Commercial RotoSeis during the continuous-push seismic sounding CRB03SEIS

4.2.7. New Orleans, LA

The final Georgia Tech RotoSeis prototype (RotoSeis V) was utilized during commercial SCPT site characterization in New Orleans, LA. During a pseudo-interval sounding, RotoSeis V was successfully tested to 30 m, which was the intended design depth. The results of NEWOR01 are presented in Figure 4.28 to illustrate the site conditions. The shear waves generated by the RotoSeis V are discussed in Chapter 5 (Section 5.5.5). At this particular site, the upper 5 m is compacted fill material, sitting on top of natural peat and organic marsh soils over low plasticity clay from 8 to 14 m. Below 14 m, predominately loose to firm sands are encountered with occasional silty lenses.

Table 4.9 Test information for sounding in New Orleans using RotoSeis V

Sounding Name	Test Type	Seismic Method	Seismic Source	Probe	Data Source
NEWOR01	$SCPTu_2$	Pseudo-interval	RotoSeis V	Hogentogler 10cm²	Southern Earth Sciences

A standard SCPTu (NEWOR01) was performed by Southern Earth Sciences, Inc. with a Hogentogler 10 cm² digital cone system and the RotoSeis V (Table 4.9) and a 200 kN capacity tracked CPT rig manufactured by Hogentogler, shown in Figure 4.29. The shear wave velocity profile was measured at 1 m intervals between rod breaks using the pseudo-interval method. The source was coupled to the ground by one of the tracks of cone rig (Figure 4.30).

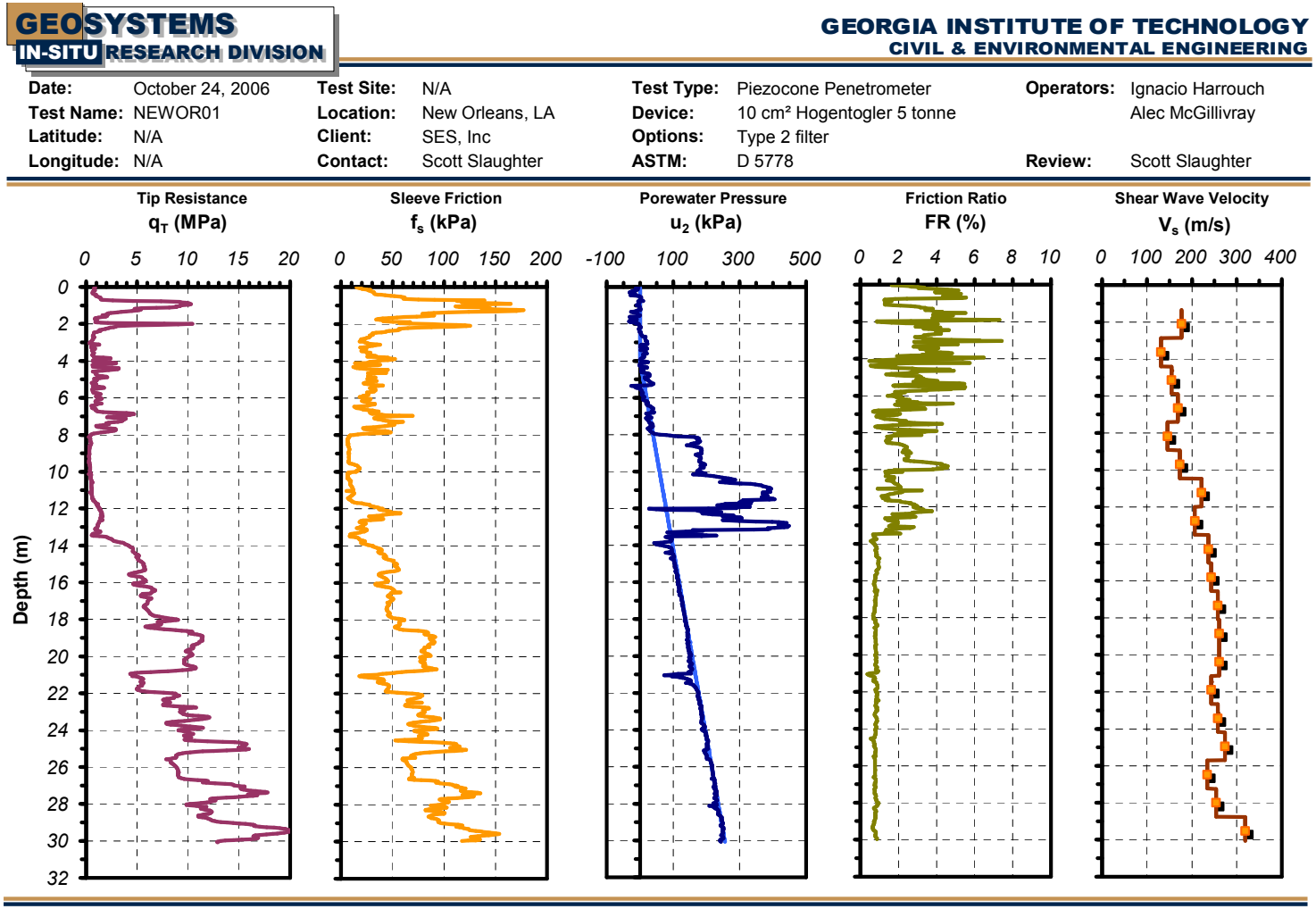

Figure 4.28 SCPTu profile NEWOR01 performed by Southern Earth Sciences, Inc. at the New Orleans test site

Figure 4.29 Southern Earth Sciences, Inc. track-mounted CPT rig

Figure 4.30 RotoSeis V coupled to the ground surface under the tracks of the CPT rig

4.2.8. St. Paul, MN

Field demonstrations of the Minnesota Department of Transportation in-situ testing equipment were conducted during a training course in St. Paul, MN. The testing took place under the I-35E overpass next to the Cayuga Pedestrian Bridge. Based on borings logs from the site, the upper 3 m consists of layered sand and gravelly sand mixtures. Below the sand and gravel is a peat layer more than 18 m thick. Nearest the surface, the peat is fibrous, and below a depth of 4 m the peat becomes more decomposed. The moisture content of the peat is around 200% with unit weights as low as 11 kN/m³. Peat is a rather unusual soil type due to its organic and fibrous contents, exhibiting relatively high friction angles and high compressibility parameters. For research dealing with peat deposits having similar properties see Boulanger et al. (1998), Kramer (2000), and den Haan and Kruse (2006).

Figure 4.31 MNDOT fleet of 3 Vertek CPT rigs

MNDOT has a fleet of three Vertek CPT rigs: one tracked rig, and two truck rigs (Figure 4.31). The biggest of the three Vertek rigs is equipped with a truck-mounted hydraulic seismic source. Using this rig, a conventional SCPTu test was performed in order to evaluate the testing procedures and make recommendations, as well as obtain recordings with the Vertek hydraulic source for comparison with the RotoSeis seismic source. Shear wave signals generated by the hydraulic seismic source were recorded with a Vertek 15 cm² pseudo-interval seismic cone. Table 4.10 lists information about the sounding. Other soundings were performed with the other rigs as part of the field demonstration, including multiple CPT soundings and a DMT, but they are not directly significant to this research effort.

Table 4.10 Test information for SCPT sounding conducted with a Vertek truck-mounted hydraulic source in St. Paul, MN

Sounding Name	Test Type	Seismic Method	Seismic Source	Probe	Data Source
F22Y0703C	$SCPTu_2$	Pseudo-interval	Vertek Hydraulic	Vertek 15cm²	MN DOT

The hydraulic source is configured for generating alternate sets of left- and right-strikes. MNDOT standard procedure is to record a left and right strike at each test depth, storing only one of the two biaxial horizontal geophone channels for each strike. At each test depth a left- strike was initiated and saved using the Channel S2 geophone. Then a right-strike was initiated, and again the Channel S2 geophone record was saved. Figure 4.32 shows the experimental test set-up. The axes of the seismic sensors are not marked on the outside of the probe, so the orientation was determined from post-processing, which is described in Chapter 5.

Although the data from the second horizontal geophone is usually discarded, in this instance, the Channel S1 geophone record corresponding to the right-strike was also saved. The sounding was performed in this way in order to capture the biaxial wave form characteristics of the hydraulic source. During the classroom session of the training course, the multi-dimensional source waves were presented, demonstrating the need to align the source with one of the horizontal receivers.

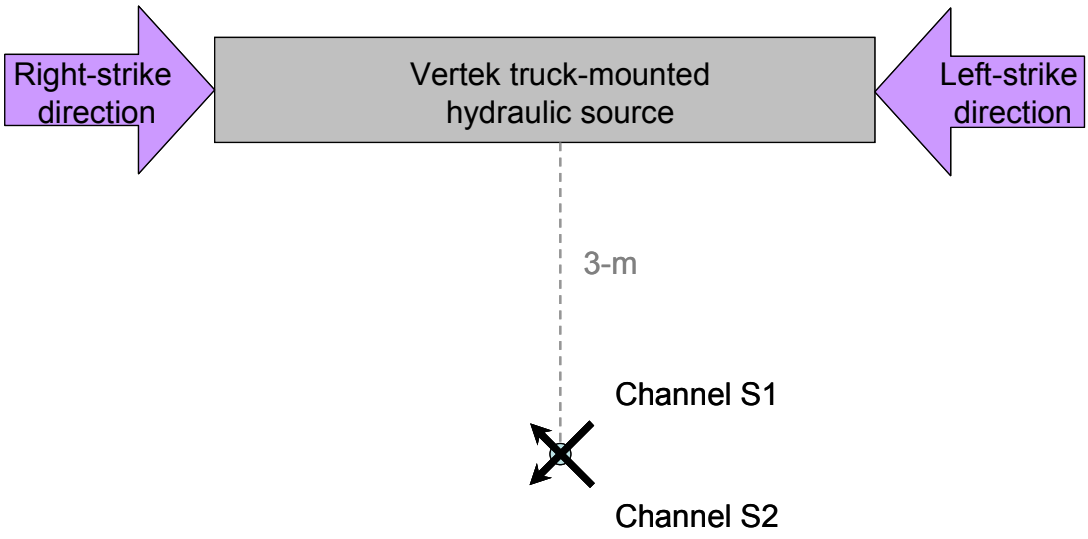

Figure 4.32 Alignment of biaxial pseudo-interval Vertek 15cm² seismic cone with the Vertek truck-mounted hydraulic source during the F22Y073C sounding

The results of the SCPTu sounding are shown in Figure 4.33. The u_2 porewater pressure data has a saw-toothed appearance due to air trapped in the cavity of the cone. This was part of the discussion during the short course related to identifying problems with field data. The cone tip resistances in the peat are extremely low, less than 1 MPa. The V_S values are also extremely low in the peat layer, at times less than 50 m/s.

There are two V_S profiles shown in the results. The points marked with circles were determined using the outdated first cross-over method of analysis which required that an extra source event (conventional paired left- and right-strikes) be captured at each

depth. The values marked with square points were determined from the cross-correlation analysis method. Only one signal is required at each depth, streamlining the field procedures. The left-strikes near the surface were saved incorrectly and as a result the first cross-over analysis gave flawed results initially.

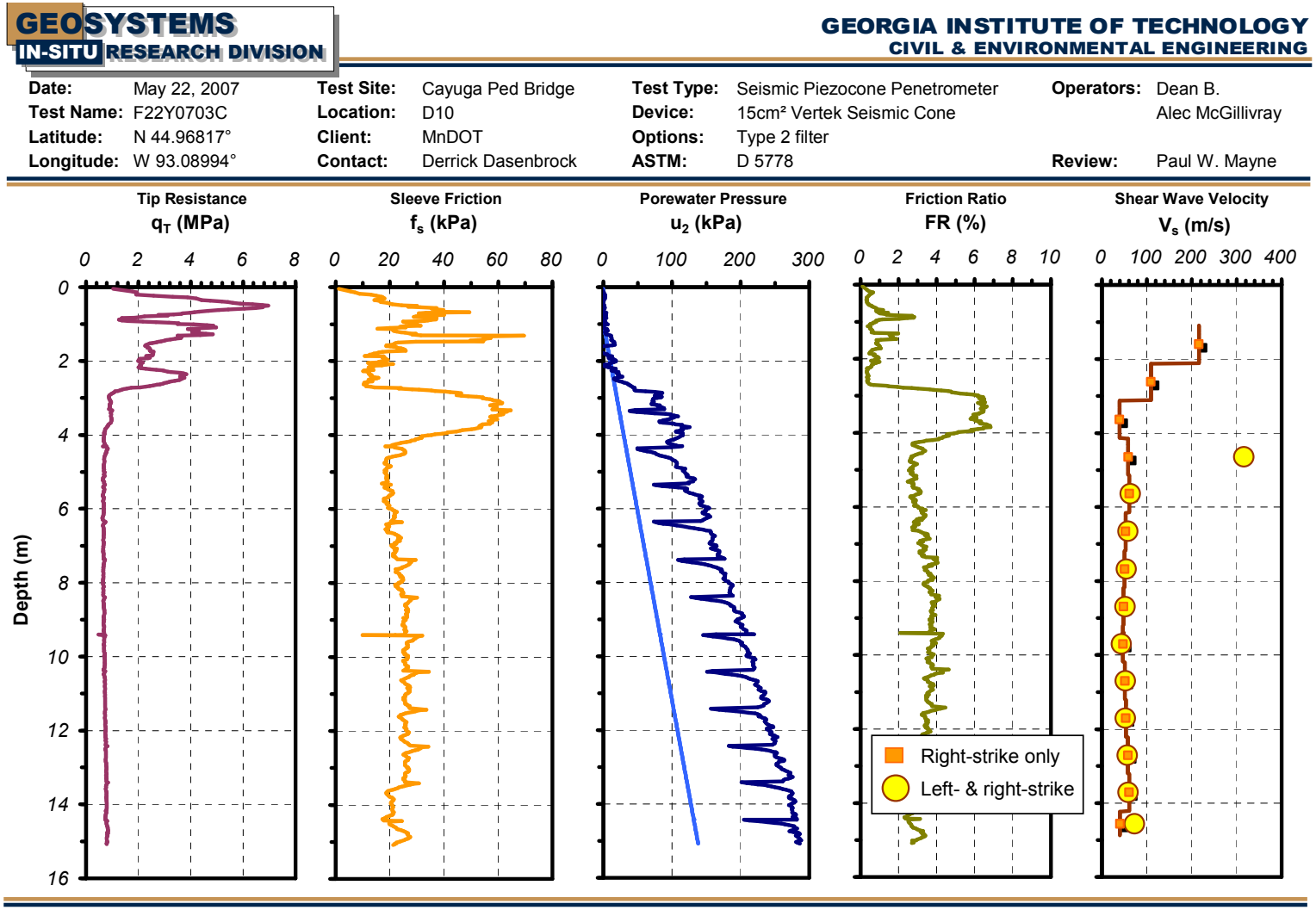

Figure 4.33 SCPTu profile F22Y0703C from the Cayuga Pedestrian Bridge test site in St. Paul, MN with V_S determined from traditional left- and right-strikes compared to V_S from just a single right strike at each depth

4.3. Summary

During this research effort, a total of 16 test sites were visited in Venice, ITA, GA, AL, SC, IL, LA, TN, and MN. The field work comprised 54 separate soundings that were performed for the evaluation of surface-generated sources, seismic probes, geophone configurations, data acquisition systems, and seismic testing methods. During this time, the testing progressed from conventional sledgehammer seismic sources and single-axis receivers to investigations of a fully automated frequent-interval continuous-push seismic system with the RotoSeis automated seismic source and biaxial true-interval probe. Of the initial 16 sites, 8 have been selected as primary test sites for detailed analyses to evaluate the testing methods and devices. These primary sites also provided results from other test methods (i.e. crosshole, downhole, reflection, refraction, surface wave, suspension logger, etc.) for comparison of shear wave velocity profiles with new methods under study.

5. EVALUATION OF SIGNALS FROM A CONTINUOUS-PUSH SEISMIC SYSTEM

5.1. Introduction

With conventional SCPT and SDMT methods, V_S is measured from time differences between seismic signals recorded by stationary receivers during breaks between rods, at progressively greater depths. The average velocity for the interval between receivers is determined from the distance traveled by the shear wave through that interval divided by the travel-time difference between the receivers. A continuous-push seismic system has been proposed which would reduce field testing times while simultaneously allowing an increased number of V_S measurements to be made during penetration.

The frequent-interval method was introduced as a means to improve the resolution of downhole shear wave velocity profiles by using overlapping true-interval measurements (Chapter 3). The components of a continuous-push system, which has been developed for this research, include the RotoSeis automated seismic source, the true-interval seismic probes and attachments, and the automated data acquisition.

This chapter discusses the effects that the characteristics of the seismic source have on the recorded shear waves, and provides an evaluation of the RotoSeis automated seismic source. The shear wave signals recorded with stationary receivers are compared to shear waves recorded with non-stationary receivers of a continuous-push seismic system. Ultimately, the velocity results obtained from a sounding with a continuous-push system are compared to results obtained during a frequent-interval test with stationary receivers.

5.2. Signal Appearance

Recorded seismic signals may not always have the expected appearance of shear waves resulting from an impulse-type seismic source. Often, there are peaks and valleys and disturbances that distort or obscure the arriving impact wavelets. In order to determine the travel-time differences between recordings, the appearance of the shear wave within each signal must be clearly identifiable and similar in appearance from one recording to the next.

In practice, any feature of the signal that deviates from the familiar source wavelet is regarded as noise. The actual reasons for the distortion of the signals during a test often remain unknown by the operator. Unexpected features in the seismic recordings can be attributed to several sources such as the data acquisition device, electromagnetic interference, ambient vibrations, mismatched sensors, reflected seismic source energy, and misaligned sensors. Moreover, for the continuous-push signals, frictional vibrations from the probe penetrating through the soil, as well as vibrations from the pushing system itself can also contribute to signal distortion.

Shear wave amplitude attenuates with depth, making the signals more susceptible to contamination from noise. For this research, the approach of increasing the source amplitude relative to noise levels is limited because of the design requirements that RotoSeis remain a portable device. Therefore, in order to maximize the quality of the recorded signals, care must be taken to minimize the appearance of noise and maximize the appearance of the shear wave component.

5.2.1. Sensor performance and position

Unmatched seismic sensor characteristics can cause differences in signal appearance between receivers. The geophones utilized in each of the seismic cones/seismic probes/seismic modules utilized in this research are all of the same type, (i.e., GeoSpace, LP model GS-14-L3 as described in Chapter 3). In order to verify the

similarity between the these geophones, and to evaluate the effect, if any, of the relative position of the receivers within the probe, signals obtained from different source events were compared at duplicate sensor depths. In Figure 5.1, a comparison between geophones of the biaxial true-interval seismic probe demonstrates the similarity of receiver responses. Channel 5 (near the probe tip) and Channel 1 (near the top of the probe) are superimposed at identical receiver depths. The signals were recorded during CRB02SEIS utilizing the sledgehammer seismic source while the probe was stationary.

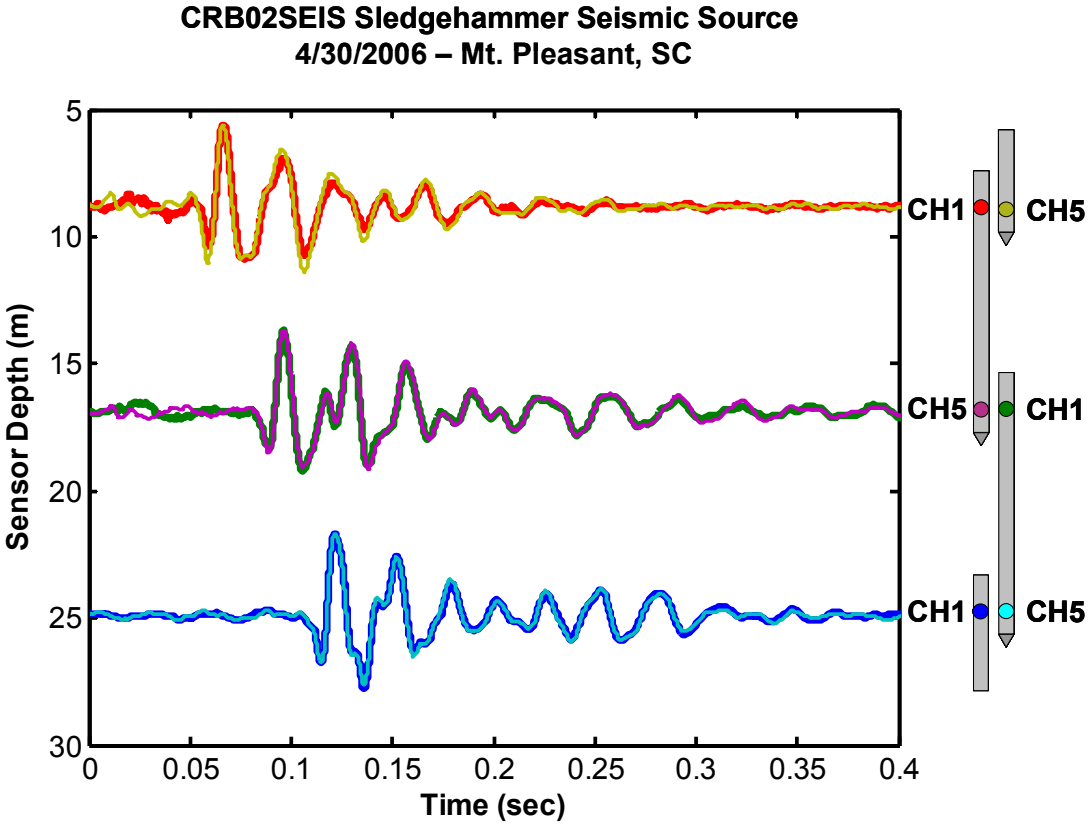

Figure 5.1 Comparison of recorded signals from biaxial true-interval probe geophones in the Channel 1 and Channel 5 positions for the same sensor depths (9 m, 17 m, and 25 m) to investigate the effect of position of the geophones within the probe

5.2.2. Sensor alignment

For each of the three sensor position depths shown in Figure 5.1 (i.e., one shallow, one mid-depth, and one deep), the output of the Channel 1 geophone at depth is nearly identical to the recording of the Channel 5 geophone when positioned at the same depth. The geophone characteristics appear to be matched and the signals are not affected by the position of the receivers within the probe. Even though there is a subtle change in appearance of the signals with depth, they are essentially identical for any particular depth. These results also call attention to the repeatability from the sledgehammer source in this instance.

The biaxial true-interval seismic probe detects particle motions in two horizontal component directions. If the receiver properties are matched, the responses should be able to be combined together to reveal multi-dimensional motion. In Figure 5.2, Channel 1 and Channel 2 are plotted together with time and overlaid by the combination of Channel 5 and Channel 6 which have been recorded at the same sensor depth.

Though the seismic source acts in a single direction, the resulting particle motions are not confined to the plane of the source alignment. Off-axis impacts may further exaggerate the out-of-plane motion, and create a more rounded spiral signal. It is not possible for a single-axis receiver to capture the full source signal. However, the majority of V_S analysis methods utilize only a single component. Therefore, it is important to align one of the axes with the primary direction of the shear wave motions.

Another way to visualize the directionality of shear wave particle motions is by plotting the x-direction horizontal component versus the y-direction component without time, to create a hodograph. This type of plot is equivalent to viewing the particle motions in plan view from the surface, with the center of the plot being the center of the probe rods. Figure 5.3 contains three hodographs of the same signals previously presented in Figure 5.1. When the component sensors are combined, changes in signal appearance with depth are more pronounced, but the signal is still consistent between sensor pairs and source events.

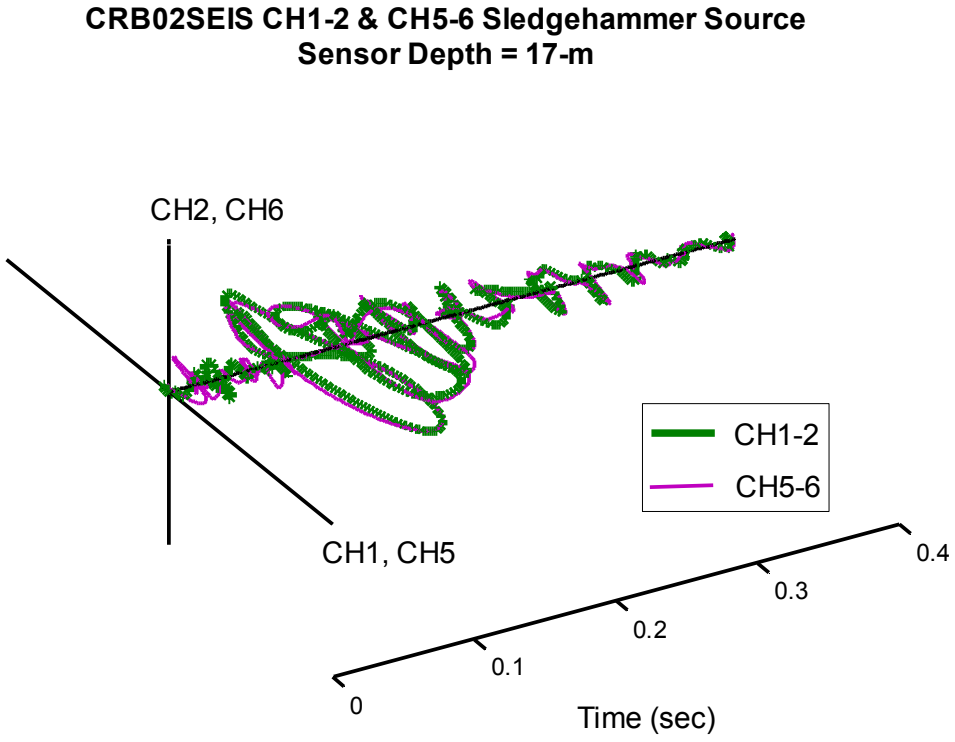

Figure 5.2 Combination of biaxial signal components Channel 1 with 2 and Channel 5 with 6 for to form a 3-dimensional view of the time history of two signals recorded at a sensor depth of 17 m

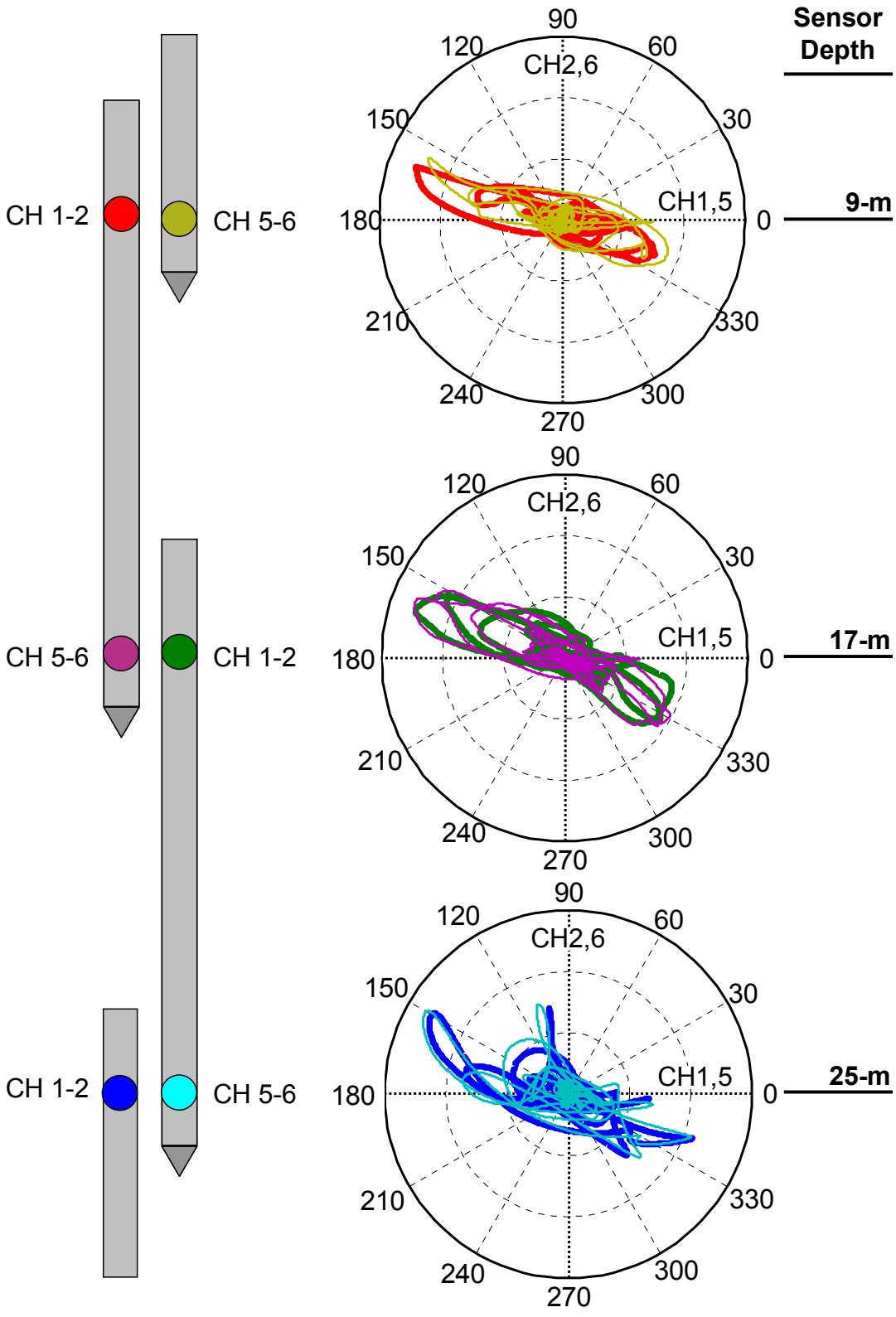

Figure 5.3 Hodographs of Channel 1-2 and Channel 5-6 pairs at three sensor depths to investigate effect of sensor position on the 2-dimensional shear wave signals

For a directional seismic source, the hodograph shows the source direction relative to the receiver orientation. If the rods rotate during the sounding, the hodograph will reveal the rotation. Even though neither component direction of CRB02SEIS was perfectly aligned with the direction of the seismic source, it is possible to re-project the results to obtain a resultant signal component aligned in the optimal direction, or any other angle.

The issue of source-receiver alignment is critical for tests performed with single axis seismic probes. Even for tests utilizing multi-axis seismic devices, the results may be affected by failure to account for misalignment. Signal quality will suffer if the sensors are not oriented to maximally capture the source wave. For the 9 m sensor depth of CRB02SEIS, the best and worst alignment possibilities are shown in Figure 5.4 to illustrate the possible extremes of orientation influence on signal quality. The upper signal is projected at the optimal angle for this particular record, -20°, and projected again in the lower signal at the angle most perpendicular to the particle motion, 70°. For the optimally-oriented signal component, the shear wave is clearly visible. The lower signal, resulting from the projection at the worst possible angle, is derived from the same original components as the upper signal, yet the shear wave is invisible within the background vibrations.

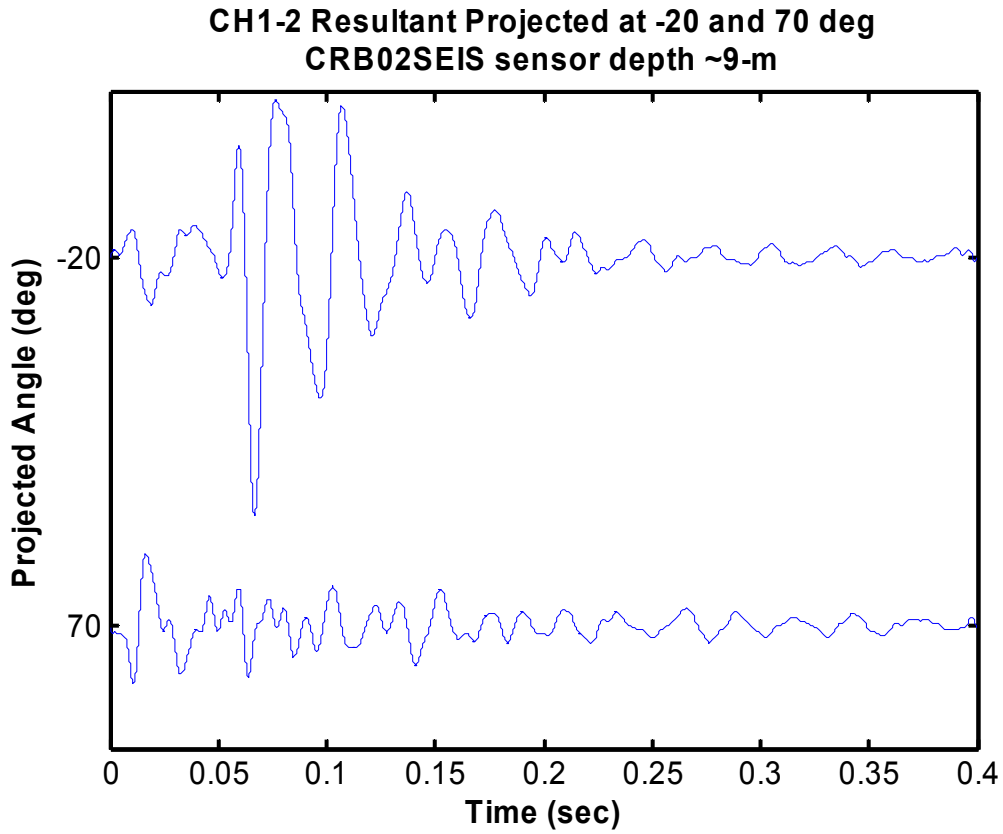

Figure 5.4 Maximum and minimum amplitude single-axis shear wave signals computed from the combination and projection of Channels 1 and 2 showing: (a) upper trace: the optimal source alignment angle (-20°) and (b) lower trace: the most out of plane angle or weakest projection angle (70°) as determined from a hodograph

Figure 5.5 demonstrates the progression of distortion associated with rotation of a sensor relative to the seismic source using the combination of Channels 1 and 2 for the 9 m sensor depth of CRB02SEIS. As the component projection angle is rotated through 360° starting from the optimum angle, the source amplitude appears to fade, reappear with reverse polarity, fade again, and as the rotation comes full circle, the original polarity and amplitude return.

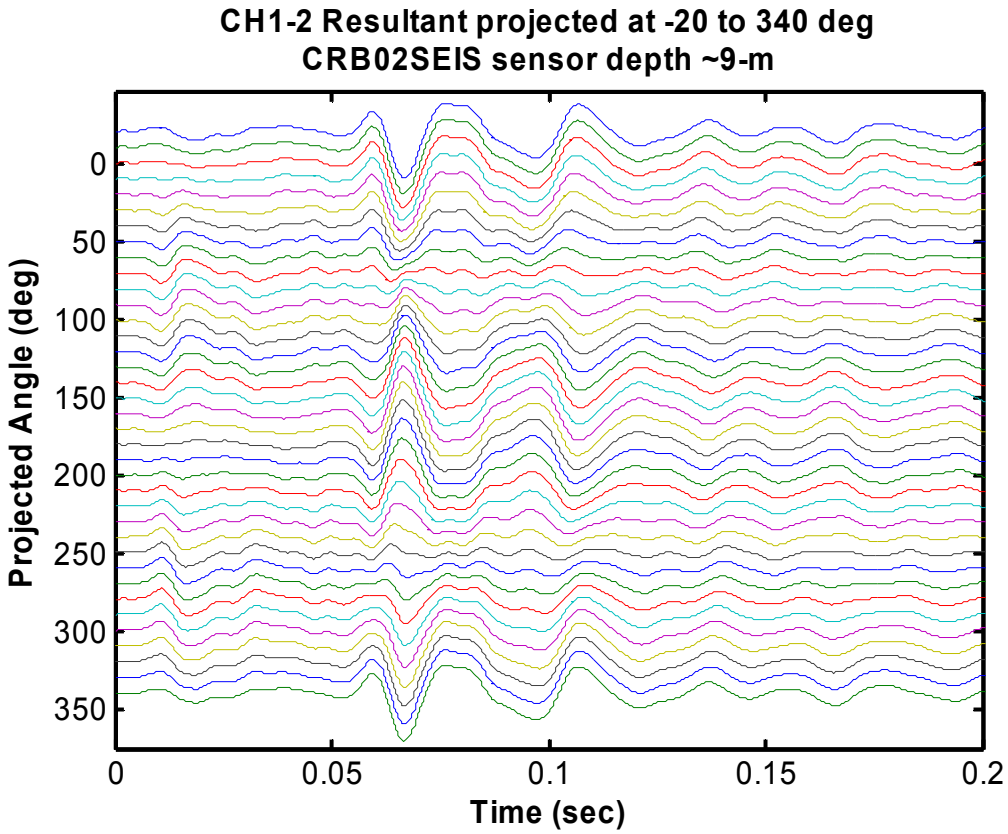

Figure 5.5 Amplitude changes caused by rotation of the 2-dimensional signal projection angle from the optimal alignment through 360°

Not only does the sensor orientation affect signal amplitude, rotation of the sensors during a sounding can cause errors in the determined travel time differences. Although it is not obvious, given the long time scale of Figure 5.5, the rotation of the sensors causes an apparent time-shift in the signal. Figure 5.6 was created by determining the absolute value of the time difference between the optimally-aligned signal from the previous figure and each of the other projected signals in that figure, from -20° to 340°. For each projection angle, there is a time difference when compared with the optimally-aligned signal, even though each signal is a component of the same source event.

If the sensors rotate during the course of the sounding, the amplitude may remain of sufficient quality for detection, but comparison between sensors having different rotation will induce error in the travel-time difference. The severity of the velocity error

caused by timing errors is dependent on the actual velocity and the interval length. Ranges were presented previously in Chapter 3 (Table 3.1 and Table 3.2), indicating that for a 1 m interval and 300 m/s V_S, an error of 0.1 ms corresponds to a V_S error of 8.7 m/s. For the particular record highlighted in Figure 5.6, a 0.1 ms error is induced by less than 30° of sensor rotation.

Manufacturers of commercial SCPT equipment normally do not mark the orientation of the sensor(s) on the probe, so neither component direction will be aligned well at the start of the test. It is possible to re-project the data later to correct for orientation problems, but this is uncommon. For one commercial system, the operations manual recommends a trial and error process to achieve optimal alignment on one of the two components of the biaxial geophone by rotating the penetrometer in 10° increments until a quality signal is obtained. Then, the other geophone component is ignored for the duration of the sounding.

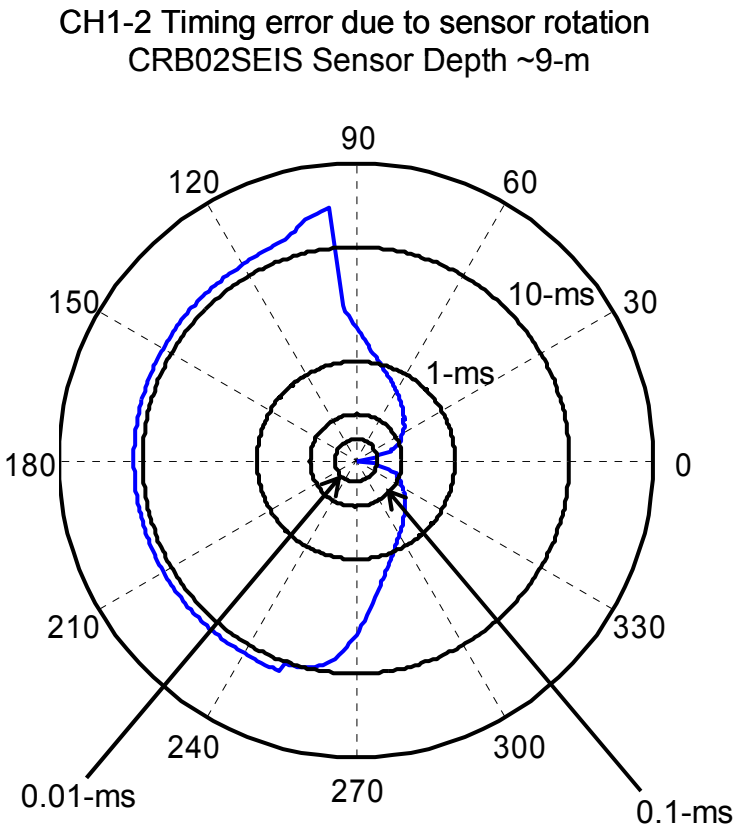

Figure 5.6 Apparent time shift of a projected signal caused by rotation of the projection angle from the optimal angle through 360°

5.2.3. Interference from reflections and noise

Aside from the orientation issues, the hodographs (Figure 5.3) also reveal changes in signal shape with depth. Changes in signal shape can be caused by interference from electromagnetic sources and from ambient vibrations. Power line noise in the U. S. will appear as a 60 Hz component, and in some cases, at multiples of 60 Hz. Electromagnetic interference can also come from nearby power supplies, generators, or inherently noisy devices like the electric motor that powers the RotoSeis. In the case of the RotoSeis, an optical isolator (Figure 3.53) was added to the data acquisition trigger circuit in order to decouple RotoSeis from any wires connected to the data acquisition.

Vibratory sources can also include construction activities, rail or road traffic, and

machinery. Even the CPT testing vehicle can be a potential source for vibratory contamination of the seismic signals. Vibrations from the testing vehicle may be especially prevalent because the vehicle is connected directly to the probe rods.

In the case of Figure 5.3, because the odd-shaped patterns are duplicated with separate source events and separate receivers, random noise can be ruled out as the cause. The change in signal appearance with depth is likely a result of interference from shear waves reflecting back on themselves from a layer boundary or buried object, overlapping the incident wave.

In Figure 5.7, compiled from Baziw (2007), a synthetic signal generated by a surface seismic source is shown which is influenced by overlapping reflections. The uppermost plot is the signal that would be recorded with a seismic sensor below ground. The middle plot indicates the arrival time of the incident wavelet and relative strength of reflected source energy. The final plot in the series describes how the recorded signal might be decomposed into a linear combination of the incident and the overlapping scaled and shifted reflections. Even reflectors several meters away (below, above, or to the side) from the sensor can reflect back wavelets that will arrive before the complete incident wavelet has passed. In this simulation, the distortion of the signal is not severe, but can be enough to interfere with comparisons between waves recorded at adjacent depths.

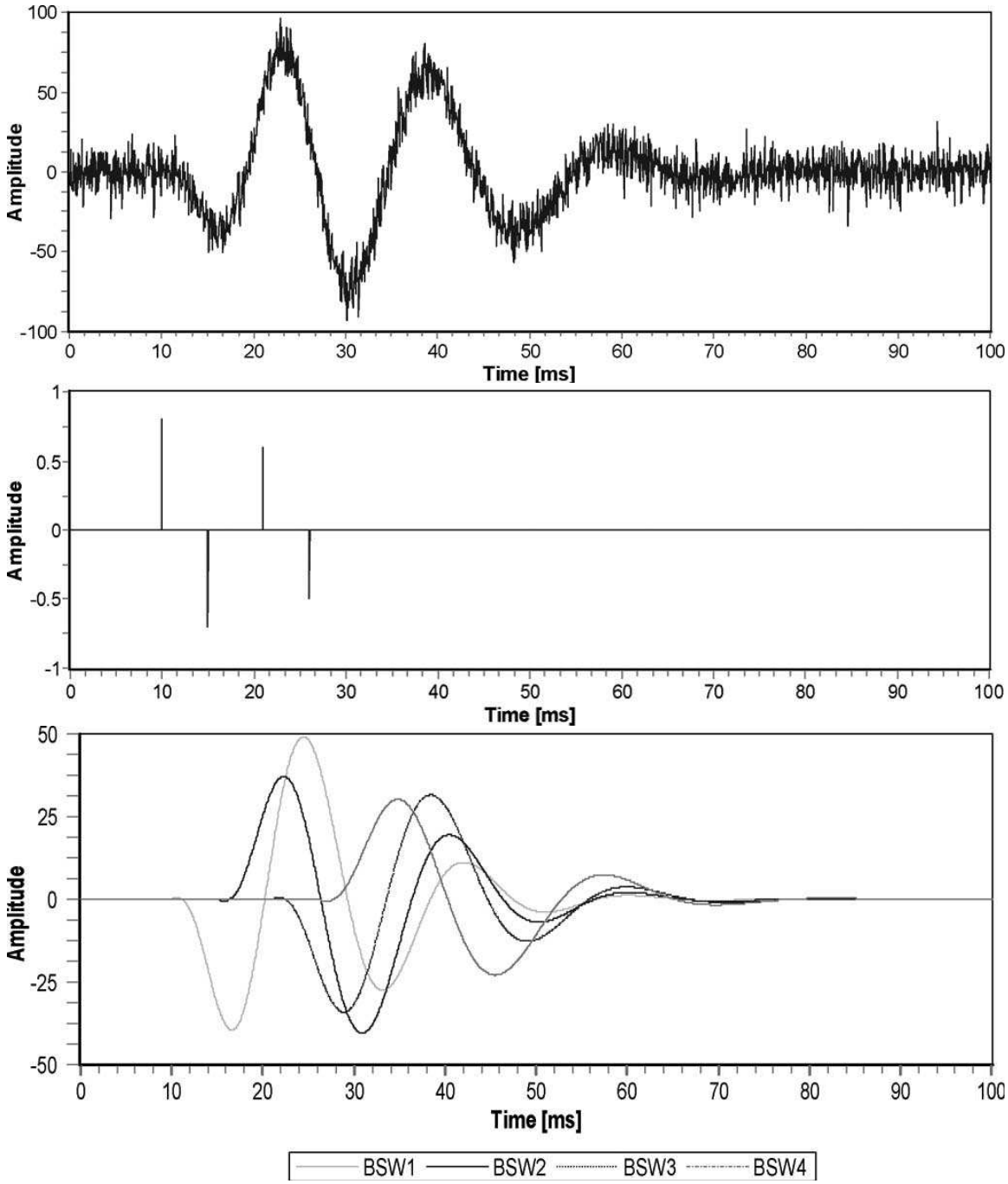

Figure 5.7 Synthetic shear wave signal shaped by reflected shear waves overlapping with the incident source wave (Baziw, 2007)

5.3. Effects Caused by the Data Acquisition System

The data acquisition system can also affect the appearance of the recorded wave signals. Data acquisition captures the analog signals from the sensors and converts them to digital signals that can be stored on the computer. If the input ranges, sampling rate and duration of the recording are not appropriate, the signals can become distorted. To avoid altering the signals during the measurement process, the voltage range, sampling rate, and recording length must be matched to the sensor and signal characteristics.

Several different data acquisition systems were utilized to record seismic signals during the field testing program. Descriptions of the systems are given in Chapter 3. A summary of the data acquisition devices and settings corresponding to specific field tests is given in Table 5.1.

5.3.1. Voltage range

If the input voltage is outside the range of the device, the signals will be clipped. This is important to consider when amplifiers are used. If the input voltage is too low, the data acquisition may not have enough resolution to capture the details of the shear waves. The recordings will appear noisy because of loss of resolution.

Resolution of the recorded data is related to the specified bit resolution of the data acquisition. The minimum change in voltage that can be detected is the range of the device divided by two raised to the number of bits resolution. The data acquisition may be bipolar so for a device capable of digitizing inputs from -10 V to +10 V, the voltage range is 20 V.

For the model GS-14-L3 geophones used for this research, the output peak-to-peak voltages range from ±0.1 V near the surface and attenuate to almost ±0.0001 V at depth. The attenuation of peak-to-peak voltage during the sounding CRB03SEIS is shown in Figure 5.8. Although there is some scatter due to noise between 9 m and 16 m, the trend is decreasing voltage by 3 orders of magnitude from the surface down to 30 m.

Table 5.1 Data acquisition systems and settings for significant field study tests

Sounding Names	Data Acquisition	Applicable Input Range (V)	Resolution (bits)	Amplification	Sampling Frequency (Hz)	Duration (sec)
VENI02 FCPT03 FCPT04 MUDB1 OPELI2 OPETRU STON1A STONO01 CRBDH1 CRBDH3 CRB01 CRB02 NEWOR01[1]	Hogentogler E3	0 - 10 (approx.)	10	× 70 (approx.)	40,000	0.20
SDMT15 SDMT19 SDMT14	FLUKE 123	(selectable) ±0.2 ±0.08 ±0.02	8	× 50	2,520 (T-I)[2] 1,260 (P-I)[3]	0.10 (T-I)[2] 0.20 (P-I)[3]
FCPT03SEIS FCPT04SEIS MUDBSEIS	HP3560A	(selectable) ±0.1 ±0.05 ±0.02 ±0.01 ±0.005	12	None	5,120	0.10
OPETRUSEIS STONOSEIS	Agilent 1432A	(selectable) ±0.2 ±0.1	16	None	5,120 40,000	0.40
STONO01SEIS CRB01SEIS CRB02SEIS	Geometrics Geode	±2.8	24	× 64	48,000	0.50
CRB03 CRB03SEIS CRB04 CRB04SEIS	National Instruments 9239	±10	24	× 100	5,000	1.40

[1] Digital Hogentogler System, [2] True-Interval, [3] Pseudo-Interval

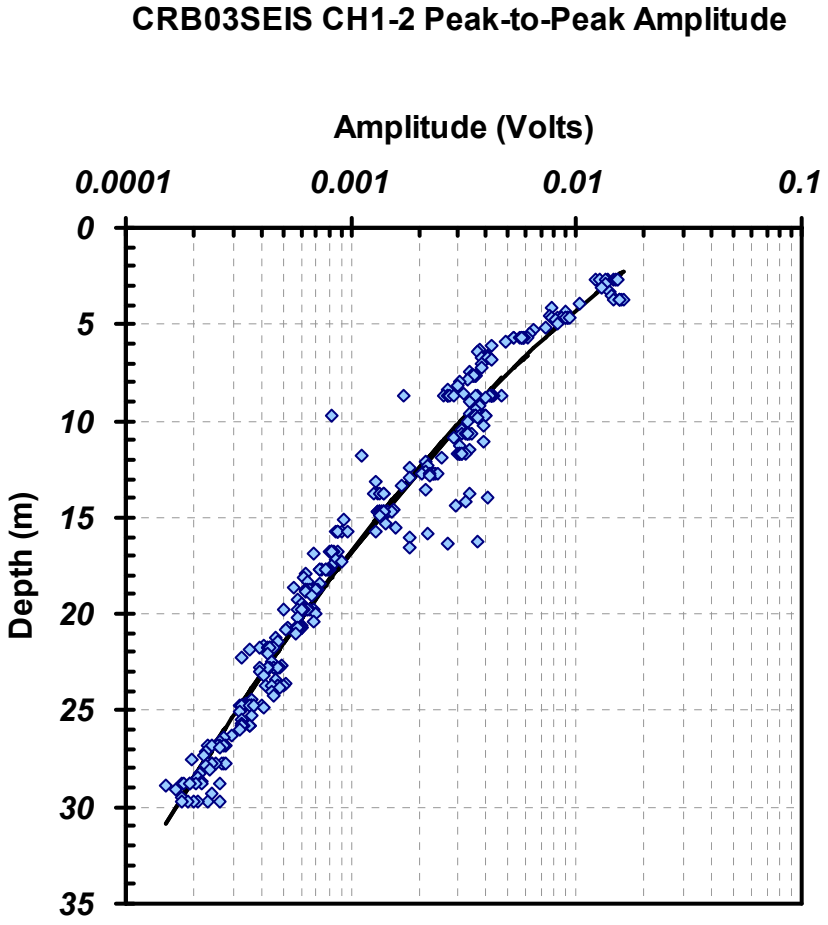

Figure 5.8 Decrease in peak-to-peak geophone output voltage with depth due to shear wave attenuation

Devices with selectable input ranges can have lower resolution because the input range can be reduced to accommodate decreasing amplitudes. The Fluke 123 hand-held battery-operated 2-channel oscilloscope, HP3560A 2-channel portable signal analyzer, and Agilent Technologies 1432A 16-channel signal analyzer data acquisition systems each have selectable input ranges that had to be adjusted with depth during the course of the soundings. The Geometrics Geode and the National Instruments 9239 have high resolution at 24-bit, so the input range can remain constant throughout the sounding. However, the input ranges are large, requiring amplification of the signals.

5.3.2. Sampling rate

The sampling rate governs the time resolution of the recorded signals. Signals containing high frequency components require high sampling rates. However, minimizing the sampling rate is desirable for reducing the demands/requirements of the data acquisition device. The Nyquist rate, which is two times the highest frequency component in the signal, is the minimum allowable sampling rate. Yet, for practical applications, a sampling rate ten times higher than the highest frequency signal component is a common recommendation for maximizing the signal quality. For surface seismic sources, the upper bound frequency is less than 200 Hz (Fernandez, 2000). Therefore a sampling rate of 2 kHz should be adequate to capture generated shear waves.

Though the source signals may be less than 200 Hz, noise components in the signals may contribute higher frequencies that are unwanted. Anti-aliasing filters are required to remove frequency components greater than twice the sampling frequency. If high frequency components are under-sampled, they may appear as low frequency noise within the source bandwidth.

The sampling rate also affects the resolution of the determined travel-time differences between signals. A sampling rate of 2000 Hz is adequate to capture all of the frequency components of a signal having a 200 Hz bandwidth, however the resolution of analysis performed in the time domain will suffer. In order to reduce the time spacing between points within the signal, it is necessary to up-sample the data to a higher rate by interpolating between data points. No new frequency information is added, but the increased time resolution allows more accurate comparisons of time differences. Karl et al. (2006) recommend up-sampling to 100 kHz utilizing the function in Matlab which adds zeros between points and then applies a low pass filter to smooth the signal. The up-sampling method utilized in these analyses is a Fourier Transform based approach which involves zero-padding in the frequency domain using the Fast Fourier Transform (Wang et al., 1992). An overview of the Fourier Transform is given in Section 5.4.

5.3.3. Duration

The duration of a recorded shear wave signal needs to be long enough to capture the arriving waveform. For the true-interval methodology, the recording may be triggered just prior to the arrival of the source wave at the uppermost sensor, ending just after the waveform passes the lowermost sensor. For the pseudo-interval method, the recording is triggered at the time of the activation of the source for the duration required to reach the sensors at depth. Only the portions leading up to and including the source shear wave are needed to determine V_S. Trimming the signals is common practice to save disk space, but longer signals will capture extra geophysical information contained in the reflections. Jarvis and Knight (2000) extended recording times to 1 second to perform vertical seismic profiling during conventional SCPT soundings.

Figure 5.9 displays the entire catalog of records recorded during the frequent-interval sounding CRB02SEIS performed with a sledgehammer seismic source. The amplitudes of the signals in the plot have been normalized by their peak amplitudes to account for the attenuation of the source signals with depth.

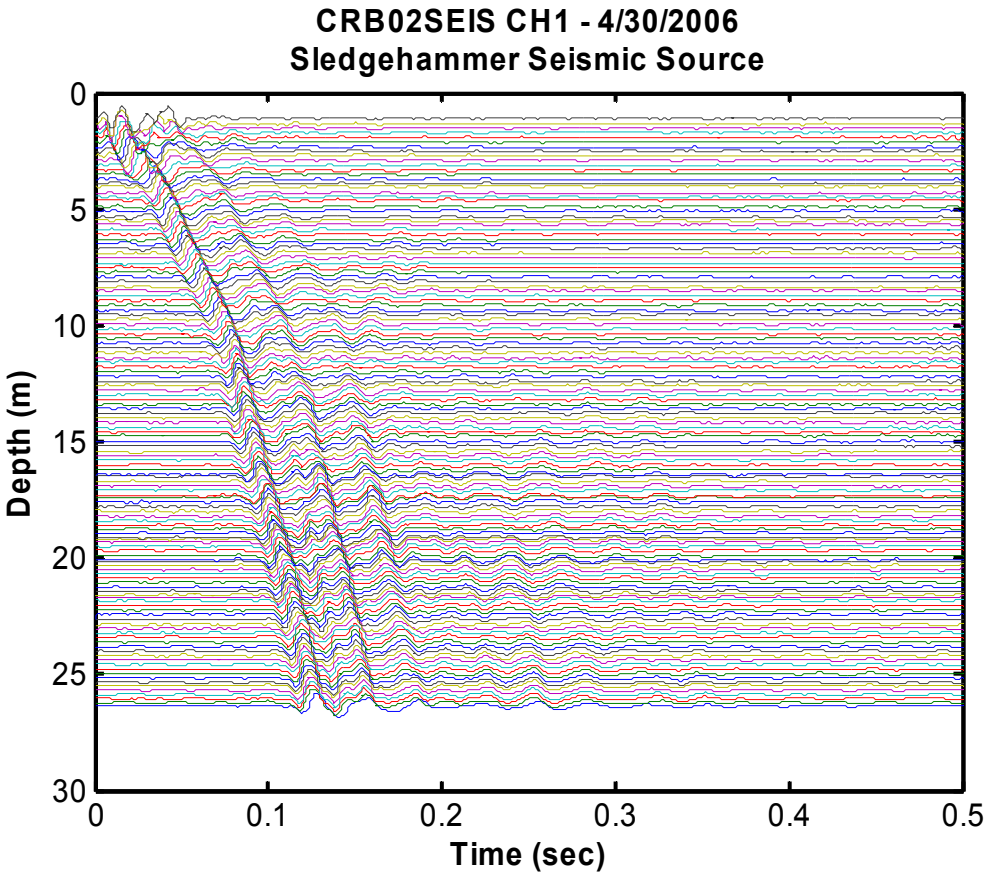

Figure 5.9 CRB02SEIS sledgehammer seismic signals recorded for 0.5 s with normalized amplitudes and shifted to their respective depths

5.4. Fourier Transform

Although shear waves are non-dispersive, meaning the velocity does not change with frequency, measurement of velocity can be influenced by the frequency content of the signals. A layered profile acts as a low-pass filter, causing high frequencies to attenuate faster with depth (Mancuso et al., 1989; Stokoe and Santamarina, 2000), and low frequencies are difficult to time accurately because of the broad peaks (Fernandez, 2000).

The Fourier Transform is the tool most commonly used to analyze frequency components of recorded time signals. In order to understand the benefits and limitations of frequency-based calculations with shear waves, it is useful to provide a brief overview

of the Fourier Transform concepts.

The Fourier Transform decomposes a time domain signal into a series of sine functions representing the frequency components in the original signal. The scale (amplitude) and time-shift (phase) of each sine function are such that summing all of the component sine functions together reproduces the original time domain signal. This concept is illustrated in Figure 5.10. The upper portion of the figure shows 32 individual sine functions, with frequencies ranging from 1 to 32 Hz, that when added together, form a wavelet similar to what would be produced by an impulse seismic source. Such a transient signal is able to be represented as a sum of continuous sine signals because the amplitudes are additive where the peaks of the sine functions line up (in phase), and where the peaks are oppositely polarized (out of phase), the amplitudes cancel out to near zero.

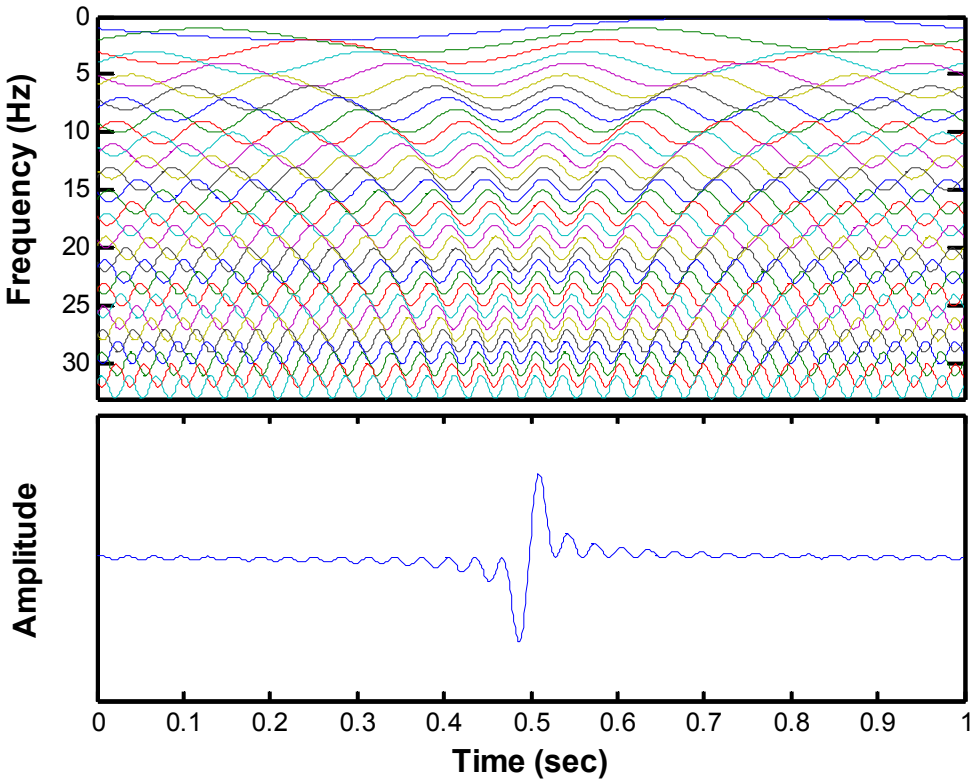

Figure 5.10 A series of sine functions varying in frequency from 1 to 32 Hz, having constant amplitude, and a constant phase shift of $-\pi/2$, summed together to form a familiar impulse-type source wavelet

Decomposition by the Fourier Transform allows the amplitude and the phase of each frequency component to be visualized independently. However, the Fourier Transform is based on the assumption that the signals are stationary. In this instance, "stationary" means that the frequency content does not change with time, and is not related to changing position of the receivers. Figure 5.11 demonstrates the frequency domain representation of the same time domain signal that was shown in Figure 5.10. The uppermost plot is the amplitude versus time. The middle plot is the amplitude of each of the sine wave components making up the transient time domain signal. In this instance, all of the sine functions have equal amplitude for all frequencies from 1 to 32 Hz. The lowermost plot describes the phase of each of the component sine functions. This

particular time signal is made up of sine waves having a constant phase shift of –π/2. The phase shifts above 32 Hz are inconsequential because the amplitudes are zero above 32 Hz. This is a stationary signal given that for each frequency component there is only a single amplitude and phase. The same frequency component cannot be represented twice in the same signal with two phases or two amplitudes. A thorough explanation of the effects of amplitudes and phase shifts on the appearance of the resulting wavelet can be found in Chapter One of Yilmaz (1987).

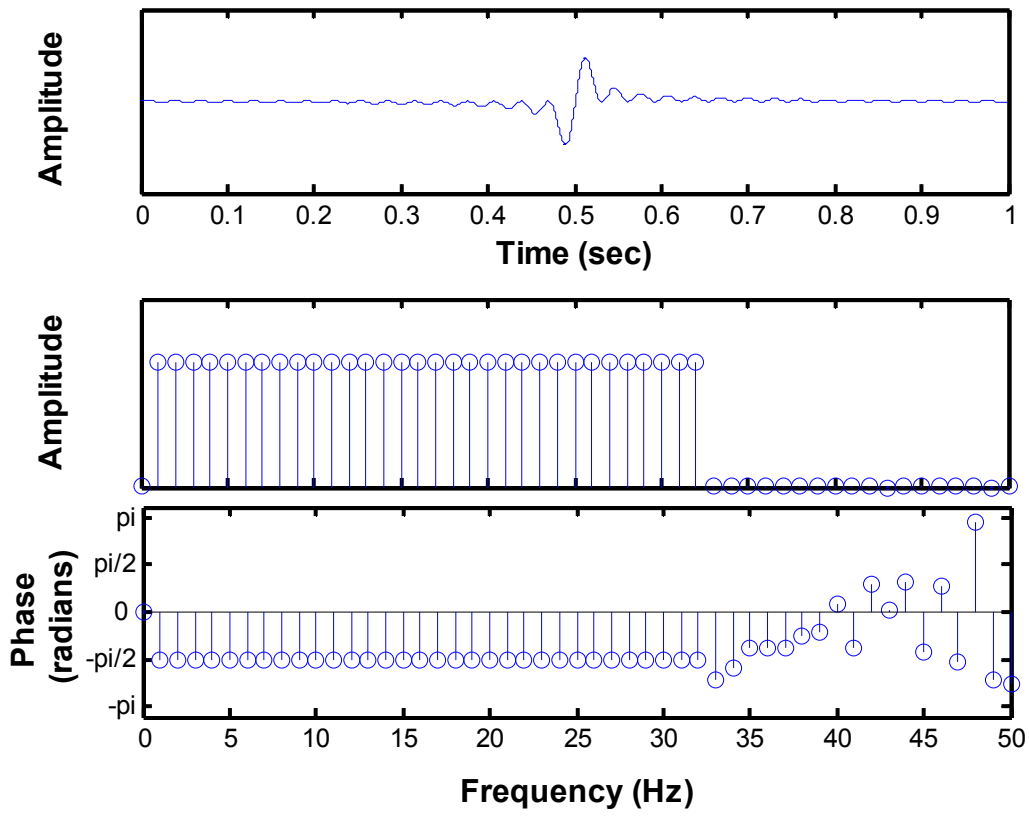

Figure 5.11 Frequency domain presentation of a familiar source wavelet containing frequencies from 1 to 32 Hz, with a constant phase shift of –π/2

The decomposed time-domain wavelet described in the previous figures is a stationary signal, having a unique amplitude and phase for each frequency component for the duration of the signal. In reality, shear wave signals associated with downhole

velocity testing are typically non-stationary. In a layered profile, shear waves reflect back on themselves with the same frequency content contained in the incident wave, but with different phase, or position in time, and with decreased amplitude. As a result of violating the assumption of stationary signals, the amplitudes and phases of the non-stationary components will be distorted and averaged out over neighboring frequencies. Resolution of frequency specific behavior may be lost.

5.5. Evaluation of RotoSeis

During the field testing program, the automated RotoSeis devices were evaluated for signal clarity, directionality, repeatability, reliability, and useful depth. Signal clarity refers to the visibility of the shear wave impulse relative to ambient noise levels. Directionality describes how well the particle motions of the shear wave move in a plane parallel to the axis of the source. The amplitude versus time and amplitude versus frequency are compared for the different seismic sources. The frequency content of the source signal affects the sharpness of the impulse, and influences how well the shear wave stands out against the background noise.

5.5.1. AutoSeis

The electromagnetic AutoSeis developed by Casey (2000) was the first automated seismic source in the series of sources developed at Georgia Tech. Figure 5.12 shows a series of time histories recorded during field studies with the AutoSeis at the Opelika, Alabama National Geotechnical Experimentation Site (NGES). The signals were weak but detectable to a depth of approximately 13 m. The recordings were made with the Hogentogler E3 field computer and a single axis, pseudo-interval 100 kN seismic cone. The original signals were trimmed at the time of recording to save disk space. The results have been zero-padded and amplitudes normalized here for display.

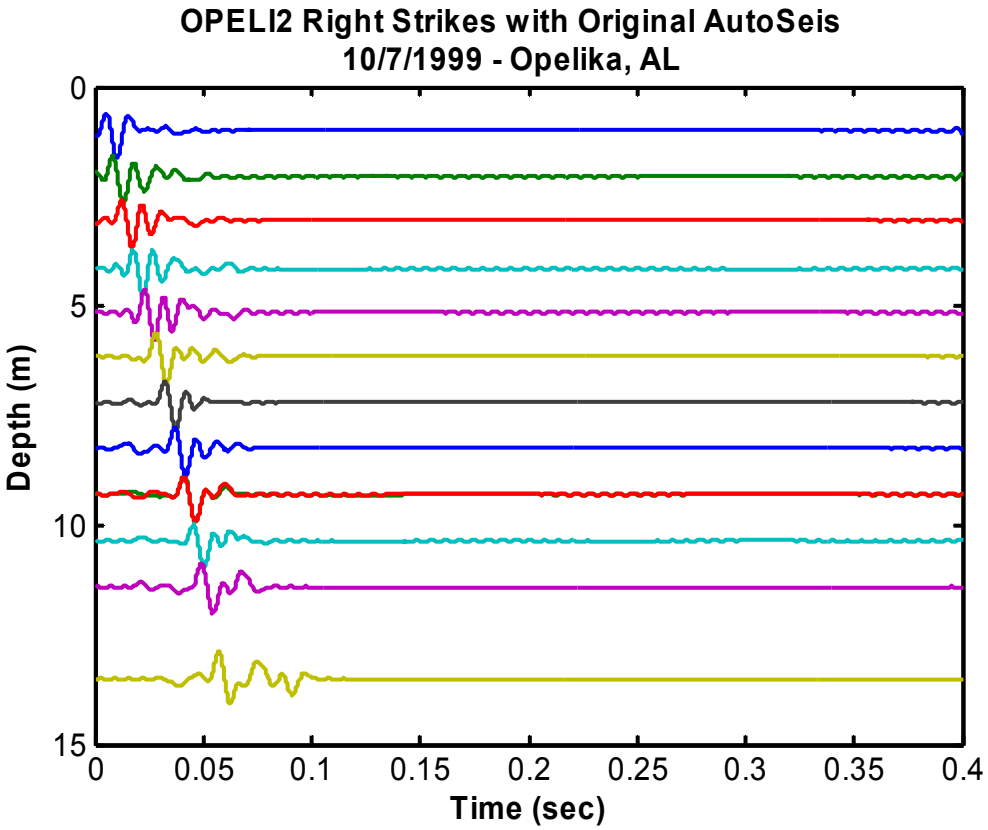

Figure 5.12 Family of time history signals collected with the original electromagnetic AutoSeis seismic source

5.5.2. RotoSeis II

The RotoSeis II was also tested at the Opelika NGES using a similarly-sized hammer mass as the electromagnetic AutoSeis (2.3 kg for AutoSeis and 2.6 kg for the RotoSeis II). The propagation depth was also similar. During the frequent-interval sounding OPETRUSEIS, RotoSeis II was tested side-by-side with the sledgehammer pendulum source, utilizing the biaxial true-interval seismic probe and the frequent-interval method to record the signals. The pendulum source was placed under an outrigger on one side of the cone truck, and the RotoSeis II was placed under the outrigger on the opposite side of the truck. At each test depth, every 20 cm, the penetration was paused, each source was activated separately, and corresponding shear

waves were recorded. Shown below in Figure 5.13 are the series of signals recorded with both sources. The signals are the optimally projected signals created by the combination of Channels 1 and 2.

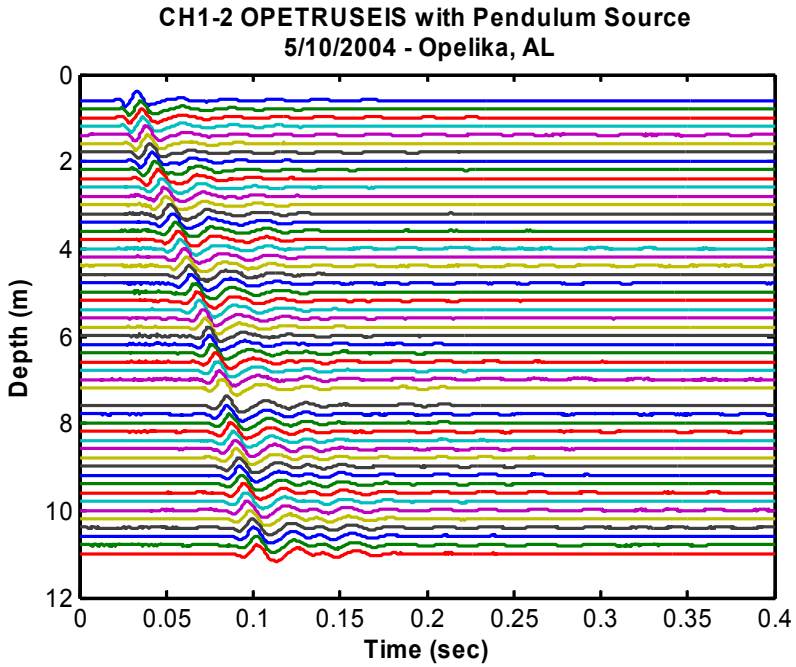

(a)

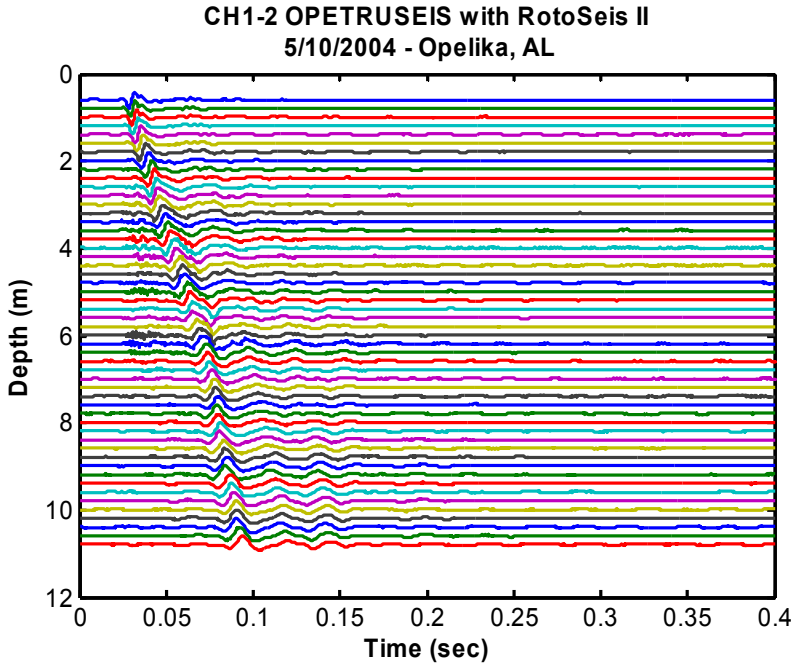

(b)

Figure 5.13 Time history signals from a frequent-interval test at the Opelika NGES using (a) the pendulum source and (b) the RotoSeis II

RotoSeis II and the sledgehammer both produced readily detectable signals down to final depths of 11 m. Yet, the family of signals generated by the RotoSeis II appeared somewhat noisier than the signals generated by the sledgehammer because the amplitude of the RotoSeis wave was as much as 70% less than the sledgehammer amplitude. Following these experiments, the RotoSeis hammer mass and internal spring stiffness were increased in subsequent models in order to increase the amplitude.

In Figure 5.14, RotoSeis II and pendulum signals are compared in the time domain and the frequency domain for the 10 m depth records. The RotoSeis II time domain amplitude is noticeably lower than the sledgehammer. The lower amplitude can also be seen in the plot of frequency content. The peak frequency of the RotoSeis II (36 Hz) is also lower than the peak frequency of the pendulum (50 Hz). RotoSeis II was slipping along the surface with each impact, which contributes to the low amplitudes and reduced bandwidth. The base of the pendulum source is textured to reduce slipping. Surface texture was applied to following RotoSeis devices.

Hodographs created by combining Channels 1 and 2 for the 10 m signals (Figure 5.15) reveal similar 2-dimensional signal shapes for the two sources as well. The hodographs also show the alignment of the probe sensors relative to each source. RotoSeis II was arranged at an angle 30° off of Channel 1, and the pendulum source was oriented at 30° in the opposite direction.

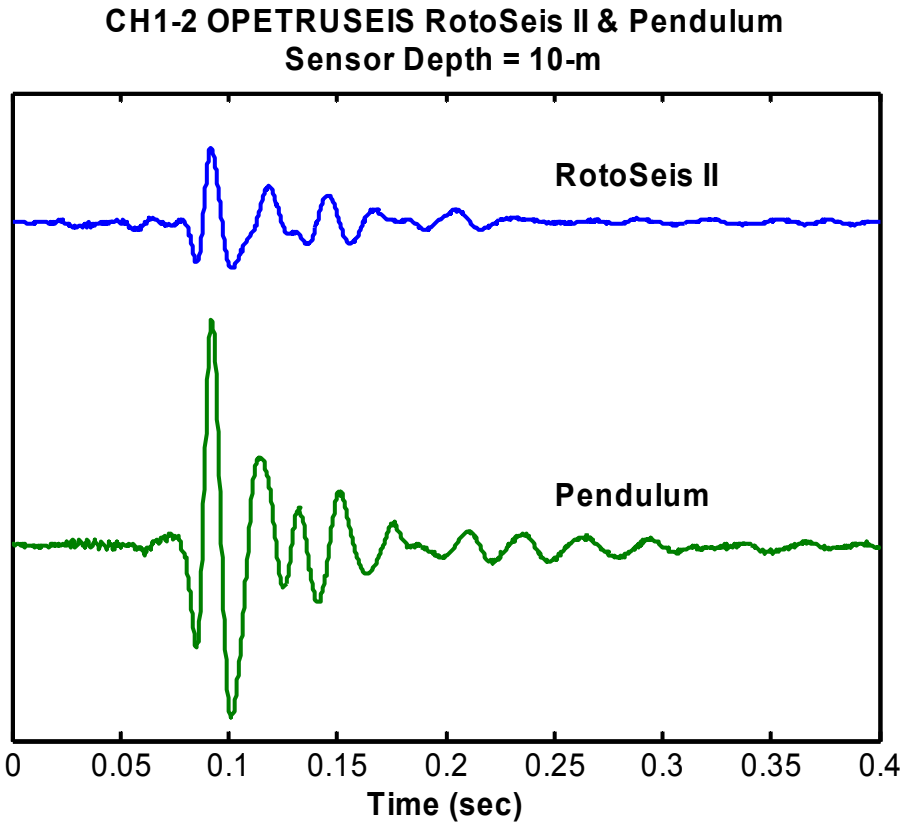

(a)

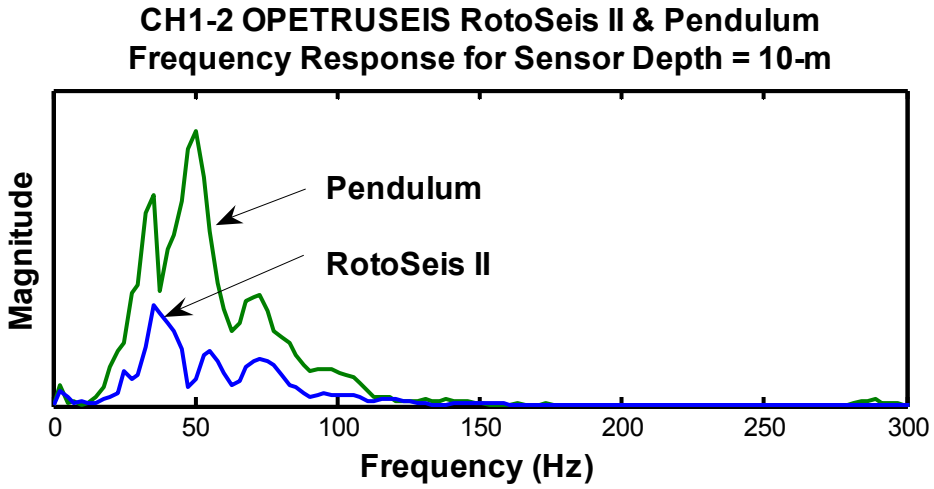

(b)

Figure 5.14 Comparison of a RotoSeis II signal with a pendulum signal recorded at 10 m depth from the Opelika NGES in (a) the time domain and (b) the frequency domain

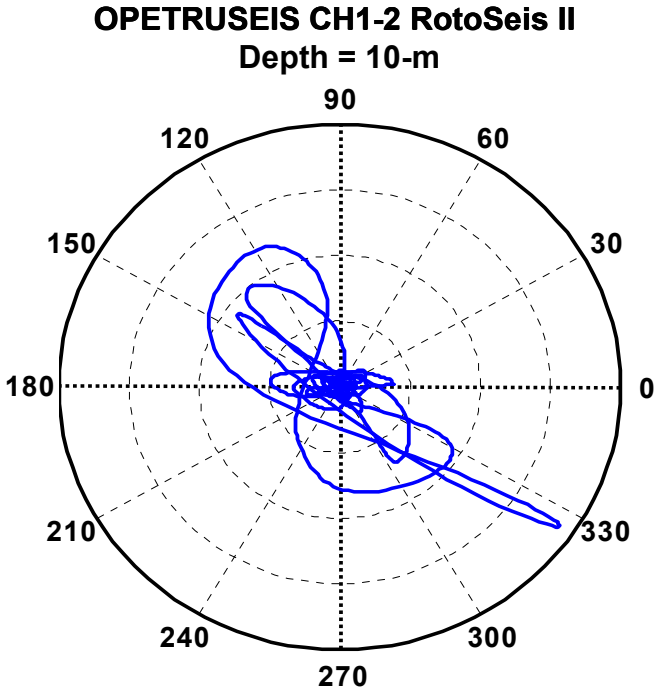

(a)

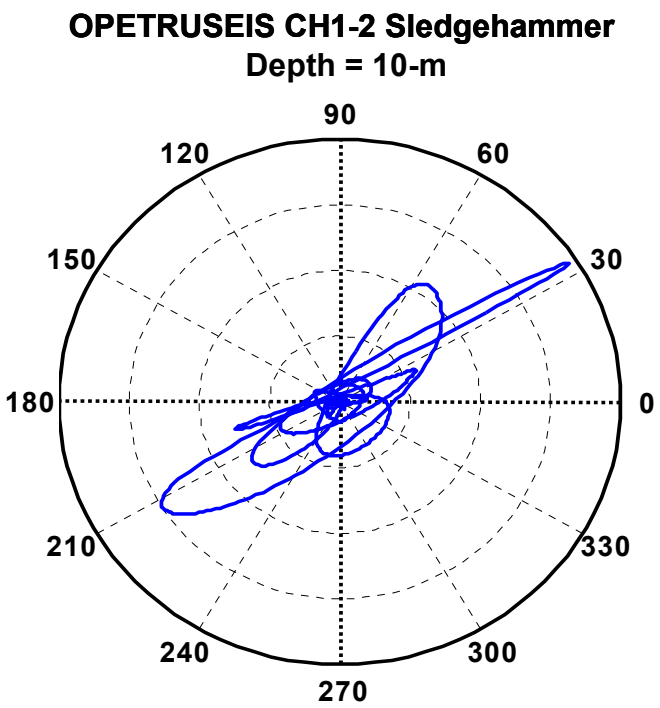

(b)

Figure 5.15 Hodographs of (a) RotoSeis II and (b) sledgehammer signals recorded during OPETRUSEIS at 10 m depth

5.5.3. Truck-mounted hydraulic seismic source

Biaxial seismic signals were recorded in St. Paul, MN using a 15 cm² Vertek seismic cone penetrometer and a Vertek cone truck with a large hydraulic source mounted beneath the truck frame just behind the cabin. The hydraulic source is capable of producing hammer impacts in opposite directions, known as left-strikes and right-strikes. However, only the family of recorded right-strike seismic signals from one of the horizontal components is shown in Figure 5.16 (a). The signals have strong amplitude which is easily identifiable. A direct comparison with other seismic sources is not possible because the data acquisition units and amplification for the Vertek system are not known. However, the magnitude of the frequency content for the hydraulic source at 6 m depth (Figure 5.16 (b)) is nearly constant from 15 Hz to 70 Hz, which is more uniform, but slightly lower bandwidth than the frequency content for the sledgehammer and RotoSeis II signals presented previously. The source is mounted to the underside of the truck, which prevents the source from sliding, but any high frequencies generated by the hydraulic source are overshadowed by the magnitudes of the low frequencies.

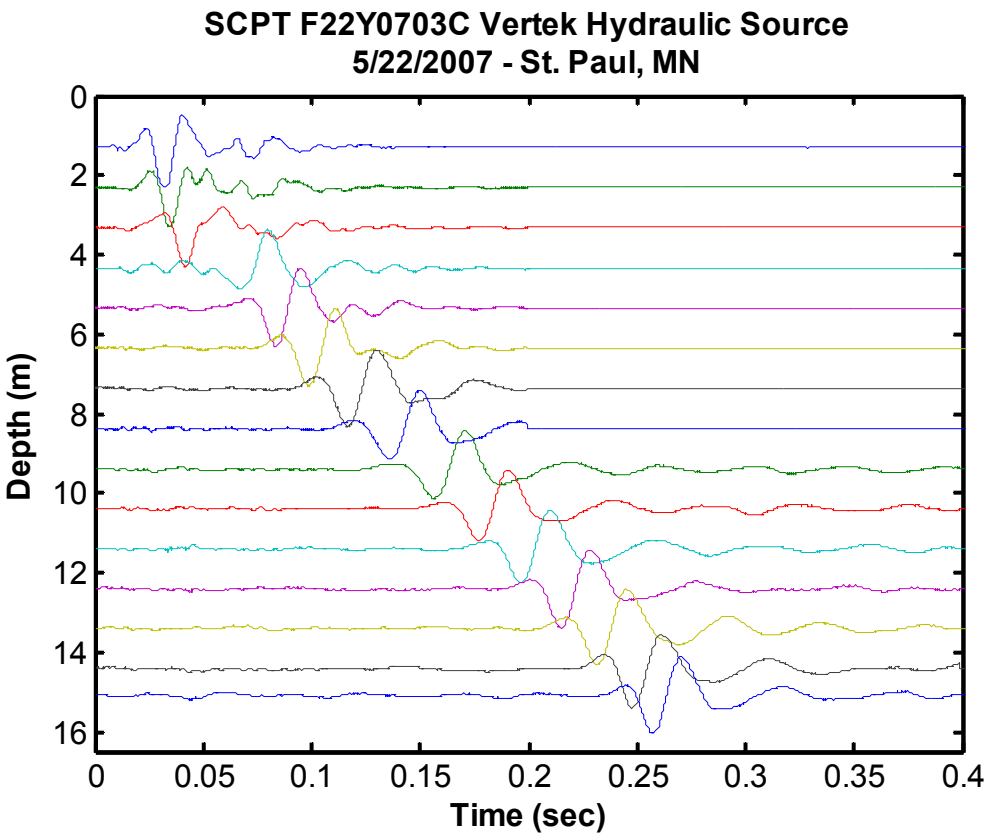

(a)

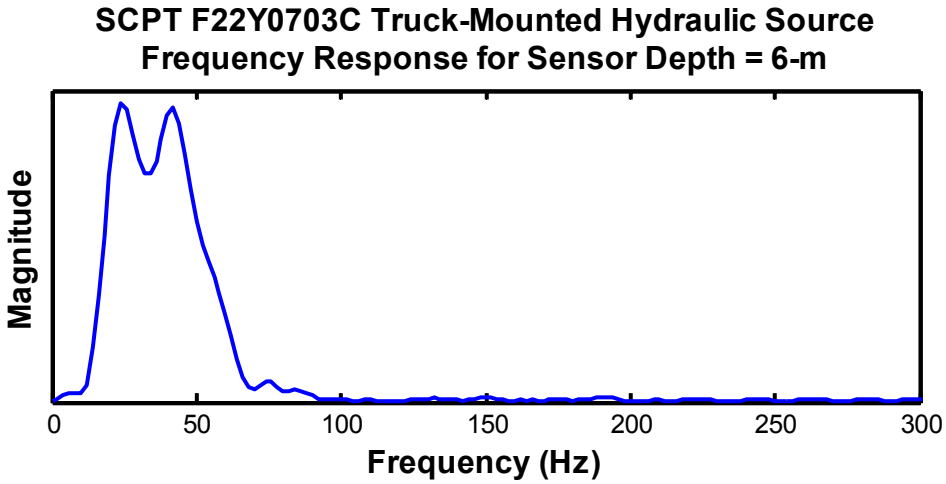

(b)

Figure 5.16 Shear wave signals generated by a truck-mounted hydraulic seismic source (a) time-domain signals normalized with depth and (b) a representative frequency response from a depth of 6 m

Though the 15 cm² Vertek seismic cone contains a triaxial geophone package at one elevation, multi-axis seismic data are not normally collected with this system. The manufacturer's recommended procedures are to activate the source to the left or right, select the strongest amplitude horizontal component and save it. Then activate the source in the opposite direction and save the same horizontal component, which is now oppositely polarized. For the sounding F22Y0703C, both horizontal components resulting from a single right-strike were saved. Combining the two horizontal components to form a 3-dimensional time-history (Figure 5.17) shows that the signal is directional, but with a rounded appearance.

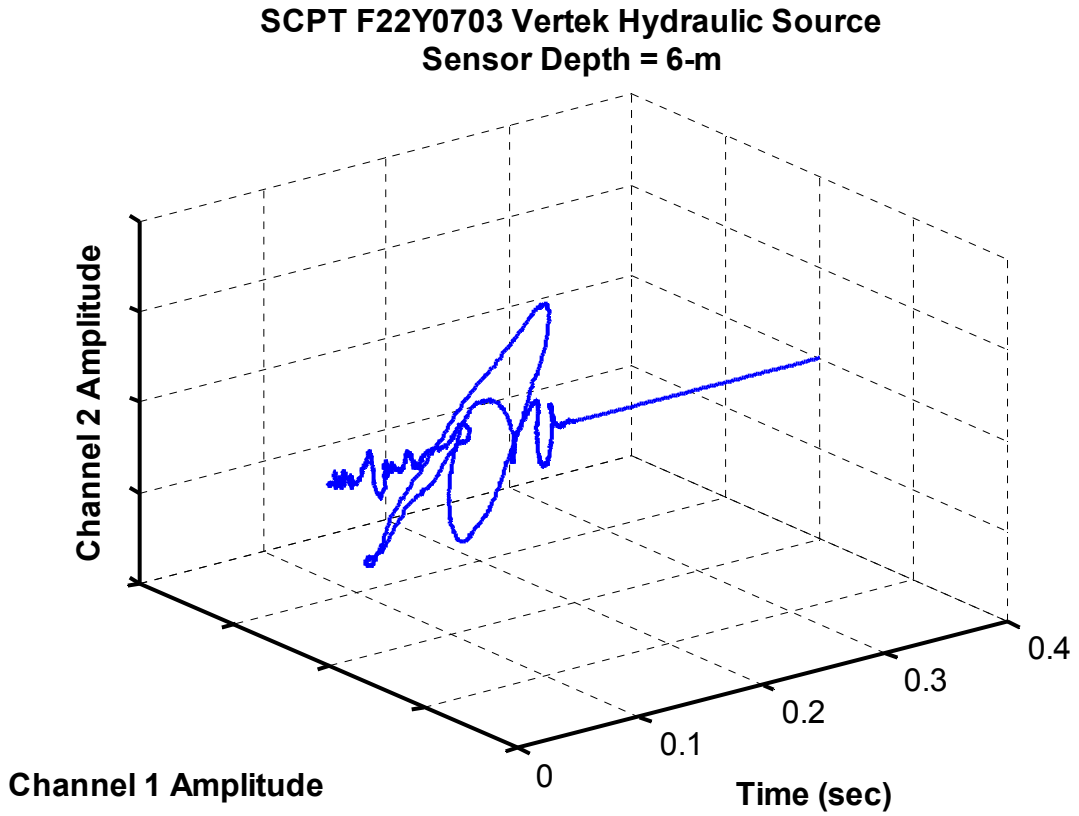

Figure 5.17 3-dimensional time-history of the hydraulic source signal recorded at 6 m depth for I-35E test site in St. Paul, MN

The hodograph of the biaxial signals from 6 m (Figure 5.18) highlights the orientation of the receivers relative to the axis of the hydraulic source. The axes of the seismic sensors are not explicitly marked on the probe, so the operators are not able to control the initial source-receiver alignment other than by rotating the rods and observing the changes in amplitude of the seismic signals. In this instance, the S1-direction horizontal component is oriented at -30° from the source axis.

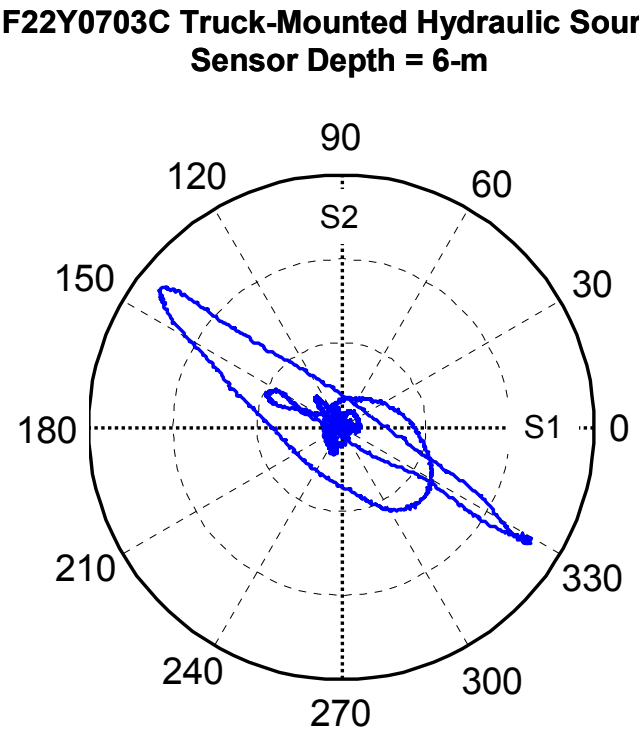

Figure 5.18 Hodograph of the 6 m depth hydraulic source signal depth for I-35E test site in St. Paul, MN

5.5.4. Sledgehammer repeatability

The sledgehammer signals presented previously in Figure 5.1 and Figure 5.3 show that the sledgehammer is, at times, capable of producing strong repeatable signals, but because it is a manually operated source, variability is common. Sledgehammer results from frequent-interval sounding STONOSEIS are presented in Figure 5.19, during which hammer strikes were repeated six times at each rod break. The results shown are the components of the combination of Channel 1 and Channel 2, projected at the optimal source angle. The upper plot contains the entire list of time records, recorded in 20 cm increments, while the lower plot displays only the repeated source signals at the rod breaks.

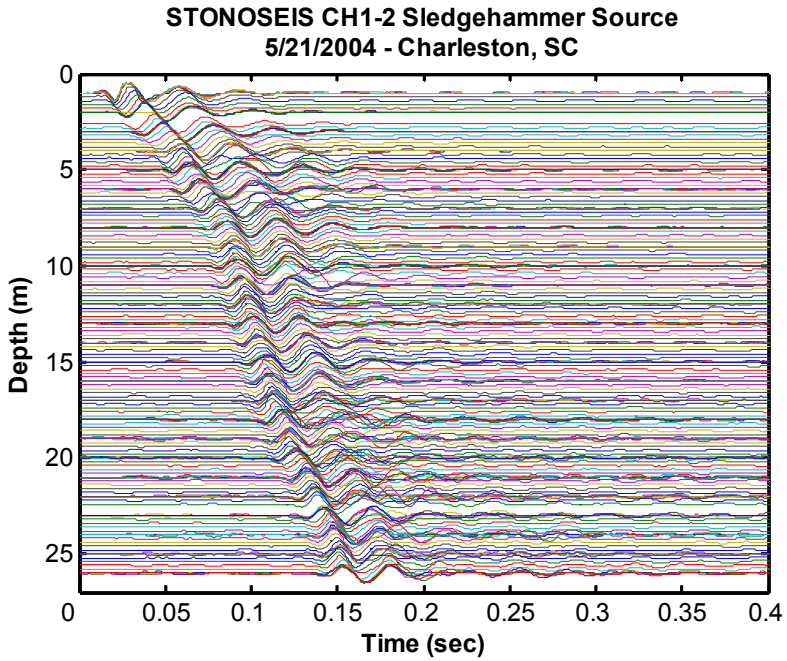

(a)

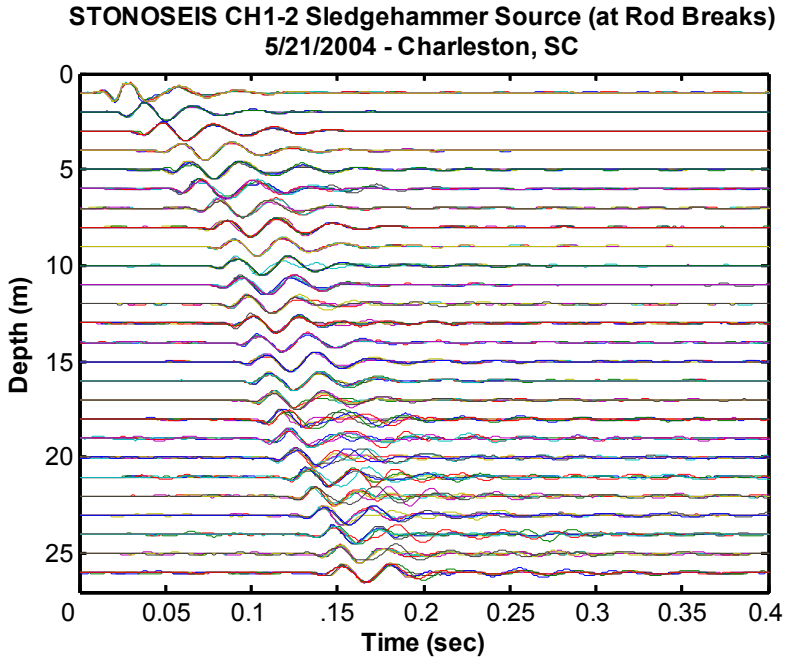

(b)

Figure 5.19 Frequent-interval shear wave signals collected at the Stono Marina with five additional hammer strikes recorded at each rod break (a) the complete record of signals and (b) repeated source events recorded at rod breaks

Plotted on the full depth scale, the waves appear to be fairly consistent, and the signals do not appear noisy. Figure 5.20 zooms in on the repeated sledgehammer signals obtained at a depth of 3 m. The upper plot contains the superimposed time records and the lower plot shows the frequency content for the same records. The bandwidth of the STONOSEIS sledgehammer signals is approximately 50 Hz, which is less than bandwidth of the hydraulic source shown in Figure 5.16 (b) as well as the RotoSeis II and sledgehammer bandwidths shown in Figure 5.14. In this instance, for the STONOSEIS sounding, the sledgehammer was impacting a steel beam having a smooth base. With each hammer strike, the source slipped significantly along the surface. The slipping at the interface apparently prevented high frequencies from being transmitted into the soil.

Three-dimensional time plots for each of the six hammer strikes at the 3 m depth for the Stono Marina, SC test site are shown in Figure 5.21. The variation in signal from one strike to the next is noticeable. Changes in signal shape were not as evident when viewing the projected component time signals from Figure 5.20. The 3-dimensional signals show that well-centered hammer-strikes produced narrow patterns, while off-center strikes resulted in more rounded, spiral-like motions.

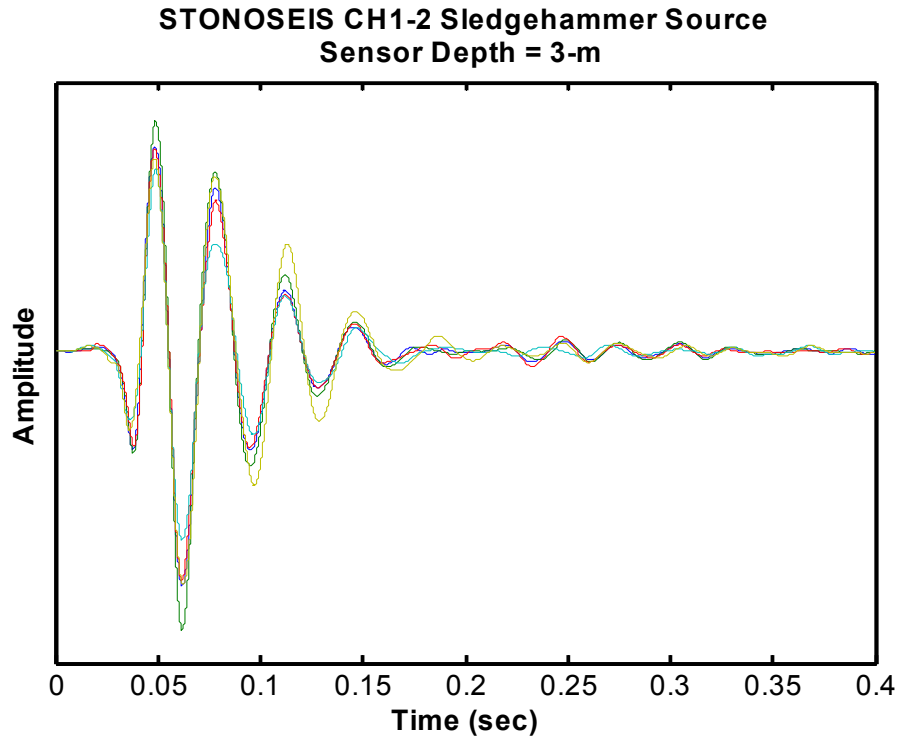

(a)

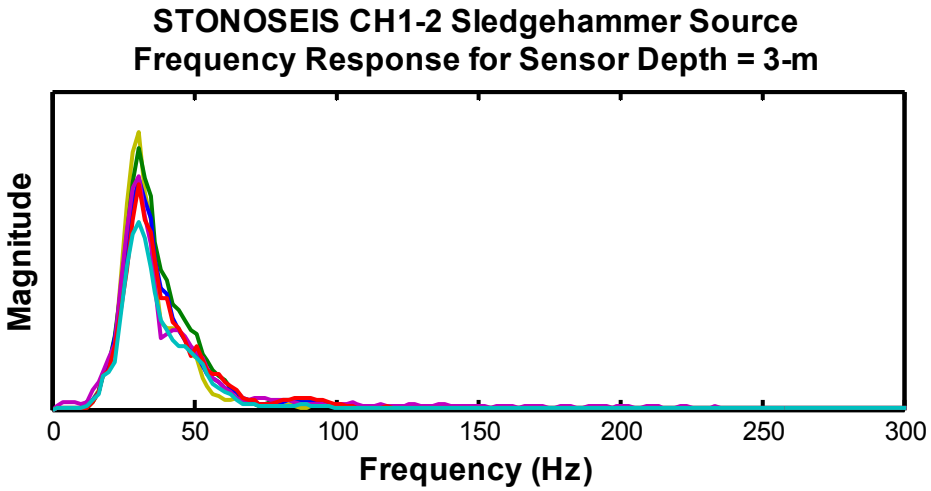

(b)

Figure 5.20 Superimposed recordings of six hammer strikes at a depth of 3 m during the frequent-interval test STONOSEIS (a) time histories (b) frequency domain representations

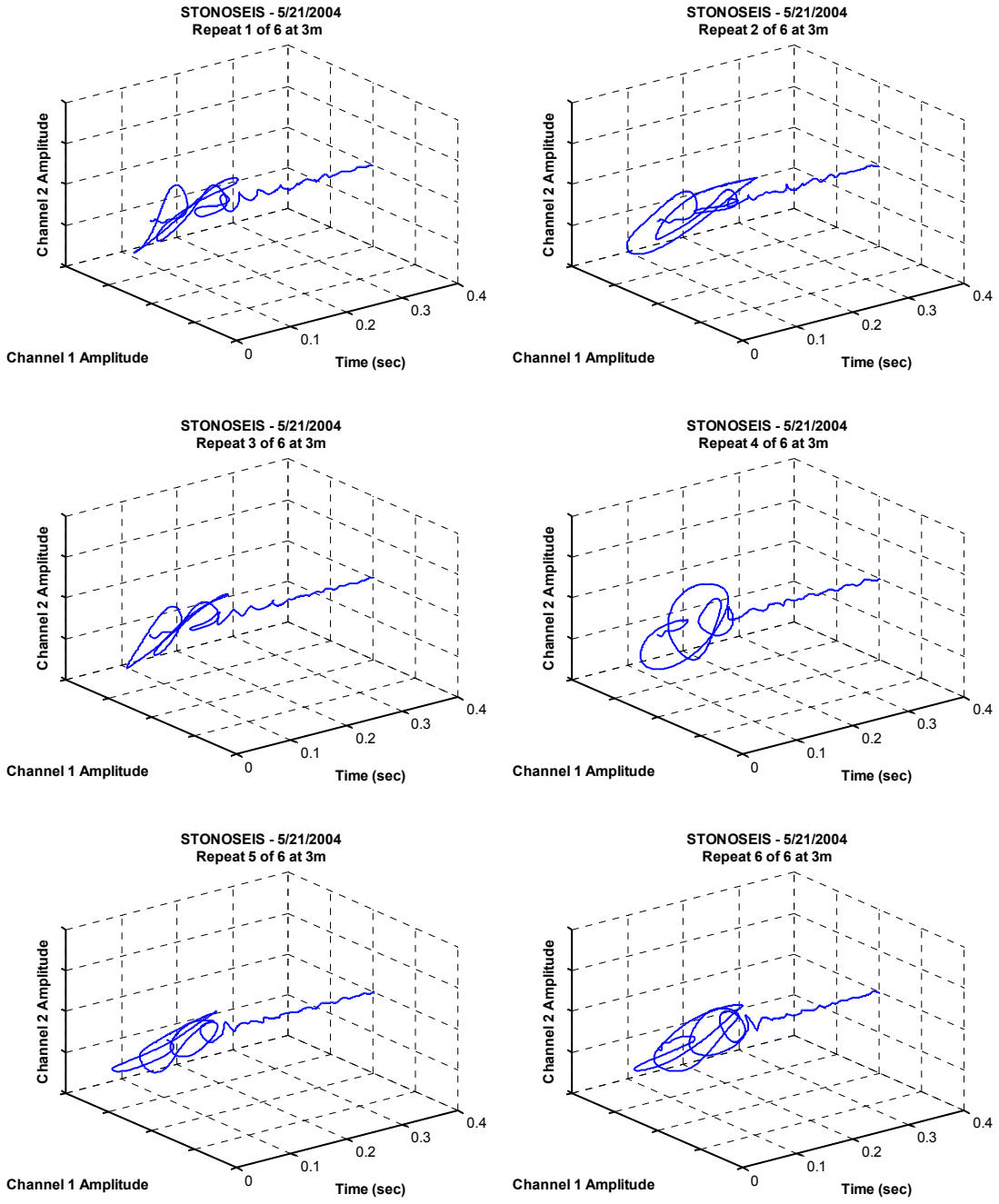

Figure 5.21 3-dimensional time-histories of six sledgehammer impacts recorded during STONOSEIS at a depth of 3 m

The angle between the source and the receivers remained constant during the repeated hammer strikes, which is evident from the hodograph (Figure 5.22). The hodograph also reveals that three of the signals are more rounded than the other three. The rounded signals correspond to off-center impacts, which also results in lower amplitude than the well-centered impacts.

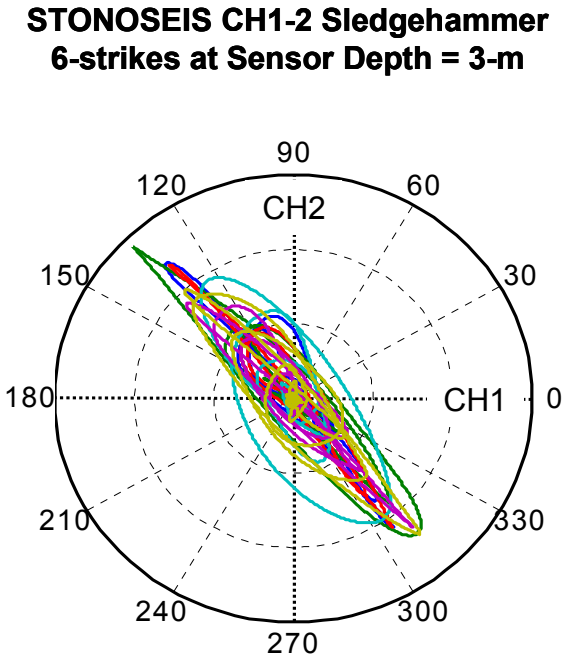

Figure 5.22 Hodograph of six superimposed biaxial recordings of sledgehammer source events at 3 m depth for Stono Marina, SC

5.5.5. RotoSeis V

Repeatability tests were conducted using the RotoSeis V seismic source which was the final Georgia Tech prototype before going into production. During continuous-push seismic sounding CRB01SEIS, several impacts were recorded during pauses in penetration at each rod break. Figure 5.23 presents the optimally-projected stationary-receiver recordings from Channels 1 and 2 down to a depth of 13 m. The test was stopped early at 13 m because of mechanical issues related to the penetration pushing system, not

due to insufficient source amplitude.

A closer look at the signals from the 5.6 m depth recording (Figure 5.24) shows that the signals are quite similar to each other in the time domain. Even the ringing at the trailing ends, which might otherwise have been considered to be random noise, is well-matched from one source strike to the next. The lower portion of the plot shows the frequency domain representation, which is also similar aside from the component at approximately 38 Hz. The rods were not released from the pushing system to make these recordings and as a result, the vibrations from the cone tuck at 38 Hz were traveling down the rods. The bandwidth for these RotoSeis V signals extends beyond 125 Hz. The textured base of the source prevented slipping, which improved the coupling and increased the bandwidth.

The three-dimensional time plots of each signal are shown in Figure 5.25. The responses are slightly rounded, but consistent. The hammer within the RotoSeis V was not perfectly centered which resulted in slightly off-center strikes. The same signals are displayed on a hodograph in Figure 5.26, and further highlight the repeatability of the RotoSeis V.

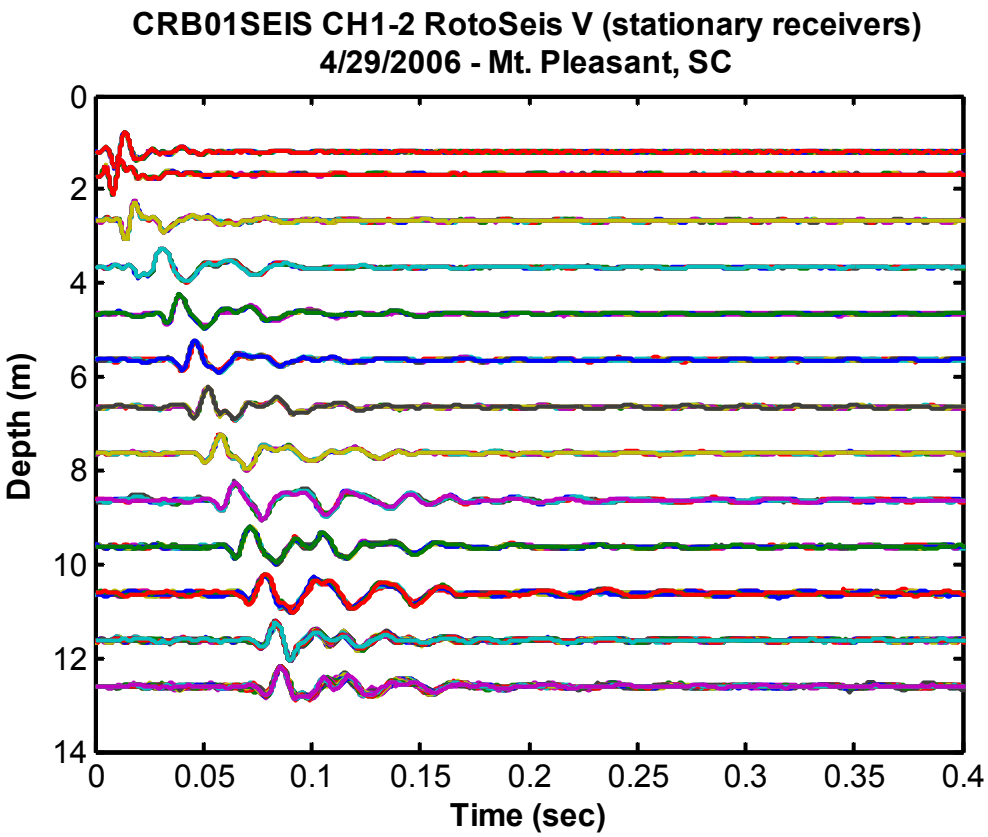

Figure 5.23 Optimal projection of duplicate RotoSeis V signals recorded while penetration stopped at rod breaks during the continuous-push sounding CRB01SEIS

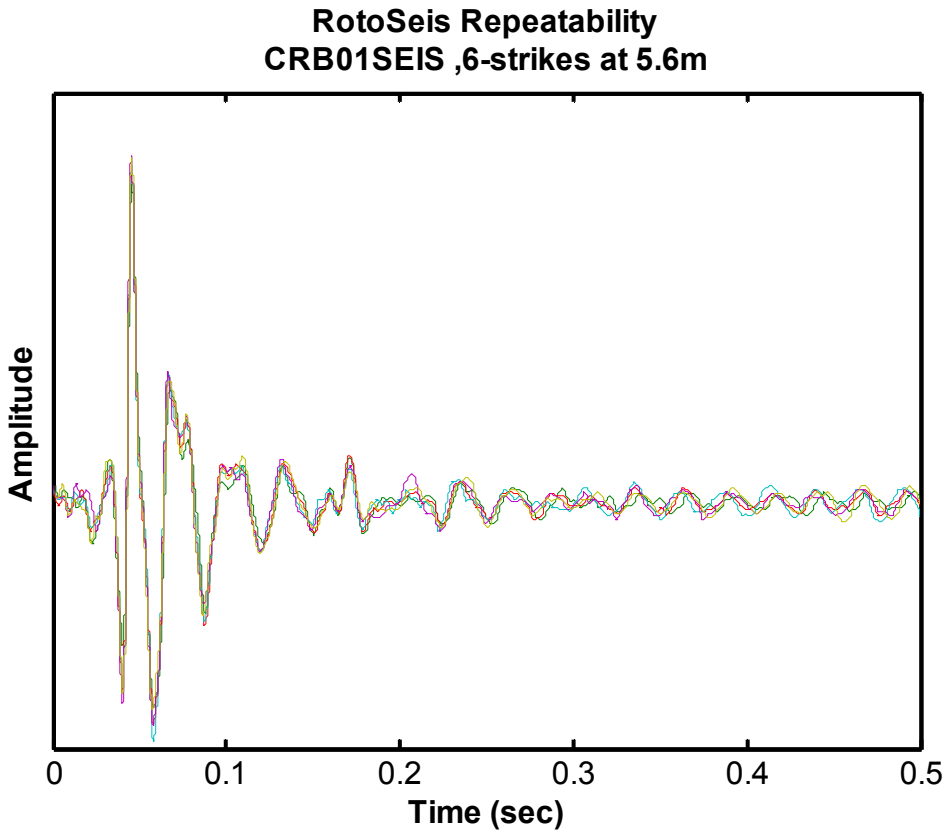

(a)

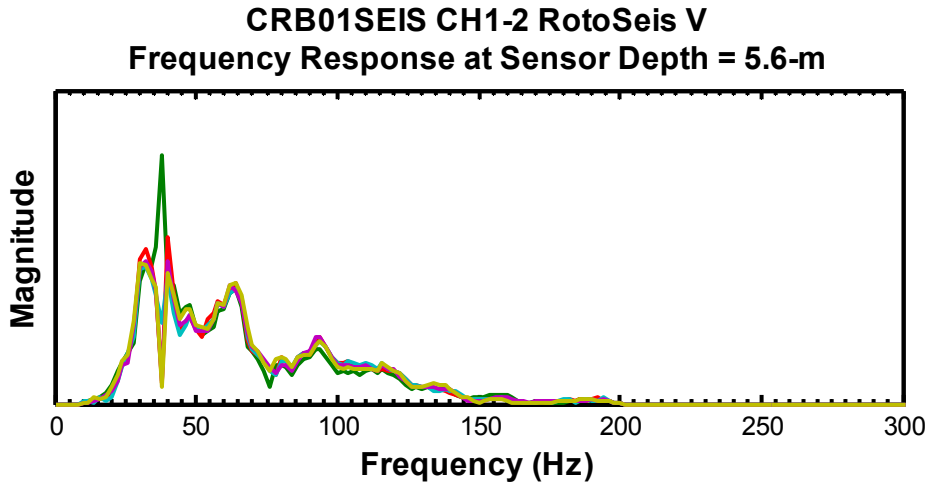

(b)

Figure 5.24 Optimal projection of six repeated hammer strikes of RotoSeis V at 5.6 m during CRB01SEIS (a) time domain and (b) frequency domain

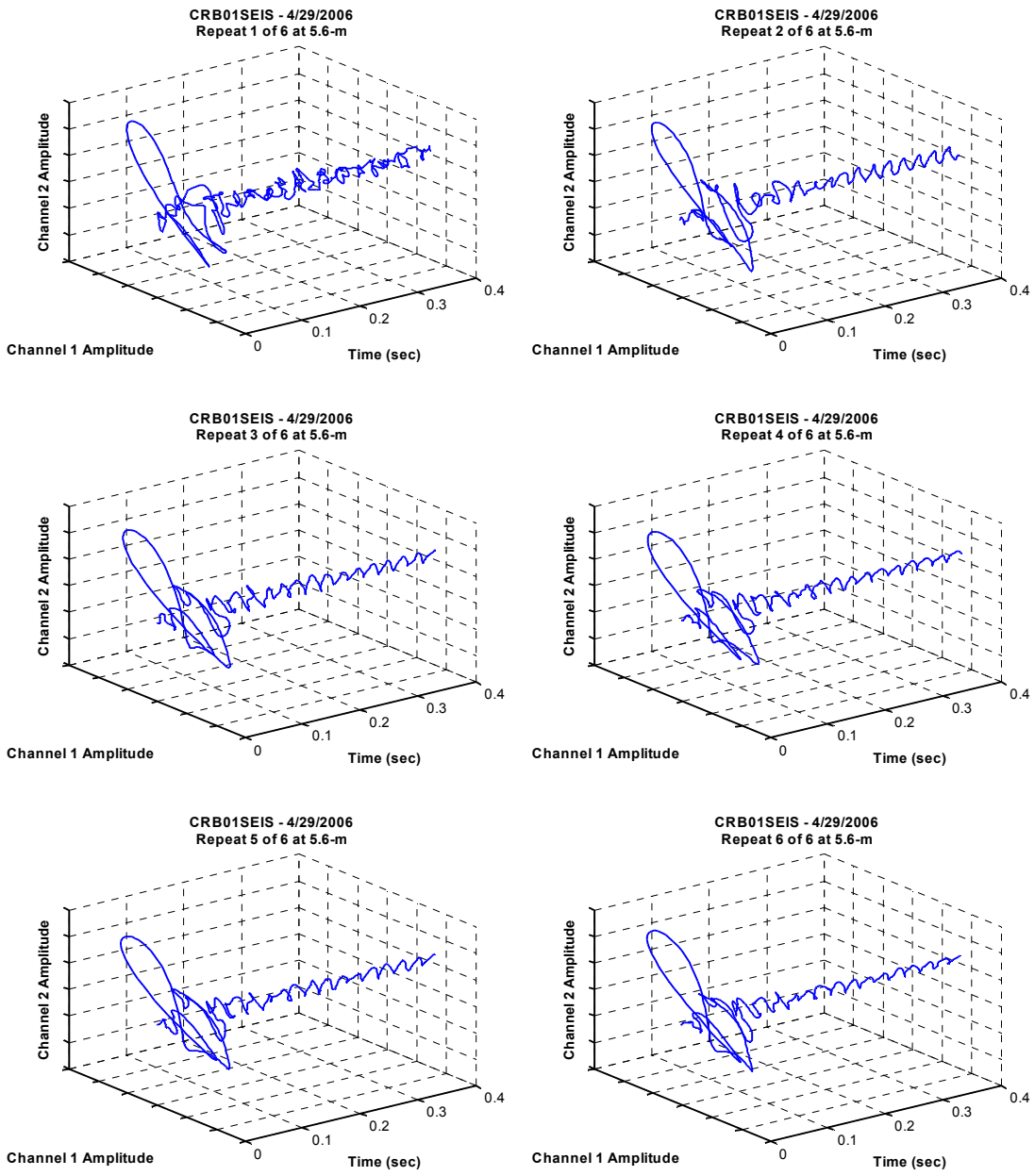

Figure 5.25 3-dimensional time-histories of six sledgehammer impacts recorded during CRB01SEIS at a depth of 5.6 m

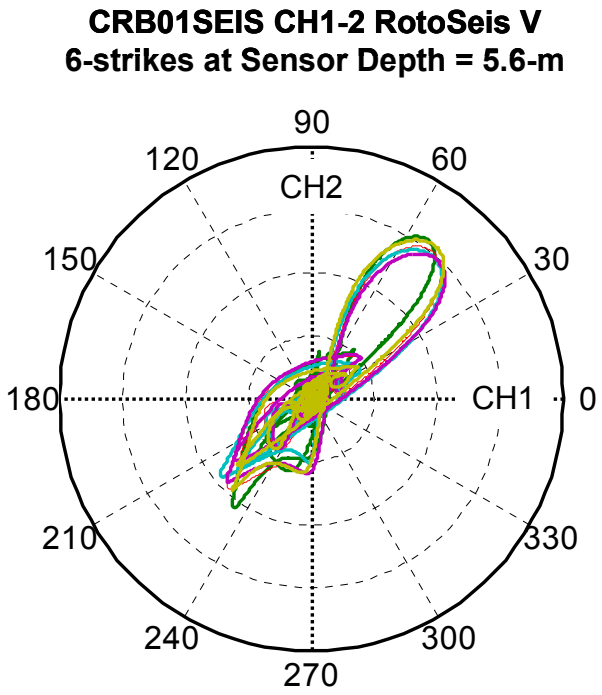

Figure 5.26 Hodograph of six superimposed biaxial recordings of RotoSeis V source events at 5.6 m depth

RotoSeis must be capable of generating shear waves that can be utilized to measure shear wave velocity at depths up to 30 m, which is a reasonable upper bound for the majority of commercial, as well as research-type, site characterization needs. The deepest seismic sounding achieved with the original AutoSeis was 21 m during SCPT sounding FORST1 (Figure 3.32). The pneumatic AutoSeis was tested to 23 m during SCPT sounding SWGA01 (Table 4.1 and Figure 3.34), and although capable of reaching 30 m, the signal quality was deteriorating, as described in Chapter 3. RotoSeis II was successfully tested to 30 m during SCPT sounding HENM (Table 4.1), but several signals had to be stacked, or added together, to sufficiently improve signal quality for analysis. Three RotoSeis prototypes later, at a test site in New Orleans, LA, RotoSeis V generated signals of sufficient quality to a depth of 30 m during the SCPT sounding NEWOR01. The test was performed with a 100 kN Hogentogler digital cone penetrometer system,

utilizing a single horizontal seismic sensor, and a CPT rig provided by Southern Earth Sciences, Inc. under the direction of the author.

The seismic recordings collected during the test, shown in Figure 5.27, do not have the appearance of ideal shear wave signals, with the peak amplitude at the first arrival, but the shear wave is able to be detected and velocity profile analyzed to depths of up to 30 m. The signal quality was likely affected by accidental rod rotation, which is a concern while pushing in soft soils (Figure 4.28). With only a single axis receiver, it is not possible to enhance the results by re-projecting to a better alignment angle. The unusual flat trailing ends of the signals are a result of zero-padding the signals for display. The original signals were trimmed significantly at the time of recording to reduce file size.

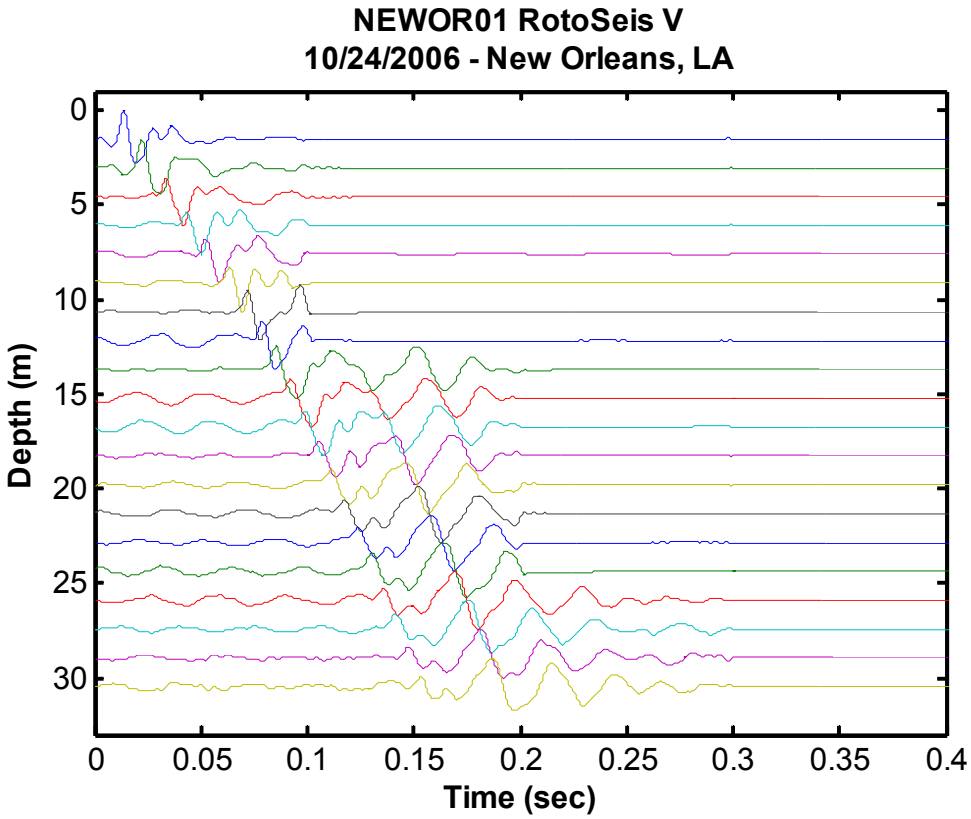

Figure 5.27 Seismic records recorded with RotoSeis V to a depth of 30 m during the SCPTu sounding NEWOR01 in New Orleans, LA

5.5.6. Commercial RotoSeis

A commercial version of the RotoSeis was developed based on the design of RotoSeis V, the final Georgia Tech prototype. During construction of the production model by Finite Precision, life-cycle testing was performed to determine the reliability of the device. The Commercial RotoSeis was tested for approximately 90,000 cycles under continuous operation until a keyway, a slot in the axle which allows the gear to be fixed to the axle, became deformed, and the gears lost alignment. For continuous-push operation, with a hammer strike occurring every 10 seconds, the number of strikes per 30 m sounding is approximately 220 to 260, depending on the haste with which new rods are added. For the tested lifespan, RotoSeis could perform more than 360 continuous-push soundings to 30 m without failure.

The downhole test at the Cooper River Bridge in Mt. Pleasant, SC with the Commercial RotoSeis was successful to a depth of 30 m. Signals are presented in Figure 5.28 from CRB03SEIS, which were recorded at rod breaks during the continuous-push seismic test. The signals shown are the combined responses of Channels 1 and 2, which have been projected at the optimal angle relative to the axis of the RotoSeis. Several repeated signals were collected during the rod breaks while RotoSeis ran continuously with hammer strikes occurring every 10 seconds.

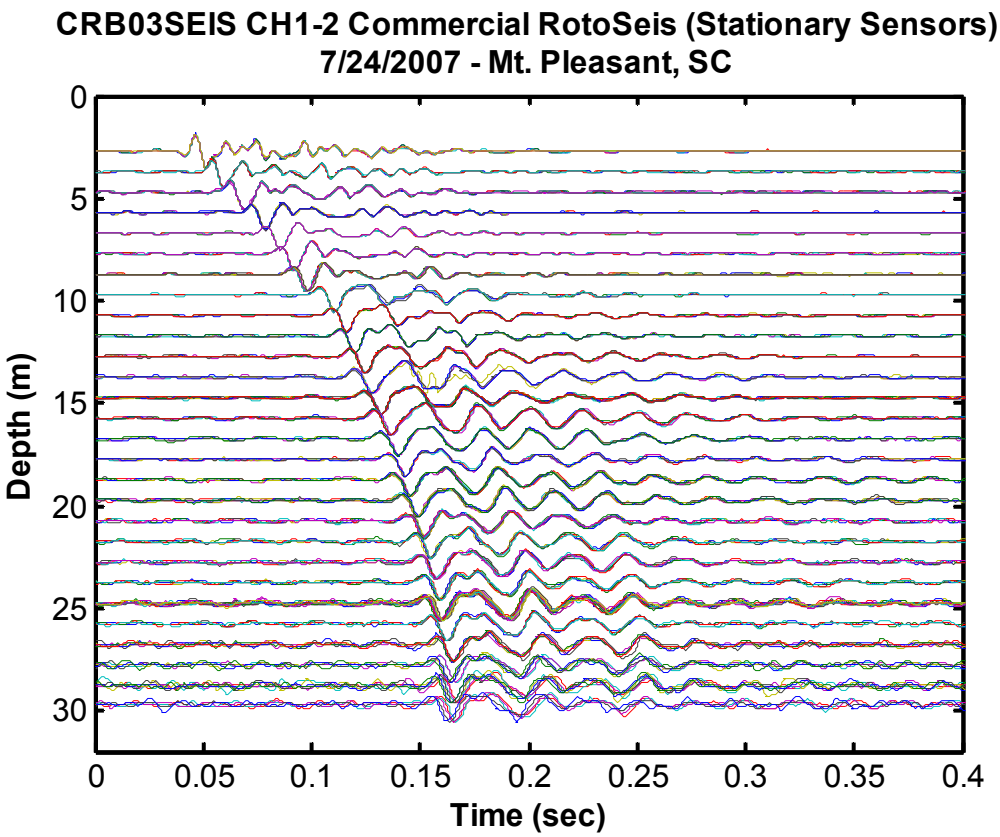

Figure 5.28 Signals recorded with the Commercial RotoSeis during pauses in penetration of CRB03SEIS conducted at Mt. Pleasant, SC test site

Signals from six CRB03SEIS repeated hammer strikes at a depth of 10.7 m are shown in Figure 5.29. The upper plot is the time domain representation of the signals, and the lower plot describes the frequency content. In both representations, the repeated signals are essentially the same. The bandwidth for the Commercial RotoSeis is about 100 Hz, which is slightly less than the RotoSeis V bandwidth at the same site. The reason for the reduced bandwidth of the commercial device is again likely related to coupling. The base surface of the Commercial RotoSeis utilizes the same textured surface as the RotoSeis V in order to minimize slipping. However, for CRB01SEIS RotoSeis V trials, the source was placed under the outrigger of the cone truck, and for CRB03SEIS the Commercial RotoSeis was anchored separately from the cone truck using earth anchors. The cone truck outrigger provides higher normal force and stiffer coupling, however the

anchors were utilized to maintain a constant normal force on the seismic source during continuous-push seismic recording.

The 3-dimensional time plots (Figure 5.30) and hodograph (Figure 5.31) again reinforce the repeatable nature of the Commercial RotoSeis. It can also be seen that the shape of the signal is directional with little out-of-plane motion. The Commercial RotoSeis appears to have a better aligned hammer than the previous prototype version. The axis of the source was aligned at approximately 60° from Channel 1.

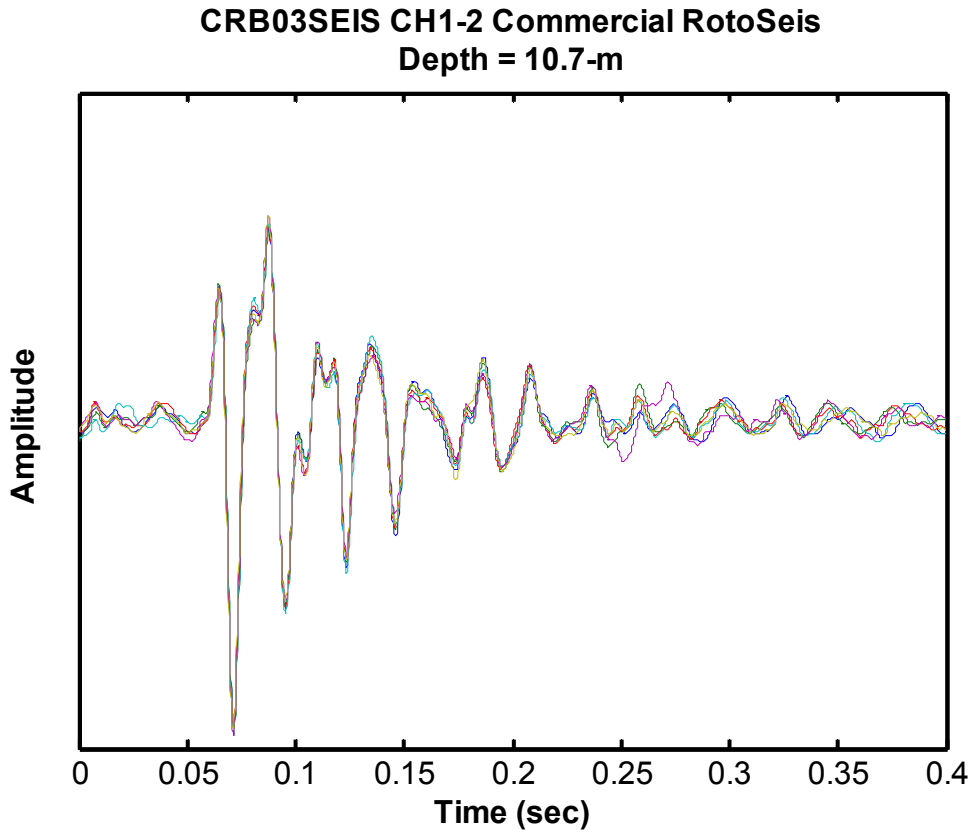

(a)

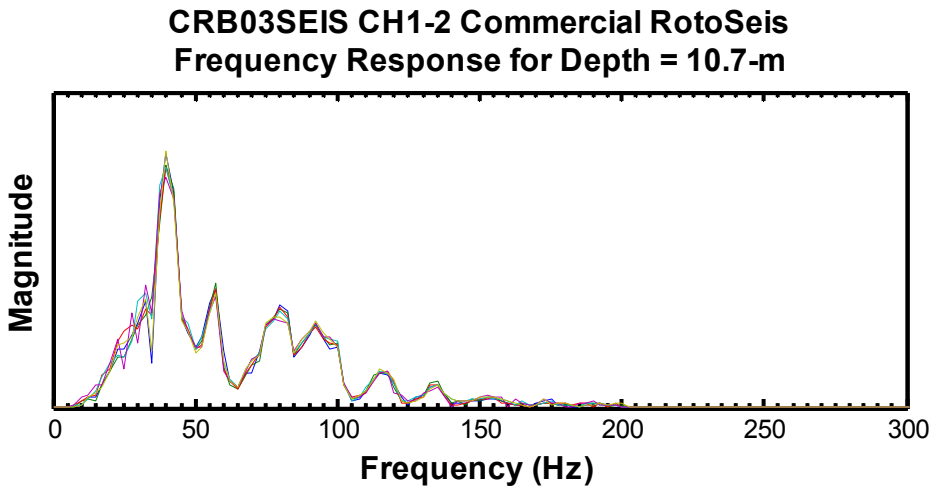

(b)

Figure 5.29 Repeated strikes of the Commercial RotoSeis performed during CRB03SEIS at 10.7 m (a) time domain signals and (b) frequency domain representation

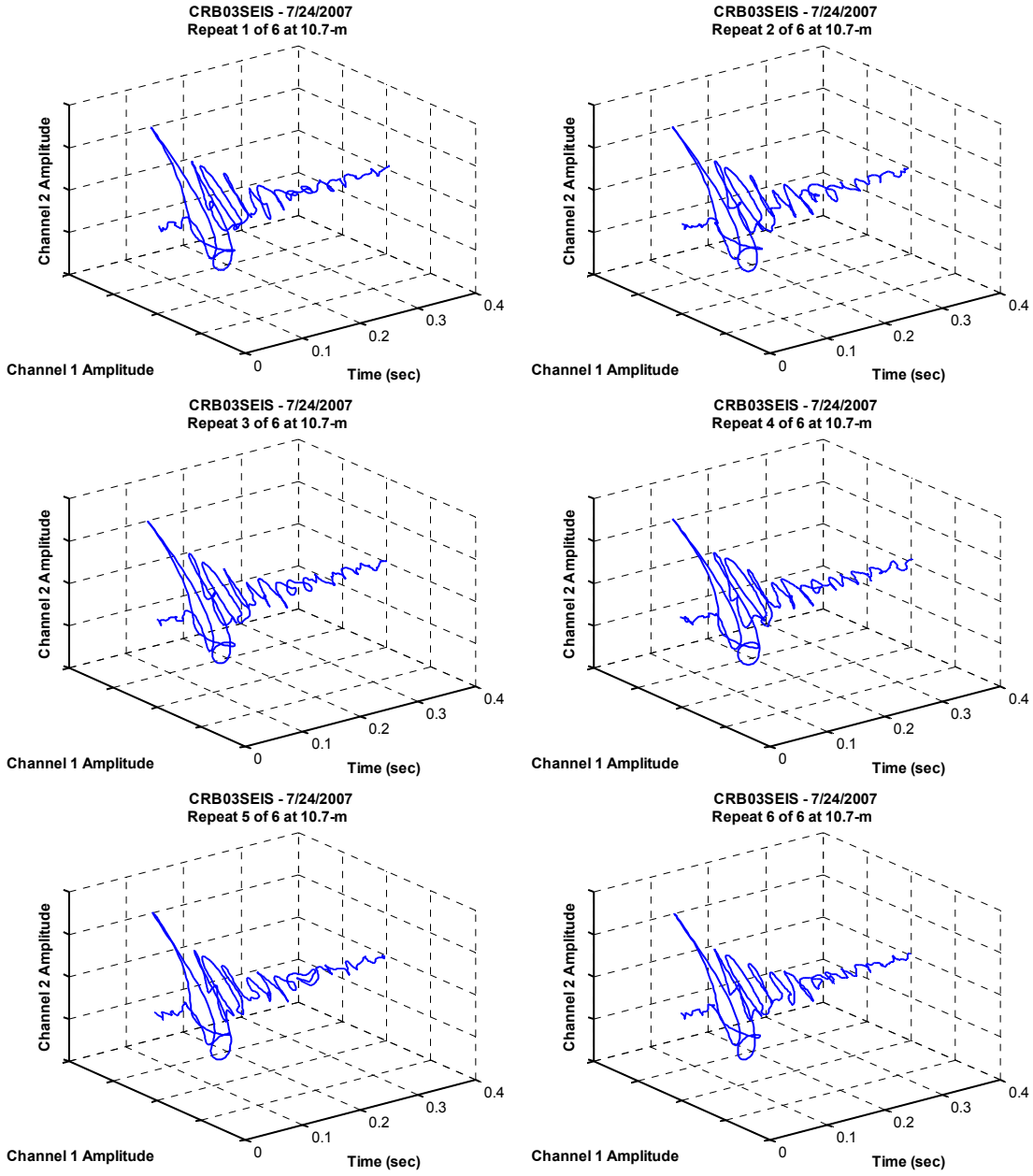

Figure 5.30 3-dimensional time-histories of six Commercial RotoSeis impacts recorded during CRB03SEIS at a depth of 10.7 m

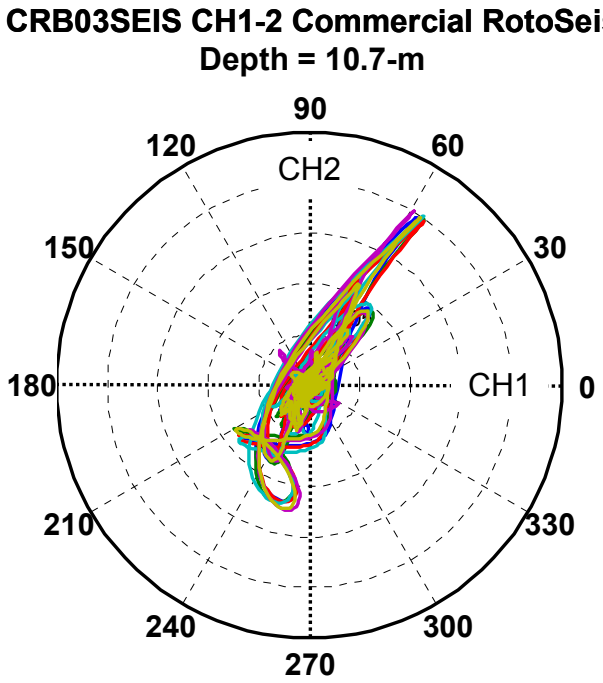

Figure 5.31 Hodograph of six superimposed biaxial recordings of Commercial RotoSeis source events at 10.7 m depth

5.6. Continuous-Push Recordings

Continuous-push seismic recordings were made during soundings CRB03 and CRB03SEIS at the Cooper River Bridge test site in Mt. Pleasant, SC. Both of the tests were conducted for the purpose of developing a continuous-push seismic system in order to reduce field testing times for SCPT while simultaneously increasing the amount and quality of data that can be obtained during direct-push in-situ testing.

The signals shown in Figure 5.32 are the non-stationary sensor recordings, which were generated using Commercial RotoSeis and collected on Channel 2 of the biaxial-true-interval probe during sounding CRB03SEIS. The number of recorded wavelets is significantly increased over conventional SCPT procedures at 1 m depth intervals. The stationary sensor recordings made at rod breaks during this same sounding were presented previously in Figure 5.28. The appearance of noise is significantly greater in

the non-stationary (moving) sensors than in the stationary sensors. For most of the sounding, the peaks of the shear wave arrivals stand out clearly against the background. In general, the quality of the wavelets appears to be quite good over most of the depth range covered. Yet, between depths of 12.5 m and 15.5 m, the ambient noise overpowers the source signals. Based on the CPTu profile at this location (Figure 5.33), the noisy seismic signals likely correspond to the granular sandy layer immediately preceding the top of the Cooper Marl (see site description in Section 4.2.6).

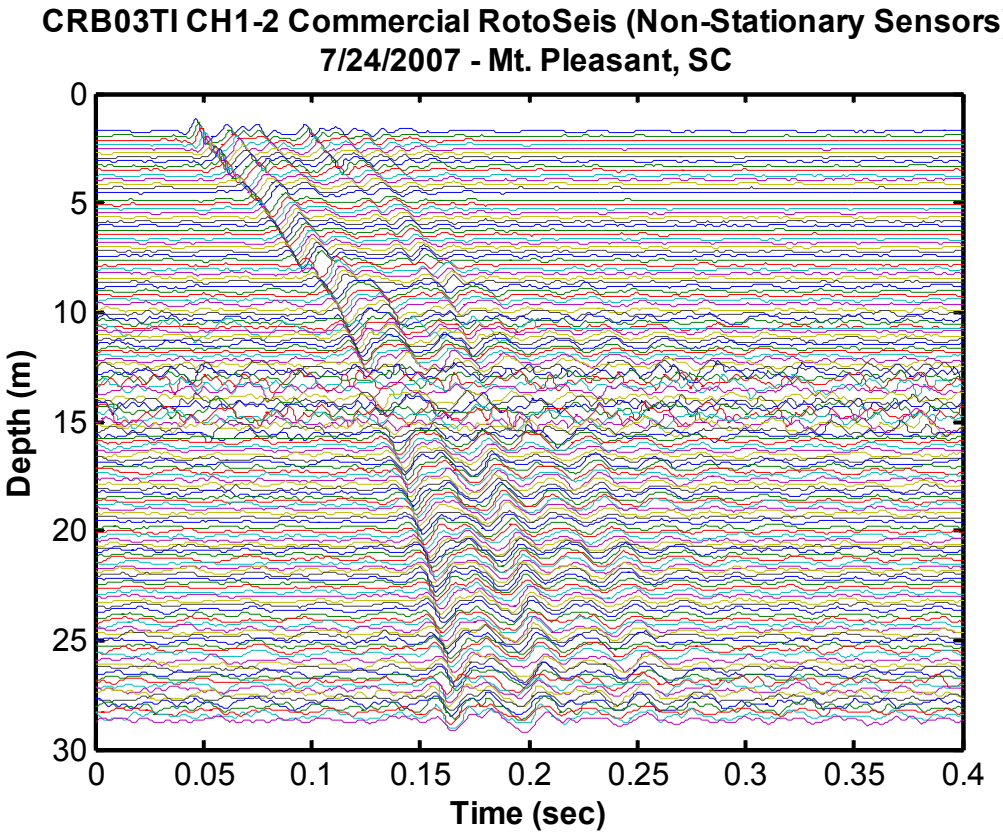

Figure 5.32 Continuous-push seismic records recorded with Commercial RotoSeis to a depth of 30 m during penetration of the sounding CRB03SEIS at the Cooper River Bridge site in Mt. Pleasant, SC

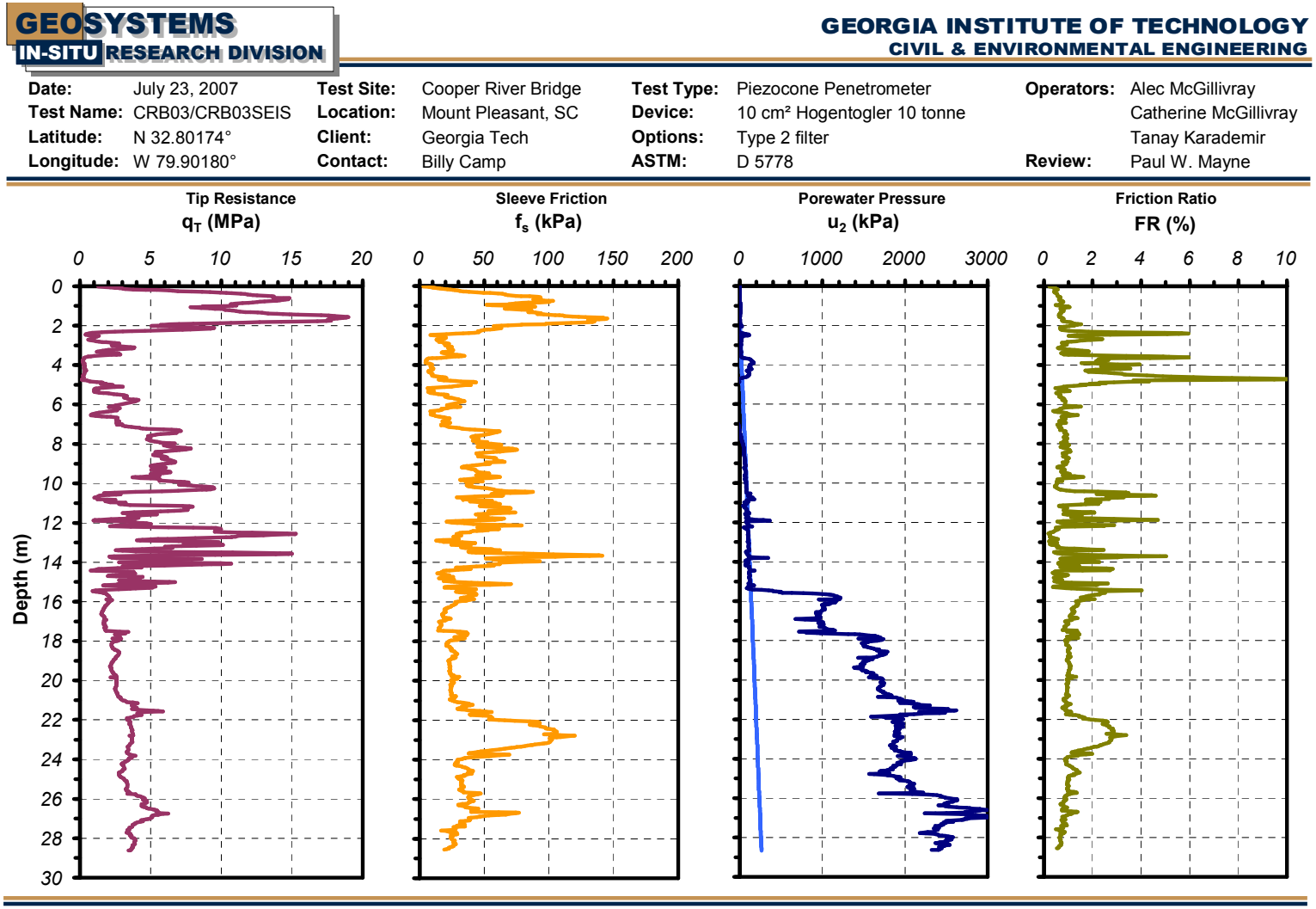

Figure 5.33 Profile of tip resistance, sleeve friction, penetration porewater pressure and friction ratio from CRB03

In order to compare the characteristics of the stationary sensors and the non-stationary sensors, non-stationary receiver signals from Channels 1 and 2 were selected which correspond to stationary receiver signals that were recorded with Channels 5 and 6 where the sensor depths are equal. The selection of signals used for comparison is illustrated in Figure 5.34. Points on the sloped portions of the lines were recorded during penetration. Points on the horizontal portions on the lines were recorded while the probe was stopped. Because the offset between the sensors is slightly less than 1 m, the sensor depths do not line up precisely, but they can be treated as the same.

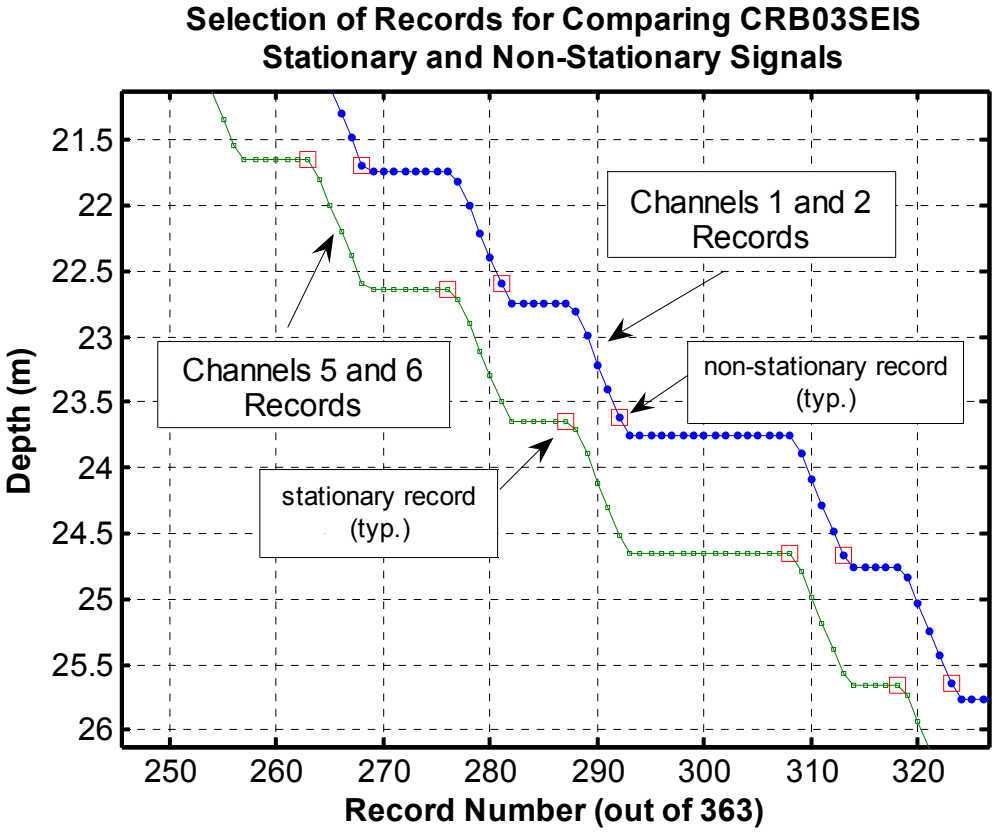

Figure 5.34 Methodology for selecting stationary receiver signals recorded by Channels 5 and 6 to compare with non-stationary receiver signals recorded by Channels 1 and 2 at the same sensor depths

The time histories for the selected stationary and non-stationary sensor recordings are shown in Figure 5.35. For the near-surface depths, the continuous-push signals appear to be identical to their stationary receiver counterparts. In the layer beginning at 12.5 m, the amplitude of the noise increases relative to the amplitude of the shear waves to the point where shear waves are no longer visible. Once the sensors penetrate into the Cooper Marl, the non-stationary sensor signals are still noisier than the stationary receiver signals, but noise levels are reduced.

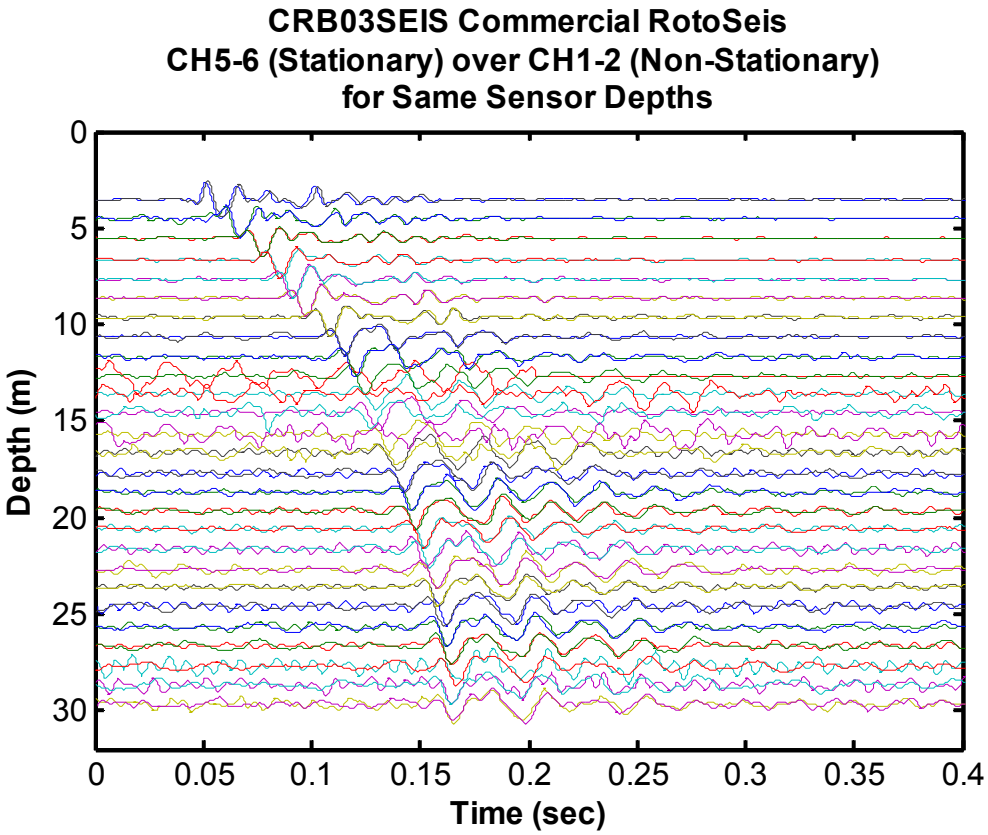

Figure 5.35 Comparison of non-stationary sensor Channels 1 and 2 signals with stationary sensor Channels 5 and 6 signals for the same sensor depths during CRB03SEIS

The time signals of stationary and non-stationary (moving) sensors are compared in the following series of figures at 3 depths of CRB03SEIS. For the sensor depth of 7.6 m (Figure 5.36), the signal appearance is not noticeably different between a continuous-push signal and one recorded with stationary receivers. However, the appearance of the hodograph is different from a previous Commercial RotoSeis hodograph (Figure 5.31). The reason for the widened appearance is a loss of normal force applied to the top of the source. As mentioned previously, the source was coupled to the ground by earth anchors. As the source vibrated on the surficial sands, settlement occurred which relaxed the load from the anchors. This was discovered and corrected at subsequent depths and the narrow hodograph returned.

Figure 5.37 shows the time signals for the sensor at a depth of 14.6 m. This depth is within the noisiest part of the profile of signals. Good agreement exists between the shear wave components of the stationary and non-stationary receiver signals, but the background noise of the non-stationary sensors is too great to allow identification of the shear wave component within the recording without the overlaid stationary receiver signal.

The final figure in the series, Figure 5.38, is a recording from 17.6 m, within the Cooper Marl, just below the noisiest part of the profile. The noise level in the non-stationary receiver signal has subsided and the shear wave impulse is again visible. The stationary and non-stationary receiver signals are nearly the same again.

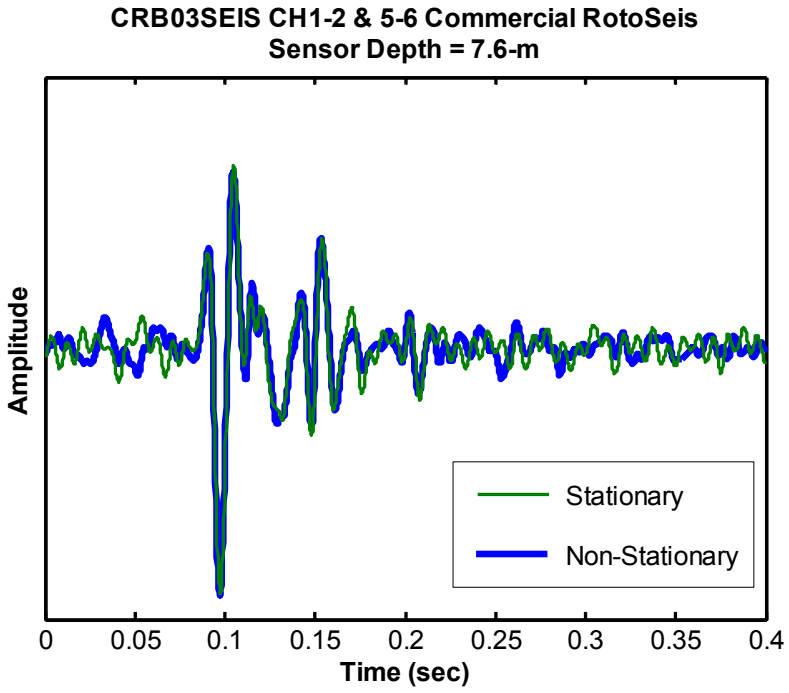

(a)

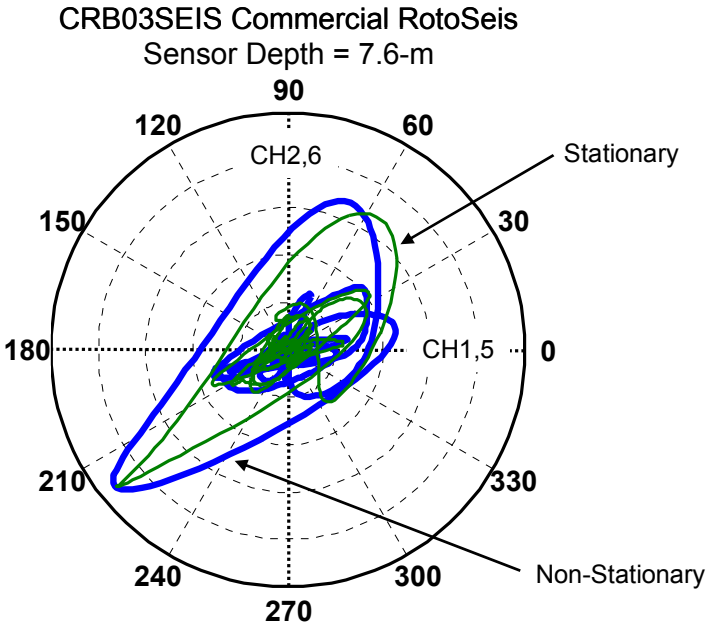

(b)

Figure 5.36 Comparison of CRB03SEIS Commercial RotoSeis signals from Channels 1 and 2 non-stationary sensors with Channels 5 and 6 stationary signals for the sensor depth 7.6 m with (a) the time histories and (b) a hodograph

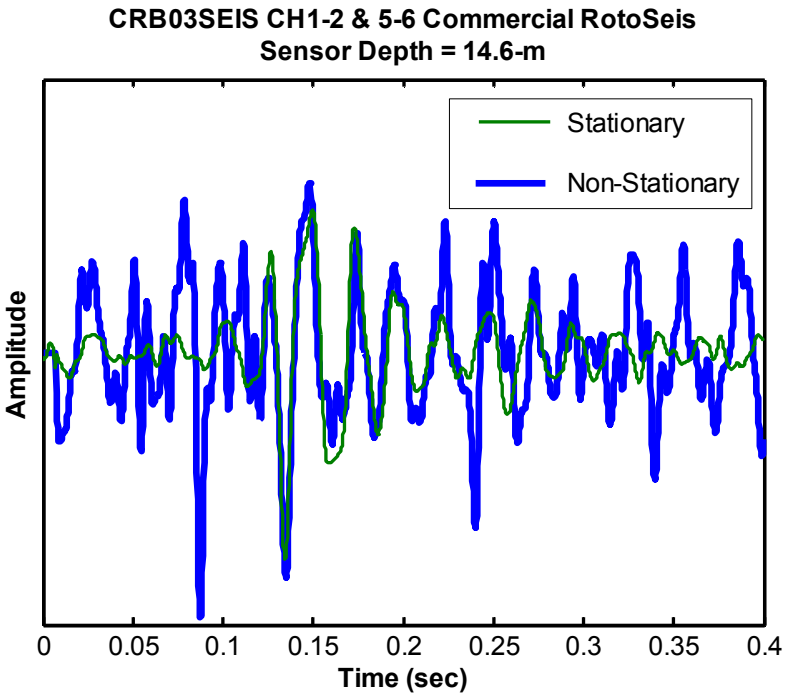

(a)

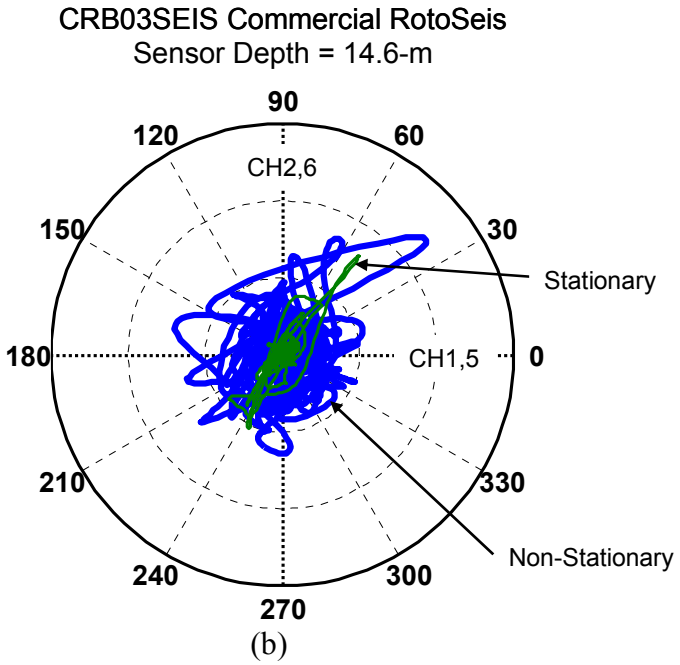

(b)

Figure 5.37 Comparison of CRB03SEIS Commercial RotoSeis signals from Channels 1 and 2 non-stationary sensors with Channels 5 and 6 Stationary signals for the sensor depth 14.6 m with (a) the time histories and (b) a hodograph

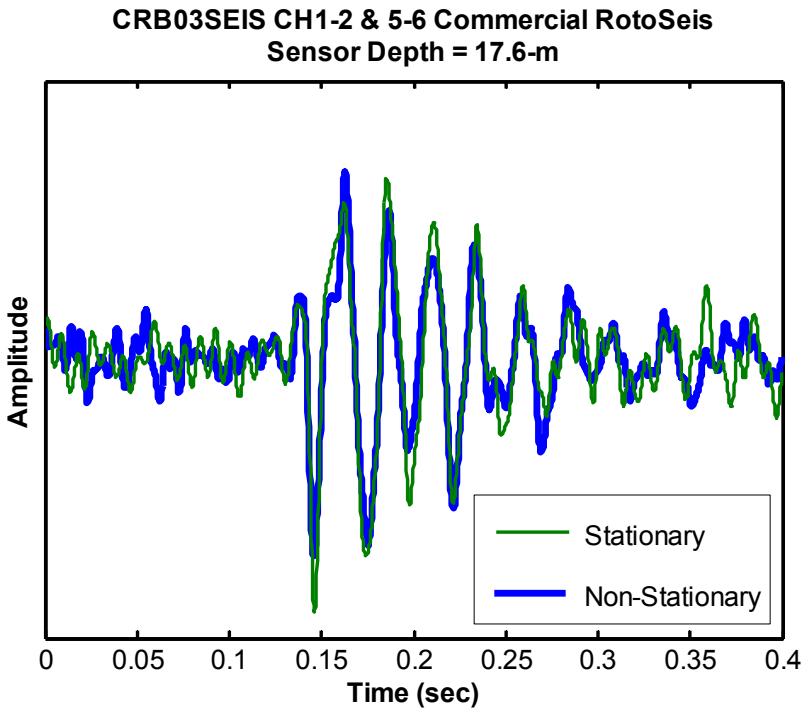

(a)

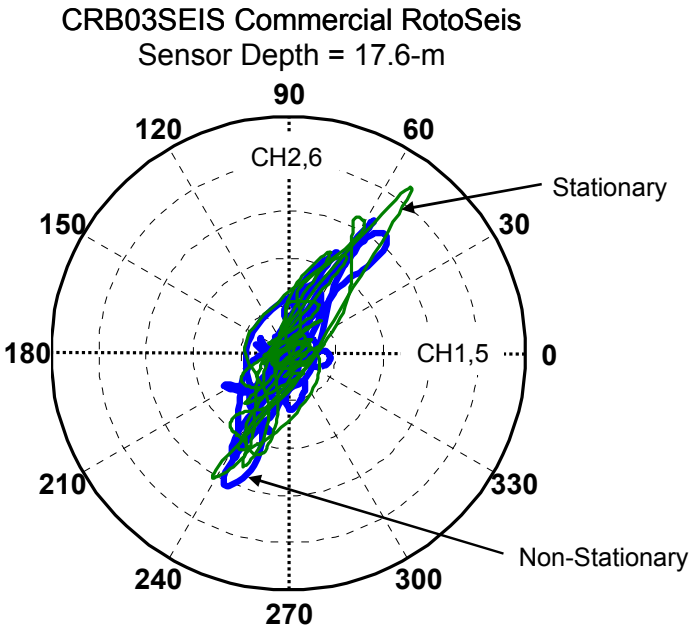

(b)

Figure 5.38 Comparison of CRB03SEIS Commercial RotoSeis signals from Channels 1 and 2 non-stationary sensors with Channels 5 and 6 Stationary signals for the sensor depth 17.6 m with (a) the time histories and (b) a hodograph

The frequency contents for the stationary and non-stationary receiver signals for depths 7.6 m, 14.6 m, and 17.6 m are compared in Figure 5.39. As expected, based on the previous time domain comparisons, the stationary and non-stationary receiver signals at 7.6 m and 17.6 m depths are relatively similar and the noisy 14.6 m signal shows elevated amplitudes within and outside of the source bandwidth. The source bandwidth is approximately 100 Hz, although by 17.6 m the amplitudes of the higher frequency components have diminished. In all of the signals, the non-stationary receiver signals show elevated amplitudes in the 26 Hz range. The low frequency noise within the source bandwidth is likely due to vibrations from the pushing system, rather than particle crushing or friction between soil particles and the probe.

Researchers working with the Acoustic Cone Penetration Test (ACPT), which was discussed briefly in Section 3.3, were concerned with frequency content of vibrations created during penetration of a probe through soil. During penetration chamber tests in sands, Houlsby and Ruck (1998) found that vibrations detected with a microphone inside the probe had broad spectrum frequency content. However, they determined that vibrations less than 3 kHz were due to mechanical vibrations related to the pushing system. Responses between 3 and 13 kHz were deemed resonances within the device itself. Frequencies between 17 and 25 kHz were considered to be the frequencies related to soil properties. The energy from an impulse-type surface seismic source has a frequency bandwidth less than 200 Hz, which is within the bandwidth considered to be affected by vibrations from the pushing system, but well below the frequencies associated with the friction affects from the soil. These were similar conclusions made by other researchers. For a device developed by Massarsch (1986), it had been found that the soil-related penetration noise occurs in the 200 kHz range and researchers chose not to use anything less to quantify soil properties.

Signals from CRB03, the continuous-push SCPTu performed with the 10 cm² Hogentogler cone, are displayed in Figure 5.40. The upper plot shows the records obtained while the probe was in motion, and the lower plot contains records obtained with the probe held stationary, while paused during breaks between rods. Again, the non-stationary receiver signals appear much noisier than the stationary-receiver signals. Except for the depths between 12.5 m and 15.5 m, the shear wave component is still readily apparent.

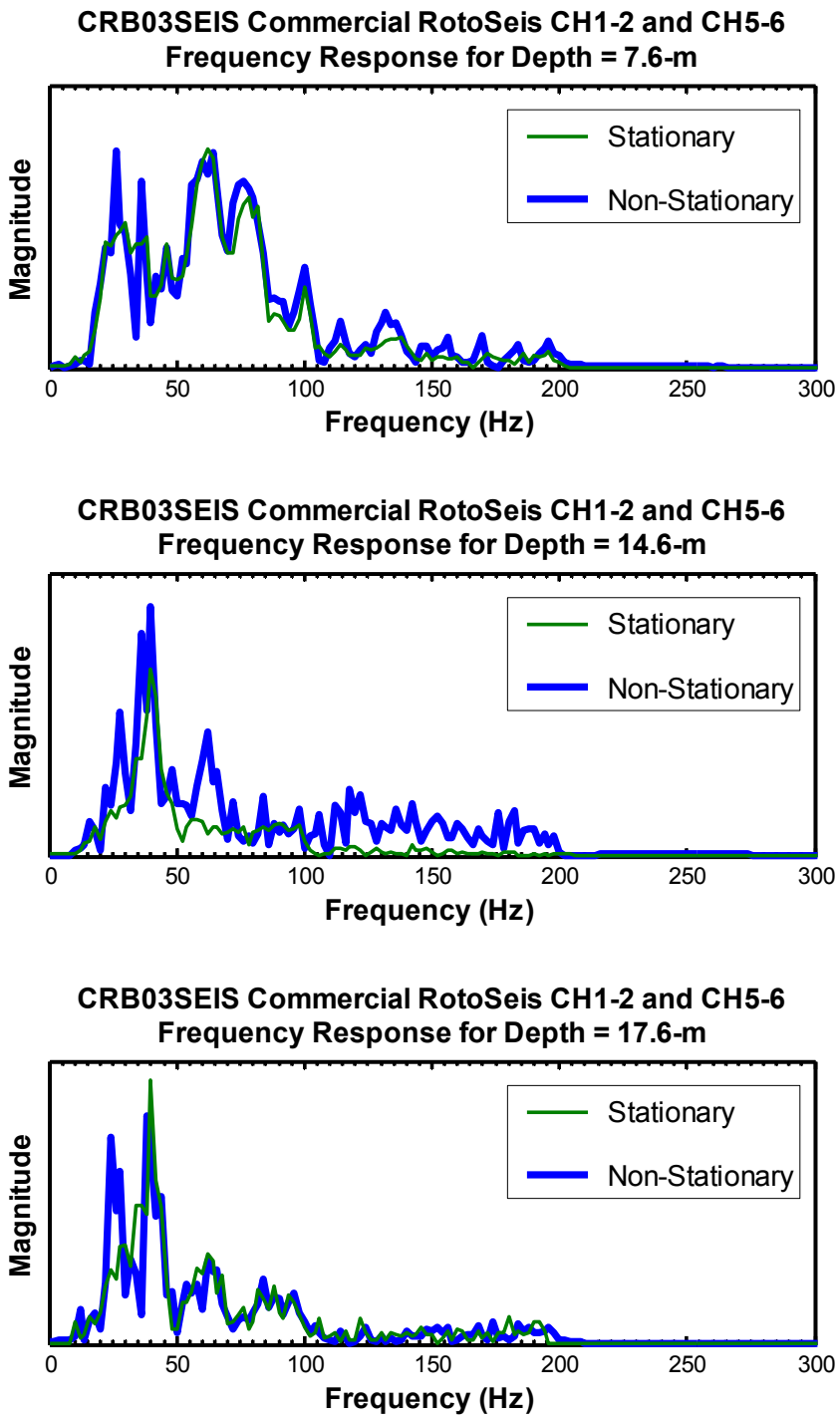

Figure 5.39 Frequency content of signals recorded with stationary and non-stationary sensors for CRB03SEIS

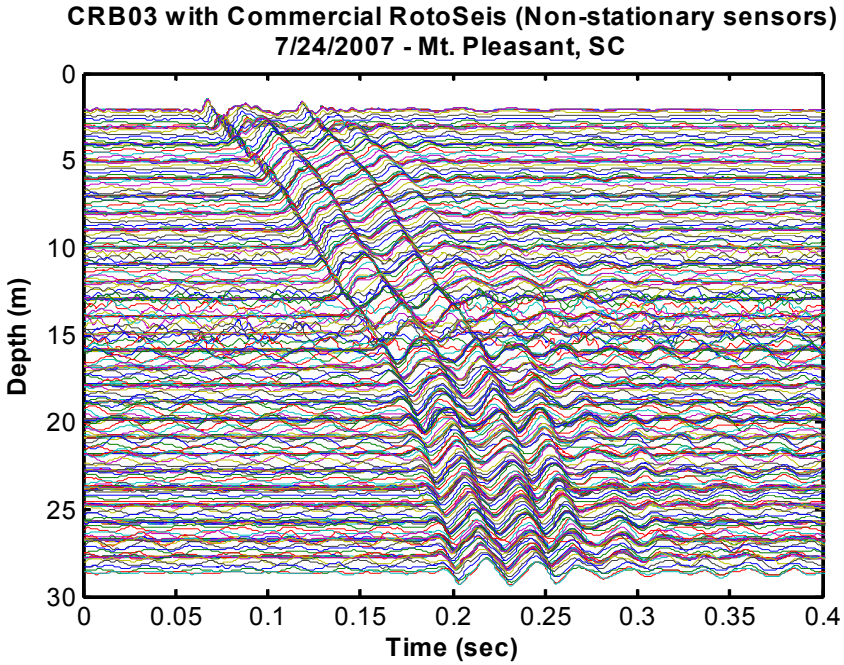

(a)

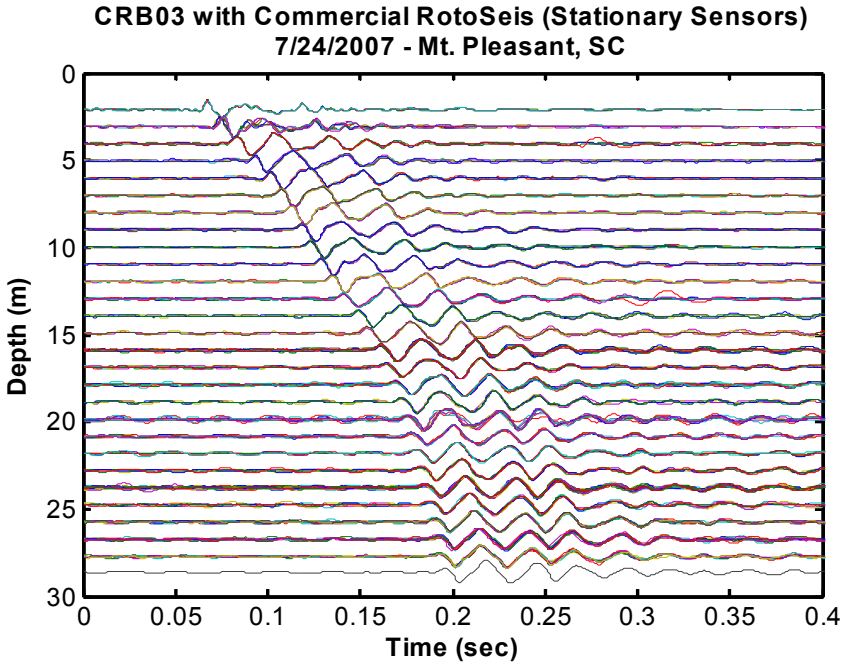

(b)

Figure 5.40 CRB03 Hogentogler cone and Commercial RotoSeis time histories for (a) non-stationary sensors and (b) stationary sensors only

In order to further study the frequency amplitude differences between the stationary and non-stationary receiver signals, the pre-trigger scans from each signal were separated from the portion of the signal containing the shear wave arrival. The duration of the original recorded signals was 1.4 s. The durations of the subdivided signals were 0.2 s interval for the noise records as well as the shear wave records. A series of surface plots were created from these signals in order to show the magnitudes of the frequency content as it changes with depth.

Figure 5.41 shows the same surface from two points of view: (a) the three-dimensional surface of the frequency content of the pre-trigger noise with depth out to more than 1000 Hz and (b) the same surface looking parallel with the frequency axis to show just the change in peak noise magnitude with depth. The noise recorded by a stationary receiver is shown as a red surface. The noise frequencies components from a non-stationary receiver are plotted as a transparent blue surface. In the upper plot, ridges are visible in the surfaces occurring at 350 Hz and 650 Hz that are well outside the typical source bandwidth of 100 Hz. There is also a ridge that runs down along 36-38 Hz, which can be problematic because this lies within the source bandwidth.

The red surface might be expected to be completely flat, but the raised portions of the red surface are due to vibrations from the cone truck. The two-dimensional view shows that the amplitude of noise vibrations recorded by a stationary receiver varies with depth, generally decreasing, but not continually. This indicates that the vibrations are transmitted through contact with the rods rather than solely through the ground by the tires and leveling pads. Even though penetration is halted, the rods are still in contact with the vibrating cone truck, confined within the guide tube.

During penetration, the pushing system is firmly connected to the rods, which results in increased noise transmission. The noise recorded by a non-stationary receiver is additive to the stationary receiver noise, so the blue noise surface lies above the red noise surface. Based on the three-dimensional view, the peak frequency components of the

pushing noise are the same as the peak components of noise recorded by a stationary receiver, indicating that the vibrations emanate from the same source. However, the amplitude of the non-stationary receiver noise varies more with depth. Within the sand layer between 12.5 m and 15.5 m (see Figure 5.33), the non-stationary sensor noise amplitude increases dramatically. Increases in the bandwidth of some of the non-stationary noise signals appear in thin layers, mimicking the spiked appearance of the q_T and f_S channels at those depths.

Although increased vibrational noise is carried down by contact of the testing vehicle with the rods during penetration, the vibrations do not affect all of the seismic sensors equally. The noise is amplified in the stiffer layers, but the increased vibration is confined within those layers. During the sounding CRB03SEIS, the tip of the seismic probe, including Channels 5 and 6, encountered the noise-causing layer at a depth of 12.5 m, yet the noise levels do not increase at the Channels 1 and 2 locations, located 1 m above the tip, until the sensors actually arrive at 12.5 m themselves. In other words, the lower non-stationary receivers experience the noise before the upper non-stationary receivers.

In Figure 5.42, the frequency range has been shortened to highlight more of the source bandwidth. The red surface is again the noise recorded by pre-trigger scans with the receiver held stationary. The transparent blue surface is the frequency content of the RotoSeis shear wave signals recorded also with a stationary receiver. The shallow noise magnitudes, which seem significant in the previous plot, almost disappear under the strong source amplitudes near the surface. The source amplitude attenuates sharply with depth, but the frequency magnitudes remain above stationary receiver noise magnitudes for the duration of the sounding.

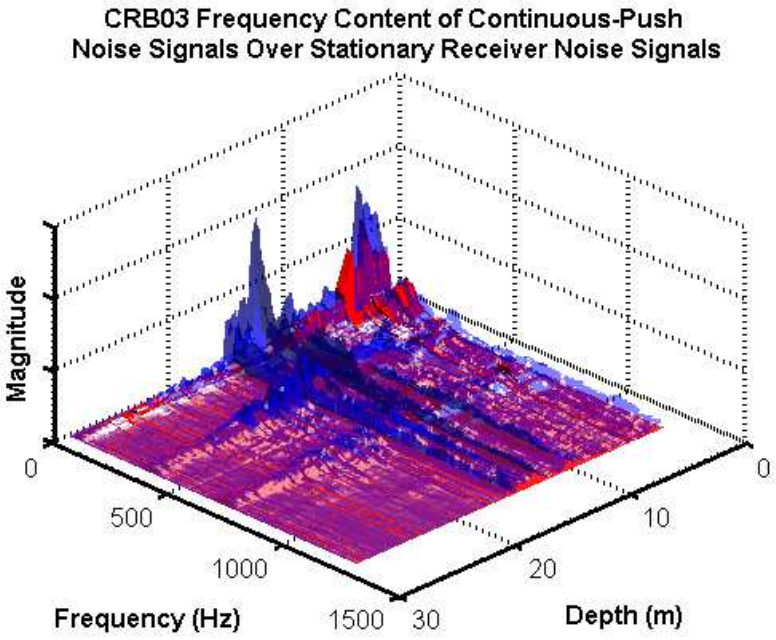

(a)

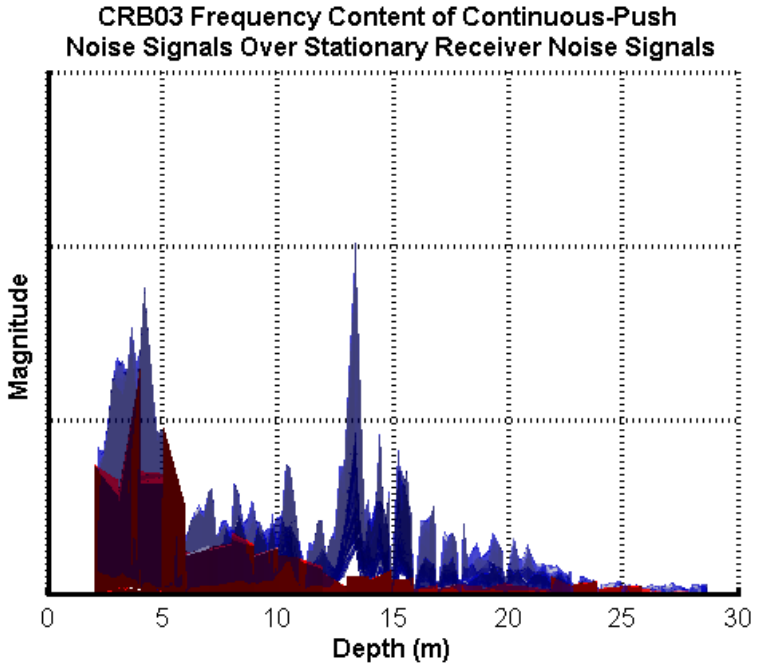

(b)

Figure 5.41 Surface plot of the frequency content of noise measured during CRB03 by a non-stationary sensor (transparent blue surface) and the frequency content of the noise measured with a stationary sensor (red surface) (a) 3-D view and (b) 2-D view of magnitude with depth

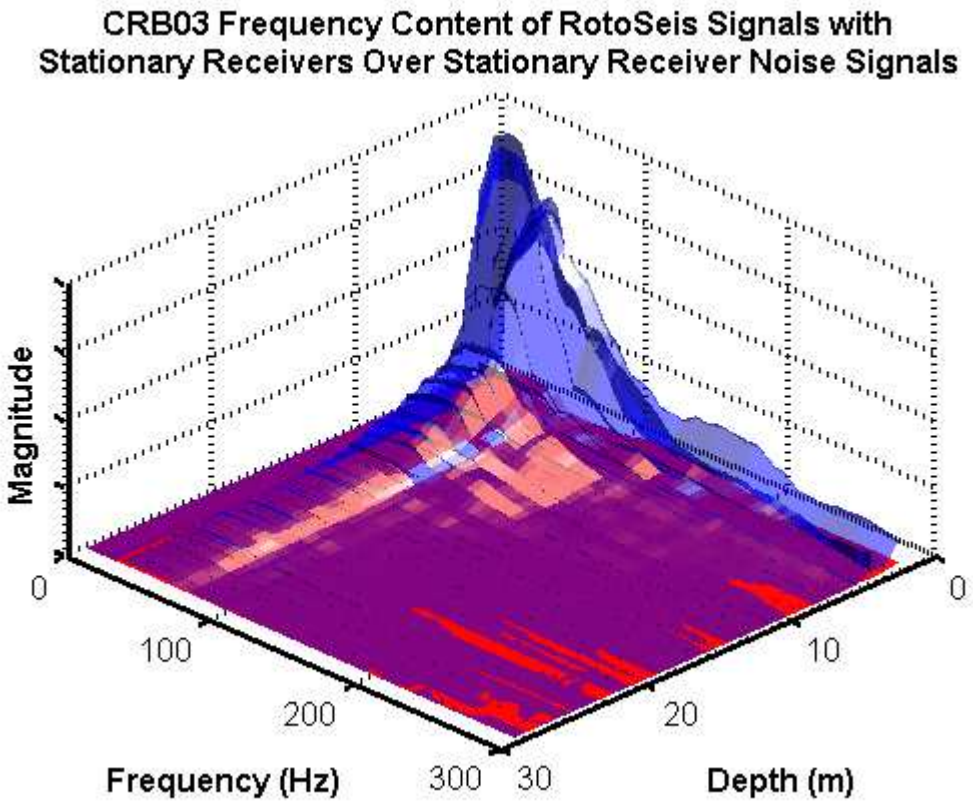

Figure 5.42 Surface plot of the frequency content with depth for CRB03 Commercial RotoSeis signals recorded with a stationary receiver (transparent blue) and the frequency content with depth for the noise measured by a stationary sensor (red surface)

Figure 5.43 shows the magnitudes of the stationary receiver RotoSeis frequencies again in blue, but this time plotted over the magnitudes of the noise recorded by the non-stationary receiver in red. Between the depths of 12.5 m and 15.5 m, the red noise surface rises above the source amplitudes. The source signals are obscured by noise in this depth range, preventing V_S analysis utilizing those signals

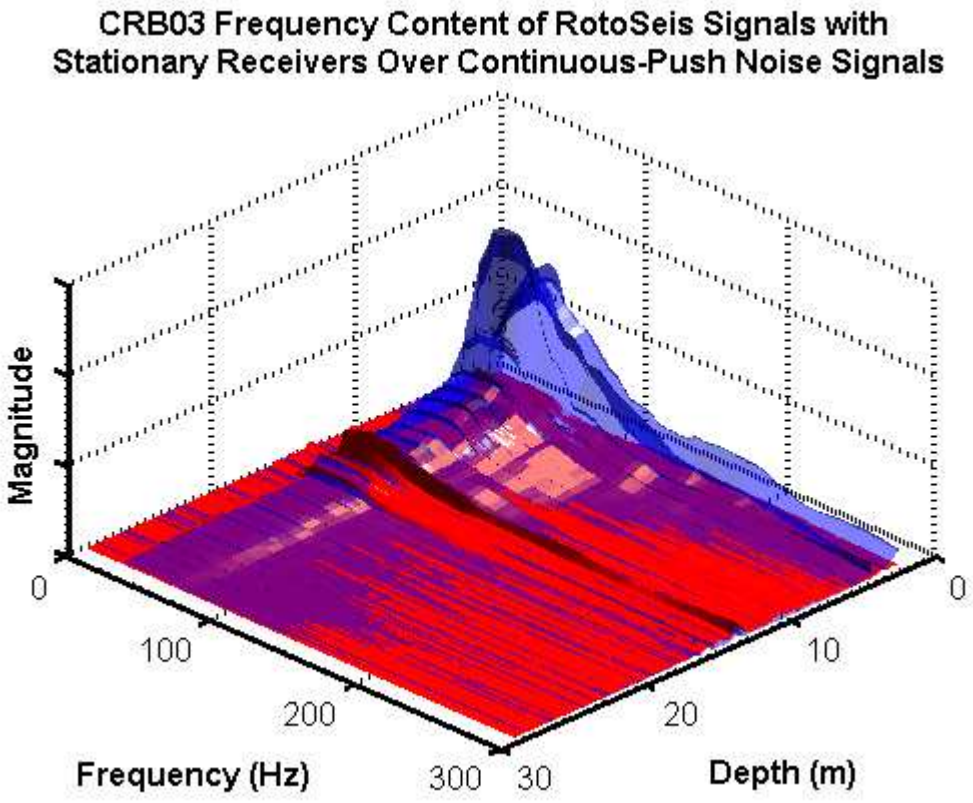

Figure 5.43 Surface plot of the frequency content with depth for CRB03 Commercial RotoSeis signals recorded with a stationary receiver (transparent blue) and the frequency content of the noise measured with a non-stationary sensor (red surface)

In the final surface plot, Figure 5.44, the frequency content of the non-stationary receiver source signals (blue) are plotted over the frequency spectrum of stationary receiver source signals in red. The relative magnitudes and frequency content are similar, but the non-stationary receiver signals contain elements of the penetration-noise signals which are similar bandwidth. As a result, the non-stationary signals plot above the less distorted surface of stationary receiver frequencies.

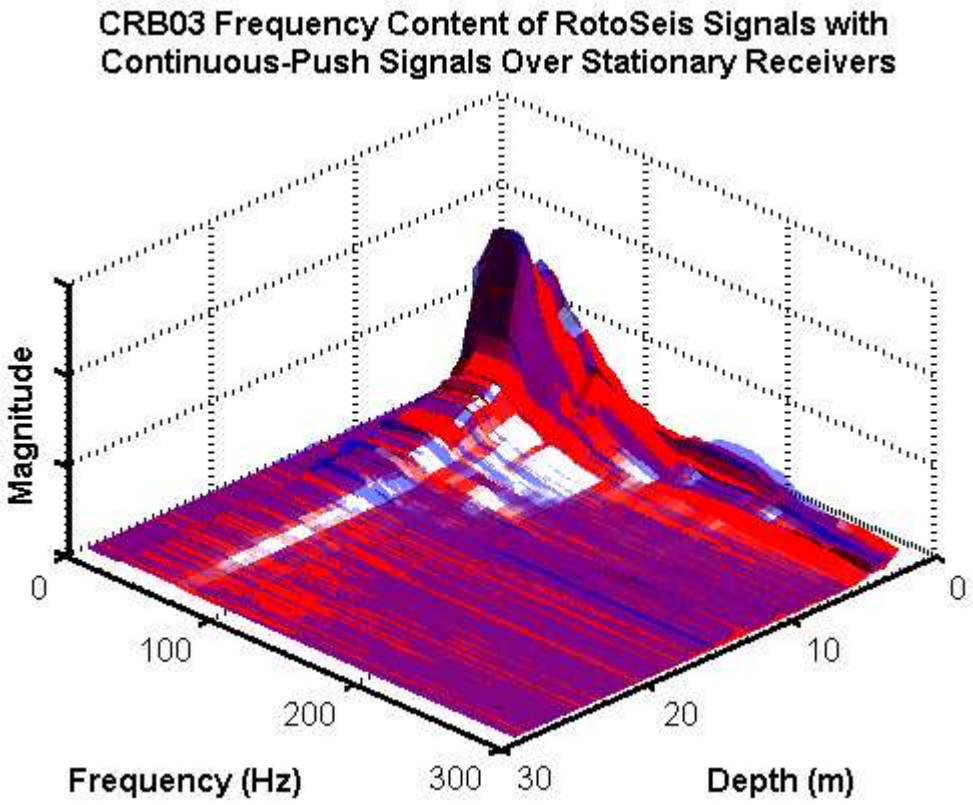

Figure 5.44 Surface plot of the frequency content with depth for Commercial RotoSeis signals recorded with a non-stationary receiver (transparent blue) and the frequency content for Commercial RotoSeis signals recorded with a stationary receiver (red surface)

5.6.1. Continuous-push shear wave velocity

The results of soundings CRB03 and CRB03SEIS including the CPT channels are presented once again in Figure 5.45, but this time with the velocity results from the continuous-push records. There are actually three V_S profiles superimposed on the plot. The green square points are the V_S values determined from the non-stationary receivers of the biaxial true-interval probe during CRB03SEIS utilizing the commercial RotoSeis. The V_S values determined with the commercial RotoSeis device with stationary receivers while the probe was stopped at rod breaks during CRB03SEIS are emphasized with yellow circles. Lastly, for comparison, the frequent-interval velocity results from the stationary receiver sledgehammer sounding CRB02SEIS are superimposed on the CRB03SEIS results. An elevation difference between the sounding locations necessitated

that the CRB02SEIS results be shifted lower by a vertical distance of 0.5 m for comparison plotting.

Despite the tens of meters between the sounding locations, the V_S profiles match reasonably well. The differences in the upper 12 m depths are due to lateral variations in the soil properties. The frequent-interval velocities in this zone, from both CRB02SEIS and the continuous-push sounding CRB03SEIS, form smooth trends as would be expected from overlapping interval measurements. Within the noisy layer above the Cooper Marl, the continuous-push V_S could not be determined due to loss of signal quality. Below the top of the marl, the signal qualities improved and continuous-push velocities could be calculated again.

The frequent-interval sledgehammer velocities demonstrate that the velocity within the marl is variable. For the continuous-push signals with the commercial RotoSeis, the source amplitudes in the marl attenuated to levels too low to avoid influence from the penetration-related noise. During continuous-push testing, penetration was halted every meter to add rods. With no additional time or effort, the system continued to record seismic signals. The V_S values determined from RotoSeis signals recorded during these rod breaks match the V_S determined with the sledgehammer during CRB02SEIS. However, the profile of V_S determined from non-stationary receivers is scattered compared to the sledgehammer signals which were recorded strictly with stationary receivers.

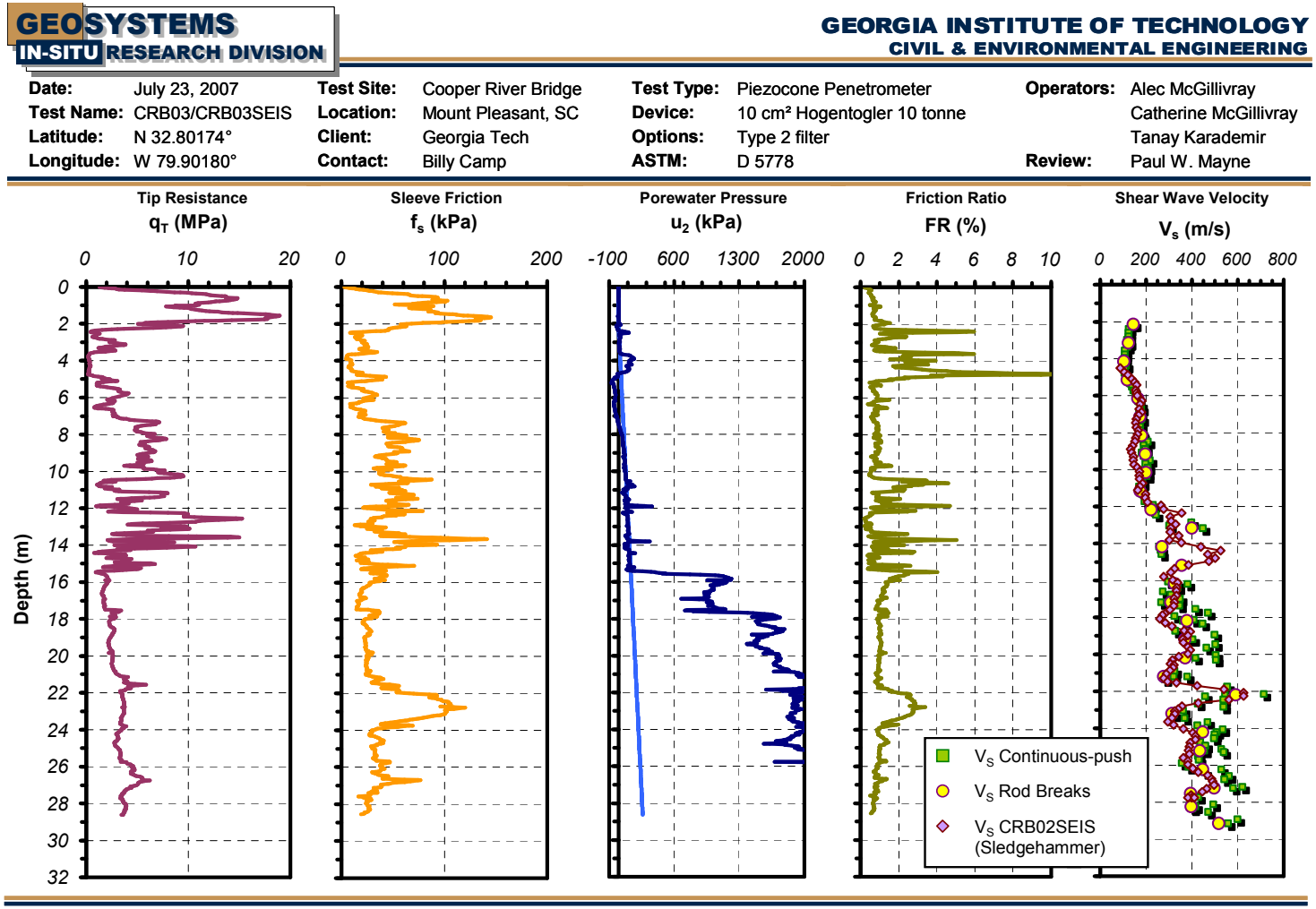

Figure 5.45 Continuous-push SCPT sounding CRB03/CRB03SEIS results with superimposed frequent-interval sledgehammer velocities measured during CRB02SEIS

5.6.2. Reduction in testing times

The amount of extra time required for making seismic measurements during direct-push site characterization depends on a number of factors including, the size of the testing crew, the type of source, the data acquisition characteristics, and efficiency of the procedures. A manual seismic source like the sledgehammer is slow to operate because of communication delays between the data acquisition operator and the source operator. Having an extra person to operate the source is faster than not having one, but adds extra man-hours to a job. Recording and storing the source signals can be a tedious multi-step process of examining the quality of the record(s), trimming the data, choosing a filename, and saving the record. Lastly, if the test procedures require multiple reversible polarity left- and right-strikes, the process will be slowed further.

The conventional SCPT sounding CRBDH1, which was performed at the Cooper River Bridge test site in Mt. Pleasant, SC, to a depth of 30 m, is a representative test lasting 66 minutes, not including time for pulling the rods back out of the ground. The sounding was performed with a two-person crew, one to operate the source, and another to operate the data acquisition and handle the rods. That time breaks down to about 2.3 minutes per rod during pushing. At the end of each 1 m pushing stroke, while penetration was stopped, the data acquisition software was switched from monitoring penetration measurements to seismic recording mode. Once the trigger was armed and ready, the signal was given to the source operator to activate the source. The sledgehammer source was then struck one time. The signal was recorded, displayed, examined, assigned a file name, and stored to the hard drive. Once the shear wave was recorded, the next rod was attached and pushing began again.

With the continuous-push seismic system, the process of generating and recording shear waves runs automatically in the background without interference from the operator. The rods are pushed in a constant rate of 2 cm/s in 1 m strokes. At the completion of each

stroke, the next rod is attached and penetration continues. The frequent-interval continuous-push SCPT sounding CRB03 to a depth of 28 m, lasted 50 minutes (subtracting time porewater pressure dissipation times), not including pulling out time. A 2-person crew was also used for this test, with one person handling the rods, and the operator focusing only on the data acquisition. That test breaks down to about 1.85 minutes per rod. The difference in time between the two methods was approximately 27 seconds per rod, or roughly 14 minutes for a 30 m sounding, resulting in more than a 20% time reduction for pushing with the continuous-push system. Typical commercial operations perform as many as 4 hammer strikes at each depth, which could easily expand the time by more than another minute per rod. The advantage of the continuous-push system is even more dramatic considering that the frequent-interval method during continuous-push recording made 5 times the number of measurements while achieving the time reduction.

5.7. Summary

A continuous-push seismic system should consist of a seismic probe, preferably true-interval type with multi-axes receivers, an automated data acquisition system, and an automated seismic source. In this chapter, the components of such a system have been evaluated in field testing and post-processing of wave signals.

The characteristics of the receivers utilized in the biaxial true-interval probe are well matched as seen in comparisons of signals recorded with different receivers for the same sensor depths. Additionally, the position of the receivers within the probe does not appear to influence the recorded signals. In order to realize the full potential of multi-axes probes as well as the maximize the quality of the shear waves for analysis, the component directions should be combined to reveal the multi-dimensional characteristics of the particle motions and allow for any needed correction due to misalignment between the source and receivers.

Misalignment can dramatically reduce signal quality as sensors are not oriented to capture the particle motions in the direction of maximum displacement. Changes in alignment during a sounding can even result in phase shifts of the signals. However, by combining the signals from biaxial horizontal components, it is possible to re-project the results to the optimal angle relative to the source direction.

The data acquisition system can also influence the performance of a continuous-push seismic system as well as the appearance of the recorded signals. The input range must not only accommodate the full range of voltages to be detected, but the resolution must be high so that the range does not have to be reset periodically due to attenuation of source amplitudes with depth. In order to maintain time resolution for the purposes of analyses, the recommended sampling frequency is 100 kHz. However, the source bandwidth is less than 200 Hz, so it is better to record at 2000 Hz and up-sample the recordings to 100 kHz during processing. The duration of the recorded signal need only capture the arriving shear wave, but extending the recording time will increase the frequency resolution and may be useful for geophysical analyses.

A sledgehammer seismic source can be used to generate quality shear waves, but there is potential for operator error to affect signal quality, and the manual nature of the device makes it unsuitable for frequent-interval continuous-push measurements. The prototype and commercial RotoSeis seismic sources were evaluated and found to be reliable as well as repeatable. The bandwidth of the source signals was found to be controlled by the stiffness of the source coupling to the ground surface. The Commercial RotoSeis device was tested successfully to a depth of 30 m utilizing recordings made with stationary-receivers. During continuous-push operation, the source amplitude below depths of 13 m was too low to avoid distortion from noise related to the pushing system and non-stationary receivers. If the amplitude and bandwidth of the RotoSeis could be improved with better coupling to reduce the appearance of noise, the potential time savings offered by a continuous-push system is significant.

6. RESULTS AND ANALYSES OF DOWNHOLE FIELD TESTING

6.1. Overview and Synopsis

The incorporation of seismic sensors within the cone penetrometer and flat dilatometer blade in order to measure shear wave velocity profiles during direct-push in-situ site characterization was first presented some two decades ago (Rice, 1984; Hepton, 1988). Yet, in that 20-year time span, the equipment and procedures for the seismic testing component of the SCPT and SDMT have remained essentially unchanged despite dramatic advances in computers and data acquisition. Because of the extra time required both in the field and post-processing phases, it is not currently cost effective to measure V_S with each test sounding. Additionally, the depth resolution of the V_S profile is insufficient to provide detailed stratigraphy and characterization on par with the "continuous" penetration measurements. Better integration of the seismic component with the direct-push site characterization systems is necessary to reduce testing times, improve the quality of the results, and ultimately, make measurement of V_S part of routine site investigation practice.

If seismic testing were to become an automated component of the SCPT and the SDMT, profiles of V_S could be measured without additional field effort. Seismic signals could also be recorded during penetration, allowing a reduction in the size of the depth increments between V_S measurements. During research toward this goal, multiple prototypes of seismic probes, data acquisition systems, and automated seismic sources were developed, leading ultimately to a continuous-push seismic system. The equipment and methodology have been described in Chapter 3, and the details of field trials, including information about the test sites, can be found in Chapter 4. This chapter presents the frequent-interval V_S results obtained from stationary as well as non-stationary receivers for comparison with velocity results obtained from conventional SCPT and SDMT, as well as crosshole, downhole, suspension-logger, surface wave,

reflection, and refraction V_S profiles from the same sites.

6.2. Frequent-Interval SDMT V_S in Venice, Italy

Detailed site characterization was needed to predict settlements for a circular test embankment constructed in the town of Treporti, near Venice, Italy. The site stratigraphy was described previously in Chapter 4 as interbedded layers of sand, silts, and silty clays, with lenses of organic peat. As part of the characterization program, a series of three SCPT and three SDMT soundings were performed across the diameter of the (then proposed) embankment prior to construction. For the SCPT soundings, measurements of q_T, f_S, and u_2 porewater pressure were made at 2.5 cm increments, and V_S was measured at the conventional 1 m depth increments during rod breaks. A portable pendulum hammer arrangement was used as the seismic source. In Figure 6.1, the SCPT results are plotted next to the profile of saturated unit weight (γ_{sat}), which was measured from borehole samples (Simonini, 2004). The highlighted depths in the figure mark the locations of peat layers as determined by low unit weights (i.e., $\gamma_{sat} < 12$ kN/m³).

The channels of the SCPT were able to delineate the peat layers, particularly by the high friction ratios (i.e., FR > 6 %). The V_S profile also reflects the presence of peat with consistently decreased V_S at those depths. As discussed in Section 4.2.8, very low V_S is characteristic of peat deposits. However, the 1 m increment between V_S measurements is too coarse to have allowed the detection and delineation of the peat layers (or lenses) solely based on velocity, without availability of γ_{sat} from the borehole samples.

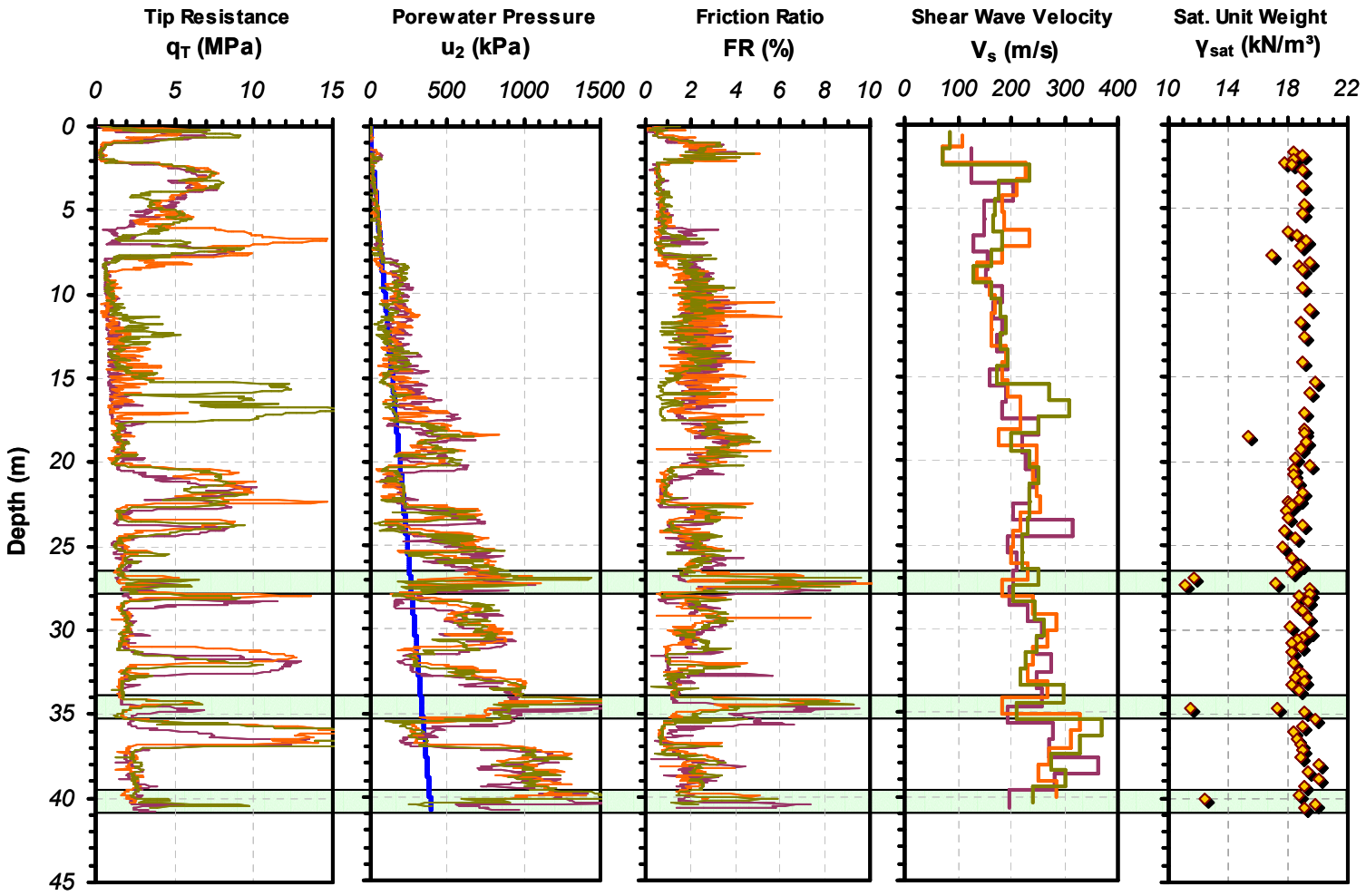

Figure 6.1 Superimposed SCPT results from Treporti Test embankment with saturated unit weights, determined from a borehole samples, highlighting peat layers (saturated unit weights from Simonini (2004))

The SDMT system, which was constructed specifically for the Treporti project, is a true-interval device with two levels of single axis geophone modules attached above the DMT blade. Dilatometer readings were made from the standard pressure panel. Seismic recording was performed with a battery-powered 2-channel FLUKE 123 ScopeMeter. Because the seismic channels were recorded independently from the DMT readings, it was possible to measure shear wave velocity simultaneously with the DMT readings.

For SDMT15 and SDMT19, dilatometer pressure readings were only made at 1 m depth increments. Consequently, V_S was only measured at 1 m intervals following true-interval as well as pseudo-interval procedures. However, during SDMT14, dilatometer readings were recorded every 20 cm. At each 20 cm test interval, measurements of the dilatometer pressures (p_0, p_1, and p_2) and overlapping true-interval (termed *frequent-interval*) shear wave signals were recorded.

In Figure 6.2, the results of the SCPT14 tip resistance (q_t) and the SDMT14 corrected pressures (p_0 and p_1) are plotted side-by-side with the superimposed velocity results of the pseudo-interval seismic cone and the frequent-interval seismic dilatometer. The enhanced detail of the frequent-interval method reveals stratigraphy within the velocity profile that is more consistent with the finer details of the cone and dilatometer measurements. The frequent-interval V_S obtained from SDMT14 detects peaks in V_S at 3 m and 7 m, which corresponds to peak values in the DMT p_0 pressures. However, during the test, groundwater infiltrated the probe below 16 m, disabling the lower geophone, so the deeper peat layers were not able to be characterized by the frequent-interval method. The sounding was continued utilizing the pseudo-interval procedure. The results presented in the figure are trimmed to the maximum depth of the frequent-interval results.

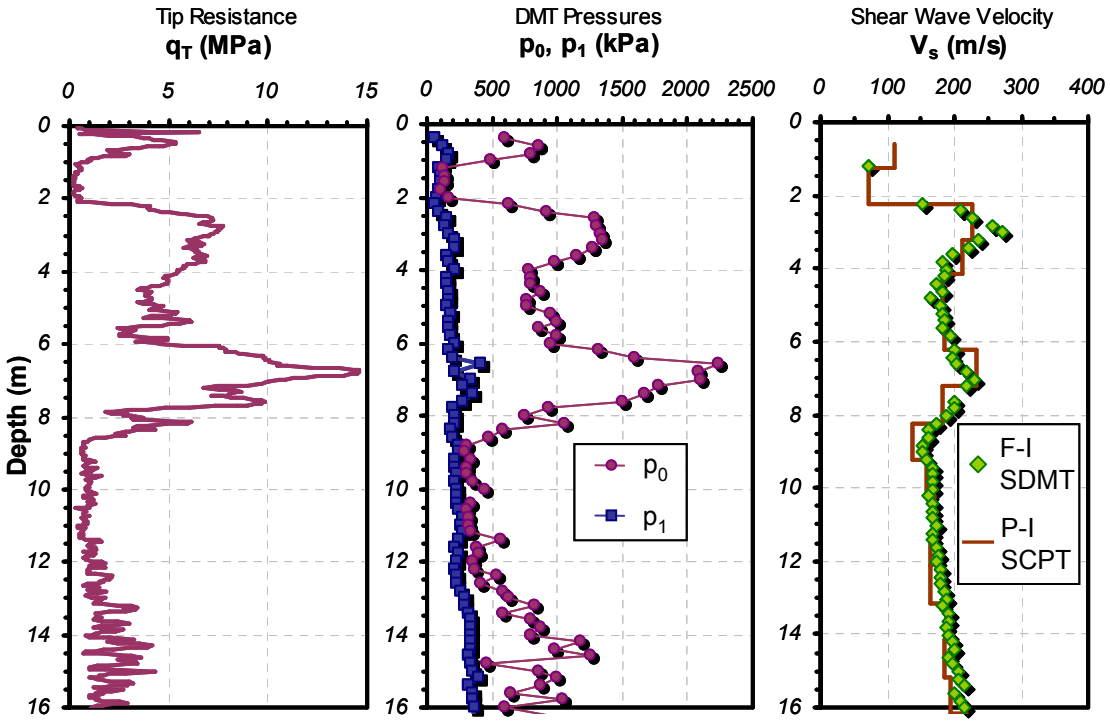

Figure 6.2 SCPT tip resistance and seismic flat dilatometer sounding pressures with frequent-interval V_S at the Treporti test embankment

An additional 3rd party direct-push downhole shear wave velocity test was performed at the site by Soil Test Inc. The results of this test and all of the Georgia Tech seismic tests obtained at the test site are presented in Figure 6.3. The SCPT results displayed previously in Figure 6.1 show some lateral variability between soundings, which is evident in the overlaid V_S profiles in Figure 6.3. Some of the variability may also be due to the sensitivity of the pseudo-interval method to errors in depth measurement, particularly with the Soil Test profile. Differences in test depths further add to the dissimilar appearance. Ultimately, the general V_S trends between soundings are mostly consistent, but the improved depth resolution of the frequent-interval V_S shows well-defined peaks with data increasing up to the peaks and then down from the peaks, rather than the abrupt oscillations of the other profiles.

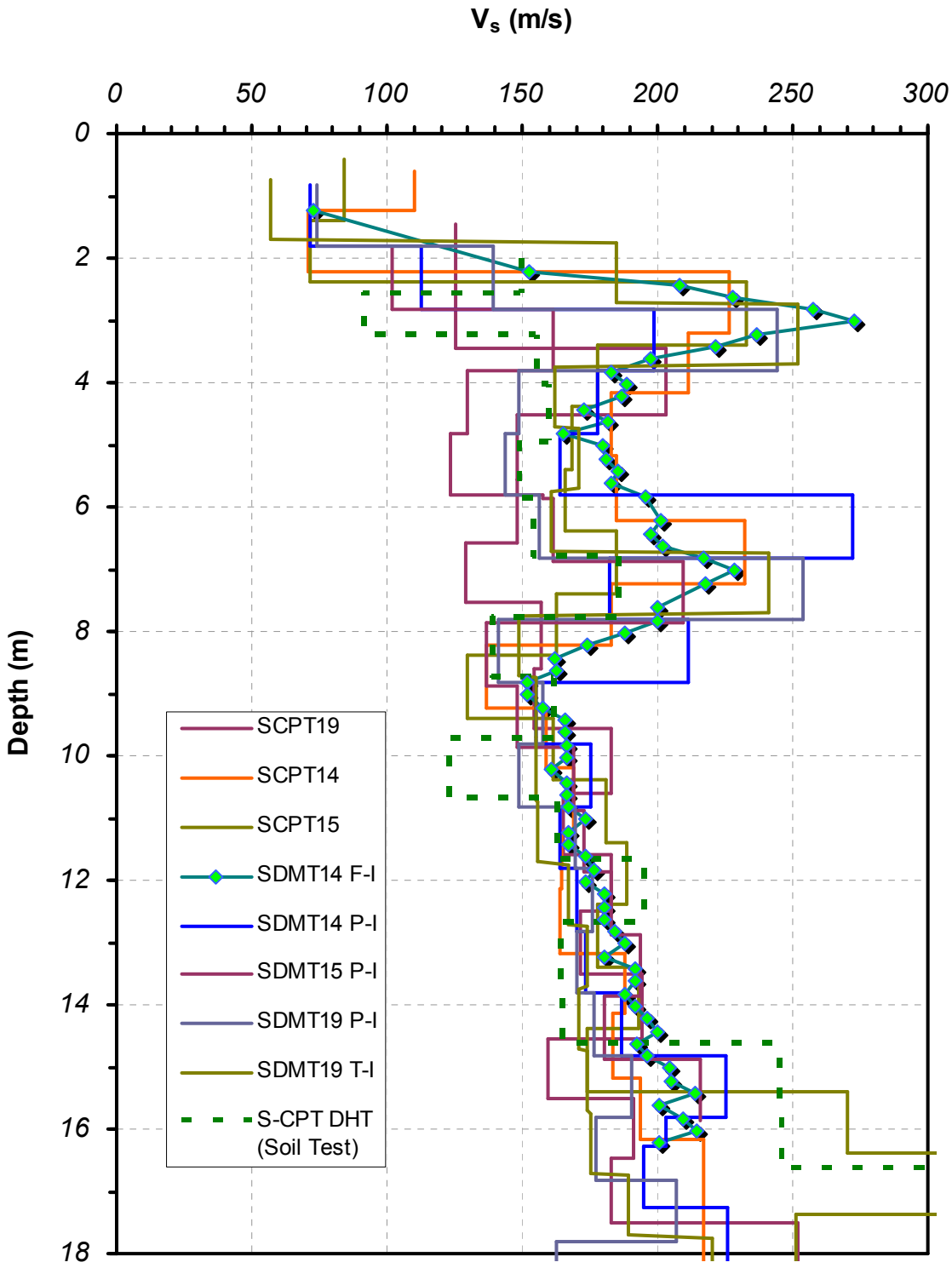

Figure 6.3 Comparison of frequent-interval, pseudo-interval, and true-interval V_S profiles from the Treporti test embankment

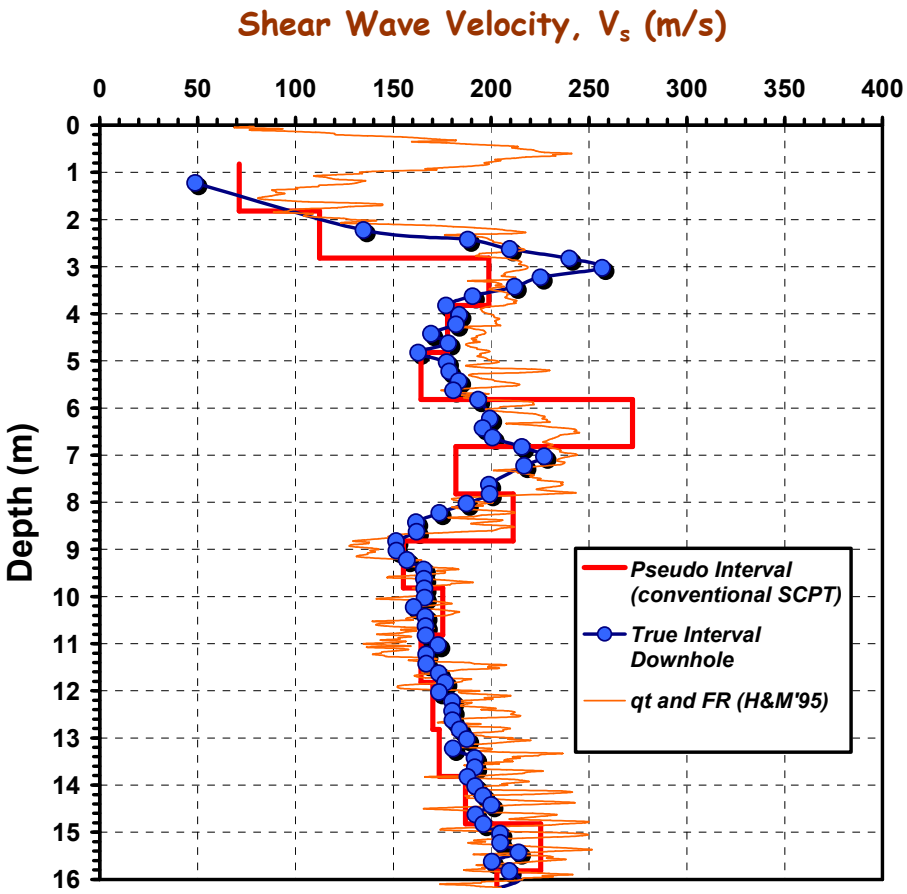

Figure 6.4 Comparison of frequent-interval, pseudo-interval, and correlated V_S profiles at the Treporti test site (McGillivray and Mayne, 2004)

In addition to comparisons between measured V_S at the Treporti test site, the frequent-interval data is compared to predicted V_S utilizing an empirical relationship proposed by Hegazy and Mayne (1995) for estimating shear wave velocity from cone tip stress and friction ratio ($FR = f_S/q_T*100\%$) shown in Equation 6.1:

$$V_S = \left(10.1 \cdot \log\left(q_T\right) - 11.4\right)^{1.67} \cdot FR^{0.3} \qquad 6.1$$

Using the data from SCPT14, Figure 6.4 shows that this empirical correlation appears to closely follow the detailed profile that was delineated by the frequent-interval shear wave results produced during SDMT14.

6.3. Frequent-Interval V_S Profiling at Northwestern University

Frequent-interval tests were next performed on the campus of Northwestern University in Evanston, Illinois. For this site, the true-interval seismic probe was utilized. The water-proofing applied to the geophones was improved after problems encountered at the Treporti test site. At each test location, a conventional pseudo-interval SCPT was conducted with the 10 cm² Hogentogler cone penetration system. After extraction of the Hogentogler cone, the larger 15 cm² true-interval seismic probe was inserted in the same hole. The larger diameter insured that the seismic sensors maintained coupling with the soil despite the hole left by the smaller CPT probe. The conventional SCPT velocities were measured at 1 m intervals. The true-interval seismic probe velocities were measured in 20 cm increments as had been done previously with SDMT14 at the Treporti test site. At each depth increment, the sledgehammer source was used to generate shear waves. The data were recorded with the HP3560A portable signal analyzer, and stored in the on-board memory. The input voltage scale had to be adjusted as depth increased in order to account for the decreasing amplitude of the surface source signal.

The superimposed SCPTu readings (q_T, f_S, and u_2) and V_S results for the five conventional soundings are shown in Figure 6.5 along with the frequent-interval velocities which were measured at two of the locations. The repeatable peak in V_S coincides with the silty organic sand between 3 m and 7 m, as identified by the boring data presented in Chapter 4 (Section 4.2.2) and the elevated friction ratio. Below that, V_S increases nearly linearly with depth, as does q_T. Figure 6.6 shows an expanded plot of V_S results. In the upper 3.5 m, FCPT04SEIS VS is significantly less than FCPT03SEIS VS, which may be due to differences in source coupling and signals resulting from the sledgehammer source. Below 3.5 m, there is little difference between the two sets of frequent-interval results. The fluctuations in the conventional results may be due to depth accuracy affects with the pseudo-interval method.

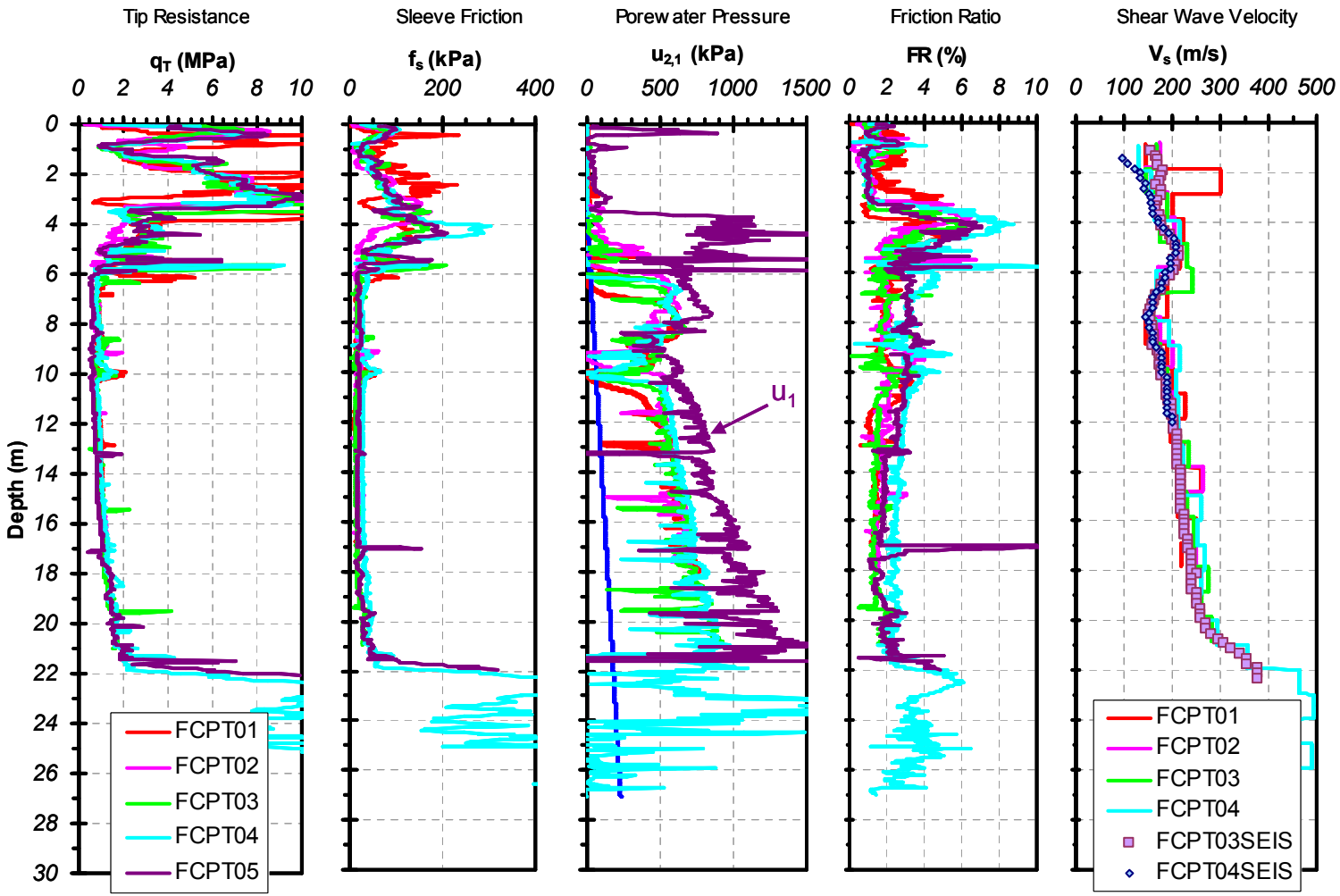

Figure 6.5 Superimposed SCPT results and frequent-interval V_S profiles determined prior to construction at the Ford Design Center on the campus of Northwestern University

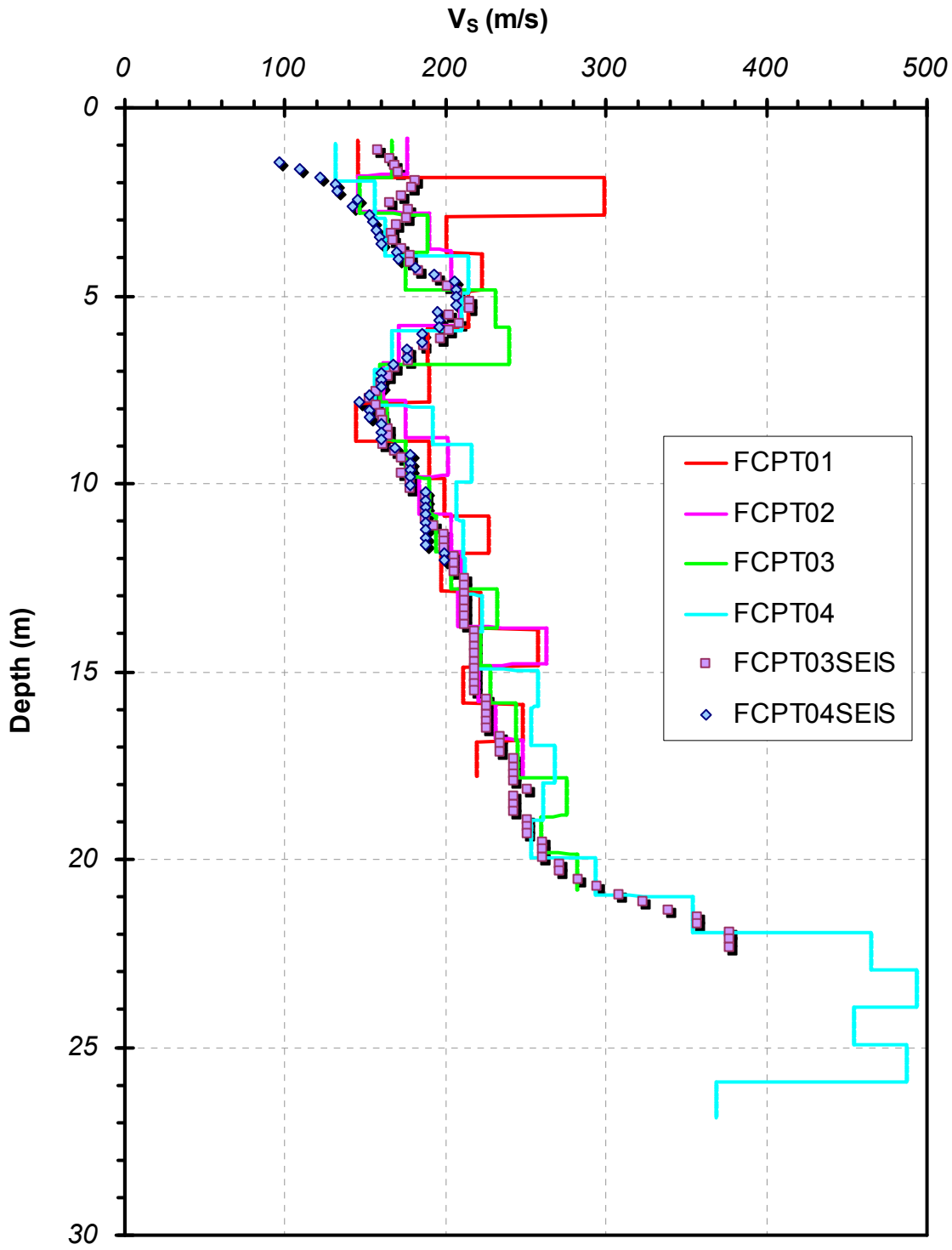

Figure 6.6 Comparison of V_S profiles from conventional pseudo-interval SCPT and frequent-interval direct-push methods at the Northwestern University test site

6.4. Frequent-Interval Results from Mud Island in Memphis, Tennessee

Following the testing at Northwestern University, the true-interval seismic probe was used to measure a frequent-interval V_S profile at Mud Island in Memphis, TN. The site is composed of layers of fill, loose sand, soft alluvial silt, and clay mixtures. Previous site investigations at this site had been performed in order to determine the site response characteristics and liquefaction potential (Schneider et al., 2001).

In the following figure (Figure 6.7), the results of a conventional seismic cone test (SCPT sounding MUDB1) are presented in comparison with the frequent-interval shear wave velocity profile (MUDBSEIS). At the Northwestern University test site, the frequent-interval tests had been conducted in the same hole as the conventional SCPT. At this location, the frequent-interval sounding was performed 3 years later than the SCPT, and was located nearly 25 m to the north. Even though the tests are separated by several meters and several years, the velocity profiles are reasonably consistent between the two soundings. There is a sand layer in the upper 5 m with V_S decreasing with depth, after which the velocity increases linearly until 21 m, then a slight drop before the frequent-interval test was concluded. Differences in the upper 8 m could be due to lateral variability and/or some error due to inaccurate depth measurement with the pseudo-interval system.

In Figure 6.8, the frequent-interval V_S profile is compared with V_S profiles determined from other field geophysical methods, including: standard refraction survey, a hybrid reflection/refraction test, and a surface wave test. The frequent-interval profile is similar to the other tests, except for the higher velocity layer implied by the surface wave results between 13 m and 19 m. Of course, the non-invasive methods are not able to match the detailing of the downhole methods, but their maximum measured depth is much greater. For the figure, the depths of the non-invasive tests have been limited to 40 m in order to be able to see the frequent-interval profile more clearly.

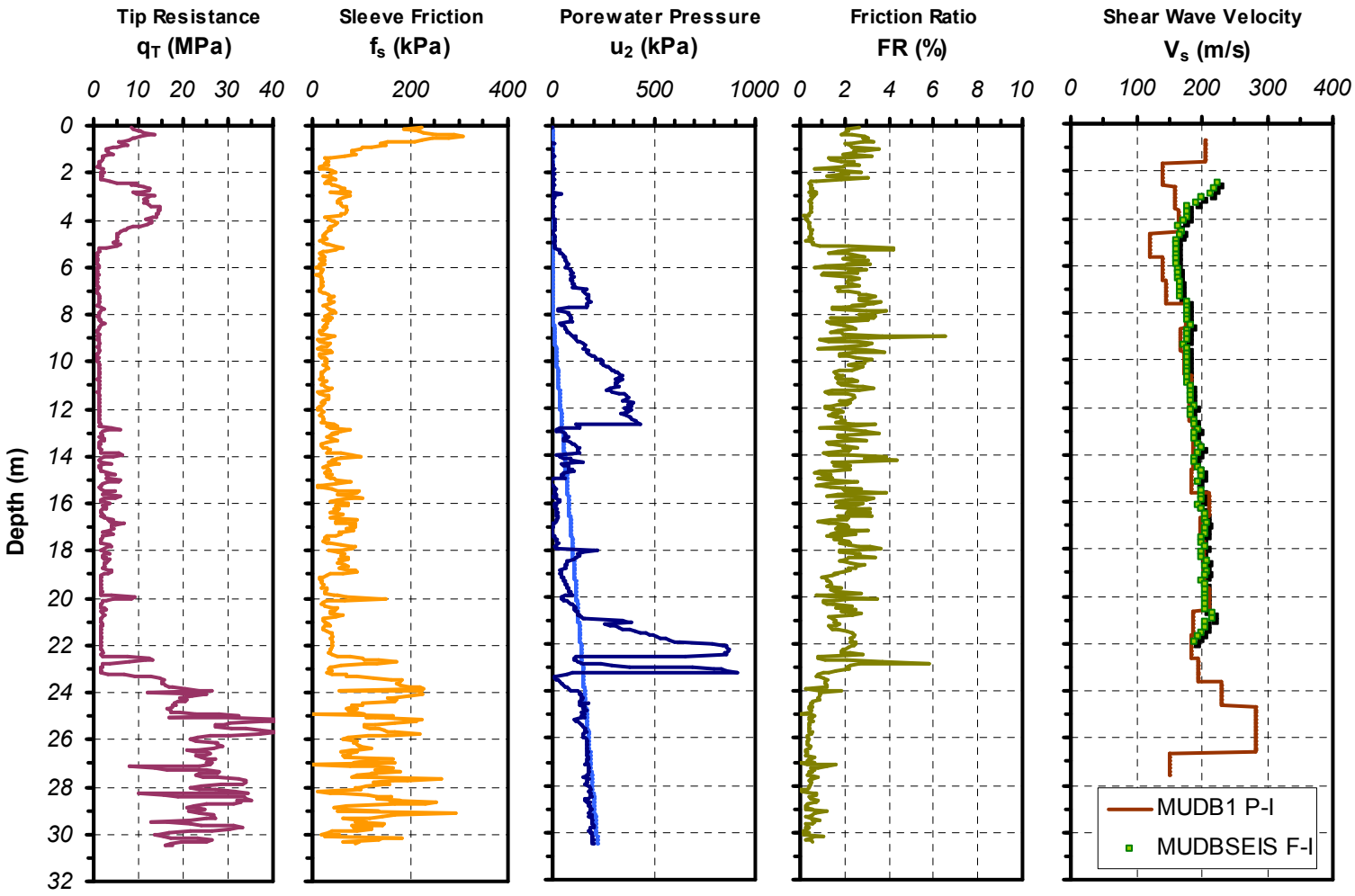

Figure 6.7 SCPT results from MUDB1 with frequent-interval V_S profile from MUDBSEIS

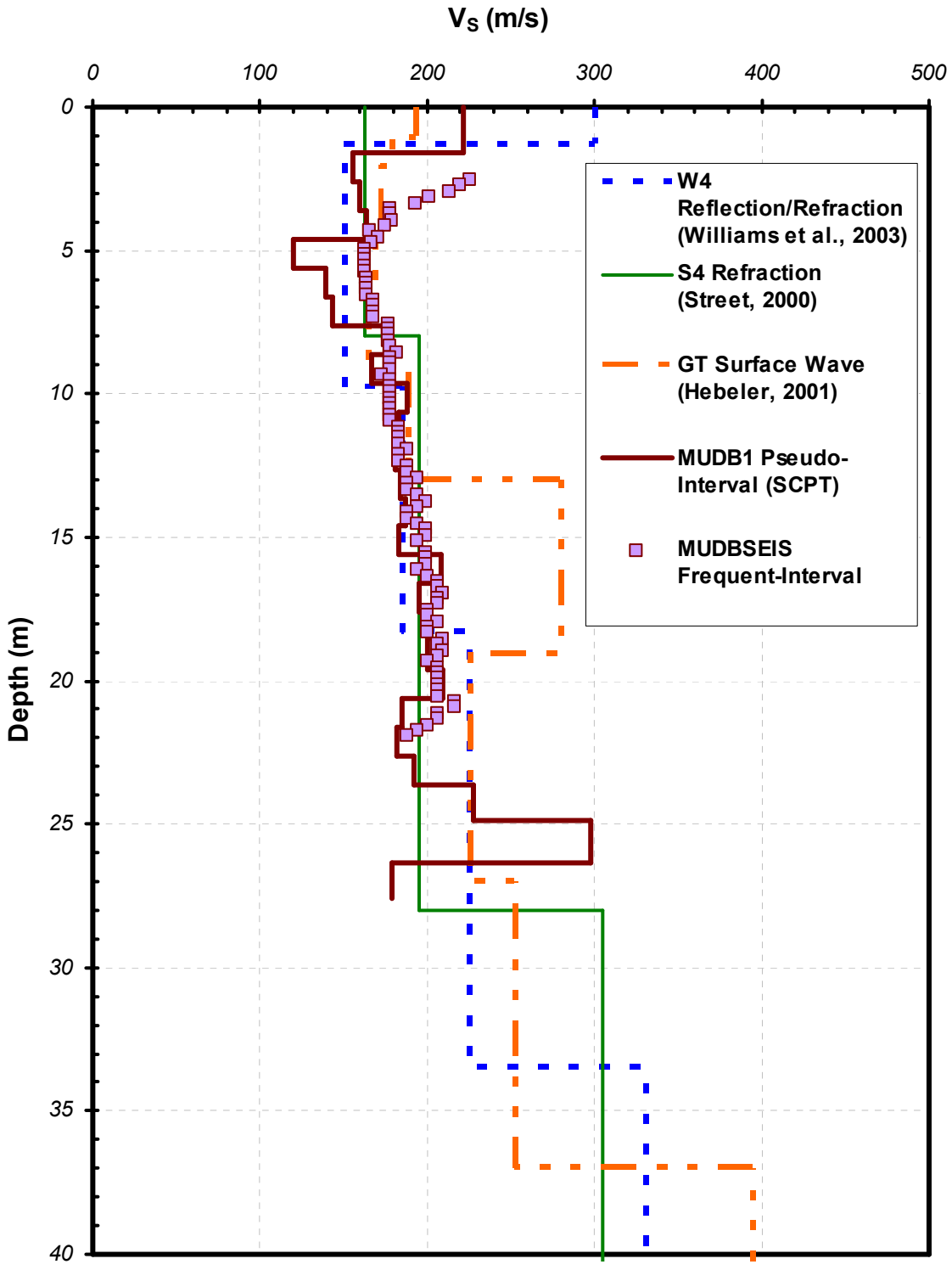

Figure 6.8 Comparison of V_S profiles from reflection, refraction, surface wave, pseudo-interval SCPT, and frequent-interval direct-push methods at the Mud Island test site

6.5. Frequent-Interval V_S at the NGES Near Opelika, AL

Auburn University manages a National Geotechnical Experimentation Site near Opelika, AL. Since testing began at the site in 1996, the site has been characterized extensively by lab and in-situ testing. The NGES has proven to be a valuable resource for evaluating new devices and test methods with respect to previously obtained data.

After construction of the biaxial true-interval seismic probe, initial trial testing was conducted at the NGES. Due to recent foundation research activities, obstructions forced the latest test location to be outside the typical test area, a few meters to the east. Rather than push the seismic probe "blind", a conventional pseudo-interval SCPT (OPETRU) was first performed using the Hogentogler system. The biaxial true-interval seismic probe was then used to measure the frequent-interval V_S profile (OPETRUSEIS) in the same hole. Penetration of the biaxial probe was halted every 20 cm, and biaxial shear wave signals were recorded. Figure 6.9 shows the results of the frequent-interval SCPT sounding (OPETRU/OPETRUSEIS) with two representative conventional pseudo-interval soundings (OPEAUT and OPELI2) performed nearby. The sounding OPETRU/OPETRUSEIS is located just 7 m to the east of OPEAUT, but in the upper 8 m, the q_T and f_S values are uncharacteristically low for this site. However, the low tip and friction sleeve measurements are confirmed by the low V_S values as determined by both pseudo-interval and frequent-interval methods. There are creeks nearby, and this sounding may be located in a creek bed that was in-filled during grading activities.

In Figure 6.10, the frequent-interval V_S profile is compared with results from a crosshole test (CHT), a pseudo-interval SDMT, an array-based surface wave profile, and other pseudo-interval SCPT soundings. Unfortunately, the dissimilar soil conditions in the upper 8 m are significant. Below 8 m, the frequent-interval matches well with the crosshole test results, considered to be the baseline comparison test in industry. The SASW is also similar, but the pseudo-interval results are more scattered.

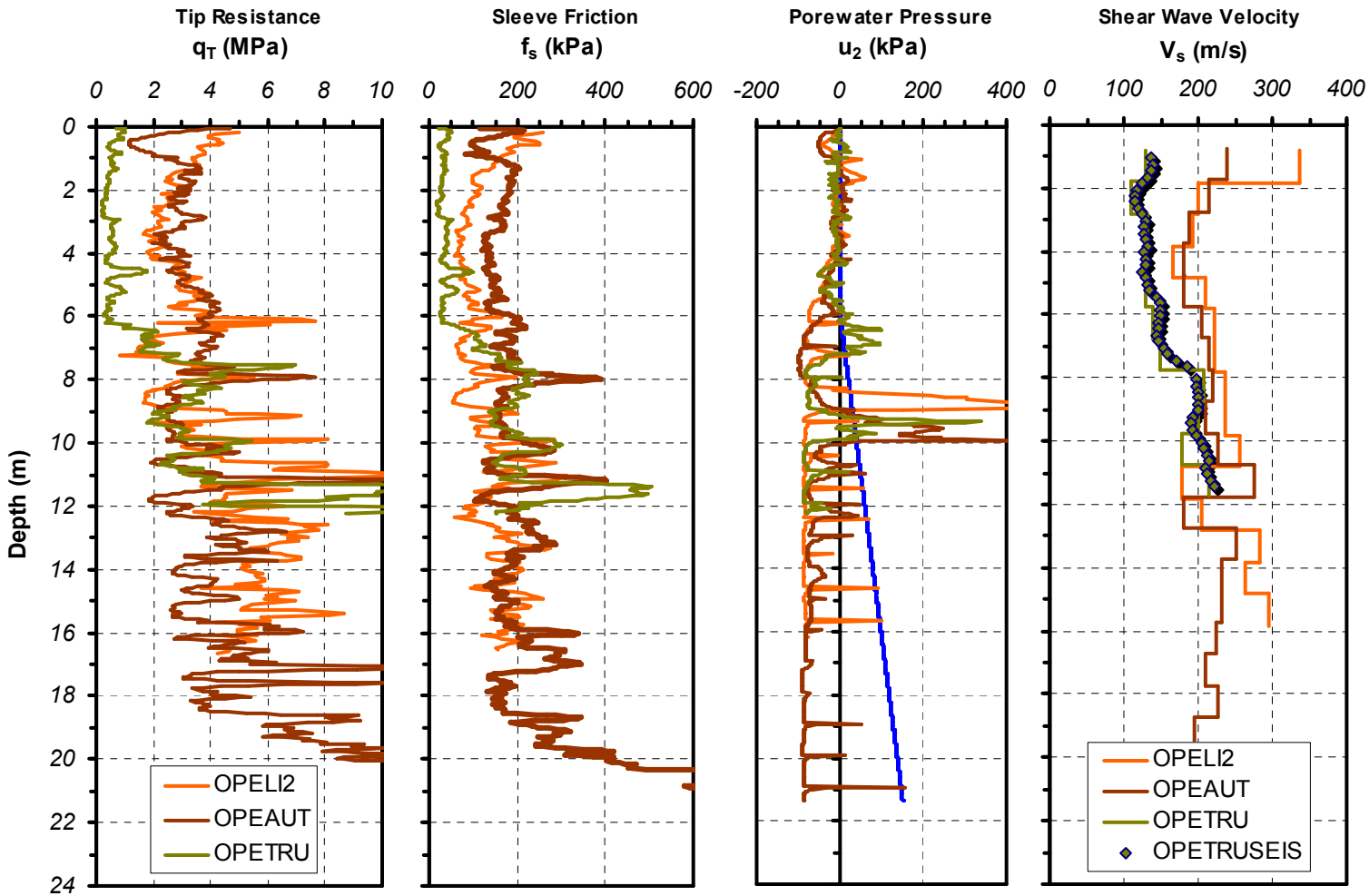

Figure 6.9 Superimposed SCPT results with frequent-interval V_S at the NGES near Opelika AL

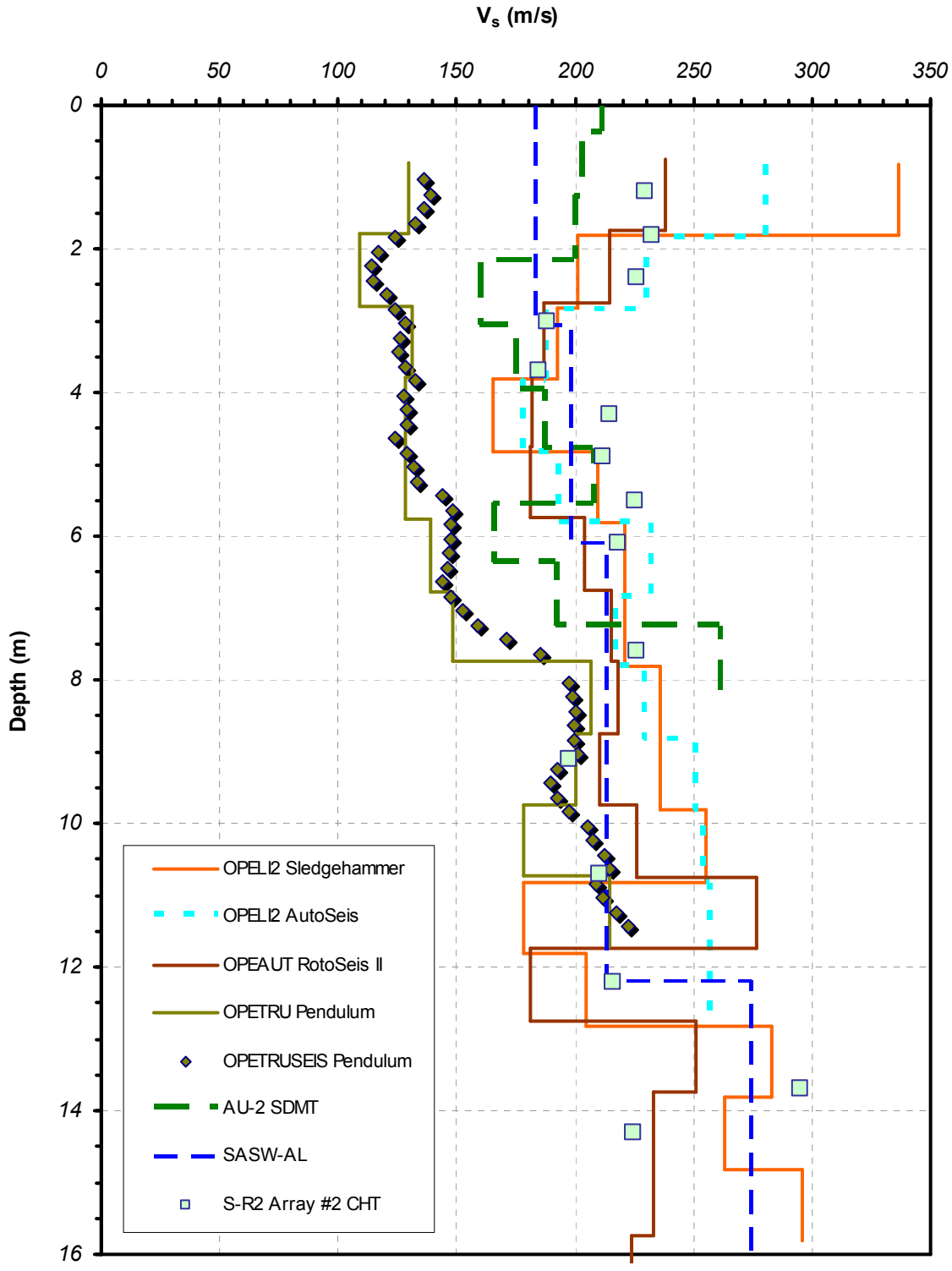

Figure 6.10 Comparison of V_S profiles at the Opelika, AL NGES using frequent-interval direct-push, conventional pseudo-interval SCPT, pseudo-interval SDMT, surface wave method, and crosshole test

6.6. Frequent-Interval and Continuous-Push V_S at the Stono Marina

After the successful trial of the biaxial true-interval seismic probe at the Opelika NGES, the probe was taken to Charleston, SC in order to collect frequent-interval V_S data in the Cooper Marl, a cemented carbonate deposit that is often misclassified as a high plasticity clay. During the frequent-interval sounding STONOSEIS, the V_S profile was measured with stationary receivers at 20 cm depth increments down to a depth of 26 m. The test was located 35 m to the south of a previous conventional SCPT (STON1A) and a deep borehole downhole velocity test (PS-1 DHT).

During a subsequent visit with the biaxial true-interval seismic probe and the final Georgia Tech RotoSeis prototype (RotoSeis V), a continuous-push frequent-interval sounding (STONO01SEIS) was conducted in the hole left after pushing an ordinary CPT sounding (STON01). The test was located 100 m to the south of the previous frequent-interval test. During the continuous-push seismic test, the RotoSeis was set to deliver a hammer strike every 10 seconds, corresponding to a 20 cm depth increment during penetration at 2 cm/s. The geophones in the biaxial true-interval probe were connected to a Geometrics Geode seismograph which recorded the signals automatically from each hammer strike. However, at a depth of 8 m, the probe encountered the top of the marl layer. Penetration forces increased sufficiently in the marl to cause the cone truck's earth anchors to pull out of the ground slightly. The RotoSeis was placed under one of the leveling pads to provide a normal force for coupling, but as the truck lifted off the ground, the coupling was lost and the sounding had to be stopped.

The results of the pseudo-interval SCPT sounding, the frequent-interval sounding, and the continuous-push frequent-interval sounding are presented in Figure 6.11. The penetration results are consistent between the two soundings, despite the distance between them. The results are also similar to the representative sounding shown previously in Chapter 4 (Figure 4.15). It is typical for the V_S profile to have a scattered appearance because the degree of cementation in the Cooper Marl varies with depth.

However, the frequent-interval actually confirms the oscillations in V_S within the marl. The increased depth resolution delineates the V_S into layers with more certainty as V_S increases gradually up towards peaks and gradually decreases coming down from peaks, as opposed to large swings between one point and the next with conventional downhole methods. The continuous-push frequent-interval results also reveal a great deal of detail in the upper 8 m, demonstrating that it is possible to acquire reliable V_S data without intervention from the operator.

In Figure 6.12, the V_S profiles are plotted at a larger scale for better examination. The results of the borehole downhole test are included for an objective comparison. The different methods yield consistent profiles, but the frequent-interval tests are considerably more detailed. The continuous-push velocities and the stationary receiver velocities differ near the surface, but this could be attributable to varying surface conditions over the 100 m distance between the tests.

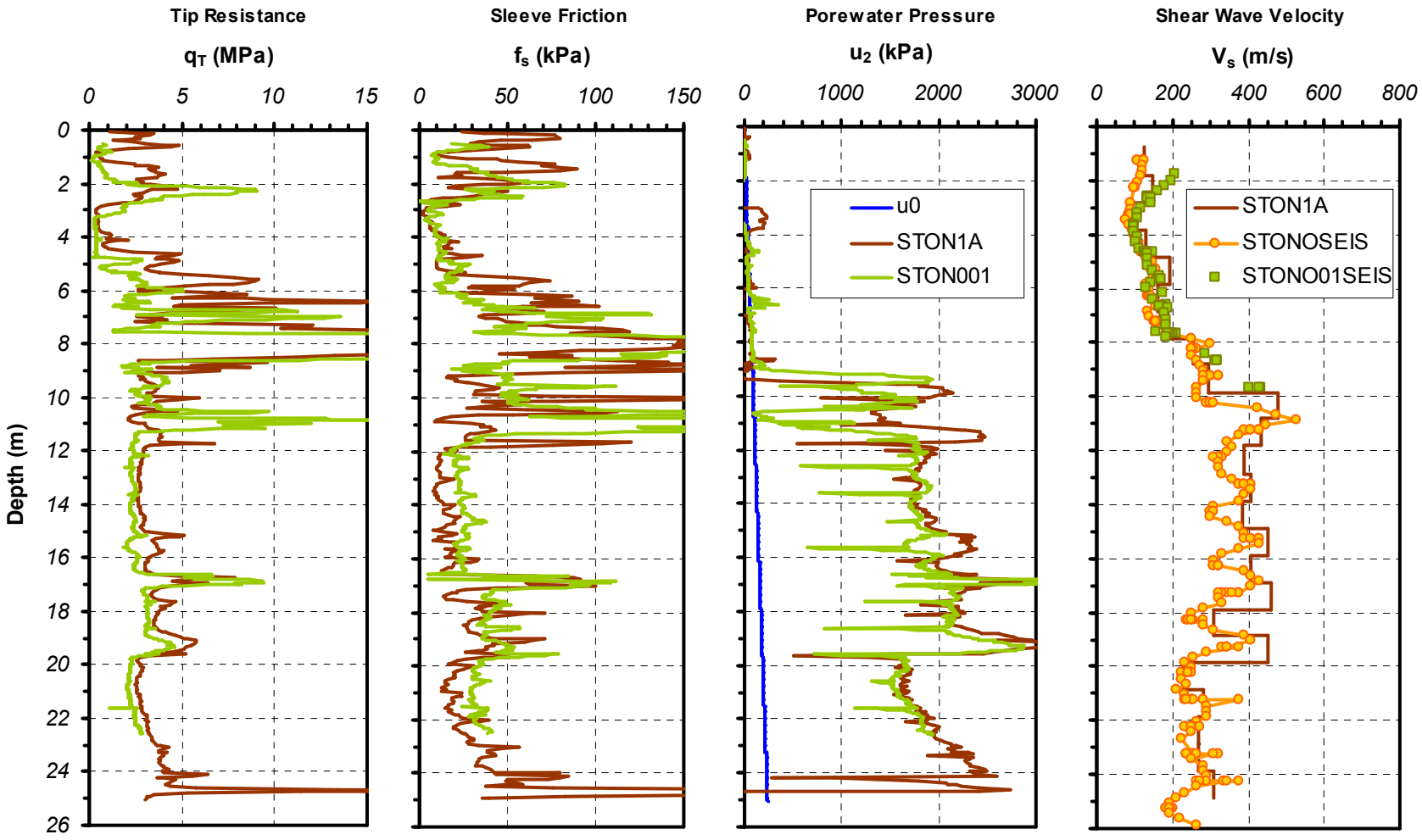

Figure 6.11 SCPT results with frequent-interval and continuous-push frequent-interval V_S profiles obtained during multiple visits to the Stono Marina test site in Charleston, SC

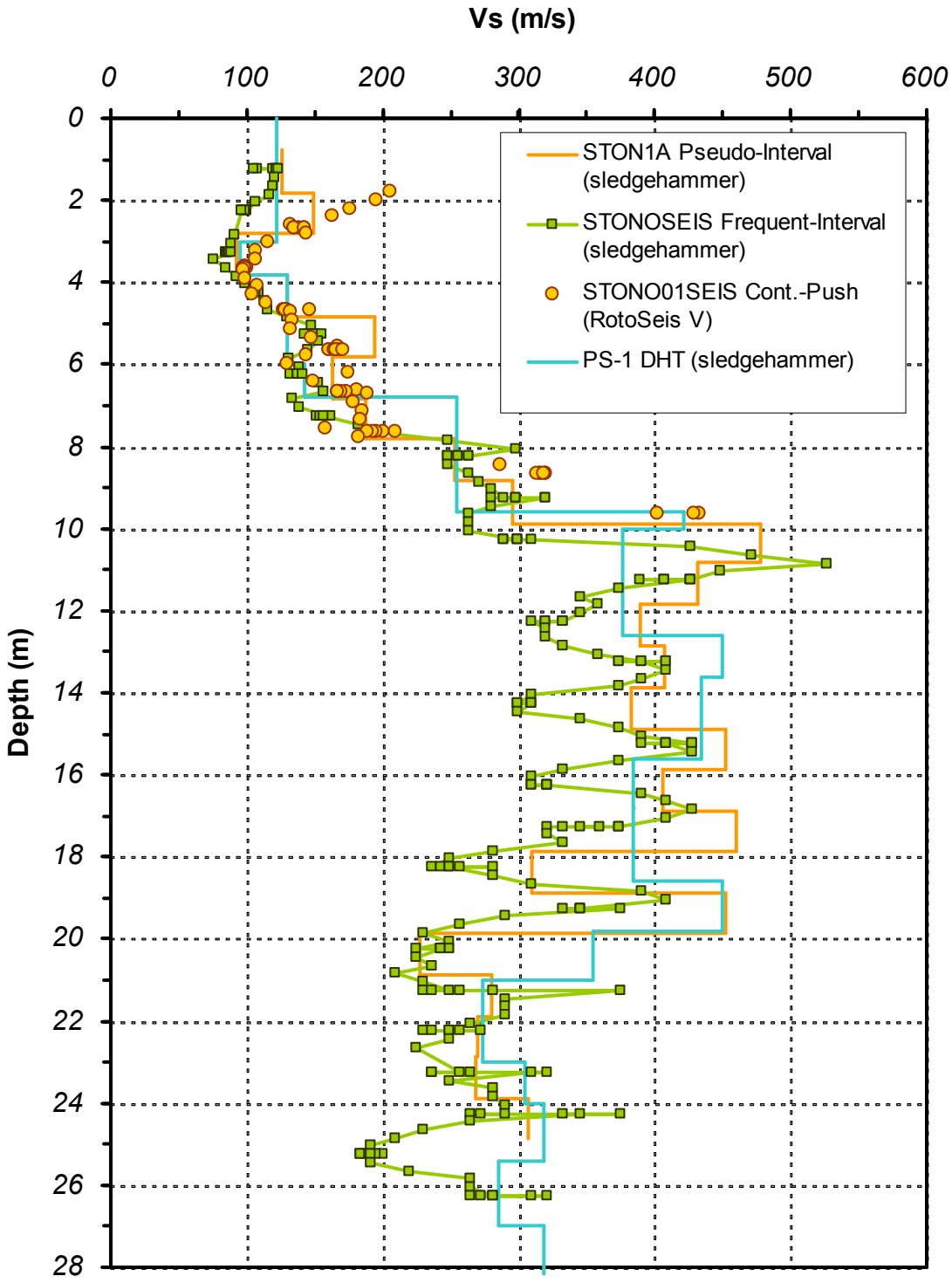

Figure 6.12 Comparison of V_S profiles obtained at the Stono Marina using frequent-interval and continuous-push frequent-interval direct-push method, as well as from a conventional cased borehole downhole test

6.7. Frequent-Interval and Continuous-Push V_S at the Cooper River Bridge

The Cooper River Bridge test site, located in Mt. Pleasant, SC, across the Cooper River from downtown Charleston, is another site underlain by the Cooper Marl. The detailed descriptions of the site and the tests conducted were presented in Section 4.2.6. The tests include a visit to the site in 2006, during which the biaxial true-interval seismic probe and the RotoSeis V were used to record continuous-push frequent-interval shear wave velocity signals during the sounding CRB01SEIS. As with the continuous-push test performed at the Stono Marina, the RotoSeis was set to generate hammer strikes automatically every 10 seconds, which corresponds to a 20 cm depth increment during penetration. The signals were also recorded automatically with the Geode seismograph. As similar to the sounding at the Stono Marina, once the probe reached the top of the marl, this time at 13 m, the normal force on the top of the RotoSeis was lost as the increased penetration force caused the leveling pads to lift off the ground. Following the shallow continuous-push seismic sounding, a stationary receiver frequent-interval sounding (CRB02SEIS) was performed utilizing the sledgehammer source to a depth of 27 m.

The test site was revisited in July of 2007 to field test the new commercial version of the RotoSeis seismic source, as well as attempt to obtain deep continuous-push shear wave velocity measurements. A continuous-push sounding (CRB03SEIS) was conducted with the Commercial RotoSeis coupled to the ground by earth anchors, rather than the leveling pad of the cone truck. The RotoSeis was set for automated operation, continually delivering hammer strikes every 10 seconds, and the signals were recorded automatically by the National Instruments CompactDAQ system.

The results of the SCPT soundings conducted with the stationary receiver frequent-interval test and the continuous-push frequent interval test are presented in Figure 6.13 with a conventional pseudo-interval SCPT (CRBDH1) performed a few years

earlier. Above the Cooper Marl, the two frequent-interval profiles are different, but both are smooth trends as are expected with frequent-interval results. There are tens of meters between the tests which may account for slight variations between the soundings. The sounding CRBDH1 is nearer to CRB03 than to CRB02, and as a result those two soundings seem to match more closely. Below the top of the marl, the stationary receiver frequent-interval velocities confirm the varying degree of cementation with depth. The continuous-push profile correlates well with the profile determined with stationary receivers, yet the continuous-push results show increased scatter. Vibratory noise transmitted through the rods by the pushing system interfered with the determination of travel time differences. The influence of the signal noise was discussed in Chapter 5.

In Figure 6.14, the V_S profiles from the various SCPT soundings are compiled into a single plot that also includes borehole downhole test results and a short segment of V_S profile measured during a suspension logger test. A high velocity layer was detected with the borehole downhole test between 4 m and 6 m that could not be confirmed by any of the other tests. The velocities from the SCPT soundings indicate a smaller and less distinct increase in V_S at these depths, which reflects the appearance of the q_T measurements seen in Figure 6.13. At this site, the downhole test was also unable to capture the variation of V_S within the marl. The resolution of the suspension logger results is high enough to capture some of the velocity variation, but the test was located almost 1 km away, in the Cooper River, so the layers do not line up perfectly. The stationary receiver frequent-interval results (CRB02SEIS) are the most detailed. At 21.5 m, an unusually high V_S layer was detected by both CRB02SEIS and CRBDH2. Examining the pseudo-interval data by itself, the measurement may have been considered unreasonable. However, with the frequent-interval results, there are two duplicate measurements supporting that value, and multiple points leading up to and down from the peak that form a convincing trend.

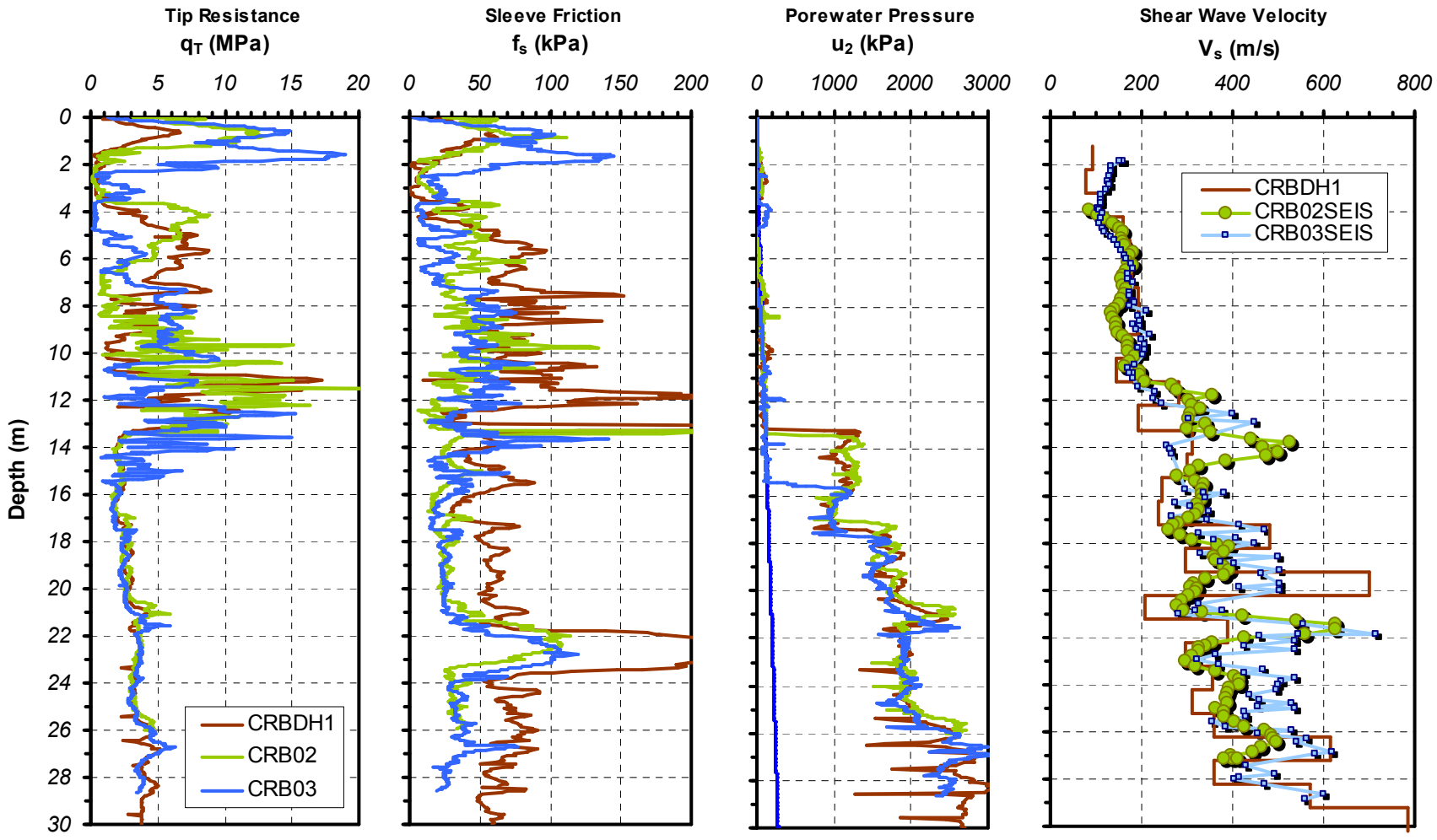

Figure 6.13 Superimposed results of three SCPT soundings with V_S profile determined from conventional pseudo-interval, frequent-interval with stationary receivers, and continuous-push frequent-interval, at the Cooper River Bridge tests site in Charleston, SC

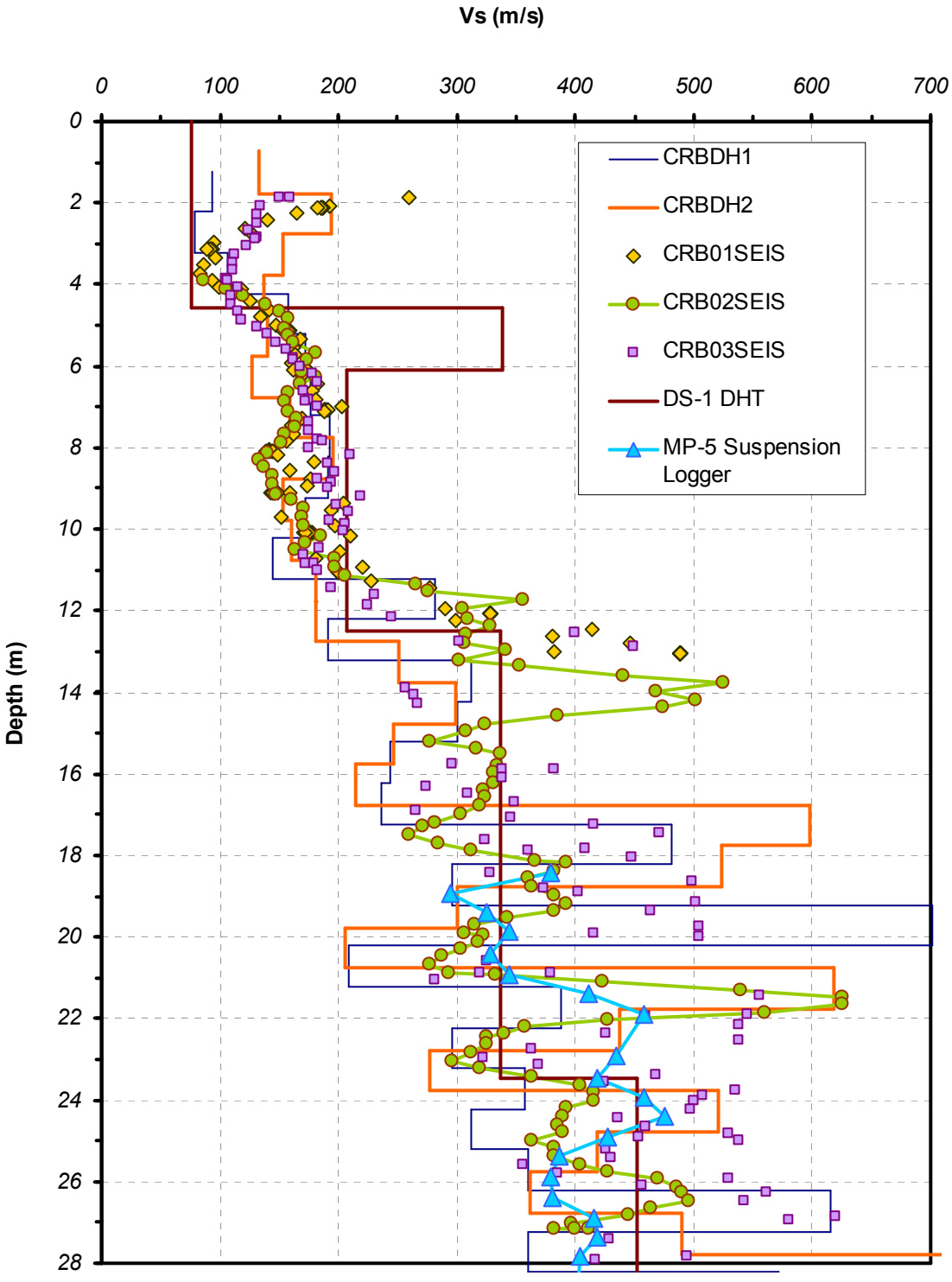

Figure 6.14 Comparison of V_S profiles determined from conventional pseudo-interval SCPT, frequent-interval with stationary receivers, continuous-push frequent-interval, borehole downhole, and suspension logger at the Cooper River Bridge test site

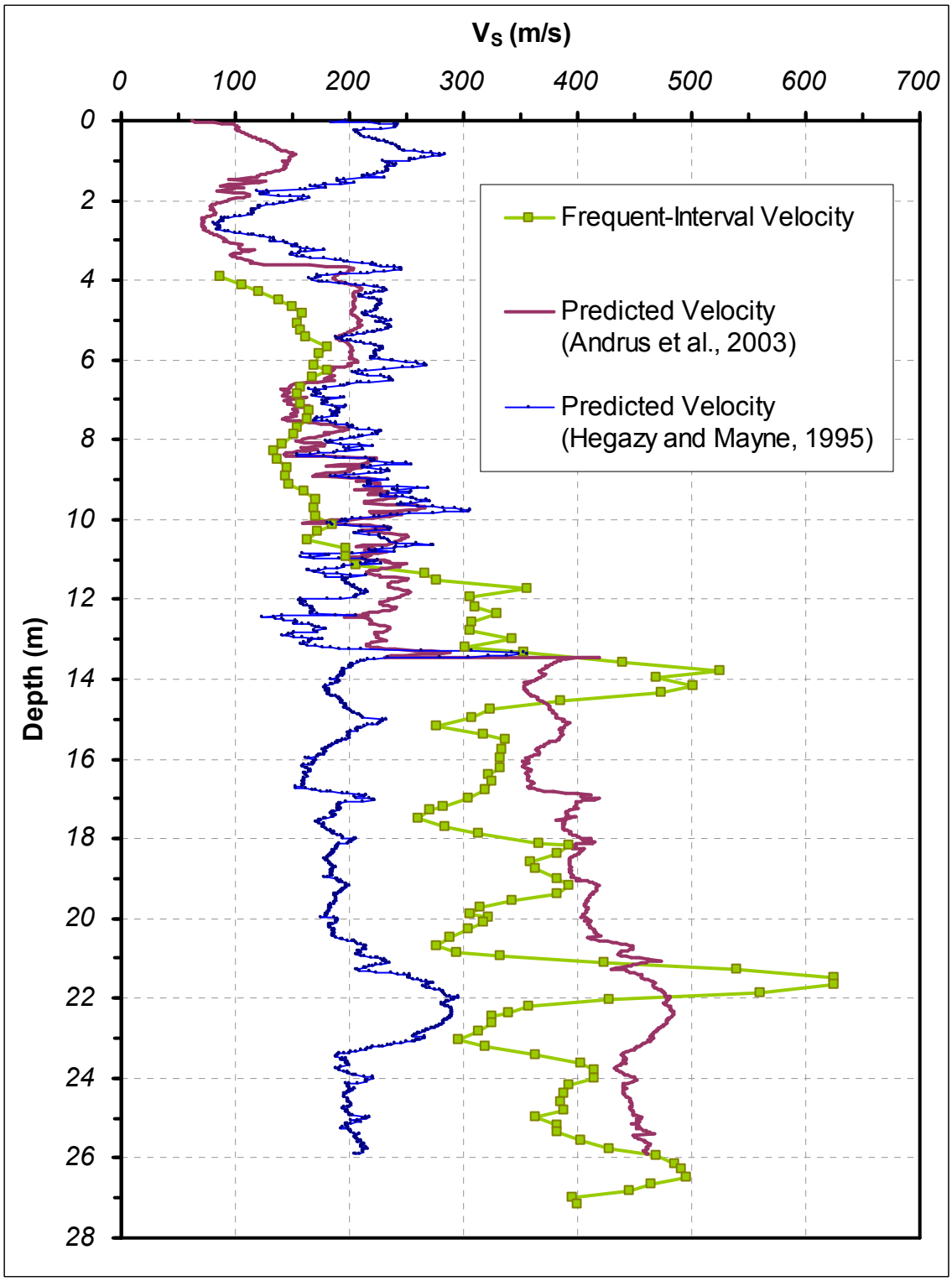

Figure 6.15 Comparison of frequent-interval V_S from CRB02SEIS with predicted V_S profiles based on correlations with CPT results

In Figure 6.15, the frequent-interval V_S profile from the sounding CRB02SEIS is compared with V_S profiles predicted from CPT-based correlation methods. The correlation by Hegazy and Mayne (1995) (Equation 6.1) was presented previously for comparison with frequent-interval SDMT data from the Treporti test site (Figure 6.4), where the predicted profile tracked well with the measured profile. The same correlation at the Cooper River Bridge test site does not perform as well. Velocities above 11 m are over-predicted by about 100 m/s, and below 11 m they are under-predicted by about 100 m/s. The top of the Cooper Marl is at 13 m. The other correlation presented in Figure 6.15 was developed by Andrus et al. (2003) from a database of SCPT soundings in South Carolina including specific soundings from the bridge test site. The relationship is given below in Equation 6.2. It is based on the CPT tip resistance, the soil behavior type index (I_C), and the depth (Z). Additionally, there is an age scaling factor (ASF) applied to compensate for increasing stiffness with age of the deposit.

$$V_S = 4.63 \cdot q_c^{0.342} \cdot I_c^{0.688} \cdot Z^{0.092} \cdot ASF \tag{6.2}$$

$$I_c = \left[(3.47 - \log(Q))^2 + (1.22 + \log(F))^2 \right]^{0.5} \tag{6.3}$$

$$F = \frac{f_s}{q_c - \sigma_v} \cdot 100\% \tag{6.4}$$

$$Q = \frac{q_c - \sigma_v}{P_a} \cdot \left(\frac{P_a}{\sigma'_v} \right)^n \tag{6.5}$$

Guidelines for choosing ASF are listed in Andrus et al. (2003). The ASF were obtained from the used for this sounding are: ASF = 1 for 0 – 3.6 m, ASF = 1.23 for 3.6 – 13.5 m, and ASF = 2.29 for 13.5 m until the maximum depth. Calculation of I_C utilized to develop this correlation is based on an iterative process described in Robertson and Wride (1998). Starting with the value of n = 1, if I_C is less than 2.6, recalculate just those I_C values for n = 0.5. If any of those recalculated I_C values are now greater than 2.6, recalculate just those for n = 0.7.

In the upper 11 m, the two correlation methods match closely. Below 11 m the correlations diverge. Within the marl, the correlation utilizing ASF is able to better predict V_S. Velocity is generally over predicted in the marl, except for the highest peaks which are the prediction is not able to replicate.

A segment of CRB02/CRB02SEIS between 20 m and 23 m is shown in Figure 6.16 to illustrate the potential for frequent-interval V_S to provide detailed information about the soil stratigraphy that may not be readily identified by the other penetration measurements. In this figure, the ends of the vertical bars on the plot of V_S represent the locations of the upper and lower seismic sensors. The point in the middle is the average V_S between the receivers. As described in Section 3.2.2, the intervals overlap so that the measured profile is essentially a smoothed version of the actual profile. A potential cemented layer between 21 m and 22 m is highlighted across all of the channels in the figure. The measured velocity increases within the cemented layer as more of the probe becomes embedded. The measured velocities then begin to decrease as the probe passes through the other side of the layer. The presence of the layer is apparently not confirmed by the tip, sleeve, or porewater pressure channels.

Although the cone penetrometer measurements are near-continuous, the measured stresses and pressures are not truly discrete. As the cone penetrates the soil, the sensors are influenced by the stiffness and stresses above the cone and below the cone as well as adjacent to the cone. Depending on the soil stiffness, the sphere of influence in front of

the cone tip may be as little as 2 or 3 tip diameters in soft soils and as much as 10 to 20 diameters in stiff soils (Lunne et al., 1997).

In this instance, the tip stress begins to increase at 20.90 m as it approaches the stiffer layer. The tip resistance reaches a peak at the top of the layer at 21.05 m, and the measured resistance promptly decreases. The diameter of the cone tip is 3.57 cm. Therefore the tip begins to "see" the upcoming stiff layer approximately 4 tip diameters in advance. Once the cone penetrates into the cemented layer, the cementation is potentially destroyed and the strength and stiffness are reduced. The shear wave propagates at a larger scale that likely includes soil outside the disturbed zone, so the elevated V_S is detected.

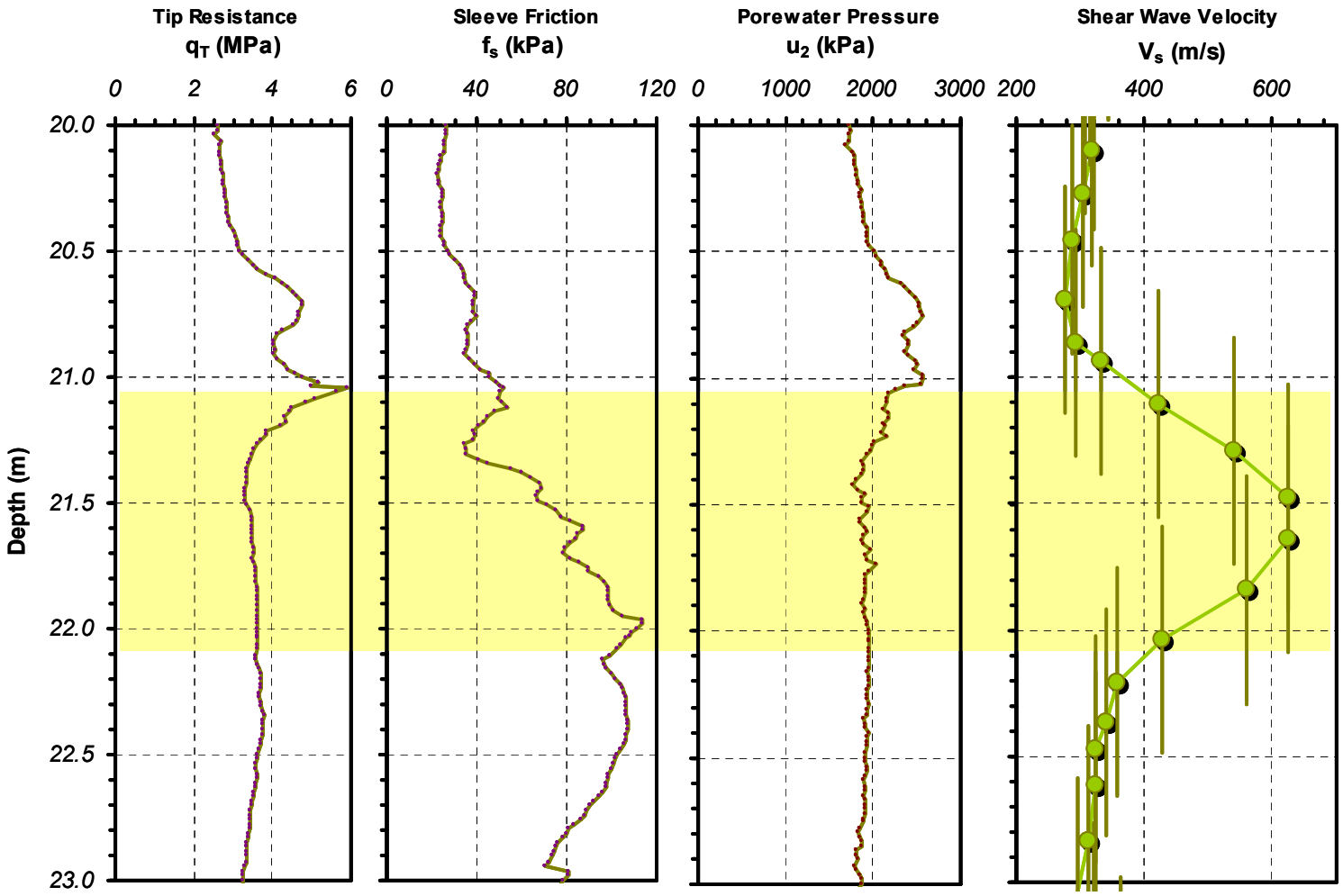

Figure 6.16 Frequent-interval SCPT results from CRB02 between 21 m and 22 m, highlighting a cemented layer within the Cooper Marl, which is well-defined by the detailed V_S, but not readily visible in the q_T, f_S, or u_2, channels

6.8. Summary

During direct-push testing by seismic cone and seismic flat dilatometer, the shear wave velocity profile is only acquired by special request, particularly on projects related to seismicity concerns, soil liquefaction, and/or ground vibrations. This is due in part because the conventional testing procedures and data handling for SCPT and SDMT are time consuming and not cost effective. Essentially, geotechnical practice for these tests has not changed for two decades, despite the improvements in automation, field data collection, and signal post-processing by computer.

In an effort to promote the integration of V_S profiling into direct-push testing, an automated continuous-push seismic system has been developed to eliminate the additional field testing time required to measure V_S. The seismic system operates independently from the CPT/DMT components, allowing V_S to be measured simultaneously with the complementary penetration measurements. This method utilizes overlapping true-interval measurements, termed frequent-interval, to improve depth resolution in the results, and possibly to identify soil behavior that may not be readily detected by the other penetration measurements.

In this chapter, frequent-interval V_S profiles from SCPT and SDMT soundings conducted at several test sites, utilizing both stationary receivers and non-stationary (moving) receivers with the continuous-push system, have been compared with V_S profiles from conventional SCPT and SDMT soundings to demonstrate the potential for improvement. At selected test sites, frequent-interval V_S profiles have also been compared with other direct V_S measurement methods such as crosshole (CHT), downhole (DHT), and suspension-logger (SL), as well as non-invasive methods such as surface wave, seismic refraction (SR), and refraction/reflection (RR). Predicted VS determined from correlations with CPT measurements were also compared with the frequent-interval profiles.

The results of these prototype tests show an enhanced depth resolution of the frequent-interval profiles that more closely match the level of detail captured by the penetration readings obtained during CPT and DMT. Frequent-interval V_S measured with the continuous-push seismic system exhibits some unwanted scatter due to noise related to the pushing system, but otherwise matches results obtained with stationary receivers. A continuous-push system is necessary to record frequent-interval data without increasing testing times.

7. CONCLUSIONS AND RECOMMENDATIONS

7.1. Research Objectives and Motivation

Shear wave velocity is a fundamental property of soils directly related to the shear stiffness at small-strains. Therefore, the shear wave velocity should be a routine measurement during everyday site characterization by soil test borings, cone penetrometer, and flat dilatometer. Instead, V_s is obtained only at special request, primarily for investigations concerned with vibratory machinery, seismic site amplification, and soil liquefaction potential. Yet, the shear modulus from shear wave velocity data ($G_0 = G_{max} = \rho_t V_S^2$) represents a fundamental initial stiffness of soils applicable to static monotonic loading, as well as dynamic loading conditions, for shallow foundations, pilings, retaining walls, and other geotechnical situations. That is, G_0 is the beginning of the stress-strain-strength curve and applies to the initial state of the soil conditions prior to loading and unloading. It is an essential ingredient for soil constitutive modeling and will become paramount for analytical and numerical simulations.

There are several lab and field methods for measuring V_S, but the SCPTu and the SDMT are the most efficient means for profiling the small-strain stiffness in addition to evaluating large-strain strength, as well as provide evaluations of the geostratigraphy, stress state, and permeability, all within a single sounding. Although the cone penetration testing (CPT) and flat dilatometer testing (DMT) have been in use for over three decades in the USA, they are only recently becoming commonplace on small-, medium-, and large-size projects as more organizations begin to realize their benefits. Primarily, the advantages of CPT and DMT include fast, continuous, and economical collection of in-situ data, when compared to the older slower augering and boring methods based on rotary drilling and sampling. The CPT and DMT methods obtain multiple readings with depth, whereas soil borings often capture a single N-value at 1.5 m depth intervals.

Productivity is the key benefit, as between 100 to 200 m of CPT soundings and/or from 50 to 60 m of DMT soundings can be completed in one day, versus a conventional soil drilling & sampling rig that may attain a lineal rate of 20 to 40 m of vertical site investigation.

Regrettably, the SCPTu and the SDMT are lagging slightly behind their non-seismic counterparts in popularity, in part because the geophysics component of the tests has not been updated during the 25 years since the tests were envisioned. With conventional SCPTu and SDMT methods, V_S is measured only during prolonged pauses in penetration at 1 m rod breaks. The original developments for field testing procedure and post-processing of wave signals were based on analog recordings. The original process required paired sets of left- and right-strikes (often duplicated to confirm repeatability) that adds to the time spent in the field, which consequently increases testing costs. Time spent for downhole testing at each shear wave velocity recordings was lost time in production CPT portions of the test. Repeatability was needed since a simple sledge hammer was employed as surface seismic source. The issue of repeatability can be solved by use of an automated source. Herein, mechanical, electro-mechanical, pneumatic, and hydraulic-mechanical sources have been discussed towards an improved field procedure.

The original SCPT and SDMT methods depended on a crossover interpretation that required judgment by the user and placed weight on a single point captured at each test depth. New developments in automation, digital data recordings, computer processing capabilities, and software are readily available to reduce field testing times and data reduction to obtain V_S in a fast, reliable, and economical manner. Finally, of additional note, the one meter V_S depth interval is much more coarse than the near-continuous penetration-type measurements.

The primary goal of this research was to develop equipment and methods to remove barriers to seismic testing during direct-push site characterization investigations.

To this end, a continuous-push seismic system has been developed which integrates V_S measurement with the SCPTu and SDMT procedures and improves the quality of the V_S results. The continuous-push system is comprised of an automated seismic source, a true-interval biaxial seismic probe, and an automated data acquisition system.

7.2. Research Findings and Conclusions

Field studies were conducted at 16 test sites of differing geologic conditions, with 8 primary sites selected for detailed examination during this research effort. Based on the field performance, prototype equipment, and analysis of the recorded wavelets, the following conclusions have been derived.

7.2.1. The use of RotoSeis for SCPT and SDMT

The RotoSeis automated seismic source was developed to reduce field testing times during conventional SCPT and SDMT soundings, as well as allow frequent-interval V_S to be measured with continuous-push operations. The device is truly automated; generating duplicate shear wave impulses at regular time intervals without interaction form the operator. RotoSeis does not generate reversible polarity shear waves. The use of left- and right-strikes is only necessary for outdated analysis methods. More advanced techniques such as cross-correlation, require only a single source event at each test depth.

The rotational motion of the RotoSeis hammer reduces the horizontal reaction forces which have been found to be problematic in portable automated seismic sources with horizontally accelerated hammers. The rotational motion also facilitates continual operation. For this research, the source was operated at 10 s intervals corresponding to 20 cm depth increments during penetration at the standard rate of 2 cm/s. The design of the RotoSeis progressed through 5 prototypes, and a patent for the device has been filed by Georgia Tech Research Corporation and is currently pending as of the time of this writing. In the meantime, the RotoSeis has been licensed for commercial production, with several units currently in use around the world. The commercial RotoSeis is based on the

final prototype, with substantial changes to the enclosure. The performance of the final prototype was proven to a depth of 30 m during a conventional SCPTu sounding in New Orleans, LA, and the commercial version of the device was successfully tested to a depth of 30 m during a continuous-push seismic test in Charleston, SC.

The frequency bandwidth of the source signals is affected by the quality of the coupling between the source and the ground surface. Sliding of the source along the surface decreases the bandwidth. To maintain normal force on the source during continuous-push seismic testing with a light weight testing vehicle, the source should be coupled to the ground by the tire of a support vehicle or earth anchors rather than the leveling pad of the testing vehicle.

7.2.2. Implementation of biaxial seismic sensors

A true-interval biaxial probe is recommended for capturing seismic signals during conventional as well as continuous-push seismic testing. Misalignment of the sensors and the source reduces the quality of the recorded seismic signals. With biaxial receivers, the two component signals can be combined to create a projected signal that is optimally aligned with the seismic source. This technique can be used to correct for any rotation of the rods that might occur during the course of a sounding. Rotating the rods causes an apparent phase shift in the component signals.

The position of the sensors within the probe, near the tip or near the back of the probe, was not found to have an effect on the recorded signals. However, the interval length between the sensors does influence the accuracy of the measured V_S. Reducing the interval length shortens the travel time difference between receivers, increasing the significance of any timing errors or uncertainties.

7.2.3. Data acquisition requirements for continuous-push SCPT and SDMT

The seismic data acquisition system should be independent from the penetration type (non-seismic) data acquisition. Currently available SCPT systems require the

operator to switch back and forth between recording applications. By separating the slow non-seismic recording device from the seismic recording device, seismic signals can be set to record automatically after each trigger event generated by the source. A timing circuit should be used to improve the consistency of the trigger detection and eliminate false triggers. Any electrical interference in the trigger circuit can be prevented from reaching the data acquisition system with the use of an optical isolator circuit. The resolution of the data acquisition system should be high enough to capture the detail of the lowest amplitude signals without having to adjust the input range. Amplifiers may be needed to maximize the input range of the system.

The maximum frequency of mechanical surface seismic sources is less than 200 Hz. To completely capture the source signal the sampling rate should be greater than 2000 Hz. The use of anti-aliasing filters is important to prevent unwanted frequencies outside the source bandwidth from being under-sampled and contaminating the signals at lower frequencies. Up-sampling techniques should be used at the time of analysis to increase the time resolution of the signals.

The duration of the recorded signals affects the frequency resolution and not the time resolution. Only the short segment of signal containing the arriving shear wave impulse needs to be stored, but increasing recording time allows for more accurate filtering. Longer recordings can also be used to capture reflections for more in depth geophysical processing. Long pre-trigger scans can be useful for sampling the background noise levels.

7.2.4. Realization of the frequent-interval method

Conventional methods for downhole seismic require the operator to visually approve each signal prior to storage, which reduces productivity. A new frequent-interval seismic method has been proposed for making overlapping true-interval measurements. By utilizing a consistent source, and a true-interval probe, the

opportunities for error are reduced, and the recording process can be automated. Signals may be monitored on the display and automatically stored, just as the other channels of the SCPTu would be monitored during penetration. The new method also significantly improves the depth resolution of V_S profiles without compromising accuracy by overlapping measurement intervals rather than shortening the interval length. The enhanced detail of the frequent-interval profile is able to capture layering and detect soils with unusual characteristics, such as peat lenses and cemented zones within the soil profile. When compared with other test methods, the frequent-interval results obtained with stationary receivers as well as non-stationary receivers during continuous-push seismic tests were found to yield similar results at the tests depths in common.

7.2.5. Effect of noise on the non-stationary receivers

In order for a continuous-push seismic sounding to be successful, the amplitude of the source signals must be higher than the amplitude of any vibratory noise generated during penetration having frequency content within the source bandwidth. The testing vehicle was found to be the most significant noise source, contaminating the seismic signals with vibrations through contact with the rods. During penetration, the noise becomes amplified in the stiffer soil layers, but the increased noise only acts at the depth of the sensor. Sensors outside the noisy layer are not affected.

7.2.6. Considerations for V_S analysis

Cross-correlation is an easily implemented analysis method that is a significant improvement over the popular first-crossover method, but interference from reflected waves and ambient noise violates the assumptions of the cross correlation method. As analysis techniques become more robust, real-time monitoring of V_S side-by-side with q_T, f_S, and u_b should be possible. The enhanced integration of V_S with common in-situ tests will allow engineers that are unfamiliar with geophysical methods a low cost option for gaining exposure.

7.2.7. Final comments

In a comprehensive review on the use of elastic waves in geotechnical engineering by Stokoe and Santamarina (2000), the authors conclude by describing four factors critical to the future growth of geophysical applications in the engineering field: (1) instruction, (2) industrialization (automation), (3) integration, and (4) innovation. This research contributes in some way to each of these factors. The advances that have been made could be considered basic by geophysics standards, but the incremental step is certainly significant for the geotechnical engineering community.

A secondary component of this research program has been the education of students and practitioners with regard to shear wave velocity profiling during site characterization with the cone penetrometer and the flat dilatometer. Outreach efforts include short course presentations and field demonstrations incorporated into research and consulting testing programs. To this end, an attempt has been made to provide the reader with practical information without overwhelming discussion of complex concepts.

The continuous-push seismic system has the ability to fully automate the measurement of V_S during penetration testing, building on the integration efforts, begun by other researchers two decades prior, to combine of seismic methods with the CPT and the DMT. Lastly, innovations have taken place in the form of a patented new type of automated seismic source and a new frequent-interval test method. Increased accessibility to detailed V_S profiling opens the door to the development of new engineering applications.

7.3. Future Directions

There are several potential applications for the continuous-push seismic system:

- The detailed depth resolution of the frequent-interval shear wave profile provides an opportunity to revisit existing relationships between measured parameters. The continuous-push seismic system encourages measurement

of V_S rather than estimation of V_S from correlations, but correlations play an important role in geotechnical engineering for developing a deeper understanding of soil behavior when the predicted values match, or do not match, the measured values.

- The redundancy of the overlapping measurements may aid in the quantification of the accuracy and precision of measured V_S values. The overlapping results might also be deconvolved into more discrete measurements.

- The closely spaced seismic signals could be utilized for more complex geophysics, such as vertical seismic profiling (VSP).

- The RotoSeis seismic source technology could be utilized to monitor time dependent V_S changes for monitoring consolidation of dredge spoils or performance of ground improvement techniques.

There are also opportunities for improving the continuous-push seismic system to improve the reliability and reduce analysis times:

- Further characterization of the penetration-related noise is needed so that a method can be developed for damping unwanted vibrations before they reach the receivers.

- New directional filter methods could be implemented to take advantage of the directionality of the source and the multi-component seismic sensors to further reduce the appearance of noise.

- The geophones utilized for the seismic probes should be replaced with small MEMs accelerometers to reduce the dimensional requirements and

make room for additional electronics. The MEMs accelerometers have linear amplitude and phase response down to 0 Hz, reducing signal distortion, and allowing them to double as inclinometers.

- A practical technique is needed for improving the stiffness of the source coupling, even in soft surficial soils. Stiffer coupling will increase the bandwidth of the source signals, which improves accuracy of travel-time estimations while making the signals less susceptible to interference from narrow-band noise, like that from the testing vehicle.

- Due to the time-varying frequency content of seismic signals, wavelet processing techniques are better-suited to the processing of seismic signals and could potentially fully automate the analysis of V_S.

The ultimate goal for the continuous-push seismic system is to incorporate the source within the probe rods along with the seismic sensors. A similar device (Figure 7.1) was conceived by Stokoe et al. (1978) for making discrete velocity measurements at the base of a borehole. The source is lowered downhole with the receivers, and the receivers are pushed into the soil beneath the bottom of the borehole. The source could be streamlined so that it could be pushed into the soil along with the receivers, eliminating the need for a borehole, and allowing continuous profiling rather than discrete measurements.

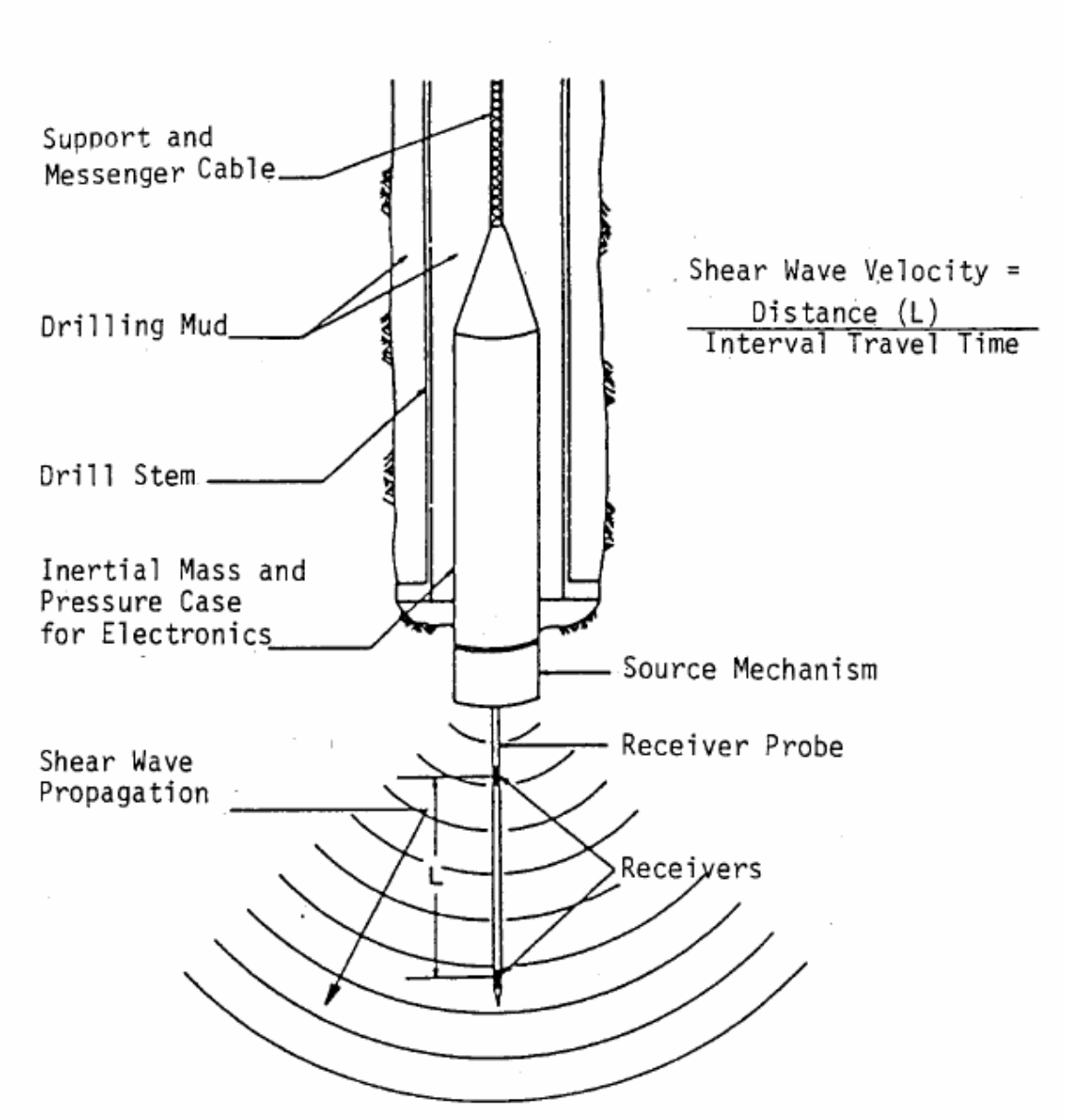

Figure 7.1 Schematic of the Bottom-Hole Seismic Device (Stokoe et al., 1978)

By building the source into the probe rods downhole with the receivers, problems associated with attenuation of the source amplitude and low bandwidth as a result of poor coupling could be eliminated. During continuous-push testing, the noise levels were found to attenuate with depth. If the seismic source were to travel downhole with the receivers, the source amplitude would not attenuate significantly before reaching the receivers, and the interference from noise would become negligible. Accuracy of

measured velocity would also improve with the use of higher frequency source signals. The use of higher frequency shear waves is possible due to the shorter source-receiver distance and improved coupling. The source coupling would improve with depth as the confinement increases. Source coupling is of particular concern for offshore applications, for which the soils near the mud line are too soft to support a surface source.

As seen in Figure 7.2, a continuous-push seismic system, containing source and receivers, is not only applicable to the SCPT and the SDMT. For offshore exploration there are other continuous-push tests such as the T-bar test and a continuous-push vane shear test (VST), both of which could benefit from continuous-push seismic measurements.

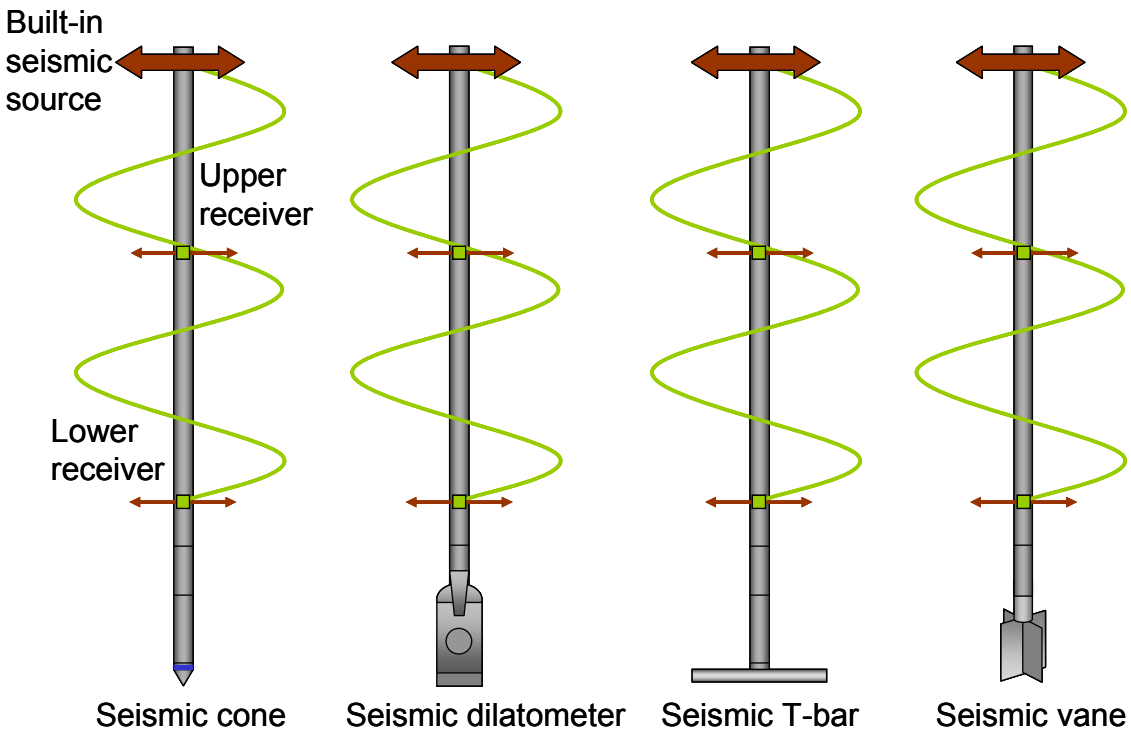

Figure 7.2 Application of continuous-push seismic to several direct-push site characterization systems

APPENDIX A. PRESENTATION OF FIELD TEST RESULTS

A total of 52 field tests were performed during this research effort. The soundings were performed to evaluate the different versions of the RotoSeis automated seismic source, to collect frequent-interval shear wave velocity profiles, to verify the components of the continuous-push seismic system, and to provide conventional results for comparisons. The majority of the soundings are SCPTu, which were performed with the Hogentogler 10 cm² seismic cone. Three SDMT soundings were conducted at the Treporti test site. Ten of the tests utilized either the true-interval or biaxial true-interval seismic probes to measure frequent-interval V_S profiles. The details of the tests are listed below in Table A.1, and the results of the soundings are shown in the following pages.

Table A.1 Summary of field tests performed which relate to the development of a continuous-push system

Sounding Name	Site	Date	Latitude N°	Longitude E°	Test Type	Seismic Method	Seismic Source	Probe	Depth (m)
SWGA01	Collierville, TN	June 5, 2001	35.09335	89.71093	$SCPTu_2$	Pseudo-interval	Pneumatic AutoSeis, Pendulum	Hogentogler 10cm²	22.9 (28.6)
SCPT19 (VENI01)	Treporti, Italy	June 10, 2002	45.46774	-12.45487	$SCPTu_2$	Pseudo-interval	Pendulum	Hogentogler 10cm²	40.8
SCPT14 (VENI02)	Treporti, Italy	June 11, 2002	45.46774	-12.45461	$SCPTu_2$	Pseudo-interval	Pendulum	Hogentogler 10cm²	40.2
SCPT15 (VENI03)	Treporti, Italy	June 11, 2002	45.46771	-12.45447	$SCPTu_2$	Pseudo-interval	Pendulum	Hogentogler 10cm²	40.6
SDMT15	Treporti, Italy	June 12, 2002	45.46770	-12.45448	SDMT	Pseudo-interval True-interval	Pendulum	True-interval Seismic DMT	15.8 (P-I) 13.2 (T-I) (32.0)
SDMT14	Treporti, Italy	June 13, 2002	45.46770	-12.45465	SDMT	Pseudo-interval Frequent-interval	Pendulum	True-interval Seismic DMT	29.8 (P-I) 16.2 (F-I) (31.0)
SDMT19	Treporti, Italy	June 14, 2002	45.46773	-12.45486	SDMT	Pseudo-interval True-interval	Pendulum	True-interval Seismic DMT	36.8 (P-I) 36.2 (T-I) (37.0)
BLST01	Mooring, TN	October 17, 2002	36.33203	89.58680	$SCPTu_2$	Pseudo-interval	Pendulum	Hogentogler 10cm²	38.9
BLST03	Mooring, TN	October 18, 2002	36.33203	89.58631	$SCPTu_2$	Pseudo-interval	Pendulum	Hogentogler 10cm²	30.9
BLST05	Mooring, TN	October 29, 2002	36.33203	89.58680	$SCPTu_2$	Pseudo-interval	Pendulum	Hogentogler 10cm²	25.8
BLST06	Mooring, TN	October 30, 2002	36.33204	89.58679	$SCPTu_2$	Pseudo-interval	Pendulum	Hogentogler 10cm²	27.9
BLST08	Mooring, TN	November 1, 2002	36.33203	89.58679	$SCPTu_2$	Pseudo-interval	RotoSeis I	Hogentogler 10cm²	21.0 (28.1)
BLST11	Mooring, TN	June 15, 2003	36.33203	89.58679	$SCPTu_2$	Pseudo-interval	RotoSeis I, Pendulum	Hogentogler 10cm²	15.0 (22.9)

( ) - indicates maximum depth of sounding, (P-I) - pseudo-interval, (F-I) - frequent-interval

Table A.1 (continued) Summary of field tests performed which relate to the development of a continuous-push system

Sounding Name	Site	Date	Latitude N°	Longitude E°	Test Type	Seismic Method	Seismic Source	Probe	Depth (m)
FCPT04	Evanston, IL	July 14, 2003	42.05679	87.67663	$SCPTu_2$	Pseudo-interval	Sledgehammer	Hogentogler 10cm²	27.1
FCPT04SEIS	Evanston, IL	July 14, 2003	42.05679	87.67663	Downhole Seismic	Frequent-interval	Sledgehammer	True-interval seismic probe	12.0
FCPT02	Evanston, IL	July 16, 2003	42.05692	87.67689	$SCPTu_2$	Pseudo-interval	Sledgehammer	Hogentogler 10cm²	17.7
FCPT03	Evanston, IL	July 16, 2003	42.05688	87.67640	$SCPTu_2$	Pseudo-interval	Sledgehammer	Hogentogler 10cm²	21.0
FCPT05	Evanston, IL	July 17, 2003	42.05679	87.67663	$CPTu_1$	None	None	Hogentogler 10cm²	22.0
FCPT05SEIS	Evanston, IL	July 17, 2003	42.05679	87.67663	Downhole Seismic	Frequent-interval	Sledgehammer	True-interval seismic probe	3.4
FCPT01	Evanston, IL	July 18, 2003	42.05704	87.67654	$SCPTu_2$	Pseudo-interval	Sledgehammer	Hogentogler 10cm²	18.0
FDMT1	Evanston, IL	July 19, 2003	42.05704	87.67654	DMT	None	None	DMT blade	23.0
FCPT03SEIS	Evanston, IL	July 20, 2003	42.05688	87.67640	Downhole Seismic	Frequent-interval	Sledgehammer	True-interval seismic probe	23.0
MUDB1	Memphis, TN	March 5, 2000	35.15647	90.05688	$SCPTu_2$	Pseudo-interval	Pendulum	Hogentogler 10cm²	31.0
MUDBSEIS	Memphis, TN	September 19, 2003	35.15669	90.05692	Downhole Seismic	Frequent-interval	Sledgehammer	True-interval seismic probe	21.9
OPEAUT	Opelika, AL	March 1, 2004	32.59394	85.29739	$SCPTu_2$	Pseudo-interval	RotoSeis II	Hogentogler 10cm²	20.9
OPETRU	Opelika, AL	May 10, 2004	32.59391	85.29746	$SCPTu_2$	Pseudo-interval	Pendulum	Hogentogler 10cm²	12.2
OPETRUSEIS	Opelika, AL	May 10, 2004	32.59391	85.29746	Downhole Seismic	Frequent-interval	RotoSeis II, Pendulum	Biaxial true-interval seismic probe	11.8

( ) - indicates maximum depth of sounding

Table A.1 (continued) Summary of field tests performed which relate to the development of a continuous-push system

Sounding Name	Site	Date	Latitude N°	Longitude E°	Test Type	Seismic Method	Seismic Source	Probe	Depth (m)
HENM	Sikeston, MO	August 11, 2004	36.71608	89.47210	$SCPTu_2$	Pseudo-interval	RotoSeis II	Hogentogler 10cm²	29.8 (30.9)
12ST01	Atlanta, GA	September 10, 2004	33.78452	84.37980	$SCPTu_2$	Pseudo-interval	RotoSeis III	Hogentogler 10cm²	16.8
12ST02	Atlanta, GA	September 10, 2004	33.78476	84.38018	$SCPTu_2$	Pseudo-interval	RotoSeis III	Hogentogler 10cm²	16.8
BMS02	Berea, SC	September 13, 2004	34.91513	82.45541	$SCPTu_2$	Pseudo-interval	RotoSeis III	Hogentogler 10cm²	18.0 (18.6)
HRES01	Atlanta, GA	February 11, 2005	33.79429	84.41091	$SCPTu_2$	Pseudo-interval	RotoSeis IV	Hogentogler 10cm²	16.8 (17.8)
PWRP1	St. Petersburg, FL	March 3, 2006	27.85923	82.60089	$SCPTu_2$	Pseudo-interval	RotoSeis V	Hogentogler 10cm²	13.7
PWRP2	St. Petersburg, FL	March 3, 2006	27.85915	82.60282	$SCPTu_2$	Pseudo-interval	RotoSeis V	Hogentogler 10cm²	18.5
PWRP3	St. Petersburg, FL	March 4, 2006	27.85970	82.60191	$SCPTu_2$	Pseudo-interval	RotoSeis V	Hogentogler 10cm²	12.4
PWRP4	St. Petersburg, FL	March 4, 2006	27.86038	82.60313	$SCPTu_2$	Pseudo-interval	RotoSeis V	Hogentogler 10cm²	14.4
PWRP5	St. Petersburg, FL	March 4, 2006	27.86032	82.60078	$SCPTu_2$	Pseudo-interval	RotoSeis V	Hogentogler 10cm²	14.2
BEAU01	Beaufort, SC	April 27, 2006	32.44004	80.68442	$SCPTu_2$	Pseudo-interval	RotoSeis V	Hogentogler 10cm²	11.0
BEAU02	Beaufort, SC	April 27, 2006	32.44006	80.68442	$SCPTu_2$	Pseudo-interval	RotoSeis V	Hogentogler 10cm²	17.0 (17.8)

( ) - indicates maximum depth of sounding

Table A.1 (continued) Summary of field tests performed which relate to the development of a continuous-push system

Sounding Name	Site	Date	Latitude N°	Longitude E°	Test Type	Seismic Method	Seismic Source	Probe	Depth (m)
STON1A	John's Island, SC	December 16, 1999	32.75241	80.01335	$SCPTu_2$	Pseudo-interval	Sledgehammer	Hogentogler 10cm²	25.1
STONOSEIS	John's Island, SC	May 21, 2004	32.75228	80.01317	Downhole Seismic	Frequent-interval	Sledgehammer	Biaxial true-interval seismic probe	26.0
STONO01	John's Island, SC	April 28, 2006	32.75123	80.01346	$CPTu_2$	None	None	Hogentogler 10cm²	22.1
STONO01SEIS	John's Island, SC	April 28, 2006	32.75123	80.01346	Downhole Seismic	Continuous-push frequent-interval	RotoSeis V	Biaxial seismic probe	9.7
CRBDH1	Mt. Pleasant, SC	December 17, 1999	32.80161	79.90153	$SCPTu_2$	Pseudo-interval	Pendulum	Hogentogler 15cm²	30.6
CRB01	Mt. Pleasant, SC	April 29, 2006	32.80162	79.90064	$CPTu_2$	None	None	Hogentogler 10cm²	24.9
CRB01SEIS	Mt. Pleasant, SC	April 29, 2006	32.80162	79.90064	Downhole Seismic	Continuous-push frequent-interval	RotoSeis V	Biaxial true-interval seismic probe	12.6
CRB02	Mt. Pleasant, SC	April 30, 2006	32.80165	79.90065	$CPTu_2$	None	None	Hogentogler 10cm²	26.0
CRB02SEIS	Mt. Pleasant, SC	April 30, 2006	32.80165	79.90065	Downhole Seismic	Frequent-interval	Sledgehammer	Biaxial true-interval seismic probe	27.7
CRB03	Mt. Pleasant, SC	July 24, 2007	32.80174	79.90180	$SCPTu_2$	Continuous-push pseudo-interval	Commercial RotoSeis	Hogentogler 10cm²	28.6
CRB03SEIS	Mt. Pleasant, SC	July 24, 2007	32.80174	79.90180	Downhole Seismic	Continuous-push frequent-interval	Commercial RotoSeis	Biaxial true-interval seismic probe	28.5
NEWOR01	New Orleans, LA	October 24, 2006	N/A	N/A	$SCPTu_2$	Pseudo-interval	RotoSeis V	Hogentogler 10cm²	29.7
F22Y0703C	St. Paul, MN	May 22, 2007	44.96817	93.08994	$SCPTu_2$	Pseudo-interval	Vertek Hydraulic	Vertek 15cm²	15.1

( ) - indicates maximum depth of sounding

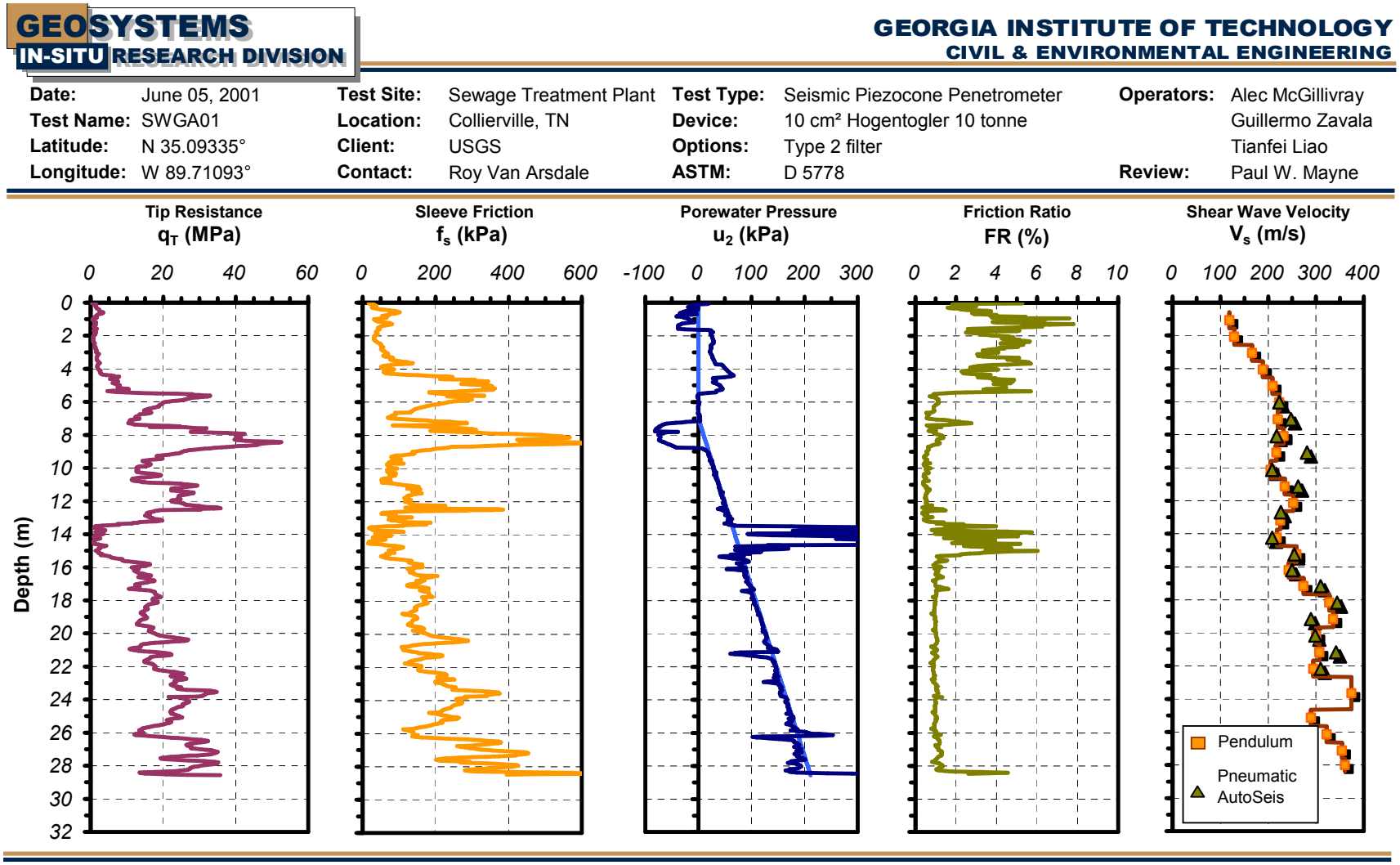

Figure A.1 Plot of SCPTu sounding SWGA01 with pendulum and pneumatic AutoSeis

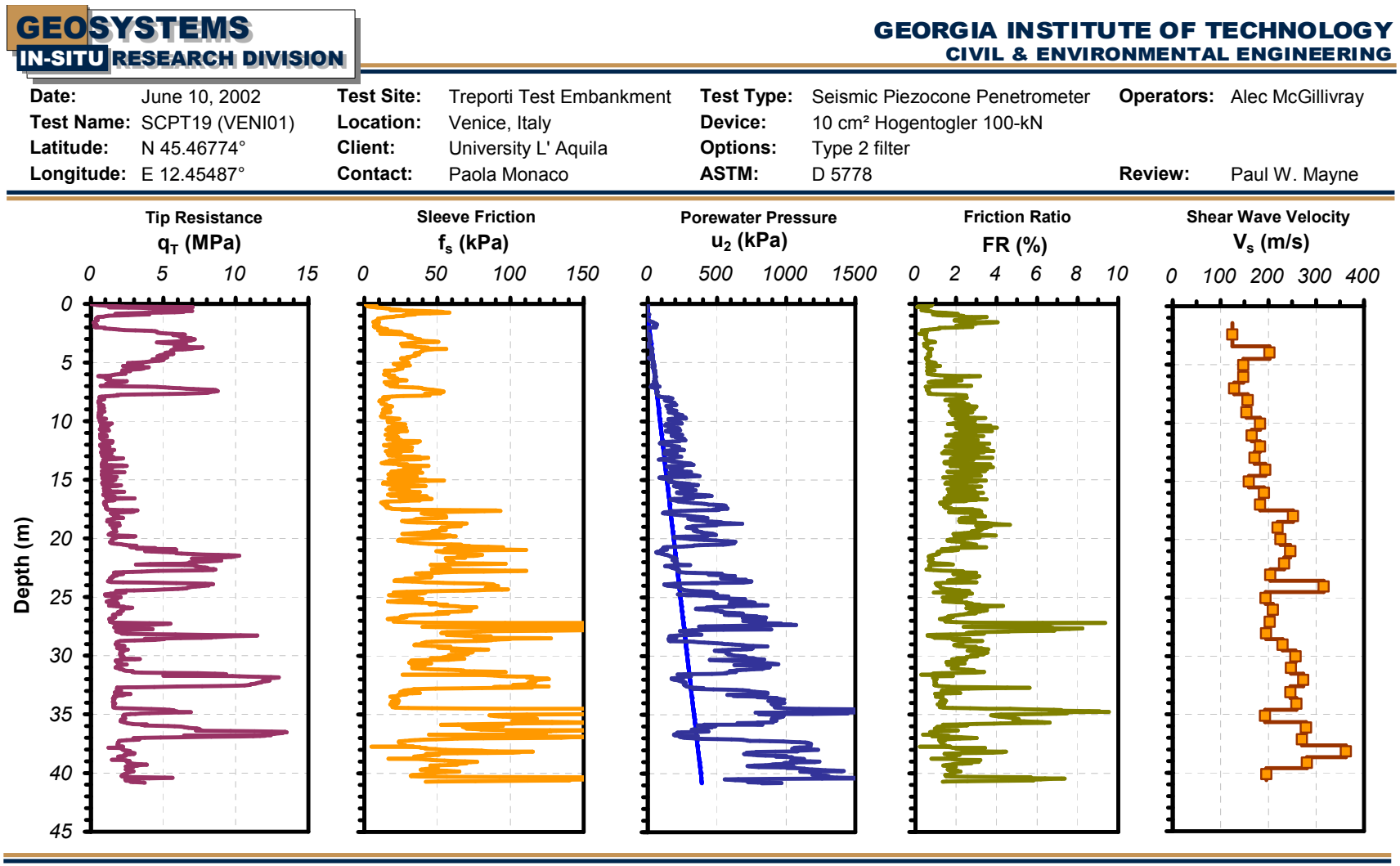

Figure A.2 Plot of SCPTu sounding SCPT19 (VENI01) with pendulum

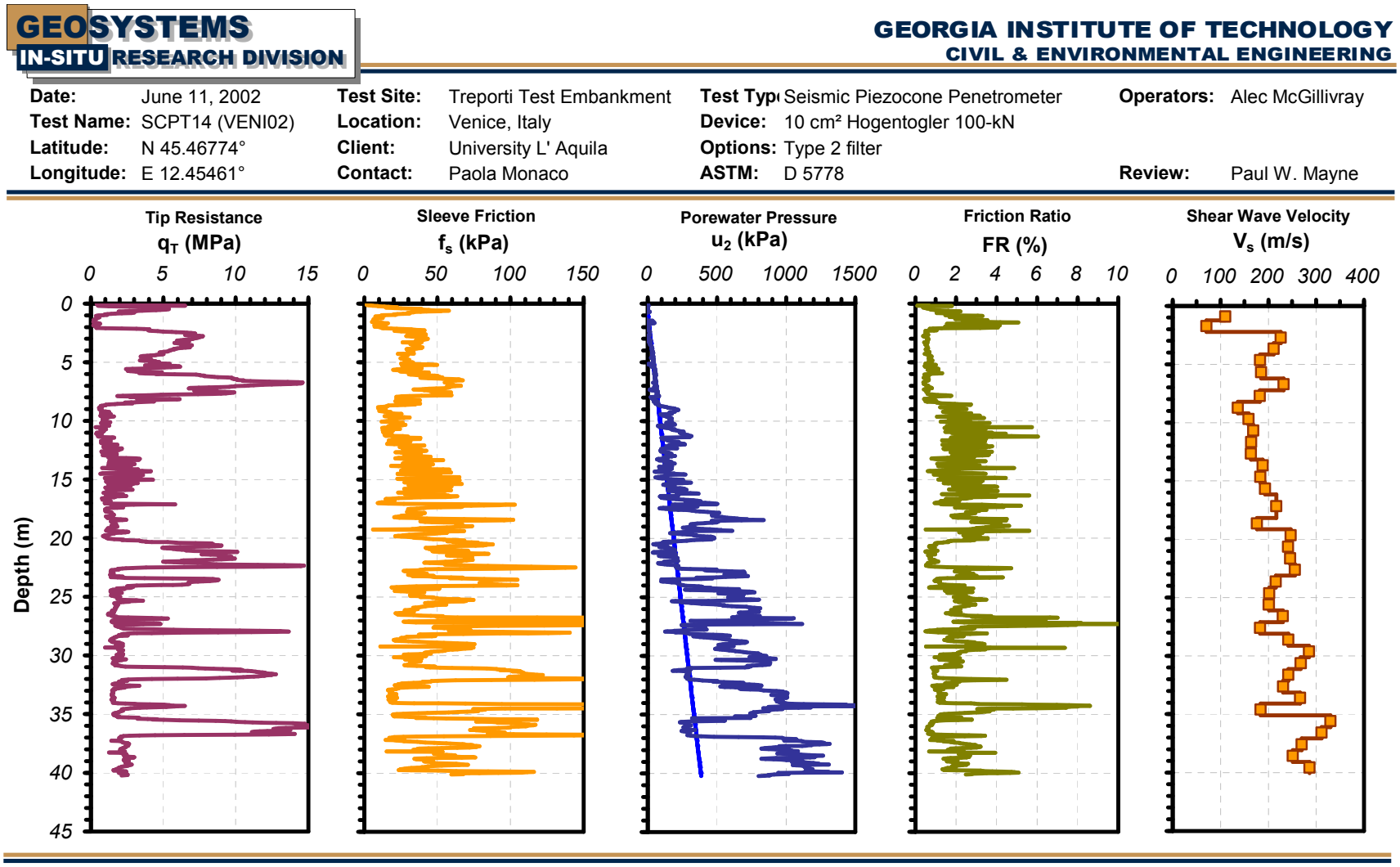

Figure A.3 Plot of SCPTu sounding SCPT14 (VENI02) with pendulum

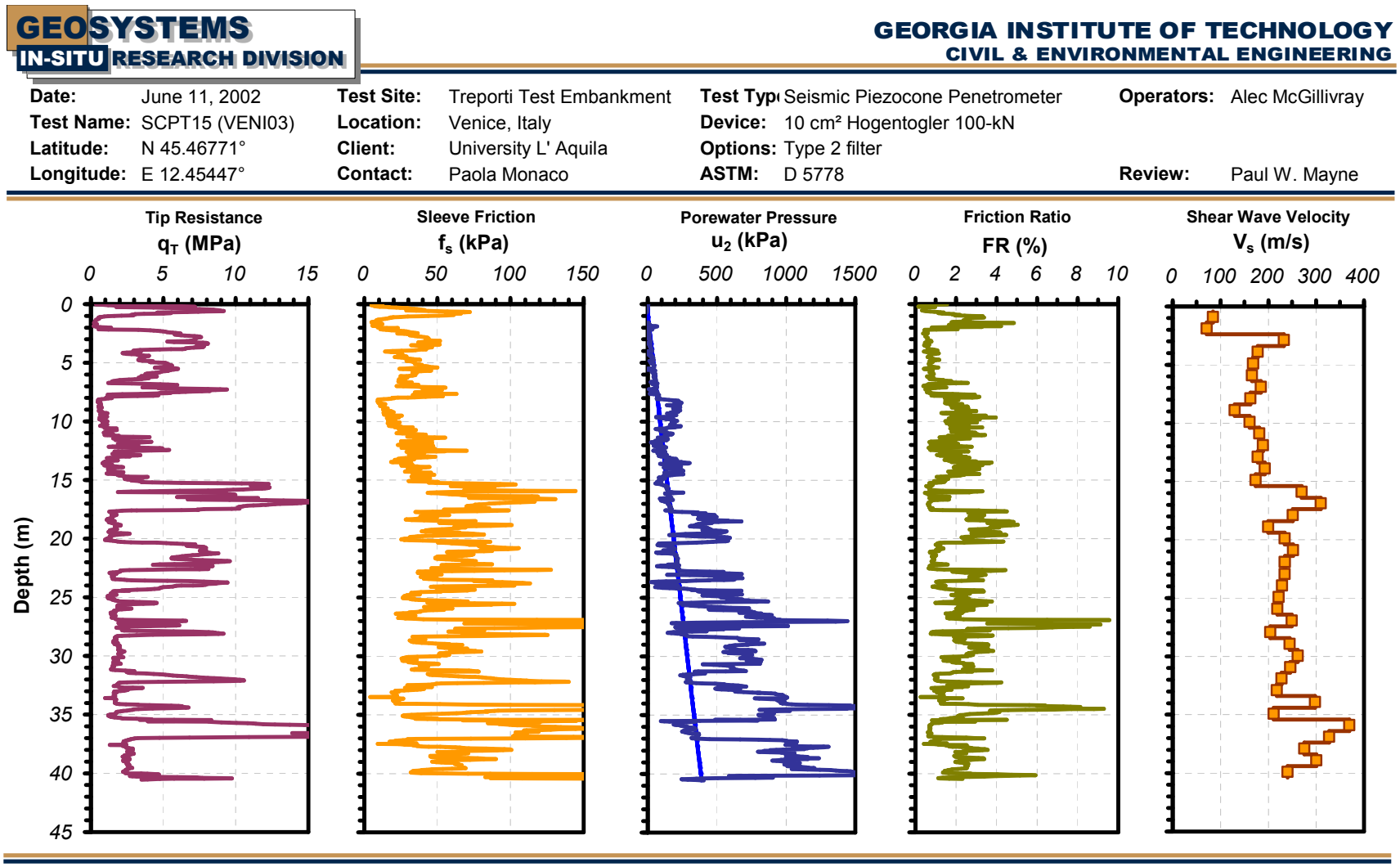

Figure A.4 Plot of SCPTu sounding SCPT15 (VENI03) with pendulum

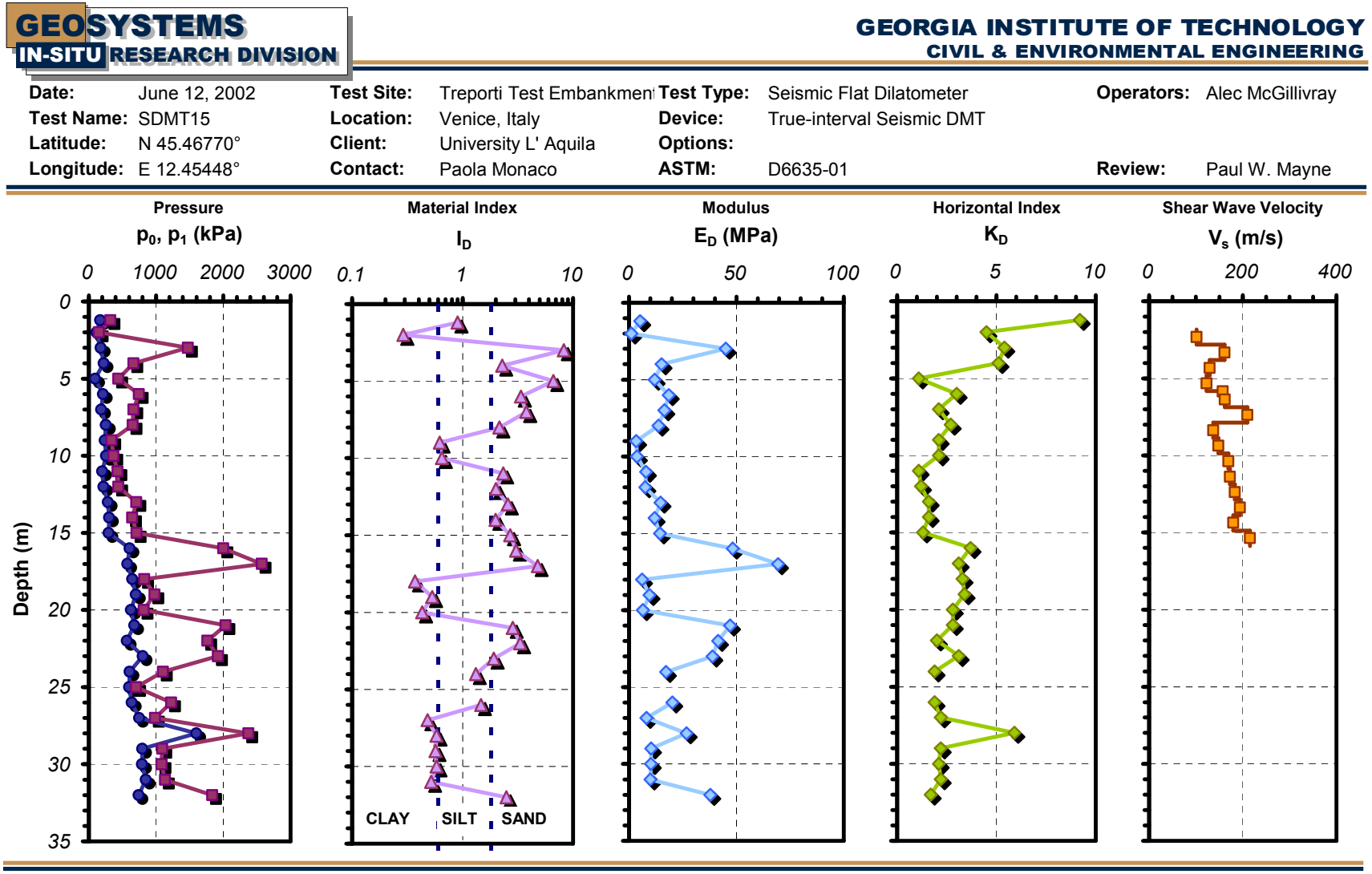

Figure A.5 Plot of SDMT sounding SDMT15 with pendulum

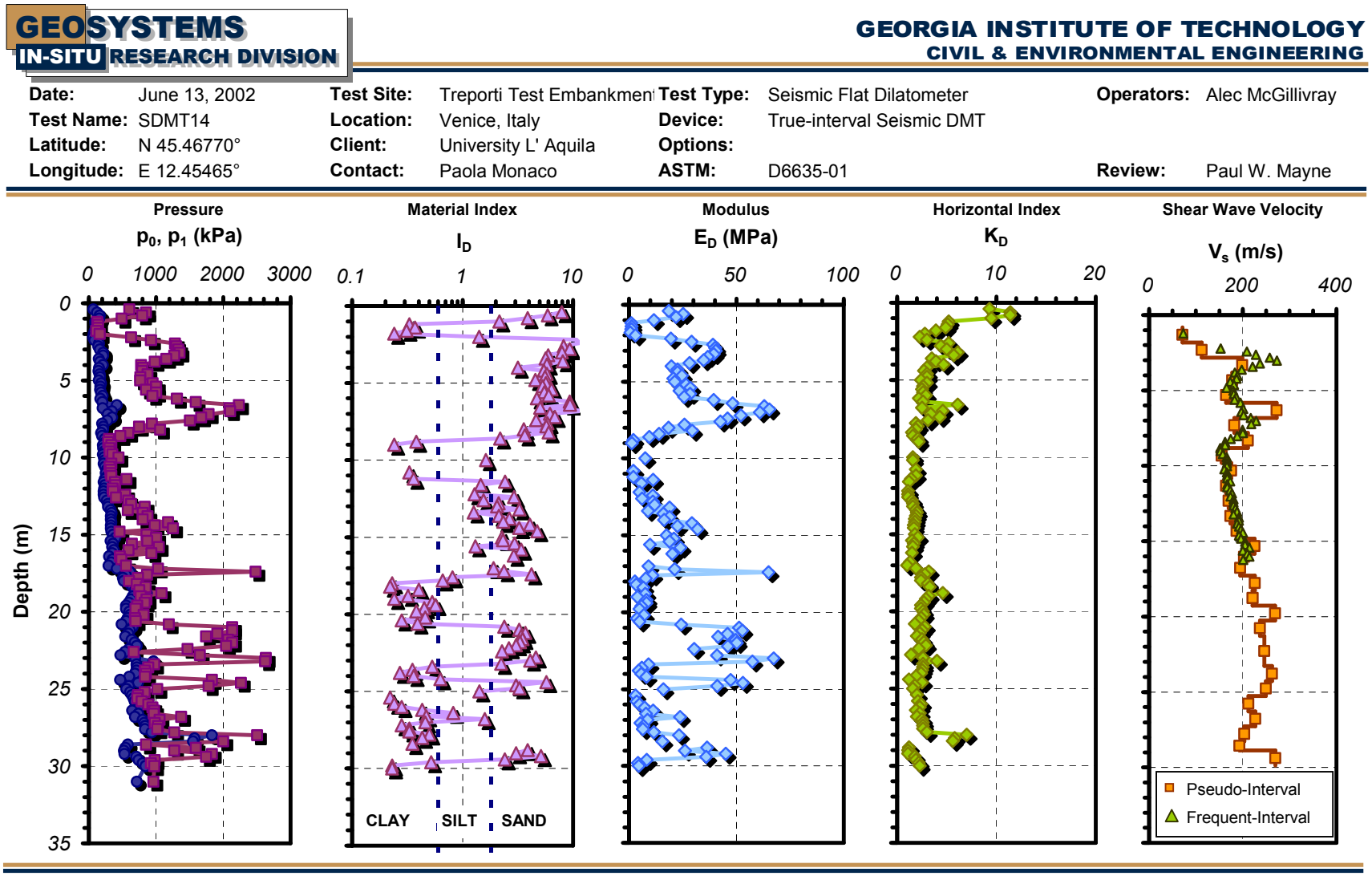

Figure A.6 Plot of SDMT sounding SDMT14 with pendulum

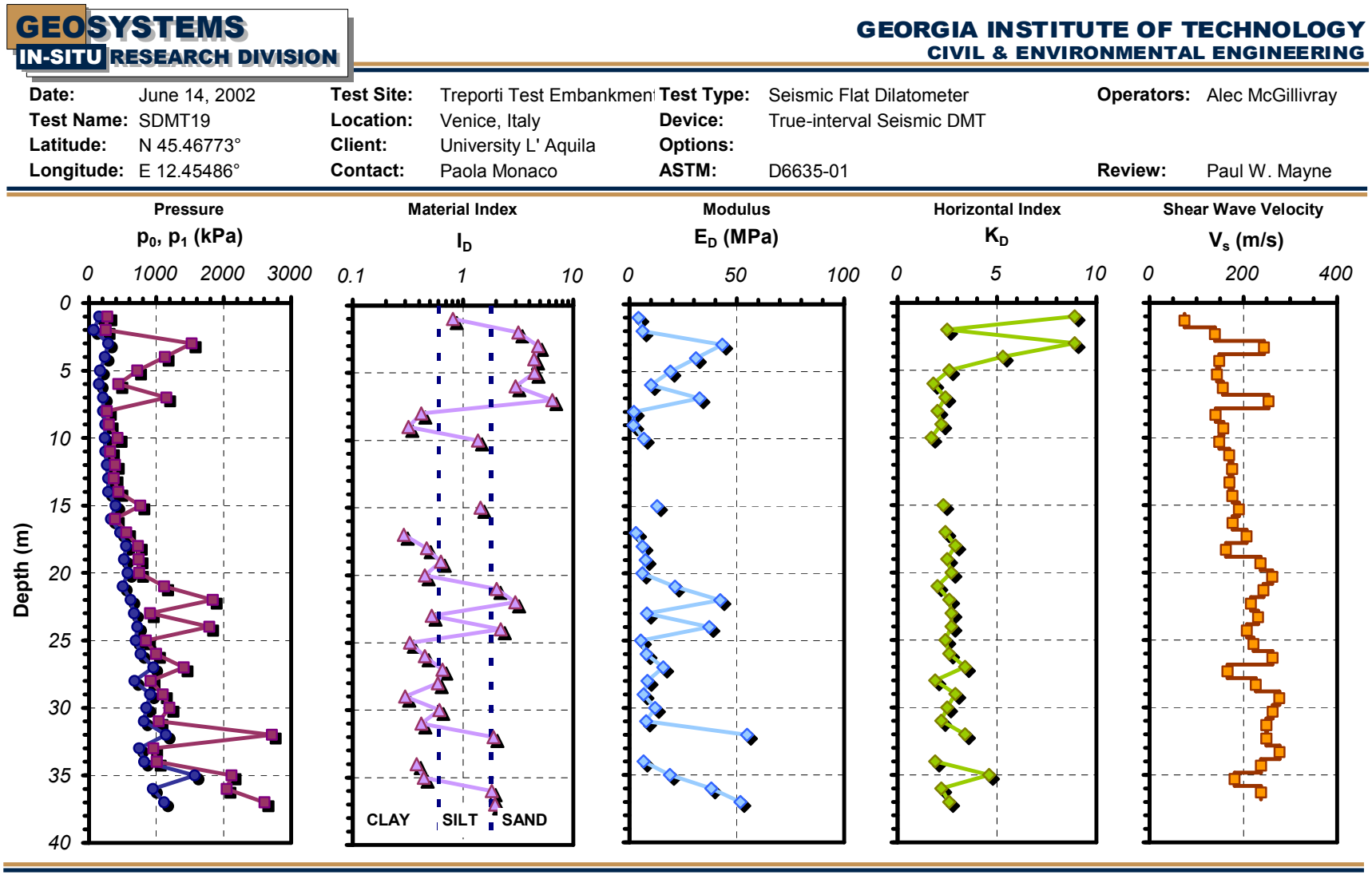

Figure A.7 Plot of SDMT sounding SDMT19 with pendulum

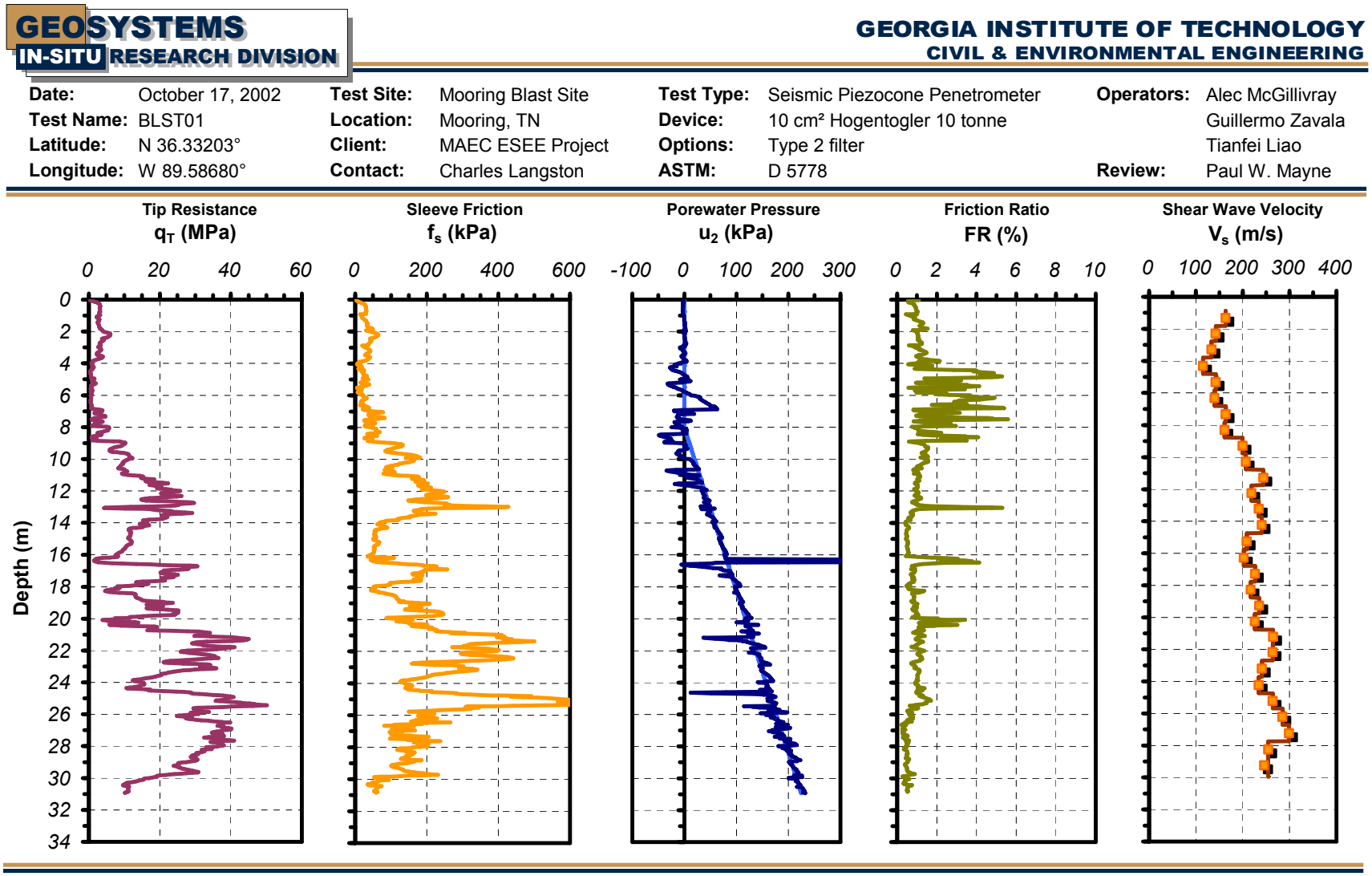

Figure A.8 Plot of SCPTu sounding BLST01 with pendulum

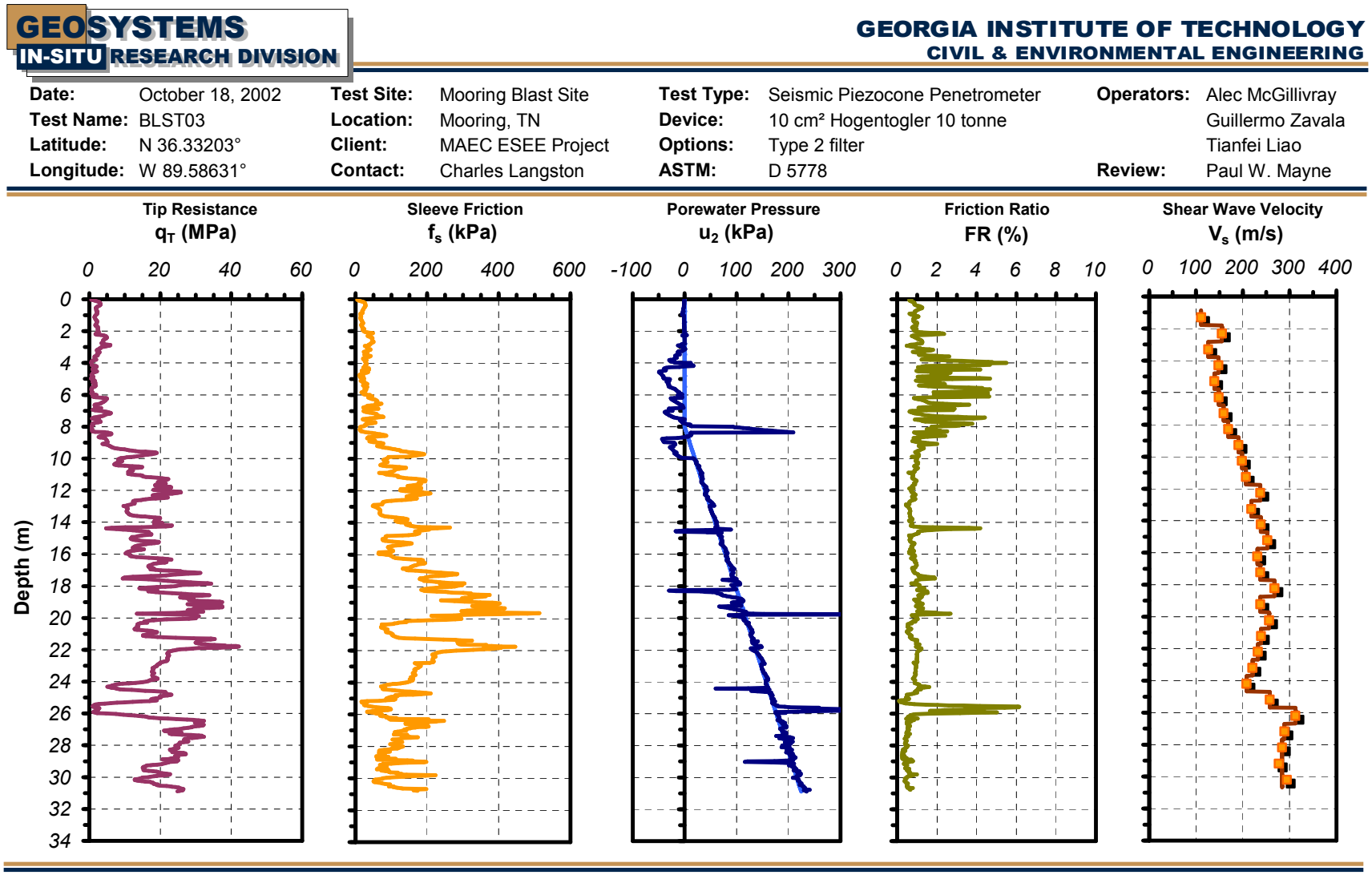

Figure A.9 Plot of SCPTu sounding BLST03 with pendulum

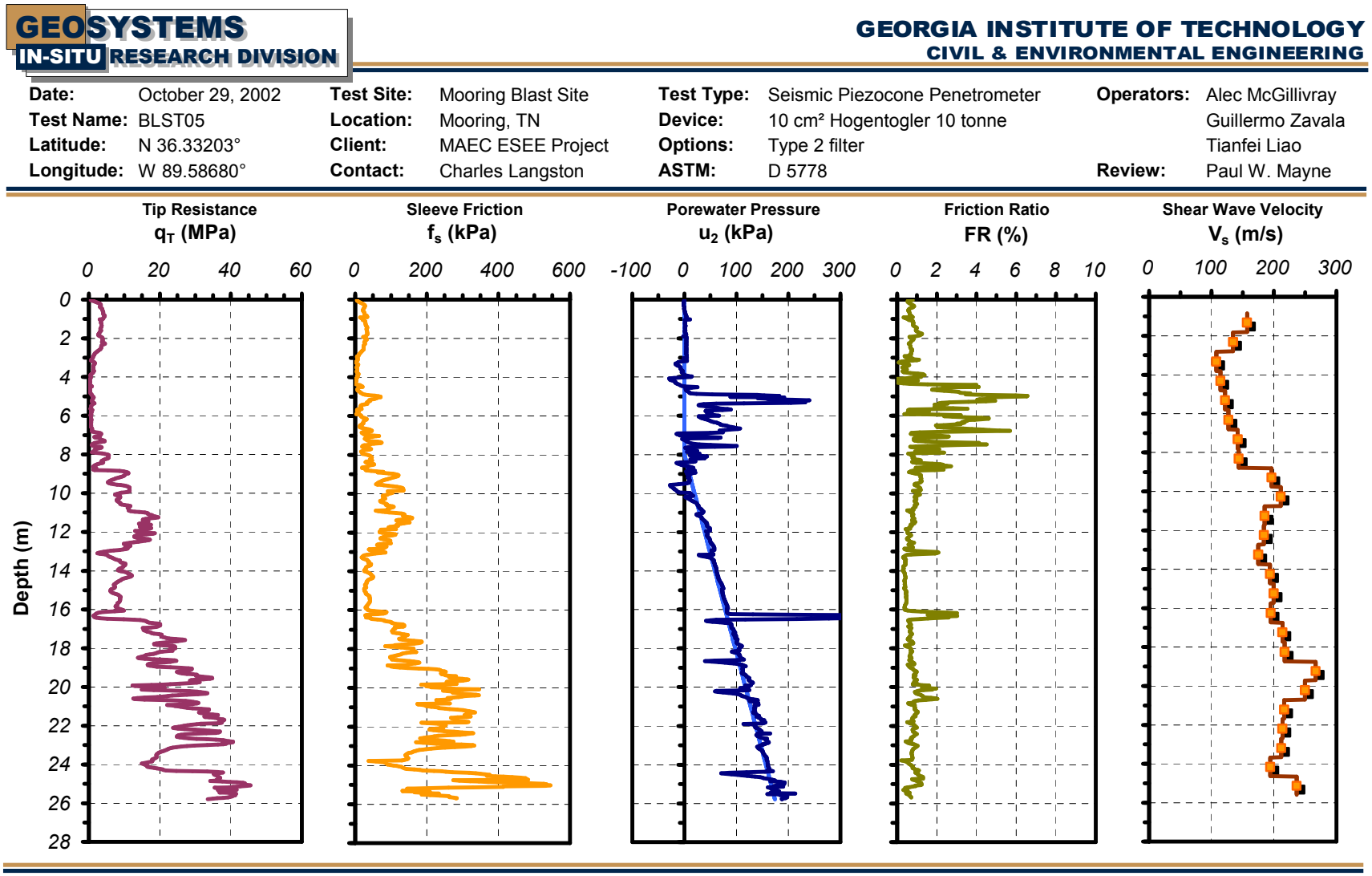

Figure A.10 Plot of SCPTu sounding BLST05 with pendulum

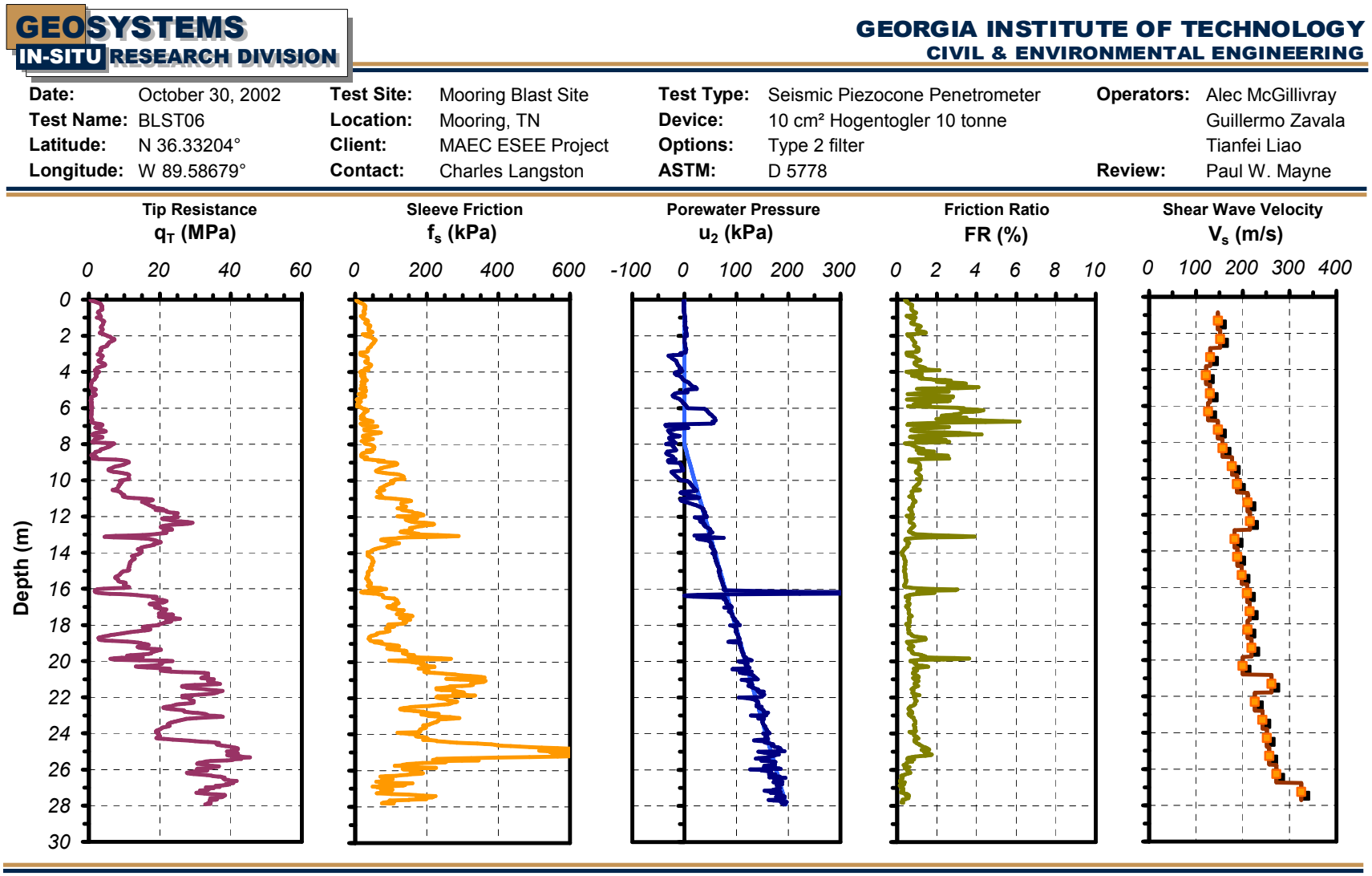

Figure A.11 Plot of SCPTu sounding BLST06 with pendulum

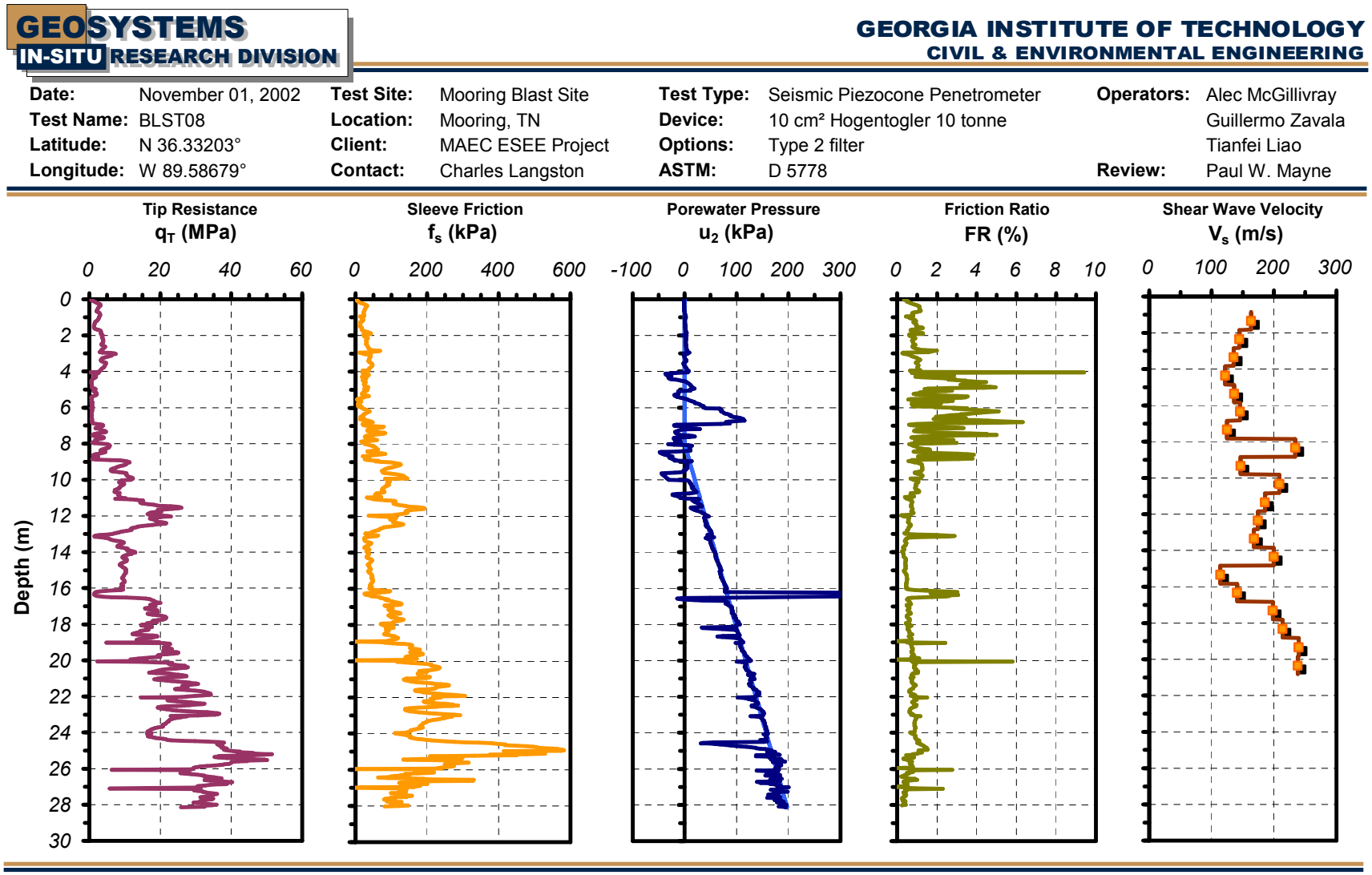

Figure A.12 Plot of SCPTu sounding BLST08 with RotoSeis I

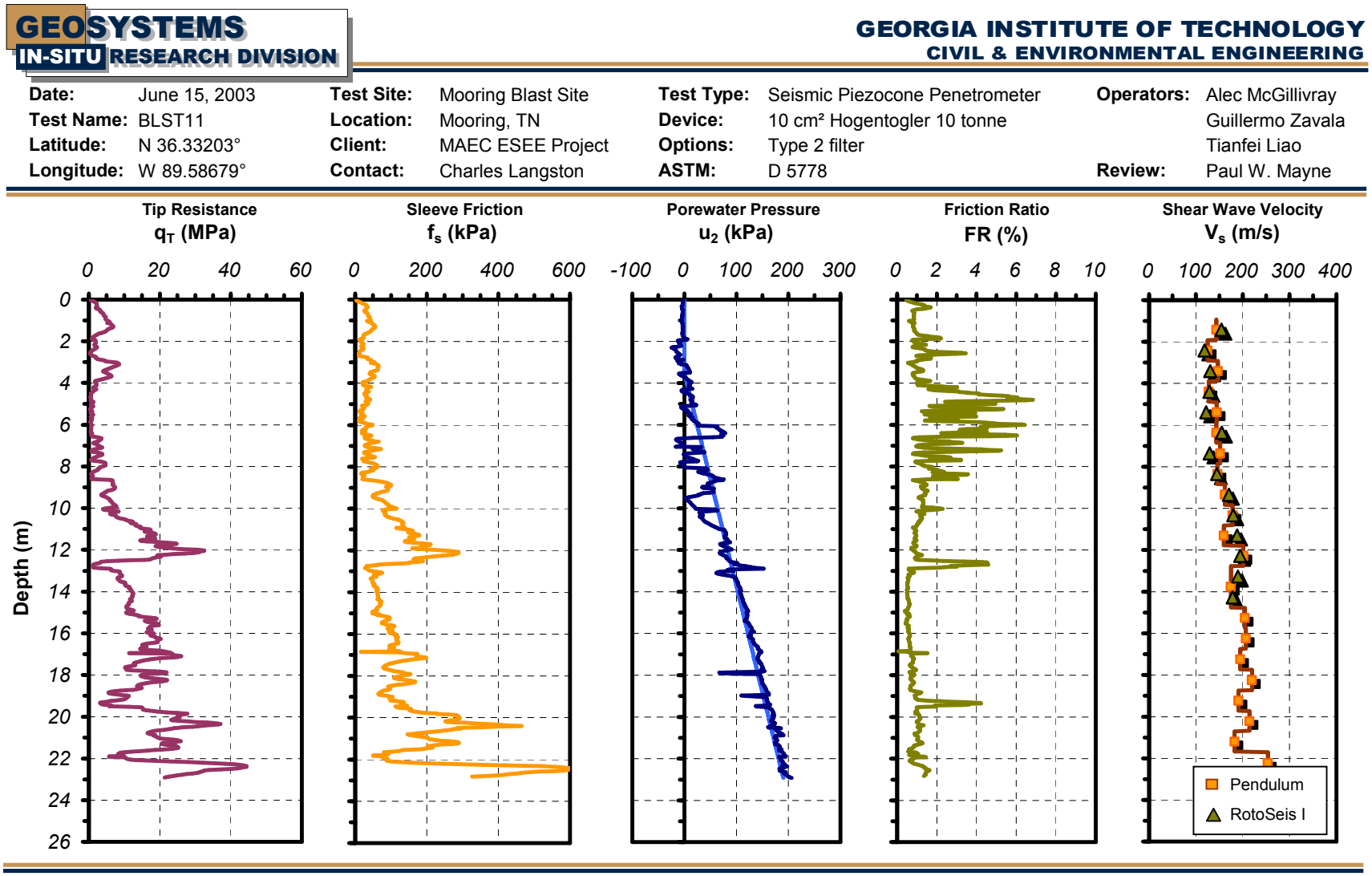

Figure A.13 Plot of SCPTu sounding BLST11 with pendulum and RotoSeis I

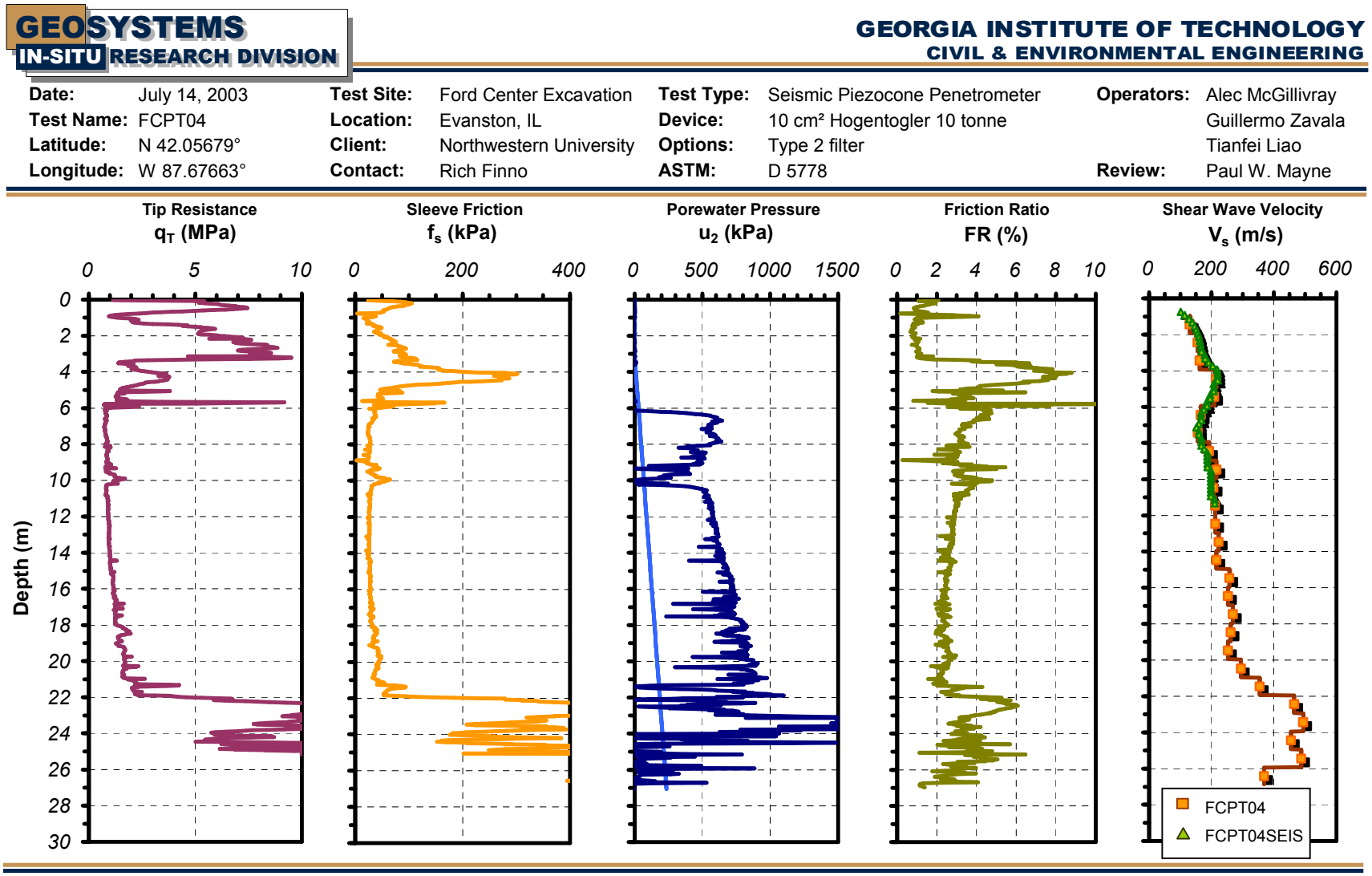

Figure A.14 Plot of SCPTu sounding FCPT04/FCPT04SEIS with sledgehammer

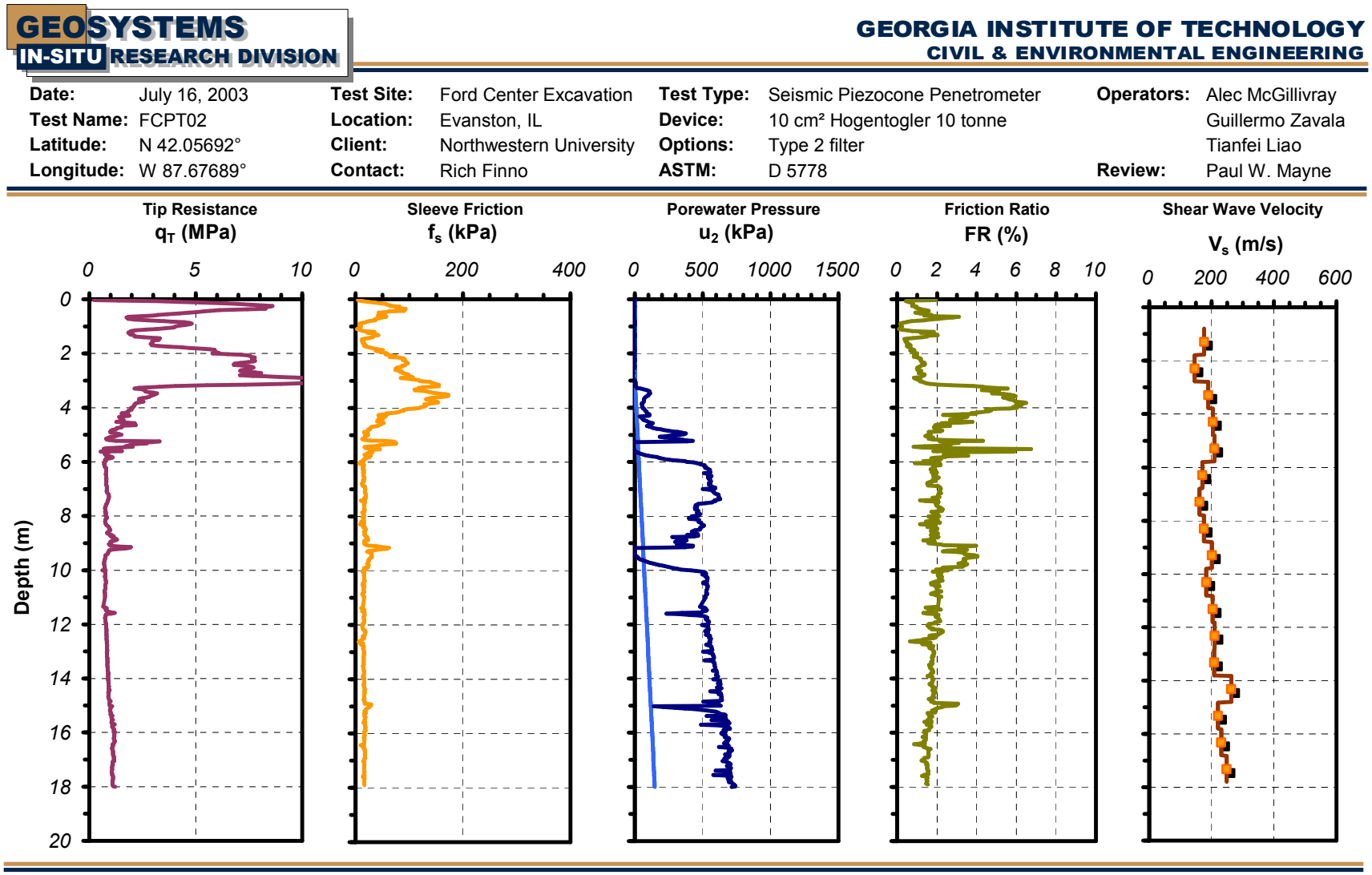

Figure A.15 Plot of SCPTu sounding FCPT02 with sledgehammer

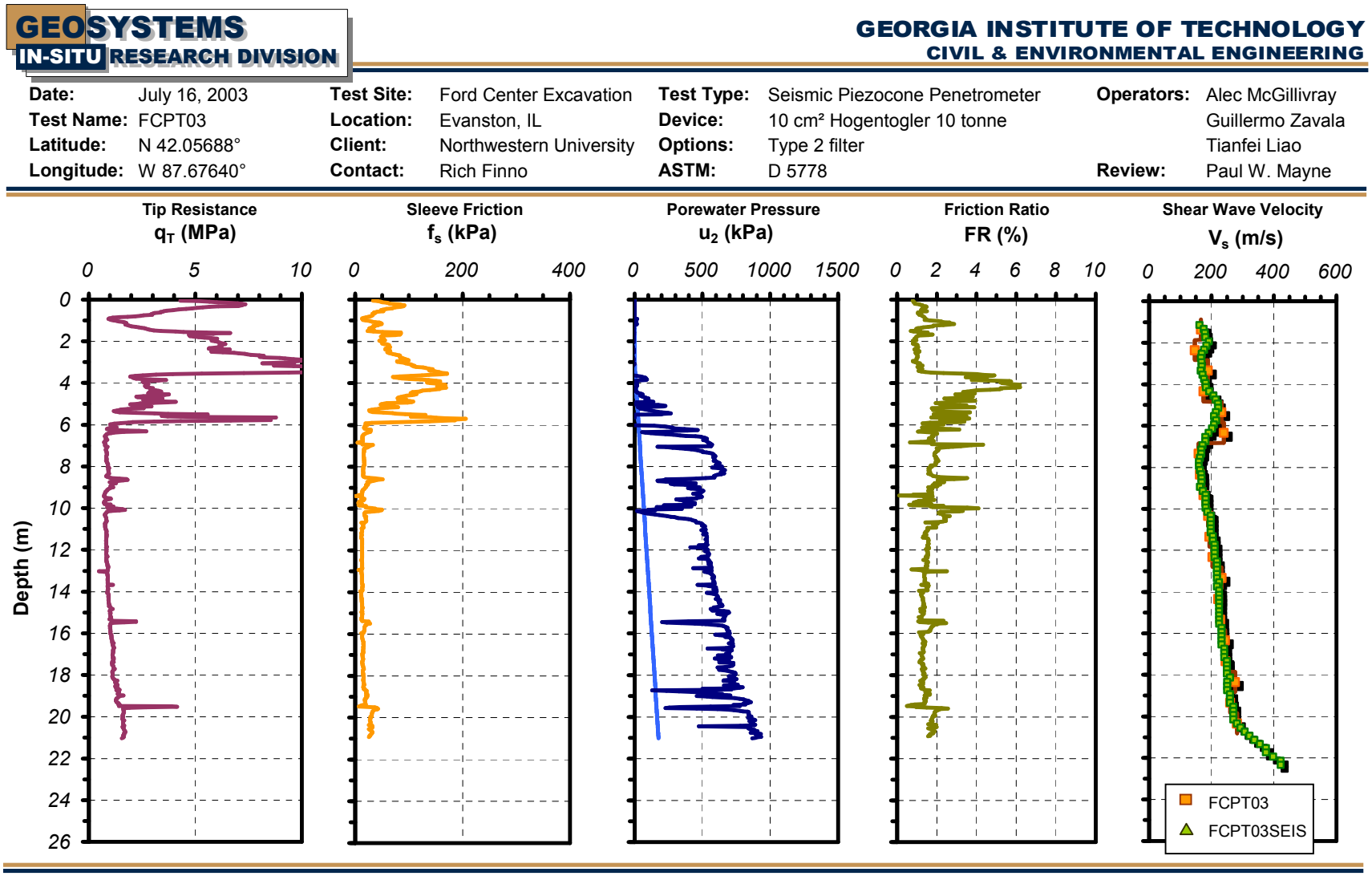

Figure A.16 Plot of SCPTu sounding FCPT03 with sledgehammer

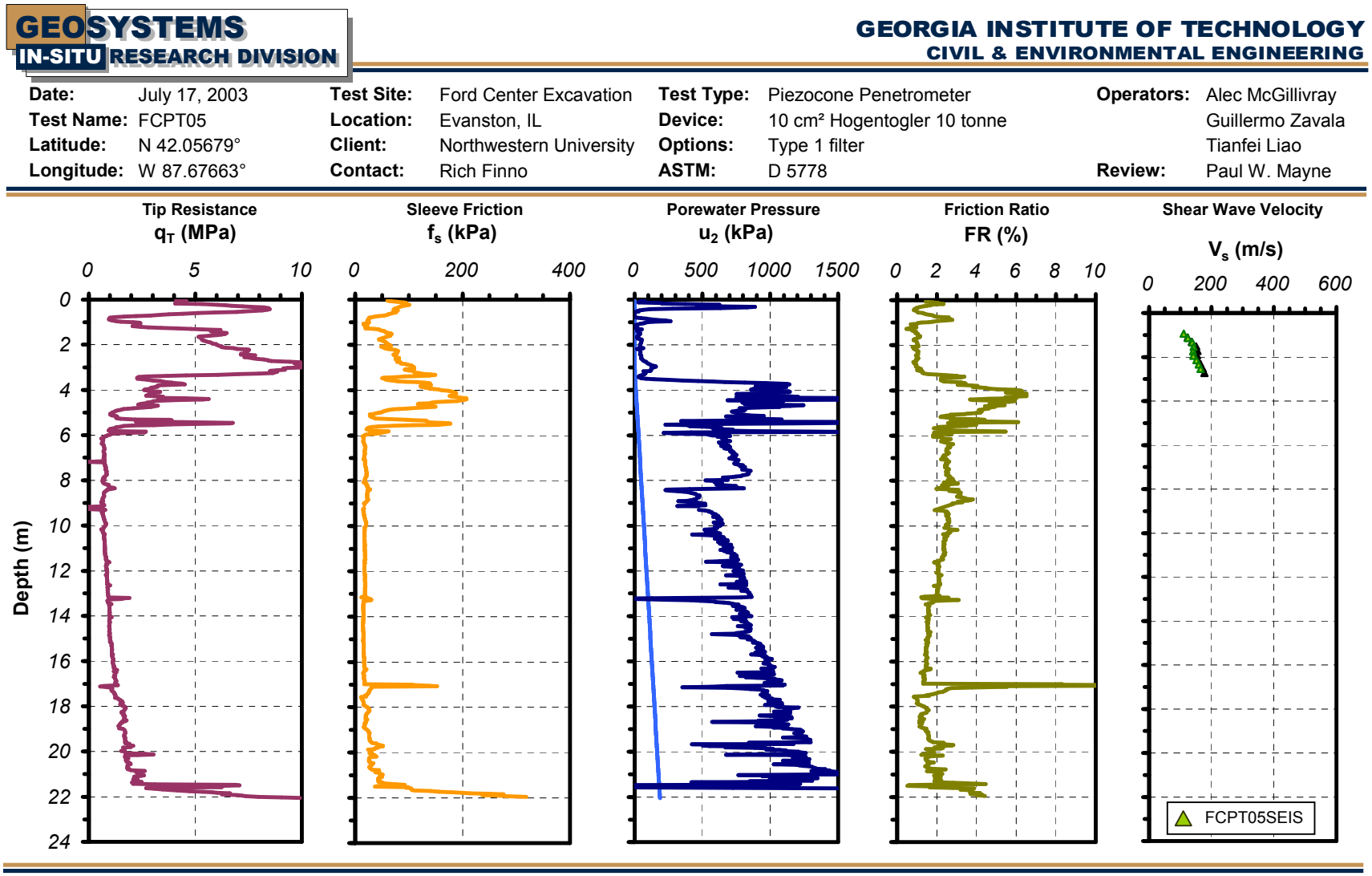

Figure A.17 Plot of SCPTu sounding FCPT05/FCPT05SEIS with sledgehammer

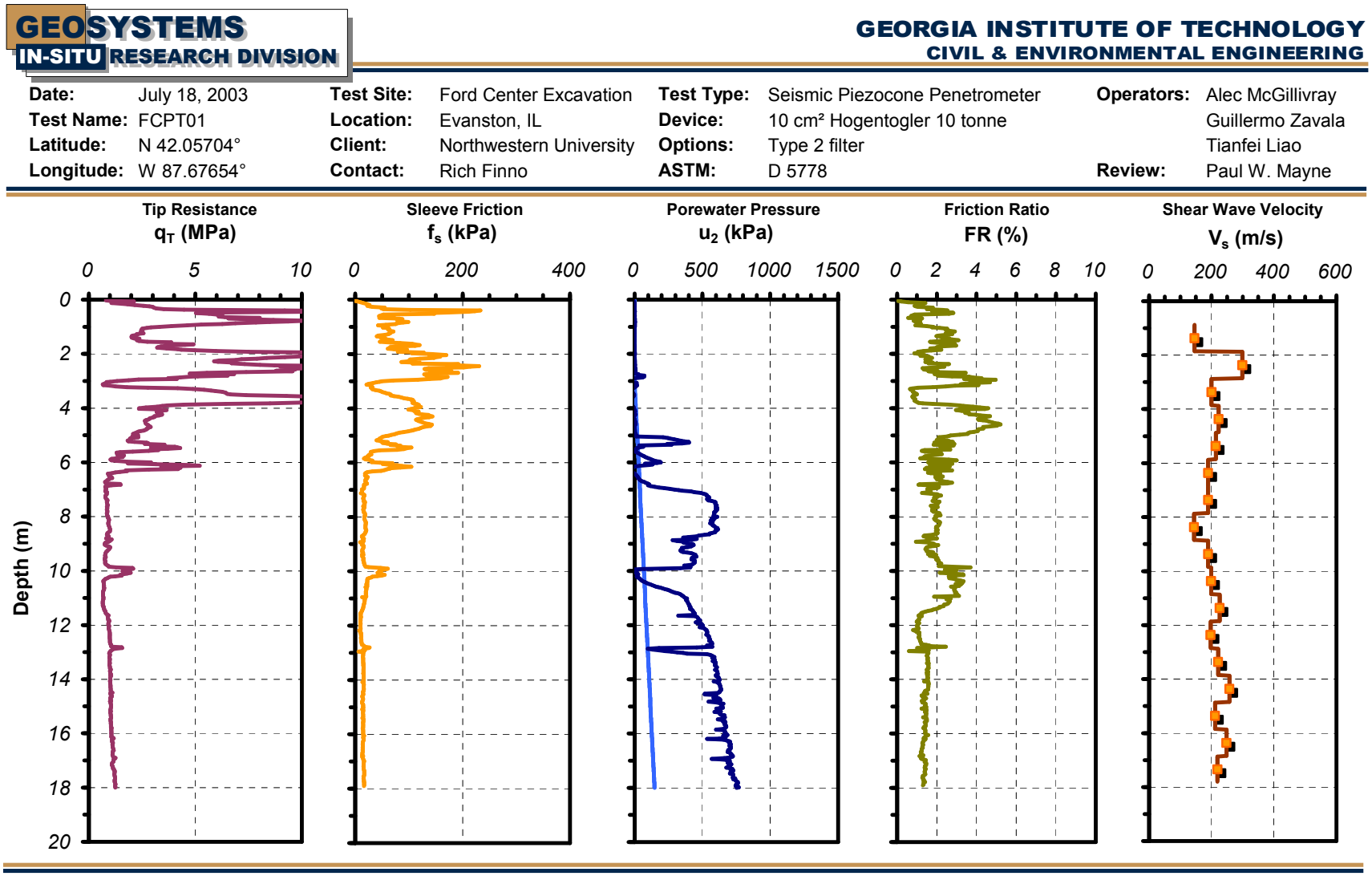

Figure A.18 Plot of SCPTu sounding FCPT01 with sledgehammer

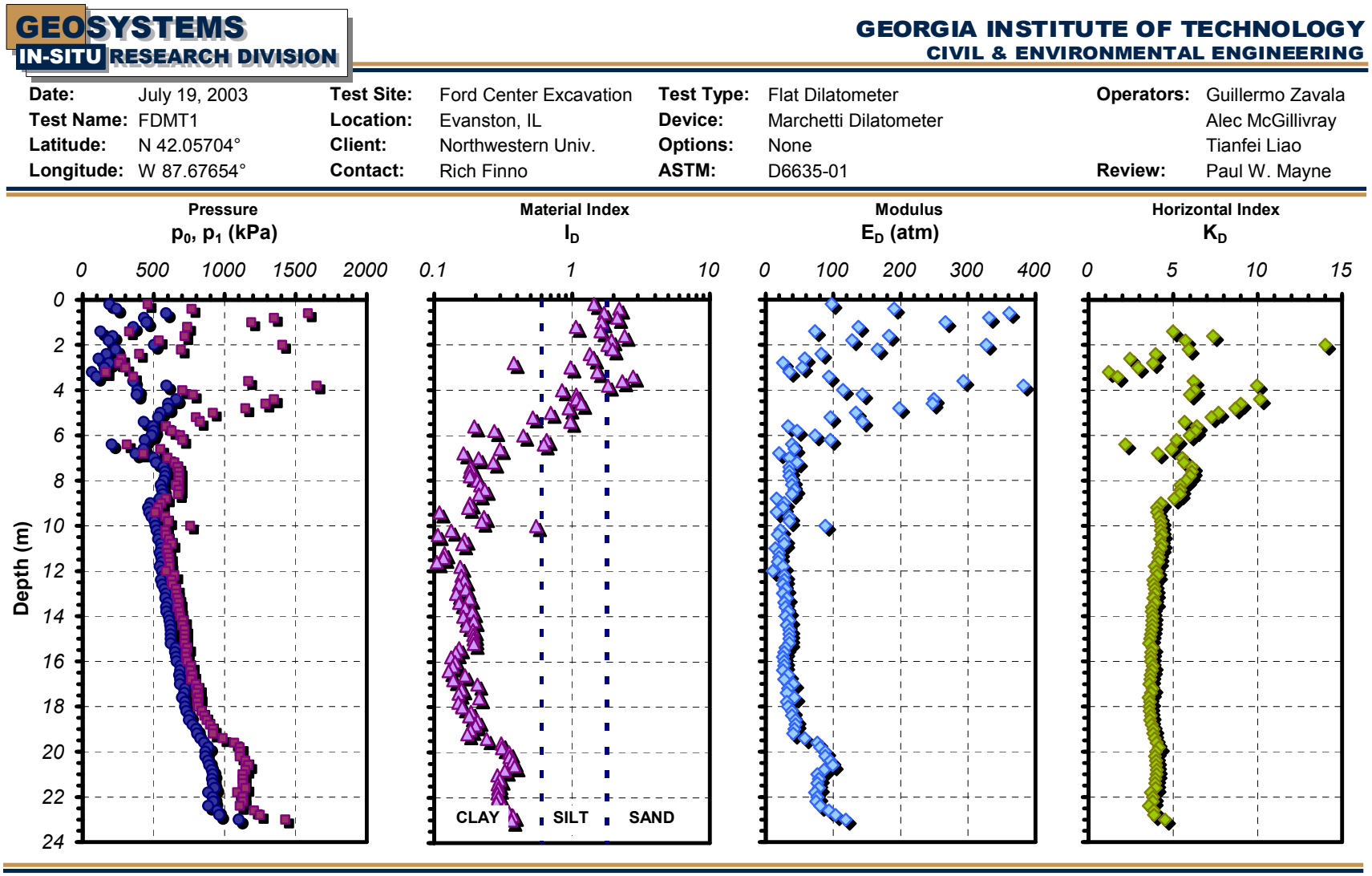

Figure A.19 Plot of DMT sounding FDMT1

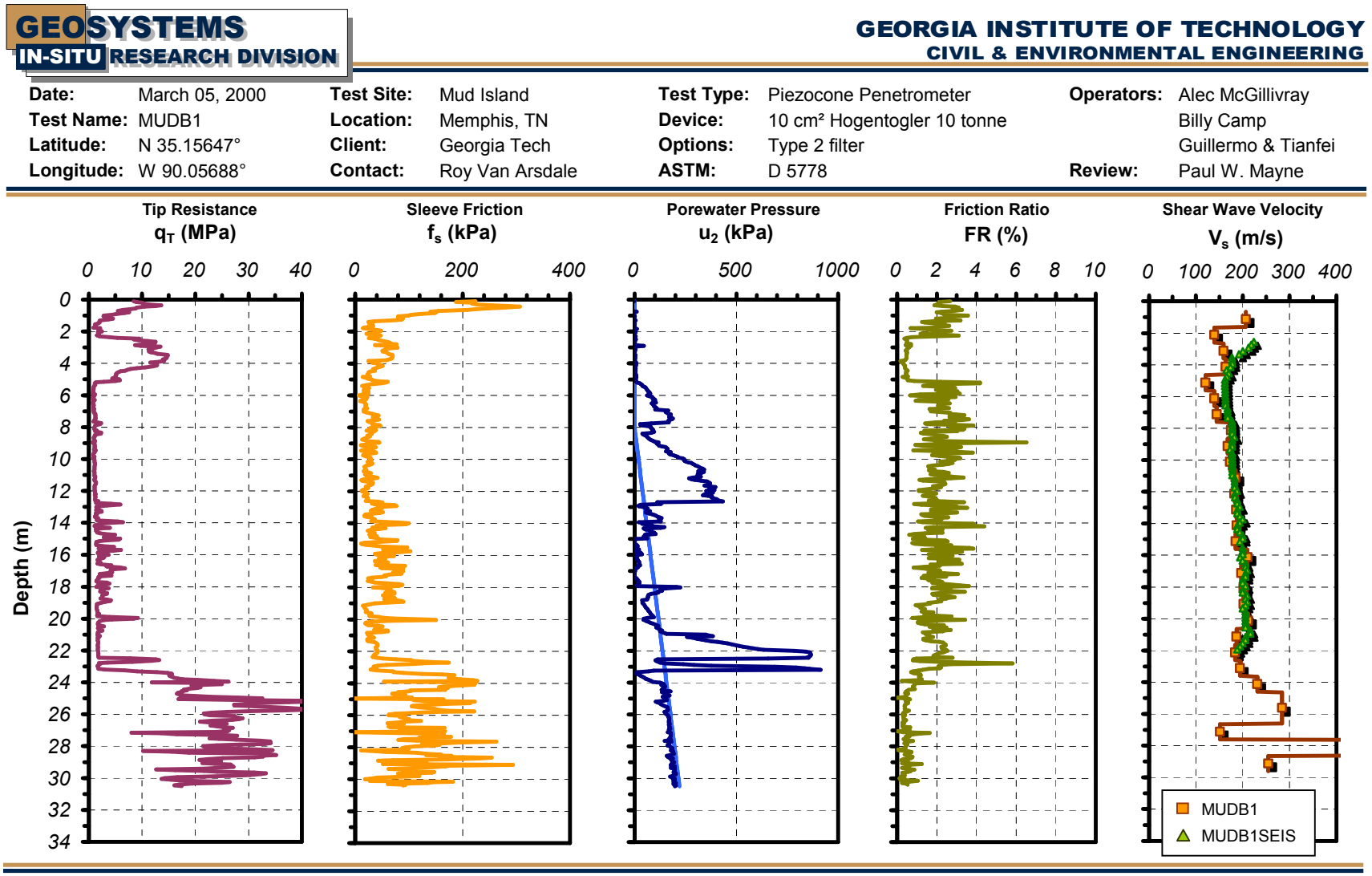

Figure A.20 Plot of SCPTu sounding MUSB1/MUDB1SEIS with pendulum and sledgehammer

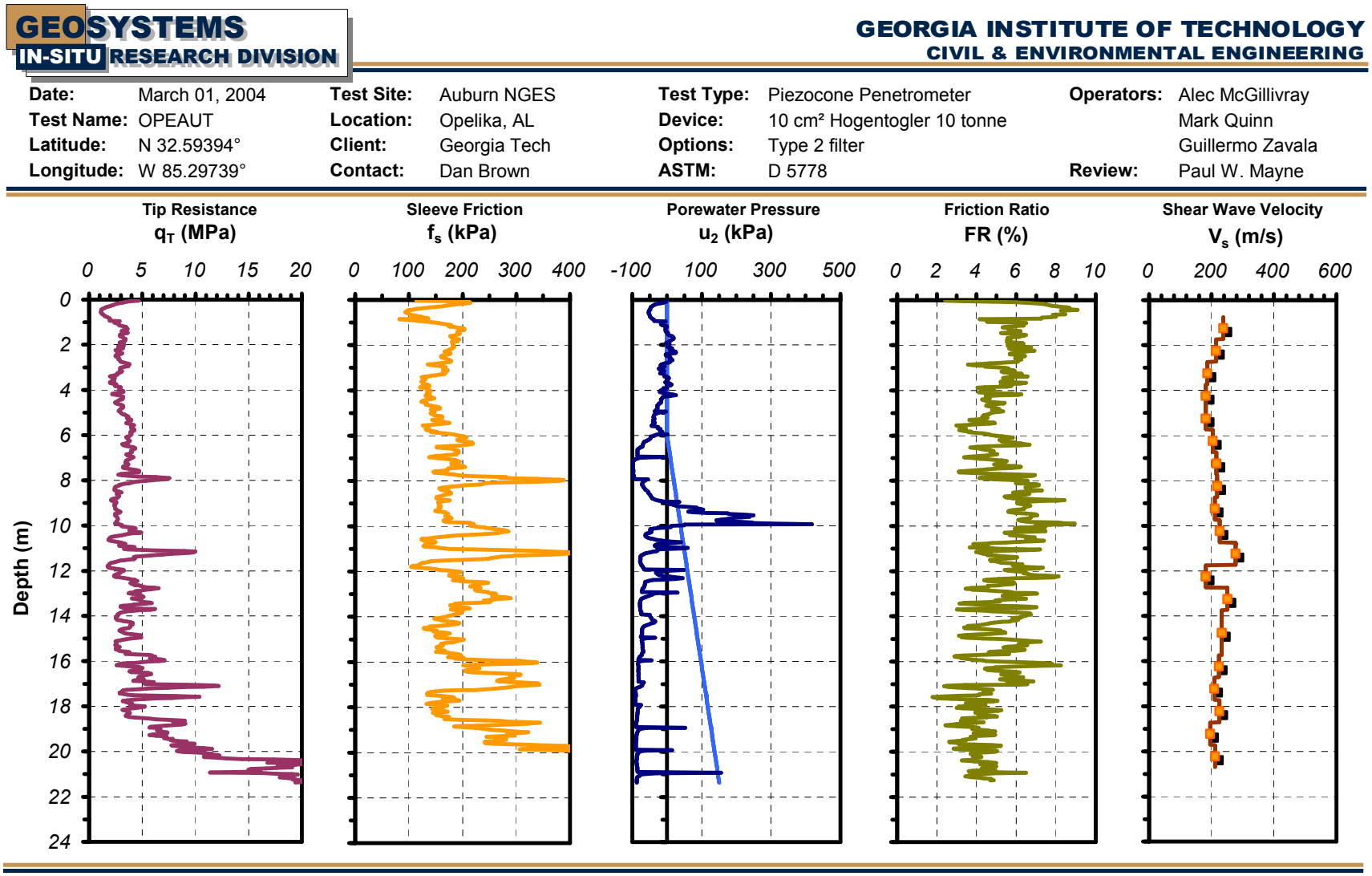

Figure A.21 Plot of SCPTu sounding OPEAUT with RotoSeis II

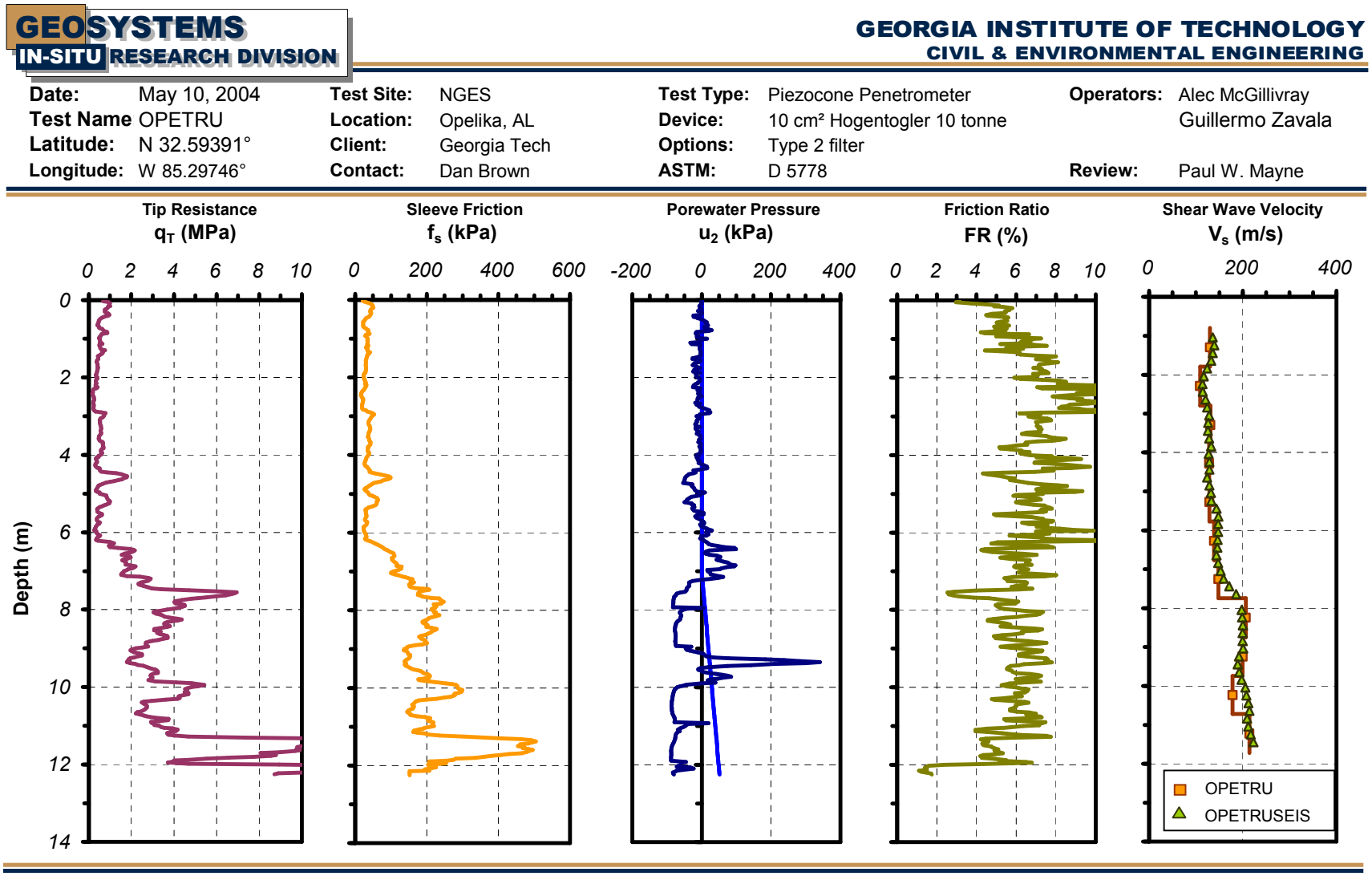

Figure A.22 Plot of SCPTu sounding OPETRU/OPETRUSEIS with pendulum and RotoSeis II

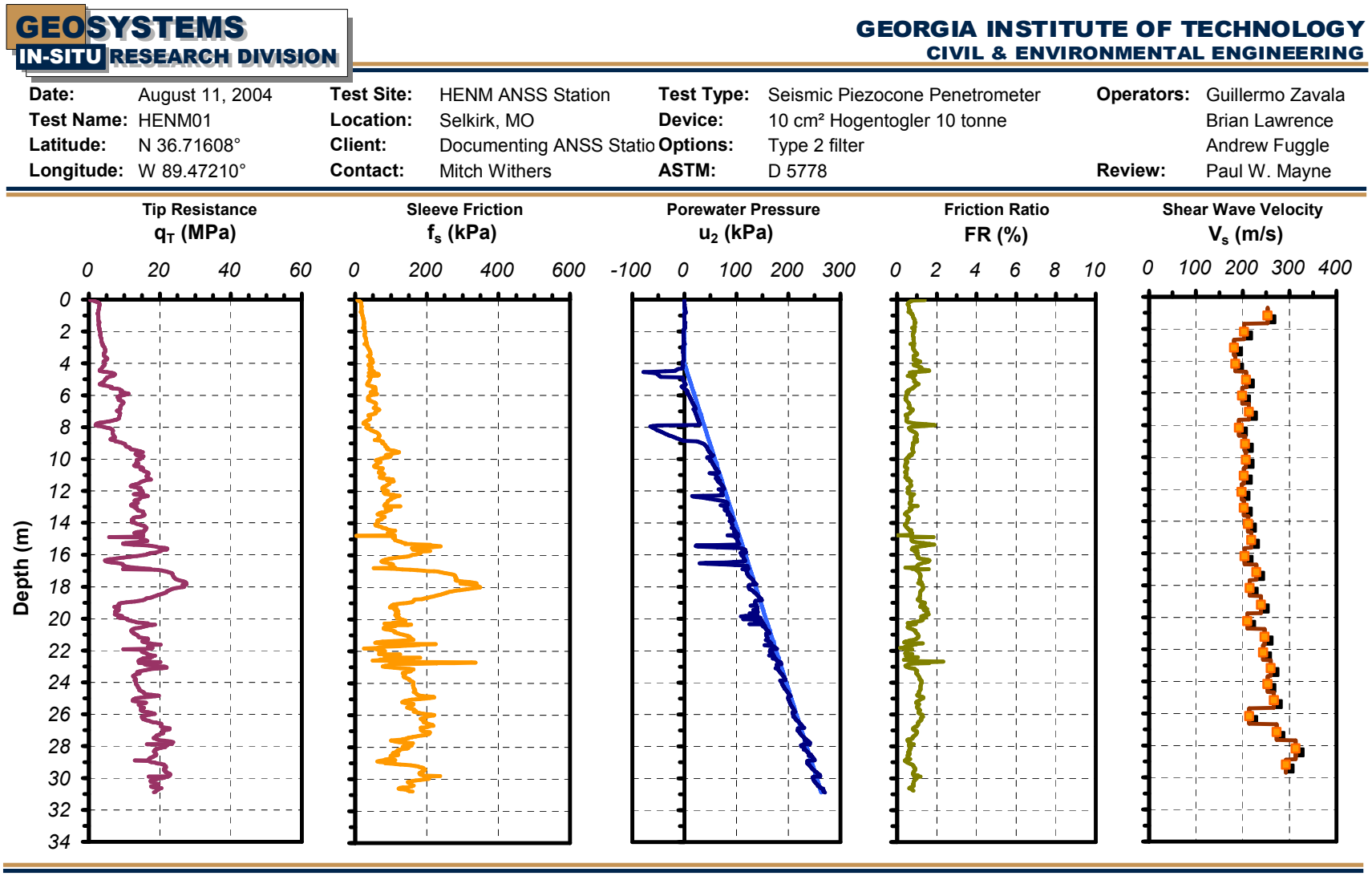

Figure A.23 Plot of SCPTu sounding HENM01 with RotoSeis II

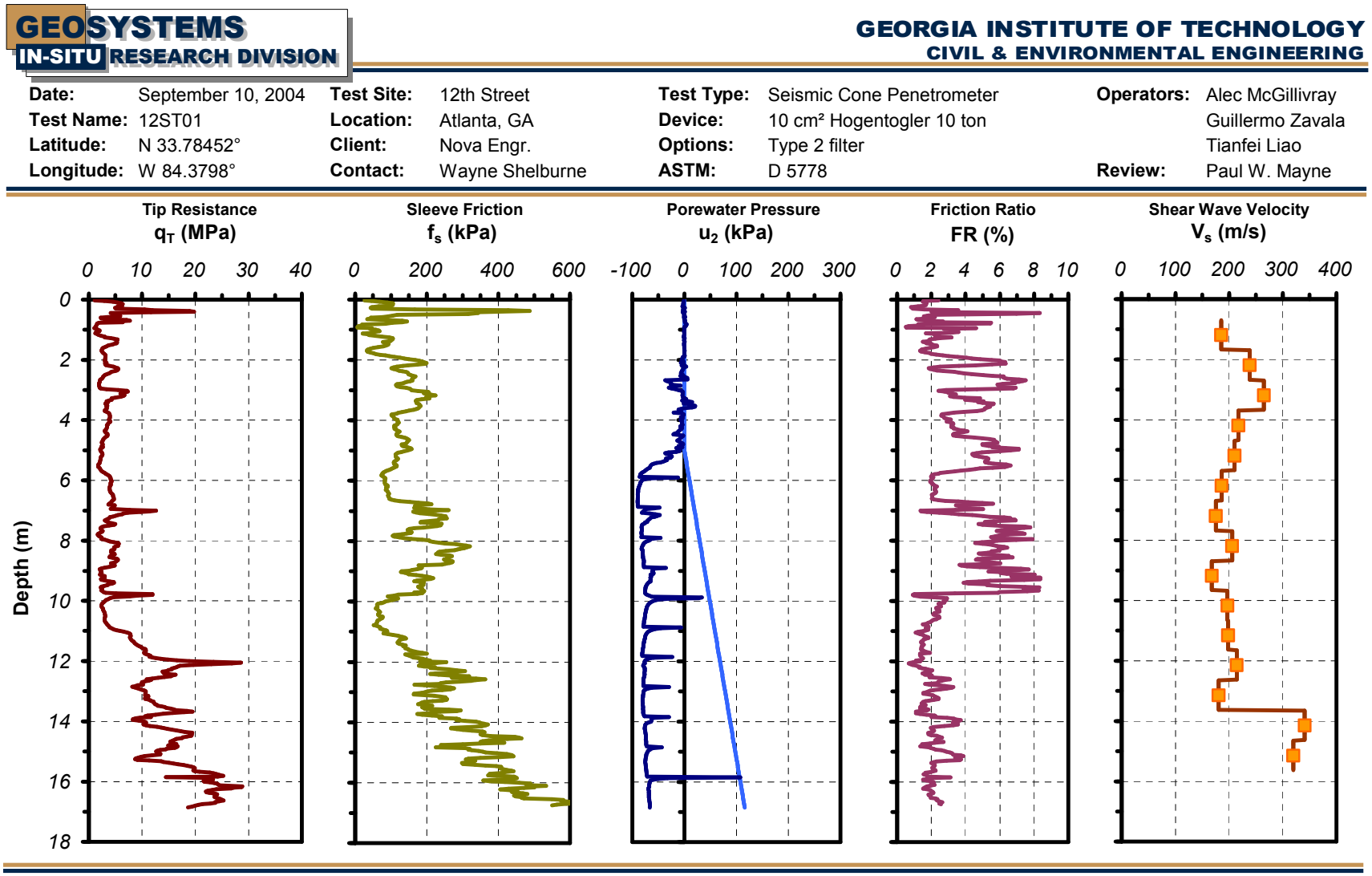

Figure A.24 Plot of SCPTu sounding 12ST01 with RotoSeis III

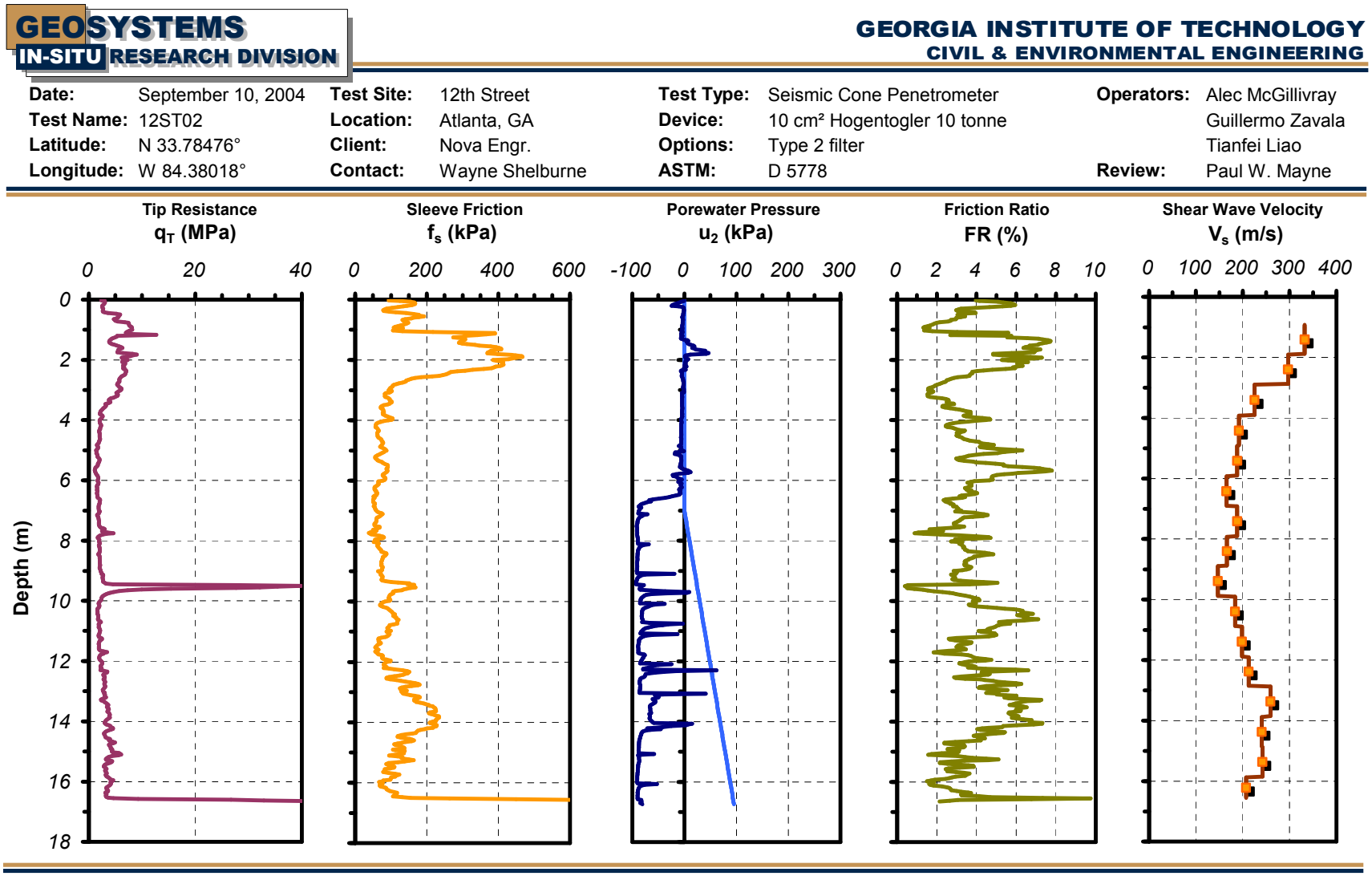

Figure A.25 Plot of SCPTu sounding 12ST02 with RotoSeis III

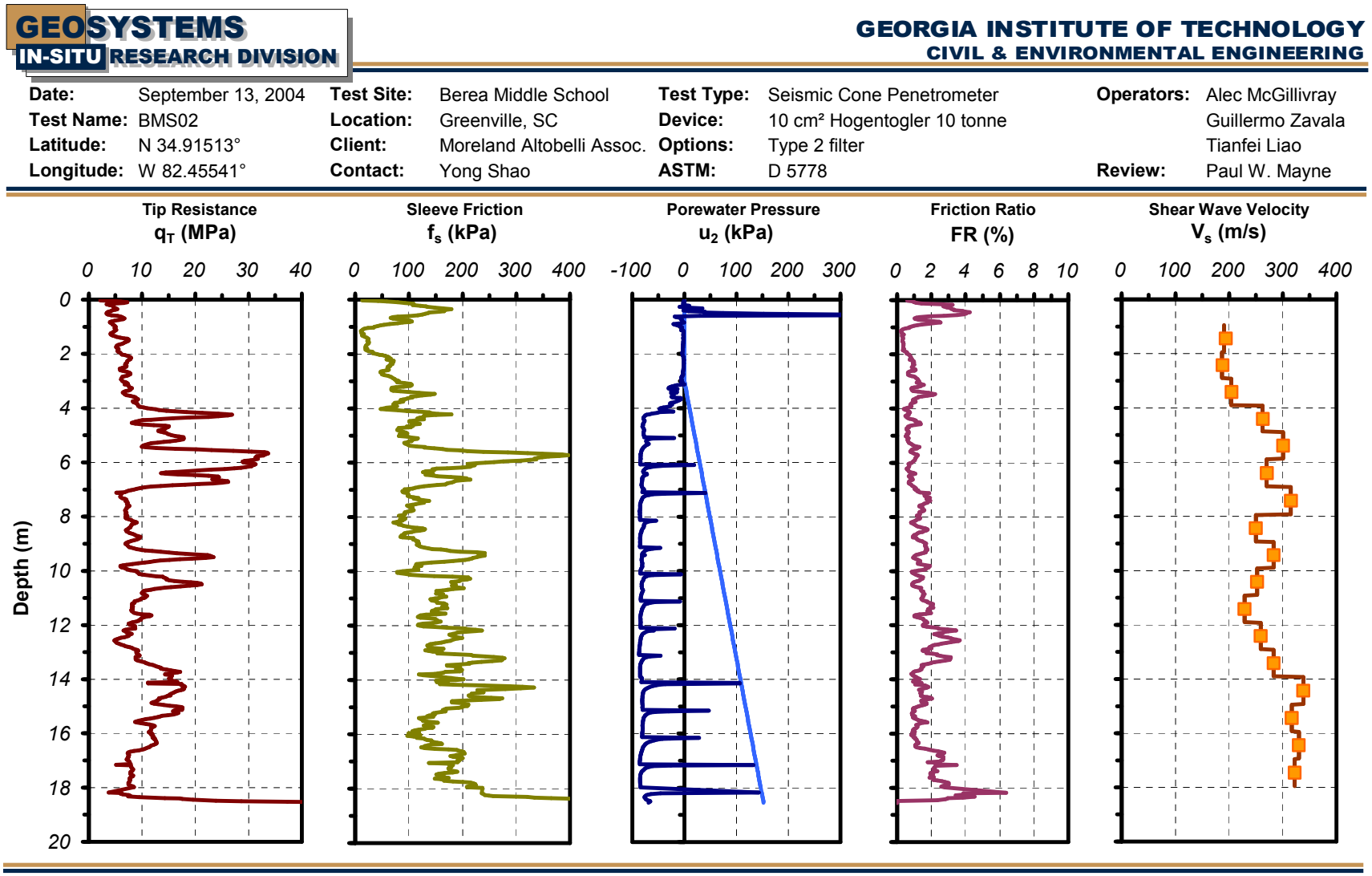

Figure A.26 Plot of SCPTu sounding BMS02 with RotoSeis III

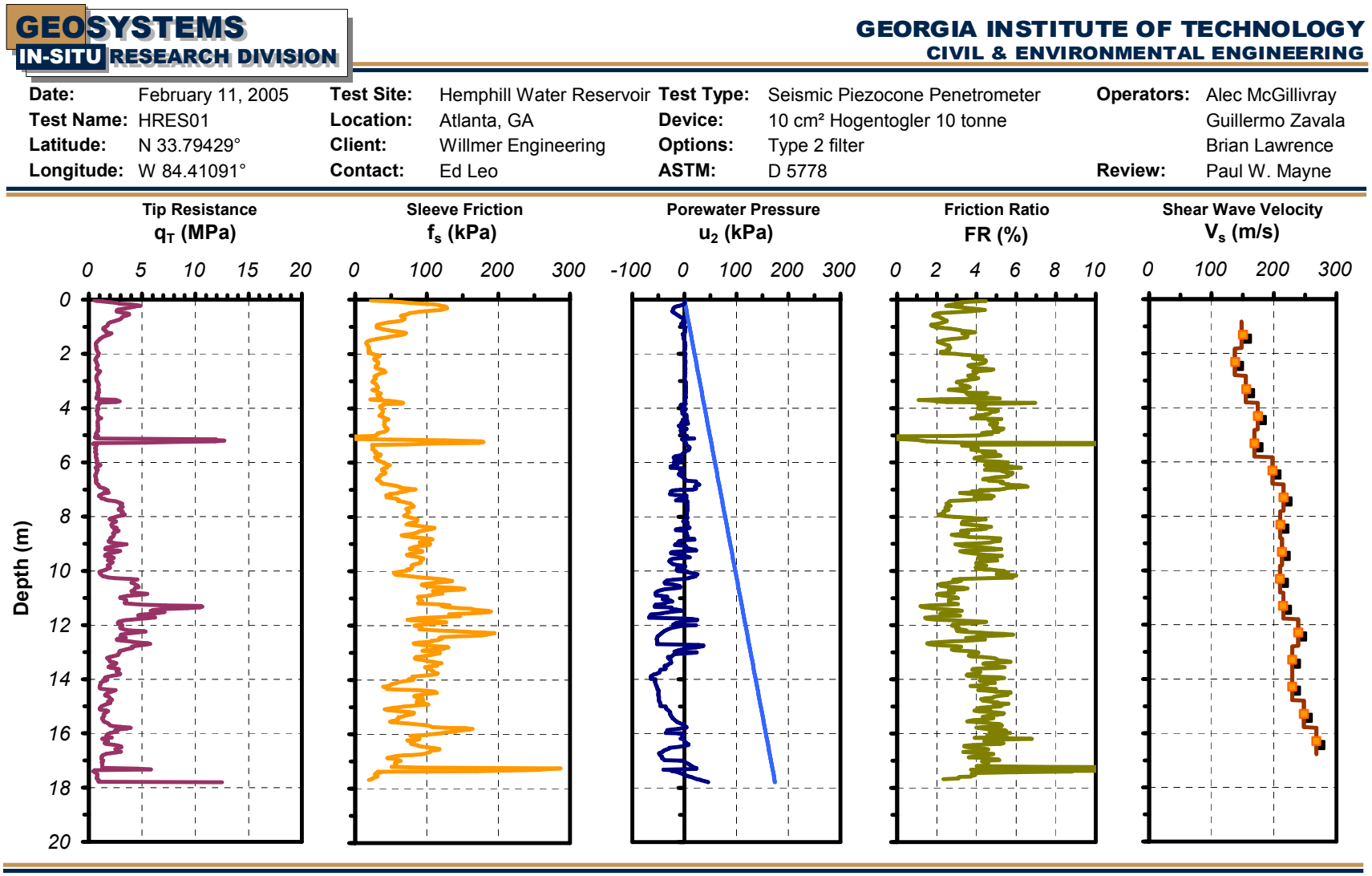

Figure A.27 Plot of SCPTu sounding HRES01 with RotoSeis IV

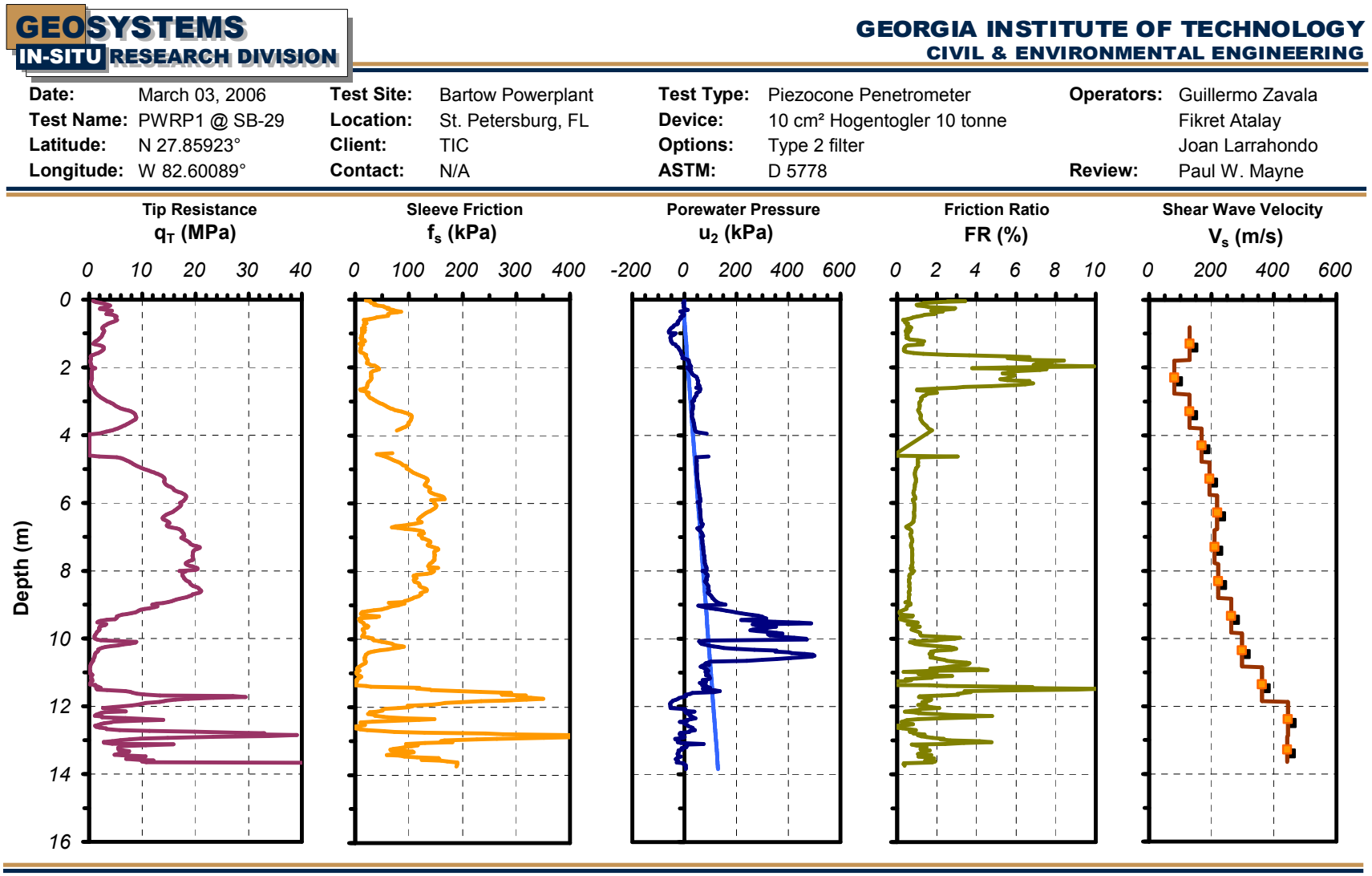

Figure A.28 Plot of SCPTu sounding PWRP1 with RotoSeis V

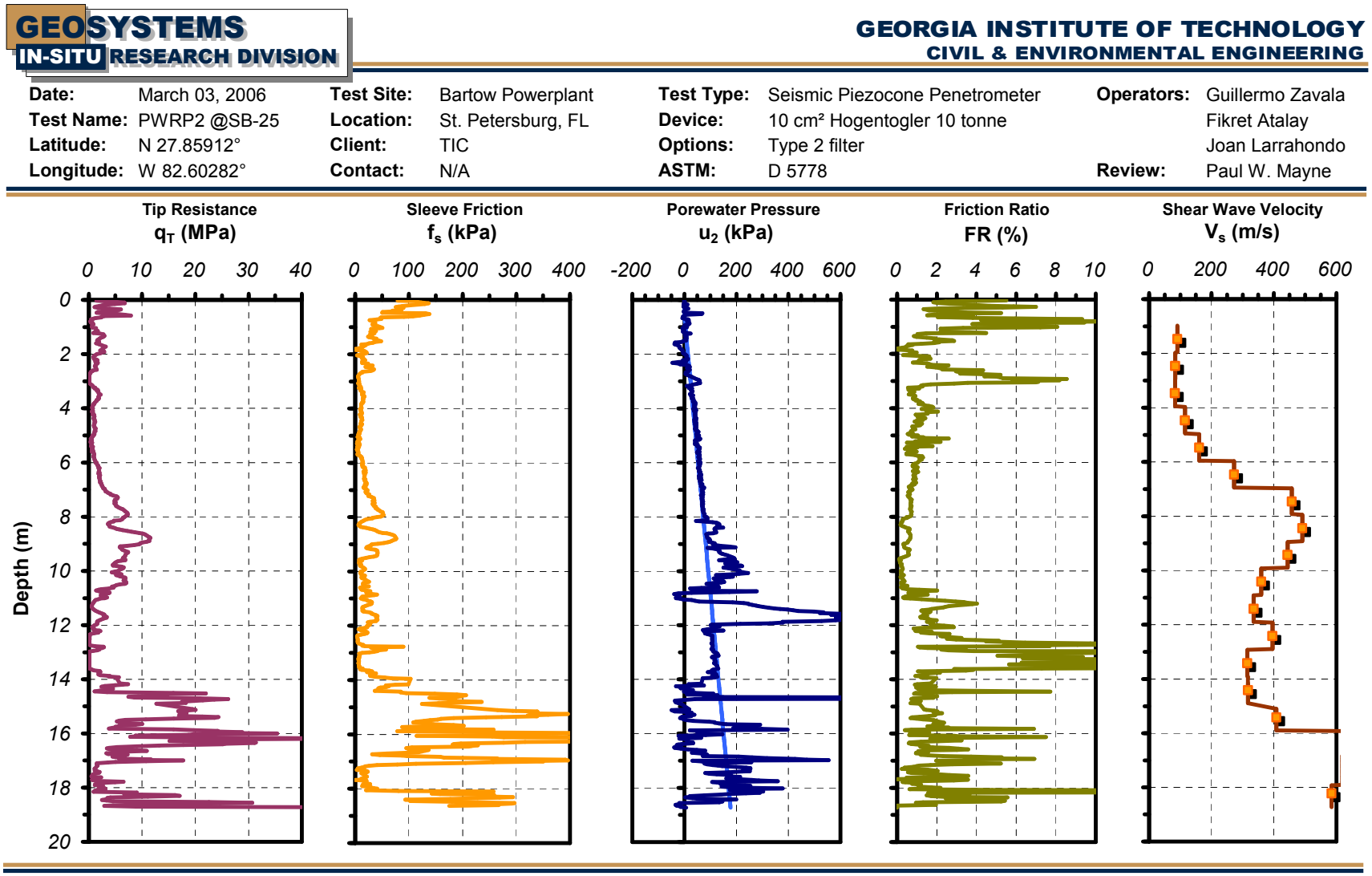

Figure A.29 Plot of SCPTu sounding PWRP2 with RotoSeis V

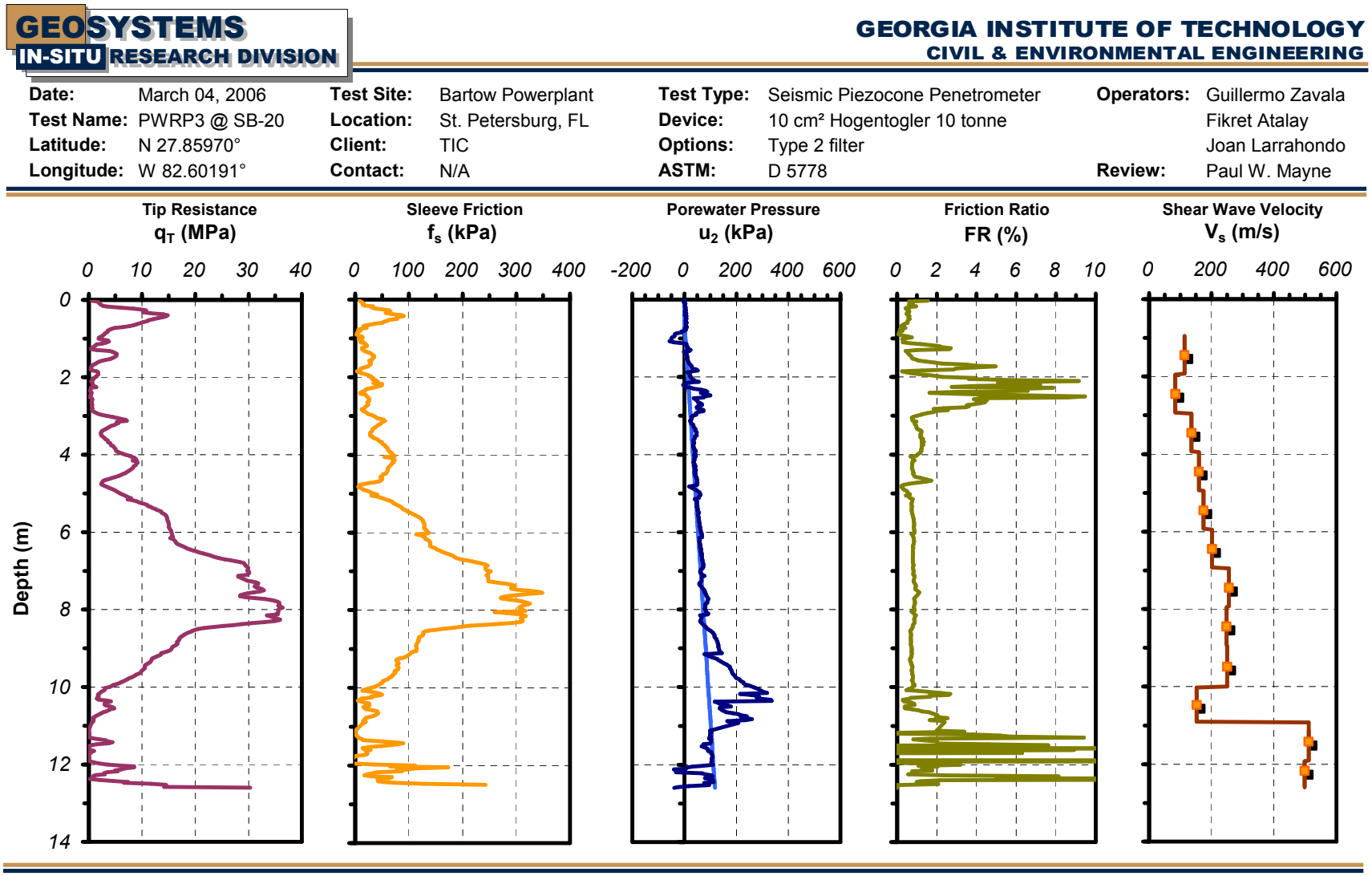

Figure A.30 Plot of SCPTu sounding PWRP3 with RotoSeis V

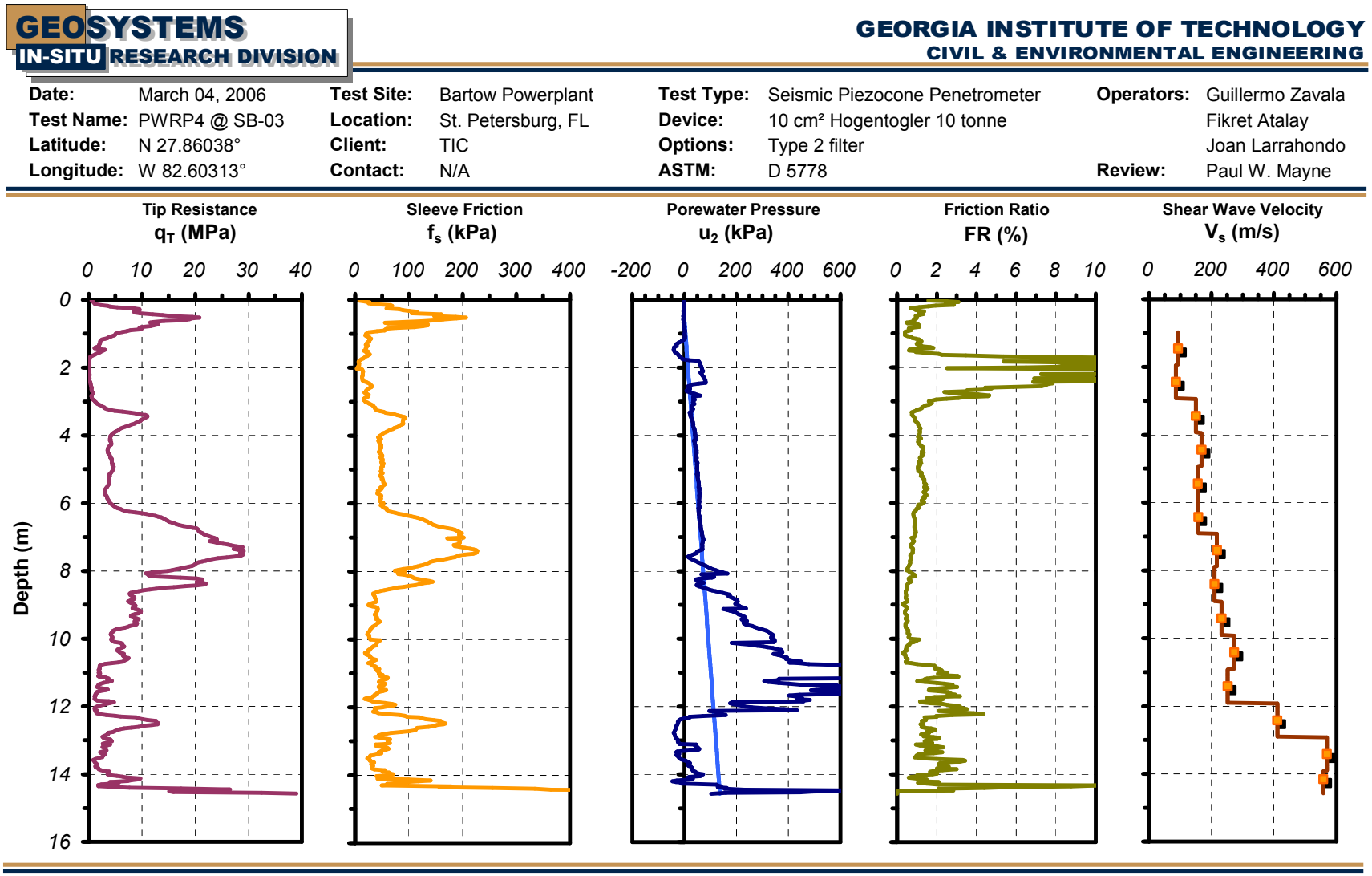

Figure A.31 Plot of SCPTu sounding PWRP4 with RotoSeis V

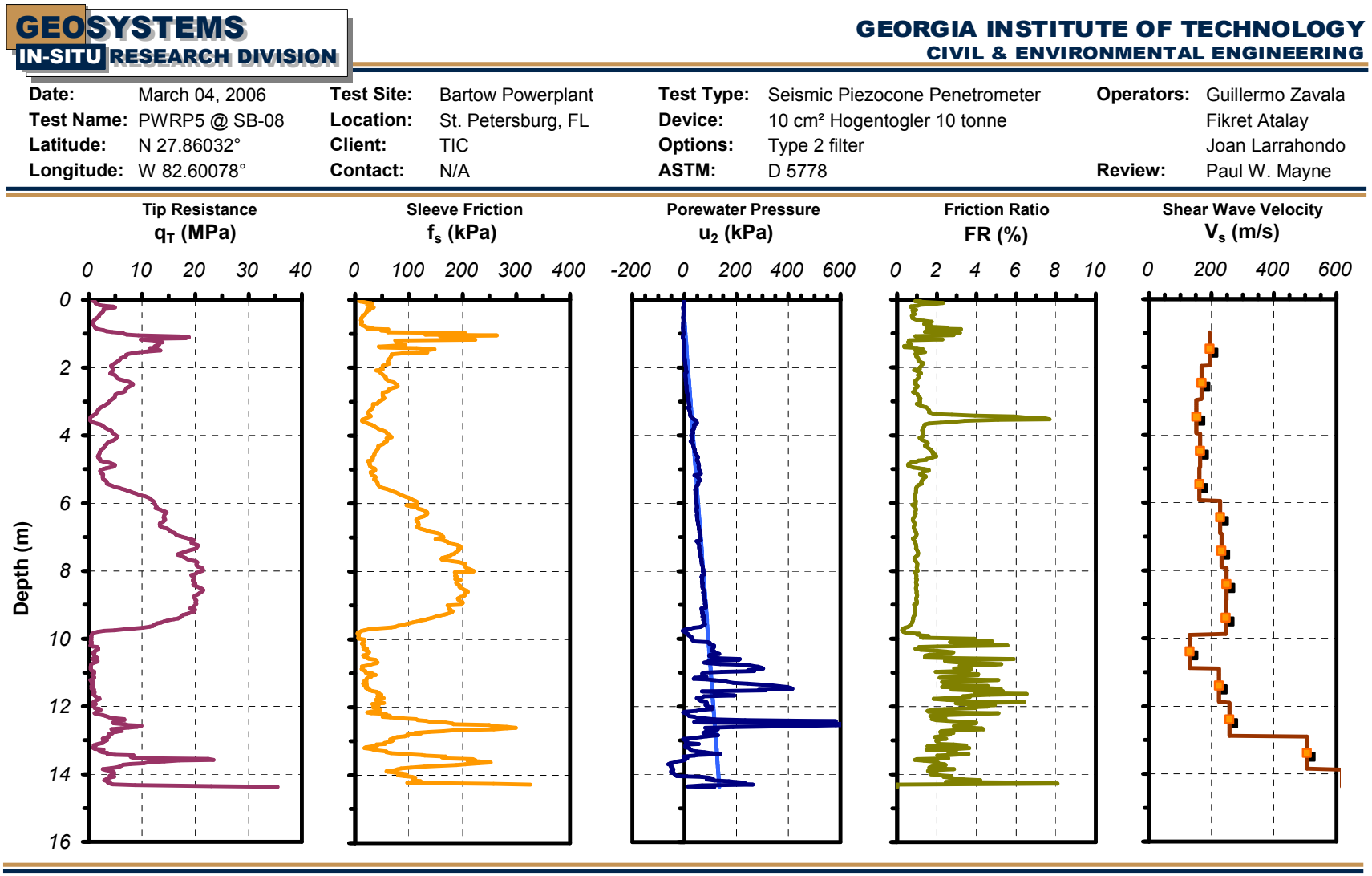

Figure A.32 Plot of SCPTu sounding PWRP5 with RotoSeis V

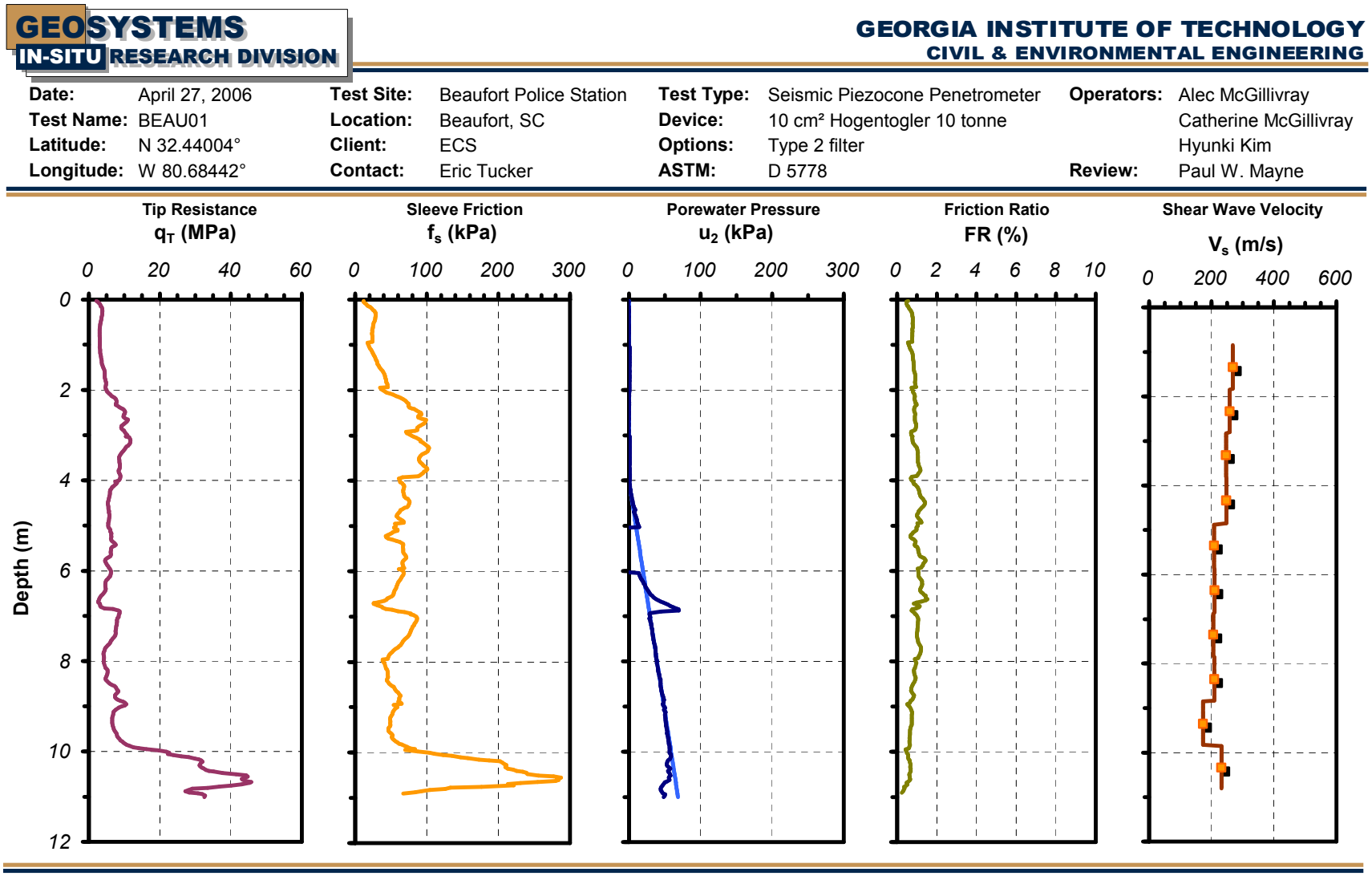

Figure A.33 Plot of SCPTu sounding BEAU01 with RotoSeis V

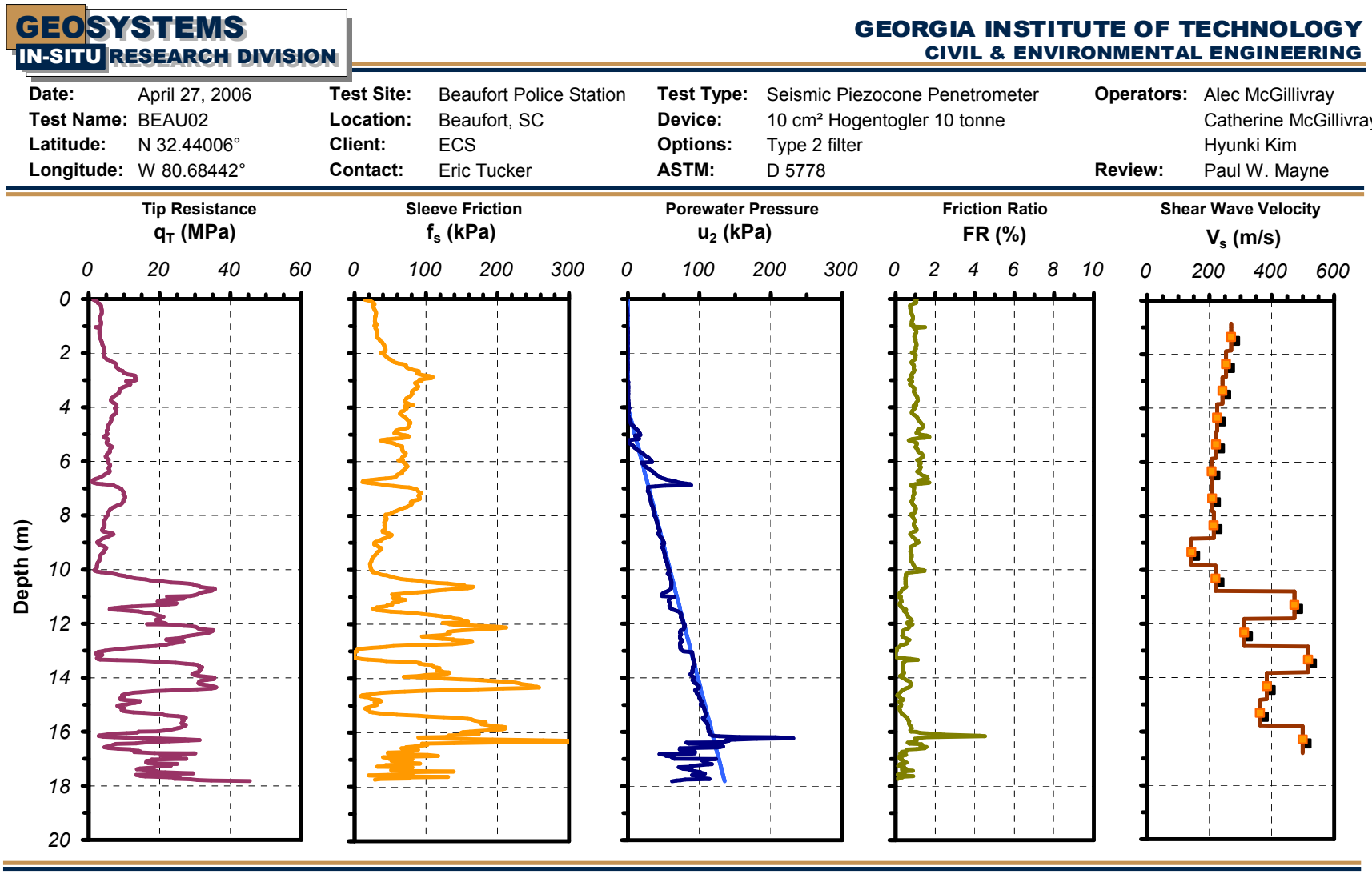

Figure A.34 Plot of SCPTu sounding BEAU02 with RotoSeis V

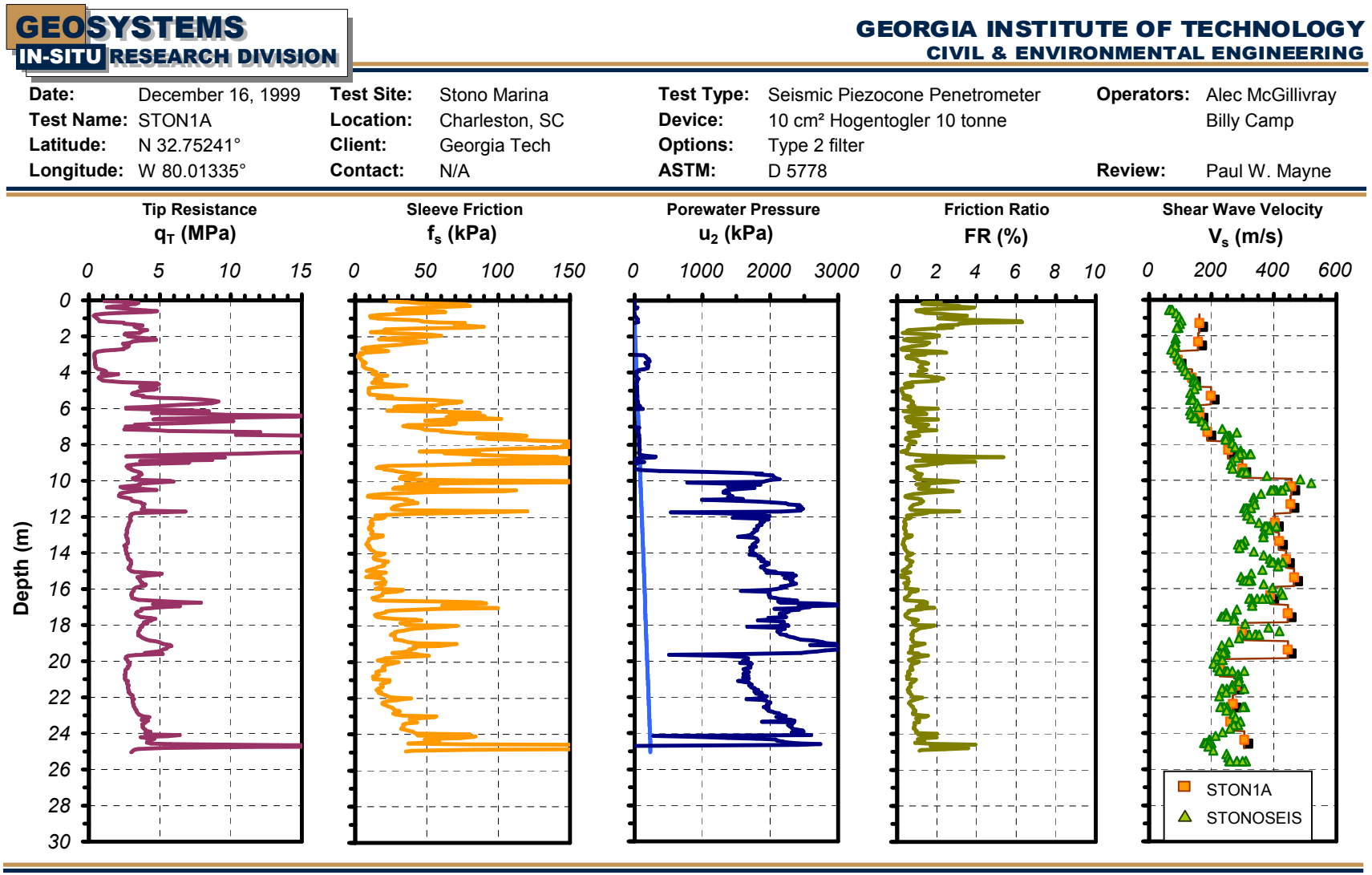

Figure A.35 Plot of SCPTu sounding STON1A/STONOSEIS with sledgehammer

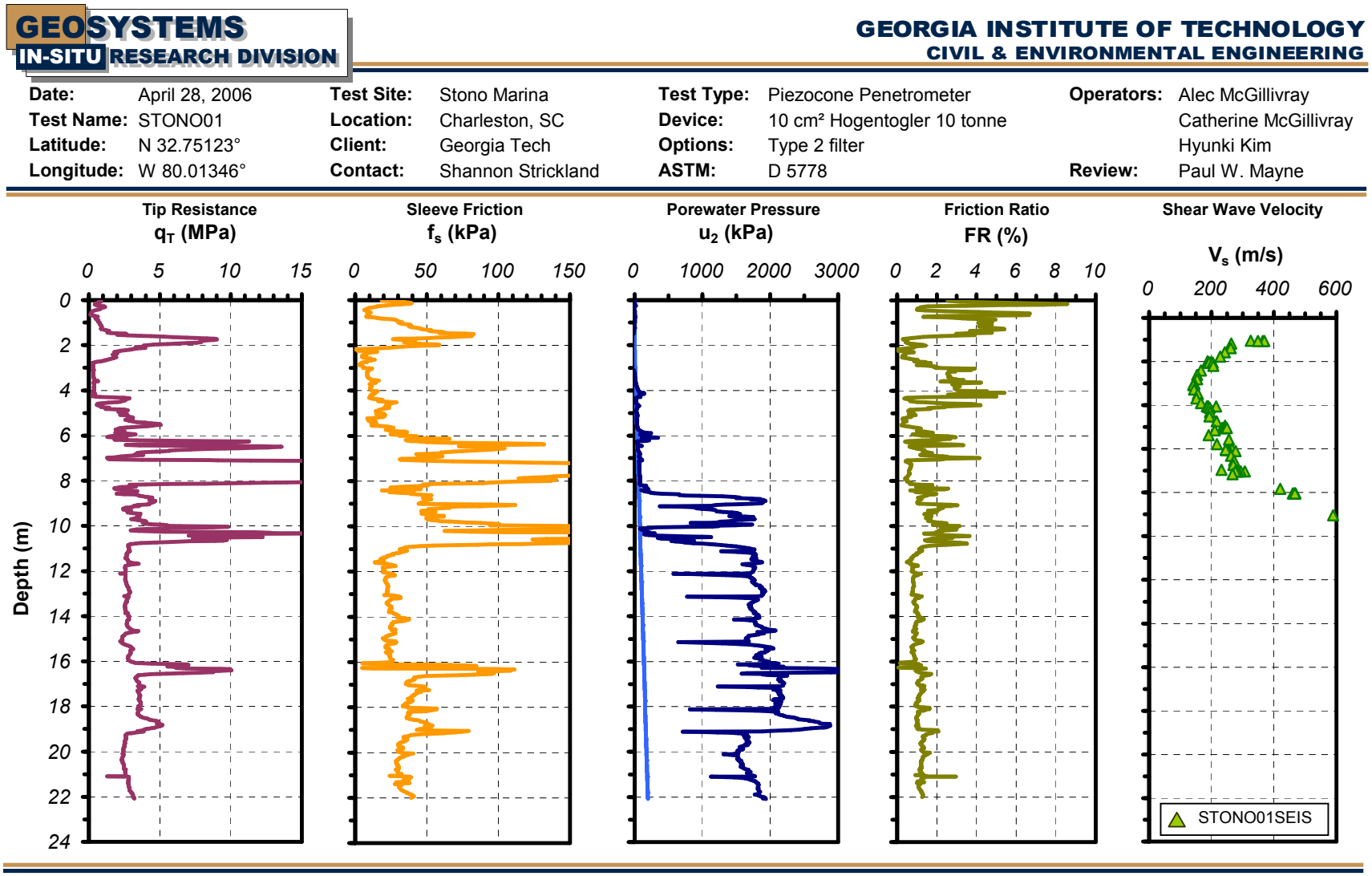

Figure A.36 Plot of SCPTu sounding STONO01/STONO01SEIS with RotoSeis V

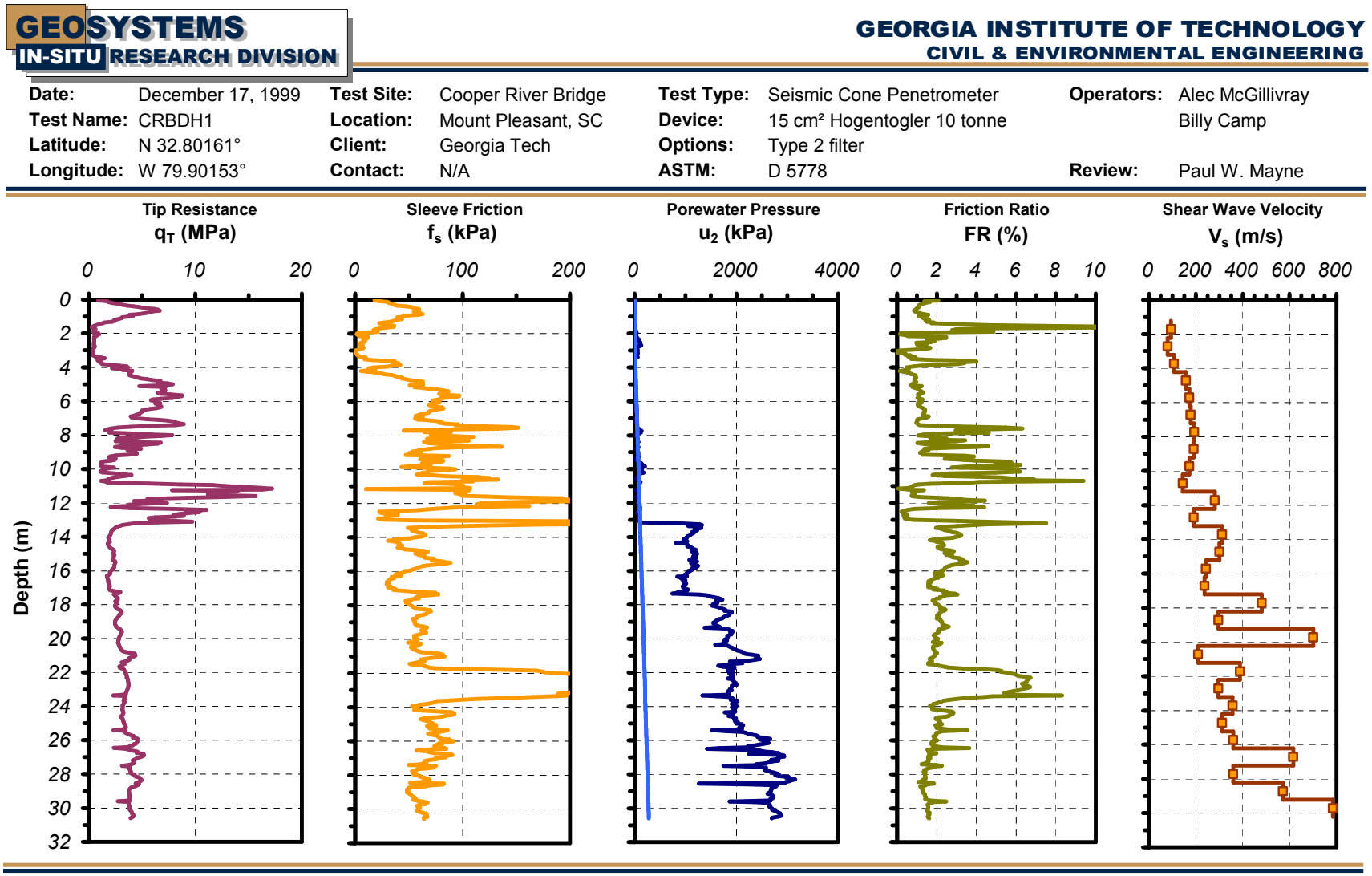

Figure A.37 Plot of SCPTu sounding CRBDH1 with pendulum

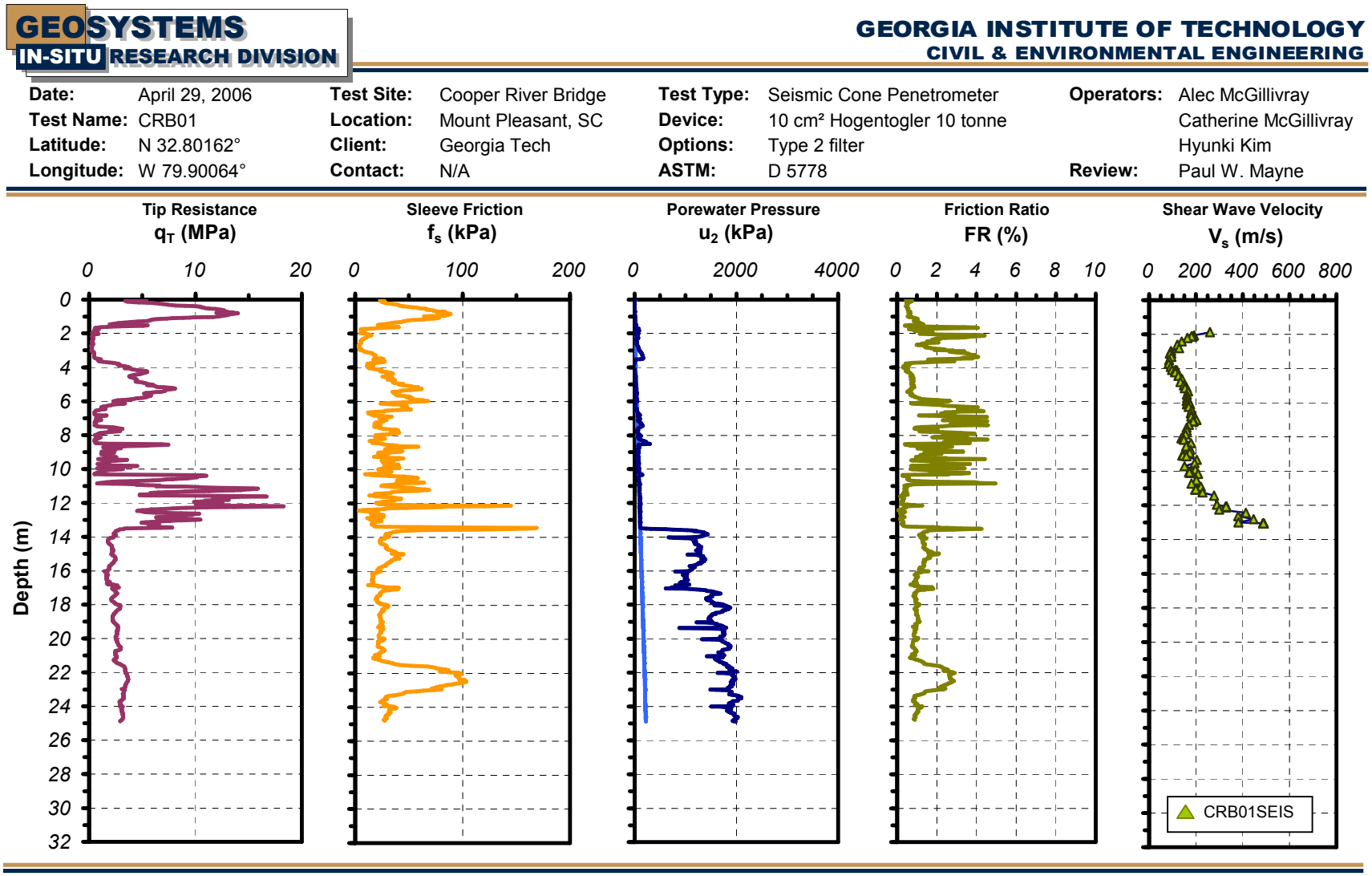

Figure A.38 Plot of SCPTu sounding CRB01/CRB01SEIS with RotoSeis V

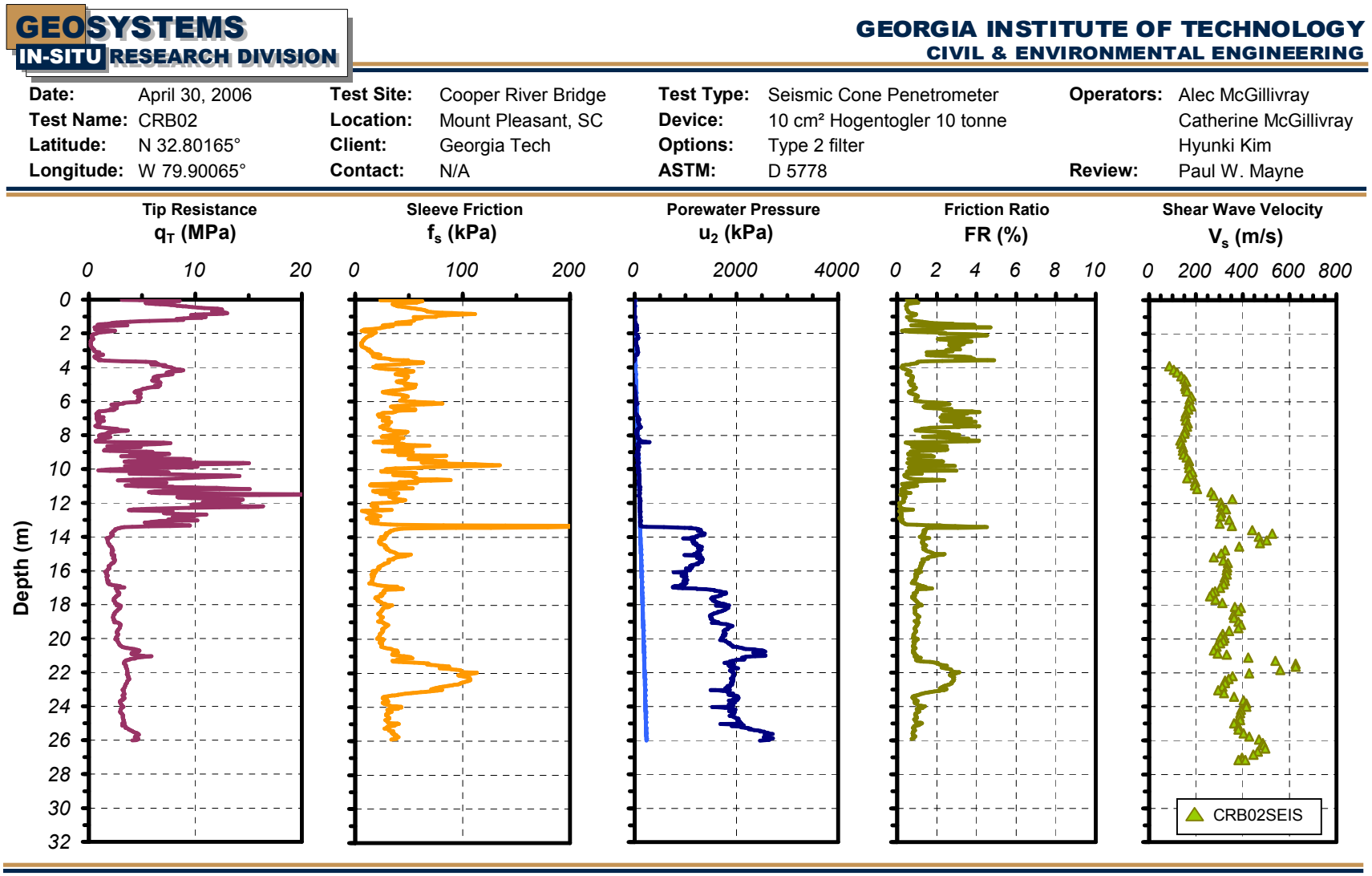

Figure A.39 Plot of SCPTu sounding CRB02/CRB02SEIS with sledgehammer

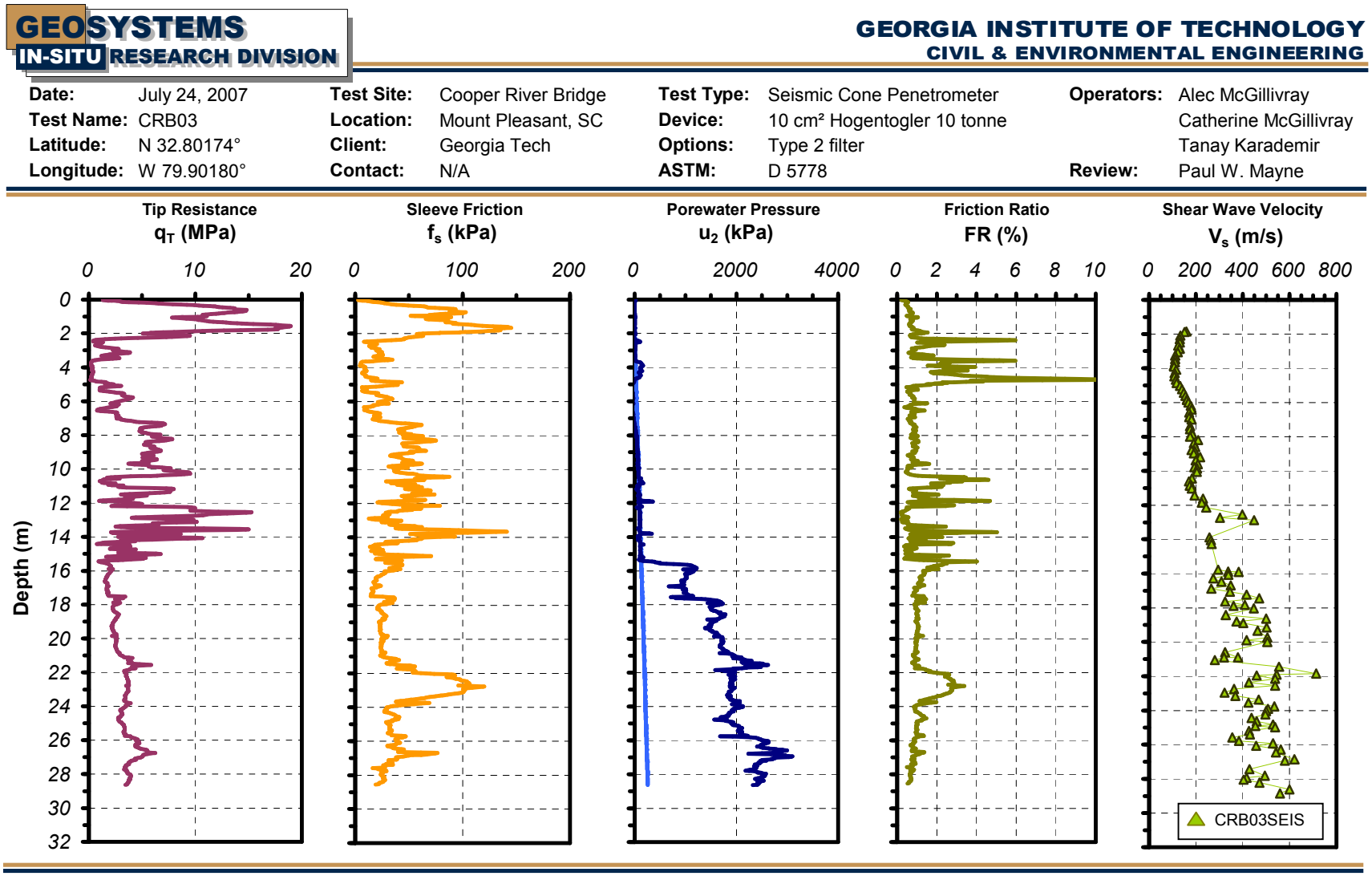

Figure A.40 Plot of SCPTu sounding CRB03/CRB03SEIS with Commercial RotoSeis

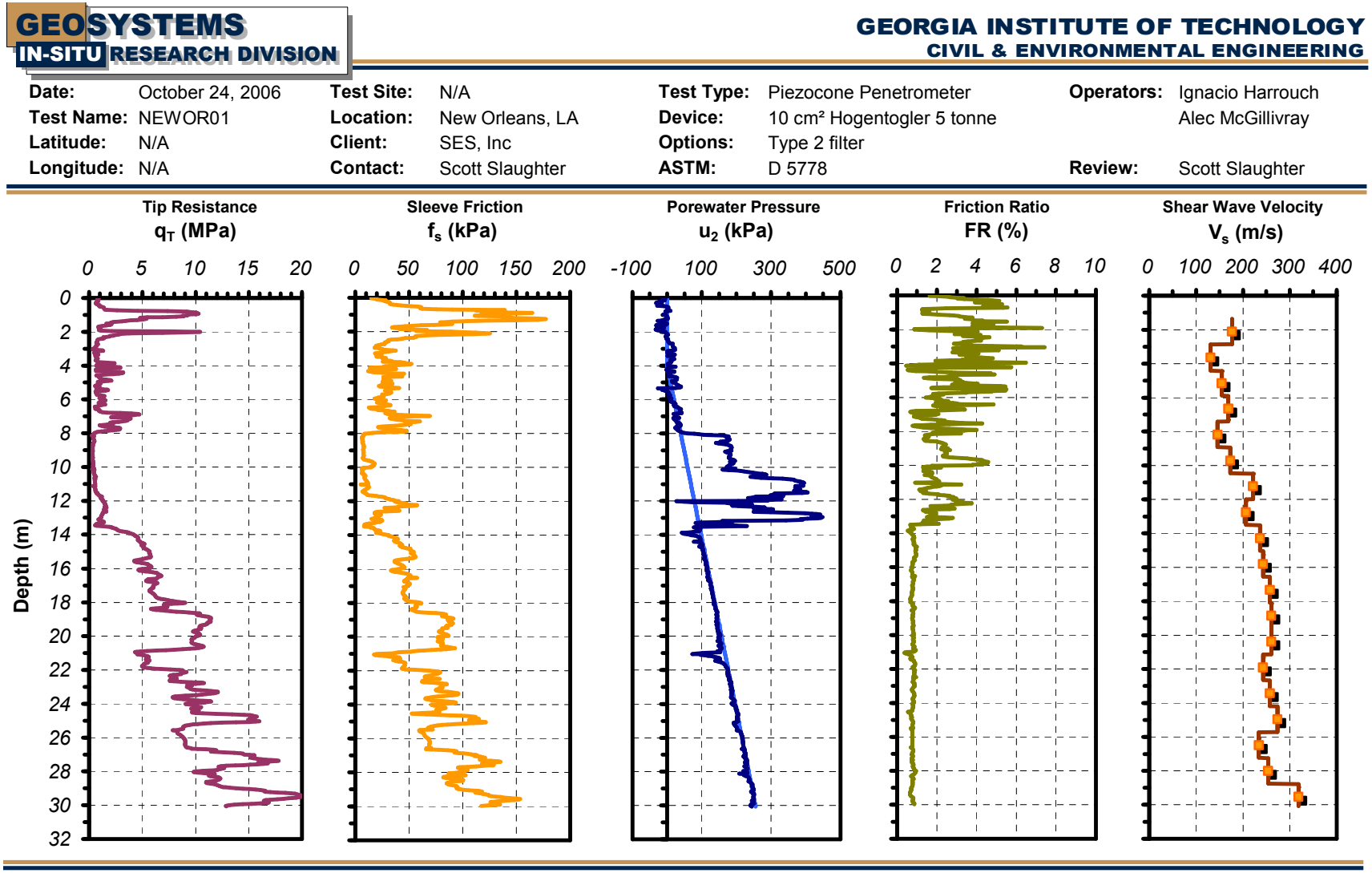

Figure A.41 Plot of SCPTu sounding NEWOR01 with RotoSeis V

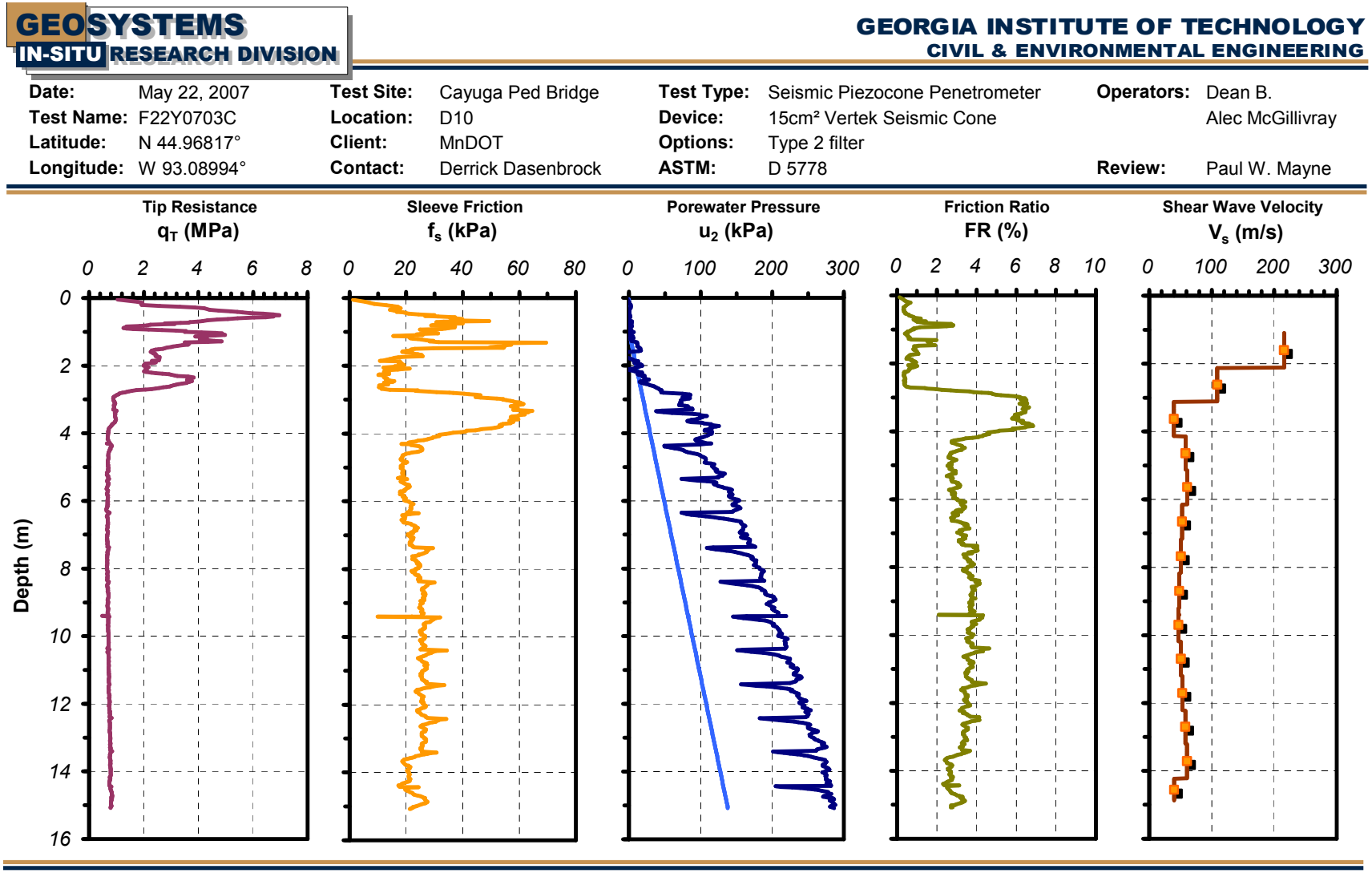

Figure A.42 Plot of SCPTu sounding F22Y0703C with truck mounted hydraulic source

APPENDIX B. DETAILS FOR ELECTRICAL CIRCUITS

Four instrumentation amplifiers were built to amplify geophone output signals from the biaxial true-interval seismic probe. The diagram for a single amplifier is shown in Figure B.1. Each amplifier consists of three common 741 op-amps, which can be purchased at neighborhood electronics stores for as little as $2 each. An instrumentation amplifier uses three op-amps in a single amplifier to increase input impedance, remove the DC offset, and greatly reduce common mode noise on the input signal lines.

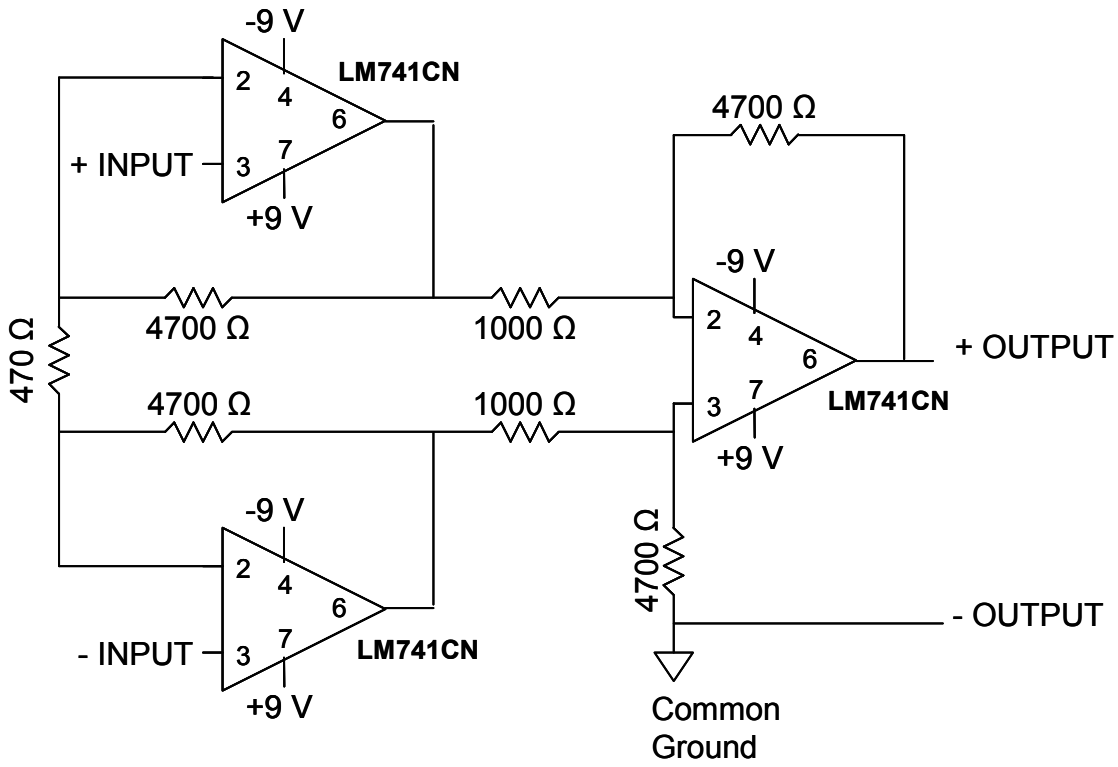

Figure B.1 Circuit diagram for a single ×100 gain instrumentation amplifier using readily available 741 op-amps

The trigger timing circuit shown in Figure B.2 is based on the circuit recommended by Stewart and Campanella (1993). A common 555 integrated circuit (IC) is used to generate a square pulse having a duration of approximately 2.5 s. The square pulse is initiated when a contact closure is detected at the hammer switch.

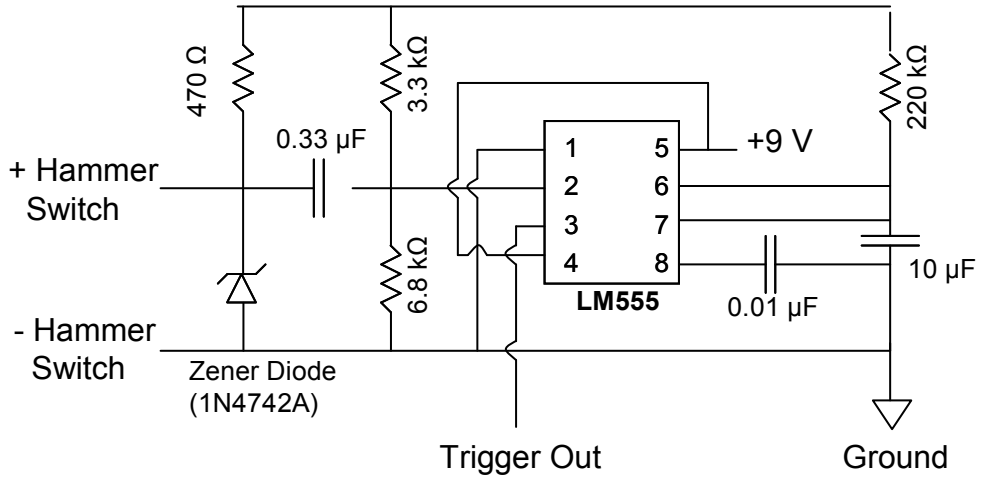

Figure B.2 Trigger timing circuit based on Stewart and Campanella (1993)

The optical isolator circuit presented in Figure B.3 utilizes an infrared LED and infrared phototransistor to detect the light from the LED. In the first half of the circuit, a battery is connected in series with the hammer switch. When the switch closes, current flows through the circuit, illuminating the infrared LED lamp. On the second half of the circuit, a phototransistor detects the light emitted from the LED, changing the state of the transistor from open to closed, which emulates the hammer switch closure. The outputs of the optical isolator can be connected directly to the trigger timing circuit to eliminate the potential for conduction of noise from the hammer switch to the trigger circuit and data acquisition system.

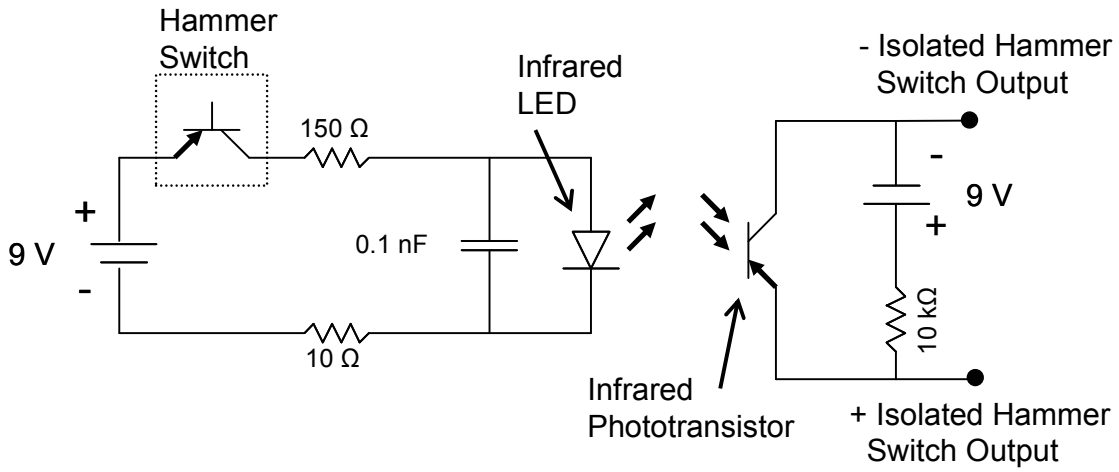

Figure B.3 Optical isolator circuit for protecting trigger circuit and data acquisition system from electrical noise produced by the RotoSeis seismic source

APPENDIX C. GIS SOUNDING LOCATION DATABASE

In-situ testing generates tremendous amounts of data relatively quickly. Data storage can become a problem, but being able to keep track of all the tests performed can be an even bigger problem. This research effort is comprised of more than 50 field tests. Since 1997, the In-Situ group at Georgia Tech has performed more than 430 field tests. The availability of handheld GPS units has made it possible to determine the global coordinates for each sounding with reasonable accuracy, which helps to organize data using geographic information systems (GIS).

In order to track the extensive Georgia Tech field testing efforts, a database was created to track important information pertaining to each test, such as latitude, longitude, country, city, state, county, test date, maximum depth, sounding name, tip area, position of the pore pressure element, and additional options such as seismic or resistivity. The locations of each of the 430 tests are displayed in Figure C.1. The database information pertaining to the soundings is listed in Table C.1.

Figure C.1 Locations of soundings performed by the In-Situ Group at Georgia Tech (created with Google Maps)

Table C.1 Summary of CPT soundings performed by the In-Situ group

Lat	Long	Country	State	City	County	Date	Depth	Int_Ref	Area	u_b	Options
17.98046100	-66.75848000	USA	Puerto Rico	Penuelas		19971217		LSP31			
17.98046100	-66.75848000	USA	Puerto Rico	Penuelas		19971218		LSP32			
17.98046100	-66.75848000	USA	Puerto Rico	Penuelas		19971218		LSP71			
32.73943000	-80.23963000	USA	SC	Charleston	Charleston	19980227	9.27	HW1	10	u1	Vibro
32.73943000	-80.23963000	USA	SC	Charleston	Charleston	19980227	9.02	HW2	10	u1	
32.73943000	-80.23963000	USA	SC	Charleston	Charleston	19980227	19.20	HW4	10	u2	Seismic
32.91875000	-80.04695000	USA	SC	Charleston	Charleston	19980227	14.40	TIS01	10	u2	Seismic
32.91875000	-80.04695000	USA	SC	Charleston	Charleston	19980227	8.92	TIS02	10	u1	Vibro
32.91875000	-80.04695000	USA	SC	Charleston	Charleston	19980227	9.13	TIS03	10	u1	
17.98046100	-66.75848000	USA	Puerto Rico	Penuelas		19980516	16.25	PRD1	10	u2	
17.98046100	-66.75848000	USA	Puerto Rico	Penuelas		19980516		PRD2	10	u2	
17.98046100	-66.75848000	USA	Puerto Rico	Penuelas		19980517		PRD4	10	u2	
17.98046100	-66.75848000	USA	Puerto Rico	Penuelas		19980517		PRS1	10	u2	
17.98046100	-66.75848000	USA	Puerto Rico	Penuelas		19980517		PRS2	10	u2	
17.98046100	-66.75848000	USA	Puerto Rico	Penuelas		19980517		PRS3	10	u2	
17.98046100	-66.75848000	USA	Puerto Rico	Penuelas		19980517		PRS4	10	u2	
17.98046100	-66.75848000	USA	Puerto Rico	Penuelas		19980518		PRD3	10	u2	
17.98046100	-66.75848000	USA	Puerto Rico	Penuelas		19980725		LSP11D	10	u2	
17.98046100	-66.75848000	USA	Puerto Rico	Penuelas		19980725		LSP11S	10	u2	
17.98046100	-66.75848000	USA	Puerto Rico	Penuelas		19980725		LSP12D	10	u2	
17.98046100	-66.75848000	USA	Puerto Rico	Penuelas		19980725		LSP12S	10	u2	
17.98046100	-66.75848000	USA	Puerto Rico	Penuelas		19980725		LSP16D	10	u2	
17.98046100	-66.75848000	USA	Puerto Rico	Penuelas		19980726		LSP16S	10	u2	
17.98046100	-66.75848000	USA	Puerto Rico	Penuelas		19980726		LSP17D	10	u2	
17.98046100	-66.75848000	USA	Puerto Rico	Penuelas		19980726		LSP17S	10	u2	

Table C.1 (continued) Summary of CPT soundings performed by the In-Situ group

Lat	Long	Country	State	City	County	Date	Depth	Int_Ref	Area	u_b	Options
		USA	DE	Dover		19980728	7.50	PC-1	10	u1u2	
		USA	DE	Dover		19980728	15.65	SC-2	10	u2	
32.59390232	-85.29722982	USA	AL	Spring Villa	Lee	19980831	14.25	AL831A	15	u2	
32.59391032	-85.29722086	USA	AL	Spring Villa	Lee	19980831	29.80	AL831B	15	u2	
32.59388508	-85.29723846	USA	AL	Spring Villa	Lee	19980901	26.40	AL901C	15	u2	
32.59388679	-85.29721578	USA	AL	Spring Villa	Lee	19980901	31.40	AL901D	15	u2	
35.02913000	-89.70566000	USA	TN	Memphis	Shelby	19980915	4.55	MEMPHA		u2	Seismic
35.02913000	-89.70566000	USA	TN	Memphis	Shelby	19980915	2.60	MEMPHB		u2	Seismic
35.02913000	-89.70566000	USA	TN	Memphis	Shelby	19980915	2.95	MEMPHC		u2	Seismic
35.02913000	-89.70566000	USA	TN	Memphis	Shelby	19980915	3.25	MEMPHD		u2	Seismic
35.11722000	-89.80555000	USA	TN	Memphis	Shelby	19980916	4.65	MEMPHE		u2	Seismic
35.11722000	-89.80555000	USA	TN	Memphis	Shelby	19980916	10.20	MEMPHF		u2	Seismic
35.11722000	-89.80555000	USA	TN	Memphis	Shelby	19980916	33.00	MEMPHG		u2	Seismic
35.10833000	-89.73052000	USA	TN	Memphis	Shelby	19980917	20.65	MEMPHH		u2	Seismic
35.09927000	-89.80247000	USA	TN	Memphis	Shelby	19980917	12.25	MEMPHI		u2	Seismic
35.19078000	-90.04502000	USA	TN	Memphis	Shelby	19980917	14.70	MEMPHJ		u2	Seismic
35.15042000	-90.12953000	USA	AR	West Memphis	Crittenden	19980918	32.00	MEMPHK		u2	Seismic
35.97276600	-89.90780000	USA	AR	Blytheville	Mississippi	19981021	37.00	BUGG01	10	u2	Seismic
35.98233000	-89.93310000	USA	AR	Blytheville	Mississippi	19981021	28.00	YARB01	10	u2	Seismic
36.09485000	-89.84831000	USA	MO	Steele	Pemiscot	19981022	31.45	DODD01	15	u2	Seismic
36.09458000	-89.84833000	USA	MO	Steele	Pemiscot	19981022	25.60	DODD02	15	u2	Seismic
35.99261600	-89.83556000	USA	AR	Blytheville	Mississippi	19981023	30.70	3MS617-A	15	u2	Seismic
36.09423000	-89.84816000	USA	MO	Steele	Pemiscot	19981023	32.60	DODD03	15	u2	
35.99276000	-89.83553000	USA	AR	Blytheville	Mississippi	19981024	30.55	3MS617-C	10	u2	
35.99266000	-89.83526000	USA	AR	Blytheville	Mississippi	19981024	15.90	3MS617-D	10	u1u2	

Table C.1 (continued) Summary of CPT soundings performed by the In-Situ group

Lat	Long	Country	State	City	County	Date	Depth	Int_Ref	Area	u_b	Options
35.97225000	-89.90792000	USA	AR	Blytheville	Mississippi	19981024	34.75	BUGG02	10	u2	Seismic
35.98353000	-89.88650000	USA	AR	Blytheville	Mississippi	19981025	26.30	HUEY01	15	u2	Seismic
36.11920000	-89.84393000	USA	MO	Steele	Pemiscot	19981025	16.50	JOHN01	15	u2	Seismic
36.11888000	-89.61493000	USA	MO	Caruthersville	Pemiscot	19981028	25.55	I15501	15	u2	Seismic
36.11888000	-89.61493000	USA	MO	Caruthersville	Pemiscot	19981028	22.00	I15502	10	u2	
36.11888000	-89.61493000	USA	MO	Caruthersville	Pemiscot	19981028	23.00	I15503	15	u2	Seismic
36.11888000	-89.61493000	USA	MO	Caruthersville	Pemiscot	19981028	18.00	I15505	10	u2	
33.78000000	-84.39955000	USA	GA	Atlanta	Fulton	19981113	9.00	GTB301	10	u2	
34.04176000	-83.39817000	USA	GA	Athens	Jackson	19981124	7.95	SCB501	10	u2	Seismic
34.04176000	-83.39817000	USA	GA	Athens	Jackson	19981125	17.10	SCB301	15	u2	Seismic
34.04176000	-83.39817000	USA	GA	Athens	Jackson	19981125	18.05	SCB401	15	u2	Seismic
35.97313000	-89.90797000	USA	AR	Blytheville	Mississippi	19981215	11.00	BUGG03	10	u1	Vibro
33.78000000	-84.39955000	USA	GA	Atlanta	Fulton	19990119	9.00	GTB302	10	u2	
33.78000000	-84.39955000	USA	GA	Atlanta	Fulton	19990119	9.00	GTB303	10	u2	
32.59432000	-85.29738000	USA	AL	Spring Villa	Lee	19990128	10.10	ALRS01	15	u2	Rough Sleeve
32.59432000	-85.29738000	USA	AL	Spring Villa	Lee	19990128	10.00	ALRS02	15	u2	Rough Sleeve
32.59432000	-85.29738000	USA	AL	Spring Villa	Lee	19990128	10.00	ALSM04	15	u2	
32.59432000	-85.29738000	USA	AL	Spring Villa	Lee	19990128	10.00	ALSM05	15	u2	
33.78000000	-84.39955000	USA	GA	Atlanta	Fulton	19990309	13.00	AMS	10	u2	
35.12916000	-89.84155000	USA	TN	Memphis	Shelby	19990322	30.55	SFSR01	10	u2	Seismic
35.12905000	-89.84030000	USA	TN	Memphis	Shelby	19990322	25.50	SFSR02	15	u2	Seismic
35.35780000	-90.01883000	USA	TN	Memphis	Shelby	19990323	21.55	SFOR01	10	u2	Seismic
35.35843000	-90.01837000	USA	TN	Memphis	Shelby	19990323	21.15	SFOR02	15	u2	Seismic
33.43351000	-84.71332000	USA	GA	Newnan	Cowetta	19990621	17.75	Cow10a	10	u2	
33.43351000	-84.71332000	USA	GA	Newnan	Cowetta	19990621	18.00	Cow10b	10	u2	

Table C.1 (continued) Summary of CPT soundings performed by the In-Situ group

Lat	Long	Country	State	City	County	Date	Depth	Int_Ref	Area	u_b	Options
35.15229000	-90.04868000	USA	TN	Memphis	Shelby	19990713	28.00	PSI1A		u2	Seismic
35.14272000	-90.04827000	USA	TN	Memphis	Shelby	19990714	18.00	PSI2A	15	u2	Seismic
35.13484000	-90.02343000	USA	TN	Memphis	Shelby	19990715	17.00	PSI3A	15	u2	Seismic
32.59390232	-85.29722982	USA	AL	Spring Villa	Lee	19990802	12.65	OP899A	10	u2	
32.59390232	-85.29722982	USA	AL	Spring Villa	Lee	19990802	8.90	OP899B	10	u2	
32.73955000	-80.14156600	USA	SC	Charleston	Charleston	19990913	35.25	SODFM1	10	u2	Seismic
32.73930000	-80.14126000	USA	SC	Charleston	Charleston	19990914	30.05	SODFM2	10	u2	Seismic
32.59390232	-85.29722982	USA	AL	Spring Villa	Lee	19991007	11.25	OPELI1	10	u2	Seismic
32.59390232	-85.29722982	USA	AL	Spring Villa	Lee	19991007	16.65	OPELI2	10	u2	Seismic
35.12891600	-89.84101600	USA	TN	Memphis	Shelby	19991012	9.55	SHOOTA	10	u2	Seismic
35.12906000	-89.84076000	USA	TN	Memphis	Shelby	19991012	15.95	SHOOTB	15	u2	Seismic
35.12925000	-89.84048000	USA	TN	Memphis	Shelby	19991012	30.80	SHOOTC	10	u2	Seismic
35.35783000	-90.01883000	USA	TN	Memphis	Shelby	19991013	31.85	FORST1	10	u2	Seismic
35.35800000	-90.01950000	USA	TN	Memphis	Shelby	19991013	30.25	FORST2	10	u2	Seismic
35.35800000	-90.01950000	USA	TN	Memphis	Shelby	19991014	32.90	FORST3	10	u2	Seismic
35.35816000	-90.01966000	USA	TN	Memphis	Shelby	19991014	32.95	FORST4	10	u2	Seismic
32.59417773	-85.29739662	USA	AL	Spring Villa	Lee	19991208	10.30	OPEL1A	15	u2	Seismic
32.59416422	-85.29740491	USA	AL	Spring Villa	Lee	19991208	10.15	OPEL1B	15	u2	Seismic
32.59390553	-85.29731153	USA	AL	Spring Villa	Lee	19991208	8.95	OPEL1C	15	u2	Seismic
32.59390380	-85.29729355	USA	AL	Spring Villa	Lee	19991208	10.25	OPEL1D	15	u2	Seismic
32.59390625	-85.29721727	USA	AL	Spring Villa	Lee	19991208	19.30	OPEL1E	10	u2	Seismic
32.75241000	-80.01335000	USA	SC	Charleston	Charleston	19991216	25.05	STON1A	10	u2	Seismic
32.80161000	-79.90153000	USA	SC	Mount Pleasant	Charleston	19991217	30.60	CRBDH1	15	u2	Seismic
32.80143000	-79.90351000	USA	SC	Mount Pleasant	Charleston	19991218	29.05	CRBDH2	15	u2	Seismic
33.77844000	-84.39561000	USA	GA	Atlanta	Fulton	20000210	7.70	Plum2	15	u2	

Table C.1 (continued) Summary of CPT soundings performed by the In-Situ group

Lat	Long	Country	State	City	County	Date	Depth	Int_Ref	Area	u_b	Options
35.14468333	-90.05931667	USA	TN	Memphis	Shelby	20000304	33.00	MUDA11	10	u2	Seismic
35.14468333	-90.05931667	USA	TN	Memphis	Shelby	20000304	31.00	MUDA12	10	u2	Seismic
35.15646667	-90.05688333	USA	TN	Memphis	Shelby	20000305	31.00	MUDB1	10	u2	Seismic
35.15971667	-90.05641667	USA	TN	Memphis	Shelby	20000305	38.00	MUDC1	10	u2	Seismic
35.15971667	-90.05641667	USA	TN	Memphis	Shelby	20000306	11.10	MUDC2	10	u1u2	
35.17780000	-90.05318333	USA	TN	Memphis	Shelby	20000306	24.00	MUDE1	10	u2	Seismic
35.17568333	-90.05538333	USA	TN	Memphis	Shelby	20000307	28.00	MUDD1	10	u2	Seismic
35.17568333	-90.05538333	USA	TN	Memphis	Shelby	20000307	25.95	MUDD2	10	u1	
10.39018000	-61.47696000	Trinidad				20000614	13.80	DSAL01	10	u2	Seismic
10.39018000	-61.47696000	Trinidad				20000615	15.35	DSAL02	10	u2	Seismic
10.39039000	-61.47569000	Trinidad				20000616	21.00	DSAL03	15	u2	Seismic
10.39138000	-61.47626000	Trinidad				20000616	20.75	DSAL04	15	u2	Seismic
10.39196000	-61.47702000	Trinidad				20000616	16.40	DSAL05	15	u2	Seismic
10.39114000	-61.47760000	Trinidad				20000617	16.10	DSAL06	15	u2	Seismic
10.39006000	-61.47694000	Trinidad				20000617	21.85	DSAL07	15	u2	Seismic
10.39028000	-61.47635000	Trinidad				20000617	15.40	DSAL08	15	u2	Seismic
10.39138000	-61.47557000	Trinidad				20000618	13.85	DSAL09	10	u2	Seismic
10.39138000	-61.47536000	Trinidad				20000620	17.15	DSAL10	10	u2	Seismic
32.77417000	-79.97069000	USA	SC	Charleston	Charleston	20000628	19.35	WPCR01	10	u2	
32.84943000	-79.85709000	USA	SC	Mount Pleasant	Charleston	20000628	15.50	WPCR02	10	u2	
32.84878000	-79.85653000	USA	SC	Mount Pleasant	Charleston	20000628	15.85	WPCR03	10	u2	
32.84956000	-79.85702000	USA	SC	Mount Pleasant	Charleston	20000628	15.90	WPCR04	10	u2	
32.89465000	-79.82000000	USA	SC	Mount Pleasant	Charleston	20000630	17.65	WPCR05	10	u2	
32.89464000	-79.82114000	USA	SC	Mount Pleasant	Charleston	20000630	7.05	WPCR06	10	u2	
32.89463000	-79.82128000	USA	SC	Mount Pleasant	Charleston	20000630	6.95	WPCR07	10	u2	

Table C.1 (continued) Summary of CPT soundings performed by the In-Situ group

Lat	Long	Country	State	City	County	Date	Depth	Int_Ref	Area	u_b	Options
32.89502000	-79.82252000	USA	SC	Mount Pleasant	Charleston	20000630	6.95	WPCR08	10	u2	
32.89495000	-79.82360000	USA	SC	Mount Pleasant	Charleston	20000630	6.95	WPCR09	10	u2	
32.89480000	-79.82410000	USA	SC	Mount Pleasant	Charleston	20000630	7.90	WPCR10	10	u2	
32.89455000	-79.82478000	USA	SC	Mount Pleasant	Charleston	20000630	7.00	WPCR11	10	u2	
32.89457000	-79.82716000	USA	SC	Mount Pleasant	Charleston	20000630	6.95	WPCR12	10	u2	
32.89455000	-79.82674000	USA	SC	Mount Pleasant	Charleston	20000701	7.25	WPCR13	10	u2	
32.89477000	-79.82537000	USA	SC	Mount Pleasant	Charleston	20000701	7.25	WPCR14	10	u2	
32.89508000	-79.82479000	USA	SC	Mount Pleasant	Charleston	20000701	7.15	WPCR15	10	u2	
32.89545000	-79.82375000	USA	SC	Mount Pleasant	Charleston	20000701	14.50	WPCR16	10	u2	
32.89558000	-79.82310000	USA	SC	Mount Pleasant	Charleston	20000701	7.25	WPCR17	10	u2	
32.89527000	-79.82148000	USA	SC	Mount Pleasant	Charleston	20000701	7.15	WPCR18	10	u2	
32.89500000	-79.82777000	USA	SC	Mount Pleasant	Charleston	20000702	15.50	WPCR19	10	u2	
35.12374000	-89.93186000	USA	TN	Memphis	Shelby	20000708	9.85	CERE	15	u2	Seismic
35.12372000	-89.93177000	USA	TN	Memphis	Shelby	20000708	11.10	CERIM	10	u2	Seismic
35.15657000	-90.05679000	USA	TN	Memphis	Shelby	20000708	32.85	MUDBR	10	u1	Resistivity
35.09949000	-89.69931000	USA	TN	Memphis	Shelby	20000709	26.25	WOLF1	15	u2	Seismic
35.09947000	-89.69919000	USA	TN	Memphis	Shelby	20000709	28.90	WOLF2	10	u2	
35.09951000	-89.69948000	USA	TN	Memphis	Shelby	20000709	25.10	WOLF3	10	u2	
35.09932000	-89.70006000	USA	TN	Memphis	Shelby	20000709	20.10	WOLF4	10	u2	
35.09982000	-89.70285000	USA	TN	Memphis	Shelby	20000710	31.70	WOLF5	10	u2	Seismic
35.09980000	-89.70301000	USA	TN	Memphis	Shelby	20000710	15.80	WOLF6	10	u2	
35.09983000	-89.70322000	USA	TN	Memphis	Shelby	20000710	20.55	WOLF7	10	u2	Resistivity
35.34582000	-80.84432000	USA	NC	Charlotte	Mecklenburg	20000717	14.95	TRIS01	10	u2	Seismic
35.34565000	-80.84445000	USA	NC	Charlotte	Mecklenburg	20000717	18.00	TRIS02	10	u2	
35.34571000	-80.84459000	USA	NC	Charlotte	Mecklenburg	20000718	17.20	TRIS03	10	u2	

Table C.1 (continued) Summary of CPT soundings performed by the In-Situ group

Lat	Long	Country	State	City	County	Date	Depth	Int_Ref	Area	u_b	Options
35.34539000	-80.84429000	USA	NC	Charlotte	Mecklenburg	20000718	15.45	TRIS04	10	u2	Seismic
35.34522000	-80.84399000	USA	NC	Charlotte	Mecklenburg	20000718	13.50	TRIS05	10	u2	
35.34521000	-80.84432000	USA	NC	Charlotte	Mecklenburg	20000718	11.35	TRIS06	10	u1	
35.34507000	-80.84502000	USA	NC	Charlotte	Mecklenburg	20000718	15.35	TRIS07	10	u2	Seismic
35.34507000	-80.84484000	USA	NC	Charlotte	Mecklenburg	20000719	16.60	TRIS08	15	u2	
35.34507000	-80.84484000	USA	NC	Charlotte	Mecklenburg	20000719	14.00	TRIS09	15	u2	
35.34489000	-80.84509000	USA	NC	Charlotte	Mecklenburg	20000719	10.40	TRIS10	15	u2	
35.34535000	-80.84514000	USA	NC	Charlotte	Mecklenburg	20000719	10.65	TRIS11	10	u1u2	
35.34549000	-80.84503000	USA	NC	Charlotte	Mecklenburg	20000720	21.75	TRIS12	10	u2	Resistivity
35.34539000	-80.84526000	USA	NC	Charlotte	Mecklenburg	20000720	19.50	TRIS13	10	u2	Resistivity
37.38298000	-77.34672000	USA	VA	Richmond	Henrico	20000725	9.75	RICH01	10	u2	Seismic
37.38320000	-77.34664000	USA	VA	Richmond	Henrico	20000726	9.25	RICH02	10	u2	Seismic
37.38320000	-77.34664000	USA	VA	Richmond	Henrico	20000726	9.10	RICH03	10	u1	Reisistivity
37.19032000	-80.57926000	USA	VA	Blacksburg	Pulaski	20000727	3.20	BLAC01	10	u2	
37.19032000	-80.57926000	USA	VA	Blacksburg	Pulaski	20000727	5.45	BLAC02	10	u2	Seismic
37.19032000	-80.57926000	USA	VA	Blacksburg	Pulaski	20000727	5.10	BLAC03	10	u1	Resistivity
37.19048000	-80.57913000	USA	VA	Blacksburg	Pulaski	20000727	5.50	BLAC04	15	u2	Seismic
33.42260000	-79.19026000	USA	SC	Pawleys Island	Georgetown	20000729	10.00	MYRT01	10	u2	
33.42287000	-79.19039000	USA	SC	Pawleys Island	Georgetown	20000729	10.05	MYRT02	10	u2	
33.42316000	-79.19024000	USA	SC	Pawleys Island	Georgetown	20000729	10.05	MYRT03	10	u2	
33.42298000	-79.18995000	USA	SC	Pawleys Island	Georgetown	20000729	10.00	MYRT04	10	u2	
33.83605000	-78.69940000	USA	SC	North Myrtle Beach	Horry	20000729	10.05	MYRT05	10	u2	
33.83351000	-78.69891000	USA	SC	North Myrtle Beach	Horry	20000729	10.10	MYRT07	10	u2	
33.83481000	-78.70179000	USA	SC	North Myrtle Beach	Horry	20000729	6.95	MYRT08	10	u2	
32.91875000	-80.04695000	USA	SC	Charleston	Charleston	20000729	9.09	TIS04	10	u1	Vibro

Table C.1 (continued) Summary of CPT soundings performed by the In-Situ group

Lat	Long	Country	State	City	County	Date	Depth	Int_Ref	Area	u_b	Options
35.58316802	-90.38906446	USA	AR	Marked Tree	Poinsett	20000814	32.05	MTREE01	10	u2	Seismic
35.58324000	-90.38912000	USA	AR	Marked Tree	Poinsett	20000815	8.95	MTREE02	10	u2	Resistivity
35.58320597	-90.38913952	USA	AR	Marked Tree	Poinsett	20000815	13.68	MTREE03	10	u2	Resistivity
35.58317044	-90.38915988	USA	AR	Marked Tree	Poinsett	20000815	15.70	MTREE04	10	u2	Resistivity
35.58313640	-90.38917940	USA	AR	Marked Tree	Poinsett	20000815	15.70	MTREE05	10	u1	Resistivity
35.58310833	-90.38919550	USA	AR	Marked Tree	Poinsett	20000815	15.80	MTREE06	10	u1	Resistivity
35.58307430	-90.38921501	USA	AR	Marked Tree	Poinsett	20000815	15.57	MTREE07	10	u1	Resistivity
35.58304051	-90.38923438	USA	AR	Marked Tree	Poinsett	20000815	15.73	MTREE08	10	u1	Resistivity
35.58383000	-90.38992000	USA	AR	Marked Tree	Poinsett	20000816	15.55	MTREE09	10	u2	Resistivity
35.58380300	-90.38996250	USA	AR	Marked Tree	Poinsett	20000816	15.65	MTREE10	10	u2	Resistivity
35.58378435	-90.38999171	USA	AR	Marked Tree	Poinsett	20000816	15.80	MTREE11	10	u2	Resistivity
35.58376081	-90.39002890	USA	AR	Marked Tree	Poinsett	20000817	25.93	MTREE12	10	u2	Seismic
35.58374056	-90.39006077	USA	AR	Marked Tree	Poinsett	20000817	8.05	MTREE13	10	u2	Resistivity
35.58371271	-90.39010460	USA	AR	Marked Tree	Poinsett	20000817	15.48	MTREE14	10	u2	Resistivity
33.77573000	-84.40018000	USA	GA	Atlanta	Fulton	20000914	9.73	Bogg01	10	u2	
32.59392979	-85.29710747	USA	AL	Spring Villa	Lee	20000926	18.23	JAG01	10	u2	Seismic
32.59390262	-85.29715208	USA	AL	Spring Villa	Lee	20000926	20.50	JAG02	10	u2	Resistivity
32.59387364	-85.29720593	USA	AL	Spring Villa	Lee	20000926	19.40	JAG03	10	u2	Resistivity
32.59390789	-85.29721308	USA	AL	Spring Villa	Lee	20000926	22.27	JAG04	10	u2	Resistivity
32.59391515	-85.29721922	USA	AL	Spring Villa	Lee	20001213	15.66	OPEMEM1	10	u2	
32.59391715	-85.29721263	USA	AL	Spring Villa	Lee	20001213	15.82	OPEMEM2	10	u2	
32.59392444	-85.29719240	USA	AL	Spring Villa	Lee	20001213	12.92	OPEMEM3	10	u2	
33.76767000	-84.39774000	USA	GA	Atlanta	Fulton	20010129	13.73	COKE01	10	u2	Seismic
33.76769000	-84.39752000	USA	GA	Atlanta	Fulton	20010129	8.85	COKE02	10	u2	
33.76767000	-84.39760000	USA	GA	Atlanta	Fulton	20010129	7.90	COKE03	10	u1	

Table C.1 (continued) Summary of CPT soundings performed by the In-Situ group

Lat	Long	Country	State	City	County	Date	Depth	Int_Ref	Area	u_b	Options
35.60202000	-89.97719000	USA	AR	Wilson	Mississippi	20010306	21.40	WILS02	10	u2	Seismic
35.60208000	-89.97713000	USA	AR	Wilson	Mississippi	20010306	16.40	WILS04	10	u2	
35.60217000	-89.97711000	USA	AR	Wilson	Mississippi	20010306	16.50	WILS07	10	u2	
35.60215000	-89.97715000	USA	AR	Wilson	Mississippi	20010307	22.93	WILS06	10	u1	Resistivity
36.92609000	-89.15822000	USA	MO	Wyatt	Mississippi	20010308	25.40	WYAT01	10	u2	Seismic
36.92685000	-89.15717000	USA	MO	Wyatt	Mississippi	20010308	12.30	WYAT03	10	u2	
36.92706000	-89.15572000	USA	MO	Wyatt	Mississippi	20010309	23.00	WYAT04	10	u2	Resistivity
36.92740000	-89.15610000	USA	MO	Wyatt	Mississippi	20010309	19.70	WYAT05	10	u2	Resistivity
28.05269000	-81.80768000	USA	FL	Auburndale	Polk	20010330	20.83	SC05	10	u2	Seismic
28.05241000	-81.80763000	USA	FL	Auburndale	Polk	20010330	22.45	SC06	10	u2	Seismic
28.05427000	-81.80783000	USA	FL	Auburndale	Polk	20010331	18.90	SC02	10	u2	Seismic
28.05371000	-81.80811000	USA	FL	Auburndale	Polk	20010331	19.70	SC03	10	u2	Seismic
28.05322000	-81.80818000	USA	FL	Auburndale	Polk	20010331	19.63	SC04	10	u2	Seismic
28.05472000	-81.80782000	USA	FL	Auburndale	Polk	20010401	18.35	SC01	10	u2	Seismic
28.05284000	-81.80856000	USA	FL	Auburndale	Polk	20010401	19.80	SC07	10	u2	Seismic
28.05247000	-81.80858000	USA	FL	Auburndale	Polk	20010401	20.78	SC08	10	u2	Seismic
35.09335000	-89.71093000	USA	TN	Collierville	Shelby	20010605	28.58	SWGA01	10	u2	Seismic
35.09333000	-89.71091000	USA	TN	Collierville	Shelby	20010605	30.35	SWGA02	10	u2	Seismic
35.23957000	-90.02412000	USA	TN	Memphis	Shelby	20010606	14.95	TRPK01	10	u2	Seismic
35.23957000	-90.02412000	USA	TN	Memphis	Shelby	20010606	15.05	TRPK02	10	u1	Resistivity
35.12366000	-89.93169000	USA	TN	Memphis	Shelby	20010607	10.18	CERI03	10	u2	Seismic
35.12366000	-89.93169000	USA	TN	Memphis	Shelby	20010607	21.33	CERI04	15	u2	Seismic
36.70038000	-90.13251000	USA	MO	Dexter	Stoddard	20010619	29.02	DEX01	10	u2	Seismic
36.70038000	-90.13251000	USA	MO	Dexter	Stoddard	20010619	19.33	DEX02	10	u2	Resistivity
38.45882000	-90.35043000	USA	MO	St. Louis	St. Louis	20010620	19.75	MER01	10	u2	Seismic

Table C.1 (continued) Summary of CPT soundings performed by the In-Situ group

Lat	Long	Country	State	City	County	Date	Depth	Int_Ref	Area	u_b	Options
38.45882000	-90.35043000	USA	MO	St. Louis	St. Louis	20010620	18.68	MER02	10	u2	
38.46538000	-90.41467000	USA	MO	St. Louis	Jefferson	20010621	12.98	MER03	10	u2	Seismic
38.46502000	-90.41460000	USA	MO	St. Louis	Jefferson	20010621	13.55	MER04	10	u2	Seismic
36.65318000	-90.13231000	USA	MO	Dexter	Stoddard	20010622	30.03	DEX03	10	u2	Seismic
36.65321000	-90.13226000	USA	MO	Dexter	Stoddard	20010622	28.90	DEX031	10	u2	Resistivity
36.53725000	-90.17570000	USA	MO	Dexter	Dunklin	20010622	26.43	DEX04	10	u2	Seismic
36.53725000	-90.17570000	USA	MO	Dexter	Dunklin	20010622	26.50	DEX05	10	u2	Resistivity
35.65993869	-89.38768563	USA	TN	Brownsville	Haywood	20010711	10.73	CALB04	10	u2	
35.65973607	-89.38948051	USA	TN	Brownsville	Haywood	20010711	10.63	CALB07	10	u2	
35.65949786	-89.38846162	USA	TN	Brownsville	Haywood	20010711	20.80	CALB09	10	u2	Seismic
35.65896120	-89.38706147	USA	TN	Brownsville	Haywood	20010711	10.83	CALB12	10	u2	
35.65893108	-89.38802639	USA	TN	Brownsville	Haywood	20010711	21.65	CALB16	10	u2	
35.66011667	-89.38859657	USA	TN	Brownsville	Haywood	20010712	10.53	CALB03	10	u2	
35.65923774	-89.38916000	USA	TN	Brownsville	Haywood	20010712	22.83	CALB14	10	u2	Seismic
35.65888453	-89.38975380	USA	TN	Brownsville	Haywood	20010712	21.50	CALB18	10	u2	
35.65837799	-89.38935906	USA	TN	Brownsville	Haywood	20010712	21.13	CALB24	10	u2	Seismic
35.65798918	-89.39003720	USA	TN	Brownsville	Haywood	20010712	9.98	CALB28	10	u2	
35.65875310	-89.38869104	USA	TN	Brownsville	Haywood	20010713	21.50	CALB20	10	u2	
35.65845739	-89.38764177	USA	TN	Brownsville	Haywood	20010713	21.10	CALB22	10	u2	Seismic
35.65818358	-89.38731788	USA	TN	Brownsville	Haywood	20010713	10.03	CALB27	10	u2	
35.65735121	-89.38759791	USA	TN	Brownsville	Haywood	20010713	9.85	CALB30	10	u2	
35.65718144	-89.38849873	USA	TN	Brownsville	Haywood	20010713	9.88	CALB31	10	u2	
35.65593288	-89.38809049	USA	TN	Brownsville	Haywood	20010713	9.85	CALB37	10	u2	
27.86435800	-82.39423000	USA	FL	Gibsonton	Hillsborough	20010918	15.00	CARG01	10	u2	Resistivity
27.86435800	-82.39423000	USA	FL	Gibsonton	Hillsborough	20010918	12.50	CARG02	10	u2	Resistivity

Table C.1 (continued) Summary of CPT soundings performed by the In-Situ group

Lat	*Long*	*Country*	*State*	*City*	*County*	*Date*	*Depth*	*Int_Ref*	*Area*	u_b	*Options*
27.86435800	-82.39423000	USA	FL	Gibsonton	Hillsborough	20010920	4.80	CARG03	10	u2	Resistivity
27.86435800	-82.39423000	USA	FL	Gibsonton	Hillsborough	20010921	6.25	CARG04	10	u2	Resistivity
28.38785000	-81.24702000	USA	FL	Orlando	Orange	20010921	18.60	DFI01A	10	u2	Seismic
32.59409966	-85.29716875	USA	AL	Spring Villa	Lee	20011120	13.98	wpcopel1	10	u2	
32.59393279	-85.29718809	USA	AL	Spring Villa	Lee	20011120	17.06	wpcopel2	10	u2	
32.59391576	-85.29722718	USA	AL	Spring Villa	Lee	20011120	18.20	wpcopel3	10	u2	
32.59421456	-85.29719454	USA	AL	Spring Villa	Lee	20020509		AMR01	10	u2	Seismic
32.59410387	-85.29716511	USA	AL	Spring Villa	Lee	20020509		AMR02	10	u2	
36.18851000	-80.26579000	USA	NC	Winston-Salem	Forsyth	20020524	12.63	sara01	10	u2	
36.18825000	-80.26544000	USA	NC	Winston-Salem	Forsyth	20020524	11.85	sara02	10	u2	Seismic
36.18844000	-80.26564000	USA	NC	Winston-Salem	Forsyth	20020524	16.08	sara03	10	u2	
36.18817000	-80.26580000	USA	NC	Winston-Salem	Forsyth	20020524	11.88	sara04	10	u2	
36.18908864	-80.26356059	USA	NC	Winston-Salem	Forsyth	20020524	8.90	sara05	10	u2	
36.18941000	-80.26344000	USA	NC	Winston-Salem	Forsyth	20020525	15.60	sara06	10	u2	Seismic
36.18933000	-80.26386000	USA	NC	Winston-Salem	Forsyth	20020525	9.20	sara07	10	u2	
45.46774000	12.45487000	Italy				20020610	40.23	veni01	10	u2	Seismic
45.46774000	12.45461000	Italy				20020611	40.82	veni02	10	u2	Seismic
45.46774000	12.45447000	Italy				20020611	40.55	veni03	10	u2	Seismic
32.74868000	-79.90089000	USA	SC	Charleston	Charleston	20020802	32.90	mehl01	10	u2	Seismic
32.88874000	-80.01118000	USA	SC	Charleston	Charleston	20020803	28.60	mcc01	10	u2	Seismic
32.85402000	-79.88695000	USA	SC	Mt. Pleasant	Charleston	20020803	31.50	mcmp01	10	u2	Seismic
32.80165000	-79.90141000	USA	SC	Mt. Pleasant	Charleston	20020805	32.52	CRBDH3	10	u1	
32.51800000	-85.03201000	USA	AL	Phenix City	Lee	20020821	14.40	SLPF01	10	u2	
32.51810000	-85.03161000	USA	AL	Phenix City	Lee	20020821	11.58	SLPF02	10	u2	
32.51762000	-85.03141000	USA	AL	Phenix City	Lee	20020821	8.05	SLPF03	10	u2	

Table C.1 (continued) Summary of CPT soundings performed by the In-Situ group

Lat	Long	Country	State	City	County	Date	Depth	Int_Ref	Area	u_b	Options
30.74525000	-81.65394000	USA	GA		Camden	20020909	9.90	stmr01	10	u2	Seismic
30.74525000	-81.65394000	USA	GA		Camden	20020909	9.60	stmr02	10	u1	Resistivity
31.33836000	-81.46584000	USA	GA		McIntosh	20020910	18.00	alts01	10	u2	Seismic
31.33836000	-81.46584000	USA	GA		McIntosh	20020910	17.93	alts02	10	u1	
31.10846000	-81.48951000	USA	GA		Glynn	20020911	14.95	sldn01	10	u2	Seismic
31.10846000	-81.48951000	USA	GA		Glynn	20020911	14.85	sldn02	10	u1	
31.66718000	-81.83751000	USA	GA		Long	20020912	22.45	altn01	10	u2	Seismic
31.66711000	-81.83746000	USA	GA		Long	20020912	13.75	altn02	10	u1	
33.61940000	-84.42041000	USA	GA	Atlanta	Clayton	20020920	21.00	RNWY01	10	u2	Seismic
33.61943000	-84.42015000	USA	GA	Atlanta	Clayton	20020920	19.55	RNWY02	10	u2	Seismic
33.62027000	-84.41868000	USA	GA	Atlanta	Clayton	20021001	8.70	RNWY03	10	u2	Seismic
33.62023000	-84.41867000	USA	GA	Atlanta	Clayton	20021001	9.45	RNWY04	10	u2	Seismic
33.62202000	-84.42361000	USA	GA	Atlanta	Clayton	20021001	15.18	RNWY05	10	u2	Seismic
33.61995000	-84.42062000	USA	GA	Atlanta	Clayton	20021002	14.07	RNWY06	10	u2	Seismic
36.33203000	-89.58680000	USA	TN	Mooring	Lake	20021017	38.95	BLST01	10	u2	Seismic
36.32481000	-89.56696000	USA	TN	Mooring	Lake	20021018	24.73	BLST02	10	u2	Seismic
36.33203000	-89.58631000	USA	TN	Mooring	Lake	20021018	30.89	BLST03	10	u2	Seismic
35.46024000	-90.56563000	USA	AR	Marked Tree	Poinsett	20021028	29.00	BLST04	10	u2	Seismic
36.33202522	-89.58680332	USA	TN	Mooring	Lake	20021029	25.80	BLST05	10	u2	Seismic
36.33204435	-89.58679005	USA	TN	Mooring	Lake	20021030	27.92	BLST06	10	u2	Seismic
35.46024754	-90.56563401	USA	AR	Marked Tree	Poinsett	20021031	28.58	BLST07	10	u2	Seismic
36.33202600	-89.58679108	USA	TN	Mooring	Lake	20021101	28.08	BLST08	10	u2	Seismic
33.75800000	-84.39600000	USA	GA	Atlanta	Fulton	20030122	20.68	CNN02	10	u2	Seismic
31.64404000	-81.39945000	USA	GA		McIntosh	20030203	25.83	GDOT-1	10	u2	
32.08302000	-81.10370000	USA	GA	Savannah	Chatham	20030204	12.85	GDOT-4	10	u2	

Table C.1 (continued) Summary of CPT soundings performed by the In-Situ group

Lat	Long	Country	State	City	County	Date	Depth	Int_Ref	Area	u_b	Options
31.64404000	-81.39945000	USA	GA		McIntosh	20030305	26.50	GDT-95	10	u2	
32.43305000	-84.03678000	USA	GA		Macon	20030326	7.83	FLNT01	10	u2	Seismic
33.96082000	-84.36655000	USA	GA	Atlanta	Fulton	20030401	14.70	WALG01	10	u2	Seismic
33.96078000	-84.36633000	USA	GA	Atlanta	Fulton	20030404	3.50	WALG02	10	u2	
33.96078000	-84.36633000	USA	GA	Atlanta	Fulton	20030404	3.85	WALG03	10	u2	
33.96084000	-84.36636000	USA	GA	Atlanta	Fulton	20030404	4.23	WALG04	10	u2	
33.62092039	-84.43140824	USA	GA	Atlanta	Clayton	20030523	3.58	ARPT01	10	u2	
33.62095166	-84.43135767	USA	GA	Atlanta	Clayton	20030523	2.78	ARPT02	10	u2	
33.62090432	-84.43135392	USA	GA	Atlanta	Clayton	20030523	5.03	ARPT03	10	u2	Seismic
33.62096013	-84.43132052	USA	GA	Atlanta	Clayton	20030523	3.15	ARPT04	10	u2	Seismic
33.62094080	-84.43133949	USA	GA	Atlanta	Clayton	20030524	6.18	ARPT05	15	u2	Seismic
33.62090512	-84.43137294	USA	GA	Atlanta	Clayton	20030524	4.08	ARPT06	15	u2	Seismic
33.62015446	-84.43285579	USA	GA	Atlanta	Clayton	20030524	13.75	ARPT07	15	u2	Seismic
33.62016670	-84.43287008	USA	GA	Atlanta	Clayton	20030524	13.43	ARPT08	10	u2	Seismic
33.62015074	-84.43281616	USA	GA	Atlanta	Clayton	20030610	8.30	ARPT09	10	u2	Seismic
33.62017845	-84.43287071	USA	GA	Atlanta	Clayton	20030610	10.35	ARPT10	10	u2	Seismic
33.62092169	-84.43135446	USA	GA	Atlanta	Clayton	20030611	1.43	ARPT11	10	u2	Seismic
33.62090976	-84.43134347	USA	GA	Atlanta	Clayton	20030611	4.72	ARPT12	10	u2	Seismic
33.62095698	-84.43132128	USA	GA	Atlanta	Clayton	20030611	3.60	ARPT13	10	u2	Seismic
35.46024000	-90.56563000	USA	AR	Marked Tree	Poinsett	20030614	22.15	BLST09	10	u2	Seismic
35.48452000	-90.55111000	USA	AR	Marked Tree	Poinsett	20030614	19.48	BLST10	10	u2	Seismic
36.33202600	-89.58679108	USA	TN	Mooring	Lake	20030615	22.93	BLST11	10	u2	Seismic
35.03836000	-89.69209000	USA	TN	Memphis	Shelby	20030616	11.82	COLT01	10	u2	Seismic
35.23019000	-89.98315000	USA	TN	Memphis	Shelby	20030616	21.68	GILT01	10	u2	Seismic
35.15775000	-89.98885000	USA	TN	Memphis	Shelby	20030617	10.63	RDST01	10	u2	Seismic

Table C.1 (continued) Summary of CPT soundings performed by the In-Situ group

Lat	Long	Country	State	City	County	Date	Depth	Int_Ref	Area	u_b	Options
33.62019322	-84.43281626	USA	GA	Atlanta	Clayton	20030626	6.45	ARPT14	10	u2	Seismic
33.62013626	-84.43286760	USA	GA	Atlanta	Clayton	20030626	13.03	ARPT15	10	u2	Seismic
33.62090402	-84.43136944	USA	GA	Atlanta	Clayton	20030626	4.90	ARPT16	10	u2	Seismic
33.62093667	-84.43130084	USA	GA	Atlanta	Clayton	20030626	8.03	ARPT17	10	u2	Seismic
42.05679000	-87.67663000	USA	IL	Evanston	Cook	20030714	27.13	FCPT04	10	u2	Seismic
42.05932000	-87.67093000	USA	IL	Evanston	Cook	20030715	26.93	NUCPT1	10	u2	Seismic
42.05932000	-87.67093000	USA	IL	Evanston	Cook	20030715	24.03	NUCPT2	10	u1	Seismic
42.05692000	-87.67689000	USA	IL	Evanston	Cook	20030716	17.68	FCPT02	10	u2	Seismic
42.05688000	-87.67640000	USA	IL	Evanston	Cook	20030716	20.02	FCPT03	10	u2	Seismic
42.05679000	-87.67663000	USA	IL	Evanston	Cook	20030717	21.95	FCPT05	10	u1	
42.05704000	-87.67654000	USA	IL	Evanston	Cook	20030718	18.00	FCPT01	10	u2	Seismic
40.28598000	-88.13008000	USA	IL	Rantoul	Champaign	20030722	10.03	UIUC01	10	u2	Seismic
38.01575000	-84.59983333	USA	KY	Lexington	Fayette	20030723	3.98	HFARM1	10	u2	Seismic
35.96172000	-89.96940000	USA	AR	Gosnell	Mississippi	20030920	24.10	GSAR01	10	u2	Seismic
36.10192000	-89.49125000	USA	TN	Dyersburg	Dyer	20030920	36.60	LNXT01	10	u2	Seismic
35.35785000	-90.01882000	USA	TN	Memphis	Shelby	20030922	21.33	SHBF01	10	u2	Seismic
33.85145000	-84.39227000	USA	GA	Atlanta	Fulton	20031020	10.43	BKHD01	10	u2	
33.85151000	-84.39235000	USA	GA	Atlanta	Fulton	20031020	12.07	BKHD02	10	u2	Seismic
33.85161000	-84.39261000	USA	GA	Atlanta	Fulton	20031020	9.13	BKHD03	10	u2	Seismic
33.85138000	-84.39239000	USA	GA	Atlanta	Fulton	20031020	11.13	BKHD04	10	u2	
32.59393500	-85.29739300	USA	AL	Spring Villa	Lee	20040301	21.38	OPEAUT	10	u2	Seismic
32.85402000	-79.88695000	USA	SC	Mt. Pleasant	Charleston	20040311	21.60	MCMP02	10	u2	Seismic
32.59391000	-85.29746000	USA	AL	Spring Villa	Lee	20040510	12.25	OPETRU	10	u2	Seismic
33.95784000	-84.53780000	USA	GA	Marietta	Cobb	20040611	22.98	BPTCH1	10	u2	Seismic
33.78024000	-84.38771000	USA	GA	Atlanta	Fulton	20040624	12.23	MACS01	10	u2	Seismic

Table C.1 (continued) Summary of CPT soundings performed by the In-Situ group

Lat	Long	Country	State	City	County	Date	Depth	Int_Ref	Area	u_b	Options
33.78048000	-84.38805000	USA	GA	Atlanta	Fulton	20040624	14.07	MACS02	10	u2	Seismic
33.77847000	-84.41244000	USA	GA	Atlanta	Fulton	20040628	10.00	MARI01	10	u2	
33.77842000	-84.41232000	USA	GA	Atlanta	Fulton	20040628	9.63	MARI02	10	u2	Seismic
33.77806000	-84.41175000	USA	GA	Atlanta	Fulton	20040628	9.98	MARI03	10	u2	
33.77800000	-84.41207000	USA	GA	Atlanta	Fulton	20040628	8.32	MARI04	10	u2	Seismic
33.77749000	-84.41158000	USA	GA	Atlanta	Fulton	20040628	4.65	MARI05	10	u2	
33.77845000	-84.41249000	USA	GA	Atlanta	Fulton	20040713	10.4	MARI06	10	u2	Seismic
33.77836000	-84.41231000	USA	GA	Atlanta	Fulton	20040713	8.8	MARI07	10	u2	Seismic
33.77850000	-84.41282000	USA	GA	Atlanta	Fulton	20040713	10.9	MARI08	10	u2	Seismic
33.77839000	-84.41210000	USA	GA	Atlanta	Fulton	20040713	9.35	MARI09	10	u2	Seismic
33.77832000	-84.41221000	USA	GA	Atlanta	Fulton	20040713	8.26	MARI10	10	u2	
33.86453000	-84.47501000	USA	GA	Vinings	Cobb	20040727	8.35	VINI01	10	u2	Seismic
33.86452000	-84.47478000	USA	GA	Vinings	Cobb	20040727	13.07	VINI02	10	u2	Seismic
36.26925000	-89.28779000	USA	TN	Dyersburg	Obion	20040809	10.93	GLAT	10	u2	Seismic
35.91071000	-89.33946000	USA	TN	Dyersburg	Dyer	20040810	26.85	HALT	10	u2	Seismic
36.11285000	-89.86240000	USA	MO	Portageville	Pemiscot	20040810	25.00	PEBM	10	u2	Seismic
36.71608000	-89.47210000	USA	MO	Sikeston	New Madrid	20040811	30.88	HENM	10	u2	Seismic
36.44971000	-89.62819000	USA	MO	Steele	New Madrid	20040811	34.18	PENM	10	u2	Seismic
36.54072000	-89.22837000	USA	KY	Hickman	Fulton	20040812	19.03	HICK	10	u2	Seismic
33.77753000	-84.41190000	USA	GA	Atlanta	Fulton	20040820	6.90	MARI11	10	u2	Seismic
33.77804000	-84.41157000	USA	GA	Atlanta	Fulton	20040820	10.28	MARI12	10	u2	
33.77844000	-84.41235000	USA	GA	Atlanta	Fulton	20040820	11.98	MARI13	10	u2	

Table C.1 (continued) Summary of CPT soundings performed by the In-Situ group

Lat	Long	Country	State	City	County	Date	Depth	Int_Ref	Area	u_b	Options
33.78452000	-84.37980000	USA	GA	Atlanta	Fulton	20040910	16.85	12ST01	10	u2	Seismic
33.78476000	-84.38018000	USA	GA	Atlanta	Fulton	20040910	16.75	12ST02	10	u2	Seismic
34.91513000	-82.45541000	USA	SC	Berea	Greenville	20040913	18.55	BMS02	10	u2	Seismic
33.79429000	-84.41091000	USA	GA	Atlanta	Fulton	20050211	17.80	HRES01	10	u2	Seismic
33.79414000	-84.41115000	USA	GA	Atlanta	Fulton	20050211	14.60	HRES02	10	u2	
33.77608000	-84.29836000	USA	GA	Atlanta	Decatur	20050509	14.15	DCAT01	10	u2	Seismic
18.44764000	-66.71471000	USA	Puerto Rico	Arecibo		20050714	15.30	CPT03	10	u2	
18.44699000	-66.71127000	USA	Puerto Rico	Arecibo		20050714	13.43	CPT04	10	u2	
18.44927000	-66.70969000	USA	Puerto Rico	Arecibo		20050714		CPT05	10	u2	
18.44927000	-66.70969000	USA	Puerto Rico	Arecibo		20050714		CPT05b	10	u2	
18.45088000	-66.70940000	USA	Puerto Rico	Arecibo		20050714		CPT06	10	u2	
18.45231000	-66.70860000	USA	Puerto Rico	Arecibo		20050714	10.38	CPT07	10	u2	Seismic
18.44670000	-66.72063000	USA	Puerto Rico	Arecibo		20050715		CPT01	10	u2	
18.44717000	-66.71899000	USA	Puerto Rico	Arecibo		20050715		CPT02	10	u2	
31.21605000	-84.19691000	USA	GA	Camilla	Mitchell	20050803	12.23	CAMI01	10	u2	
31.21604000	-84.19683000	USA	GA	Camilla	Mitchell	20050803	15.63	CAMI02	10	u2	
31.21461000	-84.19569000	USA	GA	Camilla	Mitchell	20050803	15.93	CAMI03	10	u2	
35.55500000	-90.65720000	USA	AR	Harrisburg	Poinsett	20050808	24.20	HBAR01	10	u2	Seismic
35.60429000	-90.30257000	USA	AR	Lepanto	Poinsett	20050808	26.85	LPAR01	10	u2	Seismic
36.66362000	-89.75199000	USA	MO	Parma	Stoddard	20050810	26.85	PARM01	10	u2	Seismic
36.34174000	-88.86694000	USA	TN	Martin	Weakly	20050811	12.83	UTMT01	10	u2	Seismic
18.40802000	-65.81342000	USA	Puerto Rico	Loiza		20050927	13.53	BBP02	10	u2	

Table C.1 (continued) Summary of CPT soundings performed by the In-Situ group

Lat	Long	Country	State	City	County	Date	Depth	Int_Ref	Area	u_b	Options
18.40822000	-65.81419000	USA	Puerto Rico	Loiza		20050927	14.70	BBP03	10	u2	
18.40731000	-65.81401000	USA	Puerto Rico	Loiza		20050928	14.72	BBP04	10	u2	
18.40786000	-65.81161000	USA	Puerto Rico	Loiza		20050928	13.90	BBP05	10	u2	
18.40797000	-65.81030000	USA	Puerto Rico	Loiza		20050928	13.25	BBP06	10	u2	
18.40740000	-65.81303000	USA	Puerto Rico	Loiza		20050928	14.73	BBP07	10	u2	
18.40420000	-65.81696000	USA	Puerto Rico	Loiza		20050929	29.83	BBP08	10	u2	Seismic
27.85923000	-82.60089000	USA	FL	St. Petersburg	Pinellas	20060303	13.85	PWRP01	10	u2	Seismic
27.85915000	-82.60282000	USA	FL	St. Petersburg	Pinellas	20060303	18.73	PWRP02	10	u2	Seismic
27.85970000	-82.60191000	USA	FL	St. Petersburg	Pinellas	20060304	12.60	PWRP03	10	u2	Seismic
27.86038000	-82.60313000	USA	FL	St. Petersburg	Pinellas	20060304	14.58	PWRP04	10	u2	Seismic
27.86032000	-82.60078000	USA	FL	St. Petersburg	Pinellas	20060304	14.38	PWRP05	10	u2	Seismic
27.86064000	-82.59920000	USA	FL	St. Petersburg	Pinellas	20060304	9.83	PWRP06	10	u2	
34.29280000	-84.73030000	USA	GA	White	Bartow	20060318	2.00	TOYO01	10	u2	
34.29280000	-84.73030000	USA	GA	White	Bartow	20060318	2.50	TOYO02	10	u2	
34.29280000	-84.73030000	USA	GA	White	Bartow	20060318	13.40	TOYO03	10	u2	
34.29280000	-84.73030000	USA	GA	White	Bartow	20060318	13.85	TOYO04	10	u2	
34.29280000	-84.73030000	USA	GA	White	Bartow	20060318	10.87	TOYO05	10	u2	
34.29280000	-84.73030000	USA	GA	White	Bartow	20060318	13.07	TOYO06	10	u2	
34.29280000	-84.73030000	USA	GA	White	Bartow	20060318	13.25	TOYO07	10	u2	
32.44004000	-80.68442000	USA	SC	Beaufort	Beaufort	20060427	11.00	BEAU01	10	u2	Seismic
32.44005556	-80.68442222	USA	SC	Beaufort	Beaufort	20060427	17.82	BEAU02	10	u2	Seismic
32.75123000	-80.01346000	USA	SC	Johns Island	Charleston	20060428	22.08	STONO01	10	u2	Seismic

Table C.1 (continued) Summary of CPT soundings performed by the In-Situ group

Lat	*Long*	*Country*	*State*	*City*	*County*	*Date*	*Depth*	*Int_Ref*	*Area*	u_b	*Options*
32.80162000	-79.90064000	USA	SC	Mount Pleasant	Charleston	20060429	24.89	CRB01	10	u2	Seismic
32.80165000	-79.90065000	USA	SC	Mount Pleasant	Charleston	20060430	26.01	CRB02	10	u2	Seismic
33.80752000	-84.42145000	USA	GA	Atlanta	Fulton	20060519	4.93	DIDIER01	10	u2	
33.80752479	-84.42148025	USA	GA	Atlanta	Fulton	20060519	4.03	DIDIER02	10	u2	
33.80751945	-84.42141319	USA	GA	Atlanta	Fulton	20060519	4.84	DIDIER03	10	u2	
32.89960000	-83.70824000	USA	GA	Macon	Bibb	20060801	3.17	MACO01	10	u2	Seismic
32.31925000	-84.80203000	USA	GA	Columbus	Chattahoochee	20060808	5.75	COLU01	10	u2	Seismic
30.99970000	-81.90451670	USA	GA	Brunswick	Camden	20060903	10.45	RAIN01	10	u2	Seismic
31.19653000	-81.98257000	USA	GA	Nahunta	Brantley	20060905	4.90	NAHU02	10	u2	Seismic
30.12890000	-89.87080000	USA	LA	New Orleans	Orleans Parrish	20061024	30.08	NEWOR01	10	u2	Seismic
30.88308890	-84.31865000	USA	GA	Cairo	Grady	20061108	12.73	CAIRO01	10	u2	Seismic
34.28363000	-83.84515000	USA	GA	Gainesville	Hall	20070509	8.80	HGIG01	10	u2	
32.16928000	-81.21091000	USA	GA	Savannah	Chatham	20070701	19.87	GTSAV01	10	u2	Seismic
32.16925000	-81.21088000	USA	GA	Savannah	Chatham	20070715	19.76	GTSAV02	10	u2	Seismic
32.80174000	79.90180000	USA	SC	Mt. Pleasant	Charleston	20070723	28.60	CRB03	10	u2	Seismic
32.80167000	-79.90183000	USA	SC	Mt. Pleasant	Charleston	20070725	27.47	CRB04	10	u2	Seismic

REFERENCES

Aki, K. (1965). "A note on the use of microseisms in determining the shallow structures of the earth's crust." *Geophysics*, 30(4), 665-666.

Alarcon-Guzman, A., Chameau, J. L. and Leonards, G. A. (1986). "New apparatus for investigating the stress-strain characteristics of sands." *Geotechnical Testing Journal*, 9(4), 204-212.

Alarcon-Guzman, A., Chameau, J. L., Leonards, G. A. and Frost, J. D. (1989). "Shear modulus and cyclic undrained behavior of sands." *Soils and Foundations*, 29(4), 105-119.

Andrus, R. D., Fairbanks, C. D., Zhang, J., Camp, W. M., III, Casey, T. J., Cleary, T. J. and Wright, W. B. (2006). "Shear-wave velocity and seismic response of near-surface sediments in Charleston, South Carolina." *Bulletin of the Seismological Society of America*, 96(5), 1897-1914.

Andrus, R. D. and Stokoe, K. H. (1997). "Liquefaction resistance based on shear wave velocity." *Proceedings from Workshop on Evaluation of Liquefaction Resistance*, *NCEER-97-0022*, Multidisciplinary Center for Earthquake Engineering Research, Buffalo, NY, 89-128.

Andrus, R. D., Zhang, J., Ellis, B. S. and Juang, C. H. (2003). "Guide for estimating the dynamic properties of South Carolina soils for ground response analysis." *FHWA-SC-03-07*, South Carolina Department of Transportation, Columbia, SC, 141 p.

Areias, L., Haegeman, W. and Van Impe, W. F. (2004). "New de-coupled shear wave source for the SCPT test." *Geotechnical and Geophysical Site Characterization*, *ISC-2*, Porto, Portugal, Millpress, Rotterdam, 1, 643-645.

ASTM D 5778-95 (2000). "Standard test method for performing electronic friction cone and piezocone penetration testing of soils." ASTM, West Conshohocken, PA.

ASTM D 4428/D 4428M (2000). "Standard test methods for crosshole seismic testing." ASTM, West Conshohocken, PA.

ASTM D 4015-92 (2000). "Standard test methods for modulus and damping of soils by the resonant-column method." ASTM, West Conshohocken, PA.

ASTM D 5777-00 (2006). "Standard guide for using the seismic refraction method for subsurface investigation." ASTM International, West Conshohocken, PA.

Baldi, G., Hight, D. W. and Roscoe, K. H. (1988). "A re-evaluation of conventional triaxial test methods." *Advanced Triaxial Testing of Soil and Rock*, Louisville, Kentucky, ASTM Special Technical Publication 977, ASTM, Conshohocken, PA, 219-263.

Baziw, E. J. (2007). "Implementation of the Principle Phase Decomposition Algorithm." *IEEE Transactions on Geoscience and Remote Sensing*, 45(6), 1775-1785.

Benoît, J. (2000). "The United States National Geotechnical Experimentation Sites program: The first decade." *National Geotechnical Experimentation Sites*, Geotechnical Special Publication 93, ASCE, Reston, VA, 1-25.

Boulanger, R. W., Arulnathan, R., Harder L. F., J., Torres, R. A. and Driller, M. W. (1998). "Dynamic properties of Sherman Island peat." *Journal of Geotechnical and Geoenvironmental Engineering*, 124(1), 12-21.

Burland, J. B. (1989). "Ninth Laurits Bjerrum Memorial Lecture: "Small is beautiful" - the stiffness of soils at small strains." *Canadian Geotechnical Journal*, 26(4), 499-516.

Butcher, A. P. and Powell, J. J. M. (1996). "Practical considerations for field geophysical techniques used to assess ground stiffness." *International Conference on Advances in Site Investigation Practice*, London, Thomas Telford, 2, 701-714.

Camp, W. M. (2004). "Drilled and driven foundation behavior in a calcareous clay." *Drilled Shafts, Micropiling, Deep Mixing, Remedial Methods, and Specialty Foundation Systems*, *GeoSupport 2004*, Orlando, FL, Geotechnical Special Publication 124, ASCE, Reston, VA, 1-18.

Campanella, R. G. (1994). "Field methods for dynamic geotechnical testing: An overview of capabilities and needs." *Dynamic Geotechnical Testing II*, San Francisco, CA, ASTM Special Technical Publication 1213, ASTM, West Conshohoken, PA, 3-23.

Campanella, R. G., Robertson, P. K. and Gillespie, D. (1986). "Seismic cone penetration test." *Use of In Situ Tests in Geotechnical Engineering*, *In Situ '86*, Blacksburg, VA, Geotechnical Special Publication 6, ASCE, Reston, VA, 116-130.

Cascante, G., Vanderkooy, J. and Chung, W. (2003). "Difference between current and voltage measurements in resonant-column testing." *Canadian Geotechnical Journal*, 40(4), 806-820.

Casey, T. J. (2000). "Shear wave data collection in Mid America using an automated surface source during seismic cone testing." *Master of Science*, Civil and Environmental Engineering, Georgia Institute of Technology, Atlanta, 212 p.

Casey, T. J. and Mayne, P. W. (2002). "Development of an electrically-driven automatic downhole seismic source." *Soil Dynamics and Earthquake Engineering*, 22, 951-957.

Cho, G. C. and Santamarina, J. C. (2001). "Unsaturated particulate materials-particle-level studies." *Journal of Geotechnical and Geoenvironmental Engineering*, 127(1), 84-96.

Cola, S. and Simonini, P. (2002). "Mechanical behavior of silty soils of the Venice lagoon as a function of their grading characteristics." *Canadian Geotechnical Journal*, 39(4), 879-893.

den Haan, E. J. and Kruse, G. A. M. (2006). "Characterisation and engineering properties of Dutch peats." *Second International Workshop on Characterisation and Engineering Properties of Natural Soils*, Singapore, Taylor and Francis Group, London, Vol. 4, 2101-2133.

Dyvik, R. and Madshus, C. (1985). "Lab measurements of Gmax using bender elements." *Advances in the Art of Testing Soils Under Cyclic Conditions*, *ASCE Convention*, Detroit, MI, ASCE, Reston, VA, 186-196.

Elzeftawy, A. and Cartwright, K. (1981). "Evaluating the saturated and unsaturated hydraulic conductivity of soils." *Permeability and Groundwater Contaminant Transport*, ASTM Special Technical Publication 746, ASTM, Philadelphia, PA, 168-181.

Ewing, W. M., Jardetzky, W. and Press, F. (1957). *Elastic waves in layered media*. McGraw-Hill, New York, 380 p.

Fahey, M. and Carter, J. P. (1993). "Finite element study of the pressuremeter test in sand using a nonlinear elastic plastic model." *Canadian Geotechnical Journal*, 30(2), 348-361.

Fernandez, A. (2000). "Tomographic imaging the state of stress." *Doctor of Philosophy*, Civil and Environmental Engineering, Georgia Institute of Technology, Atlanta, 297 p.

Finke, K. A., Mayne, P. W. and Klopp, R. A. (1999). "Characteristic piezocone response in Piedmont residual soils." *Behavioral Characteristics of Residual Soils*, *GeoCongress '99*, Charlotte, NC, Geotechnical Special Publication 92, ASCE, Reston, VA, 1-11.

Finke, K. A., Mayne, P. W. and Klopp, R. A. (2001). "Piezocone penetration testing in Atlantic Piedmont residuum." *Journal of Geotechnical and Geoenvironmental Engineering*, 127(1), 48-54.

Finno, R. J. (1989). "Subsurface conditions and pile installation data: 1989 Foundation Engineering Congress test section." *Predicted and Observed Axial Behavior of Piles: Results of the Pile Prediction Symposium*, Evanston, IL, Geotechnical Special Publication 23, ASCE, New York, NY, 1-74.

Finno, R. J. (1992). "Stress-strain-strength responses of compressible Chicago glacial clays." *Journal of Geotechnical Engineering*, 118(10), 1607-1625.

Finno, R. J., Gassman, S. L. and Calvello, M. (2000). "The NGES at Northwestern University." *National Geotechnical Experimentation Sites*, Geotechnical Special Publication 93, ASCE, Reston, VA, 130-159.

Frost, J. D., DeJong, J. T. and Saussus, D. R. (2006). "Analytical investigation of friction sleeve length effects on stratigraphic interpretation." *International Journal of Geomechanics*, 6(1), 11-29.

Frost, J. D. and Drnevich, V. P. (1994). "Towards standardization of torsional shear testing." *Dynamic Geotechnical Testing II*, San Francisco, CA, ASTM Special Technical Publication 1213, ASTM, Philadelphia, PA, 276-287.

Hardin, B. O. and Black, W. L. (1968). "Vibration modulus of normally consolidated clay." *Journal of the Soil Mechanics and Foundations Division*, 94(SM2), 353-369.

Hardin, B. O. and Drnevich, V. P. (1972). "Shear modulus and damping in soils: measurement and parameter effects." *Journal of the Soil Mechanics and Foundations Division*, 98(SM6), 603-624.

Hayashi, K. and Suzuki, H. (2004). "Active and passive surface-wave methods for estimating s-wave velocity structures." *International Conference on Environmental and Engineering Geophysics*, *ICEEG 2004*, Wuhan, China, Science Press, Monmouth Junction, NJ, 90-96.

Hebeler, G. L. (2001). "Site characterization in Shelby County, Tennessee using advanced surface wave methods." *Master of Science*, Civil and Environmental Engineering, Georgia Institute of Technology, Atlanta, 197 p.

Hegazy, Y. A. and Mayne, P. W. (1995). "Statistical correlations between V_S and cone penetration test data for different soil types." *International Symposium on Cone Penetration Testing*, *CPT '95*, Linköping, Sweden, Swedish Geotechnical Society, 2, 173-178.

Henke, W. and Henke, R. (1993). "Laboratory evaluation of in situ geotechnical torsional cylindrical impulse shear test for earthquake resistant design." *Bulletin of the Seismological Society of America*, 83(1), 245-63.

Hepton, P. (1988). "Shear wave velocity measurements during penetration testing." *Penetration testing in the UK*, *Geotechnology Conference*, Birmingham, UK, Thomas Telford, London, 275-278.

Hoar, R. J. and Stokoe, K. H. (1978). "Generation and measurement of shear waves in situ." *Dynamic Geotechnical Testing*, Denver, CO, ASTM Special Technical Publication 654, ASTM, Philadelphia, PA, 3-29.

Houlsby, G. T. and Ruck, B. M. (1998). "Interpretation of signals from an acoustic cone penetrometer." *Geotechnical Site Characterization*, *ISC' 98*, Atlanta, GA, Balkema, Rotterdam, Vol. 2, 1075-1080.

Hryciw, R. D. (1989). "Ray-path curvature in shallow seismic investigations." *Journal of Geotechnical Engineering*, 115(9), 1268-1284.

Hwang, S. K. (1997). "Dynamic properties of natural soils." *Doctor of Philosophy*, Civil Engineering, University of Texas, Austin.

Jamiolkowski, M., Lacellota, R., LoPresti, D. C. F. and Pallera, O. (1994). "Stiffness of Toyoura sand at small and intermediate strain." *13th International Conference on Soil Mechanics and Foundation Engineering*, New Delhi, Balkema, Rotterdam, 1, 169-172.

Jardine, R. J., Chow, F., Overy, R. and Standing, J. (2005). *ICP Design Methods for Driven Piles in Sands and Clays*. Thomas Telford, Ltd, London, 112 p.

Jardine, R. J. and Potts, D. M. (1991). "Some practical applications of a non-linear ground model." *Deformation of Soils and Displacements of Structures*, *10th European Conference on Soil Mechanics and Foundation Engineering*, Florence, Italy, Balkema, Rotterdam, 1, 223-228.

Jardine, R. J., Symes, M. J. and Burland, J. B. (1984). "Measurement of soil stiffness in the triaxial apparatus." *Geotechnique*, 34(3), 323-340.

Jarvis, K. D. and Knight, R. (2000). "Near-surface VSP surveys using the seismic cone penetrometer." *Geophysics*, 65(4), 1048-1056.

Kahler, S. and Meissner, R. (1983). "Radiation and receiver patterns of shear and compressional waves as a function of Poisson's Ratio." *Geophysical Prospecting*, 31, 421-435.

Kalinski, M. E. and Stokoe, K. H. (2003). "In situ estimate of shear wave velocity using borehole spectral analysis of surface waves tool." *Journal of Geotechnical and Geoenvironmental Engineering*, 129(6), 529-535.

Kaneko, F., Kanemori, T. and Tonouchi, K. (1990). "Low-frequency shear wave logging in unconsolidated formations for geotechnical applications." *Geophysical Methods for Geotechnical Investigations*, St. Louis, MO, ASTM Special Technical Publication 1101, ASTM, West Conshohocken, PA, 79-98.

Karl, L., Haegeman, W. and Degrande, G. (2006). "Determination of the material damping ratio and the shear wave velocity with the seismic cone penetration test." *Soil Dynamics and Earthquake Engineering*, 26, 1111-1126.

Kates, G. L. (1997). "Development and implementation of a seismic flat dilatometer test for small- and high-strain soil properties." *Master of Science*, Civil and Environmental Engineering, Georgia Institute of Technology, Atlanta, 173 p.

Keahey, J. (2002). *Venice against the sea: A city besieged*. T. Dunne Books/St. Martin's Press, New York, 296 p.

Keiswetter, D. and Steeples, D. (1994). "Practical modifications to improve the sledgehammer seismic source." *Geophysical Research Letters*, 21(20), 2203-2206.

Kim, D.-S. (1991). "Deformational characteristics of soils at small to medium strains from cyclic tests." *Doctor of Philosophy*, Civil Engineering, University of Texas, Austin.

Kitsunezaki, C. (1980). "A new method for shear-wave logging." *Geophysics*, 45(10), 1489-1506.

Klein, K. (1999). "Electromagnetic properties of high specific surface minerals." *Doctor of Philosophy*, Civil and Environmental Engineering, Georgia Institute of Technology, Atlanta, 335 p.

Kokesh, F. P. (1952). "The development of new method of seismic velocity determination." *Geophysics*, 17(3), 560-574.

Kondner, R. L. (1963). "Hyperbolic stress-strain response; cohesive soils." *Journal of the Soil Mechanics and Foundations Division*, 89(SM1, Part 1), 115-143.

Kramer, S. L. (1996). *Geotechnical earthquake engineering*. Prentice Hall, Upper Saddle River, N.J., 653 p.

Kramer, S. L. (2000). "Dynamic response of Mercer Slough peat." *Journal of Geotechnical and Geoenvironmental Engineering*, 126(6), 504-511.

Ladd, C. C. and DeGroot, D. J. (2003). "Recommended practice for soft ground site characterization: Arthur Casagrande Lecture." *12th Panamerican Conference on Soil Mechanics and Geotechnical Engineering*, *Soil and Rock America 2003*, Boston, MA, VGE, Essen, Germany, 1, 3-57.

Lai, C. G. (1998). "Simultaneous inversion of Rayleigh phase velocity and attenuation for near-surface site characterization." *Doctor of Philosophy*, Civil and Environmental Engineering, Georgia Institute of Technology, Atlanta, 370 p.

Lai, C. G., Pallara, O., Lo Presti, D. C. F. and Turco, E. (2001). *Low-strain stiffness and material damping ratio coupling in soils*. Advanced Laboratory Stress-Strain Testing of Geomaterials, Balkema, Rotterdam, 265-274.

Lehane, B. and Fahey, M. (2002). "A simplified nonlinear settlement prediction model for foundations on sand." *Canadian Geotechnical Journal*, 39(2), 293-303.

Leroueil, S. and Hight, D. W. (2003). "Behaviour and properties of natural soils and soft rocks." *Characterization and Engineering Properties of Natural Soils*, Swets & Zeitlinger, Lisse, 1, 29-254.

Li, X. S., Yang, W. L., Shen, C. K. and Wang, W. C. (1998). "Energy-injecting virtual mass resonant column system." *Journal of Geotechnical and Geoenvironmental Engineering*, 124(5), 428-438.

Liao, T. (2005). "Post processing of cone penetration data for assessing seismic ground hazards, with application to the New Madrid seismic zone." *Doctor of Philosophy*, School of Civil and Environmental Engineering, Georgia Institute of Technology, Atlanta, 470 p.

Liao, T., Zavala, G., Camp, W. M., III, McGillivray, A. V. and Mayne, P. W. (2000). "Results of seismic piezocone penetration tests performed in Memphis, Tennessee." *GTRC Projects E-20-F47/F34*, presented to the USGS and the Mid-America Earthquake Center (MAE), p.

Liu, H. P., Hu, Y., Dorman, J., Chang, T. S. and Chiu, J. M. (1997). "Upper Mississippi embayment shallow seismic velocities measured in situ." *Engineering Geology*, 46(3-4), 313-330.

Liu, H. P., Mair, R. L. and Warrick, R. E. (1996). "An improved air-powered impulsive shear-wave source." *Bulletin of the Seismological Society of America*, 86(2), 530-537.

Liu, H. P., Warrick, R. E., Westerlund, R. E., Fletcher, J. B. and Maxwell, G. L. (1988). "An air-powered impulsive shear-wave source with repeatable signals." *Bulletin of the Seismological Society of America*, 78(1), 355-369.

Lo Presti, D. C. F., Jamiolkowski, M., Pallara, O. and Cavallaro, A. (1996). "Rate and creep effect on the stiffness of soils." *Measuring and Modeling Time Dependent Soil Behavior*, *1996 ASCE National Convention*, Washington, D.C., Geotechnical Special Publication 61, ASCE, Reston, VA, 166-180.

Lo Presti, D. C. F., Pallara, O., Lancellotta, R., Armandi, M. and Maniscalco, R. (1993). "Monotonic and cyclic loading behavior of two sands at small strains." *Geotechnical Testing Journal*, 16(4), 409-424.

Lunne, T., Robertson, P. K. and Powell, J. J. M. (1997). *Cone Penetration Testing in Geotechnical Practice*. Routledge, New York, NY, 312 p.

Mancuso, C., Simonelli, A. L. and Vinale, F. (1989). "Numerical analysis of in situ s-wave measurements." *12th International Conference on Soil Mechanics and Foundation Engineering*, Rio de Janeiro, Brazil, Balkema, Rotterdam, 1, 277-280.

Marchetti, D., Marchetti, S., Monaco, P. and Totani, G. (2007). "Risultati di prove in sito mediante dilatometro sismico (SDMT)." *XXIII Convegno Nazionale di Geotecnica*, *Previsione e controllo del comportamento delle opere*, Padova-Abano Terme, 9p.

Marchetti, S. (1980). "In situ tests by flat dilatometer." *Journal of the Geotechnical Engineering Division (ASCE)*, 106(GT3), 299-321.

Marchetti, S., P. Monaco, Calabrese, M. and Totani, G. (2004). "DMT-predicted vs measured settlements under a full-scale instrumented embankment at Treporti (Venice, Italy)." *Geotechnical and Geophysical Site Characterization*, *ISC-2*, Porto, Portugal, Millpress, Rotterdam, 2, 1511-1518.

Martin, G. K. and Mayne, P. W. (1998). "Seismic flat dilatometer tests in Piedmont residual soils." *Geotechnical Site Characterization*, *ISC '98*, Atlanta, GA, Balkema, Rotterdam, 2, 837-843.

Massarsch, K. R. (1986). "Acoustic penetration testing." *Fourth International Geotechnical Seminar*, *Field Instrumentation and In-Situ Measurements*, Singapore, Nanyang Technological Institute, 71-76.

Mayne, P. W. (2005). "Integrated ground behavior: in-situ and lab tests." *3rd International Symposium on the Deformation Characteristics of Geomaterials*, *ISLyon03*, Lyon, France, Taylor & Francis Group, London, 155-177.

Mayne, P. W., Brown, D. A., Vinson, J., Schneider, J. A. and Finke, K. A. (2000). "Site characterization of Piedmont residual soils at the NGES, Opelika, Alabama." *National Geotechnical Experimentation Sites*, Geotechnical Special Publication 93, ASCE, Reston, VA, 160-185.

Mayne, P. W., Martin, G. K. and Schneider, J. A. (1999). "Flat dilatometer modulus applied to drilled shaft foundations in Piedmont residuum." *Behavioral Characteristics of Residual Soils*, *GeoCongress '99*, Charlotte, NC, Geotechnical Special Publication 92, ASCE, Reston, VA, 101-112.

Mayne, P. W., Schneider, J. A. and Martin, G. K. (1999). "Small and large strain properties from seismic flat dilatometer tests." *Prefailure Deformation Characteristics of Geomaterials*, Torina, Italy, Balkema, Rotterdam, 1, 419-426.

McGillivray, A. and Mayne, P. W. (2004). "Seismic piezocone and seismic flat dilatometer tests at Treporti." *Geotechnical and Geophysical Site Characterization*, *ISC-2*, Porto, Portugal, Millpress, Rotterdam, 2, 1623-1628.

Meng, J. (2003). "The influence of loading frequency on dynamic soil properties." *Doctor of Philosophy*, Civil and Environmental Engineering, Georgia Institute of Technology, Atlanta, 176 p.

Nazarian, S. and Stokoe, K. H. (1984). "In situ shear wave velocities from spectral analysis of surface waves." *8th World Conference on Earthquake Engineering*, San Francisco, CA, 3, 31-38.

Nigbor, R. L. and Imai, T. (1994). "The suspension P-S velocity logging method." *Geophysical Characterization of Sites*, *13th International Conference on Soil Mechanics and Foundation Engineering*, New Delhi, Oxford and IBH Publishing, 57-61.

Ohori, M., Nobata, A. and Wakamatsu, K. (2002). "A comparison of ESAC and FK methods of estimating phase velocity using arbitrarily shaped microtremor arrays." *Bulletin of the Seismological Society of America*, 92(6), 2323-2332.

Park, C. B., Miller, R. D. and Xia, J. (1999). "Multichannel analysis of surface waves." *Geophysics*, 64(3), 800-808.

Puzrin, A. M. and Burland, J. B. (1998). "Non-linear model of small-strain behaviour of soils." *Geotechnique*, 48(2), 217-233.

Puzrin, A. M. and Shiran, A. (2000). "Effects of the constitutive relationship on seismic response of soils. Part I. Constitutive modeling of cyclic behavior of soils." *Soil Dynamics and Earthquake Engineering*, 19(5), 305-318.

Ramberg, W. and Osgood, W. R. (1943). *Description of stress-strain curves by three parameters*. Technical Note 902, National Advisory Committee for Aeronautics, Washington, D.C., 34 p.

Redpath, B. B. (1973). "Seismic refraction exploration for engineering site investigations." *Technical Report E-73-4*, U.S. Army Waterways Experimentation Station, Vicksburg, MS, 60 p.

Ricceri, G., Simonini, P. and Cola, S. (1997). "Stiffness of clayey silts of the Venetian quaternary basin from laboratory tests." *14th International Conference on Soil Mechanics and Foundation Engineering*, Hamburg, Germany, Balkema, Rotterdam, 1, 391-394.

Ricceri, G., Simonini, P. and Cola, S. (2002). "Applicability of piezocone and dilatometer to characterize the soils of the Venice lagoon." *Geotechnical and Geological Engineering*, 20(2), 89-121.

Rice, A. H. (1984). "The seismic cone penetrometer." *Master of Science*, Civil Engineering, University of British Columbia, Vancouver, B.C., 112 p.

Richart, F. E., Hall, J. R. and Woods, R. D. (1970). *Vibrations of Soils and Foundations*. Prentice-Hall, Englewood Cliffs, N.J., 414 p.

Rix, G. J. (2004). *Personal communication*, Georgia Institute of Technology, Atlanta, GA, November 22.

Robertson, P. K., Campanella, R. G., Gillespie, D. and Rice, A. (1986). "Seismic CPT to measure in situ shear wave velocity." *Journal of Geotechnical Engineering*, 112(8), 791-803.

Robertson, P. K. and Wride, C. E. (1998). "Evaluating cyclic liquefaction potential using the cone penetration test." *Canadian Geotechnical Journal*, 35(3), 442-459.

Roblee, C. J., Li, X.-S., Chan, C. K., Idriss, I. M., Wang, G., Herrmann, L. R. and Jackura, K. A. (1994). "Feasibility of a tool for in situ measurement of material properties of clays over a wide strain range." *Dynamic Geotechnical Testing II*, San Francisco, CA, ASTM Special Technical Publication 1213, ASTM, West Conshohocken, PA, 134-161.

Roblee, C. J. and Riemer, M. F. (1998). "Downhole Freestanding Shear Device concept." *Geotechnical Earthquake Engineering and Soil Dynamics III*, Seattle, WA, Geotechnical Special Publication 75, ASCE, Reston, VA, 1, 201-212.

Sanchez-Salinero, I., Roesset, J. M. and Stokoe, K. H. (1986). "Analytical studies of body wave propagation and attenuation." *Geotechnical Engineering Report GR86-15*, The University of Austin, Austin, TX, 272 p.

Santamarina, J. C., Klein, K. A. and Fam, M. A. (2001). *Soils and Waves*. John Wiley & Sons, Inc., Chichester, England, 488 p.

Sasitharan, S., Robertson, P. K. and Sego, D. C. (1994). "Sample disturbance from shear wave velocity measurements." *Canadian Geotechnical Journal*, 31(1), 119-124.

Saussus, D. R., Frost, J. D. and DeJong, J. T. (2004). "Statistical analysis of friction sleeve length effects on soil classification." *International Journal for Numerical and Analytical Methods in Geomechanics*, 28(12), 1257-1278.

Schnabel, P. B., Lysmer, J. and Seed, H. B. (1972). "SHAKE: A computer program for earthquake site response of horizontally layered sites." Earthquake Engineering Research Center, University of California, Berkeley, p.

Schneider, J. A., Hoyos, L. J., Mayne, P. W., Macari, E. J. and Rix, G. J. (1999). "Field and laboratory measurements of the dynamic shear modulus of Piedmont residual soils." *Behavioral Characteristics of Residual Soils*, *GeoCongress '99, Charlotte, NC*, Geotechnical Special Publication 92, ASCE, Reston, VA, 12-25.

Schneider, J. A., Mayne, P. W. and Rix, G. J. (2001). "Geotechnical site characterization in the greater Memphis area using cone penetration tests." *Engineering Geology*, 62(1-3), 169-184.

Scholey, G. K., Frost, J. D., LoPresti, D. C. F. and Jamiolkowski, M. (1995). "A review of instrumentation for measuring small strains during triaxial testing of soil specimens." *Geotechnical Testing Journal*, 18(2), 137-156.

Schwarz, S. D. and Conwell, F. R. (1974). "A technique for the in-situ measurement of shear wave velocities (Vs) for deep marine foundations." *6th Annual Offshore Technology Conference*, Houston, TX, IEEE, 1, 755-762.

Seed, R. B., Cetin, K. O., Moss, R. E. S., Kammerer, A. M., Wu, J., Pestana, J. M., Riemer, M. F., Sancio, R. B., Bray, J. D., Kayen, R. E. and Faris, A. (2003). "Recent advances in soil liquefaction engineering: A unified and consistent framework." *26th Annual ASCE Los Angeles Geotechnical Spring Seminar*, Long Beach, CA, ASCE, Reston, VA, 71.

Shibuya, S., Mitachi, T., Hosomi, A. and Hwang, S. C. (1996). "Strain rate effects on stress-strain behaviour of clay as observed in monotonic and cyclic triaxial tests." *Measuring and Modeling Time Dependent Soil Behavior*, *1996 ASCE National Convention*, Washington, D.C., Geotechnical Special Publication 61, ASCE, Reston, VA, 214-227.

Shibuya, S., Yamashita, S., Mitachi, T. and Tanaka, H. (1995). "Effects of sample disturbance on G_{max} of soils - a case study." *1st International Conference on Earthquake Geotechnical Engineering*, Tokyo, Japan, 1, 77.

Shima, E. and Ohta, Y. (1967). "Experimental study on generation and propagation of S-Waves: I., Designing of Sh-Wave generator and its field tests." *Bulletin of the Earthquake Research Institute of Tokyo*, 45, 19-31.

Simonini, P. (2004). "Characterization of the Venice lagoon silts from in-situ tests and the performance of a test embankment." *Geotechnical and Geophysical Site Characterization*, *ISC-2*, Porto, Portugal, Millpress, Rotterdam, 187-207.

Simonini, P., Ricceri, G. and Cola, S. (2006). "Geotechnical characterization and properties of Venice lagoon heterogeneous silts." *Second International Workshop on Characterization and Engineering Properties of Natural Soils*, Singapore, Taylor and Francis Group, London, Vol. 4, 2289-2330.

Simons, N. E., Menzies, B. K. and Matthews, M. C. (2002). *A Short Course in Geotechnical Site Investigation*. Thomas Telford, London, 353 p.

Stam, J. C. (1962). "Modern developments in shallow seismic refraction techniques." *Geophysics*, 27(2), 198-212.

Stewart, W. P. and Campanella, R. G. (1993). "Practical aspects of in situ measurements of material damping with the seismic cone penetration test." *Canadian Geotechnical Journal*, 30(2), 211-219.

Stokoe, K. H., II, Arnold, E. J., Jr., Hoar, R. J., Shirley, D. J. and Anderson, D. G. (1978). "Development of a bottom-hole device for offshore shear wave velocity measurement." *10th Annual Offshore Technology Conference*, Houston, TX, OTC 3210, 1367-1375.

Stokoe, K. H. and Santamarina, J. C. (2000). "Seismic-wave-based testing in geotechnical engineering." *International Conference on Geological and Geotechnical Engineering*, *Presentation*, Melbourne, Australia.

Summers, G. C. and Broding, R. A. (1952). "Continuous velocity logging." *Geophysics*, 17(3), 598-614.

Tan, T.-S., Lee, F.-H., Chong, P.-T. and Tanaka, H. (2002). "Effect of sampling disturbance on properties of Singapore clay." *Journal of Geotechnical and Geoenvironmental Engineering*, 128(11), 898-906.

Tatsuoka, F., Jardine, R. J., LoPresti, D., DiBenedetto, H. and Kodaka, T. (1999). "Characterizing the pre-failure deformation properties of geomaterials." *14th International Conference on Soil Mechanics and Foundation Engineering*, Hamburg, Germany, 4, 2129-2164.

Tatsuoka, F. and Shibuya, S. (1992). "Deformation characteristics of soils and rocks from field and laboratory tests." *Report of the Institute of Industrial Science*, The University of Tokyo, 37(1), 136.

Tokimatsu, K. (1995). "Geotechnical site characterization using surface waves." *1st International Conference on Earthquake Geotechnical Engineering*, *IS-Tokyo '95*, Balkema, Rotterdam, 1333-1368.

Tokimatsu, K., Tamura, S. and Kojima, H. (1992). "Effects of multiple modes on Rayleigh wave dispersion." *Journal of Geotechnical Engineering*, 118(10), 1529-1543.

Triantafyllidis, T., Wichtmann, T. and Niemunis, A. (2004). "On the determination of cyclic strain history." *International Conference on Cyclic Behaviour of Soils and Liquefaction Phenomena*, *CBS04*, Bochum, Balkema, Rotterdam, 321-334.

Tringale, P. T. and Mitchell, J. K. (1982). "An acoustic cone penetrometer for site investigations." *Second European Symposium on Penetration Testing*, *ESOPT II*, Amsterdam, Balkema, Rotterdam, Vol. 2, 909-914.

Villet, W. C. B., Mitchell, J. K. and Tringale, P. T. (1981). "Acoustic emissions generated during the quasi-static cone penetration of soils." *Acoustic Emissions in Geotechnical Engineering Practice*, ASTM Special Technical Publication 750, ASTM, Conshohocken, PA, 174-193.

Vinson, J. L. and Brown, D. A. (1997). "Site characterization of the Spring Villa Geotechnical Test Site and a comparison of strength and stiffness parameters for a Piedmont residual soil." *Research Report No. IR-97-04*, Civil Engineering Dept., Auburn University, Auburn, AL, 385 p.

Vogel, C. B. (1952). "A seismic velocity logging method." *Geophysics*, 17(3), 586-597.

Vucetic, M. (1994). "Cyclic threshold shear strains in soils." *Journal of Geotechnical Engineering*, 120(12), 2208-2228.

Wang, Y.-H. (2001). "Attenuation in soils and non-linear dynamic effects." *Doctor of Philosophy*, Civil and Environmental Engineering, Georgia Institute of Technology, Atlanta, 281 p.

Wang, Z. W., Soltis, J. J. and Miller, W. C. (1992). "Improved approach to interpolation using the FFT." *Electronics Letters*, 28(25), 2320-2322.

White, J. E. (1983). *Underground sound: Application of seismic waves*. Elsevier, New York, 253 p.

Williams, R. A., Wood, S., Stephenson, W. J., Odum, J. K., Meremonte, M. E., Street, R. and Worley, D. M. (2003). "Surface seismic refraction/reflection measurement determinations of potential site resonances and the areal uniformity of NEHRP site class D in Memphis, Tennessee." *Earthquake Spectra*, 19(1), 159-189.

Woods, R. D. (1978). "Measurement of dynamic soil properties." *Earthquake Engineering and Soil Dynamics*, Pasadena, CA, ASCE, Reston, VA, 1, 91-178.

Woods, R. D. (1994). "Laboratory measurement of dynamic soil properties." *Dynamic Geotechnical Testing II*, San Francisco, CA, ASTM Special Technical Publication 1213, ASTM, Philadelphia, PA, 165-190.

Woolery, E., Street, R., Wang, Z. and Harris, J. (2000). "NEHRP soil classifications and 1-d site effects in the upper Mississippi embayment." *Seismological Research Letters*, 71(1), 114.

Yamamoto, T., Rogers, A. and Trevorrow, M. (1991). "Experimental verification and application of bottom shear modulus profiler (BSMP) method." *Ocean Technologies and Opportunities in the Pacific for the 90's*, *Oceans '91*, Honolulu, HI, IEEE, Piscataway, NJ, 1, 123-128.

Yilmaz, Ö. (1987). *Seismic Data Processing*. Society of Exploration Geophysicists, Tulsa, OK, 526 p.

Zhang, J. and Toksoz, M. N. (1998). "Nonlinear refraction traveltime tomography." *Geophysics*, 63(5), 1726-1737.

Zywicki, D. J. (1999). "Advanced signal processing methods applied to engineering analysis of seismic surface waves." *Doctor of Philosophy*, Civil and Environmental Engineering, Georgia Institute of Technology, Atlanta, 357 p.